UNIVERSITY of STIRLING

Sandstone Heritage in a Climate Change(d) Future: Weathering of Torridonian and Devonian building stone and its implications for conservation

David Crawford McCaughie

BSc (Hons)

June 2021

Thesis submitted for the degree of Doctor of Philosophy

Biological and Environmental Science

School of Natural Sciences

University of Stirling

Scotland

Table of Contents

List of Figures

List of Tables

Commonly used Acronyms

CEF	Controlled Environment Facility.
HES	Historic Environment Scotland.
IPCC	International Panel on Climate Change.
PPL	Plane Polarised Light.
SEM-EDX	Scanning Electron Microscope with Dispersive X-Ray analyser.
SMC	Scheduled Monument Consent.
UKCP09	United Kingdom Climate Projections 2009.
UKCP18	United Kingdom Climate Projections 2018.
UNESCO	United Nations Educational, Scientific and Cultural Organisation.
XPL	Crossed Polarised Light.
XRD	X-Ray Diffraction.
XRF	X-Ray Fluorescence.

Acknowledgements

Fresh out of school in 2012, I did not think university was for me. After a year out, I decided to give it a go and from my very first lecture at the University of Stirling, which I recall was on the formation of the solar system, I knew I had made the correct decision.

In the third year of my undergraduate studies, I selected ‘Geoarchaeology’ as one of my modules, coordinated by Professor Ian Simpson. This turned out to be among the most astute academic choices I made while at university. Without Ian, I would have thought myself completely out of my depth in pursuing a PhD straight after completing my undergraduate degree in Environmental Science. As well as setting up fantastic opportunities including my visit to Kyoto University, Japan, in 2018, his support, guidance, motivation, expertise, friendship and confidence in my research has been unwavering.

I owe a great deal of thanks to Dr Clare Wilson, who has stepped up at extremely short notice in the final stages of my PhD to provide valuable comments, suggestions, and guidance ahead of my thesis submission. Clare, in no small part, has ensured that I have been able to complete and submit a PhD that I am proud of.

Within Biological and Environmental Sciences, I am grateful to have had excellent technical assistance from Mr George MacLeod and Mr James Weir. Throughout my PhD, George produced over 60 high quality petrographic thin sections, completed XRF analysis for salts and provided extensive thin section and SEM-EDX training and support. James briefed me on the use of the University of Stirling’s CEF, he programmed all required chambers to the exact climatic parameters provided and was always there to make sure the chambers were running smoothly, which ensured that the experimental phase of my research was successful.

The University of Stirling and HES jointly provided funding for my PhD which I am extremely grateful for. Enormous credit is due to both organisations who permitted me a 6-month funding extension to account for pandemic related delays.

Before the pandemic, I was fortunate to be able to work closely with HES’s Science Team at The Engine Shed in Stirling. I owe particular thanks to Dr Callum Graham who took time out of his extremely busy schedule on numerous occasions to share his expertise in describing petrographic thin sections, as well as provide comprehensive XRD training and assist in conducting sandstone physical characterisation tests. I would also like to thank Dr Ewan Hyslop and Dr Aurelie Turmel, also of HES. Their wealth of experience was extremely

valuable, particularly as I developed my research design. I very much hope to have the opportunity to work with colleagues at HES again in the not-too-distant future.

Although our time together in person was interrupted due to COVID, I was lucky enough to be part of an excellent PhD cohort. I have shared an office for the majority of my PhD with some fantastic people from around the world, each with their own interesting and unique research project, fascinating life experiences and genuine passion for what they do. Every cloud has a silver lining and working from home prompted the creation of the 'Heritage' and 'Living Landscapes' lab groups which I looked forward to attending every week.

I owe a massive thank you to my parents, Isabel, and Crawford, who go above and beyond to support me in everything that I do, and my siblings, Scott, and Caitlin who I can always rely on for a good laugh. It has been an eventful few years, but I can always count on my family.

Finally, my wonderful fiancée, Rebecca, I bet you learned more about brochs and sandstone than you ever cared to! I could not have completed this thesis without you; whether from 3000 miles away in your hometown of Albany, NY, or from right by my side, your loving support and ability to see the good in any situation has kept me going through all the ups and downs of my PhD.

Abstract

Sandstones are important to Scotland's heritage as a traditional building stone from the Neolithic to the present day and are particularly susceptible to weathering. This thesis focuses on two Scottish sandstones; Torridonian Sandstone and Stromness Flagstone, found in Clachtoll and Borwick Brochs, respectively. Culturally significant sandstones of these types were obtained from archaeological spoil associated with each site, and are weathered stone initially exposed above ground during the Scottish Middle Iron Age (Clachtoll C14 date; ca. 2025 ± 30 BP). Samples of each sandstone were also collected from geological outcrops as unweathered control rock. The baseline condition of control rock and broch stone has been determined with focus placed on how the stone had weathered since their emplacement above surface. Petrographic thin section analysis, X-Ray diffraction (XRD) analysis, and scanning electron microscope with dispersive X-Ray analyser (SEM-EDX) analysis results have identified weathering features brought about by exposure above surface, particularly in the Stromness Flagstone. Conversely, the Torridonian Sandstone broch stone appears robust. These findings formed a baseline of each sandstone type and how they have weathered to date. Through exposure to warmer, wetter winters and warmer, drier summers in a climate changed future in Scotland, the weathering of these sandstones may accelerate. To understand this, innovative controlled environment facility (CEF) experiments have been conducted, whereby sub-samples of control rock and broch stone were subjected to systematic accelerations of climate change parameters, informed by UKCP18 data. In both the 'Climate Changed Year' and '30-Year Seasonal Climate Change' experiments, broch stone, particularly from Borwick, is seen to weather at an increased rate under climate changed conditions, compared to the present day. This is evidenced by surface failures, salt formation and dolomite dissolution exacerbated by sulphide weathering in Stromness Flagstone samples, as well as increased granular loss and vertical cracking in Torridonian Sandstone.

Quotation

“We must never forget that the natural environment is a collective good, the patrimony of all humanity and the responsibility of everyone”

Pope Francis, 2017.

1 Introduction and Literature Review

1.1 Introduction

The environmental implications of climate change are multifaceted and include threats posed to cultural, historic environments, manifested through a forecast increase in chemical, physical and biological weathering of significant stone buildings, structures, and monuments (Hulme *et al.*, 1999; Adger *et al.*, 2012; Parmesan and Yohe, 2003). Observations made, such as from the Mauna Loa Observatory in Hawaii have highlighted an irrefutable, increasing global output of CO_2 since the 1950s, primarily from anthropogenic sources, contributing to a changing global climate (Keeling *et al.*, 1976). The International Panel on Climate Change (IPCC) published a special report in 2018 on the effects of a 1.5°C increase in global temperature above pre-industrial levels. The report showed that currently, anthropogenic activity has resulted in around 1.0°C of global warming above pre-industrial levels, and states with high confidence that this increase is likely to reach 1.5°C between 2030 and 2052 if warming continues at the present rate (IPCC, 2018). As a consequence, heritage scientists and organisations are beginning to recognise that culturally important structures will be exposed to new climatic conditions, having a potentially destructive, but as yet unknown impact on the historic environment (Viles and Cutler, 2012). An intrinsic theme of this thesis is to elucidate more precisely the effect that climate change will have on the historic environment, with a specific focus placed on the rich and diverse sandstone heritage of Scotland that is investigated, cared for, and promoted by Historic Environment Scotland (HES).

In order to produce a robust and comprehensive literature review, extensive discussion occurred with conservation practitioners as well as geology, stone weathering, and climate science experts at HES. A series of key concepts were highlighted, and a targeted literature search was conducted through a series of academic research databases, including SCOPUS, Web of Science and ScienceDirect. Furthermore, publications produced by relevant organisations including HES, UNESCO and the IPCC were also consulted. The key components of this literature review are outlined in depth below.

To highlight the relevance and significance of this research, the following literature review firstly showcases Scotland's traditional building landscape and its once-booming building stone industry. Scottish heritage structures are then contextualised within the growing belief that through anthropogenic climate change, we have entered a new geological epoch, The Anthropocene. The global importance of this study field is then highlighted, with specific

culturally significant sandstone sites throughout the world being discussed, including those inscribed by the United Nations Educational, Scientific and Cultural Organisation (UNESCO) as World Heritage Sites. With an emphasis on sandstones, the focus of this thesis, a synthesis of advancements made in understanding rock weathering processes are put forward. This is achieved by outlining some of the most prevalent processes in rock decay. Literature emerging from temperature extremes are appraised, and the role of climate change in altering rock weathering processes is discussed. Leading on from this, the classification and protection of cultural heritage is appraised before the threats posed to such heritage by climate change are outlined. The importance of this study is then highlighted once more by illustrating how it ties in with future cultural heritage and climate change agendas set out by relevant organisations, namely UNESCO and HES. The aims of this thesis are then provided at the conclusion of this chapter through a synthesis of highlighted gaps in the literature.

1.2 Scotland's Building Stones

Stone has been a fundamental building material in Scotland from the Neolithic to the present day, with world-renowned archaeology and architecture reflecting the diverse geology of the country, encompassing rocks that date back as far as 3 billion years. Showcasing Scotland's diverse and widespread building stone, granites from Aberdeenshire have been utilised as building stone for centuries, with Aberdeen itself nicknamed 'The Granite City'. Thickly bedded flagstone is abundant in Orkney and Caithness, utilised as paving and building stone. On the Western Isles, including Arran and Mull, locally sourced granite and Mesozoic sandstones have been used to build villages and towns. In the Midland Valley, Devonian and Carboniferous sandstone is plentiful and has provided building stone for many places throughout the country. Volcanic lavas surround Glasgow and Edinburgh, although these are difficult to build with, they have been used in rubble walls and the construction of roads. Greywackes of Ordovician and Silurian age located in the Scottish Borders have likewise been used for rubble wall construction, while Galloway granite is incorporated in a wide array of structures from homes to monuments to harbours (British Geological Survey, 2005).

The building stone industry in Scotland began with local stone quarries, usually exploited close to settlements where the stone could be obtained and transported with relative ease to be utilised in the construction of nearby buildings. The use of locally available stone coupled with Scotland's rich and diverse geology has resulted in distinct and variable building stone characteristics throughout the country (Gillespie and Tracey, 2016). In the 19th century, Scotland had more than 700 operational quarries that fulfilled domestic and international

demand with Scotland's stone being transported across the world. By the end of the 20th century, however, only 20 quarries remained, with only 12 of those producing sandstone as a building stone (Mcmillan and Hyslop, 2008). Presently, Scotland has around 450,000 traditional buildings and the drastic reduction in quarried sandstone from which the majority are constructed, has made finding adequate replacement stone for building repairs considerably more difficult. Furthermore, a loss of traditional building knowledge compounds the vulnerability of buildings to decay without sufficient repair work being conducted. There is still demand for stone in both building construction and repair work, however, this demand is typically met by stone imports owed to the fact that almost all historic building quarries now lie abandoned in Scotland (Historic Environment Scotland, 2011; Gillespie and Tracey, 2016). To overcome the need to import and to ensure the stone used in any repair work matches well with the type used in the building originally, the re-opening of old quarries has been sought. This was successful at Cullalo Quarry in Fife, which was re-opened in 2003 to provide Carboniferous sandstone to be used for repair work on Edinburgh's buildings (Mcmillan and Hyslop, 2008).

1.3 Climate Change and The Anthropocene

To understand key weathering processes, it is important to set the context of heritage within a changing climate. Scientific study on the influence of atmospheric absorption on the climate developed in the late 19th century and it is perhaps Arrhenius, 1896, who made the most crucial breakthrough in understanding the greenhouse effect. Arrhenius discovered that increasing atmospheric CO_2 causes increased surface temperature on earth, with the opposite being true if atmospheric CO_2 is decreased. Crucially, Arrhenius outlined that anthropogenic activity such as fossil fuel burning caused the amount of atmospheric CO_2 to rise, triggering global warming. Since then, greater awareness has developed relating to how humans influence the earth's climate. Modelling by Manabe *et al.,* 1967 produced evidence to robustly support that doubling atmospheric CO_2 has a warming effect on the earth of around 2°C. Keeling *et al.*, 1976 analysed atmospheric CO_2 data from the Mauna Loa Observatory, Hawaii, a program designed to monitor the influence of fossil fuel burning on atmospheric CO_2 levels. The analysis found that from 1959-1971, annual average CO_2 concentration in the atmosphere increased by 3.4%. Manua Loa data is still being collected at present and the trend discovered in the 1970s is still reflected in 2020 data (Global Monitoring Laboratory, 2020).

Pioneering research over the last two centuries has helped shape our understanding of climate change and the role humans play in its prevalence. Now, scientists and the general public are aware that anthropogenic activity is changing climate patterns on a global scale. Scientific literature is vast on the effects that a rise in temperature by only a few degrees can have on varied ecosystems and environmental processes. There is growing literature suggesting that the mounting interference of humans on earth's most fundamental functions with little sign of reversal, has caused the planet to transition from the post-glacial geological epoch of the Holocene into a new epoch, The Anthropocene. The inception of this transition was popularised by Paul Crutzen, a Nobel Prize-winning atmospheric chemist, in 2002. Since then, the proposed new epoch has made its way progressively into geological literature and is now commonly recognised, with debate arising as to its legitimacy, and start point.

Proposals for delineating the base of the Anthropocene include an 'early Anthropocene', aligning with the advancement of agriculture and deforestation; the Industrial Revolution, occurring at ca.,1800 CE; and the Great Acceleration, taking place during the mid-20th century, characterised by rapid population growth and industrialisation. Formal acknowledgement of a transition into the Anthropocene rests on whether human activity has become a sufficiently recognisable force, enough to leave a distinct stratigraphic marker in sediment and ice, significantly different from that of the Holocene. The idea for an Industrial Revolution defined transition into the Anthropocene has become increasingly favoured (Steffen *et al*., 2007; Zalasiewicz *et al.*, 2008; Waters *et al.*, 2016).

The proposed new epoch, therefore, can be characterised by such processes as rapid population growth, urbanisation, the exhaustion of fossil fuels with associated CO_2 emissions, the transformation of land and the release of harmful substances. Each of these processes, and more, leaving their mark on the planet, not least through climate change. Regardless of a formal definition or acceptance of the Anthropocene as a new epoch, the notion of the Anthropocene highlights that the earth, and of particular relevance to this thesis, its climate, has changed as a direct result of anthropogenic activity, so much so, the delineation of recent geological time is under question. This climate change is robustly supported through pioneering scientific efforts and research, as highlighted, such as the IPCC's special report on the impacts of global warming of 1.5°C above pre-industrial levels (IPCC, 2018).

Concerning building stone weathering, stone will be exposed to new pressures associated with The Anthropocene. As outlined by Gomez-Heras and McCabe, (2015), stone surfaces

themselves can be used as a proxy for understanding past anthropogenic change due to their exposure above surface, in some instances, for millennia. From this 'memory effect' embedded in the stone, the past weathering of the stone can be understood, from which predictions can be made as to how the stone will proceed to weather. Additionally, Goudie and Viles, (2016) highlight that it is important for global change research to be undertaken to understand the effects of a potential epoch transition on varying systems. The impacts, principally through climate change, are vast, arguably affecting all processes on earth to some degree. These impacts can be difficult to recognise, as climate change does not necessarily bring about new processes influencing an environmental function, but instead accelerate existing ones. Disentangling this acceleration from underlying processes is a difficult but vital task for heritage scientists.

The exposure history or 'memory effect' of samples utilised in this research forms a fundamental and vital aim of this thesis. Through the understanding of how past climatic conditions have influenced specific sandstone types, predictions can be made as to how the same sandstone types will be influenced by new, more extreme climate conditions. This research focuses specifically on the weathering of culturally significant stone, whereby present and past alterations will influence to a considerable extent any future climate-induced weathering. This thesis seeks to discover whether exposure of already weathered sandstone to more extreme climates will be destructive enough to result in a loss of important sandstone heritage in Scotland.

1.3.1 Climate Change in Scotland

The principal source of climate projection data for Scotland is obtained from the United Kingdom Climate Projections frameworks released in 2009 and 2018 (UKCP09 and UKCP18 respectively). UKCP09 climate projections for variables such as temperature, humidity and precipitation were available under three emission pathways of low, medium, and high. Data could be obtained for 25km sections of the UK, and entire regions. This data was utilised by HES in their pioneering 'Climate Change Risk Assessment of the Properties in Care of HES'. Within this report, it is noted that Scotland's climate has already changed markedly since the 2009 analyses and is continuing to do so. Compared with the 1960s, Scotland is currently experiencing 27 fewer days of frost, 32 fewer days of snow cover, a 1°C increase in temperature, 21% more rainfall and a sea-level rise of 3mm. Utilising UKCP09 data under a high emission scenario at 50% probability, by 2050, Scotland's sea level could rise between 16.5cm and 28.1cm, with a temperature increase of 2.8°C in summer and 2.2°C in winter

while rainfall will decrease by 13% in summer and increase by 16% in winter. Of course, under different emission pathways, these figures fluctuate and regional variations would also occur; however, HES, through this risk assessment identified that of 352 analysed sites, 89% are at high or very high risk of damage as a direct result of climate change (Historic Environment Scotland, 2017a).

The UKCP18 framework has recently updated the UKCP09 (no longer available in its full format), and this now provides the most current data on how the UK's climate is likely to change through to 2100. The UKCP18 database provides higher-resolution data than the previous framework, with global projections available at 60km and UK projections at 12km and 2.2km resolution. Although generally consistent with UKCP09, a greater depth of information is available from the updated framework.

By 2100, the UK is predicted to be warmer, particularly in the summer months, in keeping with global trends in temperature change. UKCP18 climate projections, like the UKCP09, provides local low, central, and high changes throughout the UK, equivalent to 10%, 50% and 90% probability. Under a high emission scenario, the range of projected temperature increase is between 0.9 °C and 5.4 °C in summer, and 0.7 °C to 4.2 °C in winter, by 2070. Similarly, for precipitation under a high emissions scenario, a -47% to +2% change in summer precipitation is expected, and a -1% to +35% change in winter precipitation by 2070 (UKCP, 2019).

It is clear, therefore, that Scotland's climate is changing. This thesis explores the potentially destructive effects that a changing climate may have on the country's stone-built heritage, which is poorly understood at present.

1.4 Global Cultural Significance of Sandstone

Sandstone is prevalent worldwide, both in natural geological features and in built structures, some of which have been inscribed as UNESCO World Heritage Sites due to their outstanding universal value, meeting criteria outlined by UNESCO in their 1972 convention (UNESCO, 1972). Among these sites is The Karnak temple complex in Egypt, one of the largest of its kind, comprising around 20 temples. Evidence from recent studies suggests that the complex was first inhabited between 2160 and 2055 BC (Turkington and Paradise, 2005; Ghilardi and Boraik, 2011; Marey Mahmoud *et al.*, 2011). Research has been undertaken to limit heritage loss through weathering at the Luxor temple, one of the minor temples within the complex. Lower Campanian/upper Cretaceous sandstone known as Gebel el-Silsila, or

'Nubian Sandstone' has been used in the construction of the temple, as well as for any necessary repairs. There is considerable variation in sandstone composition within the temple and 4 types of Gebel el-Silsila are characterised by Fitzner *et al.,* (2003) in terms of porosity and existing stone damage, where, through mapping techniques, a model characterising the extent of weathering on specific sections of the temple could be produced. Using the model, it was determined that while some areas displayed evidence of severe weathering, other areas within the same structure remained in a good or acceptable condition. This allowed the study to conclude that the severity of weathering does not correlate with age, but rather with the environmental microclimates found throughout the temple, a conclusion of fundamental relevance to stone sites throughout the world.

Similarly, within the Karnak temple complex, Saleh *et al.,* (1992) investigated the particularly severely weathered Temple of Amun-Ra, where entire layers of sandstone have failed, resulting in the loss of ancient wall paintings. This process occurs through the dissolution of key cementing agents within the stone. The paper provides evidence to suggest that the application of silane compounds to the structure, at times of the year when it is most vulnerable, could consolidate the sandstone, reduce water ingress, and help manage weathering at the site.

The ancient city and inscribed UNESCO World Heritage Site of Petra, Jordan, is a particularly spectacular example of sandstone heritage under threat from weathering. The site is predominantly composed of Lower Palaeozoic sedimentary rocks, with middle and upper Cambrian Umm Ishrin and Ordovician Disi sandstones comprising the majority of the monuments. Hundreds of monuments carved directly into sandstone bedrock are seen at the site which dates back to approximately 2000 BP (Heinrichs, 2008). Alarmingly, greater than 50% of the carved sandstone monuments at Petra have been damaged, primarily by salt weathering, with close to 12% of structures being destroyed by cavernous tafoni formation, also referred to as honeycomb weathering, owed to the physical appearance of the feature. Due to the destructive effects that salt weathering has had on the ancient city, efforts have been made to understand this complex process at the site, while generating potential mitigation strategies to reduce heritage loss at Petra (Wedekind and Ruedrich, 2006). Additionally, the controlling factors of mortar type, temperature, humidity, moisture and human impacts on the weathering of Petra monuments has been documented since 2001 (Al-Saad and Abdel-Halim, 2001; Paradise, 2002, 2005).

Further exemplifying the severely detrimental impact that weathering has on built sandstone heritage, The Angkor Temple, Cambodia, likewise an inscribed UNESCO World Heritage Site, has been studied in recent years. The Temple is constructed from primarily three sandstone types, these include grey to yellowish-brown sandstone, red sandstone, and greenish greywacke, supplied from numerous local quarries. Like Petra, there is a growing concern for the future of the site, particularly due to the prevalence of salt weathering. Salt, derived from the calcite cement of the sandstone as well as from bat guano, are identified as important sources from which salt infiltrates into pore space, crystallises and expands, increasing stone porosity (Hosono *et al.,* 2006). Further work by Siedel *et al.*, (2010), concludes that the main source of weathering at the temple is as a consequence of wetting and drying cycles that impact the salt weathering regime and that anthropogenic impacts are negligible. It must, however, be noted, that with future climate change, wetting and drying periods could be altered, having implications on the severity of weathering at the site through this process (Brimblecombe *et al.,* 2011).

With the realisation that weathering, and sandstone degradation has led to a loss of heritage at some of the world's most significant sites, there is an increased drive in the literature to understand and, where possible, mitigate the effects of weathering on stone-built sites throughout the world, emphasising the importance of the research undertaken in this thesis. Of note, in the referenced literature, no attention is paid to the future role that climate change will play in potentially exacerbating weathering processes on already vulnerable UNESCO World Heritage Sites. Addressing this highlighted knowledge gap, this thesis aims to understand the vulnerability of culturally and historically significant sandstone sites in Scotland to climate change. In doing so, this contributes to literature pertaining to the way sandstone degrades, while providing vital insight into the yet unknown implications that climate change has on sandstone heritage. This thesis sees the future impact of climate change as a principal threat to sandstone heritage and offers ways of building relevant climate change scenarios into the analyses of heritage monument weathering.

1.5 Rock Weathering

Weathering is an intrinsic process in long-term rock formation and destruction processes and must be explored extensively in the effort to comprehend in what manner rock degradation will occur as a result of climate change, both in underlying geology and in the built, historic environment (Hall *et al.,* 2012). The complexities of weathering at the rock–atmosphere interface is well documented. Interactions between physical, chemical and biological

processes that underpin rock weathering and the dynamic nature of these processes which operate under fluctuating environmental conditions is being increasingly understood (Moses *et al.,* 2014; Røyne *et al.,* 2008).

The interactions of different weathering and environmental processes are highlighted by Viles, (2013) and the author's elucidation between the terms 'weathering' and 'erosion' is important to outline due to their often interchangeable application. Hall *et al.,* (2012) similarly convey the important distinction between the two processes. These semantic issues notwithstanding, weathering has been defined (Yatsu, 1988; Pope *et al.,* 1995), as the *in-situ* breakdown and subsequent release of materials, generating a new and dynamic set of characteristics that the rock proceeds to exist in, under continued atmospheric and climatic conditions. Erosional processes subsequently remove and transport these released materials.

Weathering occurs by physical, chemical and biological means, which result in the development of an altered rock surface, allowing erosion, i.e. the removal of material, to take place (Moses *et al.,* 2014). It can be said, therefore, that weathering controls the rate of erosion, and the greater the weathering susceptibility of a lithology or structure, the greater erosion will occur. The relatedness of weathering and erosional processes continues to be contested in the literature. There is a clear synergy between the two processes, however, it is essential to understand their fundamental differences.

Exemplifying the synergy between weathering and erosion, cryptoendolithic organisms, through photosynthesis, caused bioalkalisation to occur in Tshipise Sandstone, a fine-grained, late Triassic outcrop in South Africa. This gave rise to chemical weathering, releasing sandstone constituents. Subsequently, the released material was exposed to erosional mechanisms, namely wind, water and trampling which removed the material from the rock, leaving behind a new surface with inherent susceptibility to future weathering (Budel *et al.,* 2004).

Technological advancements have been made in recent years, whereby state of the art methods have been employed to understand the decay of stone on the micro-scale, particularly through a greater understanding of micro-porosity and the role it plays in stone weathering. Dewanckele *et al.,* (2012), researched the development of a gypsum weathering crust by exposing a calcareous sandstone to gaseous sulphur dioxide. X-ray tomography was employed at differing stages of the sulphur dioxide treatment to envisage crust formation and pore modification resulting from the stone's exposure to a strong acid.

Micro-CT was utilised by De Kock *et al.,* (2015) to better understand the process of freeze-thaw and through this analytical technique fracture systems developing in porous limestone were more clearly understood. Furthermore, the precise type and nature of pores most vulnerable to fracture induced by freeze-thaw were identified, giving a fresh and innovative perspective on pore-scale study of the freeze-thaw process.

Finally, water distribution in sedimentary rocks was visualised through neutron radiography and microtomography by Boone *et al.,* (2014). This technique showcased the benefits of utilising a non-destructive technique to better understand water uptake in porous rock, a factor greatly influencing weathering.

It is evident, therefore, that advancements have been made on the general comprehension of rock weathering in recent decades, exemplified in the above studies. New understandings have begun to emerge surrounding weathering's complex and manifold interactions with other environmental processes and the controlling influence that climate has on decay processes (Moses *et al.,* 2014).

1.5.1 Role of Moisture and Temperature

New understandings relating to the influence of moisture on sandstone weathering have emerged in recent decades. Work by Hall and Hall, (1996) focused on the occurrence of wetting and drying cycles and subsequent weathering. It was noted that the cycle affected the type of weathered materials found in the rock. Additionally, rock characteristics such as porosity were altered, in turn influencing other weathering mechanisms. Ruedrich *et al.,* (2011) explored the role of moisture regimes in increasing the volume of sandstone, influencing rock deterioration. By examining eight different sandstone types from Germany, the study showed a direct correlation between pore size, the magnitude of water inundation, the severity of rock swelling and the resultant degradation of sandstone. In the field, work conducted in South Africa by Mol and Viles, (2010, 2012) at the Golden Gate Reserve, illustrated the poorly understood relationship between sandstone weathering and moisture regimes. Their research monitored tafoni features, showing that varying internal moisture regimes dictate to a significant degree, the extent and nature of tafoni found on the sandstone surface. Moisture regimes were mapped using non-destructive techniques, and it was discovered that flaking and resultant tafoni formation occurred due to pockets of water within the sandstone instigating the weathering process.

McCabe *et al.*, (2015) explored the interrelatedness of moisture with temperature and the implications this relationship has on sandstone weathering, noting that both factors are vital aspects of the weathering process. It was determined that stone temperature and moisture influence one another, should a change occur in one, it will be reflected in the other. Studies related to the fluctuation of temperature and the implications for sandstone weathering in extreme environments are common (Warke and Smith, 1998; McKay *et al.*, 2009; Smith *et al.*, 2011). On a more domestic level, studies are limited as highlighted by Jamison *et al.*, (2010) who focused their fieldwork in Belfast, Northern Ireland. Their findings, under temperate conditions, show that the reaction of stone to different temperature and moisture regimes is characterised by subtle, short-term variations occurring within more predictable, larger-scale fluctuations. Identifying smaller-scale changes that influence weathering is complex and more work is required to investigate these fluctuations to understand the underlying forces affecting sandstone degradation. Additionally, as weathering occurs, the complexity of sandstone increases with changing physical characteristics, greatly modifying how moisture penetrates sandstone. Jamison *et al.*, (2010) explain that with changing rock structure, moisture can penetrate deeper into the sandstone and be held there longer, exacerbating weathering.

1.5.2 Freeze-thaw Weathering

Freeze-thaw is a process intrinsically linked to climate, whereby repeated cycles of freezing and thawing influence how water and saline liquids are held within porous material. Since the inception of stone weathering studies, the process has been considered one of the most important weathering mechanisms affecting material in both the natural and built environment. Water behaves similarly in porous material where it is held under pressure, as it does in the environment. When water freezes, its volume is increased by 9% and when held in pore space this expansion can exert pressure on the physical constituents of the stone, increasing porosity. The physical characteristics of stone subjected to freeze-thaw is a determining factor in the level of decay that occurs through this process, with more porous stone being most vulnerable. Recent studies, such as by Martínez-Martínez *et al.*, (2013), demonstrate that freeze-thaw induced stone decay in carbonate rocks is non-linear, material can appear robust and stable for long periods before decay occurs at a rapid rate. Work by Nicholson and Nicholson, (2000) highlights that pre-existing weaknesses within a stone do not dictate the extent of stone breakdown by freeze-thaw. Instead, the paper finds that flaws within stone will influence where decay will take place. Exemplifying this, experimental

work found that in sandstones, decay is influenced by the textural characteristics of the stone, while in crystalline limestone, fractures tended to occur along distinct linear planes and in chalk, decay was random.

Concerning climate change, Grossi *et al.,* (2007) utilised climate predictions to understand how the process of freeze-thaw will influence culturally significant sites throughout Europe in a climate changed future. They discover that the majority of Europe will see a reduction in freeze-thaw due to exposure to warmer temperatures, however, in Northern Europe, where monuments are preserved by permafrost, they may become vulnerable to freeze-thaw weathering (Grossi *et al*., 2007).

1.5.3 Salt Weathering

Knowledge and technology-based advancements in rock weathering have resulted in a pronounced shift in the literature during the twentieth century. Previously focused on the physical weathering of rock, through the identification of features, literature is now centred on the underlying processes, particularly chemical weathering that results in the formation of specific features. In recent decades, salt weathering literature has increased greatly as more is being understood about how salts interact with moisture in porous rock to produce a plethora of weathering features such as tafoni. Salt weathering is acknowledged as one of the principal diagenesis agents in culturally significant structures and archaeological sites. Therefore, formulating methods of reducing damage to buildings as a result of salts, is at the forefront of heritage science. Salt weathering research is perhaps one of the most multidisciplinary fields in stone decay, highlighted by Goudie and Viles, (1997), with research conducted on building stone, geological outcrops and geomorphological processes. Advancements in salt weathering knowledge have been made by environmental scientists, geomorphologists, material scientists, geochemists and, perhaps of most relevance to this thesis, conservation heritage scientists. Through increased research, the process of salt weathering is now recognised as a key driver in stone decay related to structures of cultural and historical significance (Doehne, 2002).

Laboratory experiments were developed towards the end of the twentieth century to explore the effects of salt on sandstone. Williams and Robinson, (1981) showed that weathering by frost is enhanced by the presence of specific salts including sodium chloride and sodium sulphate, resulting in tafoni formations developing on rock surfaces. Similarly, McGreevy,

(1985) recognised that calcium sulphate crystallised in sandstone pore space cause the rock structure to expand, dislodging quartz grains, leading to the formation of tafoni features.

Fieldwork in the arid environments of Western Australia and New South Wales supports these laboratory observations; Young, (1987) found similar correlations between salt crystallisation and the formation of cavernous features. Turkington, (1998), through research undertaken in Nevada, further highlighted the prevalence of tafoni in salt-rich environments; however, illustrated that these features are not restricted to a singular climatic range, making clear the need for more work to be undertaken on sandstone in what can be considered non-extreme climatic regions.

Salt weathering is controlled by factors such as temperature and humidity, as established, these factors are being altered through climate change. Wetter winters in a climate changed future will facilitate 'deep wetting' of stone, meaning salts will travel further into stonework (Smith *et al.*, 2011). While salts transported deep into the stone will remain in solution for longer, delaying crystallisation, once temperature increases and precipitation decreases in summer months, crystallisation will occur. This crystallisation event can be more severe than if the process occurred frequently, potentially exacerbating the deterioration of the stone (McCabe *et al.*, 2013). Furthermore, the 'memory effect', as mentioned earlier is a crucial component when considering how a stone monument will proceed to weather, this is particularly crucial with regards to salt weathering, whereby seemingly negligible differences in the decay history of a stone can result in significantly different responses to salt weathering (McCabe *et al.*, 2007).

1.5.4 Biological Growth

The complexity of how weathering processes interact synergistically with climate is highlighted throughout this chapter, however; it is biological growth that perhaps epitomises these complex interactions. The intricacy of biological colonisation of structures is exemplified by de la Torre *et al.*, (1991) who were able to isolate and identify 26 different fungi in weathered sandstone at a cathedral in Salamanca. The rate, extent and type of biological growth are determined by many factors including the physical properties and mineralogy of the stone. Fundamentally, different types of sandstone hold differing species and abundances of biological growths; furthermore, changing mineralogies influence the surface roughness, porosity, pH, and nutrient availability of sandstone, all of which are vital for species growth. These factors influence the availability of moisture, for example, rough

and porous stone can slow runoff and concentrate water in the stone, meaning greater moisture availability for biological growth.

Microclimates become more prevalent after the colonisation of stone by algae and other biological growths as they can retain moisture, influencing the moisture regime in the stone. Furthermore, their colonisation increases local humidity, adding to the complexity of the initial microclimate (Cameron *et al.*, 1997). Over time and with continued exposure to weathering, it is shown that surface heterogeneity increases, leading to more complex and diverse stone properties that suit the formation of more diverse and abundant biological species (McCabe *et al.*, 2015).

As established, the synergistic processes involved in rock weathering are extensive and can be seen to generally degrade rock constituents, however, it must be noted that the same processes can, to a certain degree, stabilise and strengthen rock faces through the formation of biological crusts, at least temporarily (Oguchi, 2013). Extensive organism cover has been shown in some instances to protect the rock that it occupies, reducing weathering prevalence, which in turn controls erosional processes on the stone surface. Conversely, sporadic organism cover can exacerbate weathering (Papida *et al.*, 2000). Communities such as climbing plants can protect structures and control microclimates, while in some instances add to the visual appeal of the building occupied. In the same way, biological communities can detract from the visual appeal of sites by covering significant archaeological material such as sculptures and carvings (Viles and Cutler, 2012). Additionally, biological growth can promote a greening of stone, enhanced particularly in wetter months (McCabe *et al.*, 2011). As Scotland moves towards warmer, wetter winters in a climate changed future, the greening of monuments could increase. Finally, in relation to heritage and climate change, atmospheric chemistry fluctuations are forecast to modify the structure and function of biological communities. With an already complex relationship existing between biological communities and heritage sites, any change could have multifaceted outcomes.

1.5.5 Rock Weathering in Temperature Extremes

A significant number of rock weathering advancements have occurred thanks to studies that have been conducted in temperature extremes, primarily arid and arctic environments, where weathering processes are at their most severe. However, field-based studies in temperate regions are lacking (Dixon *et al.*, 2009).

In the Namib desert, rock surface microclimates were observed at 4 sites across a 100km transect for 3 years by Viles, (2005). The paper emphasises that uncertainty exists surrounding the principal weathering processes that occur in desert environments, and why these environments see the fastest weathering rates. Samples for this study were taken from fresh-cut stone with a smooth surface. Each site on the 100km transect exhibited similar results, whereby the weathering rate observed was extremely slow. The most prevalent weathering was apparent in marble located in an area of the study transect that displays the highest temperature fluxes and lowest surface wetness. Hypothesised in the paper, the smooth surface of the sample blocks likely resulted in the slow rate of weathering observed. Relating to the 'memory effect', surface roughness is a key component influencing weathering of any stone type, increasing the vulnerability of a stone to weathering. Conversely, the production of micro-scale cracks in smooth blocks by weathering can take many years (Viles, 2005).

A Mediterranean semi-arid climate was investigated by Martínez-Martínez *et al.*, (2017), in particular, porous limestone weathering in the fortress of Nueva Tabarca island, Spain. It is highlighted in the paper that salt crystallisation, particularly Halite (NaCl), is responsible for most of the weathering at the site. This action is driven by strong winds and high relative humidity that dictate to an extent the salt crystallising process.

In hyper-arid environments where water and salt are lacking, thermal stress is proposed as a significant factor in the rock weathering process. McKay *et al*., (2009) emphasise that rocks found in hyper-arid localities show evidence of severe cracking. The study recorded the surface temperature of rocks in the Atacama Desert as well as two sites on the continent of Antarctica at a rate of 1 recording per second for several days. It was found that there is a similar interval of thermal change across all sites, albeit with a 30°C difference between hot and cold sites. An approximately 2°C shift in temperature in the space of a minute can cause cracks to form in rocks. The data collected in this study exceeds this threshold and so it was determined that although an isolated shift in temperature may not cause immediate damage to the rock, repeated fluctuations could, over time, bring about weathering in low water and low salt environments (McKay *et al.*, 2009).

In a study in East Antarctica, Kanamaru *et al.*, (2018) found that weathering of granitic rocks in this cold hyper-arid environment is largely driven by oxidation, such as iron hydroxide development in cracks and fissures caused by thermal expansion and contraction of key rock constituents. The paper goes on to highlight the importance of water in the weathering

process, illustrating that for weathering to occur in earnest, a source of water is required. The lack of water available in hyper-arid regions, therefore, brings about a relatively slow rate of weathering.

Extensive work has been conducted by Hall in cold environments, his early work in the Antarctic was pioneering, concerning the interaction between rock moisture and the physical process of freeze-thaw. Using a plethora of differing fresh-cut rock types, an understanding of the freeze-thaw vulnerabilities of particular rock types was determined by their capacity to retain water, relative to their environmental position (Hall, 1986).

In Northern Canada, Hall and André, (2003) discovered that there is no set temperature where freezing occurs in sandstone, finding it to vary. Hall *et al.*, (2005), provided insight into the rate of weathering between differing lithologies relating to their albedo, in that lower albedo rocks will become warmer, faster. Crucially, the same study found that when warmer than the air, both high and low albedo rocks must release energy to the air, concluding that this finding contradicts long-standing ideas of albedo-controlled temperature differences in lithologies, a finding not previously evidenced in weathering studies.

The cited literature has improved rock weathering knowledge greatly, however, as is portrayed, a large portion of the literature comes from studies conducted in extreme climatic reaches, to facilitate a relatively quick determination of how different rock types are weathered. A clear gap in the literature, therefore, is the need for subsequent studies to focus on less extreme environments. This thesis, therefore, has a temperate, oceanic climate setting in Scotland. The country is characterised through the Köppen-Geiger classification as predominantly Cfb (oceanic climate) in main cities such as Edinburgh, Glasgow, Aberdeen, and Dundee. Slight variation is found, for example in the Cairngorms National Park the classification changes to Dfc (subarctic climate). This thesis contributes to and builds on existing rock weathering knowledge by exploring a currently underrepresented geographical area in the literature. However, as weathering processes are non-linear and intensified in more extreme environments, compounded with the recognition that weathering of stone in temperate environments will occur at a time scale where observing changes will be problematic, it is important to consider a new approach (Colman, 1981; Smith *et al.*, 2008).

1.5.6 Rock Weathering and Climate Change

Some of the principal factors regulating weathering are outlined above. These processes function at varying spatial and temporal scales, a subtle change in any of the abovementioned

factors influences other factors due to their complex interrelationships (Pope et al., 1995; Viles, 2013). Considering this, a changing climate will influence the rate and extent of weathering, by altering the existing relationship between weathering and other environmental processes; however, the specifics of how these changes will be manifested remain unknown (Hulme et al., 1999).

Studies have developed relating to the forecast influence of climate change on varying topics. Such studies include the adaptation of farming and fishing to climate change, the increased prevalence of landslides as a result of climate change, more frequent and extreme weather events as well as changing social structures resulting in the prevalence of 'climate change refugees' (Mirza, 2003; Reidsma *et al.*, 2010; Sumaila *et al.*, 2011; Gariano and Guzzetti, 2016; Berchin *et al.*, 2017). Despite the acknowledgement that climate change will affect widely varying environmental systems globally, as is clear through the emergence of diverse literature highlighted above, rock weathering is underrepresented in the literature concerning how weathering processes will alter or intensify as a result of climate change.

One of the principal aims of this thesis is to address this gap in the literature by integrating synergistic relationships that rock weathering has with other environmental processes, to understand more precisely how these processes are altered by future climate change, while considering the implications this carries for the built historic environment in Scotland. Through investigating this aim, this research serves as an example of the importance of including future climate change scenarios in subsequent studies relating to rock and stone weathering.

To achieve this aim, and as alluded to above, a new approach is vital to firstly understand the effect that climate change will have on the weathering process and secondly, how these effects can be mitigated in the built, historic environment. This research incorporates a methodology that can systematically accelerate climate parameters seen to control weathering. This allows both an assessment of stone weathering in temperate climates to be made, alongside an insight into how stone weathers with the onset of future climate change as defined by climate change scenarios. The outlined approach could transform how weathering studies are conducted, providing fresh and vital knowledge surrounding stone weathering that could prove crucial in preventing the destruction of historically and culturally significant monuments, not only in Scotland but globally.

1.6 Sandstone Weathering

Sandstone, despite its global spatial extent, is acknowledged as under-represented in stone weathering literature, with a greater focus placed on the weathering of other rock types such as granite or limestone which occupy a similar proportion of the earth's surface as sandstone (Young and Young, 1992). Comparable to rock weathering studies outlined above, research that has explored the weathering of sandstone to date is very much concentrated in extreme environments. Furthermore, the use of fresh-cut stone in sandstone weathering studies is widespread, giving them limited applicability to the decay of sandstone in historic monuments.

Manifested in, and controlling the weathering processes to an extent are the physical attributes of the stone itself; sandstone, like any sedimentary rock, is diverse and heterogeneous, with weathering making it even more so (McCabe *et al.*, 2015). Warke *et al.*, (2006) found that even slight differences in structure and mineralogy between sandstones can have a profound influence on weathering, generating observable variations in the way in which the sandstone degrades. Encompassing this, a model by Turkington and Paradise, (2005) shows that sandstone is influenced predominantly by weathering processes, environmental conditions and material characteristics which all operate with exposure to time. The process of weathering alters the material characteristics of the stone, in turn altering the way that the stone will proceed to weather. Additionally, environmental conditions are shifting through climate change, changing the rate and manner in which a given stone will weather.

1.6.1 Scale of Sandstone Weathering

It is vital to consider the diverse scale of sandstone weathering features, from mega-scale to meso-scale and micro-scale. Mega-scale features are seen in natural exposures, such as coastal arches or caves; in built sandstone, mesoscale and micro-scale features are commonplace (Turkington and Paradise, 2005). As discussed above, cavernous tafoni, a mesoscale formation is particularly prevalent in salt-rich environments. Evidence in the literature suggests that the physical properties of differing sandstones types, such as porosity and grain size are crucial in determining the stone's susceptibility to tafoni, with the critical role of microclimates also highlighted as a controlling factor (Turkington, 1998). Tafoni formation remains somewhat enigmatic, owed to its widespread incidence in vastly differing environments (Hall *et al.*, 2008). Physical sandstone characteristics, for example, can result in tafoni forming in arid desert environments such as in Utah, as well as oceanic environments

such as in the Pacific Northwest of Washington state, encapsulating the feature's ubiquitous nature (Mustoe, 1983).

Micro-scale weathering, manifested in observable mineralogical changes to sandstone, is witnessed commonly through the application of petrographic micromorphology, XRD and SEM-EDX among other techniques. Mineral constituents of sandstone are exposed to factors such as moisture and temperature fluxes which drive chemical changes in the sandstone constituents, through weathering. Studies about the chemical weathering of sandstone minerals tend to focus on geological features, rather than sandstone in the built environment.

Seen in the geology with depth, rock is exposed to increased temperature and pressure, with changing groundwater flow patterns, resultantly, chemical weathering process differs from that seen in sandstone emplaced above the surface. In geological outcrops, the weathering of K-feldspar has been monitored. Bjørlykke, (1998) examined the North Sea basin and illustrated an observable change in that; rock (feldspar, mica) + water = clay + cations. Yuan *et al.*, (2017) similarly portrayed that the weathering of K-feldspar produced secondary minerals including clays, specifically kaolinite ($Al_2(OH)_4Si_2O_5$) and illite ($(K,H_3O)(Al,Mg,Fe)_2(Si,Al)_4O_{10}[(OH)_2,(H_2O)]$). The study found that with increasing depth, greater quantities of secondary minerals were produced. There is very much a requirement, therefore, to understand mineralogical changes to sandstone that is not limited to subsurface geology, and instead investigates the valuable cultural and historical applications of sandstone. Therefore, this thesis proposes that a new approach should be taken to understand micro-scale chemical and physical changes in built sandstone over time, with a consideration made for the future effects of climate change. Chemical and physical change are important indicators of stone quality and with this knowledge, a conceptual model can be outlined, delineating pathways in which specific sandstone types are weathered. This model can incorporate differing samples across varying localities, producing a large-scale picture of the changing chemical and physical constituents of sandstone induced by climate change. The implication of observed changes in the integrity of significant cultural and historic structures can subsequently be understood.

1.7 Cultural Heritage

The concept of protecting and characterising significant landmarks, landscapes and practices, considered to be examples of 'natural' or 'cultural' heritage has been discussed in various conventions and papers since the early 1900s (Rössler, 2006; Vecco, 2010). However, until

the International Charter of Venice in 1964, there remained semantic issues surrounding the meaning of cultural heritage concerning significant sites and practices. The charter addresses the concept of cultural heritage in a succinct and encompassing manner, conveying that culturally significant sites must hold within them or display a significance relating to former times; the sites themselves can, therefore, provide a present representation of a previous lifestyle or period (ICOMOS, 1964). Therefore, the degradation of significant sites would culminate in a loss of tangible heritage. For sites to retain their cultural identity and significance, it is incumbent on present and future generations to ensure their longevity and authenticity. The development of the UNESCO 1972 World Heritage Convention has driven to an extent the protection of natural and cultural sites considered to be of 'outstanding universal value' that we desire to pass on to future generations. The convention provides a comprehensive framework and structure for identifying, inscribing, and safeguarding natural and cultural heritage on a global scale. The framework has been updated substantially since its inception, through changes to rules, guidelines and procedures that are involved in inscribing UNESCO World Heritage Sites (UNESCO, 1972; Francioni and Lenzerini, 2008). Moreover, exemplifying the complexity of identifying heritage, literature has developed in recent years highlighting that heritage is not simply tangible, present in a natural feature or cultural structure, but also intangible. This can be manifested in developmental components of specific communities or practices that are distinctive and exclusive to that group of people, therefore definitively representing the community's heritage and uniqueness (Lenzerini, 2011).

Not without its flaws, the application of the term 'universal value', which underpins the inscription of World Heritage Sites as part of the 1972 framework has received criticism in the literature due to its ambiguity and lack of distinction. Questions have been raised about what can truly be classed as universally valuable (Titchen, 1996). Furthermore, the ambitious aims of the framework to develop a sense of worldwide commonality through the inscription of World Heritage Sites has caused disapproval. It has been suggested that the framework is Eurocentric, contradicting the concept of universal value (Tucker and Carnegie, 2014).

These flaws notwithstanding, the implementation of such a relatively recent, unique, and substantial framework focused solely on the recognition and protection of outstanding heritage, highlights a global acknowledgement in recent decades about the importance of such sites. Further manifested in the framework, is the necessity to protect significant sites or suffer the consequences of failing to do so.

Related to this thesis, the inscription of World Heritage Sites, paired with a developing global mentality surrounding the importance of culturally significant sites, provides a rationale for studies to explore the threats not only to UNESCO World Heritage Sites, but to historically and culturally significant sites on a wider scale.

1.7.1 Climate Change and Cultural Heritage

As noted throughout this literature review, there is a growing concern among heritage scientists for the longevity of significant sites as a result of ensuing climate change, expected to exacerbate the degradation of monuments and buildings that can be considered unique and irreplaceable (Haugen and Mattsson, 2011). Additionally, throughout this chapter, it has been made clear that the impacts of climate change on rock and stone weathering are poorly understood. Present knowledge and studies based on the effects of climate change on cultural heritage are lacking, despite growing knowledge of probable climate scenarios (Bonazza *et al.*, 2009).

Fatorić and Seekamp, (2017) provide the first systematic review of the literature concerned solely with the link between future climate change and cultural heritage. Their findings illustrate through a review of 124 relevant papers, the growing realisation in the literature that climate change is critical to the sustainability and future integrity of important heritage sites on a global scale. The lack of studies in the field, when compared with the effects of climate change on natural, social and economic systems, is also clear (Bonazza *et al.*, 2009). Literature concerned with climate change and cultural heritage only began to emerge in 2003, with a paper that explored, among other things, the role of climatic change on coastal heritage (Vallega, 2003). From 2003-2015, studies have steadily increased as reported by Fatorić and Seekamp, (2017), highlighting the developing nature of the link. Furthermore, 41 of the 124 analysed papers are highlighted as site-specific studies, the remaining either do not reference any specific site or resource or are studies conducted at a general landscape level, illustrating that literature, although growing, remains relatively sparse on the topic. Additionally, given the global focus that UNESCO has placed on the importance of tangible heritage through the inscription of World Heritage Sites, there are disproportionally few studies focused on the effects of climate change on tangible heritage.

Although sparse, studies relating to site-specific examples of building degradation as a result of climate change provide insight into the exacerbating effect that climate change has on building deterioration, while delivering potential means by which the negative effects of

climate change can be mitigated. Georgescu *et al.*, (2017), used infrared thermography to record air temperature and relative humidity at the St. Nicholas Church of Densus, Romania, a site that has been proposed to be added to the UNESCO World Heritage list since 1991. Their work discovered that high levels of humidity within the church posed the main threat to the integrity of the structure. Biological growths and structural damage such as cracks at areas of elevated humidity were also discovered. Alongside these findings, it is noted that humidity is expected to rise across Europe in the coming years. Considering these findings, remediation techniques were put in place, specific to the building, including increasing ventilation in the church as well as implementing floor heating and drainage to prevent the capillary rise of water, reducing humidity within the structure.

Mosoarca *et al.*, (2017) make the important point that when sites considered today as culturally significant were under construction, they were built with the present and past climate of building localities taken into consideration. Climate change, which is expected to intensify present risks, while generating new threats through alterations to factors such as temperature, humidity, precipitation, wind, and biological growth, will expose buildings to an intensity of change not previously experienced. Through a case study conducted in Oravita, a mountain town in Romania with a plethora of culturally significant buildings, Mosoarca *et al.*, (2017) explore the impact of climate change on built heritage in the area. The paper explores the damage caused to structures through high-speed wind and wind-driven rain, shown to increase the penetration of water into the building stones and leading to increased weathering and subsequent erosion on historic buildings. With more frequent, high-intensity rain events in the future induced by climate change, damage to historic surfaces will increase. Additionally, a tipping point in historic structures can be seen, where the continued exposure to more extreme climatic events such as amplified rainfall, can cause partial structural collapses, as seen in retaining walls in Oravita, in the wake of intense rainfall events of 2014 and 2015. The paper concludes that the link between climate change and cultural heritage is real and complex, unless structures are protected and more studies are conducted to facilitate the protection of sites, there could be a catastrophic loss of heritage on a global scale. Mosoarca *et al.*, (2017) point out that historic buildings are inherently vulnerable to climate change and therefore subsequent studies must assess the effects of future climate change on sites, for protective frameworks and management plans to be put in place.

Likewise, studies focused on the general impact of climate change on heritage can be seen as important for the management and longevity of significant monuments and landscapes.

Dupont and Van Eetvelde, (2013) address the vulnerability of two landscape in Flanders, Belgium, to future climate change. The sites are managed and considered to be important relics of traditional land use, with scientific, natural, and aesthetic values. The incorporation of climate change in management plans pertaining to potential landscape threats is absent, prompting Dupont and Van Eetvelde, (2013) to address this. They highlight the impending threat of climate change, and through vulnerability maps, discovered that both study sites are under threat from climate change. Threats include forest destruction, soil erosion and intense flooding that could significantly deteriorate cultural landscapes, detracting from their authenticity and value. Through developed vulnerability maps, suggestions were put forward to incorporate climate change in management plans to prevent a loss of heritage in the area. The paper recognises that although the implementation of mitigations will themselves alter the landscape, they will, more importantly, preserve heritage at the locality.

In a similar study conducted on a landscape level in Newcastle, Australia; Forino *et al.,* (2016) endeavoured to construct a Cultural Heritage Risk Index (CHRI) for the area. This was achieved by conducting analyses on the nature and type of hazards that a site could be exposed to in a climate changed future, the vulnerability of sites to existing hazards and finally a risk analysis which encompassed all the mentioned factors, to generate a CHRI score. There are around 700 cultural sites in Newcastle, the study focused on results obtained when the CHRI was applied to one site, Burwood Beach Wastewater Treatment Works. The site is listed on the New South Wales State Heritage Inventory, and it was shown through the CHRI, to be at moderate risk from degradation as a result of climate change-induced events. From the obtained data, it could be suggested that a monitoring framework should be put in place to prevent the site from declining. The CHRI could be applied to enhance understanding about how sites could be lost or damaged as a result of climate change and from knowledge gained site-specific mitigations can be suggested to prevent damage.

Climate change is by nature, a slow onset process, meaning there is time to arrest its prevalence. Consequently, heritage scientists are in a unique position, as highlighted through examples from Belgium and Australia, where the future impacts of climate change on cultural heritage can be understood before they occur. This puts researchers in a position of control, where studies can portray the future impacts of climate change, while there is still time to avoid or at least limit its effects. An acknowledgement must be made that there will be a loss of heritage if climate change is not addressed and acted upon promptly. As portrayed throughout the literature, there is a lack of relevant studies highlighting the link between

cultural heritage and the critical role climate change plays in site longevity. This thesis, therefore, seeks to understand the future threats of climate change to culturally significant sandstone sites in Scotland, before they take hold. The link between cultural heritage and climate change is elucidated and rather than dealing with the aftermath of the disaster, findings from this study can aid the prevention of a cultural disaster in Scotland as a result of climate change.

1.8 Aims of UNESCO and HES

Characterising the relatively recent acknowledgement that cultural heritage is under threat from climate change, the threat was first highlighted to the UNESCO World Heritage Committee in 2005. Eight publications have been released from the organisation surrounding the impact of climate change on World Heritage, encompassing both natural and cultural sites. Three of the publications, in particular, relate well with the research undertaken in this thesis. The organisation recognises that built heritage is under severe threat from climate change, which could culminate in the loss of archaeological evidence and severely hamper efforts to gain deeper insight into past communities from historically and culturally significant sites, while detracting from the authenticity of such sites (UNESCO, 2007a). Through UNESCO's 'Climate Change and World Heritage' report, predictions are made surrounding the impact of climate change on various aspects of heritage, including built heritage, highlighting how some of the world's most treasured features could degrade. Through this, the paper provides ways in which sites can be managed as a result of their vulnerability to degradation (UNESCO, 2007b). Finally, through the 'Policy Document on the Impacts of Climate Change on World Heritage Properties', UNESCO paves the way for future research to be conducted on the link between climate change and cultural heritage. Specific needs are placed on research focused on understanding the vulnerability of materials, monitoring changes driven by climate change, accurately modelling and predicting climatic change, managing cultural heritage and preventing damage to culturally significant sites (UNESCO, 2007c). This thesis, although a standalone research project, synchronises well with current global agendas on the topic of climate change, emphasising the necessity of this study in a world where cultural heritage is at risk of ruin from climate change, in ways not fully appreciated at present.

On a more local scale, this research project works closely with HES and fits directly with their present and future agendas concerning climate change and cultural heritage. Although generated while operating as Historic Scotland, now HES, has reached the end of a five year

(2012-2017) climate change action plan, one of the aims of which was to prepare the historic environment for ensuing climate change (Historic Environment Scotland, 2012). Following on from this, HES released annual operating plans for 2017/18, 2018/19 and 2019/20, understanding the impacts of climate change on the sites under their care remains a key theme. HES is very much at the forefront of investigating the impacts of climate change on the cultural landscape of Scotland (Historic Environment Scotland, 2017b, 2018a, 2019b). Short Guides are also published regularly by HES on a multitude of topics concerning cultural heritage, including climate change adaptation for traditional buildings, highlighting the organisation's desire to safeguards structures from climate change (Historic Environment Scotland, 2016). As highlighted earlier in this literature review, HES produced a climate change risk assessment of the properties in its care, concluding that of the 336 properties, 160 are at high risk and 28 are at very high risk from impacts stemming directly from climate change (Historic Environment Scotland, 2018b). Building on this, a climate risk assessment was published, exclusively focused on the World Heritage property that is part of the 'Heart of Neolithic Orkney'(Historic Environment Scotland, 2019c). Finally, HES's guide to climate change impacts was published in late 2019, serving as a guide on how historic sites in Scotland can adapt to withstand the impacts of climate change. While acknowledging that sites are inherently at risk, the report also highlights that some have great resilience and with the generation of action plans, the impacts of climate change can be limited (Historic Environment Scotland, 2019a). This thesis builds on HES's comprehensive climate change-related publications and desire to generate a deeper understanding of how Scotland's rich sandstone heritage is affected by climate change.

1.9 Established Gaps in the Literature

As portrayed, awareness is growing that the weathering of culturally significant stone structures will likely be altered through climate change in ways not completely understood at present. Significant advancements have been made in referenced literature on stone material decay and the role of such factors as changing moisture content, temperature fluctuations, salt crystallisation and biological growth, however, gaps in the literature remain. Rock weathering studies were found in this literature review to largely neglect the implications of climate change on the severity of sandstone weathering. With a changing global climate, it is becoming increasingly crucial that this factor is considered in any subsequent studies pertinent to rock weathering. Additionally, existing knowledge has the potential to become redundant over time, with the growing awareness of the overarching significance of climate

change on the historic environment. There is an urgency, therefore, to understand how climate change will alter sandstone weathering processes.

It has been established that numerous studies in the literature are concerned solely with weathering in extreme climatic regions where processes are expedited due to the severe climatic setting. With the acknowledgement that weathering will become increasingly prevalent in various climatic extents, it is important to investigate more diverse localities, such as temperate regions. The use of smooth, fresh-cut stone samples when observing stone degradation, as seen in the literature, delivers information on how differing stone types degrade generally. However, factors such as surface roughness are vital in the rate of stone weathering and smooth-cut samples provide limited insight into the weathering of above surface sandstone that has been exposed to climate variations for centuries or even millennia, in the form of culturally and historically significant monuments.

The future effects of climate change on specific areas and sites can be modelled and predicted, showing that climate change could drive a huge loss of heritage. Due to the comparably slow onset of climate change, the effects on the historic environment can be prevented. Therefore, there is a unique opportunity to mitigate the future impacts of climate change on the historic environment before they take hold. Finally, there is a necessity for more research to be conducted to understand more fully how this can be achieved.

1.9.1 Research Aims and Objectives

As a result of gaps in the literature, this thesis seeks to define and evaluate the complex processes involved in weathering with future climate change scenarios, establishing the effect that climate change will have on weathering processes. From this, a determination can be made regarding whether there will be an increase in weathering severity as a result of climate change, and if so, how will the increased severity be manifested on specific culturally and historically significant sandstone structures in Scotland. In doing so the analyses contribute to and build on existing rock and building stone weathering knowledge by exploring a currently under-represented lithology and geographical area in the literature.

The need for a new approach in observing the weathering of sandstone has been highlighted thus far. This thesis takes an innovative approach to make both knowledge-based and technology-based advancements in the understanding of sandstone weathering. Findings from a systematic acceleration of specific climate change parameters provide timely information on the degradation of specific sandstone types in the future from climate change. From this, a

conceptual model is generated that postulates in what manner these sandstones will weather, particularly on the micro-scale, manifested through chemical, physical, and mineralogical change.

As established, there is an undoubted necessity to understand future alterations to sandstone that is not 'fresh-cut'. This thesis, therefore, utilises building stone associated with Iron Age sandstone broch sites in Scotland to address this gap in the literature.

Furthermore, the relatively slow onset of climate change provides an opportunity for the potentially destructive effects of climate change on the built historic environment to be understood through scientific research and prevented where possible. This thesis aims to understand the future impacts of climate change on cultural heritage, in a timely manner, for relevant mitigation and management plans to be implemented before the effects of climate change irreparably degrade historic monuments in Scotland.

Finally, this thesis can be seen to integrate well with the agendas of relevant organisations on a global and local scale, namely UNESCO and HES.

Summary of aims and objectives:

- Generate a new and innovative research design that retains relatability to the built environment and climate projection data
    - Obtain SMC to access culturally significant sandstone samples from Clachtoll and Borwick Brochs as well as associated geology samples.
    - Incorporate relevant climate projection data from UKCP18 in the creation of controlled environment facility experiments.

- Understand the effects of climate change on the weathering of sandstone heritage sites in Scotland
    - Conduct in depth petrographic analyses on Torridonian Sandstone and Stromness Flagstone to determine their key characteristics, degree of weathering to date and specific strengths/weaknesses
    - Undertake two innovative climate change experiments, exposing samples to simulated weathering conditions anticipated between 2025 and 2055
    - Analyse sample response using a suite of analytical techniques to create sandstone specific decay models for the next century and provide information on potential conservation strategies

- Evaluate the effectiveness of this research design and make suggestions for the future that can enhance this study area
    - Evaluate the effectiveness of the CEF in exposing samples to climate change conditions
    - Evaluate the SMC process and the limitations it has on stone weathering research

1.9.2 Thesis Plan

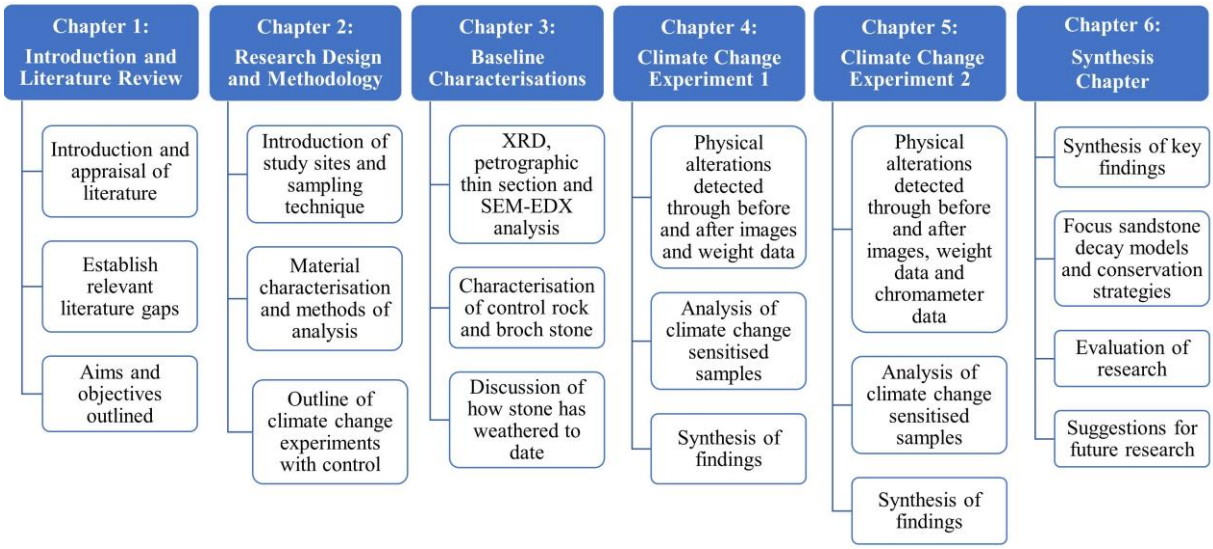

Figure 1.1 - Flowchart depicting thesis structure

Each chapter is outlined in Figure 1.1. Chapter 1 has provided an appraisal of relevant literature, from which associated gaps in the literature and resultant aims have been outlined. Chapter 2 contextualises study sites concerning the geology of Scotland and the cultural significance of stone-built heritage. The research design implemented in this study is also put forward. Chapter 3 provides a characterisation of each stone type, from which understandings are gained into how the control rock and broch stone has weathered to date. Chapter 4 and 5 provide results and discussions from two separate climate change experiments. Finally, Chapter 6 synthesises the work undertaken, linking results from previous chapters. This allows an overall interpretation of the effects of climate change on sandstone heritage in Scotland to be made from which recommendations for future conservation are given.

2 Research Design and Methodology

2.1 Chapter Introduction

This chapter provides an overview of Scotland's geology before focussing on the formation of Torridonian Sandstone in the NW Highlands and Stromness Flagstone on the Western Mainland of Orkney. These sandstone types form the building blocks of Clachtoll and Borwick Brochs; the two study sites associated with this research project.

A comprehensive and innovative research design that addresses significant gaps in rock weathering and heritage science literature is presented, adhering to relevant guidelines relating to historic monuments and their role in scientific research. A complete methodological approach is set out, incorporating sample collection and processing, the set-up of two CEF experiments and the analytical tools used in this study.

2.2 Geology of Scotland

The geology of Scotland is complex, owing to the country's exposure to vastly ranging environments spanning deep geological time. Geology plays an important role in this thesis concerning the formation of sandstone successions that have served as building stones for many of Scotland's most culturally and historically significant structures. This study examines two contrasting sandstone types, manifested in Clachtoll Broch in the NW Highlands of Scotland, constructed from Torridonian Sandstone (1000-750 million years old) and Borwick Broch, Orkney, constructed from primarily Stromness Flagstone, a Devonian Middle Old Red Sandstone (419.2-358.9 million years old).

Scotland's geological past has been studied extensively, with detail emerging over the last century surrounding the age and complexity of the country's rocks. The theory of terrane assembly explains that the country's basement geology is comprised of five sections of rock that formed as long as 3 billion years ago (gya), with each terrane punctuated by a series of northeast-southwest trending faults. The Hebridean is the northernmost terrane and is comprised of an Archaean basement of Lewisian Gneiss derived from a time when NW Scotland formed part of the ancient continent, Arctica, alongside North America, Greenland, and Siberia. Successions of Torridonian Sandstone overlay the Lewisian Complex and are in turn overlain by Cambro-Ordovician sediments. The Moine Thrust separates the Hebridean Terrane from the North Highland Terrane which is similar to the Grampian Terrane. Both are composed of thick sequences of high-grade metamorphic rocks, separated by the Great Glen Fault. The North Highland Terrane is composed of the Moine Supergroup, formed between 1

gya and 870 million years ago (mya) with the Grampian Terrane made up of the Dalradian supergroup which formed around 800 mya. The Highland Boundary Fault splits the Grampian from the Midland Valley Terrane which is dominated on the surface by Old Red Sandstone of Devonian age. Finally, the Southern Uplands Fault marks the transition into the Southern Uplands Terrane which is predominantly composed of Ordovician and Silurian greywackes and shales (Trewin, 2002; Oliver *et al*., 2008). The collision of these terranes firstly triggered the closure of the Iapetus Ocean around 400 million years ago (mya), which once separated the ancient continents of Laurentia, Baltica and Avalonia. The ensuing Caledonian Orogeny saw Himalayan sized mountains form in what became Scotland, the heavily eroded remnants of which are visible today (Craig and Geological Society of London., 1991; McKerrow *et al.,* 2000; Park, 2005).

Scotland's journey from being part of the larger continental landmass of Laurentia in the Southern Hemisphere, to its present-day location has exposed the country to drastically varying climatic conditions and environments, facilitating the formation of vast and varying lithologies. Scotland's separation from the Laurentian continent around 65 mya prompted the opening of the Atlantic Ocean, stretching the continental crust as Scotland moved east, eliciting a surge of molten rock and the formation of volcanoes extending from St Kilda to Ailsa Craig. More recently in geological time, Scotland has gone through distinct glaciation periods, which removed and transferred enormous quantities of weathered rock, shaping the landscape seen today (Mckirdy and Crofts, 2010).

This comprehensive knowledge of Scotland's geology provides a foundation for emerging research to adopt a more focused analysis of specific rock types, allowing a deeper understanding to be gained of their key structural features, chemistry, mineralogy, and integrity as building stones in Scotland within a climate changed future.

2.2.1 Torridonian Sandstone of the Northwest Highlands

Part of the UNESCO Northwest Highlands Geopark, this region is characterised by spectacular scenery and ancient geology, dominated by large, isolated mountains of Torridonian Sandstone, separated by long, deep valleys of Lewisian Gneiss. Torridonian Sandstone consisting predominantly of alluvial red arkoses unconformably overlay the Lewisian Complex, the oldest rocks in the UK and amongst the oldest in the world, composed chiefly of pyroxene gneisses that formed in the Archean between 3 and 2.7 gya. Studies based in Greenland and Canada have highlighted that the Lewisian complex is

essentially a fragment of the ancient Laurentian landmass (Johnstone and Mykura, 1989; Craig and Geological Society of London., 1991). The Lewisian complex has been divided stratigraphically into a northern, central and southern region by Sutton and Watson, (1950), with Clachtoll Broch located in the central area, characterised by pyroxene gneisses that formed during the early Scourian, an Archaean metamorphic event (Fettes and Mendum, 1987).

Scotland's geographical position when the large continental landmass of Laurentia collided with the smaller continent of Baltica and the microcontinent of Avalonia is the reason why the geology of Northern Scotland is comparable to that of Eastern Greenland and the Northwest Appalachians in the United States of America. Watt and Thrane, (2001) highlight that the Krummedal supracrustal succession in Eastern Greenland and the Upper Torridonian were deposited at around the same time when both localities comprised part of the larger Laurentian landmass. Detrital zircon analysis highlights that the successions found in Eastern Greenland date to between 1 and 0.95 gya, a time concordant with large sediment input to the Northern Atlantic. Similarly, the Torridonian successions can be seen to be derived from the same sediment input, analogous too with lithologies in Svalbard and Siberia. A detailed study of Torridonian Sandstone from a heritage perspective is beneficial not only to Scotland but to other countries that once formed the continental landmass of Laurentia and which have similar sandstone outcrops, lying predominantly within the North Atlantic region.

The Torridonian is predominantly a reddish-brown terrestrial sedimentary rock, primarily laid down in a fluvial environment and less commonly in lacustrine conditions. The sandstone type has 'Lower' and 'Upper' subdivisions, the former is comprised solely of the Stoer Group and the latter is made up of the Sleat and Torridon Groups. The Stoer Group is around 2km thick and rests unconformably on the underlying Lewisian Gneiss. The Group has lower facies containing breccia conglomerates as well as planar and cross-bedded sandstones while the upper facies are comprised of cross-bedded red sandstones and mudstones. The Sleat Group of the Upper Torridonian is exclusive to the Isle of Skye and the adjacent mainland and is generally grey in colour, laid down in a freshwater environment. There are four formations associated with the Group (Figure 2.1 Johnstone and Mykura, 1989); The Rubha Guail Formation, a coarse pebbly stone derived from the Lewisian Gneiss. The Loch na Dal Formation made up of dark grey siltstones and sandy shales with some coarse sandstone beds. The Beinn na Seamraig Formation consisting of current bedded sandstones and fine-grained grits and The Kinloch Formation which is dominated by grey siltstones and

sandstones. The Torridon Group which is the main Torridonian Sandstone succession likewise has four formations associated with it; The Diabaig Formation composed of basal breccia derived from underlying Lewisian Gneiss. The Applecross Formation comprising fluvial, cross-bedded arkose sandstones and pebbly sandstones. The Aultbea Formation of fine to medium-grained arkose sandstones. Finally, the Cailleach Head Formation dominated by grey shale and red sandstone (Johnstone and Mykura, 1989).

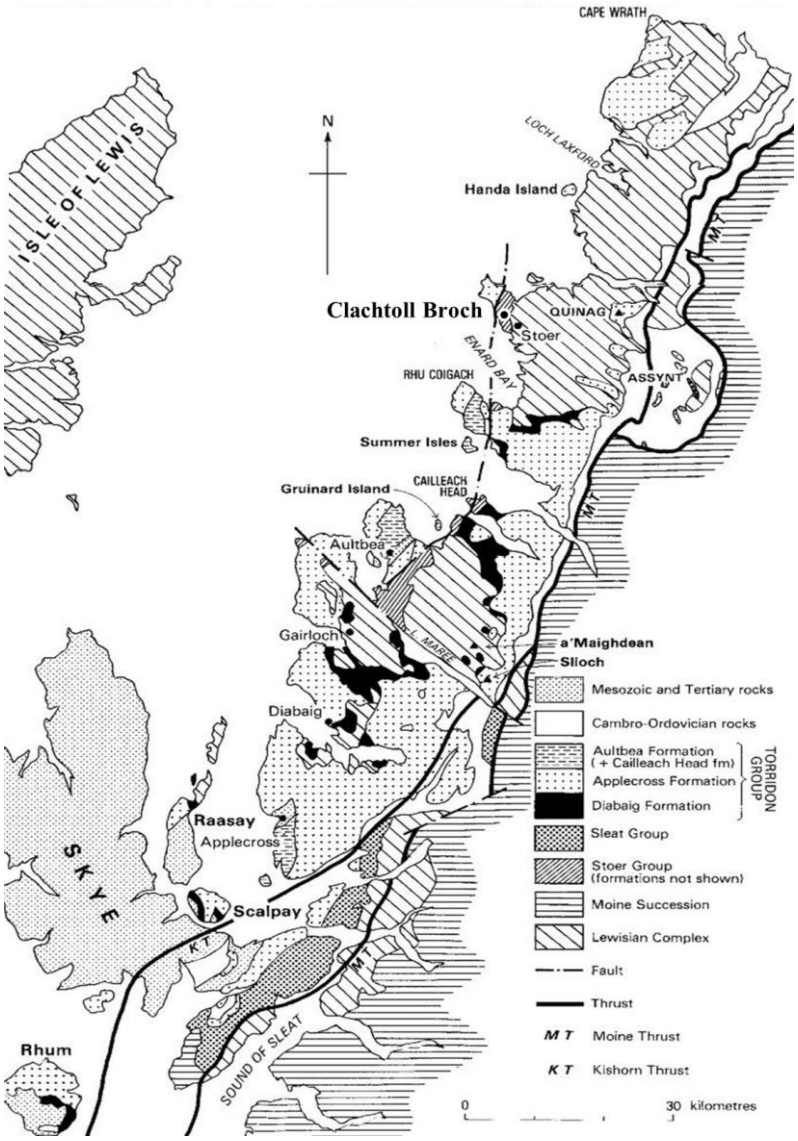

Figure 2.1 - Geological map of the area taken from Johnstone and Mykura, 1989 showing the geographical distribution of groups and formations associated with the Torridonian. The location of Clachtoll Broch is added to the map

Through its aesthetic value, ancient geological history, and unconformable location above the oldest rocks in the UK, Torridonian Sandstone has a real significance to Scotland, highlighted by the foundation of the UNESCO Northwest Highlands Geopark which incorporates the

natural features of the Torridonian successions. The rock type has been the subject of valuable scientific study from varying disciplines (Ielpi and Ghinassi, 2015). Research has developed surrounding the sedimentology of the Torridonian (R. C. Selley, 1965; George E. Williams, 1966; Owen, 1995; Owen and Santos, 2014), as well as its palaeomagnetic properties (Irving and Runcorn, 1957; Williams and Schmidt, 1997). Most importantly for this research, its petrographic mineralogy, geochemistry and geochronology have been understood through papers by (Selley, 1966; Stewart and Donnellan, 1992; Rainbird, 2001). Through analysis of the literature, the geology of the Northwest Highlands of Scotland is particularly complex, however, it is clear that significant characteristics of the sediment that formed the Torridonian successions are derived from the underlying Lewisian Gneiss. The research undertaken in this thesis can add to and enhance existing knowledge by examining the mineralogy and structure of the sandstone with advanced methods, such as XRD and SEM-EDX. Additionally, no research has been undertaken to understand the application of Torridonian Sandstone as a building stone in ancient monuments, meaning this research will provide a new analytical perspective, linking geology with building stone longevity and fluctuating weathering processes under changing climatic conditions.

2.2.2 Old Red Sandstone of Orkney

This study will likewise investigate Stromness Flagstone, a Middle Old Red Sandstone on the Western Mainland of Orkney that has been utilised in the construction of Borwick Broch. It is found in abundance in outcrops surrounding the site, including in sections of the spectacular coastline on the Western Mainland, north of the Yesnaby Cliffs. It is important initially to understand the wider context of this lithology within the geological setting of the Northern Isles.

Orkney, alongside Shetland, comprises the Northern Isles of Scotland and represents the northernmost reaches of the once Himalayan sized mountains that formed in the wake of the Caledonian Orogeny. Although grouped as the Northern Isles, the geophysical features of Orkney and Shetland contrast sharply, reflected in their respective geology. The eroded remains of the ancient mountain range can be observed on Shetland; conversely, on Orkney, the mountain roots have been covered by layers of sedimentary rock. The Northern Isles have been shaped primarily by glaciation over the last 2.6 million years (Ma), the result of which is particularly pronounced on Shetland.

The Orkney Islands are comprised of a metamorphic and granitic basement, overlain by sedimentary rocks primarily of Devonian, Middle and Upper Old Red Sandstone age, deposited by Lake Orcadie, a freshwater body that formed in the locality during the Caledonian Orogeny. At that time, Scotland was lying south of the equator and Lake Orcadie expanded, collecting desert sands which deposited in large quantities in the lake. The sediments that were deposited in the shallow areas of the lake lithified over geological time, forming the Old Red Sandstones seen today. The Middle Old Red Sandstones have 5 stratigraphic subdivisions: basal breccia, Lower Stromness Flagstones, Sandwick Fish Bed Cycle, Hoy Cycle and Upper Stromness Flagstones. Relevant to this thesis, Borwick Broch is located on the western seaboard of Orkney Mainland, south of the Sandwick Fish Bed that separates the Upper Stromness Flagstone to the north and the Lower Stromness Flagstone to the south, depicted below in Figure 2.2 taken from Mykura, 1976.

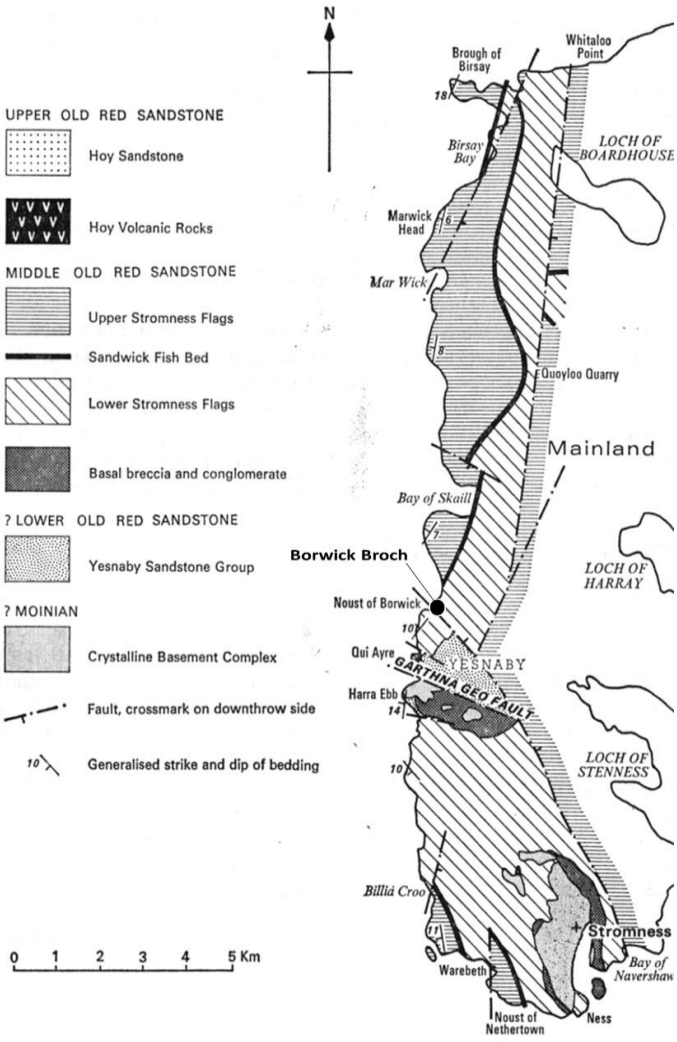

Figure 2.2 - Geological map of the area taken from Mykura, 1976 showing the geographical distribution of groups and formations associated with Orkney's Middle Old Red Sandstone. The location of Borwick Broch is added to the map

The Stromness Flagstones are characterised by over 50 cycles, each around 5-10m in depth, typically composed of thinly bedded siltstones rich in carbonate as well as silty mudstones, with alternating layers of fine-grained sandstone. The cycles can be divided into two facies, the Lower Stromness Flagstones which were laid down while covered with water and the Upper Stromness Flagstones that were deposited in shallow water as well as dry conditions. The Lower and Upper facies are separated by the Sandwick Fish Bed which is 60m in depth. The Lower Stromness Flagstones are Upper Eifelian age (393.3 Ma – 387.7 Ma) and are characterised as being abundant in dark silty mudstone, interbedded with siltstone and fine sandstone. The facies have high pyrite and ferroan dolomite content, causing it to turn a yellow/red colour upon weathering (Mykura, 1976; Craig and Geological Society of London., 1991; Mckirdy, 2010).

This research project is highly important in that it endeavours to understand the significance of Lower Stromness Flagstones within Scotland's heritage landscape. In doing so, the mineralogy, chemical characteristics, structure, and longevity of the material as a building stone will be appraised. Crucially, new insight will be gained into the extent to which the Lower Stromness Flagstone will be altered in the future through climate change, from which relevant conservation practices can be generated.

2.2.3 Torridonian and Devonian Sandstone Reference Images

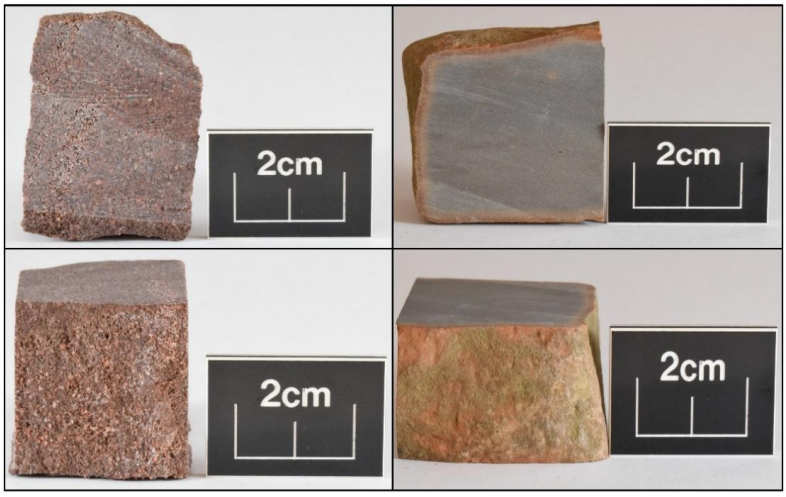

Figure 2.3 - Reference images of Torridonian Sandstone, Clachtoll Broch (L) and Stromness Flagstone, Borwick Broch (R)

Figure 2.3 serves as a general reference image depicting the two focus sandstone types of this study that are described in detail above. Both sandstones appear to be very tightly packed, particularly the extremely fine-grained Lower Stromness Flagstone.

2.3 Brochs as Culturally Significant Sites in Scotland

Remnants of the Iron Age form a vital part of Scotland's cultural landscape, with an abundance of brochs, crannogs, forts and wheelhouses preserved to varying degrees across the country. This thesis utilises the archaeological remains of two aforementioned broch towers to assess the effects of climate change on specific culturally significant sandstones in Scotland. Brochs are particularly iconic, ubiquitous, and enigmatic structures, unique to Scotland. Various hypotheses have been offered regarding their original use, and how, despite their intricacy, they were constructed in the Iron Age to such an extensive scale, with more than 500 built with a concentration across the Highlands and Islands (Hedges and Bell, 1980; Barrett, 1981). Invariably constructed with locally available drystone masonry, brochs are highly sophisticated structures, with large foundations of up to 18 metres in diameter and support a height of stone that tapers in and up to 13 metres. Within the structure, cells and staircases were constructed with scarcements supporting upper timber levels. The intricacy and skill required to construct a broch more than 2000 years ago continues to puzzle stonemasonry experts, historians and architects today, further highlighting their enigmatic nature as structures representing the development of the Iron Age in Scotland (Theodossopoulos *et al.*, 2012; Romankiewicz, 2016).

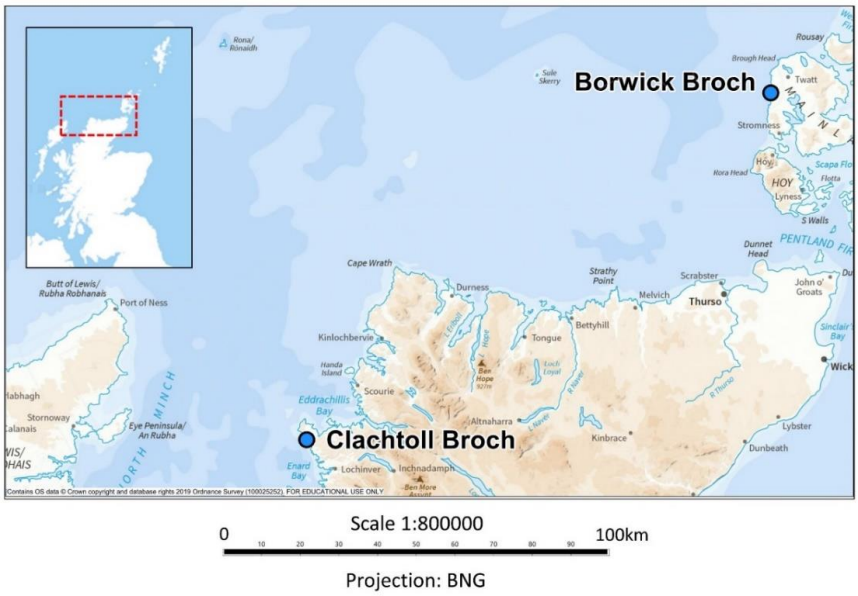

Figure 2.4 - Location of Clachtoll Broch, NW Highlands and Borwick Broch, Orkney

It is apparent in the literature that uncertainties surround broch construction and use; however, their cultural and historic significance is undeniable. The study of two brochs (Figure 2.4) comprised of different sandstone types serves as an important assessment of the

future integrity of brochs while helping to inform how sandstone types exploited as building stone for millennia will degrade under predicted climate changed futures.

2.3.1 Clachtoll Broch, Northwest Highlands

To arrest decomposition and record significant Iron Age deposits, AOC Archaeology undertook excavation work at Clachtoll Broch (Figure 2.5 and Figure 2.6), commencing in 2015 through to September 2017. Inspection of the site before excavation work noted that the broch was heavily damaged with loss of the south wall through coastal erosion and additional damage inflicted by visitors, largely through trampling.

Figure 2.5 - Clachtoll Broch entrance and surrounding archaeological spoil

Figure 2.6 - Collapsed seaward facing wall of Clachtoll Broch

The significance of Clachtoll Broch on a cultural and historical level is clear, with a radiocarbon date obtained from charcoal dating the broch to around the time of the BC/AD transition. HES's Canmore database quotes the radiocarbon date as 2025 ± 30 years BP. Moreover, there is no evidence of secondary occupation at the site, with the broch likely being destroyed by fire. Therefore, it is probable that Clachtoll Broch contains undisturbed Iron Age deposits, from which more can be understood surrounding the use and practices associated with brochs, giving the site significant cultural and historical value.

Despite there being an abundance of brochs in the Northwest Highlands, there are comparably few in-depth excavations and published research of sites. AOC Archaeology highlight that the excavation work at Clachtoll provides major insight into broch structure and architecture which can greatly enhance current understandings of broch construction while preserving the tower (Cavers *et al*., 2011; Cavers *et al*., 2015).

2.3.2 Borwick Broch, Orkney

Borwick Broch (Figure 2.7) was first described in the late nineteenth century by Watt, (1882), who detailed a broch situated on an 80-90ft promontory and that took the appearance of a grassy mound of around 20ft in height. The location of the structure at a cliff edge gave the site significant defensive qualities and an area for boats to dock. Furthermore, a freshwater burn nearby brought a source of clean water for the broch dwellers, while added protection was achieved by the inclusion of a wall on the landward side of the structure (Ritchie and Royal Commission on the Ancient and Historical Monuments of Scotland., 1996).

Figure 2.7 - Borwick Broch, located on a large promontory, Western Mainland, Orkney

Watt noted that the broch was part of a larger network of outhouses located within around 60ft of the main tower. Similar to Clachtoll, the prevalence of marine erosion at Borwick and its impact on the site was noted; measurements taken in 1882 indicate that the broch stood at a height of between 11 and 16ft, subsequent measurements, such as in 1935, detailed the broch to be significantly smaller, around 8.5ft in height, highlighting the relatively rapid rate of degradation and material loss.

Work conducted at the site dates back to the late nineteenth and early twentieth century, with later work in 1986 detailing the discovery of a midden located northeast of the broch, towards the cliff, where material dating to the Middle Iron Age was discovered which included pottery and animal bone fragments.

More recently, between 2008 and 2011, a large-scale walkover of the site hinterland was undertaken, covering around 750ha, where over 200 sites were recorded, ranging from the Bronze Age to post-medieval structures. Most notably, a field system was discovered, believed to pre-date the broch and be of Bronze Age origin. Moreover, a survey of 3.75ha around the broch produced results suggesting rig and furrow techniques being applied to the land which incorporated large amounts of anthropogenic soil associated with the broch (Historic Environment Scotland, 2018c).

The cultural significance of Borwick Broch is therefore clear, having been studied periodically for more than 130 years. The area is associated with varying practices from the Bronze Age to post-medieval times, indicating that a wide range of knowledge can be gained from the site, pertaining to land use and function, developing through distinct occupation periods.

2.4 Research Design

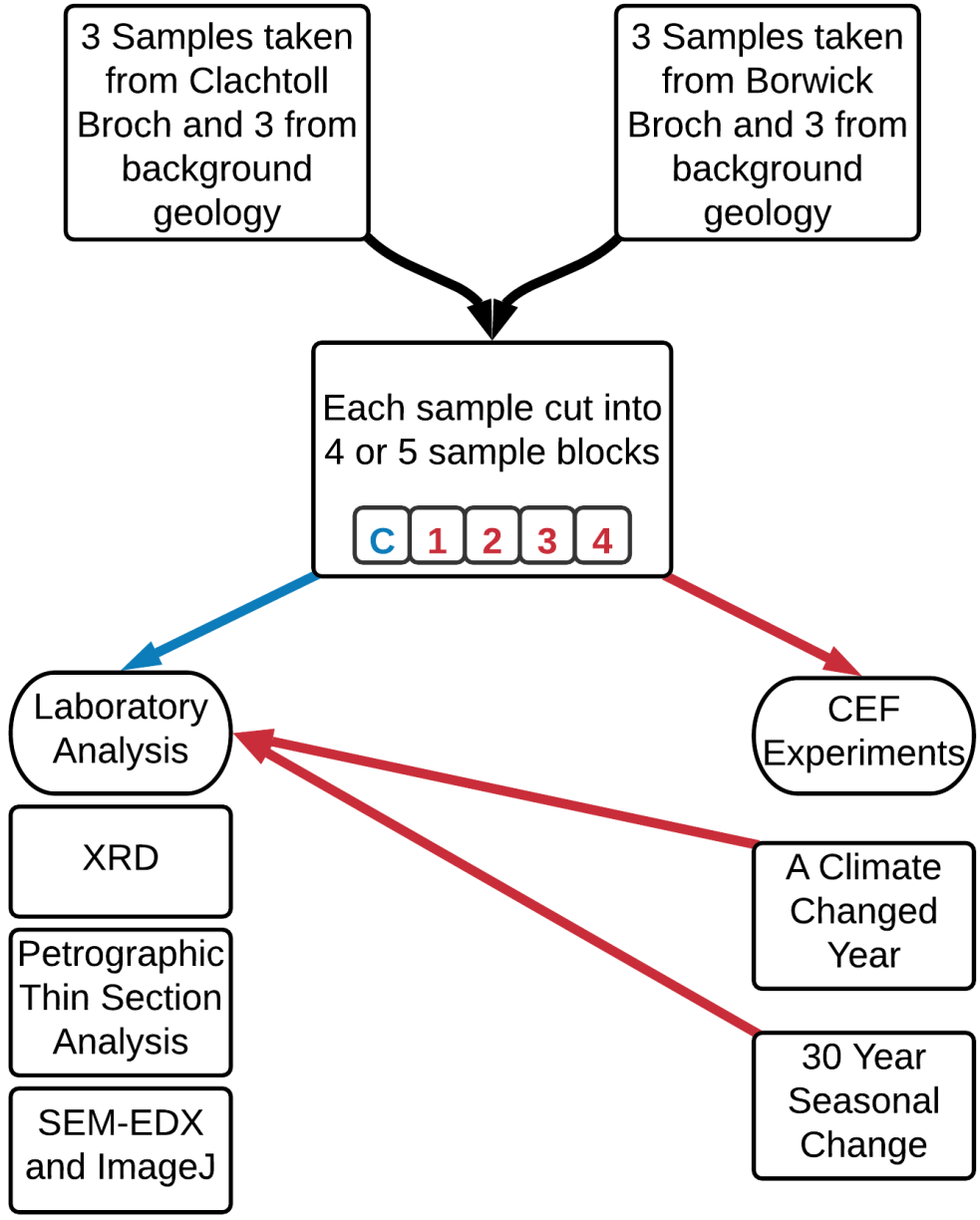

Figure 2.8 - Research design flowchart showing sample collection, processing, and analyses

The foremost aim of this thesis is to understand the future effects of climate change on the weathering of culturally significant sandstone in Scotland. The research design integrates a range of innovative, primarily laboratory-based methods to achieve this, highlighted in Figure 2.8 and detailed extensively below.

Held within the natural environment, background geology rock samples that have not been exposed above surface display a reduced prevalence of weathering than stone emplaced

above the surface in the built environment. These samples, therefore, provide insight into the unweathered 'baseline' characteristics of each sandstone type. Conversely, influenced by earth-surface environmental and anthropogenic conditions, weathering processes occur at a more pronounced rate in broch structures (Pope and Rubenstein, 1999; McCaughie *et al.*, 2020). Parallels made between the natural environment 'baseline' rock and cultural broch stone, therefore, provide insight into how the focus sandstones have weathered over the last c.2000 years during their above surface exposure. This is an essential comparison as the historical modification of stone greatly influences present and future deformation pathways (Johnston *et al*., 2019).

To achieve this, three samples of each sandstone type from Clachtoll and Borwick brochs as well as unweathered baseline samples were collected. Depending on the size of the original block, each sample obtained was cut into 4 or 5 sub-sample blocks of similar dimensions to facilitate laboratory analyses and CEF experiments. It is of note that samples of the same lithology, despite appearing homogenous, display heterogeneous characteristics when considering their physical structure, chemical constituents, and degree of weathering to date. Often, the inherent heterogeneities across samples can determine their durability as a component of a culturally significant monument (Johnston *et al*., 2019). Therefore, the sub-sample from each block labelled 'C' is the control for the block it has been cut from. Analysis of the 'C' block provides a control baseline of each sample type and individual block's present condition, while the numbered sub-sample blocks are exposed to different treatments under climate changed conditions in the CEF, based on temperature, humidity, and precipitation cycles. Exposure to a salt solution treatment is also explored in-depth below (Section 2.4.5.3 Simulating Salt Spray). Through CEF experiments, these become 'climate change sensitised' samples, subsequent analyses allow knowledge to be gained firstly on how, in a climate changed future, two types of unweathered baseline sandstone samples weather, assuming they are exposed above the surface. Secondly, how the same two sandstone types, having been pre-weathered since their incorporation in the built environment, proceed to weather under markedly different climate conditions.

Through the range of samples obtained and the methodological approach used, the weathering of two sandstone types with progression from their unweathered baseline state to a climate change sensitised state is presented in this thesis. Upon completion of CEF experiments, micro-scale, early warning indications of how the sandstones will likely weather

in the future are identified. These findings help to inform whether Scotland's sandstone heritage is under threat from climate change, and if so, to what degree.

2.4.1 Scheduled Monument Consent: Obtaining Culturally Significant Sandstone

SMC is required for any work conducted to a scheduled monument in Scotland, such as Clachtoll and Borwick Brochs. The Historic Environment Scotland Act 2014 revised the Ancient Monuments and Archaeological Areas Act 1979, giving HES the responsibility of overseeing and ruling on applications for SMC.

SMC is necessary to ensure the future protection of significant monuments, to ensure that they remain authentic and avoid degradation. However, as is intrinsic to this thesis and forms the basis of the research proposed in this study, ancient monuments, such as sandstone structures are subject to decay and the threat of destruction through climate change. Of importance to this research, climate change is one of the main threats to Scotland's sandstone heritage. Scientific research is therefore vital to ensure more knowledge is gained on how sandstone will decay in a climate changed future, to ensure the longevity of stone-built monuments.

An application was submitted to HES for sandstone to be removed from archaeological spoil heaps associated with each site, assuming material found in these heaps were once incorporated in the historic monument and have therefore been exposed above the surface for c.2000 years at their respective sites. This application was successful with conditions as follows:

- Clachtoll Broch – Archaeological spoil heap located outside the boundary of the scheduled monument; therefore, SMC is not required to obtain this material.
- Borwick Broch – Archaeological spoil heap located within the boundary of the scheduled monument. Removal of 3 x pre-selected samples of sandstone (10cm x 10cm x 5cm) from rubble associated with the broch with a geology hammer allowed.

2.4.2 Sandstone Sampling Regime

The decision process for choosing samples was as follows. To account for the compositional variation of building stone within each structure and to ensure representative samples were taken, a full site investigation occurred at Clachtoll. At Borwick, this was restricted to the landward side of the structure. A visual stone matching exercise occurred, this involved the analysis and characterisation of key stone surface features as well as an assessment of the

degree of stone weathering in the broch. Samples from spoil heaps associated with each site were then matched with the stone in the broch.

To obtain relatively pristine control samples from the background geology that were relatable to the samples taken from each spoil heap, extensive desk-based research occurred, focussed on geological maps of the areas. Relevant maps were downloaded for field work, and understanding was gained as to where outcrops of Torridonian Sandstone and Stromness Flagstone were located. Sampling was also discussed with geologists within HES's science team and climate science team. Given the proximity of rock outcrops to the brochs themselves, spoil heap samples taken served as a comparison when sampling from the background geology, to ensure that samples obtained were compositionally as similar as possible to the broch stone, albeit less weathered. The success of this sampling technique is reflected in key features identified across samples throughout Chapters 3-5 of this thesis.

2.4.2.1 Clachtoll

Clachtoll Broch lies upon the Bay of Stoer Formation of Torridonian Sandstone (Figure 2.9). Arriving on-site, the broch was examined by a walk around of the site to understand the current condition of the structure after extensive, and at the time of visit, ongoing archaeological excavation by AOC Archaeology and Historic Assynt.

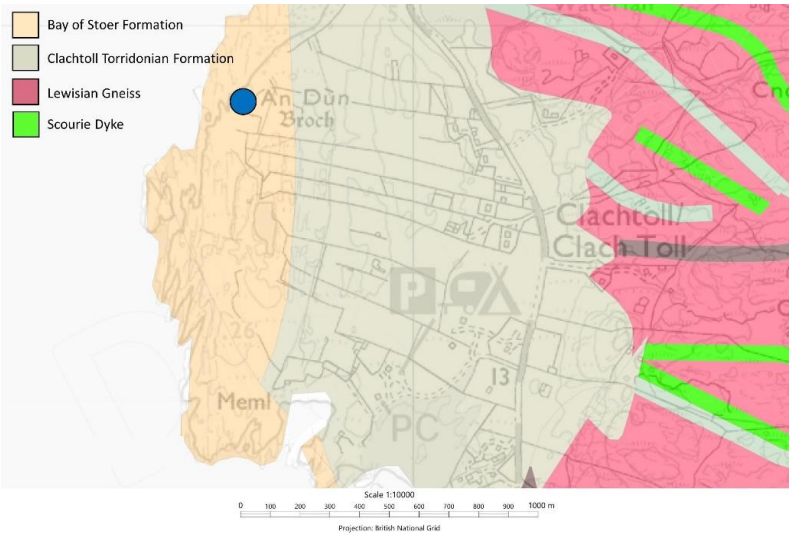

Figure 2.9 - Geological map of Clachtoll Bay, NW Highlands – Broch sandstone composed of Torridonian Sandstone (Bay of Stoer Formation). Site 'An Dun Broch' marked on the map

Figure 2.10 - Spoil heap (NC 03675 27858) at Clachtoll with Clachtoll Broch in the background (L), spoil heap (R) viewed from Clachtoll Broch

The spoil heap at Clachtoll is extensive and easily identifiable on the northern side of the structure (Figure 2.10), stretching around 10m in length and varying in height (NC 03675 27858). Given the instability of the spoil heap and its proximity to a rocky slope leading into the ocean, care was taken not to step on the heap, or to be too investigative of stone lying underneath the immediate heap surface. Through an examination of stones on the surface, care was taken to gather a sample range in keeping with the compositionally varying nature of the Torridonian Sandstone present in the broch.

Figure 2.11 - Torridonian Sandstone outcrop in Clachtoll Bay, immediately south of the broch. Background geology samples were obtained here using a geology hammer at NC 03648 27836.

Background geology samples to accompany the broch material were collected at a Torridonian outcrop immediately south of the broch (NC 03648 27836). It can be seen from Figure 2.11 that the exposed rock face has been affected by biological colonisation, therefore, where possible, the non-exposed face of rock obtained is examined as it remains relatively pristine.

2.4.2.2 Borwick

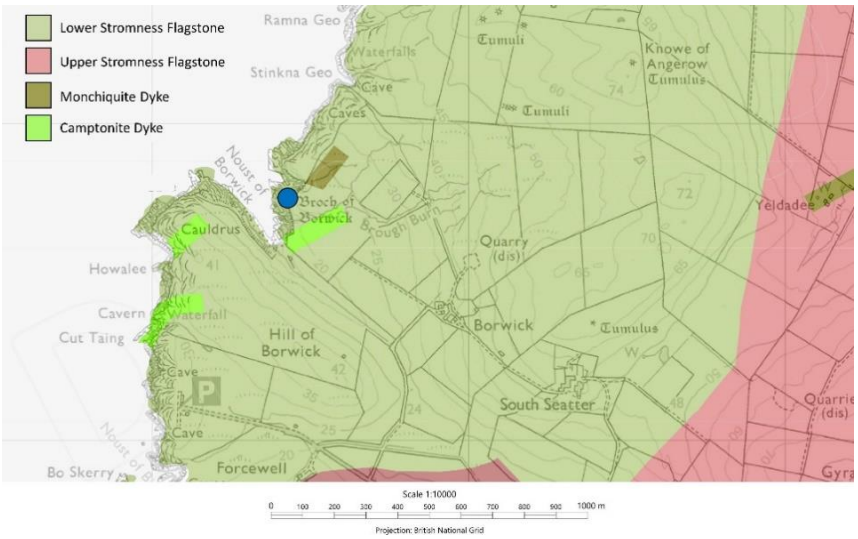

Figure 2.12 - Geological map of Borwick, Western Mainland, Orkney – Broch Sandstone composed of Lower Stromness Flagstone, Site 'Broch of Borwick' marked on the map

A similar approach was taken at Borwick Broch, whereby the geology of the area was studied before the field visit. It can be seen from Figure 2.12 that the area where the broch is located is dominated by Lower Stromness Flagstone. Unlike Clachtoll, an extensive walk-around of Borwick Broch was not possible due to its location on top of a promontory, care was taken not to step within the broch and instead to remain on the landward, spoil heap side of the structure (Figure 2.13). The spoil heap is easily spotted on the main path leading to the broch entrance, on the north-east side of the structure (HY 22428 16781).

Figure 2.13 - Spoil heap at Borwick with Borwick Broch in the background on top of a promontory

The same procedure occurred at Borwick as at Clachtoll, with stone from the surface of the excavation spoil heap being removed (Figure 2.13). The constraints placed on the research through SMC meant only 3 pre-selected samples of sandstone (10cm x 10cm x 5cm) from rubble associated with the broch could be removed. Therefore, three compositionally varying samples, encompassing a range of stone found on the surface of the spoil heap and fitting the size restrictions were photographed and sent for approval to HES, which was accepted, allowing samples to be collected the following day.

Borwick Broch is located at the top of the promontory pictured above (Figure 2.14), therefore control samples of relatively pristine Lower Stromness Flagstone were obtained with the use of a geology hammer on safely accessible areas of the outcrop which was accessed from the rocky beach on the southern side of the broch (HY 22415 16625).

Figure 2.14 - Stromness Flagstone outcrop on the Western Mainland of Orkney, background geology samples obtained from here with a geology hammer (HY 22415 16625).

As discussed in Section 2.2.2 Old Red Sandstone of Orkney, the Stromness Flagstones are characterised by over 50 cycles, each around 5-10m in depth. Therefore, hand specimens taken from archaeological spoil were used to ensure an accurate match of control sandstone was safely obtained from the cliff side close to Borwick Broch.

2.4.3 Determining the Physical Characteristics of Focus Sandstones

Fundamental to any geology research project, a series of basic laboratory tests were conducted to determine the key physical characteristics of each sandstone type, adhering to guidelines set out in relevant British standards.

2.4.3.1 Apparent Density and Open Porosity

Six homogenous and pristine control samples of Torridonian Sandstone and Stromness Flagstone were utilised in the following experiments. Ideally, for these tests, specimens are in the form of a cylinder, cube or prism measuring 70mm or 50mm in size, however, due to the non-fresh-cut nature of samples used, these specifications could not be met. Samples were, however, cube-shaped and of similar size, taken from the same lithology. Samples were dried at 70°C for a constant mass to be achieved, i.e., when the difference between two weight readings at a 24hr interval was not greater than 0.1%. Samples were stored in a desiccator until room temperature was obtained.

Each sample was weighed (m_d) then placed in an evacuation vessel where the pressure was lowered to 2kPa which was maintained for 2hrs to remove the air contained in the sample's open pores. Over 15 minutes. Demineralised water was introduced into the vessel until the

samples were immersed, while a pressure of 2kPa was maintained. After immersion, the vessel was returned to atmospheric pressure and samples were left immersed for 24hrs. Each sample was then weighed under water (m_h), quickly wiped with a damp cloth to remove excess water and weighed while saturated with water (m_s) (British Standard Institution, 2006) (Figure 2.15).

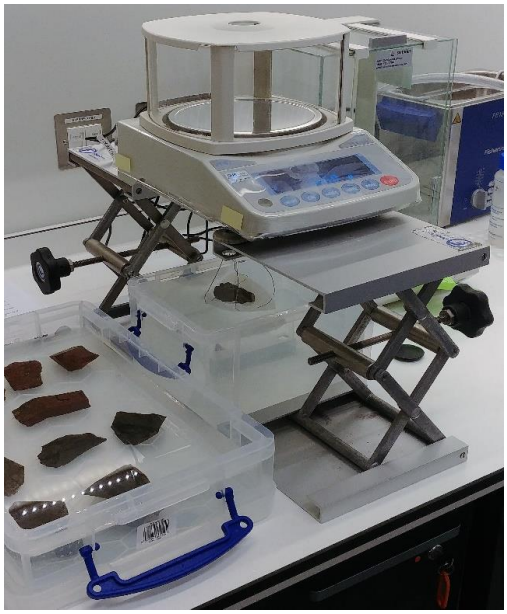

Figure 2.15 - Sample being weighed under water by hanging a cradle from the underside of the weighing scales and placing the specimen in the cradle submerged under water

Apparent density was calculated using the following formula:

$$P_b = \frac{m_d}{m_s - m_h} \, x \, P_{rh}$$

P_b – apparent density of the sample (kg/m^3)

m_s – mass of saturated sample (g)

m_d – mass of dry sample (g)

m_h – mass of sample immersed in water (g)

P_{rh} – density of water (977 kg/m^3)

Open porosity was calculated using the following formula:

$$P_o = \frac{m_s - m_d}{m_s - m_h} \text{ x } 100$$

P_o – open porosity of the sample (%)

m_s – mass of saturated sample (g)

m_d – mass of dry sample (g)

m_h – mass of sample immersed in water (g)

2.4.3.2 Water Absorption

Like samples used in apparent density and open porosity measurements, samples were dried at 70°C for a constant mass to be achieved before being weighed (m_d) and placed in a tank at least 15mm apart. Tap water was then added up to half the height of the samples, after an hour the water level was increased to three-quarters of the way up the samples, an hour later they were completely immersed. The samples were removed from the water 48hrs later, quickly wiped with a damp cloth to remove excess water and weighed (m_i) before being immersed again. Samples were re-weighed every 24hrs until a constant mass was achieved. The last weight is the mass of the saturated sample (m_s) (British Standard Institution, 2008).

Water absorption was calculated using the following formula:

$$A_b = \frac{m_s - m_d}{m_d} . 100$$

A_b – water absorption at atmospheric pressure (%)

m_s – mass of saturated sample (g)

m_d – mass of dry sample (g)

2.4.4 Sample Block Preparation

Following the collection of samples, each large sample block was named (shown in bold below) corresponding to its origin before being cut into sub-sample blocks (shown in italics below), the list of samples are as follows:

- Clachtoll Broch – **CB1** (*C,1,2,3,4*), **CB2** (*C,5,6,7,8*), **CB3** (*C,9,10,11*).
- Clachtoll Control – **CC1** (*C,1,2,3.4*), **CC2** (*C,5,6,7,8*), **CC3** (*C,9,10,11*).
- Borwick Broch – **BB1** (*C,1,2,3,3*), **BB2** (*C,5,6,7*), **BB3** (*C,8,9,10,11*).
- Borwick Control – **BC1** (*C,1,2,3,4*), **BC2** (*C,5,6,7*), **BC3** (*C,8,9,10,11*).

The heterogeneous state of each sample proved problematic when cutting them into sub-samples, care was taken to ensure the size of each block remained relatively constant, however, cutting each block to the same dimensions was not feasible; a trade-off when using non-fresh-cut stone. There is, therefore, deviations in the weight of each sample (Figure 2.16), in part owing to differing rock characteristics and deviations too in the size of the face that is exposed in the CEF (Figure 2.18).

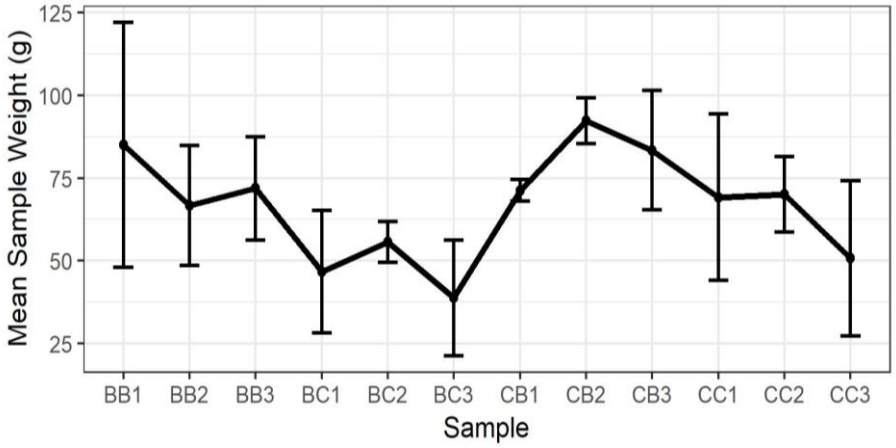

Figure 2.16 - Mean sample weight of each sub-sample block with added weight range

After cutting, high-definition photographs of samples were taken, (an example is shown below in Figure 2.17) from which image analysis could occur using ImageJ software, such as calculating the exposed sample area size (Figure 2.18).

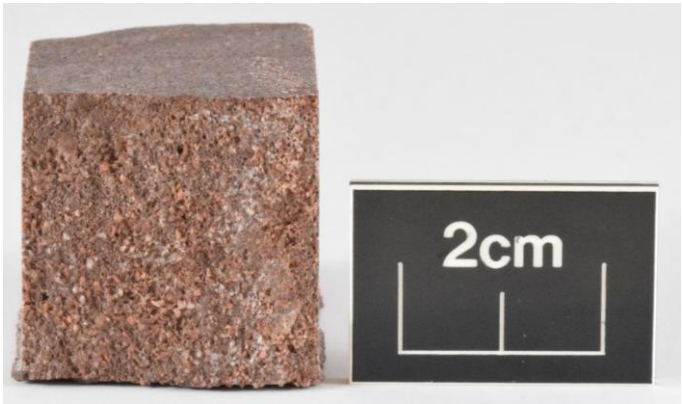

Figure 2.17 - Photograph of CB1 (1), showing the face of the block exposed in the CEF

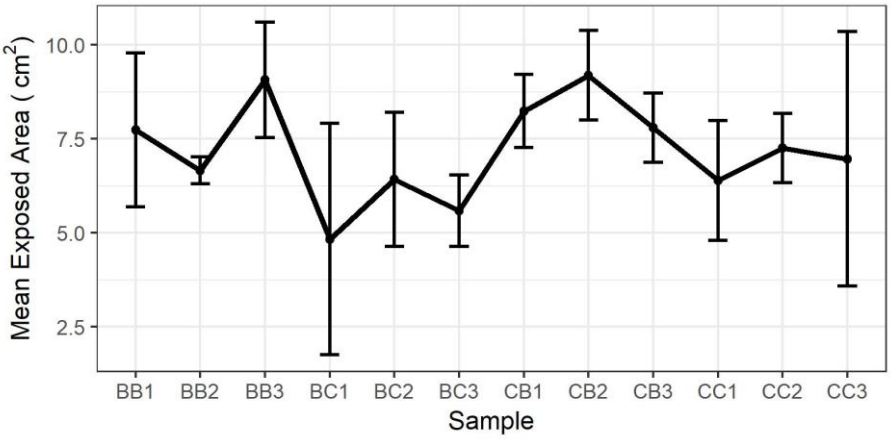

Figure 2.18 - Measured using ImageJ, mean exposed sample area with added range representing the difference within sub-samples in the size of the sample face that has been exposed in the CEF

Excluding the 'C' block, each sub-sample has been incorporated in a CEF experiment with one exposed face to allow more precise results to be gained on the behaviour of a single face which has been exposed to climate change conditions. Conversely, if the entire block were to be exposed, dubiety would arise about which exact sections of the block would have been in contact with the desired temperature, humidity, and precipitation fluctuations.

To ensure only the desired face has been exposed in the experiment, the non-exposed faces of each block were firstly wrapped in a waterproof, non-adhesive film and secondly with a waterproof adhesive tape that stuck to and held in place the waterproof film. The wrapping was conducted in such a manner that left the desired face exposed, and the remainder of the sample protected. Furthermore, the application of the non-adhesive film acted as an important boundary between the adhesive tape and the sandstone sample, it ensured no adhesive residue was left on the sample after the removal of the tape while preventing the tape from dethatching any particulate material from the sample upon its removal.

2.4.5 Climate Change Experiments

To understand the threat posed to sandstone heritage from climate change, hypothesised as a forecast increase in weathering severity, two innovative CEF experiments and subsequent laboratory analyses took place. As highlighted in Chapter 1, innovative new approaches to the complex relationships between building stone heritage, climate changed futures and weathering are needed, particularly in the geographical extent and focus lithology of this study.

Simulated laboratory conditions have been utilised in the literature to understand the behaviour of rocks in a range of settings, including pressure tests, salt weathering and freeze-thaw simulations (Přikryl *et al*., 2003; McCabe *et al*., 2007; Nong and Towhata, 2017); however, despite extensive investigation, no published research could be found that has integrated this method in understanding the effects of future climate change on built sandstone heritage. This research is innovative and different, in that climate change is regarded as having overarching influence on the weathering of culturally significant stone material. Therefore, this thesis addresses this gap through the creation of robust laboratory experiments, exposing sandstone samples to climate changed futures, informed by robust climate projection data. In line with limitations of environments that can be feasibly constructed within a laboratory, sub-samples of each larger sample block have been exposed to fluctuations in temperature and humidity with added precipitation.

Data utilised in the experiments described below mimics IPCC scenarios, integrated within the UKCP18, the official source of information detailing how the UK climate may change over the coming century. To remain consistent with HES's recent climate change risk assessment report (Historic Environment Scotland, 2018b), data were gathered through Representative Concentration Pathway 8.5 (RCP 8.5), equivalent to a high emissions scenario from global projection data at a 60km resolution for the administrative region of Northern Scotland. This data set provides information on the main drivers that influence weather patterns within the UK and is particularly useful when analysing climate data at more than one location at the same time, i.e., Clachtoll and Borwick. Additionally, utilising projections across Northern Scotland allows results from this research to be applied to similar sites within the same region, composed of the same sandstone type (Met Office, 2018, 2019).

2.4.5.1 Climate Change Experiment 1: 'Climate Changed Year'

For CEF Experiment 1, temperature, humidity, and precipitation data were obtained for the year 2055 in N. Scotland through UKCP18 RCP8.5. This year was chosen to remain constant with HES's climate change risk assessment report which used UKCP09 data on a high emission scenario in Scotland at a 50% probability level for a given year from 2040-2069. The development of high-resolution data within UKCP18 meant that a specific year could be chosen.

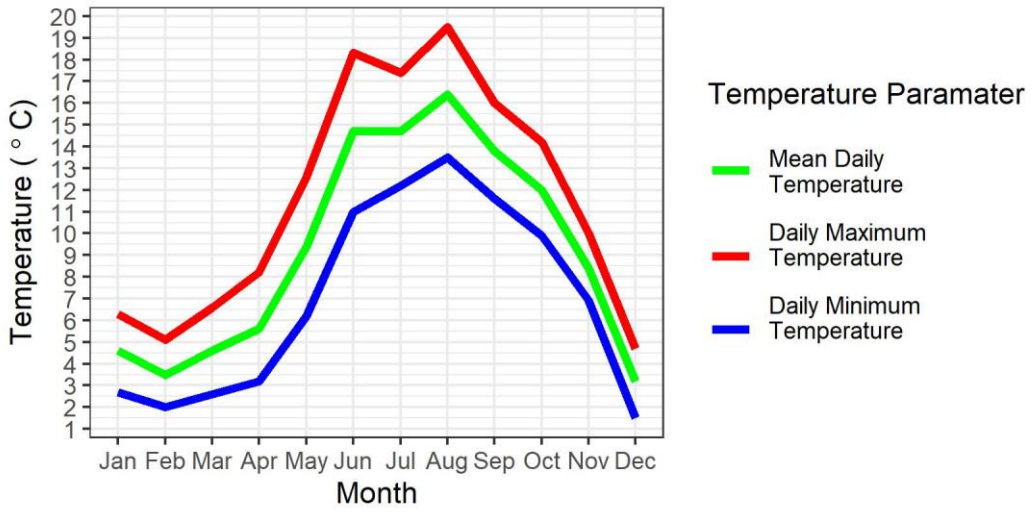

Figure 2.19 - Climate changed temperature at study sites in N. Scotland, 2055 (UKCP18)

A theoretical 'Climate Changed Year', condensed into 12 weeks was generated. Each week of the experiment corresponded to a month of real-time exposure. Temperature, humidity, and precipitation fluctuated throughout the experiment, in line with the way it is anticipated to fluctuate under future climate change conditions. Samples were exposed to precise hourly temperature fluctuations from the daily minimum to daily maximum temperature (Figure 2.19) while remaining exposed to a constant humidity for each week (Figure 2.20).

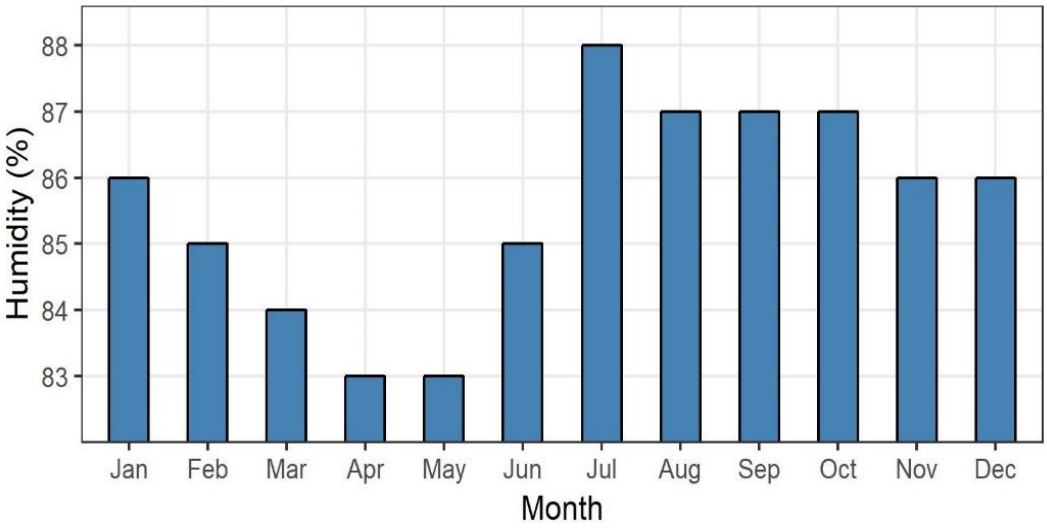

Figure 2.20 - Climate changed humidity at study sites in N. Scotland, 2055 (UKCP18)

Similarly, the monthly rainfall rate was obtained for 2055. To condense this into a week, the number of days of rain for each month at both study sites was obtained from MET office historical data (Figure 2.21).

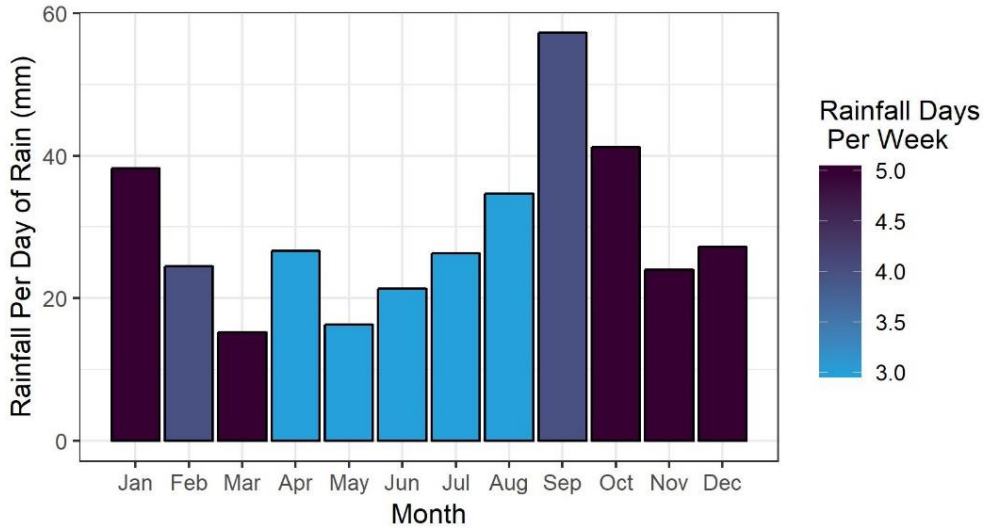

Figure 2.21 - Rainfall quantity per day of rain in each climate changed week that represents a month

Utilising January as an example, there are typically 21 days of rain at each site – the equivalent of 5 days of rain per week. Anticipated rainfall for January 2055 is 191mm, this was divided by 5, and therefore, 38.2mm of rain had to fall on 5 days of the week representing January. The same calculation was made for each month (Figure 2.21). Samples exposed to precipitation were kept separate to samples only being exposed to temperature and humidity fluctuations. Rainwater was gathered at the University of Stirling and filtered to remove large particulate material. Samples were sprayed with rainwater using a Hozelock 7L portable shower, which allowed control over which samples were sprayed and expedited the process of spraying while keeping the experiment as similar to the intensity of real rainfall as possible. Analysis of rainwater could not be conducted due to restricted laboratory access during the coronavirus pandemic. However, the UK Department for Environment Food & Rural Affairs (DEFRA) collects fortnightly rainwater data from 38 sites in the UK and daily rainwater data from 2 sites in the UK. All of the following are measured: Rainfall amount, pH, conductivity, Na^{+}, Ca^{2+}, Mg^{2+}, K^{+}, PO_4^{3-}, NH_4^{+}, NO_3^{-}, SO_4^{2-}, Cl^{-} and are readily available on Precip-Net (DEFRA, 2021). Based on data obtained from 'Balquhidder 2' in 2018, approximately 36km from the University of Stirling, pH of rainwater is typically between 5 and 7.5 and conductivity is typically between 5 and 21 μS/cm.

Before experimental work, the shower was tested on its lowest setting to discover how long it took to spray a given volume. Approximately 1mm of water was sprayed every second, therefore the length of spraying time was equivalent to 1 second per mm on each sample.

Although the use of the shower was quicker than real-time precipitation, it prevented the chamber from being open for too long and allowed each sample to be exposed to the correct amount of simulated precipitation in a manageable time. During spraying, rainwater used was gathered in a tray placed at the bottom of the CEF chamber, allowing it to be re-used in subsequent days.

A sub-sample of each larger sandstone block was exposed to differing treatments under laboratory simulated climate changed conditions (Figure 2.22).

Sandstone Block	Temperature and Humidity	Temperature, Humidity and Precipitation
Clachtoll Broch: C 1 2 3 4 / C 5 6 7 8 / C 9 10 11	1 5 9	2 6 10
Clachtoll Control: C 1 2 3 4 / C 5 6 7 8 / C 9 10 11	1 5 9	2 6 10
Borwick Broch: C 1 2 3 4 / C 5 6 7 / C 8 9 10 11	1 5 8	2 6 9
Borwick Control: C 1 2 3 4 / C 5 6 7 / C 8 9 10 11	1 5 8	2 6 9

Figure 2.22 - 'Climate Changed Year' experimental CEF chamber layout

As a control for the experiment, a second chamber was run using 2018 data, allowing the effects of climate change to be distinguished from the effects on the stone that would take place if there was no climate change between 2018 and 2055 (Figure 2.23).

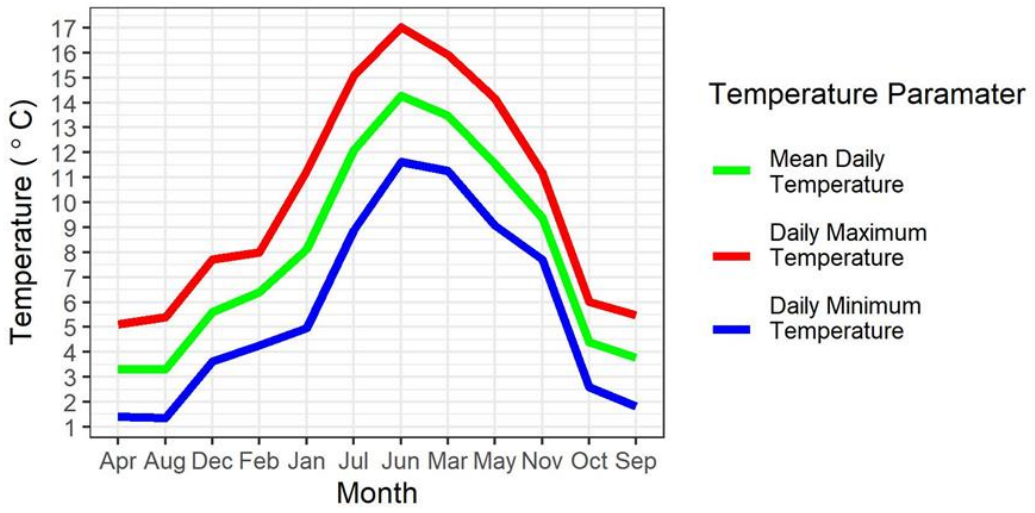

Figure 2.23 - Temperature at study sites in N. Scotland, 2018 (UKCP18)

Like the experimental chamber, each month of 2018 was condensed into a week and samples were exposed to temperature fluctuations ranging from the minimum to maximum daily temperature. The key difference between the chambers was that samples in the experimental chamber were exposed to warmer winters and summers, analogous with anticipated climate changed conditions in Scotland. Humidity remained constant for each week (Figure 2.24) and it can be seen that humidity in the control chamber is generally lower than in the experimental chamber (Figure 2.20).

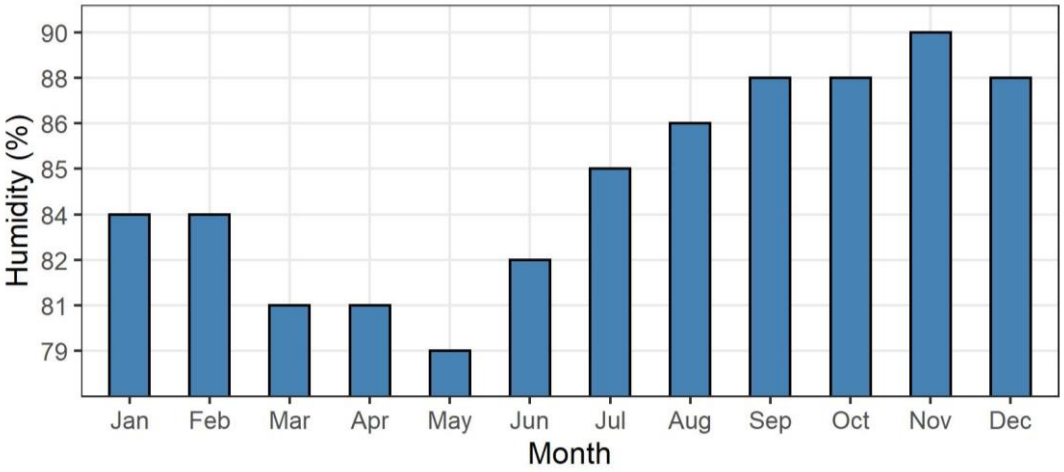

Figure 2.24 - Humidity at study sites in N. Scotland, 2018 (UKCP18)

Following the same methodology as described for the experimental chamber, a rainwater component was utilised in the control chamber (Figure 2.25)

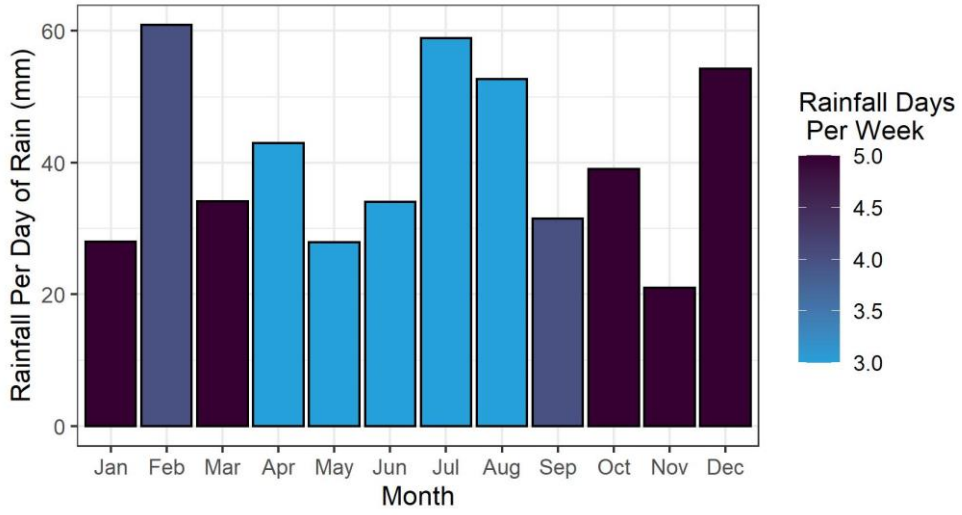

Figure 2.25 - Rainfall quantity per day of rain in each week that represents a month in 2018

As described above, data for rainfall was based on historical data for the number of days of rain at the study sites. Therefore, the number of days of rain is the same in each chamber but the volume of rainfall is different. Crucially, it is drier in the summer months in the experimental chamber, in keeping with warmer, drier summers. However, in the winter, the control chamber has more rainfall in two of the three winter months (December and February), varying slightly from anticipated warmer wetter winters in Scotland in a climate changed future.

Due to restrictions placed on obtaining culturally significant material, only one sub-sample could be utilised in each section of the control chamber, however, each of these is relatable to samples used in the experimental chamber (Figure 2.26).

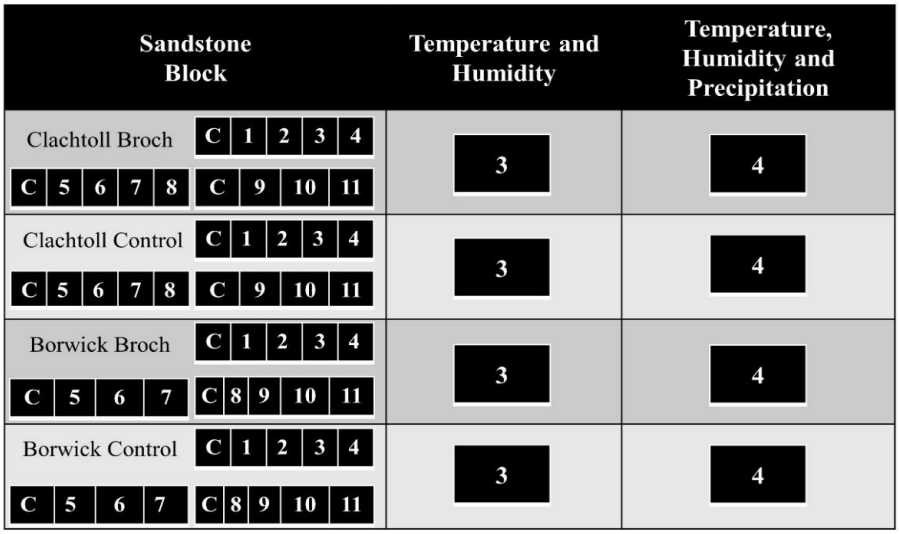

Figure 2.26 - 'Climate Changed Year' control CEF chamber layout

2.4.5.2 Climate Change Experiment 2: '30-Year Seasonal Climate Change'

For experiment two, seasonal data of minimum, mean and maximum air temperature, as well as mean relative humidity were obtained from the year 2025 to 2055. Each day in the CEF corresponds to a season, the experiment ran for 120 days to mimic 30 years of seasonal cycling. No precipitation data was utilised, instead, samples were wetted on the winter days of the experiment with rainwater, using the Hozelock 7L portable shower in the same way as experiment 1. Samples utilised in this experiment are relatable to samples utilised in experiment 1 and a control experiment run in a separate chamber, whereby sub-samples were exposed to repeat 2018 seasonal temperature and humidity fluctuations with winter wetting (Figure 2.27). This experiment was constructed in order to expose samples to more prolonged weathering, focussing on rapid seasonal transitions, while remaining within temperature and

humidity parameters that are anticipated in a climate changed future at study sites, obtained from the UKCP 18 database. This experiment aims to bridge the gap between present day and 2055, which was the chosen year for experiment 1, while stressing the samples to a higher level than in the 'Climate Changed Year' experiment.

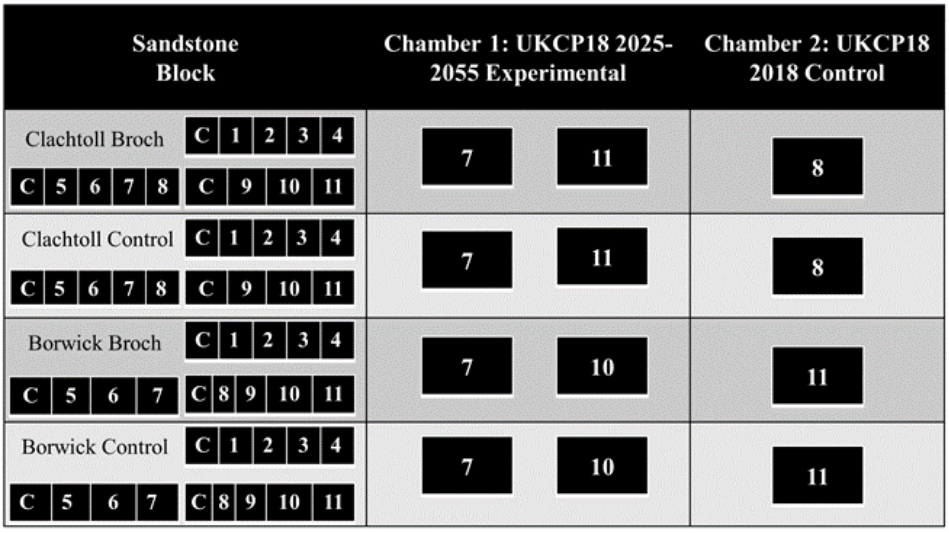

Figure 2.27 – '30-Year Seasonal Climate Change' experiment: CEF chamber 1 and 2 layouts

Resulting from the CEF experiments, a range of 'climate sensitised' Torridonian Sandstone and Stromness Flagstone samples were obtained:

- 2018 sensitised geological control rock.
- 2018 sensitised broch stone.
- 2055 climate change sensitised control rock and broch stone.
- 2025-2055 climate change sensitised control rock and broch stone.

2.4.5.2.1 Climate Change Experiment 2: Chroma Meter

Due to the subjective nature of determining colour and its susceptibility to becoming altered through weathering, a Konica Minolta CR-400 Chroma Meter was utilised in the second CEF experiment to determine the colour of each sample's exposed surface before and after their use in the experiment. The instrument flashes a light onto a specific target area and by comparing the reflectance to a standard, colour is determined (Figure 2.28).

The use of the chroma meter in the literature related to stone weathering focuses largely on colour change induced through extreme temperature events such as fire. Under exposure to

such temperatures, sandstone L* values increase, and the stone becomes much lighter in colour. In such experiments, samples are exposed to different heating regimes, reaching as high as 1000°C which commonly destroys the sample (Hajpál, 2002; Hajpál and Török, 2004; Ozguven and Ozcelik, 2013). The most apparent colour change on heat-treated sandstones in a study by Kompaníková *et al.*, (2014) occurred at temperatures above 400 °C, whereas samples heated to 60°C and 200°C showed only negligible change.

Figure 2.28 - Konica Minolta Chroma Meter CR-400 being used to determine sample surface colour. Sample locations marked on exemplar block

The instrument measures L* - lightness value, a* - red-green colour value, b* - yellow-blue colour value, all of which can be visualised on a colour coordinate diagram (Figure 2.29). Five readings were taken at five different points on each stone surface, from which mean L*, a* and b* values were obtained. These numerical colour codes were then converted into Munsell notation allowing them to be plotted on a colour wheel. Any change in colour after the experiment can be defined and related to the treatments that the samples have been exposed to.

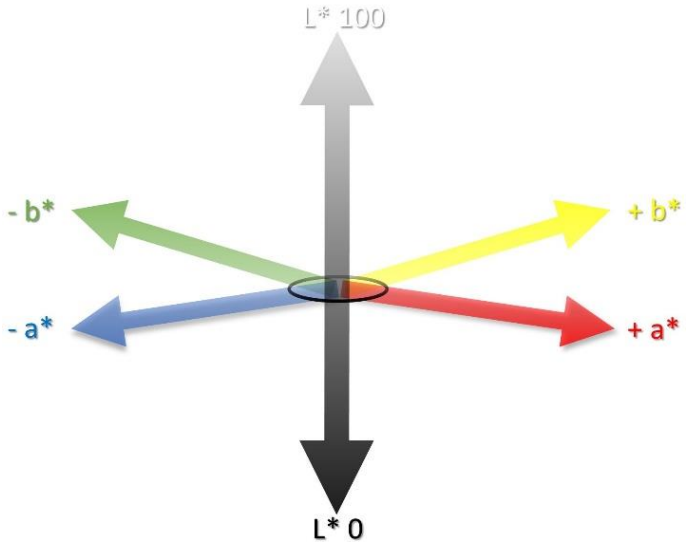

Figure 2.29 - Colour coordinate diagram for the Chroma Meter

2.4.5.3 Simulating Salt Spray

Due to the coastal location of each study site and the prominence of heritage sites located within proximity to the coast in Scotland, salt weathering was noted as a potentially important factor in the overall weathering of sandstone manifested within heritage sites. The extent and severity of salt weathering is largely dictated by variation in temperature and moisture cycles. Under wetter climate changed conditions, the stone will remain wetter for longer, resulting in 'deep wetting', which facilitates the transportation of salts deeper into stone (Smith *et al.*, 2011). Although the salts carried deeper into the stone remain wetter for longer, delaying crystallisation, once drying and subsequent crystallisation does occur, it can be more severe, detrimentally impacting the sandstone and exacerbating its weathering (McCabe *et al.*, 2013).

To discover if salt is an important weathering factor at each site, salt extraction of samples for XRD analysis was undertaken. Between 4g and 5g of material from the surface of 3 large samples from each site was chipped off and crushed using a mortar and pestle. The crushed material was then added to a centrifuge tube, topped up with 40ml deionised water and placed in an ultrasonic bath for 10 minutes. The samples were then placed in the centrifuge cradles and run at 4000 rpm for 30 minutes. The resultant clear liquid was then pipetted into a pre-weighed crystallising dish. Once dry, the crystallising dish was re-weighed to calculate the percentage of salt in each sample.

Due to the small quantity of salt crystals present, the crystals for each of the three stones from each site were combined for analysis. The combined salts were scraped into a mortar and mixed with several drops of acetone. The salt and acetone were ground with a pestle until a smooth consistency of sample was left, this was then dried and placed on an XRD sample holder for analysis to occur.

It is of note that XRD analysis is not the most robust methodological approach to test for salt, more favourable techniques include ICP-OES and ICP-MS. In this study, XRD was employed to gain an initial understanding of the presence and amount of salt within samples, from which a more robust analysis could occur if it was determined that salt is present at a level that could have detrimental impacts on the sandstones.

2.4.6 Sandstone Laboratory Analyses

Upon completion of outlined CEF experiments, the unique sample set spans the lifecycle of focus sandstones, from their deposition and incorporation in underlying geology to their extraction and use as building stones in culturally significant structures and to their subsequent exposure to future climate change scenarios in weathering experiments. It was predicted that each of these distinct stages would have observable impacts on the sandstone's appearance, microstructure, mineralogy, and petrography that could be identified and interpreted through laboratory analyses, helping to determine the future integrity of sandstone heritage in Scotland. Key physical, chemical, micro-stratigraphical and mineralogical alterations in each sandstone type and sample set were identified and understood primarily through a combination of XRD, petrographic thin section and SEM-EDX analyses. These techniques have been documented in the literature as being powerful and robust in fully characterising entire microstructures of sedimentary samples (Liu *et al.*, 2017; Lai *et al.*, 2018).

2.4.6.1 X-Ray Diffraction (XRD) Analysis

XRD is a laboratory technique applied in the characterisation and understanding of crystalline minerals held within a material and has varied application in the literature, including in geological studies. Knowledge has been gained on the formation and diagenesis of minerals over time, with exposure to different environmental or simulated conditions (El-Gohary, 2017; Geng *et al.*, 2018).

The equipment has three fundamental components (Figure 2.30), an X-ray tube (A), a sample holder (B), and an X-ray detector (C). X-rays produced from the tube are accelerated towards a sample, bombarding it with electrons.

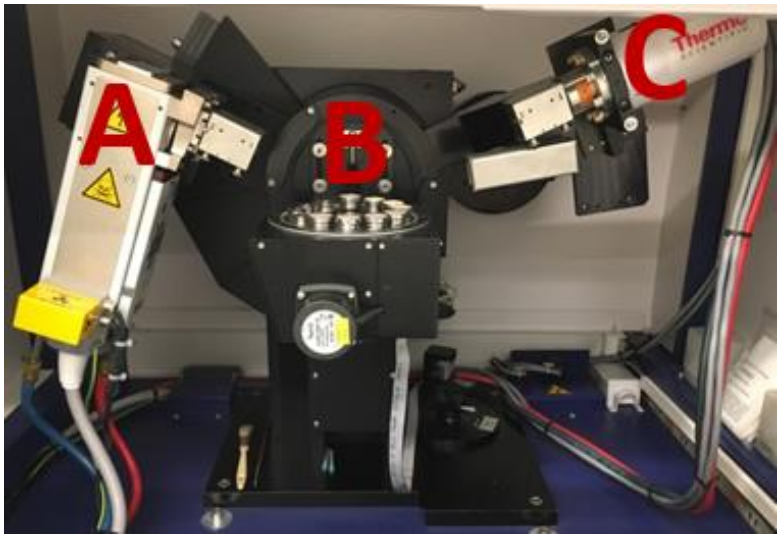

Figure 2.30 - X-ray diffractometer with X-ray tube (A), sample holder (B) and X-ray detector (C)

Upon reaching the required level of energy, electrons of the sample are diffracted off the atomic structure of the minerals they encounter, and X-ray spectra are produced, distinct to each crystalline mineral detected. The X-ray detector records the X-ray, producing a count rate or intensity, which is received on a computer in the form of peaks, specific to a detected mineral. Within the diffractometer, the sample holder rotates and the arms that the X-ray tube and detector are mounted on, rotate between an angle of 5 degrees and 70 degrees. For the purpose of this research, the analysis was run from 5 degrees to 70 degrees, with a step size of 0.02 degrees and a scan rate of 1 degree per minute. The analysis is undertaken with CuKα radiation of 1.540562 wavelength, at 45mA and 44kV on continuous scan mode.

Figure 2.31 - Fine powder Torridonian Sandstone samples in their sample holders before XRD analysis

Sample preparation is key in the analysis, ensuring the correct particle size is vital in achieving a good signal-to-noise ratio. Fine particle size also maximises the amount of particle detection in the analysis process, therefore, sandstone samples from Clachtoll and Borwick were ground to a fine powder (typically below 63μm) using a mortar and pestle. Ground sandstone was placed on a standard XRD sample holder, care was taken to ensure the holders were packed with a flat surface to maximise the analysis (Figure 2.31).

For smaller samples, an acetone backpack technique was utilised, whereby ground sandstone was mixed with acetone until a sample of slurry consistency was achieved, this was pipetted onto a glass slide and placed in the sample holder for analysis to take place (Bunaciu *et al.*, 2015).

In the literature, XRD has proved crucial in the understanding of the mineral composition of materials, from which knowledge can be gained on the formation and diagenesis of minerals over time, with exposure to different environmental or simulated conditions.

2.4.6.2 Petrographic Thin Section Analysis

The principal analytical technique applied in this thesis within the field of geoarchaeology is micromorphology, whereby petrographic thin sections have been manufactured at the University of Stirling and analysed under a polarising microscope.

Samples were initially cut using an abrasive cutter, on each sample, a line was marked, and the first cut was made, making a smooth surface, a parallel cut was then made 1cm in from the freshly cut surface ensuring a section of sandstone with two flat surfaces was produced. This was then trimmed down to size to fit on a glass slide. The side from which the thin section was to be made was polished to remove marks from the blade before the section of sandstone was glued to a glass slide using opti-tec epoxy resin and left overnight to cure. The section now mounted on a glass slide was then placed in the abrasive cutter and as much excess rock as possible was cut off. The remaining sample mounted to the slide was then ground down to the correct size using a Logitech LP50 lapping plate with 15μm calcined aluminium oxide. The desired thickness of a thin section is between 30 and 40 microns, this is verified under a polarising microscope, if the quartz present in the sample goes pale yellow under cross polarised light, then the sample is at the desired thickness. Slides were polished with 3μm diamond oil on a Logitech CL40 polishing plate to ensure maximum clarity. In this research, samples were not impregnated, furthermore, a coverslip was not applied to the

samples so that SEM-EDX work could occur. The final thin sections provide a cross-section through each sample from the exposed outer surface to the more pristine inner material.

The technique of micromorphology, or thin section analysis, allows in-depth analysis to occur on in situ materials. Samples are collected and processed in such a manner that ensures they remain undisturbed and hold within them a representation of the material as seen in the field. Furthermore, as the material is observed on a microscopic scale, micro-scale features can be identified, allowing insight to be gained into the formation, alteration, and degradation of the material. The method allows the relationship of sediments within a matrix to be understood, their interaction with one another is identifiable and factors influencing their formation and diagenesis can be clearly understood. Furthermore, the internal structure of a sedimentary material can be comprehended more fully and processes leading to the formation of the structure observed can be postulated; pertinent to this study, a particular microstructure can be related to a process such as weathering. As a consequence of the technique's benefits, its application is widespread and varied (Menzies *et al.*, 2010; van der Meer and Menzies, 2011; Bendle *et al.*, 2015).

Reedy, (1994) highlights the broad use of petrographic thin section analysis in cultural materials, including stone sculptures, architectural stone, and ceramics. The manufacture of petrographic thin sections has allowed the characteristics of different stone types to be documented, particularly those present in significant cultural relics and archaeological material, such as sandstone present in the Karnack Temple complex in Egypt (Saleh *et al.*, 1992).

Petrographic thin section analysis occurred at the University of Stirling microscopy laboratory on an Olympus BX51 mounted with a Colourview III soft imaging system camera, allowing image analysis to occur in analySIS.

Due to an error in the white balance during image acquisition, some petrographic thin section photomicrographs appear too orange in colour. This was particularly prevalent in chapter 4 thin section analysis. Badly effected images have been recalibrated in GIMP (2.10.14), an image editor software. This has improved photomicrograph quality and reduced the prevalence of discoloured images.

2.4.6.3 Scanning Electron Microscope with Emission Dispersive Spectroscopy (SEM-EDX) Analysis

Alongside structural alterations identified through petrographic thin section analysis, changes in the chemical composition of the sandstones and evidence of weathering have been understood through the utilisation of SEM-EDX. The University of Stirling thin section and micromorphology laboratory is equipped with a Zeiss Evo Ma15 Scanning Electron Microscope, fitted with a motorised 5 axis stage with large XY and Z travel and variable pressure capability. The system is fitted with SE, Backscatter and VP-SE detectors, as well as an Oxford Instruments 80 mm2 silicon drift X-ray detector for fast quantitative X-ray analysis. The machine is optimised for use at an accelerating voltage of 20 KeV and a working distance of 8.5mm. This is an extremely valuable method of analysis, applied widely and successfully in the literature. A significant advantage of using SEM-EDX is that it allows extremely high magnification images to be taken, ideal in this study looking at early indicator, micro-scale signs of weathering (Bull and Morgan, 2013).

A typical SEM-EDX has several main components, the electron source (usually a tungsten filament), a column that contains electromagnetic lenses, an electron detector, a sample chamber, and a computer display with interpretational and analytical software. A focused electron beam from the electron source scans the surface of the sample, reacting with it, generating a highly magnified topological image. Of particular importance in material analysis, the EDX component of the SEM-EDX allows the elemental composition of specific areas of interest within a sample to be determined. When the focused electron beam collides with the sample, secondary electrons and characteristic X-ray spectra are emitted. No two elements have the same X-ray spectrum, meaning that any element with a higher atomic number than boron can be detected and quantified in terms of its concentration within the focus area. The electron beam interacts with the nucleus of atoms within the sample, exciting the electron and removing it from the nucleus. The resultant electron hole is filled by an electron from the outer shell of the atom, releasing the X-ray. This X-ray is made up of the continuum and characteristic X-rays. The former is produced by the slowing of the electron, the latter is produced by the electron-hole being filled and is the crucial X-ray in determining elemental composition (Abd Mutalib *et al.*, 2017).

El-Gohary, 2017 utilised SEM-EDX analysis on sandstone samples from Petra, Jordan. Features identified in the stone were indicative of a heavily degraded material, with processes such as wetting and drying as well as contraction and expansion of the stone highlighted as

key weathering agents. Dissimilarities in grain and pore size were noted as well as prevalent fissures at the surface and deeper within the sandstone, it was concluded that their presence was due to pressure in the sample arising from the crystallisation of salts (El-Gohary, 2017).

In this research, SEM-EDX particularly compliments petrographic thin section analysis. The chemical composition of features of interest that are identified on the thin section using a polarising microscope can be understood more fully with the application of SEM-EDX. After testing different analytical techniques available on the Aztec software that works alongside the SEM, ArcMap was determined to be the most useful in this research. Through SEM-EDX mapping, the distribution of elements within samples can be visualised and quantified. Furthermore, the complex interrelationships between grain contacts, cement and porosity can be seen while variances in the relationship and composition of elements in different areas of the samples can be quantified. This is a particularly powerful analytical tool in determining weathering phenomena and in identifying pre-existing weaknesses within samples. SEM-EDX mapping has been favoured over a point analysis so that a greater depth of insight into each sample could be obtained. Fully qualitative data is gathered from a point analysis, and it is often not representative of an area or the spatial changes in relative elemental composition across a sample area. Therefore, very little can be inferred from a point analysis and limited understanding is gained into the overall chemical structure of the sample or specific areas of interest. Count times for elemental maps were between 5 and 10 minutes depending on many different factors, including SEM dead time and the size of area being scanned.

Elemental spectra are presented alongside map data in Chapters 3-5, these are normalised to 100% meaning comparisons across different samples have an associated error as these values are influenced by such factors as the amount of resin detected. However, they are nonetheless useful as a guide, showing the mineral composition of mapped areas. Additionally, during mapping, a series of key rock elements are focused on, such as silicon (Si), which is used as an indicator of the presence of quartz (SiO_2), with the caveat that Si also represents other trace minerals such as mica, feldspar, and alumino-silicate clay. The same applies to such elements as aluminium (Al), which is used as an indicator of plagioclase feldspar ($NaAlSi_3O_8$), although it also represents other trace minerals such as alumino-silicate clay and some micas. Finally, carbon (C) is used as a proxy for porosity and granular loss as this is the signal received from the resin that mounts the sample to the glass slide, therefore, the carbon signal is seen in porous areas. It must be noted, however, that although the resin is the

dominant carbon source, minerals such as carbonate could account for trace amounts of carbon identified in SEM-EDX mapping.

2.4.6.3.1 ImageJ Analysis

Key features within samples are analysed using SEM-EDX mapping as discussed above. To further quantify these results, ImageJ software has been implemented. In each SEM-EDX map, different elements are shown in unique colours, making it easy to visualise their distribution throughout a sample. In ImageJ, however, the auto-thresholding function allowed the focus element to be segregated from the image background, meaning that the distribution of key elements could be quantified and graphed to accompany map data.

Maps of particular interest were converted to 8-bit grayscale in order for the image to be segmented into two classes of pixels, one class depicting the element of interest and the other depicting the remainder of the sample. The thresholding process can be done manually, however, this can incur a high user bias due to the subjective selection of a threshold value. Moreover, for a manual threshold to be applied, image acquisition must be identical, however, in this research, acquisition varies across SEM-EDX maps through the use of different magnification, brightness, contrast and stage height between samples. Therefore, applying the same set threshold to each image would be inaccurate and incur user bias. Therefore, the 'Auto-Threshold function' has been used, eliminating user bias, and ensuring that pixel segments are fully reproducible, i.e., on the same image, the auto-threshold will always produce the same segmentation of the image. This technique was applied to all analysed images, meaning that although the threshold values are different for each image, they are generated in the exact same way through the default automatic threshold feature within ImageJ, guaranteeing a threshold that is specific to each image and fully reproducible.

After auto-thresholding, graphs could be generated, showing the intensity of the focus element across the mapped area. The intensity is represented as a 'Grey Value', which quantifies the brightness of a pixel. The value can range from a minimum of 0 to a maximum of 255; the higher the brighter. This value is utilised in this research to understand fluctuations in the intensity and prevalence of a given element within selected areas of a sample. There are a number of benefits obtained from using this technique alongside SEM-EDX work. From intensity graphs, any trends such as increasing or decreasing grey value (element abundance) can be easily identified, that may not be clear from element maps alone. Additionally, grey scale intensity graphs provide greater insight into the fluctuation of focus

element abundance with depth, allowing subtle variations to be picked out, that cannot be seen in SEM-EDX maps alone. From this, known depths of weathering features can be identified, which is particularly useful in the identification of surface weathering fronts, a key feature in Stromness Flagstone samples. Additionally, it allows graphs from different samples to be compared to one another, removing the subjectivity that arises from simply comparing SEM-EDX generated maps.

A summary for generating grey value intensity plots: Open image in ImageJ > Select 'Straight' line tool and insert a straight line over the scale bar already burned to image > Analyse > Set Scale > Insert known distance of straight line (e.g., 1mm) > Select rectangle tool and crop image to desired size (Image > Crop) > Image > Type > Convert to 8-bit > Image > Adjust > Auto-threshold > Default > Select area with rectangle tool > Analyse > Plot Profile > Save as high resolution plot.

2.5 Chapter Conclusion

The research design implemented in this study is particularly innovative, in that two sandstone types from culturally significant brochs are exposed to climate changed futures, simulated under laboratory conditions. To assess sandstone response, this study combines multiple macro/micro-scale analytical techniques, which highlight how, with the onset of climate change, the weathering of Torridonian Sandstone and Stromness Flagstone will potentially alter and accelerate.

Petrographic comparisons are made between samples collected from pristine background geology deposits, sandstone that has been exposed in archaeological monuments for millennia and stone which has been subjected to climate changed conditions in a CEF. From these comparisons, fresh insight is gained into sandstone weathering, which has allowed indicative decay models to be generated that are specific to each sandstone type and are robustly supported by observations made. This research also contributes new methodological approaches to the assessment of future climate change impacts on built heritage, through the application and assessment of CEF chambers as simulators of climate change.

3 Baseline Study of Geological Rock and Broch Stone

3.1 Chapter Introduction

This chapter characterises Torridonian Sandstone and Stromness Flagstone sampled from the background geology and archaeological spoil associated with Clachtoll and Borwick Brochs, respectively. An innovative and varied methodological approach is detailed in Chapter 2, which incorporates primarily XRD, petrographic thin section and SEM-EDX analyses to generate a robust characterisation of both sandstone types. In doing so, an understanding of how these sandstones have weathered since their removal from the geology and emplacement in the built environment has been gained. This comprehensive baseline of the sandstone types at two distinct phases provides comparative analyses from which transformations associated with climate change futures in subsequent chapters are evaluated (McCaughie *et al.*, 2020).

Firstly, the physical characteristics of each sandstone are outlined before XRD bulk and salt analysis results are presented, highlighting the key mineral constituents of each sandstone as well as determining whether salts play a significant role in their weathering. Subsequently, through petrographic thin section analysis, a micro-scale, visual understanding of the sandstones is achieved, particularly relating to their fabric, grain size, mineralogy, porosity, grain contacts and cementing agents. From observations made, specific weathering features of interest are quantified through SEM-EDX analysis and associated ImageJ work.

3.2 Sandstone Physical Characteristics

The characteristics of each sandstone type (Table 3.1) has been determined using six off-cut samples of background geology rock. Correct procedures outlined in relevant British Standards were followed where possible. Data obtained relating to the key physical characteristics of each stone type are presented below.

Table 3.1 - Mean apparent density, water absorption and open porosity of each sandstone type

Sandstone Type	Apparent Density kg/m^3	Water Absorption (%)	Open Porosity (%)
Torridonian Sandstone	2565.2	0.9	2.3
Stromness Flagstone	2674.2	1.3	3.6

The density of both sandstone types is on the higher end of typical sandstone density, while water absorption and open porosity values are very low compared with other sandstone types. To contextualise these values, Locharbriggs Sandstone, a popular building stone from Dumfries and Galloway in the Scottish Borders has a density of 2006 kg/m^3, a water absorption value of 8.3% and an open porosity value of 24.1%. Clashach, another popular sandstone building stone found along the Grampian Coast, has a density of 2084kg/m^3, a water absorption value of 6.9% and an open porosity value of 21.4% (BRE, 2020).

3.3 XRD Analysis

The application of XRD in this research is two-fold, firstly, for bulk analysis on geology rock and broch stone to understand their mineral constituents and to highlight any apparent differences between them. Secondly, due to the coastal location of each study site, salt extraction was undertaken for XRD analysis. From the results obtained, a decision was then made on whether a CEF experiment was appropriate, exposing samples to a salt spray solution, alongside climate change temperature, humidity, and precipitation parameters.

3.3.1 Clachtoll

3.3.1.1 Clachtoll Control

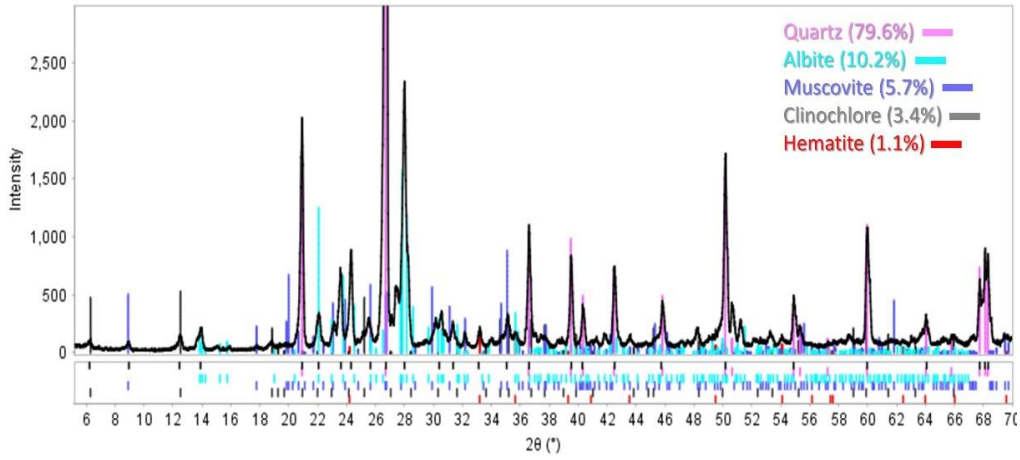

Figure 3.1 - XRD Bulk analysis of CC1, control material taken from the background geology close to Clachtoll Broch

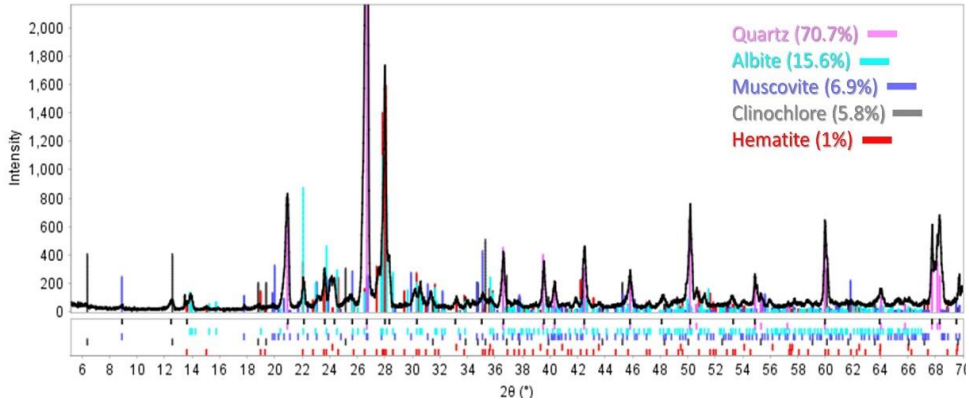

Figure 3.2 - XRD Bulk analysis of CC2, control material taken from the background geology close to Clachtoll Broch

XRD results from the analysis of two background geology samples of Torridonian Sandstone are shown above (Figure 3.1 and Figure 3.2). The primary mineral constituents are quartz, plagioclase feldspar (albite) and mica (muscovite $KAl_2(AlSi_3O_{10})(F,OH)_2$), with a trace amount of clinochlore ($Mg_5Al(AlSi_3O_{10})(OH)_8$) and hematite ($Fe_2O_3$) detected.

3.3.1.2 Clachtoll Broch

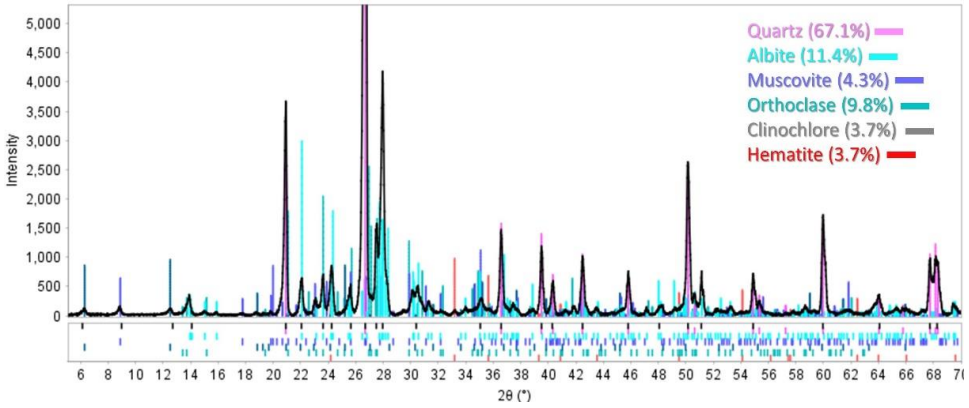

Figure 3.3 - XRD Bulk analysis of CB1, material from Clachtoll Broch archaeological spoil

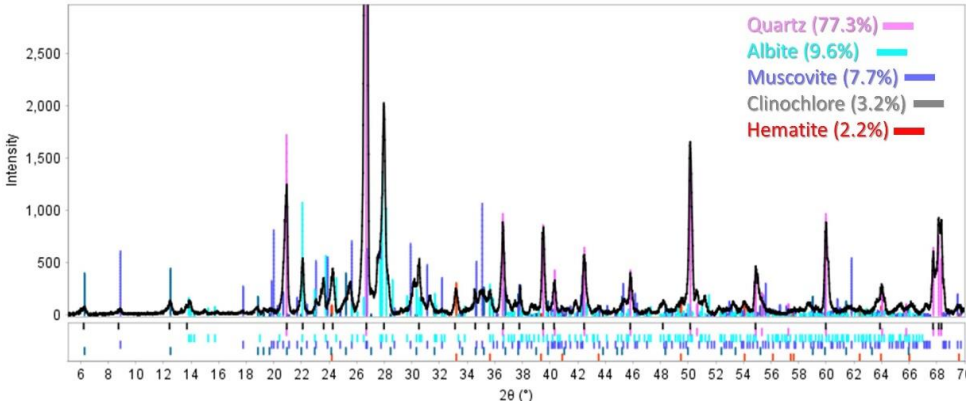

Figure 3.4 - XRD Bulk analysis of CB2, material from Clachtoll Broch archaeological spoil

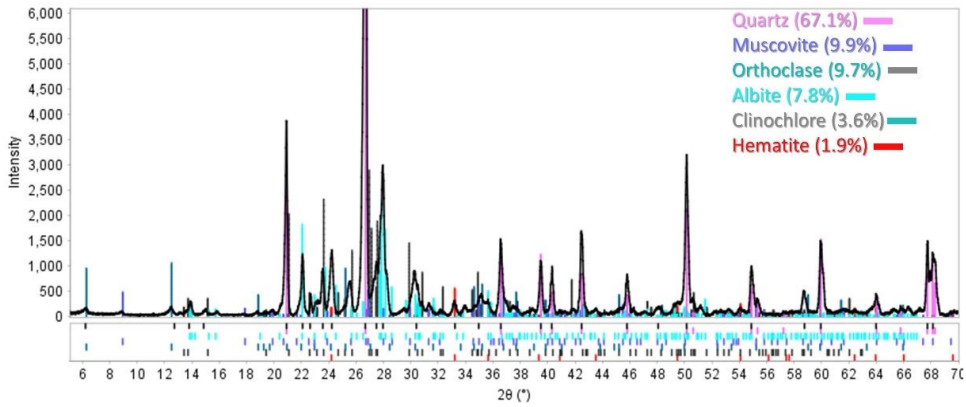

Figure 3.5 - XRD Bulk analysis of CB3, material from Clachtoll Broch archaeological spoil

Figure 3.3 - Figure 3.5 shows XRD results from the analysis of three stone samples once part of Clachtoll Broch. Each stone exhibits similar mineral characteristics to the control rock, dominated by quartz, alkali, and plagioclase feldspars as well as mica and traces of clinochlore and hematite.

3.3.1.3 XRD Bulk Analysis Clachtoll: Discussion

XRD results obtained in this study are concordant with past findings relating to Torridonian Sandstone (Selley, 1966; Rainbird, 2001). The sandstone units are clearly defined by inclusions derived from underlying Lewisian Gneiss, which contributes greatly to the physical characteristics of the sandstone, in particular the large feldspar content, meaning that much of the Torridonian can be defined as arkosic. Minimal cementing agents are identified, indicating that the successions are grain supported, explored further, and visualised through petrographic thin section and SEM-EDX analysis (Sections 3.4 Petrographic Thin Section Analysis and 3.6 , respectively). Supporting this observation, Selley, (1966) highlight the presence of quartz alongside trace amounts of chlorite, carbonate and iron oxides as cementing agents. It is likely, therefore, that although compact quartz and feldspar dominate the cementing of the Torridonian Sandstone, chlorites such as clinochlore and iron oxides such as hematite, expressed in XRD results above, act as minor cementing agents.

Muscovite comprises the main mica component of the stone, it is anticipated that trace amounts of biotite may be observed under thin section as it is a major constituent of gneiss (Coleman *et al.*, 1963; Abollino *et al.*, 2008).

Albite and orthoclase are identified, these are plagioclase and alkali feldspars, respectively. Plagioclase feldspars exist as a group of feldspars ranging from albite ($NaAlSi_3O_8$) to anorthite $Ca(Al_2Si_2O_8)$, with intermediates of oligoclase, andesine, labradorite and bytownite,

while alkaline feldspars exist as a group of feldspars, ranging from albite ($NaAlSi_3O_8$) to orthoclase and microcline ($KAISi_3O_8$) with intermediates of anorthoclase and sanidine. Orthoclase typically forms through the crystallisation of magma into primarily igneous rocks such as granite.

The aforementioned feldspars are key rock-forming minerals found commonly in metamorphic rocks, such as Lewisian Gneiss. Through the weathering of Lewisian Gneiss and resultant mobilisation of these minerals into stream and lake systems, they have become incorporated in sedimentary facies, including the Torridonian Sandstone observed at Clachtoll.

3.3.2 Borwick

3.3.2.1 Borwick Control

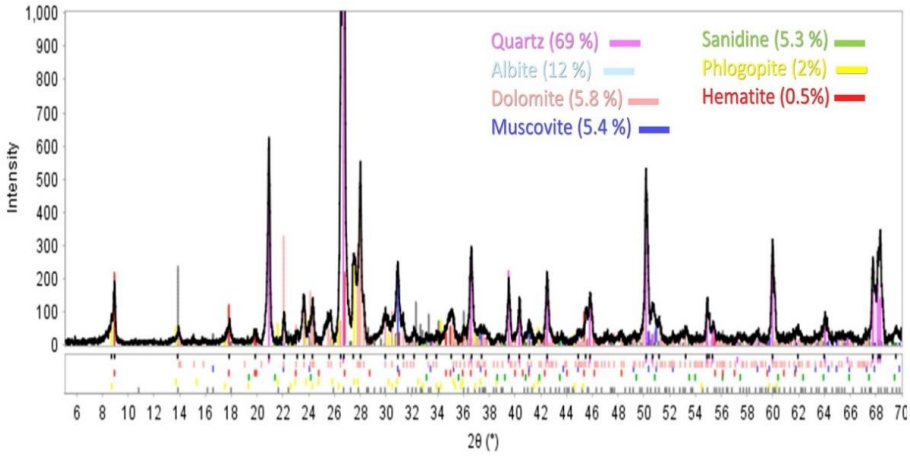

Figure 3.6 - XRD Bulk analysis of BC1, control material taken from the background geology close to Borwick Broch

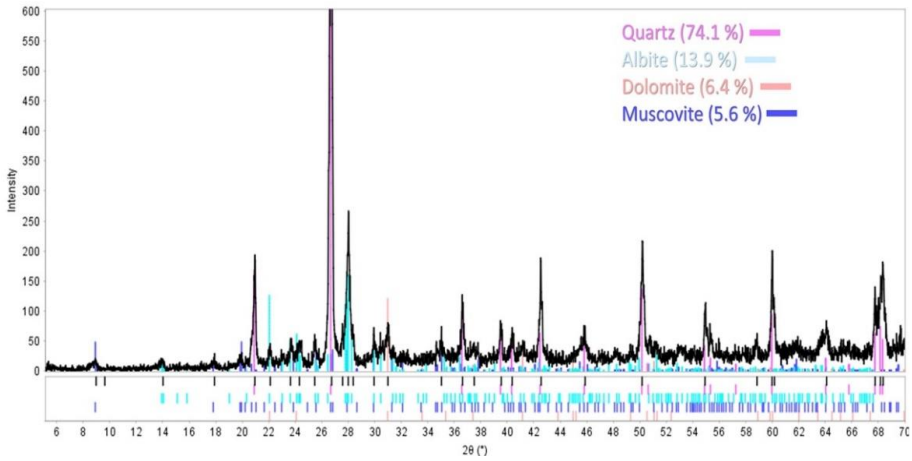

Figure 3.7 - XRD Bulk analysis of BC2, control material taken from the background geology close to Borwick Broch

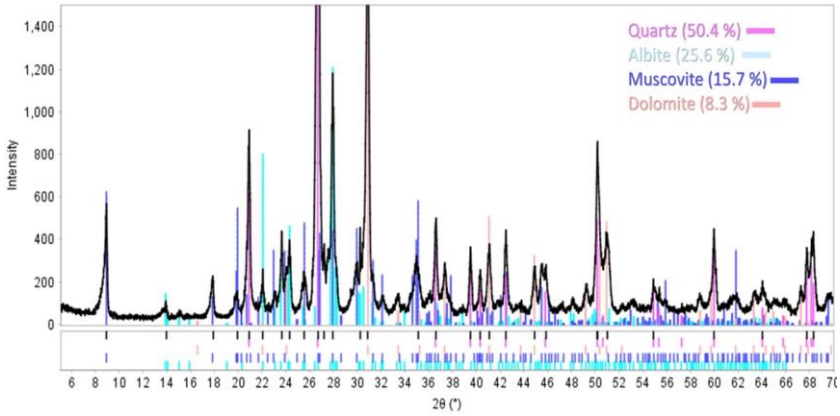

Figure 3.8 - XRD Bulk analysis of BC3, control material taken from the background geology close to Borwick Broch

XRD results from the analysis of background geology samples of Stromness Flagstone (Figure 3.8) shows that the primary constituents of the sandstone are quartz, albite, muscovite, and dolomite ($CaMg(CO_3)_2$).

3.3.2.2 Borwick Broch

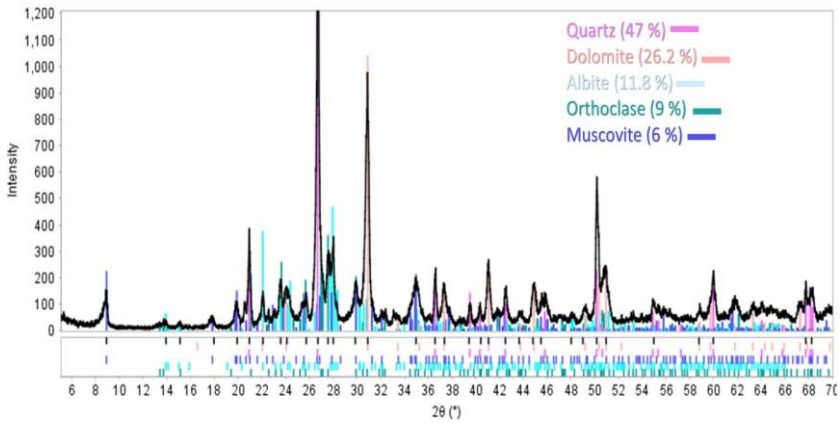

Figure 3.9 - XRD Bulk analysis of BB1, material from Borwick Broch archaeological spoil

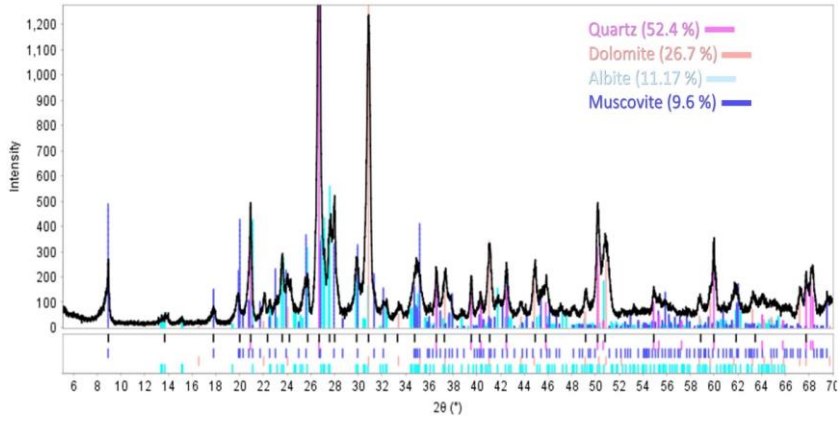

Figure 3.10 - XRD Bulk analysis of BB2, material from Borwick Broch archaeological spoil

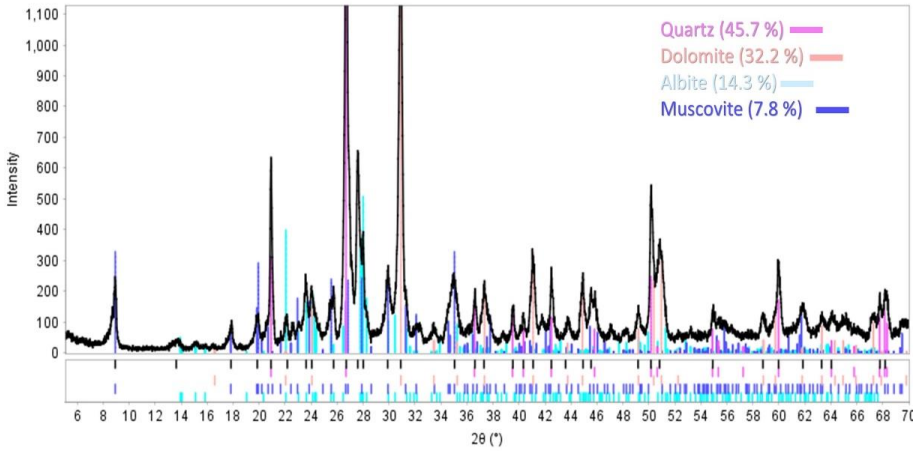

Figure 3.11 - XRD Bulk analysis of BB3, material from Borwick Broch archaeological spoil

Similarly, XRD results from the analysis of three stone samples once part of Borwick Broch (Figure 3.9 - Figure 3.11) show too that the sandstone type is dominated by quartz, feldspar, muscovite, and dolomite. Traces of phlogopite ($KMg_3(AlSi_3O_{10})(F,OH)_2$) and hematite are seen exclusively in BB1.

3.3.2.3 XRD Bulk Analysis Borwick: Discussion

XRD results presented above show that the Stromness Flagstone is a quartz dominated sandstone with feldspathic and mica inclusions, cemented by dolomite. This corresponds to the site's geological past described in Chapter 2 (Section 2.2.2 Old Red Sandstone of Orkney). The constituents of the sandstone are entirely derived from a lacustrine environment and mineral characteristics, therefore, are determined by the nature of sediment influx into the lake system from sources including the weathering of rock types that surrounded Lake Orcadie.

Quartz, as anticipated, is the dominant mineral present, as seen in any sandstone, due to its durability and resistance to weathering. The abundant presence of dolomite indicates that the Stromness Flagstone at Borwick is cement supported. Dolomite is a complex mineral that can occur in sandstones as a primary precipitate in the case of Stromness Flagstone or as a diagenetic replacement. Relevant to the Stromness Flagstones, dolomite forms in lacustrine environments, where there is a plentiful supply of magnesium, as well as suitable pore space within the sediment, where calcite is modified by magnesium to form dolomite. Dolomite evolution at depth is characterised by the repeated dissolution of early, weaker crystals that facilitate the re-precipitation of more stable crystals. Dolomite, therefore, changes

significantly over time at depth, influencing sandstone porosity and permeability as well as generating new crystals within the material (Warren, 2000).

Like the Torridonian Sandstone, albite is prevalent, as is sanidine, an alkali feldspar similar to orthoclase. Sanidine forms at higher temperatures than the other alkali feldspars and is commonly found in felsic volcanic rocks. As indicated above, the weathering of these rocks allows their constituent minerals to become incorporated within sedimentary facies.

3.3.3 XRD Bulk Analysis: Conclusion

XRD bulk analysis has generally characterised each sandstone type, with understandings gained into the dominant mineral constituents and how they became incorporated within each sandstone type. Other trace minerals are likely present in each stone type, which have gone undetected through a bulk analysis, such as differing feldspars, clays and, especially in the case of Torridonian Sandstone, other minerals derived from Lewisian Gneiss. The bulk analysis has, however, provided general insight into the mineralogy of the samples, which is enhanced through subsequent petrographic thin section and SEM-EDX observations.

3.3.4 XRD Analysis for Salts

3.3.4.1 Clachtoll Broch

Table 3.2 - Salt content (%) extracted from Clachtoll Broch stone samples

Sample Number	Sample Weight (g)	Salt Weight (g)	Salt Content (%)
CB1	4.2928	0.0056	0.13
CB2A	6.0644	0.0083	0.13
CB2B	5.1305	0.008	0.15
CB3	6.1821	0.0075	0.12

Two samples were taken from CB2, labelled as CB2A and CB2B. It can be seen from Table 3.2 that only 0.12-0.15% of the ~4.2-6.2g of crushed stone is made up of salt, with the highest quantity seen in CB2B. As described in Chapter 2 (Section 2.4.5.3 Simulating Salt Spray), salt samples were combined for the XRD analysis.

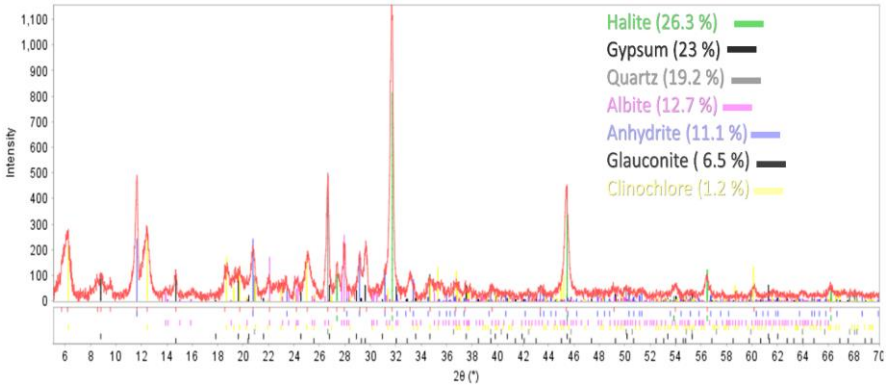

Figure 3.12 - XRD analysis result from salt extracted from Clachtoll Broch stone samples

Figure 3.12 highlights that the salts present are gypsum ($CaSO_4 \cdot 2H_2O$), halite and anhydrite ($CaSO_4$), accounting for 60.4% of the salt extracted, with the rest made up of trace, non-salt minerals, including quartz, albite, glauconite ($(K,Na)(Fe^{3+},Al,Mg)_2(Si,Al)_4O_{10}(OH)_2$) and clinochlore.

3.3.4.2 Borwick Broch

The same procedure was undertaken for Borwick samples, in that two samples were taken from BB2, labelled as BB2A and BB2B.

Table 3.3 - Salt content (%) extracted from Borwick Broch stone samples

Sample Number	Sample Weight (g)	Salt Weight (g)	Salt Content (%)
BB1	4.9395	0.0195	0.39
BB2A	5.6827	0.0059	0.10
BB2B	5.4215	0.0062	0.11
BB3	4.9647	0.0055	0.11

From Table 3.3, of the ~4.9-5.7g of crushed stone, BB1 had the highest salt content; BB2A, BB2B and BB3 had considerably less. Salt samples were combined for the XRD analysis.

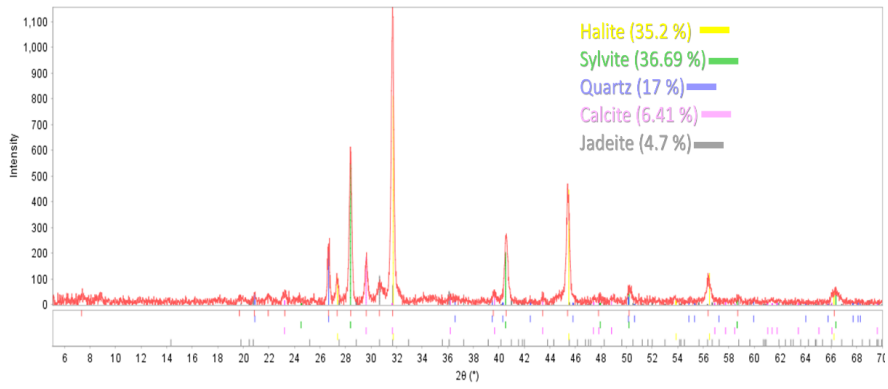

Figure 3.13 - XRD analysis result from salt extracted from Borwick Broch stone samples

The salts present in the analysed sample (Figure 3.13) are halite and sylvite (KCl) which account for 71.89% of the salt extracted, with the rest made up of trace, non-salt minerals.

3.3.4.3 XRD Analysis for Salts: Discussion

The hypothesis that salt plays a prevalent role in the weathering process at study sites used in this thesis has been disproved, to an extent, by the XRD results presented above. Trace amounts of salt were extracted from the culturally significant stone, inferring that salt is not held within the first few mm of the stone's surface to any considerable degree. It must be noted that a possible reason for this observation is simply a result of sampling, whereby the material obtained from spoil heaps in line with SMC guidelines, may not have been exposed to the coast as extensively as other building stones in the broch. The location of a building stone within a structure plays a crucial role in controlling the microclimate and weathering agents that the block is exposed to, highlighted in Chapter 1 (Fitzner *et al.*, 2003; Viles, 2005).

Relating to the physical structure of the sandstone, pore space (Table 3.1) is extremely low in both of the focus sandstones. The densely packed fabric of the samples is apparent through hand specimen inspection and thin section analysis. Salt cannot persist in the samples or penetrate to any sort of depth, impeding its weathering effect.

Given the low values detected, it is likely that the role of salt in the weathering of stone at Clachtoll and Borwick is minor. Furthermore, this thesis is principally concerned with the impacts of climate change on the weathering of sandstone, and as climate change and salt weathering are not intrinsically linked, the salt aspect of this research is not pursued in CEF experiments.

This has, nevertheless, been a useful experiment, aiding in the characterisation of the stone types. As a result of this analysis, it can be argued that although the broch sites are coastal, salt weathering is not playing a dominant role in the degradation of the stone analysed, due to the physical structure of the stone. It is noteworthy, as highlighted in Chapters 1 and 2, that hypotheses have developed suggesting that climate change could intensify the role of salt in stone weathering, whereby crystallisation will be less frequent due to wetter conditions, but more severe when it does occur (Smith *et al.*, 2011; McCabe *et al.*, 2013). Additionally, with sea-level rise brought about by climate change, coastal sites of historic significance will suffer from greater exposure to seawater and inherent salt spray. Furthermore, increased

prevalence and intensity of storms would likely increase the level of saltwater interacting with the broch stone (Historic Environment Scotland, 2017a).

The role of salt weathering could become a more significant weathering vector at the sites in the coming years; however, based on the XRD results above, there is no robust scientific backing to suggest salt weathering should be simulated in this thesis. Focus instead is placed on predicted temperature, humidity and precipitation fluctuations which are crucial in the weathering of sandstone at both study sites.

3.3.5 XRD Conclusion

The principal rationale behind XRD work was to identify the key mineral components of each sandstone type and give an understanding of the presence of salts in the material to inform experimental work.

The technique has proved insightful in highlighting that the bulk of minerals found in the Torridonian Sandstone are derived from the underlying Lewisian Gneiss. Quartz and feldspar particularly dominate the arkose sandstone, with mica and other minor inclusions identified. Stromness Flagstone samples are quartz, feldspar and mica dominated, cemented with dolomite.

This analysis technique provides limited insight into potential weathering patterns which can only be inferred from the presence/absence of peaks and interpretation of counts per second for given minerals. Therefore, this technique's prime benefits lie in producing a robust baseline of the minerals expected to be seen, and in what abundance within each sample. With the added application of petrographic thin section and SEM-EDX analysis, the presence of weathering indicators are more clearly quantified.

Finally, analysis for salts through XRD highlighted that salts occur to a very limited extent in the stones analysed and will not increase weathering at each site to the degree hypothesise, therefore, a salt spray related CEF experiment has not been pursued.

3.4 Petrographic Thin Section Analysis

In the following section, all 'C' (Figure 2.8) sub-samples associated with larger sample blocks have been analysed to determine their baseline characteristics. For each, completed petrographic analysis tables are provided, which focus on rock/stone fabric, grain size, grain contacts and cementing agents, mineralogy, porosity, and permeability. Alongside this, estimates of each sample's percentage composition are provided. These were determined

using visual percentage composition guides provided in Bullock *et al.*, 1985. Additionally, petrographic thin section scans and associated photomicrograph displaying key sample features are provided before a discussion section, specific to each sandstone type and exposure history.

3.4.1 Clachtoll

3.4.1.1 Clachtoll Control

Table 3.4 - Petrographic thin section analysis of Clachtoll control sample CC1

Site	Clachtoll, NW Highlands, Scotland
Sample Number	**CC1 (Clachtoll Control 1)**
Sample Location	**Clachtoll Bay NC 03667 27846**
Rock Fabric	Tightly compacted quartz grains bind the stone constituents together. There is a distinct clay layer, likely detrital, acting as a boundary between the fine-grained surface of the rock, and the coarse fabric of the majority of the sample.
Grain Size	Fine-grained at the surface of the sample, with a very fine clay layer. The remainder of the sample is predominantly highly compacted coarse-grained material. Medium grain sorting with sub-angular clasts throughout.
Grain Contacts and Cement	Grain supported rock, with some opaque grain coatings. Grain contacts are primarily long and tangential with a lesser occurrence of sutured and concave/convex contacts. Crushed quartz cement, with iron oxide cement at depth. Opaque minerals are present throughout.
Mineralogy	Quartz dominated, high feldspar content (arkose sandstone), primarily plagioclase and microcline with orthoclase present to a lesser extent. Traces of mica and monozyte throughout. Lithic fragments derived from Lewisian Gneiss are also present.
Porosity and Permeability	Extremely low to zero, with no sign of micro cracks. There are a few grain shaped holes in the thin section.

Table 3.5 - Percentage components Clachtoll control sample CC1

Components	Total (%)
Quartz	65
Feldspar	20
Lithic Fragment	5
Mica	3
Detrital Clay	2
Authigenic Clay	0
Carbonate	0
Opaque Minerals	5
Total	**100**

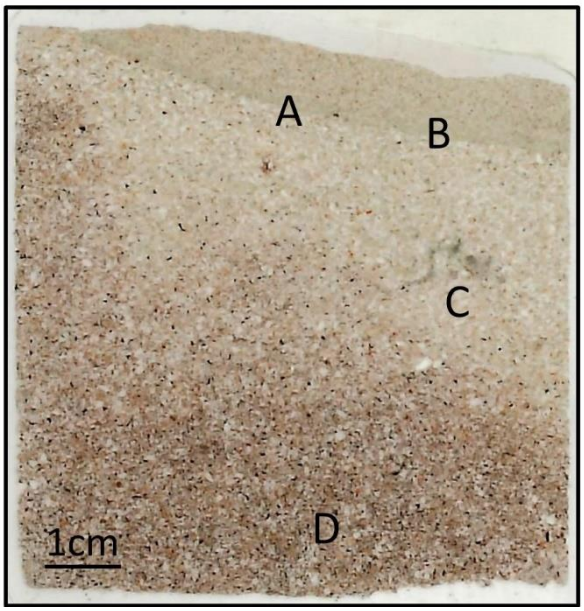

Figure 3.14 - Petrographic thin section scan of CC1, Clachtoll Control rock

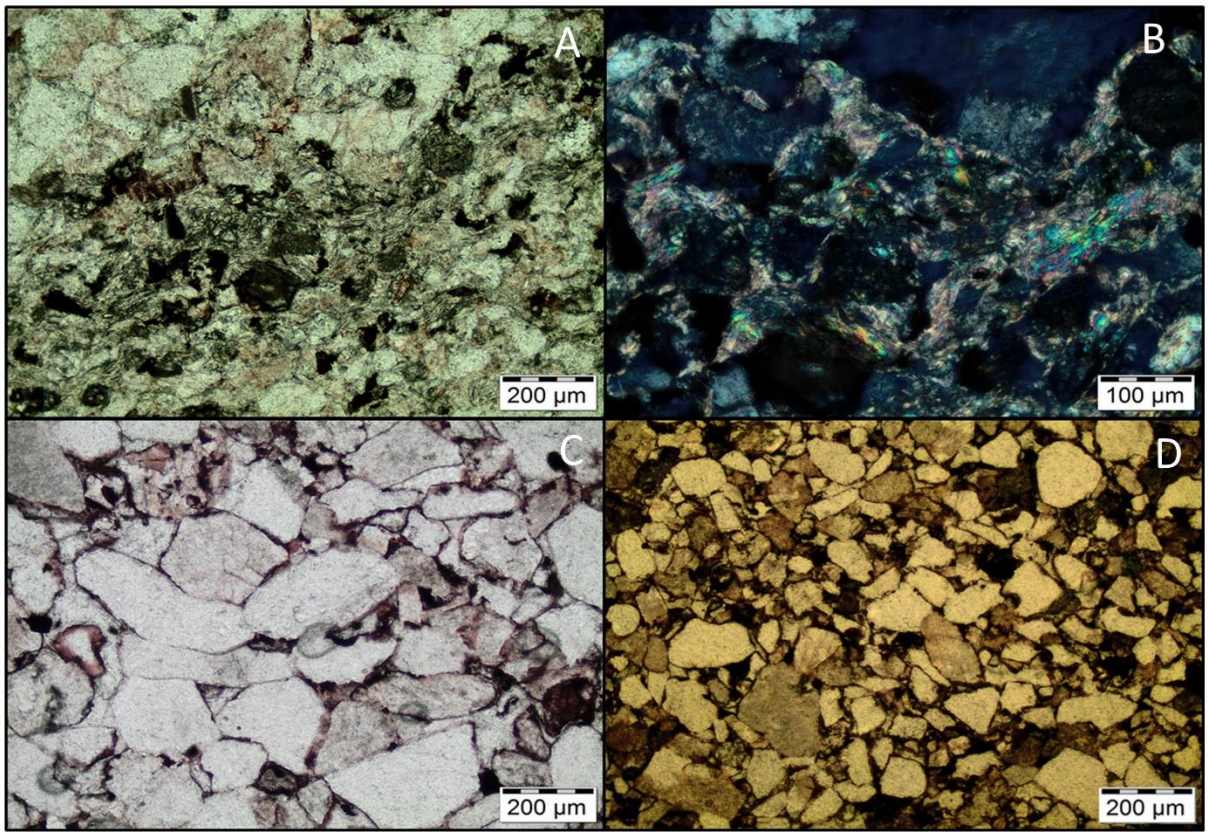

Figure 3.15 - Three distinct bands can be seen at the stone surface (A)(PPL), the uppermost layer is composed of fine-grained quartz, feldspar, and mica, in the middle, there is a very fine detrital clay layer (B)(XPL) before the sample becomes coarser and more grain supported (C)(PPL). Opaque minerals and grain coatings increase with depth (D)(PPL)

Table 3.6 - Petrographic thin section analysis of Clachtoll control sample CC2

Site	Clachtoll, NW Highlands, Scotland
Sample Number	**CC2 (Clachtoll Control 2)**
Sample Location	**Clachtoll Bay NC 03667 27846**
Rock Fabric	Similar in characteristics to CC1. There is a distinct, likely detrital clay layer acting as a boundary between the fine-grained surface of the rock, and the coarse material that dominates the rest of the sample.
Grain Size	Fine-grained at the rock surface, with a very fine detrital clay layer. Increasingly larger grain size with progression through the rock. Medium grain sorting with sub-angular clasts throughout.
Grain Contacts and Cement	Grain supported rock with a mixture of grain contacts, predominantly tangential and long with some examples of sutured as well as concave/convex contacts. Crushed quartz cement, opaque mineral coatings become more observable with progression through the rock.
Mineralogy	Quartz and feldspar dominate the rock constituents. Plagioclase is the most occurring feldspar type. Lithic fragments are scattered throughout the sample, so too is mica. Trace monozyte also present.
Porosity and Permeability	Extremely low to zero, no sign of cracks. There are a few grain shaped holes in the thin section.

Table 3.7 - Percentage components Clachtoll control sample CC2

Components	Total (%)
Quartz	65
Feldspar	20
Lithic Fragment	5
Mica	3
Detrital Clay	2
Authigenic Clay	0
Carbonate	0
Opaque Minerals	5
Total	**100**

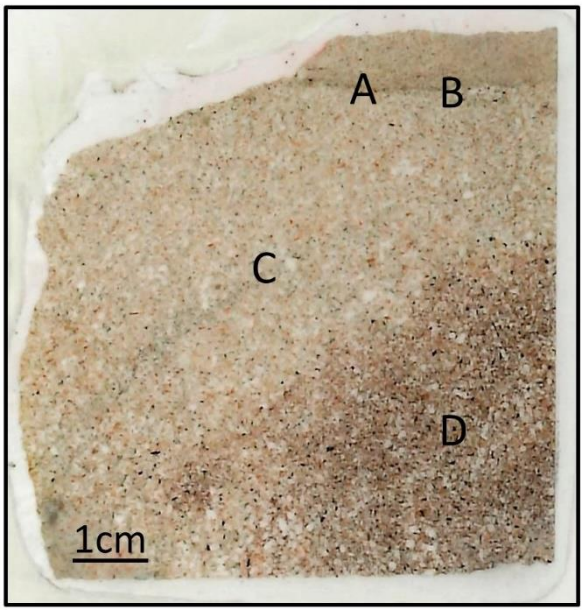

Figure 3.16 - Petrographic thin section scan of CC2, Clachtoll Control rock

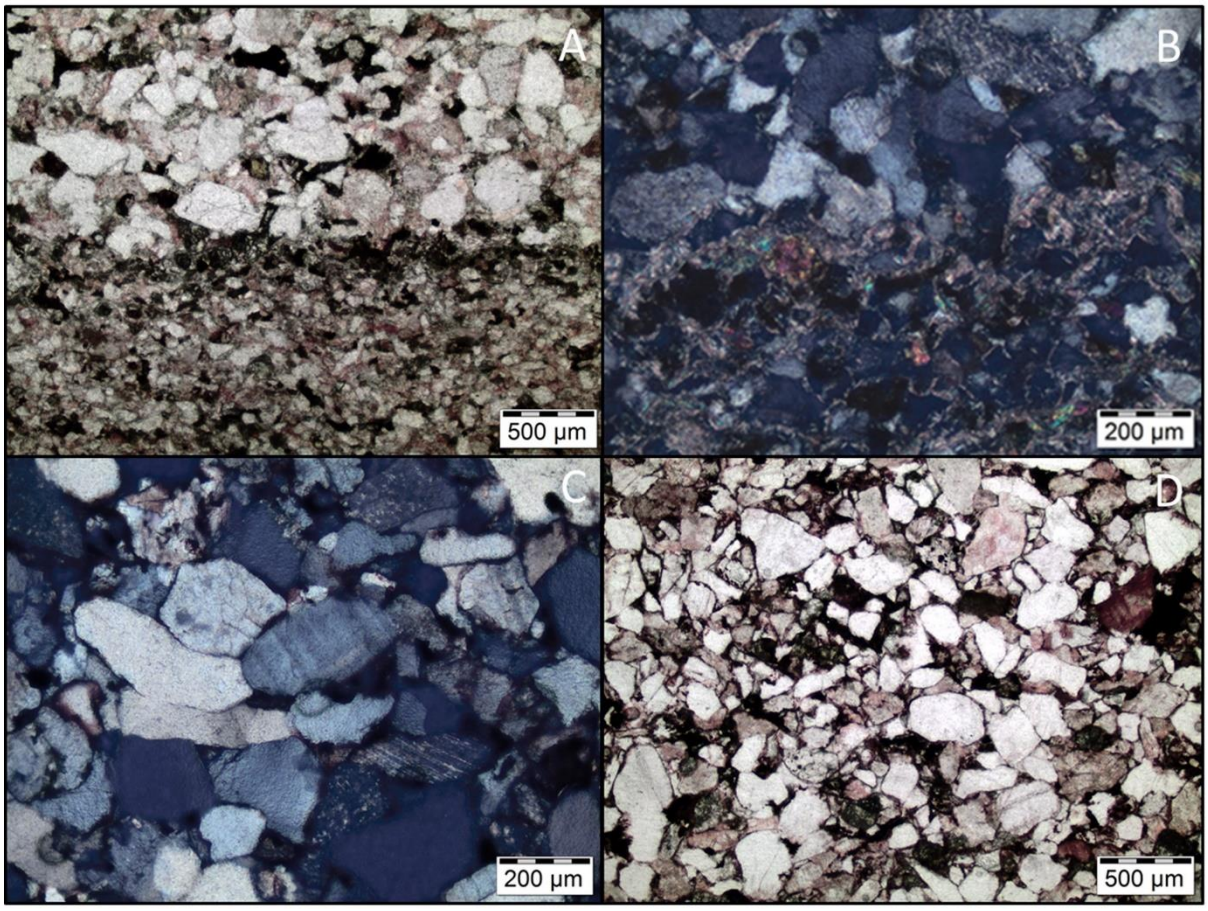

Figure 3.17 - Similar to CC1, there are three distinct bands of material, from fine-grained material at the surface, to detrital clay, to coarse material with depth (A)(PPL), (B)(XPL) and (C)(XPL). Opaque minerals and grain coatings increase with depth (D)(PPL)

Table 3.8 - Petrographic thin section analysis of Clachtoll control sample CC3

Site	Clachtoll, NW Highlands, Scotland
Sample Number	**CC3 (Clachtoll Control 3)**
Sample Location	**Clachtoll Bay NC 03667 27846**
Rock Fabric	This is a well compacted, grain supported rock. The sample varies in several ways from CC1 and CC2. No evidence of a clay layer. There is a distinct surface microcrack, running the length of the sample which could lead to material loss. No clay layer evident in the sample.
Grain Size	There are distinct fine-grained and coarse-grained areas within the sample in an unsorted manner. Generally sub-angular clasts.
Grain Contacts and Cement	Primarily tangential grain contacts with examples of sutured as well as concave/convex and long. The rock is cemented by crushed quartz with some opaque grain coating.
Mineralogy	Dominated by quartz, feldspar and opaque minerals with some lithic fragments and a low mica content. Opaque minerals appear concentrated in specific areas rather than spread throughout the sample as seen in CC1 and CC2.
Porosity and Permeability	Low porosity, however, a microcrack runs across the sample.

Table 3.9 - Percentage components Clachtoll control sample CC2

Components	Total (%)
Quartz	70
Feldspar	16
Lithic Fragment	5
Mica	3
Detrital Clay	0
Authigenic Clay	0
Carbonate	0
Opaque Minerals	6
Total	**100**

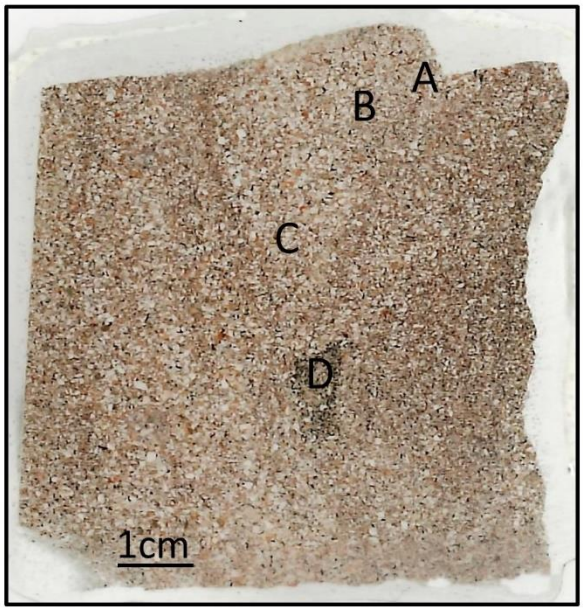

Figure 3.18 - Petrographic thin section scan of CC3, Clachtoll Control rock

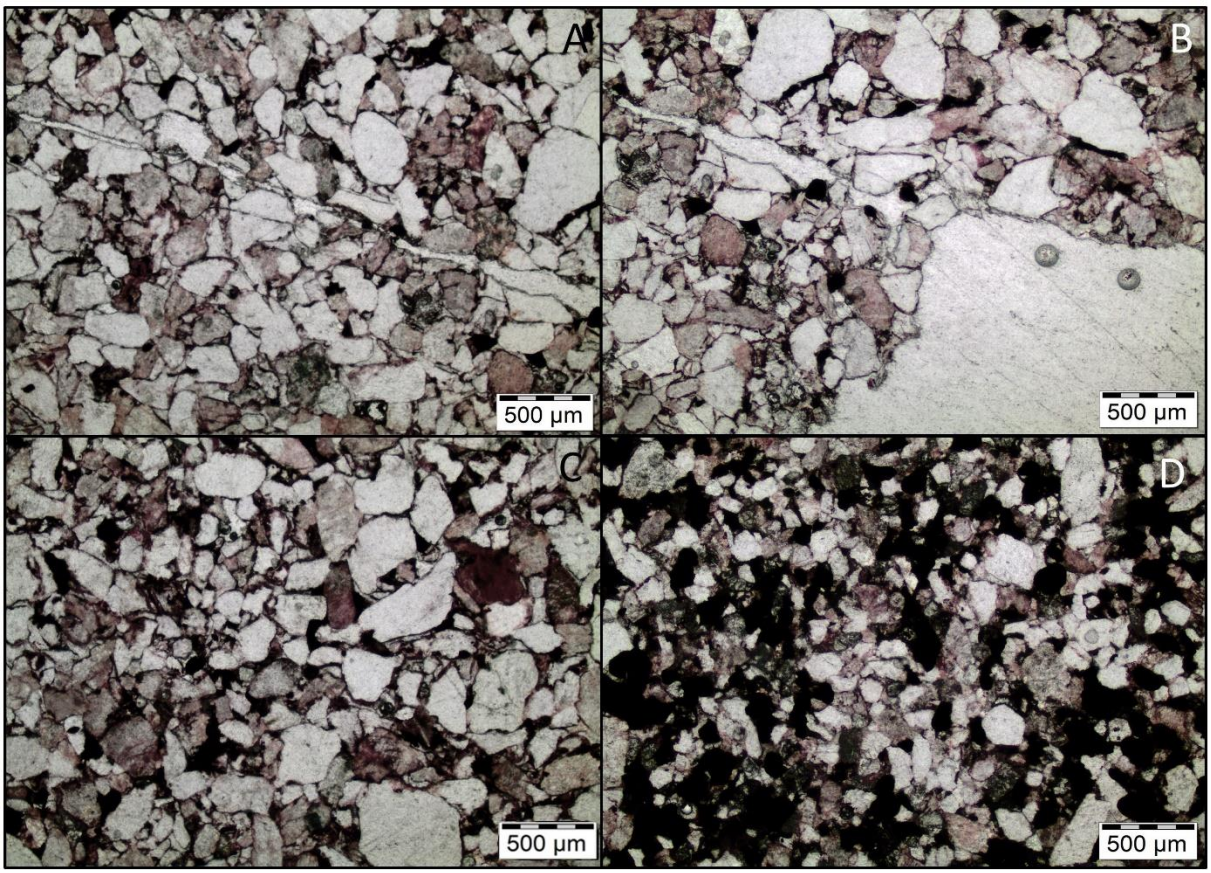

Figure 3.19 - There is a surface microcrack extending the length of the near-surface and extending deep into the rock, fracturing quartz grains (A) and (B). The sample is generally homogenous and robust (C) with a distinct opaque mineral-rich pocket at depth (D) (All PPL)

3.4.1.2 Clachtoll Broch

Table 3.10 - Petrographic thin section analysis of Clachtoll Broch sample CB1

Site	Clachtoll, NW Highlands, Scotland
Sample Number	**CB1 (Clachtoll Broch 1)**
Sample Location	**Clachtoll Broch NC 03667 27846**
Stone Fabric	Highly compacted stone fabric. The most striking feature in this sample is a microcrack running laterally across the middle of the sample and appears to be a crush zone/healed fault, perpendicular to the bedding of the stone.
Grain Size	Above the crack, there are channels of fine grains with opaque coatings and channels of coarse material. Below the crack, the sample is almost entirely coarse-grained. In the lower half the grains are coarser and generally sub-angular/rounded in appearance. Poor to moderate sorting throughout.
Grain Contacts and Cement	Long quartz grain contacts dominate, very compacted grains with some sutured and concave/convex contacts. Cemented predominantly by crushed quartz and to a lesser extent by opaque minerals.
Mineralogy	Quartz and feldspar dominate with lithic fragments and mica scattered throughout. Opaque minerals are abundant in fine grained areas and below the microcrack in the centre of the sample.
Porosity and Permeability	Very minimal porosity, some microcracks present close to the crush zone/healed fault running through the sample.

Table 3.11 - Percentage components Clachtoll Broch sample CB1

Components	Total (%)
Quartz	70
Feldspar	15
Lithic Fragment	5
Mica	2
Detrital Clay	0
Authigenic Clay	0
Carbonate	0
Opaque Minerals	8
Total	**100**

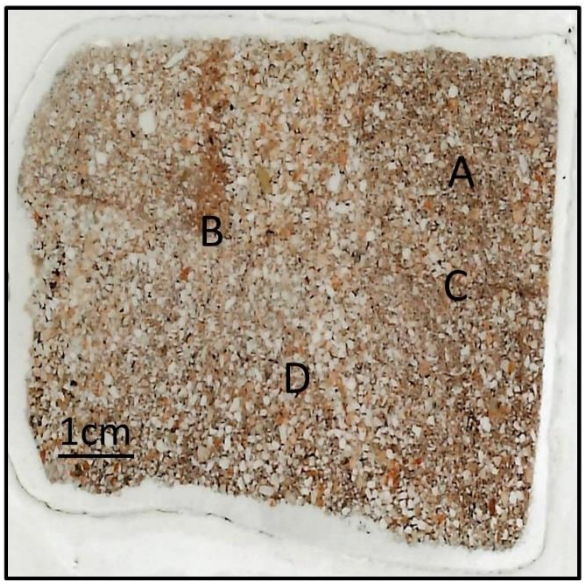

Figure 3.20 - Petrographic thin section scan of CB1, Clachtoll Broch stone

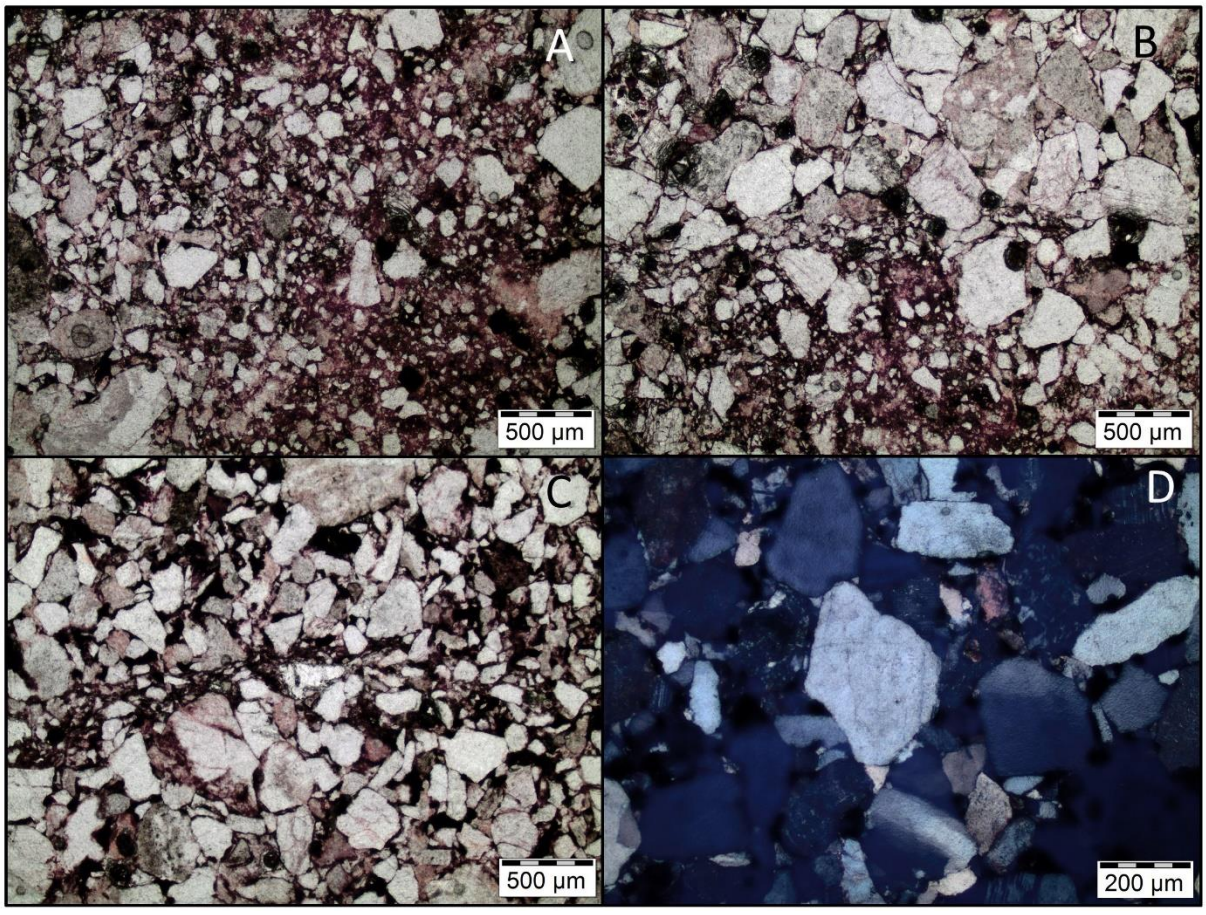

Figure 3.21 - (A)(PPL) Stone surface is characterised by channels of coarse and fine material. (B)(PPL) and (C)(PPL) show a crush zone/healed fault that extends through the middle of the sample at roughly 90°, infilled with fine crushed quartz, beyond the microcrack the sample is coarse-grained and rich in *opaque minerals (D)(XPL)*

Table 3.12 - Petrographic thin section analysis of Clachtoll Broch sample CB1

Site	**Clachtoll, NW Highlands, Scotland**
Sample Number	**CB2 (Clachtoll Broch 2)**
Sample Location	**Clachtoll Broch NC 03667 27846**
Stone Fabric	Extremely homogenous sample, contrary to CB1. The stone appears robust and compact with no weaknesses present.
Grain Size	Fine-grained throughout with some coarse outliers located in the middle of the sample. Generally well sorted with sub angular clasts.
Grain Contacts and Cement	Predominantly tangential and long. Crushed quartz cement with a low amount of opaque grain coating.
Mineralogy	Dominated by quartz and feldspar, lithic fragments and mica scattered throughout. There is a distinct reduction in opaque minerals compared with CB1.
Porosity and Permeability	Low to zero, no sign of cracks/weaknesses within the stone.

Table 3.13 - Percentage components Clachtoll Broch sample CB2

Components	Total (%)
Quartz	80
Feldspar	15
Lithic Fragment	2
Mica	1
Detrital Clay	0
Authigenic Clay	0
Carbonate	0
Opaque Minerals	2
Total	**100**

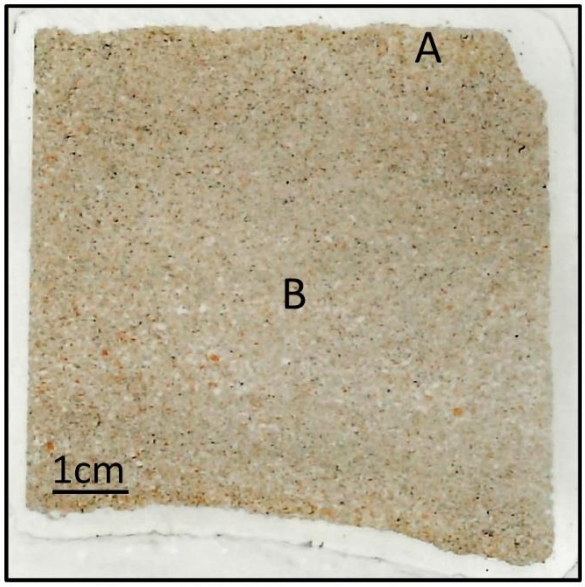

Figure 3.22 - Petrographic thin section scan of CB2, Clachtoll Broch stone

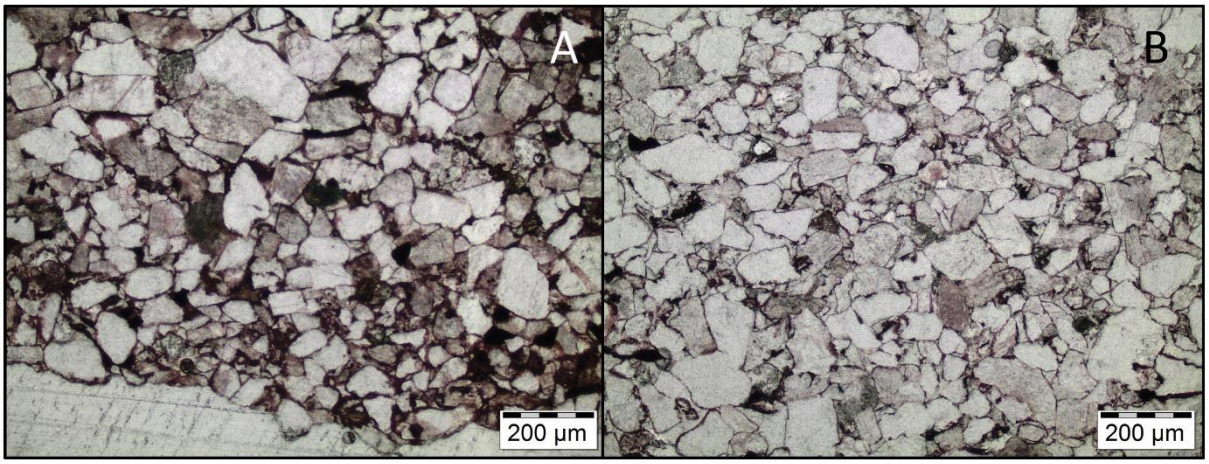

Figure 3.23 - Robust, homogenous stone with a slight weathering front (A) with opaque coatings on individual grains. (B) shows the homogenous, grain supported nature of the stone fabric with no signs of weathering at depth (Both PPL)

Table 3.14 - Petrographic thin section analysis of Clachtoll Broch sample CB3

Site	Clachtoll, NW Highlands, Scotland
Sample Number	**CB3 (Clachtoll Broch 3)**
Sample Location	**Clachtoll Broch NC 03667 27846**
Stone Fabric	Very similar in characteristics to CB2, this sample has a homogenous fabric throughout. There appears to be a very slight weathering front on the exposed surface, characterised by a reddish-orange colour.
Grain Size	Relatively coarse, subangular grains with medium sphericity. Grain size remains constant throughout the sample, indicative of a well-sorted stone.
Grain Contacts and Cement	This is a compact, grain supported stone, with little other cementing influence. Grains are highly compacted. Long and tangential grain contacts are prevalent.
Mineralogy	Dominated by quartz, feldspar and lithic fragments, mica scattered throughout.
Porosity and Permeability	Low to zero, no sign of cracks/weaknesses within the stone.

Table 3.15 - Percentage components Clachtoll Broch sample CB3

Components	Total (%)
Quartz	80
Feldspar	15
Lithic Fragment	2
Mica	1
Detrital Clay	0
Authigenic Clay	0
Carbonate	0
Opaque Minerals	2
Total	**100**

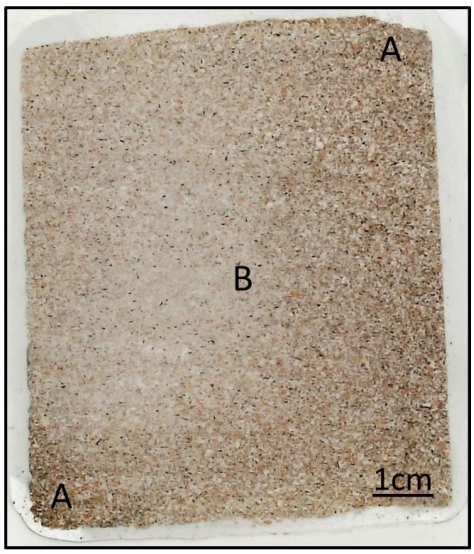

Figure 3.24 - Petrographic thin section scan of CB3, Clachtoll Broch stone

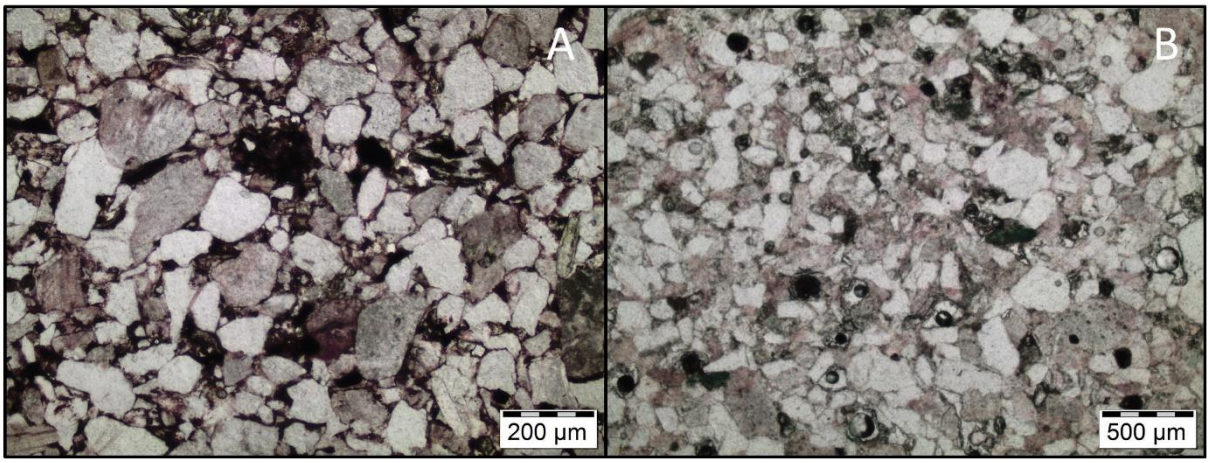

Figure 3.25 - (A) There is a slight weathering front characterised by a reddish colour in the top right and bottom left corner of the sample. With depth, the sample becomes robust and homogenous, similar to CB2 (B) (Both PPL)

3.4.1.3 Clachtoll Discussion

Through petrographic thin section analysis of Clachtoll control rock and broch stone, a visual understanding of the sandstone has been gained. Based on estimated percentage composition, the samples obtained can be seen to range from arkose to subarkose, based on Folk's sandstone classification (Folk, 1980). As anticipated, both sample types are composed of the same mineral suite, albeit with fluctuating abundance, held together by tightly compacted crushed and larger intact quartz grains. Subtle, microscopic fluctuations between the control and broch samples become clear through thin section analysis. Furthermore, natural weaknesses within the rock, stemming from the geological past of the lithology can be

identified and the implications these carry for the longevity of the sandstone can be understood.

The most striking feature within the control samples CC1 and CC2 (Figure 3.14 - Figure 3.17) is the transition within the top few millimetres of rock from predominantly fine-grained detrital clay-rich material to a much coarser, blockier structure, punctuated by an opaque clay band. This transition confirms that the Torridonian series of sandstone strata is variable, in that although the material comprising Clachtoll Broch will be of the same lithology throughout, variations within the rock relating to grain size as well as type and abundance of clay, will result in a complex and varied weathering regime within the structure. This variation, coupled with the range of factors influencing the speed and destructiveness of weathering, showcases clearly, the manifold way in which sandstone degrades within a structure in relation to its climatic setting.

The clay layer between the fine and coarse-grained areas of the samples could conceivably be a plane of weakness running the entire width of the near surface of CC1 and CC2 which could lead to surface loss. Under the microscope, the formation of these layers appears natural and likely related to the fluctuating depositional environment associated with sedimentary facies. However, a potential authigenic influence through the breakdown of K-feldspar is explored through SEM-EDX analysis presented in section 3.6 of this chapter. Authigenic clay is complex to identify, forming after deposition and usually manifested within the sandstone as linings, fillings or replacements (Wilson and Pittman, 1977).

Although the samples appear robust with no other signs of deformation or weathering, this potential weakness will have an inherent tipping point where exposure to new climatic conditions or more frequent and intensified storm events could cause the loss of an entire surface. The result of a surface loss is twofold, firstly, there are obvious negative aesthetic implications, however, the loss of this layer along a relatively lateral plane would expose the coarse area of rock beneath the clay which appears more robust and resistant to weathering, potentially consolidating the sandstone. This process is perhaps indicative of a weathering cycle present in some Torridonian building stone, whereby the initial surface once quarried is relatively pristine, containing only minor weakness areas such as a clay layer. Through the exposure of this surface to weathering, diagenesis occurs, and this weakness reaches a tipping point and is lost, exposing a deeper section of the rock that is, as the original stone was, relatively pristine and more resistant to weathering than the surface that has been lost.

Epitomising the complexity of weathering, it may be the case that the loss of a surface layer could increase surface roughness, which, as discussed in Chapter 1, can exacerbate future weathering.

CC3 (Figure 3.18 and Figure 3.19) varies from the other control samples discussed above in that it is coarser and blockier in structure with no pronounced deviations in grain size. However, of significance is a surface microcrack a few millimetres from the immediate surface. This microcrack appears similar to the clay band seen in CC1 and CC2, albeit without the clay material present. This helps to affirm the idea that Torridonian sandstone, although generally robust, is punctuated with distinct, relatively lateral oriented cracks/faults that are recognisable weaknesses within the sandstone. The microcrack present in CC3 has occurred after deposition, confirmed by the quartz grains that have been split either side of the microcrack, which appears to have originated in the top right corner of the sample, which has been lost before sampling. Through changing climate exposures, it is conceivable that this microcrack will deepen, running across the length of the near surface, eventually resulting in the loss of the rock's surface.

Through petrographic thin section analysis of broch samples, no significant deterioration of the stone can be seen that is relatable to its emplacement above the surface in Clachtoll Broch. This indicates that ca. 2000 years of exposure to climatic fluctuations have left the stone largely unscathed. The distinct cracks seen at the surface of the control samples and highlighted as significant planes of weakness are not present at the surfaces of the broch stone. A potential reason for the lack of surface cracks/weaknesses and apparent robustness of the broch sandstone is that over 2000 years as part of a broch structure, the surface layers have failed, exposing the relatively pristine stone beneath. This idea leads on from an aforementioned weathering cycle whereby failure of an inherent surface weakness such as a crack, removes the weaker stone surface and exposes a more pristine, unweathered surface, implying that weathering of this stone is cyclic, although linear in the sense that it is removing 'layers' of the stone. A key theme in this thesis, therefore, is whether through climate change this cycle increases in frequency, resulting in more rapid surface loss and stone degradation.

A weakness is seen towards the middle of CB1, running the width of the sample at an approximate angle of 90°, however, this takes a significantly different appearance to the cracks observed in control samples and is more likely a crush zone or healed fault,

characterised by fine-grained material, particularly crushed quartz, infilling and consolidating the fault.

A distinct feature that the control and broch sandstones have in common is the presence of opaque minerals, seen in the thin section scans and photomicrograph presented above. The impact of these minerals on the weathering of stone is poorly documented, however, Weibel and Friis, (2004) highlight the significance of opaque minerals as vulnerable to environmental change. Through petrographic thin section analysis, the type of opaque mineral is likely an iron oxide such as hematite, however, SEM-EDX work in section 3.6 aids in their identification.

As highlighted, no major alteration of the stone results from its removal from the background geology and subsequent emplacement above the surface. Petrographic thin section analysis shows the Torridonian Sandstone to be extremely robust, with 2000 years as part of a coastal broch structure having had little impact on the stone. Crucially, the baseline analysis presented has proved successful in identifying features in the sandstone that give inherent susceptibility to climate change. These weaknesses appear in the form of cracks/faults within the bedding of the stone, relating to its geological past as well as distinct clay layers. With exposure to increased weathering in a climate changed future, this sandstone could change. Identified weaknesses carry within them an inherent tipping point, which, when reached, will trigger the failure of the stone or sections of the stone, having implications on its longevity. It is the purpose of this research, therefore, to understand if climate change futures can trigger these weaknesses.

3.4.2 Borwick

3.4.2.1 Borwick Control

Table 3.16 - Petrographic thin section analysis of Borwick control sample BC1

Site	Borwick, Orkney
Sample Number	**BC1 (Borwick Control 1)**
Sample Location	**Borwick Geology HY 22421 16647**
Rock Fabric	This is a highly compacted sample. The rock fabric has a distinct lensoid structure with soft-sediment deformation features present and microcracks throughout. The fabric becomes homogenous with depth. There is a slight weathering front at the exposed surface, characterised as a reddish colour.
Grain Size	Extremely fine, separated into fluid bands of silt/clay with very few discernible individual grains to bands of crushed quartz with more easily distinguishable grains. Some outliers including random large quartz grains held in the fine matrix. Within each band, grains are well sorted and rounded where distinguishable.
Grain Contacts and Cement	Few identifiable grains, coarse bands are generally long contacts, indicative of the tightly packed nature of the sample. The sample is cemented with dolomite.
Mineralogy	Quartz dominated, particularly crushed. Flecks of mica are seen throughout, and randomly distributed opaque minerals are present.
Porosity and Permeability	Very low porosity, however, microcracks are present and align with abrupt shifts from extremely fine to more coarse material. Bubbles present at the exposed surface indicate surface secondary porosity.

Table 3.17 - Percentage components Borwick control sample BC1

Components	Total (%)
Quartz	62
Feldspar	2
Lithic Fragment	Trace
Mica	8
Detrital Clay	0
Authigenic Clay	0
Carbonate	25
Opaque Minerals	3
Total	**100**

Figure 3.26 - Petrographic thin section scan of BC1, Borwick Control rock

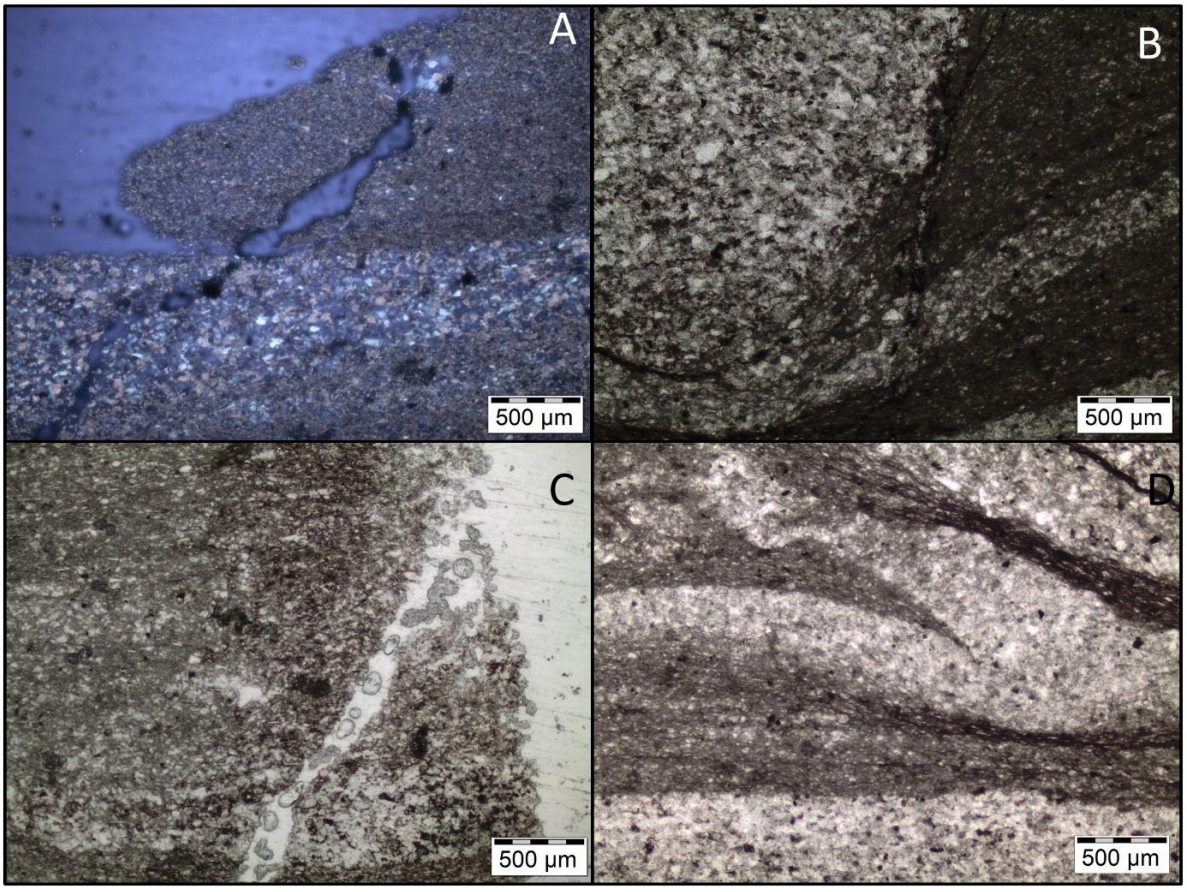

Figure 3.27 - Microcracks are visible at the sample surface (A)(XPL) and the exposed sample edge, running perpendicular to bedding (C)(PPL). Fluid, lensoid structure with evidence of soft-sediment deformation (seen throughout Borwick Control *samples) (B)(PPL) and (D)(PPL)*

Table 3.18 - Petrographic thin section analysis of Borwick control sample BC2

Site	Borwick, Orkney
Sample Number	**BC2 (Borwick Control 2)**
Sample Location	**Borwick Geology HY 22421 16647**
Rock Fabric	Very similar to BC1 in that this is a highly compacted rock. Distinct lensoid structure with soft-sediment deformation features. At depth, the sample becomes homogenous with no distinguishable material bands.
Grain Size	Extremely fine, separated into fluid bands of carbonate/silt with few discernible grains to bands of crushed quartz. Within each band, grains are well sorted and rounded where distinguishable.
Grain Contacts and Cement	Contacts are only visible in coarse sections, typically tightly packed – long and tangential contacts. There is a high dolomite content, indicative of a cement supported rock.
Mineralogy	Quartz dominates with mica and randomly distributed nodules of opaque material throughout.
Porosity and Permeability	Very low porosity, however, there are a few microcracks visible at the rock surface, these diminish with depth.

Table 3.19 - Percentage components Borwick control sample BC2

Components	Total (%)
Quartz	67
Feldspar	2
Lithic Fragment	Trace
Mica	8
Detrital Clay	0
Authigenic Clay	0
Carbonate	20
Opaque Minerals	3
Total	**100**

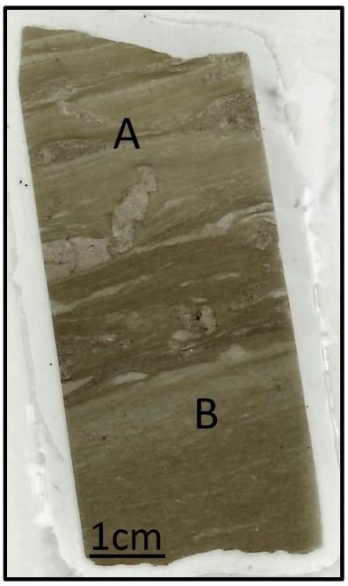

Figure 3.28 - Petrographic thin section scan of BC2, Borwick Control rock

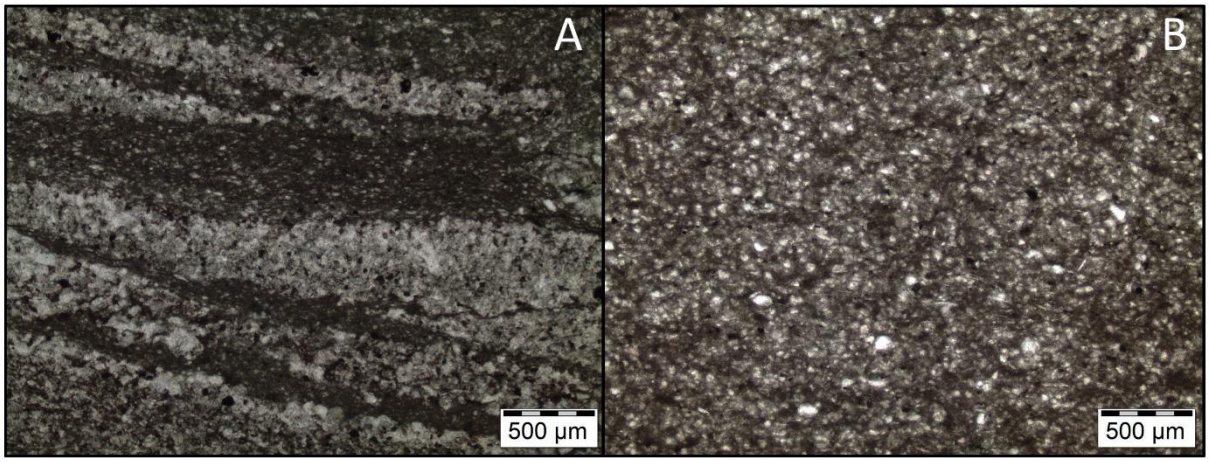

Figure 3.29 - Fluid, lensoid structure with distorted bedding planes indicative of soft-sediment deformation (A). With depth, the sample becomes more homogenous, less banding is present and there is a slight increase in grain size (B) (Both PPL)

Table 3.20 - Petrographic thin section analysis of Borwick control sample BC3

Site	Borwick, Orkney
Sample Number	**BC3 (Borwick Control 3)**
Sample Location	**Borwick Geology HY 22421 16647**
Rock Fabric	Depositional environment is seen most clearly in this sample, evidenced by extremely fine and highly compacted material. There is a lensoid structure throughout with evidence of soft-sediment deformation.
Grain Size	Layered structure throughout with bands of extremely fine material and bands of slightly coarser material. Within each band, grains are well sorted and rounded where distinguishable.
Grain Contacts and Cement	Contacts are only visible in coarse sections, typically tightly packed – long and tangential contacts. Cemented by dolomite.
Mineralogy	Quartz dominates with mica flecks throughout. Few fine opaque minerals are also present. Feldspar content is low, so too are lithic fragment inclusions.
Porosity and Permeability	Very low, however, there are a few microcracks visible at the rock surface.

Table 3.21 - Percentage components Borwick control sample BC3

Components	Total (%)
Quartz	62
Feldspar	2
Lithic Fragment	Trace
Mica	8
Detrital Clay	0
Authigenic Clay	0
Carbonate	25
Opaque Minerals	3
Total	**100**

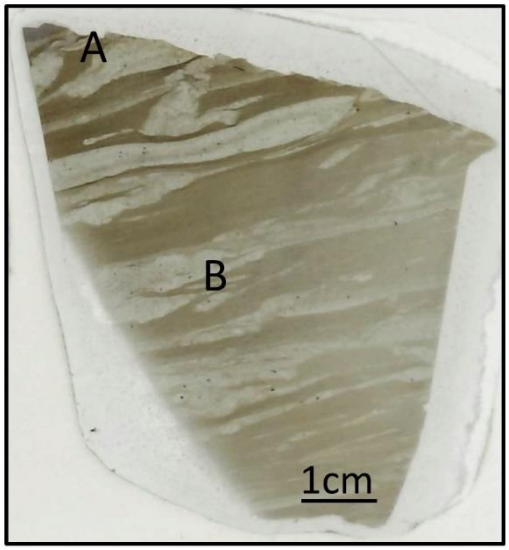

Figure 3.30 - Petrographic thin section scan of BC3, Borwick Control rock

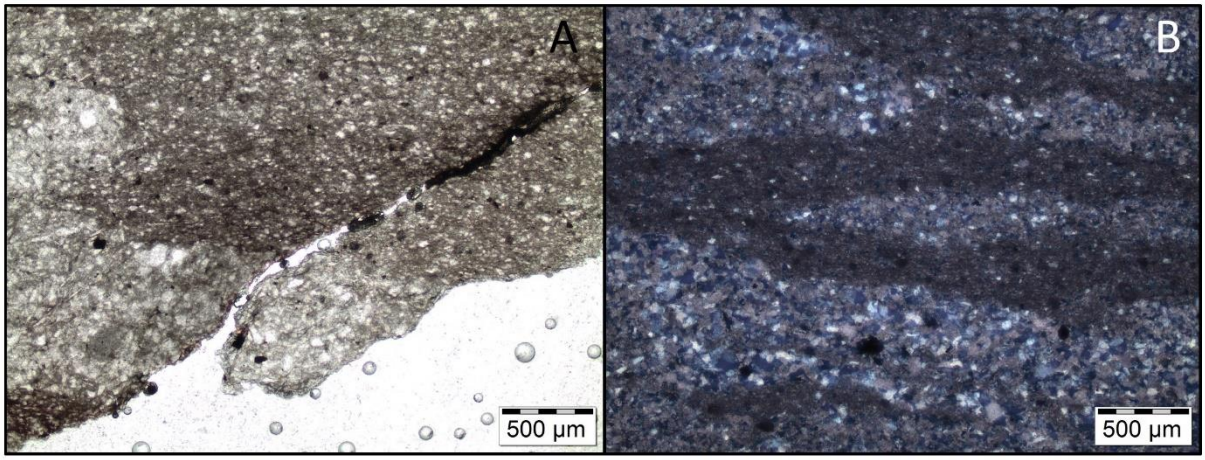

Figure 3.31 - Surface microcrack, perpendicular to bedding (A)(PPL), infilled by opaque material (B)(XPL). This sample is a clear example of the depositional environment of the stone in a fluid low/medium energy environment with evidence of soft-sediment deformation

3.4.2.2 Borwick Broch

Table 3.22 - Petrographic thin section analysis of Borwick Broch sample BB1

Site	Borwick, Orkney
Sample Number	**BB1 (Borwick Broch 1)**
Sample Location	**Borwick Broch HY 22421 16647**
Stone Fabric	Generally homogenous stone fabric, however, the structure differs from the control rock with a distinct absence of layers and soft-sediment deformation features. There are distinct reddish-brown layers towards the surface of the sample, indicative of a weathering front. Several surface microcracks are also present towards. There is an abrupt change from the weathering front to crushed quartz in a dolomite matrix.
Grain Size	Very fine-grained, similar to the non-layered sections of control samples. Homogenous throughout. Grains are well sorted and rounded/crushed in shape.
Grain Contacts and Cement	There are very few observable grain contacts due to the fine nature of the material. Cemented by dolomite.
Mineralogy	Quartz is the dominant mineral, with mica present throughout. Very few discernible feldspars and lithic fragments.
Porosity and Permeability	Surface cracks provide some laminar porosity, potentially resulting in scaling, otherwise, the porosity is very low.

Table 3.23 - Percentage components Borwick Broch sample BB1

Components	Total (%)
Quartz	60
Feldspar	3
Lithic Fragment	Trace
Mica	7
Detrital Clay	0
Authigenic Clay	0
Carbonate	30
Opaque Minerals	Trace
Total	**100**

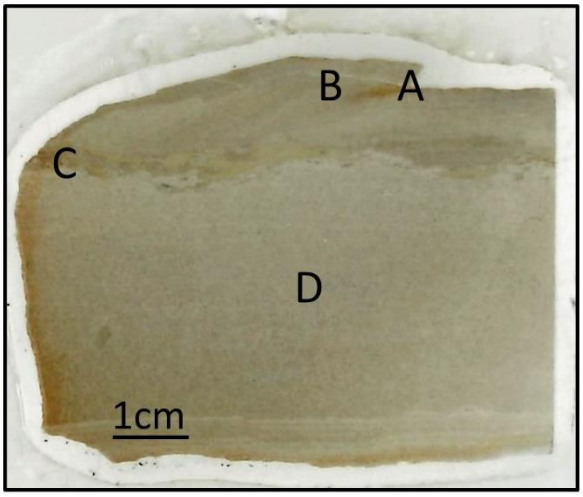

Figure 3.32 - Petrographic thin section scan of BB1, Borwick Broch stone

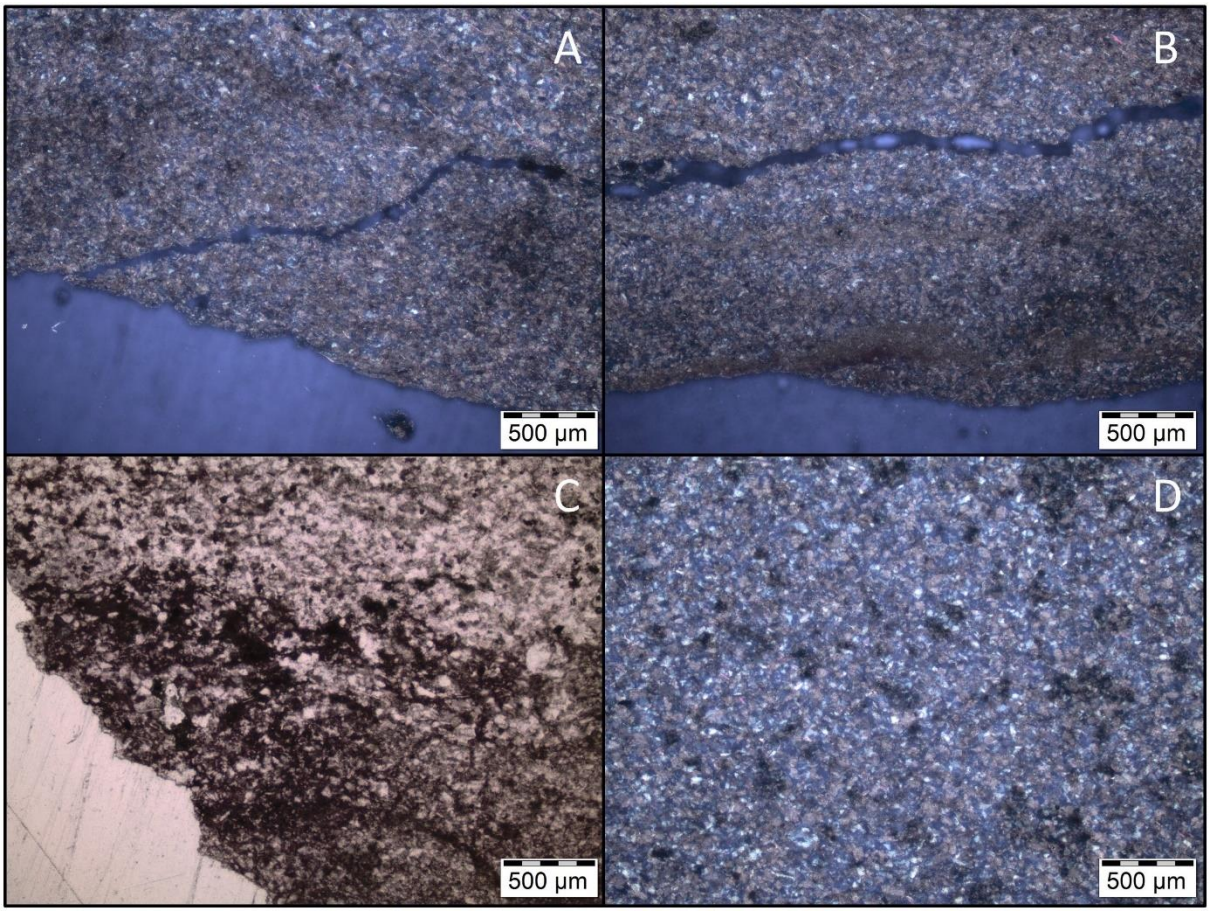

Figure 3.33 - There is a distinct microcrack within the weathered surface, running the length of the near-surface (A)(XPL) and (B)(XPL). There appears to be a secondary weathered layer at a depth of around 1cm (C)(PPL). The remainder of the sample is homogenous with no signs of weathering (D)(XPL)

Table 3.24 - Petrographic thin section analysis of Borwick Broch sample BB2

Site	**Borwick, Orkney**
Sample Number	**BB2 (Borwick Broch 2)**
Sample Location	**Borwick Broch, Orkney HY 22421 16647**
Stone Fabric	This sample is characterised by its very distinct weathering front present around the exposed perimeter of the sample, characterised by a dark red colour. The remainder of the sample is homogenous, similar to BB1. There are dark coloured nodules present throughout.
Grain Size	Extremely fine-grained, homogenous throughout. Grains are well sorted and rounded/crushed in shape.
Grain Contacts and Cement	Very few observable grain contacts due to the fine nature of the material. Cemented by dolomite.
Mineralogy	Quartz is the dominant mineral, with mica present throughout. Like BB1, there are very few discernible feldspars and lithic fragments. There are distinct opaque nodules scattered throughout the sample.
Porosity and Permeability	No microcracks or pores visible – some secondary porosity within the weathered perimeter.

Table 3.25 - Percentage components Borwick Broch sample BB2

Components	Total (%)
Quartz	60
Feldspar	2
Lithic Fragment	Trace
Mica	8
Detrital Clay	0
Authigenic Clay	0
Carbonate	25
Opaque Minerals	5
Total	**100**

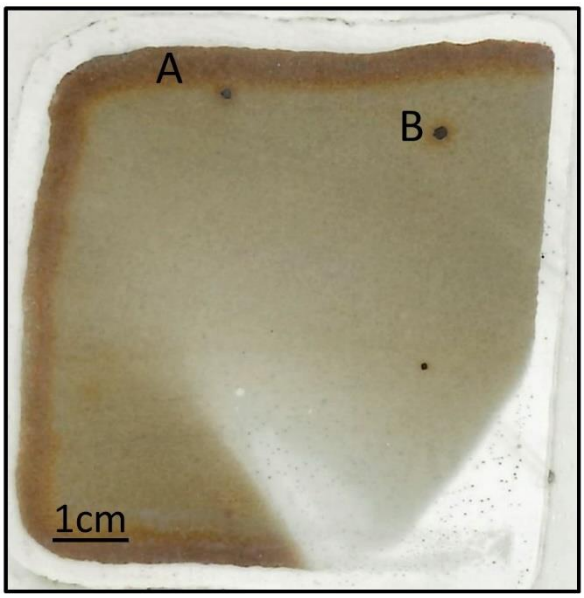

Figure 3.34 - Petrographic thin section scan of BB2, Borwick Broch stone

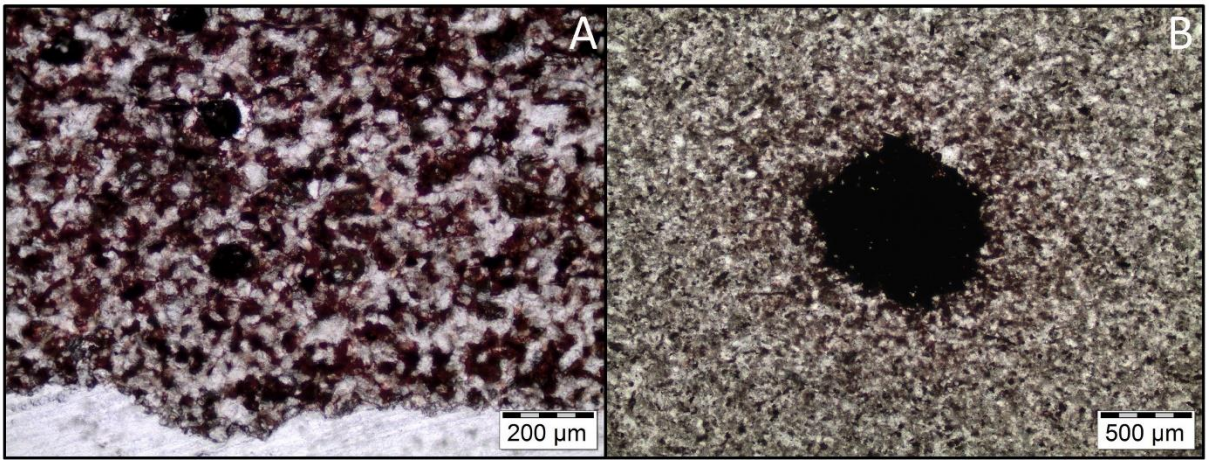

Figure 3.35 - There is a distinct weathering front surrounding the perimeter of the sample, characterised by a reddish-brown colour (A). The remainder of the sample is homogenous, containing several dark coloured nodules (B) (Both PPL)

Table 3.26 - Petrographic thin section analysis of Borwick Broch sample BB3

Site	Borwick, Orkney
Sample Number	**BB3 (Borwick Broch 3)**
Sample Location	**Borwick Broch, Orkney HY 22421 16647**
Stone Fabric	Similar to BB1 and BB2 in that the stone fabric is generally homogenous and similar to non-layered sections of control samples. Particularly like BB1, there are several distinct reddish-brown layers towards the stone surface, indicative of weathering. Several surface microcracks are also present. There is an abrupt change from the weathering fronts to crushed quartz in a dolomite matrix.
Grain Size	Extremely fine, homogenous throughout, grains are well-rounded/crushed and well sorted.
Grain Contacts and Cement	Very few observable grain contacts due to the fine nature of the material. Cemented by dolomite.
Mineralogy	Quartz is the dominant mineral, with mica present throughout. Very few discernible feldspars and lithic fragments.
Porosity and Permeability	Very low porosity, surface microcracks align with weathering front.

Table 3.27 - Percentage components Borwick Broch sample BB3

Components	Total (%)
Quartz	60
Feldspar	0
Lithic Fragment	0
Mica	5
Detrital Clay	0
Authigenic Clay	0
Carbonate	30
Opaque Minerals	5
Total	**100**

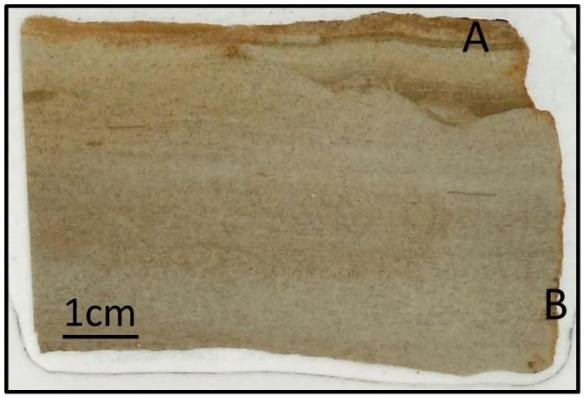

Figure 3.36 - Petrographic thin section scan of BB3, Borwick Broch stone

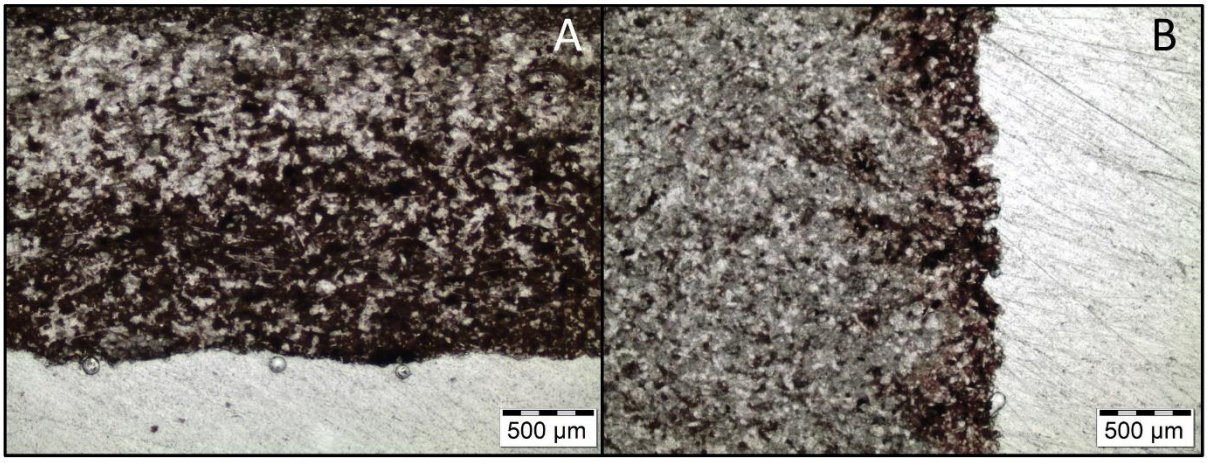

Figure 3.37 - Sample is characterised by multiple defined weathering fronts within the first centimetre of the stone surface (A). The remainder of the sample is homogenous with a slightly weathered area at the edge of the sample (B) (Both PPL)

3.4.2.3 Borwick Discussion

Based on estimate percentage composition of Borwick samples, it falls into the Wacke category of sandstone based on Folk's classification, due to its high carbonate content and extremely fine-grained matrix (Folk, 1980). Distinct differences between Borwick control and broch material are visualised through petrographic thin section analysis. The control samples (Figure 3.26 - Figure 3.31) are characteristic of typical Devonian sediment deposition and subsequent lithification. Literature on the formation of the Stromness Flagstone has already been discussed; through petrographic thin section analysis, their formation in these samples is visualised clearly as a low to medium energy lacustrine deposit. There are distinct fluid beds of primarily fine quartz held in a dolomite cement, with grain size varying slightly between layers. Seen in BC1 and BC2 (Figure 3.26 & Figure 3.29), beyond these layers the sample becomes homogenous, similar in characteristics to the broch samples. Microcracks are visible along bedding planes in the control rock, indicating areas of

weakness within the sandstone. The bedding planes are somewhat distorted, taking on a lensoid structure with signs of soft-sediment deformation, a process that occurs through varied and complex triggers. With relevance to Borwick, soft-sediment deformation occurs commonly through liquefaction in water-saturated sediments at the point of, or immediately following, deposition. In lacustrine environments, high and rapid accumulation of sediment causes material such as sand and silt to be poorly consolidated and loose in structure. When stress is applied to these sediments, liquefaction occurs leaving behind soft-sediment deformation features characterised by distorted bedding planes, as seen in the Borwick control samples (Allen, 1982; Owen and Moretti, 2011; Topal and Özkul, 2014).

Few signs of weathering are seen in the control rock, aside from a slight reddish discolouration on an exposed surface of BC1 (Figure 3.26 and Figure 3.27). This colour change is observed more clearly in the broch samples (Figure 3.32 - Figure 3.37) where there are distinct weathering crusts around the perimeter of the stones, particularly BB2, characterised by a reddish colour and indications of secondary porosity. A probable reason for the crust's formation is the dissolution of dolomite, whereby iron is liberated and attaches to clays in the mobile phase, water then evaporates at the surface of the stone, leaving behind the iron bound to clay at the stone's surface manifested as a reddish crust (Vincent *et al.*, 2018). Crust formation can be common in sandstones, particularly those in more urban environments that are exposed to pollutants, causing the stone surface to take on a very dark soot coloured appearance. Crucially, the weathered crust of a stone behaves differently from the rest of the stone and can become extremely hard and brittle, eventually leading to crust detachment (Veerle *et al.*, 2009).

In contrast with control samples, there is a clear lack of fluid deposition layers in the broch samples. The samples analysed in this thesis suggests that on exposure above surface the weaker layers, which have been shown to display microcracks within them, have been lost. Alternatively, broch builders realised the potentially negative implications of using a building stone with rapidly fluctuating layers and altered the rock in such a way that only homogenous material was utilised as a building stone in the broch.

Dark coloured nodules are prevalent in the broch stone, seen particularly in BB2 (Figure 3.34 and Figure 3.35). SEM-EDX analysis determines the chemical composition of these nodules, however, under thin section, they appear to be highly reactive sulphide nodules. Such

sulphides can weather, releasing sulphur and therefore corrosive sulphuric acid, exacerbating the degradation of stone (Rimstidt and Vaughan, 2003).

Stone weathering is accelerated after the sandstone's removal from the geology to be emplaced above the surface as Borwick Broch. Over geological time, the control sample shows very little if any sign of weathering while incorporated in a geological deposit, in marked contrast with the broch sandstone exposed for a comparably short period of around 2000 years. This comparison highlights the relatively rapid weathering of Stromness Flagstone within the built environment.

3.5 XRD Analysis Borwick: Inner vs Outer Dolomite

As highlighted in the previous section, dolomite is a complex mineral that evolves through dissolution and re-precipitation at depth (Warren, 2000), and is the main cementing agent in the Stromness Flagstone, present as a primary precipitate. The red coloured crust that surrounds the Borwick Broch stone seen in Figure 3.32 - Figure 3.37 can likely be attributed to the process of dedolomitization or dolomite dissolution.

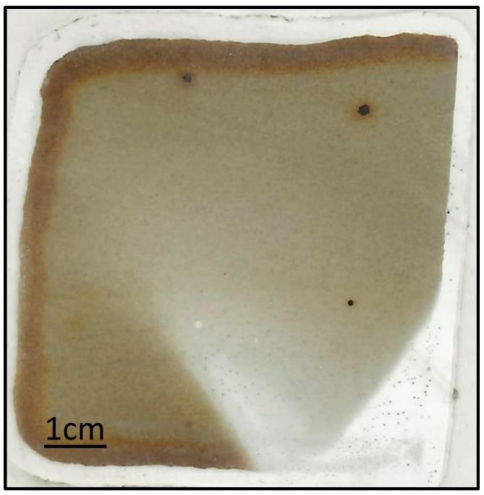

Figure 3.38 – Petrographic thin section scan of BB2 showing a distinct observable difference between the inner and outer material of the stone, characterised by a red crust

To determine the process that has caused this feature, specific XRD testing occurred, focused on the clear difference between the outer exposed stone and the inner non-exposed stone. Material from both areas of the stone was collected and prepared for separate XRD bulk analysis, the results of which are expressed below (Figure 3.39).

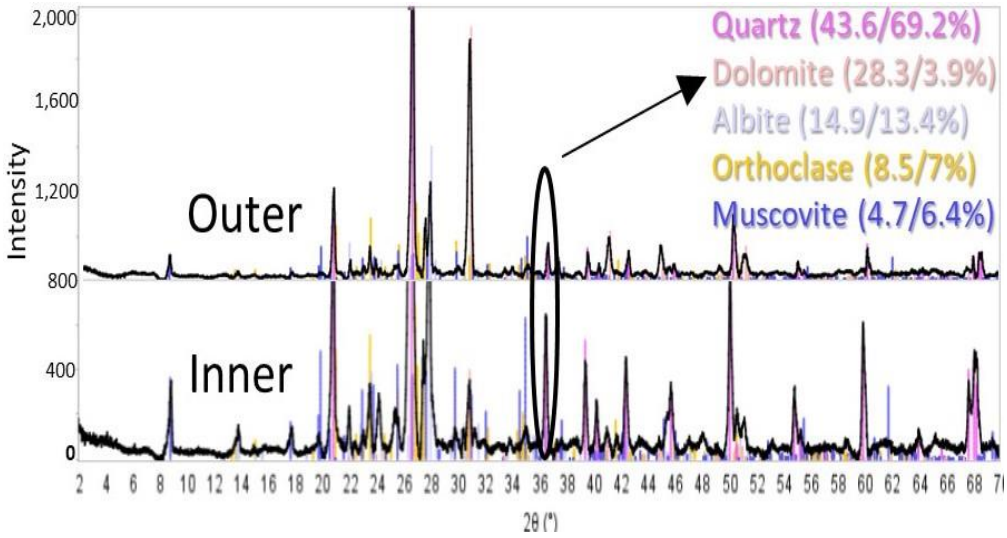

Figure 3.39 - XRD results from the analysis of pristine (Inner) and weathered (Outer) stone, Borwick Broch. Composition marked (Inner/Outer%). Dolomite peak circled

Dedolomitization is described in the literature as a process whereby dolomite is replaced by calcite, however, calcite is not observed in the XRD spectra expressed above. Furthermore, as is demonstrated in Figure 3.39, there is a considerable difference in dolomite abundance between the inner and outer stone. This indicates that dolomite dissolution has taken place without subsequent precipitation of calcite, ruling out dedolomitization in this instance. Instead, crust formation can be solely attributed to dolomite dissolution.

It must be noted that this is an important process that can stimulate dedolomitization, particularly within geological deposits. When dolomite dissolution occurs, secondary porosity is formed, where precipitation of calcite can occur. It is apparent that above surface as part of the broch, dolomite dissolution occurs on the exposed faces of the sandstone, however, calcite precipitation does not occur. Therefore, through dissolution, the stone surface is altered with the generation of secondary porosity but there is no calcite precipitation to occupy this porosity as there would be at depth. Consequently, the reddish crust differs in characteristics from the remainder of the non-exposed stone, meaning that the surface of the stone will behave differently from the bulk of the stone (Veerle *et al.*, 2009).

Additionally, dolomite dissolution is a slow reaction that can be exacerbated by acidic conditions as demonstrated by Singurindy and Berkowitz, (2003). SEM-EDX work in the following section characterises the chemistry of the dark nodules present in the Stromness Flagstone, which, through thin section observations, appear to be sulphide nodules. As

highlighted, their weathering can speed up the dissolution process by generating acidic conditions through the formation of sulphuric acid.

3.6 SEM-EDX Analysis

As discussed in Chapter 2, SEM-EDX analysis is used in this research to build on observations made during petrographic thin section work. A particular focus in this chapter is placed on understanding the general chemical composition of each unique sample, where attention is paid to micro-structures and distinct features within samples.

Additionally, key differences between the unweathered rock and broch stone that can be attributed to weathering as part of a culturally significant structure are outlined. This work culminates in the identification of potential micro-scale weaknesses. The likelihood of these vulnerabilities decaying more rapidly and destructively in a climate changed future is discussed and forms the basis of experimental work presented in subsequent chapters.

The structure of this section is as follows; firstly, for each sample, a thin section scan is provided with mapped areas delineated, reasons for why these areas have been selected are given. SEM-EDX maps for key elements in a specific analysed area are then presented. A large number of maps have been produced for each sample, therefore, only the most significant areas that are key to the understanding of the sample are presented. Likewise, some samples display similar characteristics, therefore, in some instances, a mapped area from one sample is presented as a representative map that can be applied to several samples.

3.6.1 Clachtoll

3.6.1.1 Clachtoll Control

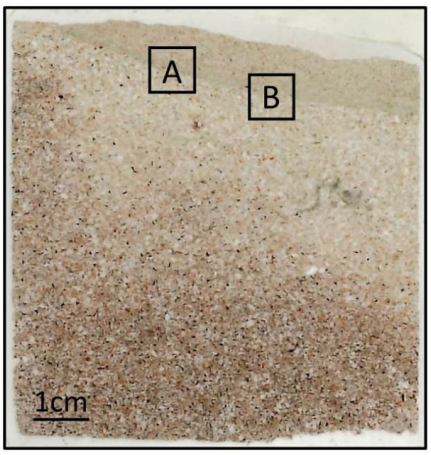

Figure 3.40 - Scan of CC1 with mapped areas highlighted

As established through petrographic thin section analysis of CC1, the feature of primary interest in this sample is the distinct transition from crushed quartz to coarse quartz punctuated by a clay band at the upper surface of the rock. Two separate areas were mapped at different magnifications to understand the chemical composition of the clay layer. Maps and associated spectra are presented below with greater colour intensity representing greater element concentration.

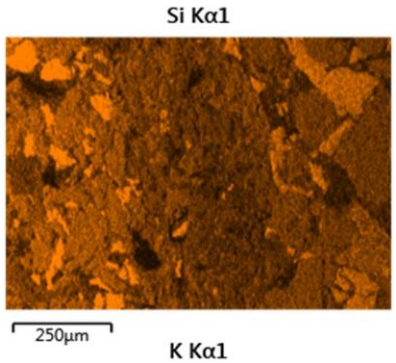

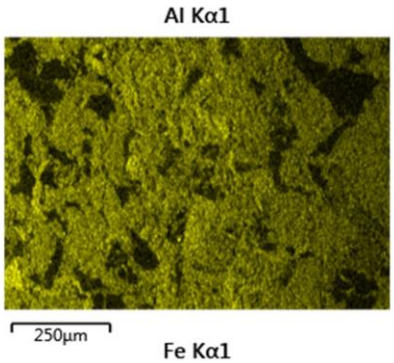

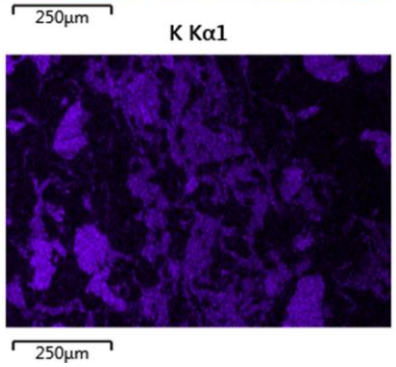

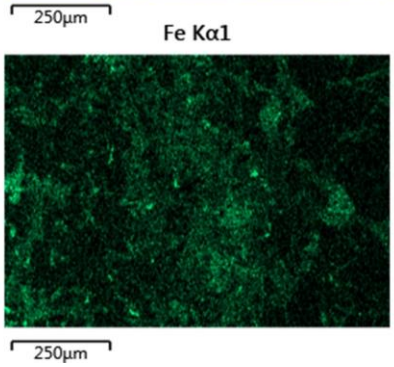

Element	Wt%
O	43.4
Si	23.4
C	12.5
Al	7.7
K	3.5
Na	2.1
Fe	2
Ti	1.8
Mg	1.6
Ca	1.6
Ni	0.1

Figure 3.41 - Quartz (Si), plagioclase feldspar (Al), K-feldspar (K) and Fe distribution in mapped section A of CC1 with normalised elemental proportion (%) of the mapped area

From Figure 3.41, the three bands of material can be identified, particularly in the quartz map, where crushed material on the left and coarse material on the right of the map are separated by the clay layer. Within the clay band, key feldspar minerals including aluminium and potassium are seen, however, they take on a fluid-like structure, potentially indicative of feldspar dissolution. Similarly, the iron cement appears to be more diffuse and finer in texture within the clay band, compared with iron located in the coarser sections of the rock.

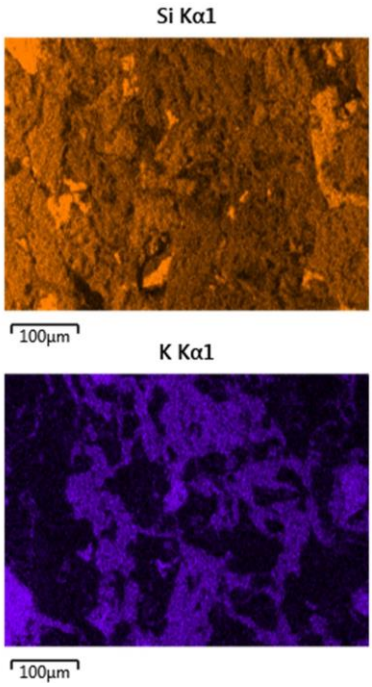

Element	Wt%
O	43.2
Si	21.8
C	12.7
Al	8.5
K	3.6
Fe	2.4
Na	2.1
Ti	2
Ca	1.9
Mg	1.6
Ni	0.1

Figure 3.42 - Quartz (Si), plagioclase feldspar (Al), K-feldspar (K) and Mg distribution in mapped section B of CC1 with normalised elemental proportion (%) of the mapped area

Figure 3.42 provides a higher magnification map of the clay band, highlighting the fluid nature of aluminium and potassium within the clay layer.

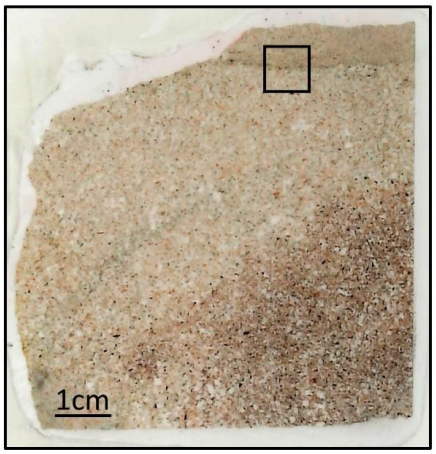

Figure 3.43 - Scan of CC2 with the mapped area highlighted

Similar to CC1, the mapping of CC2 was focused on the surface transition from crushed quartz to clay, to coarse quartz. Maps and associated spectra are presented below.

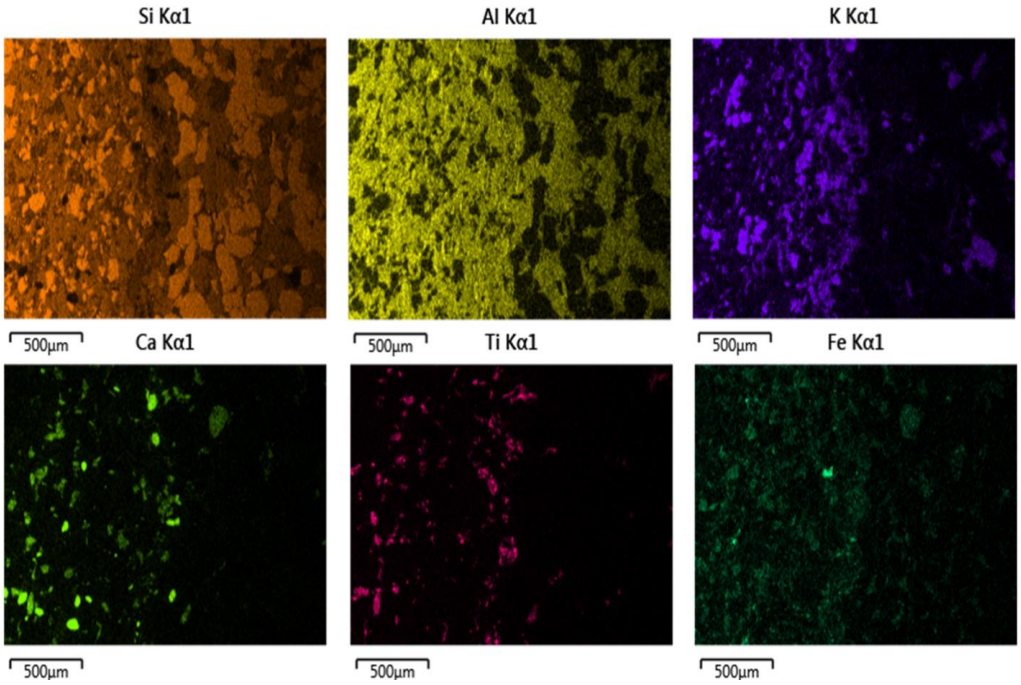

Figure 3.44 - Quartz (Si), plagioclase feldspar (Al), K-feldspar (K), Ca, Ti and Fe distribution in the mapped section of CC2

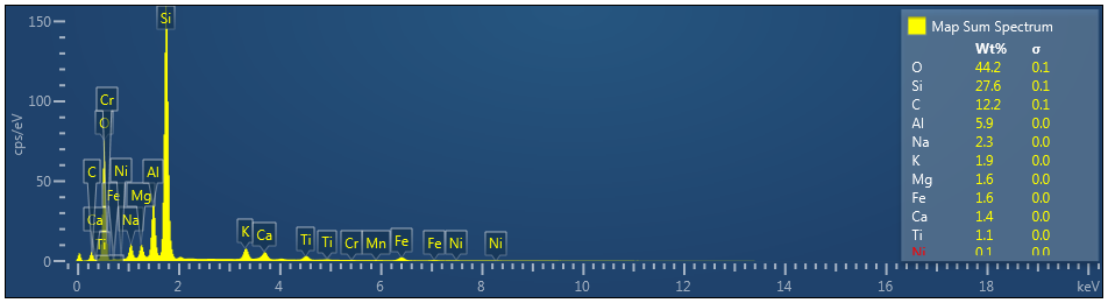

Figure 3.45 - Spectra associated with the mapped section of CC2 with normalised elemental proportion (%)

The three surface layers are particularly distinct in mapping work of CC2 (Figure 3.44). Clear differences can be picked out between the layers. Potassium is low in the coarse section on the right-hand side of the maps, appears fluid within the central clay layer and is present in small, discrete grains within the finer-grained material. Aluminium is present throughout, towards the surface of the stone it appears fragmented with some connectivity between individual grains, while in the clay layer it forms a fluid band and dominates the area beneath the clay band. Titanium and calcium also appear within the clay band and crushed quartz area but are not seen to any considerable amount above the clay layer. Iron is present throughout as a minor cementing agent.

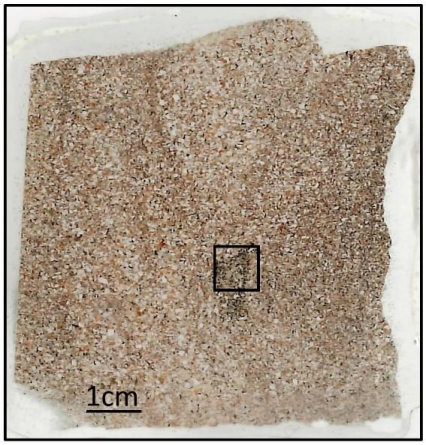

Figure 3.46 - Scan of CC3 with the mapped area highlighted

CC3 is similar in characteristics to the areas of CC1 and CC2 that are beneath the clay to coarse quartz transition. Therefore, mapping here was focused on the dark area at depth to understand the relationship between different grains and cementing agents within the Torridonian Sandstone. Maps and associated spectra are presented below.

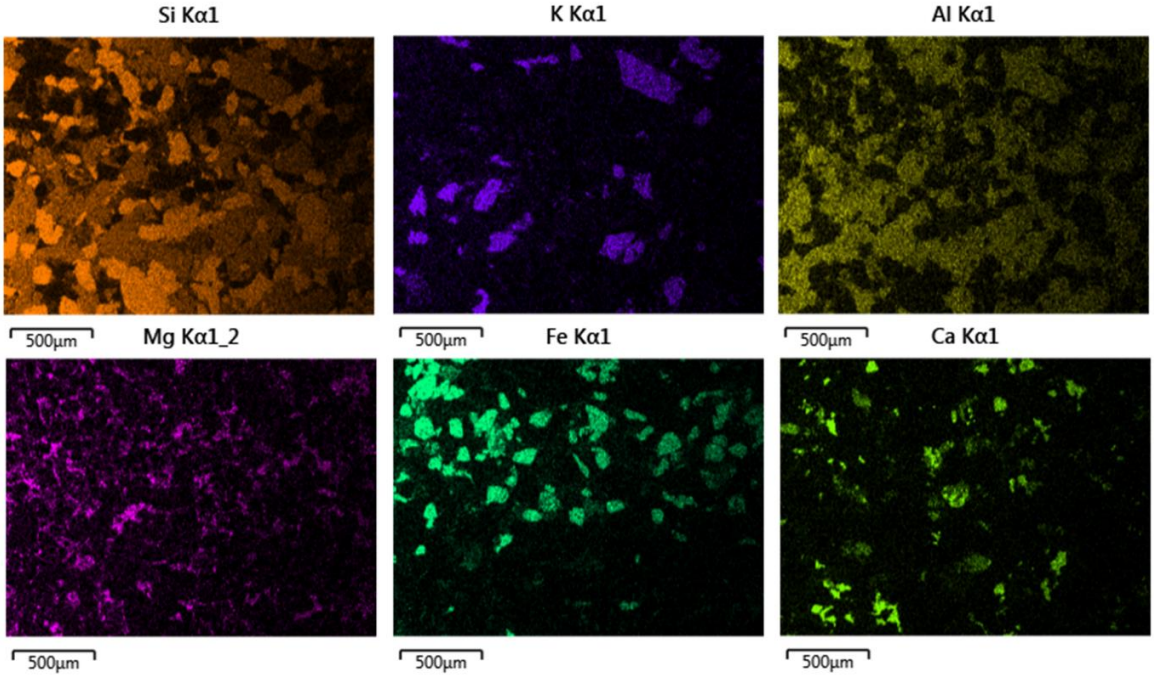

Figure 3.47 - Quartz (Si), K-feldspar (K), plagioclase feldspar (Al), Mg, Fe and Ca distribution in the mapped section of CC3

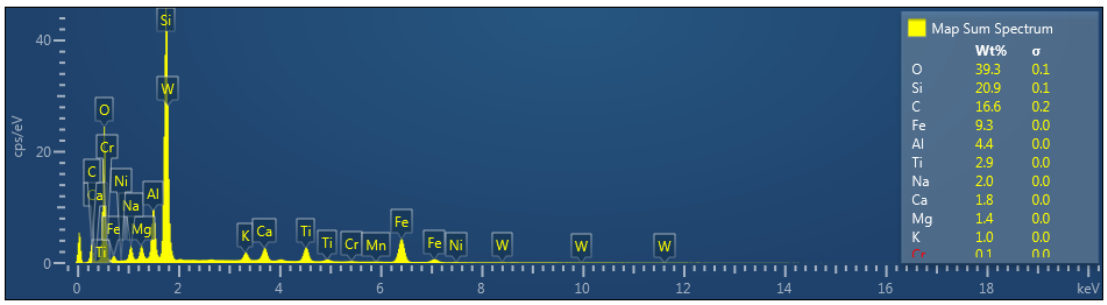

Figure 3.48 - Spectra associated with the mapped section of CC3 with normalised elemental proportion (%)

Maps shown in Figure 3.47 encapsulate the general fabric of the rock, however, the iron present appears more grain-like in structure, rather than following a similar cementing pattern to magnesium. This indicates that the function of iron within the Torridonian Sandstone is variable.

3.5.1.2 Clachtoll Broch

Figure 3.49 - Scan of CB1 with the mapped area highlighted

No apparent weathering indicators were identified in CB1 through thin section analysis, the main feature of the sample is the distinct lateral crush zone which appeared robust under the microscope. Mapping, therefore, focused on the general fabric of the broch stone to compliment thin section work. Key elements from the mapping analysis are presented below.

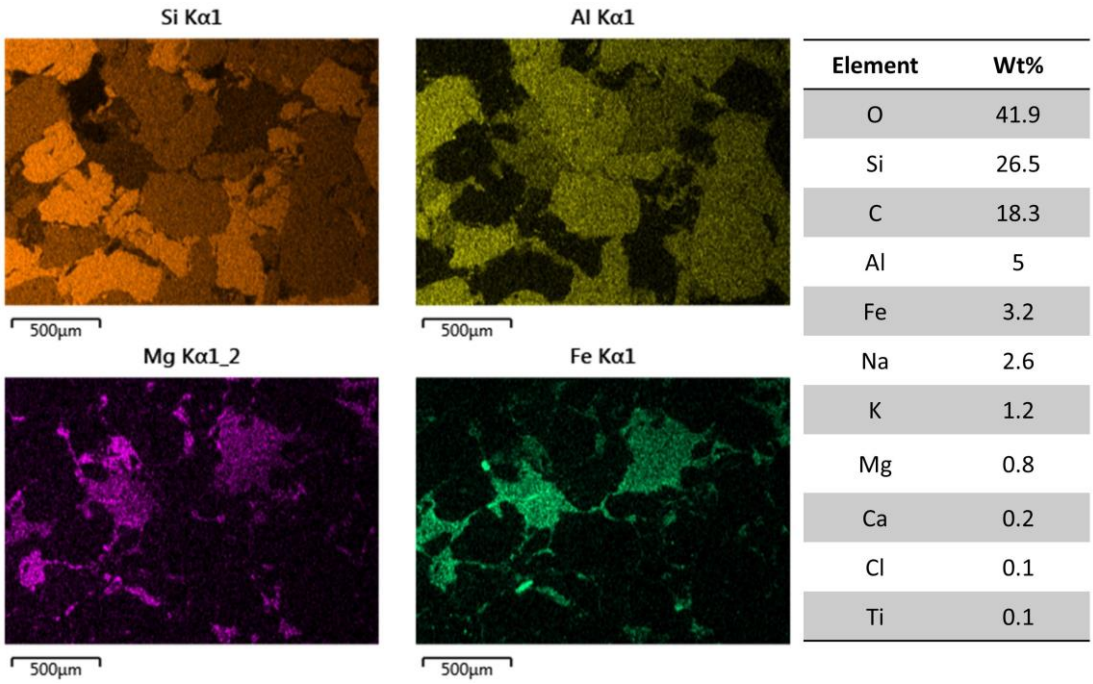

Element	Wt%
O	41.9
Si	26.5
C	18.3
Al	5
Fe	3.2
Na	2.6
K	1.2
Mg	0.8
Ca	0.2
Cl	0.1
Ti	0.1

Figure 3.50 - Quartz (Si), plagioclase feldspar (Al), Mg and Fe distribution in the mapped section of CB1 with normalised elemental proportion (%) of the mapped area

Figure 3.50 reinforces understanding of the general fabric of the Torridonian Sandstone. Quartz and feldspar appear robust and tightly packed, affirming the grain supported nature of the stone. The minor cementing influence of magnesium and iron is clear to see, connecting the thin pore space between grains, accounting for 0.8% and 3.2% of the mapped sample, respectively.

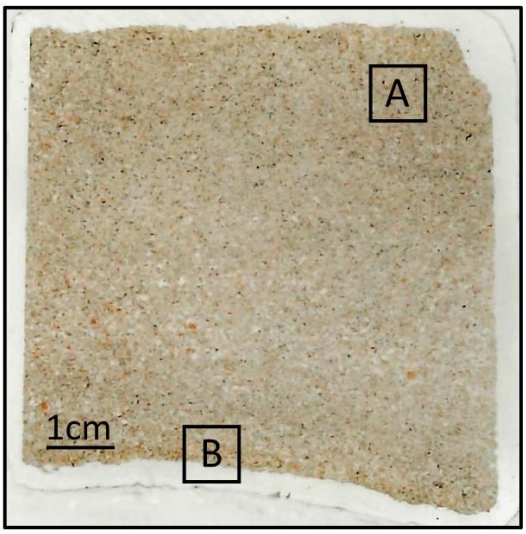

Figure 3.51 - Scan of CB2 with mapped areas highlighted

With few distinctive features, the section marked A was chosen as a means of understanding the general fabric of the stone and to compliment thin section work. Area B was chosen as there is a slight reddening on the lower edge of the sample, perhaps attributable to weathering. Maps and spectra associated with these areas are presented below.

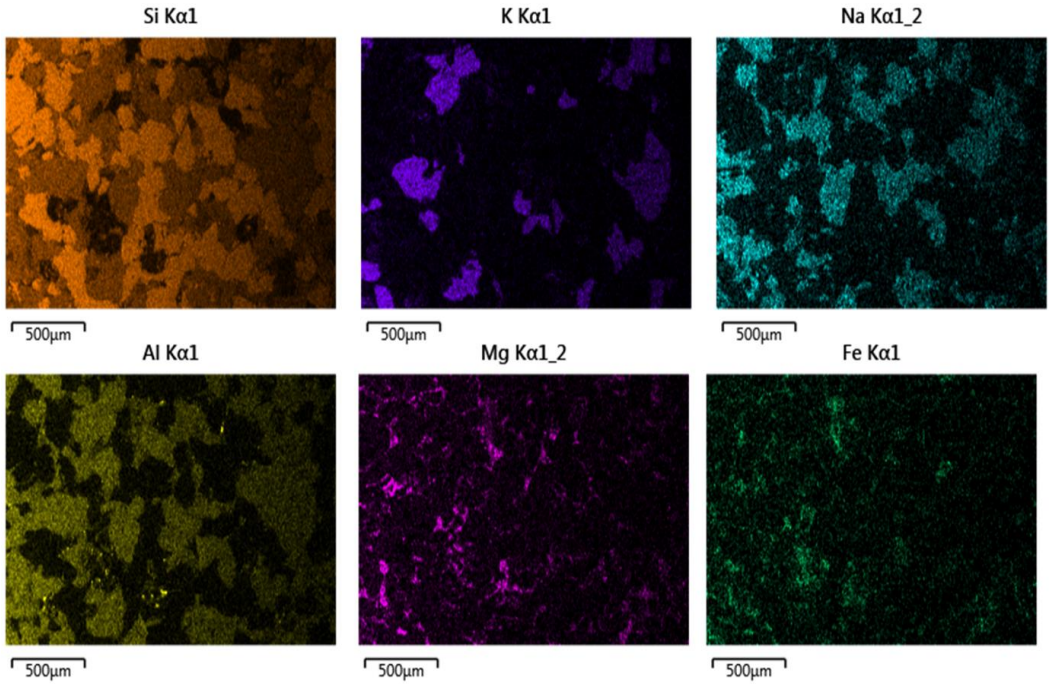

Figure 3.52 - Quartz (Si), K-feldspar (K), plagioclase feldspar (Na and Al), Mg and Fe distribution in mapped section A of CB2

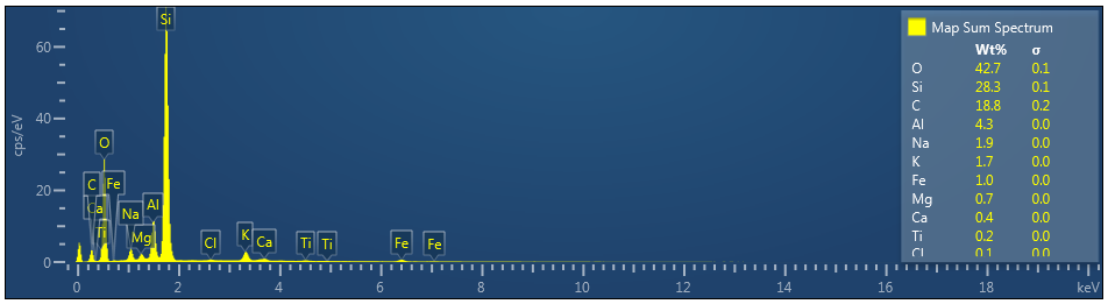

Figure 3.53 - Spectra associated with mapped section A of CB2 with normalised elemental proportion (%)

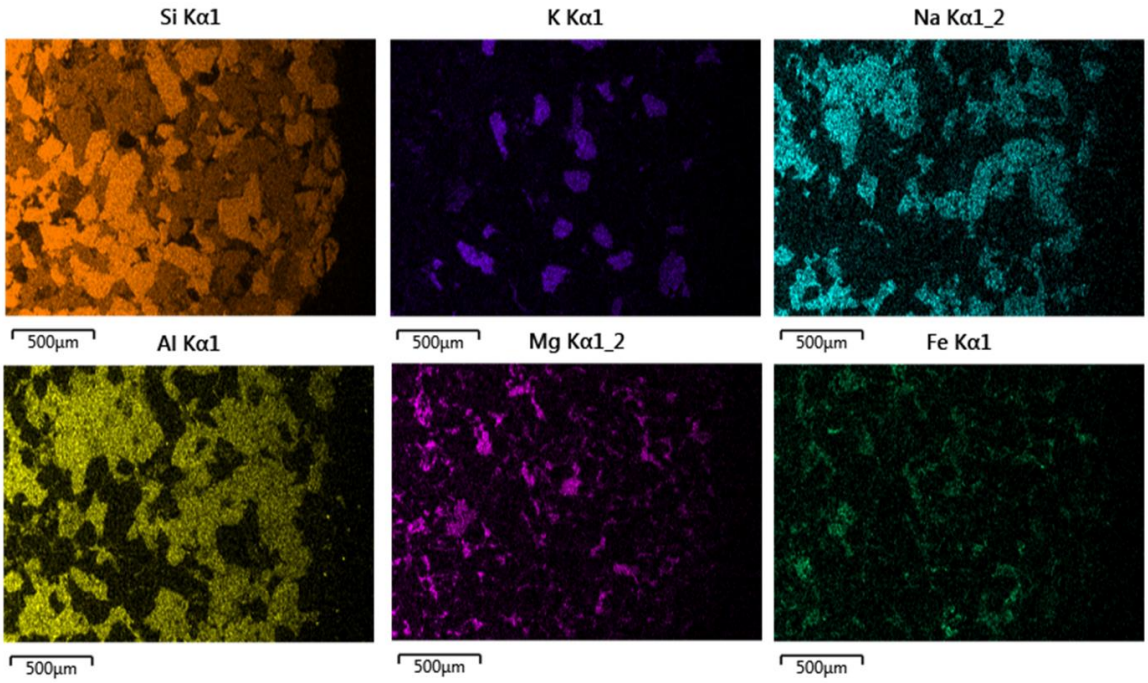

Figure 3.54 - Quartz (Si), K-feldspar (K), plagioclase feldspar (Na and Al), Mg and Fe distribution in mapped section B of CB2 with normalised elemental proportion (%) of the mapped area

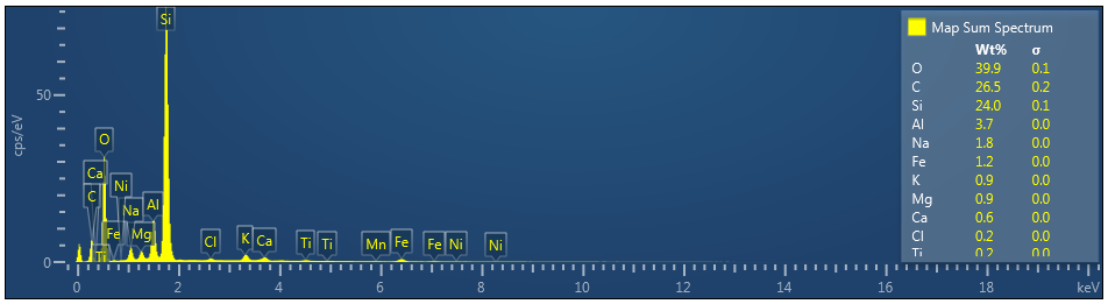

Figure 3.55 - Spectra associated with mapped section B of CB2 with normalised elemental proportion (%)

Despite the slight discolouration at the lower surface of the sample, results from mapping do not highlight any weathering indicators, instead, the sample appears robust in both mapped sections. Quartz is tightly packed, so too are the plagioclase feldspar elements of aluminium and sodium. K-feldspars are slightly sparser while magnesium and iron occupy the thin pore space between the grains (Figure 3.52 - Figure 3.54).

Figure 3.56 - Scan of CB3 with the mapped area highlighted

Similar to other broch samples, there are very few distinctive features. The upper surface of the stone appears slightly discoloured compared with the rest of the sample, therefore, mapping focused on this area. Maps and spectra are presented below.

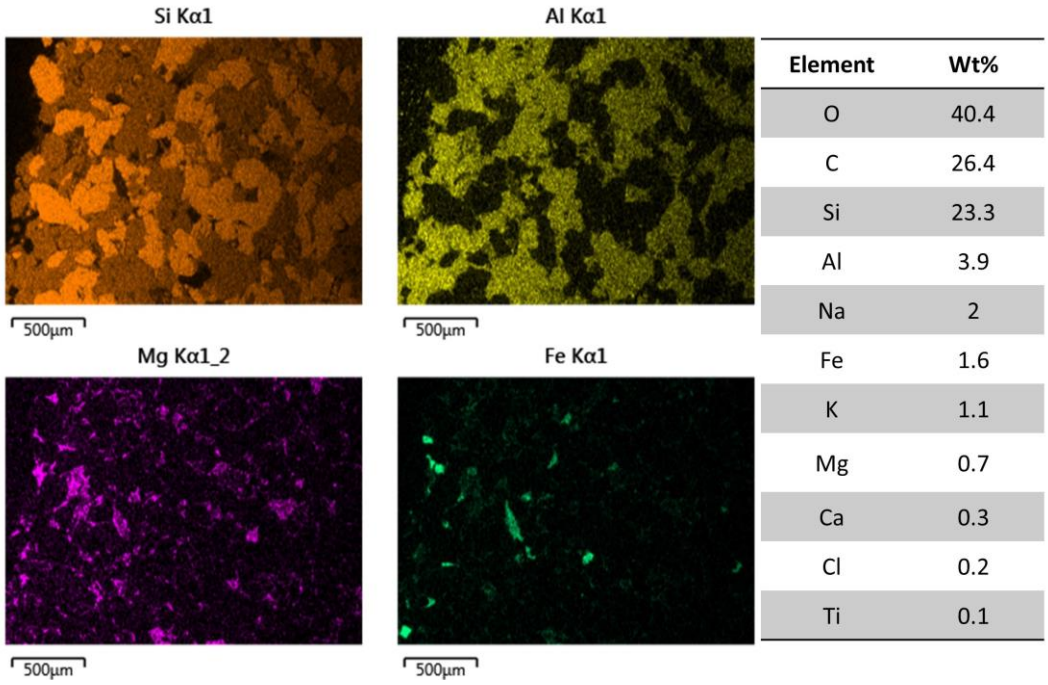

Element	Wt%
O	40.4
C	26.4
Si	23.3
Al	3.9
Na	2
Fe	1.6
K	1.1
Mg	0.7
Ca	0.3
Cl	0.2
Ti	0.1

Figure 3.57 - Quartz (Si), plagioclase feldspar (Al), Mg and Fe distribution in the mapped section of CB3 with normalised elemental proportion (%) of the mapped area

As expected, CB3 follows the same pattern as CB1 and CB2. Looking closely at the iron map in Figure 3.57, the mineral appears to be concentrated in specific areas, taking a more grain-like structure than seen in other broch samples. Furthermore, the percentage composition of key elements in the sandstone remains analogous with other broch sample spectra.

3.5.1.3 Clachtoll SEM-EDX Discussion

SEM-EDX mapping has proved to be a powerful analytical tool that compliments petrographic thin section analysis. Results obtained have enhanced understanding of Torridonian Sandstone that is manifested in control and broch samples utilised in this study from Clachtoll. The ability to visualise elements separately through mapping, a feat not possible utilising thin section analysis alone, has proved crucial in understanding the role of individual minerals and grains within samples. Quartz is ubiquitous in each sample, contributing to the grain supported nature of the sandstone, so too are plagioclase feldspars characterised by aluminium and sodium which occupy the same areas in maps shown in Figure 3.52 and Figure 3.54. K-feldspars signalled by the presence of potassium are also common, albeit to a lesser extent than plagioclase feldspars, a finding anticipated through XRD and petrographic thin section work.

Mapping has highlighted the previously undetected presence of magnesium as a minor cementing agent alongside iron. Through thin section work, it was determined that the low cement content was comprised entirely of iron, however, upon close inspection of Clachtoll Broch maps for CB1 and CB2 (Figure 3.50, Figure 3.52 and Figure 3.54), magnesium can be seen to occupy thin pore space between grains, in the same way as iron. From spectra associated with the map figures mentioned above, iron occupies 3.2% of CB1 while magnesium occupies 0.8%. In CB2 A, iron and magnesium occupy 1% and 0.7% respectively, while in CB2 B these numbers rise slightly to 1.2% and 0.9%. Although these percentage values are low, it is apparent that iron and magnesium compounds together comprise the trace cement found in the Torridonian Sandstone, an observation that only became clear through mapping, showcasing the importance of this analytical technique.

The most significant SEM-EDX finding related to Clachtoll has been in determining the characteristics, structure and percentage composition of the clay layers present in CC1 and CC2. In mapping figures presented for CC1 areas A and B (Figure 3.41 and Figure 3.42) key feldspar minerals including aluminium and potassium are present, notably, they take on a very fluid structure, contrasting the distinct grain structure of the feldspars seen in other areas of the sample, indicating feldspar dissolution has occurred, giving rise to the clay layer. Feldspar dissolution is common in geological deposits, literature that explores this phenomenon typically focus on rock reservoirs which are important resources in the petroleum industry, where feldspar dissolution has considerable implications on reservoir quality. Although not intrinsically linked to this thesis, the literature surrounding reservoir

feldspar dissolution is extensive (Stoessell and Pittman, 1990; Yuan et al., 2015; Yuan et al., 2017; Zhu, 2005), both in determining the driving forces behind mineral dissolution and the effect that dissolution itself has on the overall physical properties of a geological deposit.

Research has emerged showing that factors such as temperature and pH have significant effects on feldspar dissolution, with dissolution rate increasing with temperature and when pore water has an acidic or alkali pH. Feldspar dissolution initially increases secondary porosity, while triggering the formation of clay minerals, with illite and kaolinite typically forming in alkali and acidic conditions, respectively. Studies show that in geological reservoirs, temperatures of between 70°C–140°C cause smectite and kaolinite to be converted to illite. Contrasting views persist in the literature with evidence presented to suggest that dissolution can both strengthen and weaken the physical properties of a reservoir. Notably, with continuous feldspar dissolution, ion concentrations in the pore water increases and once saturated, precipitation occurs. It is at this point when authigenic clays form, which chokes up pore space, negatively impacting the quality of the reservoir (Xiao *et al.*, 2018).

Through SEM-EDX analysis, an effort has been made to determine the clay type present in the Clachtoll control samples. To that end, a selection of key elemental spectra associated with CC1 and CC2 maps are presented in the table below (Table 3.28), alongside clay mineral data for illite and kaolinite obtained from a mineralogy database (Barthelmy, 2012).

Table 3.28 - Percentage composition of analysed samples compared to illite and kaolinite standards

Element (%)	CC1 A	CC1 B	CC2	Illite	Kaolinite
Potassium	3.5	3.6	1.9	6.03	-
Magnesium	1.6	1.6	1.6	1.87	-
Aluminium	7.7	8.5	5.9	9.01	20.9
Iron	2	2.4	1.6	1.43	-
Silicon	23.4	21.8	27.6	25.25	21.76
Hydrogen	-	-	-	1.35	1.56
Oxygen	43.4	43.2	44.2	55.06	55.78

From percentage compositions provided in Table 3.28, it can be seen that the distinct clay bands in CC1 and CC2 are likely composed of illite, a non-expanding phyllosilicate that is commonly formed through the alteration of feldspar and mica (Galán and Ferrell, 2013; Dayal and Varma, 2017). In particular, percentages of silicon, magnesium, aluminium, and iron match well with values seen in a 100% illite standard. Some notable discrepancies must be highlighted; lower values of potassium and oxygen are seen in samples than anticipated, which is likely attributable to the presence of traces of other clays such as kaolinite. If kaolinite was the dominant clay, however, then a higher percentage of aluminium would be seen in the results.

Feldspar dissolution and subsequent illite precipitation within Torridonian Sandstone is mentioned in papers by Stewart, 1982 and Turnbull et al., 1996, without a clear conclusion being drawn. From feldspar dissolution literature referenced above Table 3.28 and the percentage composition of the clay layers in CC1 and CC2, a narrative can be built up relevant to this research. As established, the Torridonian Sandstone is an arkose sandstone with high feldspar contact, extremely tightly packed grains, and very low porosity which in turn means that pore water within the sandstone is scarce. Therefore, feldspar dissolution will be an extremely slow process that is limited in extent, however, given the age of the sandstone, dissolution has had time to occur sporadically within the rock. There are likely distinct planes where K-feldspar, in particular, has undergone dissolution, initially creating secondary porosity which has been filled over geological time with a predominantly illite rich clay. The feature seen in CC1 and CC2 is evidence of a diagenetic process that has likely taken tens of millions of years to take place, while the sandstone was held under high pressures and temperatures. In samples analysed, the clay layer does not appear to be integral to the robustness of the stone, however, it remains to be seen whether the clay layer could be a potential weak point that could be exacerbated through exposure to weathering simulations undertaken in this research.

3.6.2 Borwick

3.6.2.1 Borwick Control

Figure 3.58 - Scan of BC1 with the mapped area highlighted

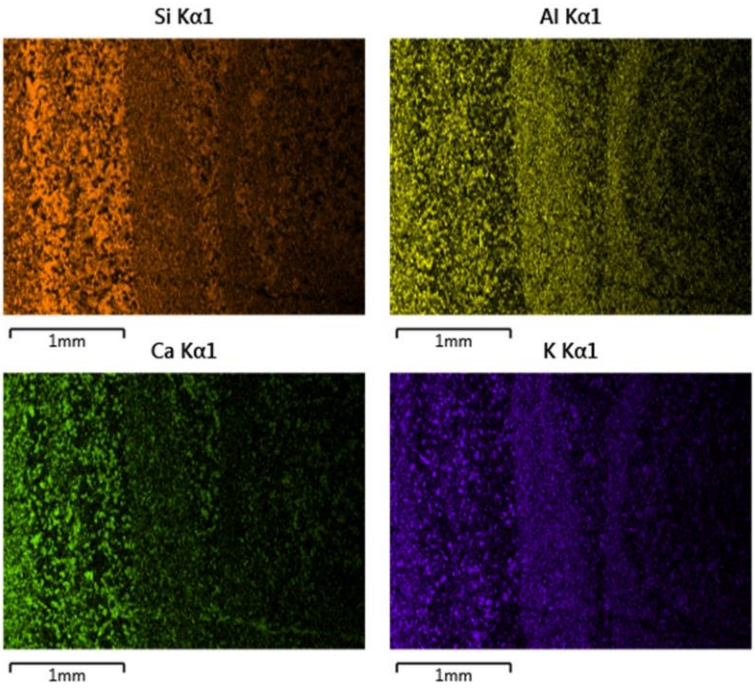

Element	Wt%
O	43.1
Si	21.1
C	16.5
Ca	5.7
Al	4.7
K	3.1
Fe	2.5
Mg	1.8
Na	1
Ti	0.3
Mn	0.1

Figure 3.59 - Quartz (Si), plagioclase feldspar (Al), Ca and K-feldspar (K) distribution in the mapped section of BC1

As highlighted through thin section work, the Borwick control samples are extremely similar, characterised by fluctuating layers of fine-grained quartz and feldspar in a dolomite cement, with signs of soft-sediment deformation. Therefore, the mapping of BC1 is representative of all Borwick control samples. Figure 3.59 highlights the subtle bedding variations in the

Stromness Flagstone. Quartz and feldspar are extremely fine-grained with calcium and magnesium comprising the dolomite cement within the stone.

3.6.2.2 Borwick Broch

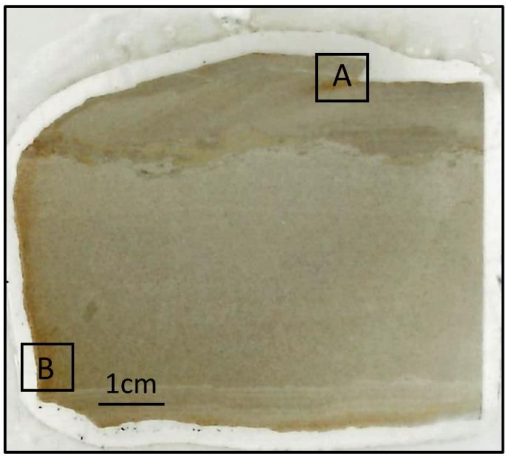

Figure 3.60 - Scan of BB1 with the mapped areas highlighted

Two distinct features are seen in BB1, a microcrack at the upper surface of the stone (A) and apparent dolomite dissolution in sections of the stone's perimeter (B), both features are mapped, and relevant figures and spectra are presented below.

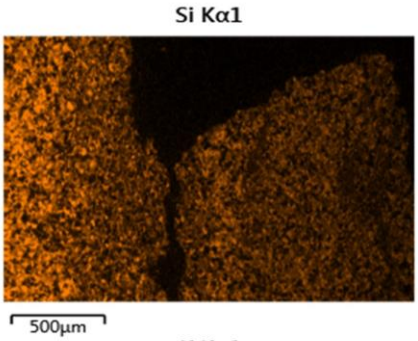

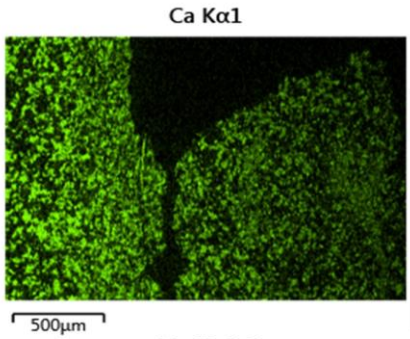

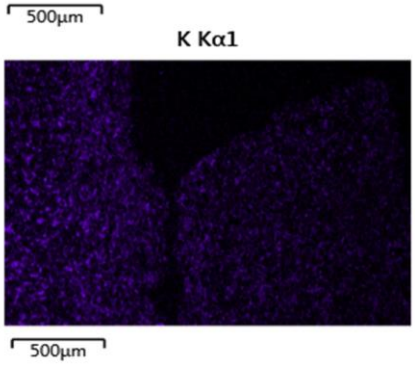

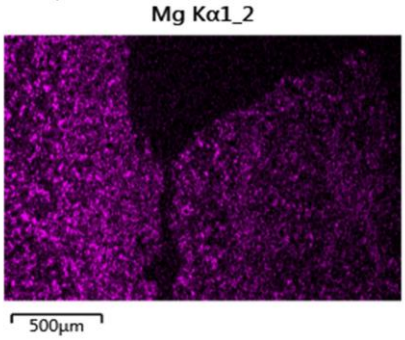

Element	Wt%
O	38
C	32.5
Si	13.3
Ca	5.3
Al	3.5
Fe	2.5
K	1.9
Mg	1.5
Na	0.8
Cl	0.4
Ti	0.2

Figure 3.61 - Quartz (Si), Ca, K-Feldspar (K) and Mg distribution in the mapped section A of BB1

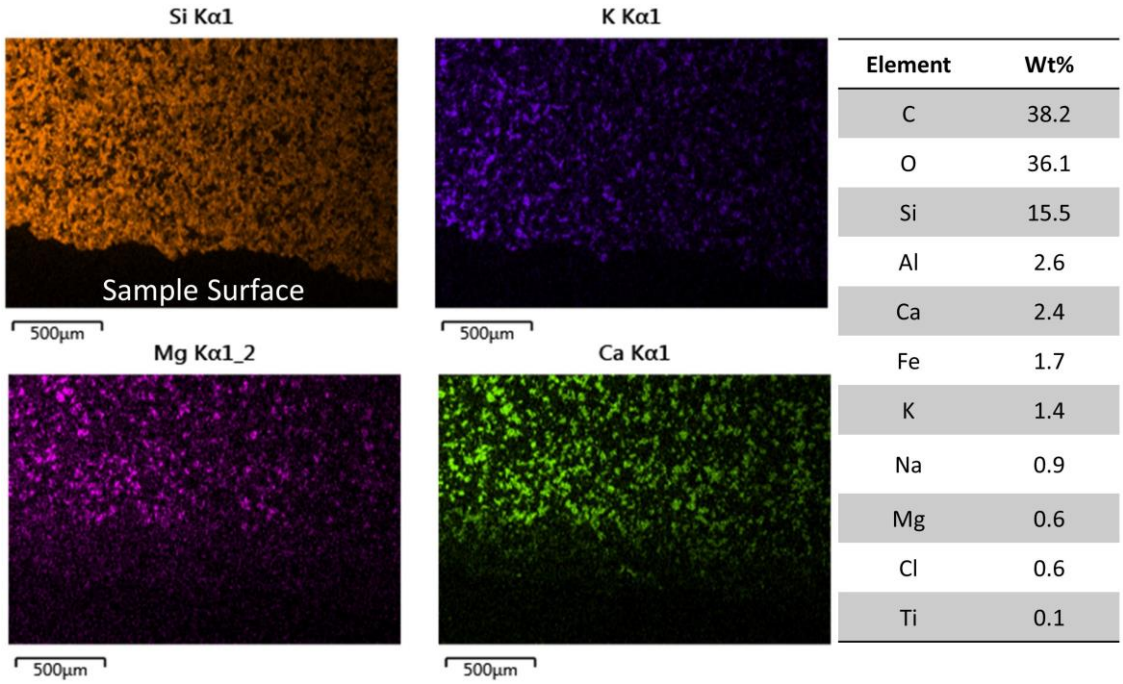

Element	Wt%
C	38.2
O	36.1
Si	15.5
Al	2.6
Ca	2.4
Fe	1.7
K	1.4
Na	0.9
Mg	0.6
Cl	0.6
Ti	0.1

Figure 3.62 - Quartz (Si), K-feldspar (K), Mg and Ca distribution in the mapped section B of BB1

In mapped section A of BB1 (Figure 3.61), there appears to be no indication of chemical breakdown surrounding the microcrack, indicating that this is a physical weakness at the surface of the stone. A clear chemical change can be seen in the mapped section B of BB1 (Figure 3.62). At the upper surface, there is a distinct loss of calcium and magnesium, the main constituents of dolomite, indicating that dolomite dissolution has occurred (Figure 3.62). Furthermore, the quantity of calcium and magnesium appear significantly lower than in Figure 3.61 where there is no evidence of dolomite dissolution. To quantify this further, image analysis has taken place and is presented in Section 3.6.2.3 Borwick ImageJ Analysis.

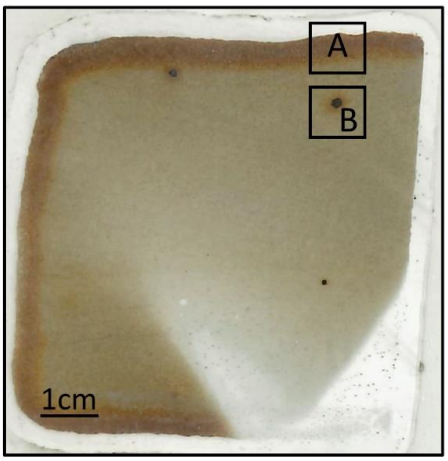

Figure 3.63 - Scan of BB2 with the mapped areas highlighted

There is a distinct weathered surface around the perimeter of BB2 (A), this was mapped at various points, however, site A as marked in Figure 3.63 was chosen as a representative map of the entire weathered front. Similarly, site B is representative of all dark coloured nodules found in BB2. Relevant maps and spectra are provided below.

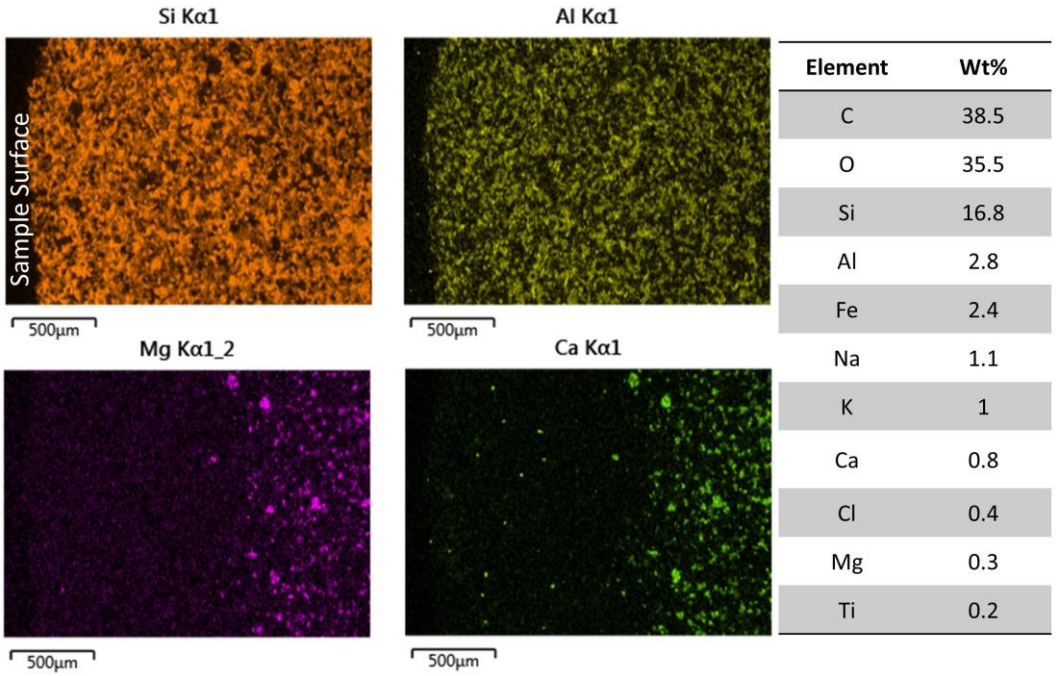

Element	Wt%
C	38.5
O	35.5
Si	16.8
Al	2.8
Fe	2.4
Na	1.1
K	1
Ca	0.8
Cl	0.4
Mg	0.3
Ti	0.2

Figure 3.64 - Quartz (Si), plagioclase feldspar (Al), Mg and Ca distribution in the mapped section A of BB2

Dolomite dissolution is clear on the surface of the mapped area A (Figure 3.64), quartz and feldspar appear intact, conversely, very low levels of key dolomite minerals are seen in the upper millimetre of the stone.

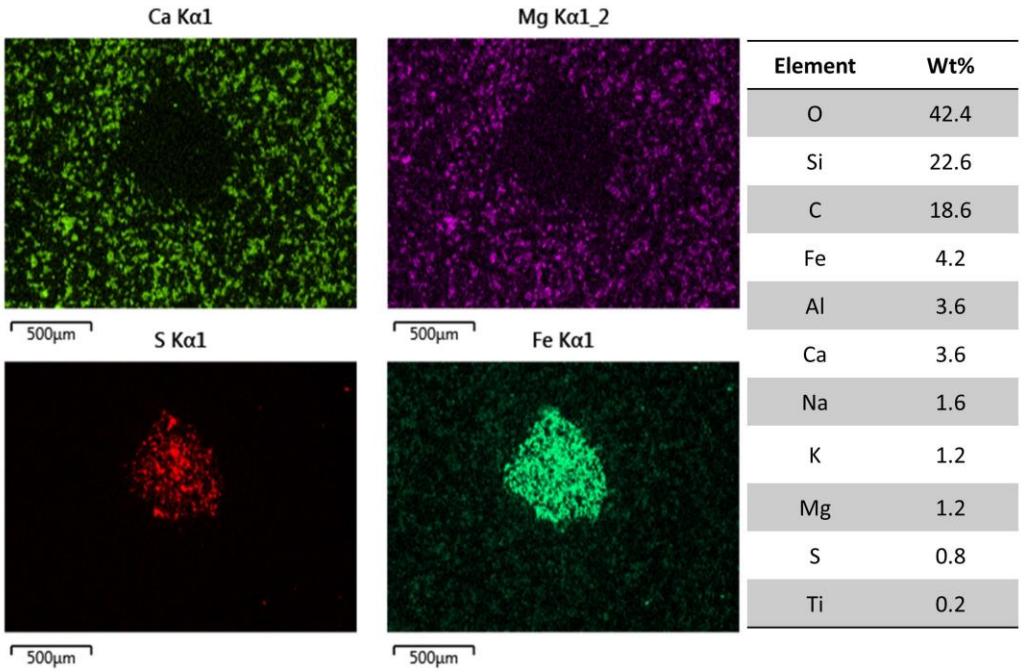

Element	Wt%
O	42.4
Si	22.6
C	18.6
Fe	4.2
Al	3.6
Ca	3.6
Na	1.6
K	1.2
Mg	1.2
S	0.8
Ti	0.2

Figure 3.65 - Ca, Mg, S and Fe distribution in the mapped section B of BB2

Mapping of section B of BB2 (Figure 3.65) has confirmed the chemistry of the dark nodules scattered throughout the Stromness Flagstone broch samples. As anticipated, they are composed of predominantly sulphur and iron, making them highly reactive sulphide nodules.

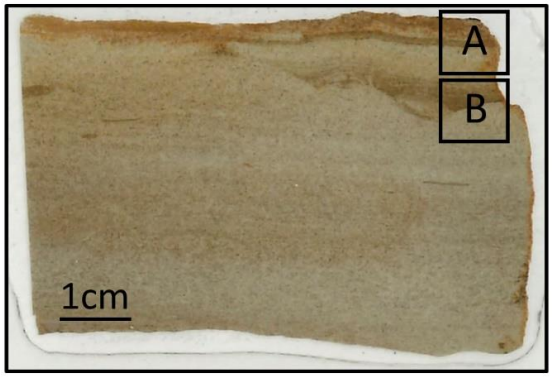

Figure 3.66 - Scan of BB3 with the mapped areas highlighted

The surface of BB3 appears complex, with two distinct dissolution fronts (A) and (B). To understand the progression between the weathered areas, two maps were generated side by side. From this, understanding is gained into how the elemental composition of the sample varies with depth and any differences in the weathered areas are identified. The maps are presented in Figure 3.67, maps from site A are on the left-hand side of the figure and maps from site B are on the right-hand side, forming a transect of the upper surface of the stone.

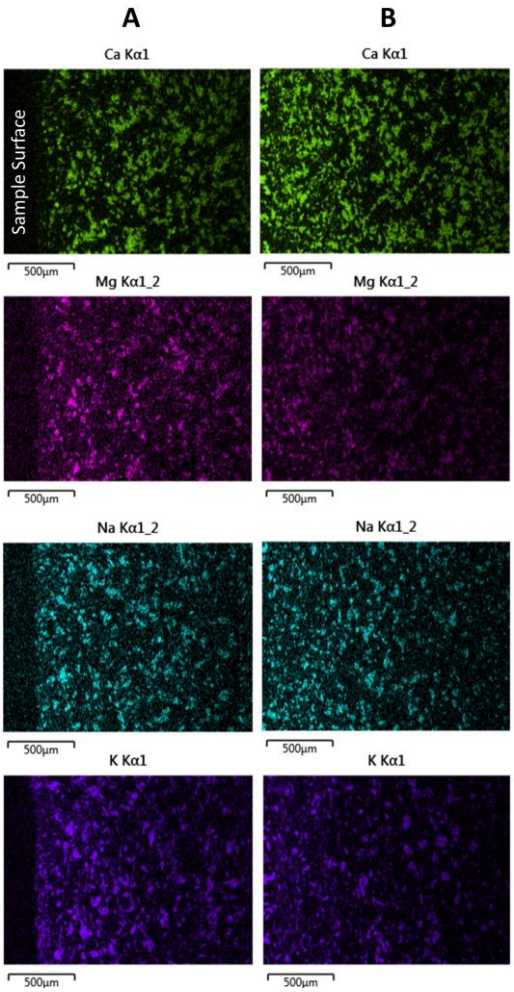

Figure 3.67 - Amalgamation of BB3 mapped sections A and B to form surface profile of Ca, Mg, Na and K

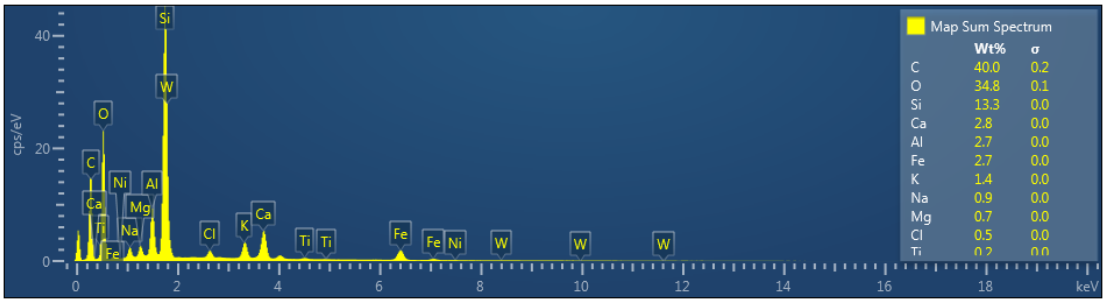

Figure 3.68 - Spectra associated with the mapped section A of BB3

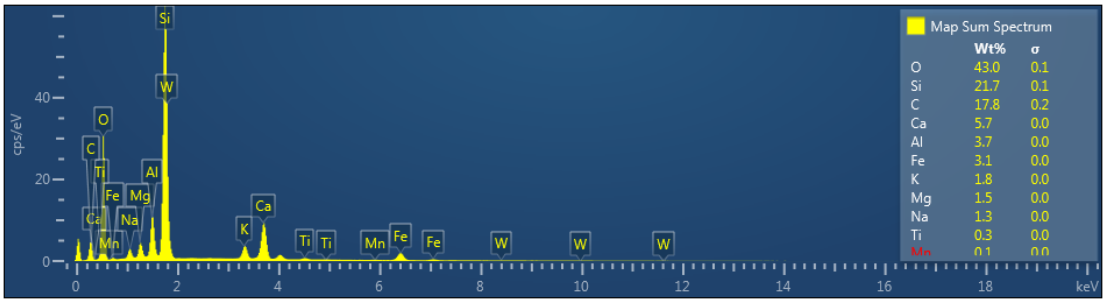

Figure 3.69 - Spectra associated with the mapped section B of BB3

There is slight evidence from mapping (Figure 3.67) to suggest dolomite dissolution has occurred on the upper surface of the sample, however, it is difficult to detect the second weathering front (section B). Further image analysis has been conducted and is presented in the following section.

3.6.2.3 Borwick ImageJ Analysis

ImageJ analysis was performed on Borwick broch samples, where insights beyond the scope of SEM-EDX mapping have been gained. Focus was placed on quantifying dolomite dissolution by thresholding magnesium and calcium separately to understand their distribution within the weathered edge of broch samples. Below are auto-threshold images of magnesium and calcium SEM-EDX maps for BB1-3 with associated graphs showing the intensity of grey pixels that represent the focus elements within the first few millimetres of the sample surface. In threshold images, the focus element is white, and the remainder of the sample is black.

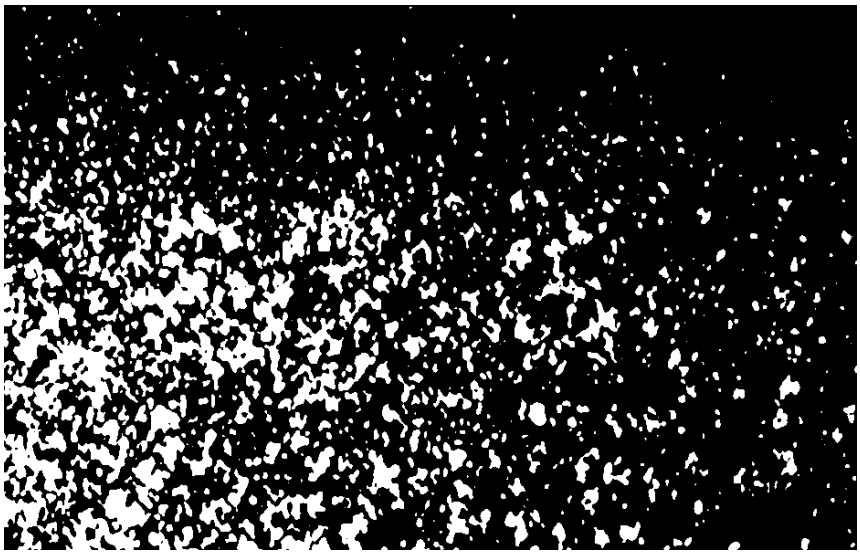

Figure 3.70 - BB1 mapped section B auto-threshold image of Mg distribution. The map has been rotated vertically and cropped to the immediate surface of the sample

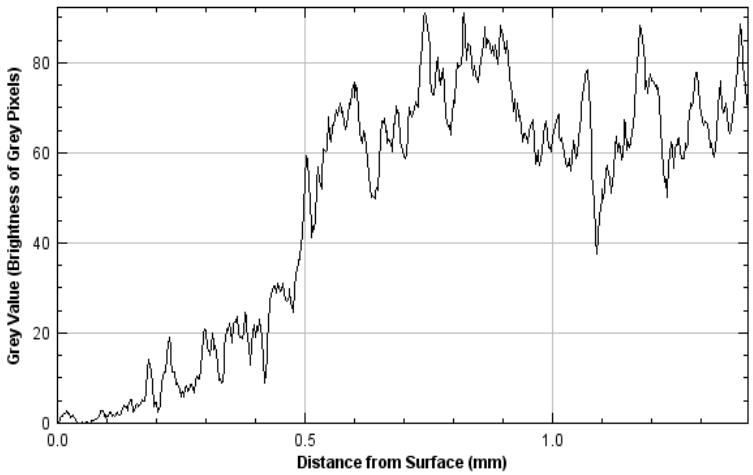

Figure 3.71 - Intensity of grey pixels (Mg) with progression from the sample surface to 1.4mm depth

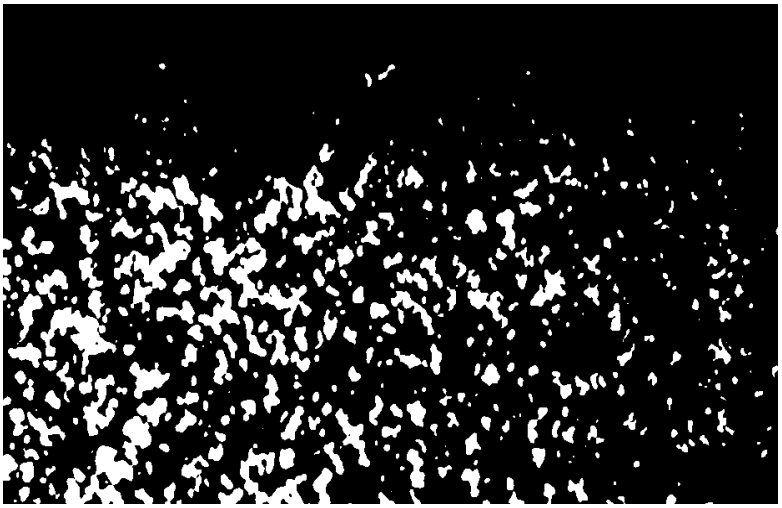

Figure 3.72 - BB1 mapped section B auto-threshold image of Ca distribution. The map has been rotated vertically and cropped to the immediate surface of the sample

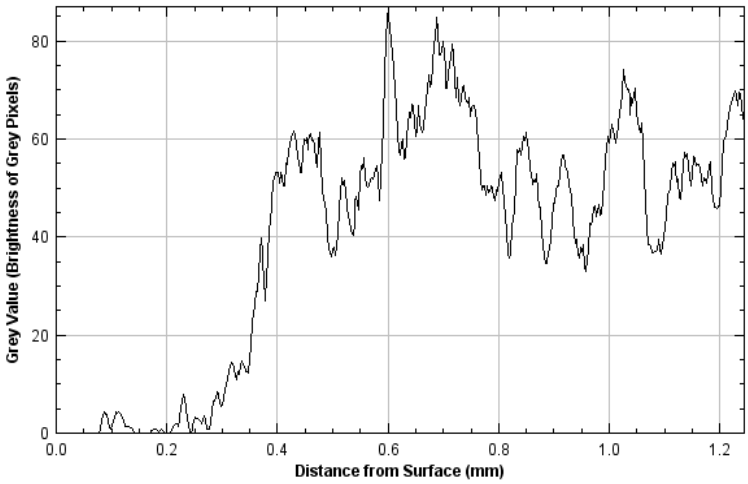

Figure 3.73 - Intensity of grey pixels (Ca) with progression from the sample surface to 1.3mm depth

In BB1 auto-threshold images for magnesium and calcium (Figure 3.70 and Figure 3.72), both elements appear sparse at the surface and increase in intensity with depth. Graphs presented (Figure 3.71 and Figure 3.73) affirm this and show that magnesium and calcium follow a similar pattern to each other, whereby in the first ~0.5mm of the sample, their grey value is low (below 20), thereafter it increases to between 35 and 80.

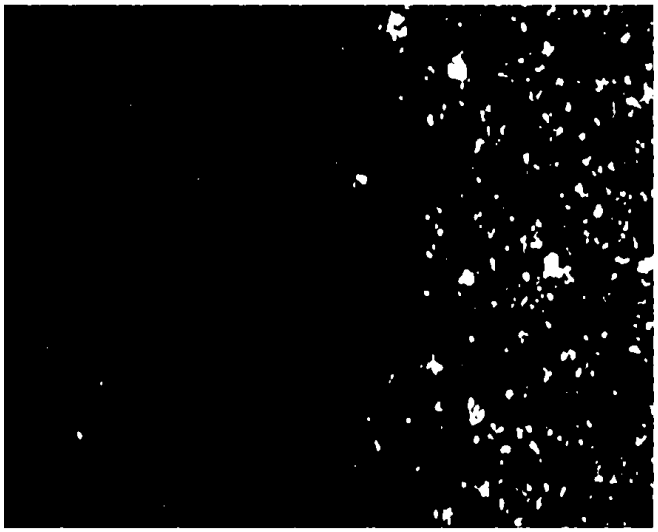

Figure 3.74 - BB2 mapped section A auto-threshold image of Mg distribution. The sample surface is at the left-hand side of the image

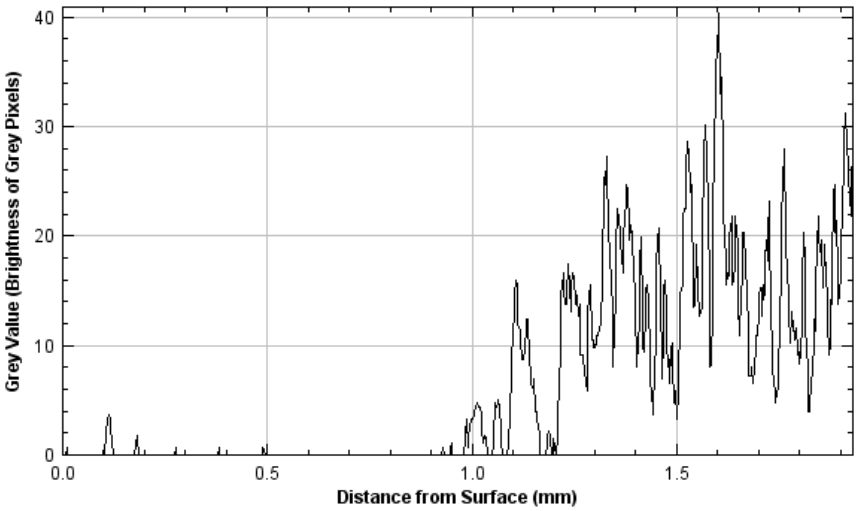

Figure 3.75 - Intensity of grey pixels (Mg) with progression from the sample surface to 1.9mm depth

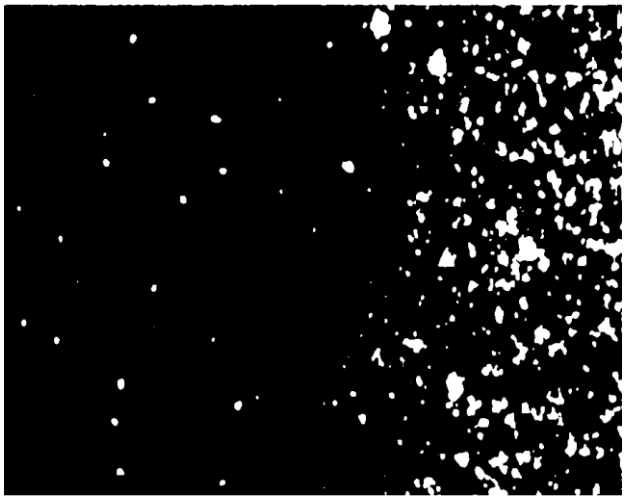

Figure 3.76 - BB2 mapped section A auto-threshold image of Ca distribution. The sample surface is at the left-hand side of the image

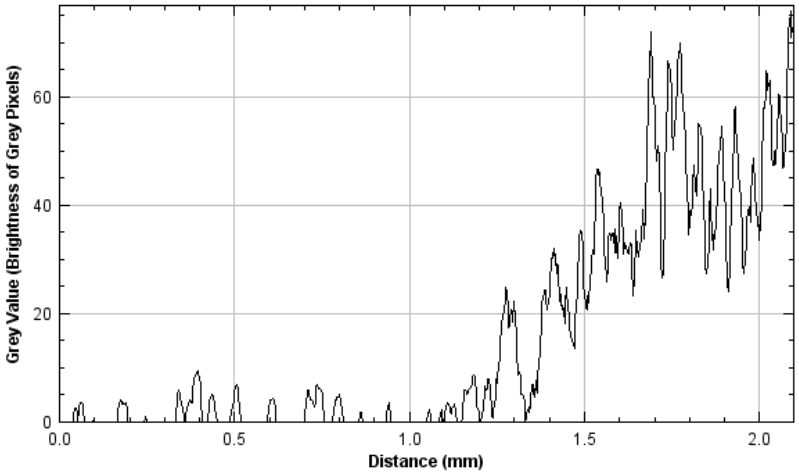

Figure 3.77 - Intensity of grey pixels (Ca) with progression from the sample surface to 2.1mm depth

In BB2, magnesium and calcium levels are low at the surface of the stone as visualised in Figure 3.74 and Figure 3.76, respectively. From Figure 3.75 and Figure 3.77, the grey level for magnesium remains predominantly below 5 in the first mm of stone, while in calcium it remains below 10. Beyond this depth magnesium begins to increase towards a grey value of between 10 and 30, with considerable fluctuation, bringing the value back to zero in places. It is not until beyond 1.5mm depth that the grey value increases to between 10 and 40. Conversely, the calcium grey value begins to increase at around 1.1mm, it increases quicker and to a higher level than magnesium. Between 1.5mm and 2mm the grey value remains comfortably within the 20-75 range.

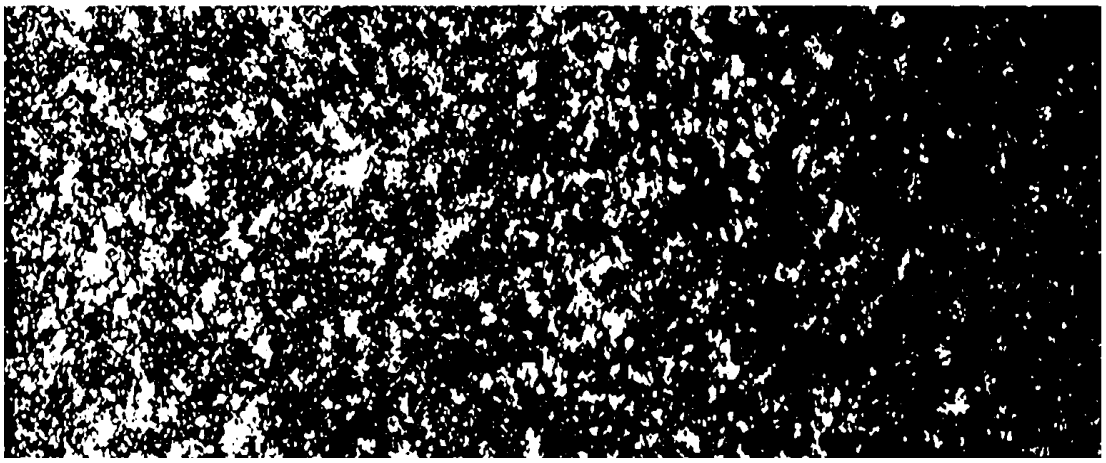

Figure 3.78 - BB3 mapped section A and B stitched together. Auto-threshold image of Mg distribution. The sample surface is at the left-hand side of the image

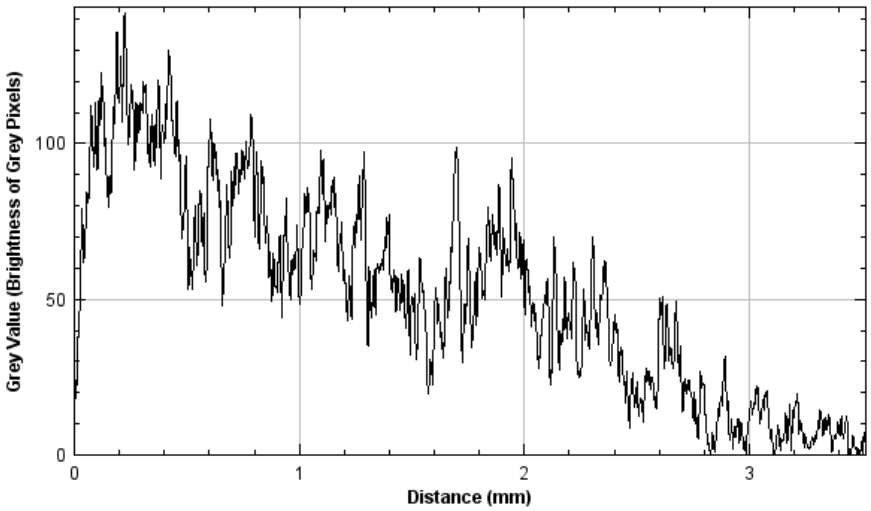

Figure 3.79 - Intensity of grey pixels (Mg) with progression from the sample surface to 3.3mm depth

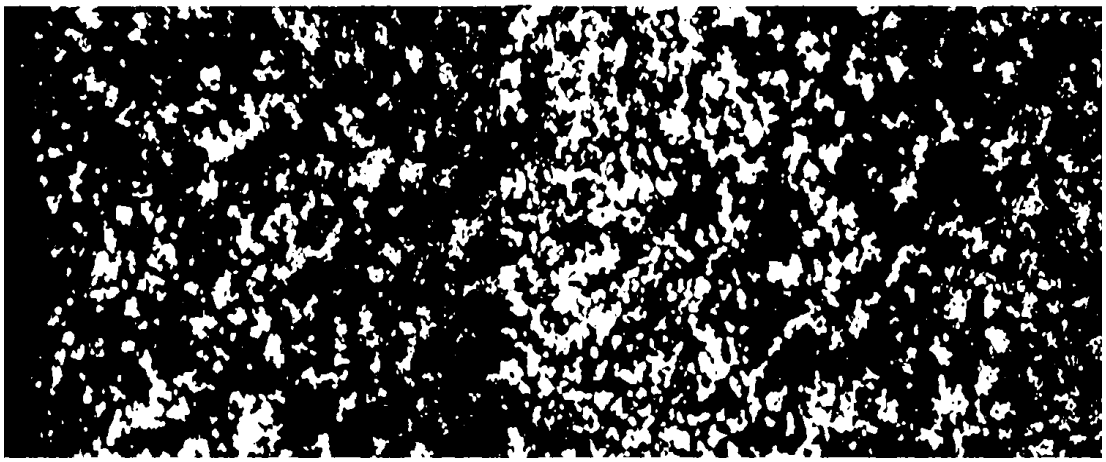

Figure 3.80 - BB3 mapped section A and B stitched together. Auto-threshold image of Ca distribution. The sample surface is at the left-hand side of the image

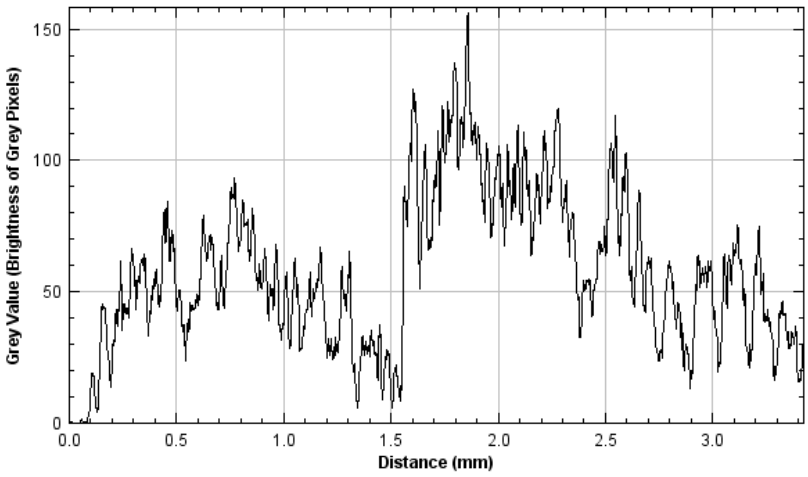

Figure 3.81 - Intensity of grey pixels (Ca) with progression from the sample surface to 3.4mm depth

For BB3, two images were stitched together from areas A and B (Figure 3.67) to aid in the detection of two potential weathering/dissolution areas. From Figure 3.78 and Figure 3.79, there is no evidence of magnesium dissolution at the surface, instead, the grey value appears to steadily decrease. Conversely, Figure 3.80 and Figure 3.81 for calcium show clear evidence of two dissolution areas. At the immediate surface and 1.5mm depth, calcium concentrations appear relatively sparse (Figure 3.80) reflected in the low grey values shown in Figure 3.81 at both locations.

3.6.2.4 Borwick SEM-EDX Discussion

The successful application of SEM-EDX mapping is most demonstrable upon observation of Borwick Broch samples. Mapping results from the control sample are nonetheless useful, the ubiquitous presence of magnesium and calcium making up the dolomite cement component is clear (Figure 3.59). The associated spectra also prove insightful, the dominance of quartz within the sample is clear with silica accounting for 64.2% of the mapped section. Elements associated with feldspars are comparably low, with aluminium, potassium and sodium together occupying 8.8% of the overall percentage composition of the map.

Mapping occurred on the broch sample surfaces where dolomite dissolution became apparent through the petrographic thin section and XRD analysis presented earlier in this chapter. The process of dolomite dissolution and its implications on stone weathering has been discussed extensively in previous sections of this chapter (Section 3.4.2.3 Borwick and 3.5 XRD Analysis Borwick: Inner vs Outer Dolomite). Only through mapping, however, has it been possible to visualise and accurately quantify this important surface change. In BB1 section B,

quartz and potassium remain intact, however, a very slight weathered edge can be seen where magnesium and calcium are absent (Figure 3.62). From associated spectra, a considerable reduction in both elements is apparent. Compared with control sample spectra (Figure 3.59), elemental composition values for each element are down 3.3% and 1.2% respectively, demonstrating a reduction in the cementing component at the surface of BB1. Surface dissolution is further exemplified in BB2 section A, in Figure 3.64 quartz and aluminium are intact but there is a very distinct loss of magnesium and calcium, reflected in the associated spectra where together they only account for 1.1% of the sample. Dolomite dissolution is less apparent in maps stitched together from BB3 (Figure 3.67), on inspection of the associated spectra, however, the surface map has considerably less magnesium and calcium than the area mapped further from the surface (Figure 3.68 and Figure 3.69).

Another clear finding from mapping work and analysis of spectra is the fluctuation of carbon, which represents the resin that bonds the sample to the glass slide that the petrographic thin section is mounted on and is used in this research as a proxy for secondary porosity. In areas where dolomite dissolution is prevalent, carbon percentages increase. In the control sample spectra (Figure 3.59), carbon occupies 16.5% of the mapped section. However, in BB1 section B (Figure 3.62) and BB2 section A (Figure 3.64) where dolomite dissolution has occurred, the carbon percentage increases to 38.2% and 38.5% respectively, indicating the formation of secondary porosity. It must be noted that these percentages will be inflated slightly since a small section of the glass slide beyond the sample surface is present in the map.

To further quantify findings from mapping, ImageJ was used where a more accurate depiction of how far dolomite dissolution extends into samples and how quickly key dolomite forming elements increase in abundance with depth beyond the weathered edge could be gained. In BB1, magnesium (Figure 3.71) and calcium (Figure 3.73) are almost completely absent from the first 0.4mm of stone before there is a sharp increase in both elements over the next 0.2mm. This sharp transition indicates that the surface of the stone is very different from the remainder of the stone, there is no buffer zone where dolomite recovers gradually. This finding affirms the idea that surface dissolution could lead to surface failure as the weathered edge is starkly different in characteristics to the remainder of the stone and will therefore behave differently (Veerle *et al.*, 2009). This is a key focus area in climate sensitised samples to determine whether exposure to climate changed futures in laboratory weathering simulations further enhances the surface weathered edge or potentially leads to surface

failure. Similarly, in BB2, magnesium (Figure 3.75) and calcium (Figure 3.77) are sparse at the surface for the first 1mm and 1.2mm, respectively. Moving between 0.3 and 0.5mm further into the stone, both elements are present to a considerable extent indicating the dolomite cement is well intact just below the weathered edge. It can be said, therefore, based on findings from BB1 and BB2 that beyond the weathered edge, the stone is relatively pristine within approximately half the distance of the weathered area. For example, if the weathered edge is 1mm in depth, within approximately 0.5mm beyond that, dissolution is no longer observable.

BB3 is mapped slightly differently from the other broch samples to detect two dissolution zones. A very slight dissolution area can be seen on the edge of the sample in the map, and this is reflected in ImageJ analysis (Figure 3.79 and Figure 3.81) where the grey value for magnesium and calcium is low at the immediate surface before quickly spiking with depth. A second dissolution area at a depth of 1.5mm is only detectable in the calcium grey value intensity. It is unusual to see a dolomite dissolution zone, albeit a small one, at such a depth within the stone, however, from the thin section scan of BB3 (Figure 3.66), it has likely developed along a distinct weakness plane or microcrack where water can penetrate the minor pore space and facilitate dolomite dissolution.

From results obtained and subsequent interpretation, it can be seen that above surface exposure for approximately 2000 years has caused a weathered edge of between 0.5mm and 1.50mm to form on broch samples through the dissolution of dolomite. As mentioned previously, this could result in surface loss. A key question that is addressed in subsequent experimental work, is whether exposure to climate change futures will deepen this weathered edge or cause it to fail. Crucially, SEM-EDX mapping and quantification through ImageJ provides a robust baseline that the climate sensitised samples are compared to, allowing the effects of climate change on the samples to be determined.

3.6.3 SEM-EDX Conclusion

SEM-EDX analysis has contributed greatly to the baseline understanding of control rock and broch stone associated with Clachtoll and Borwick. The ability to visualise elements separately and together when desired has allowed insight to be gained into the role that each element plays within the greater stone fabric. New findings have emerged from each sandstone type; in Torridonian Sandstone, the minor cementing influence of magnesium alongside iron which had gone unnoticed in XRD, and petrographic thin section work has

been discovered. Additionally, the clay layers seen in control samples have been characterised as a predominantly illite rich clay with minor kaolinite inclusions as a result of K-feldspar dissolution.

In Stromness Flagstone where dolomite dissolution is clear in broch samples, mapping work has allowed the interaction of magnesium and calcium to be more closely analysed and defined. Crucially, their abundance with depth has been quantified through associated SEM-EDX spectra and the successful use of ImageJ auto-thresholding software. Additionally, dark nodules throughout the stone fabric have been chemically characterised as being composed of primarily iron and sulphur – making them sulphide nodules (pyrite). These are inherently volatile nodules that could significantly accelerate the weathering of the Flagstone.

As indicated, the findings obtained through SEM-EDX analysis provide new insights and contribute to the overall understanding of each sandstone type. Key strengths and weaknesses within samples have been highlighted and the potential for weak areas to be exacerbated through exposure to climate changed futures becomes clear in subsequent chapters.

3.7 Chapter Conclusion

The principal aims of this chapter have been to characterise both sandstone types and understand, through the comparison of control rock and broch stone, how each sandstone has weathered over the last ca 2,000 years as part of culturally significant brochs. Crucially, from this comparison, strengths alongside potential vulnerabilities within each sandstone have been identified (Table 3.29).

Table 3.29 - Vulnerabilities and strengths associated with each sandstone type and passage of time from unearthed control rock to broch stone exposed above surface for ca. 2000 years

Sandstone Type	Control		Broch	
	Vulnerabilities	**Strengths**	**Vulnerabilities**	**Strengths**
Torridonian Sandstone	Distinct clay banding at sample surfaces	Tightly packed grain supported fabric	Microcracks	Tightly packed grain supported fabric
Stromness Flagstone	Rapidly alternating bedding structure	Intact cement	Dolomite dissolution Sulphide nodules of varying sizes Microcracks	The effect of dissolution is limited to the immediate surface of the stone

As a key foundation to any geological study, the physical characteristics of each sandstone were determined by following relevant British standards, revealing the high density and low porosity nature of both the Torridonian Sandstone and Stromness Flagstone. Following on from this, a suite of analytical techniques has helped robustly characterise the samples.

XRD firstly revealed the key bulk crystalline minerals which make up each sandstone, results from this technique were used as a route map for subsequent petrographic thin section observations. Additionally, XRD helped to inform that due to the highly compacted nature of the study sandstones, salt does not play a significant enough role in their degradation to be included in any CEF experiment.

Petrographic thin section work gave the first in-depth look at each sample type, from which grain relationships could be understood and any weathering indicators identified. Among other features, distinct clay layers in Torridonian Sandstone control rock were identified as well as clear dissolution features around the perimeter of Borwick broch stone. Furthermore, the occurrence of distinct pyrite nodules in Stromness Flagstone was noted. Additionally, physical weaknesses such as microcracks were identified in both sandstone types, although more prevalent in Borwick samples.

XRD analysis was implemented once again to quantify the clear dissolution feature in the Borwick Broch stone. A drastic reduction in dolomite, the key cement in Stromness Flagstone, is seen in the comparison of ‘inner’ and ‘outer’ stone material.

It was not until SEM-EDX mapping work that quantification of features and phenomena identified through thin section work could occur. Evidence was presented to suggest that the distinct clay layers in the Torridonian samples are likely not detrital and have instead formed through primarily K-feldspar dissolution, which produced an illite rich clay with traces of kaolinite. In the Stromness Flagstone, dolomite dissolution could be quantified, with detail emerging as to the depth of the feature and the implication it has for future surface failure.

Results indicate that Torridonian Sandstone broch stone appears robust despite above surface exposure. Interestingly, the clay layers identified in control rock could be potential weak points that are monitored in the experimental phase of this research. Conversely, the Borwick control rock is robust, while significant dissolution weaknesses attributable to exposure in Borwick Broch have been identified (Table 3.29).

Moving forward, the key aim of this research is to determine how these samples respond chemically and physically when exposed to climate changed futures derived from UKCP18 climate projections in CEF experiments. Specific attention is paid to weaknesses identified throughout this chapter (Table 3.29); however, it is anticipated that new understandings surrounding the robustness of each sandstone type will emerge, with important implications on the longevity of Scotland's historic environment in a climate changed future.

4 A Climate Changed Year

4.1 Chapter Introduction

This chapter focuses on analyses of sandstone samples utilised in a 'Climate Changed Year' CEF experiment. Incorporated within this are a range of experimental samples that have been sensitised to temperature, humidity and precipitation fluctuations associated with data obtained from UKCP18 RCP8.5 for the year 2055 in Northern Scotland (experimental chamber), together with control samples exposed to 2018 climate parameters for the same region, also obtained from UKCP18 RCP8.5 (control chamber). Comparisons made between these sets of samples allow the impacts of climate change on the focus sandstones to be determined from changes that would have occurred had there been no change in climate between 2018 and 2055.

Macro-scale physical changes have been identified through close examination of high-quality sample images taken before and after the experiment, while surface salt formation has been explored through XRD and X-Ray Fluorescence (XRF) analyses. Similarly, samples have been weighed before and after the experiment, allowing any change in mass to be understood, moreover, an indicative decay model has been extrapolated from this data. Thin section and further SEM-EDX work with image analysis have been implemented to study micro-scale alterations in the samples. These techniques aid in the identification of early indications of a weathering change or acceleration in the focus sandstones, attributable to climate change.

4.2 Visible Alterations

Each sample used in the CEF was photographed before and after the experiment, these images have been compared to determine any visible surface alterations. Images provided focus on samples showing observable alterations that are detectable by the naked eye, with those showing no change serving as a comparison where necessary.

4.2.1 Control Chamber

4.2.1.1 Temperature and Humidity

Of the four samples exposed to temperature and humidity fluctuations akin to those experienced in Northern Scotland in 2018, physical alterations are seen solely in BB1 (3) (Figure 4.1).

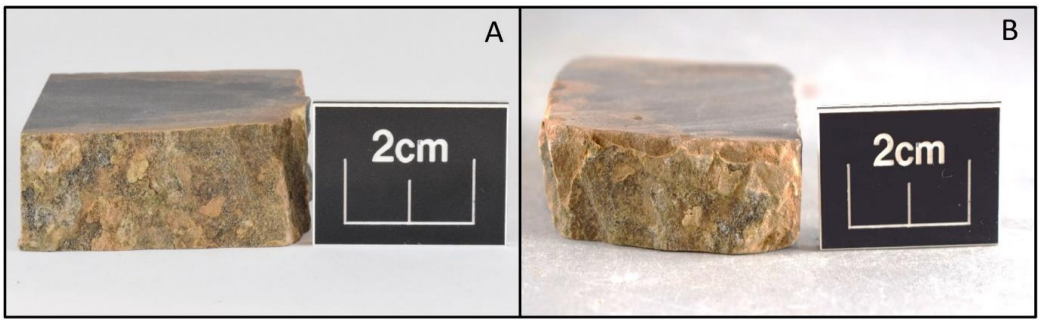

Figure 4.1 - Surface alteration on BB1 (3) before (A) and after (B) CEF control experiment showing flaking of surface material

Surface loss can be visualised through a comparison of Figure 4.1 A and B. The stone surface has altered noticeably as a result of the control experiment with distinct signs of flaking. Conversely, a Torridonian sample from Clachtoll Broch exposed to the same treatment shows no discernible surface change (Figure 4.2).

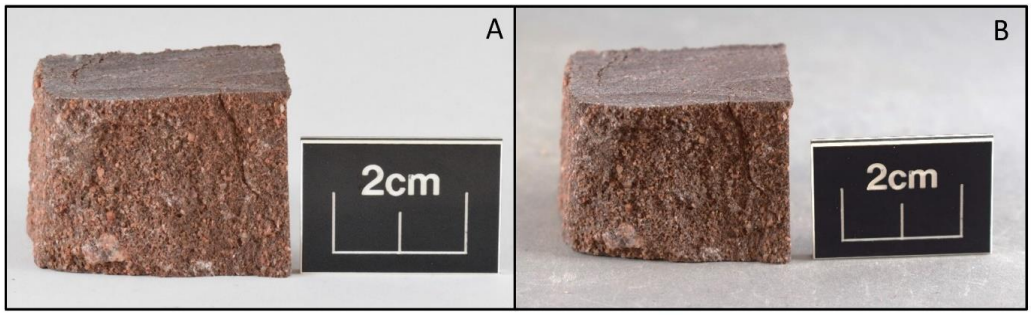

Figure 4.2 - CB1 (3) before (A) and after (B) CEF control experiment

4.2.2.2 Temperature, Humidity and Precipitation

A broch sample associated with Borwick and a background geology sample from Clachtoll exhibit surface change as a result of the control temperature, humidity, and precipitation experiment (Figure 4.3 and 4.4).

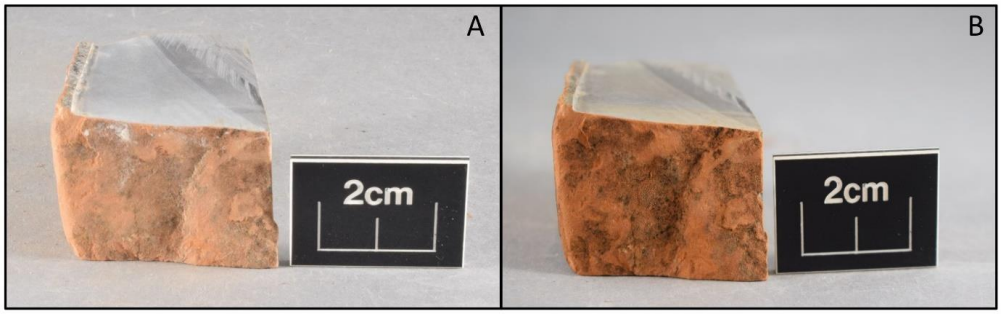

Figure 4.3 - BB1 (4) before (A) and after (B) CEF control experiment. Surface darkening is seen on the 'after' sample

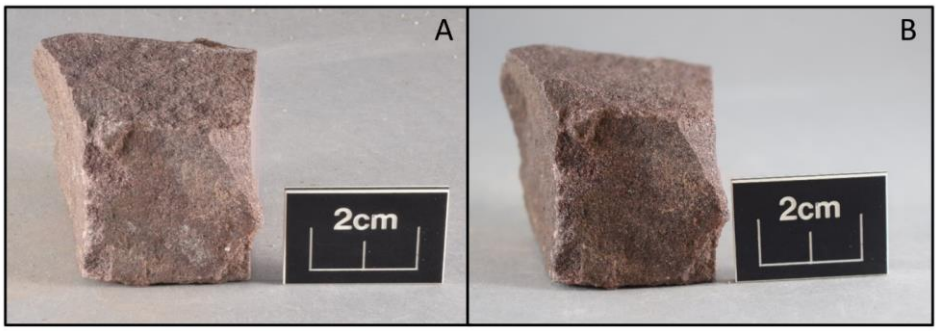

Figure 4.4 - CC1 (4) before (A) and after (B) CEF control experiment. Surface darkening is seen on the 'after' sample

A clear colour change can be seen on the surface of both BB1 (4) and CC1 (4), the samples appear to have darkened through exposure in the CEF. This is particularly apparent on the surface of the Borwick sample.

4.2.2 Experimental Chamber

4.2.2.1 Temperature and Humidity

Two of the three Borwick Broch samples exposed in the CEF to temperature and humidity conditions predicted for 2055 failed, as shown in Figure 4.5 and Figure 4.6.

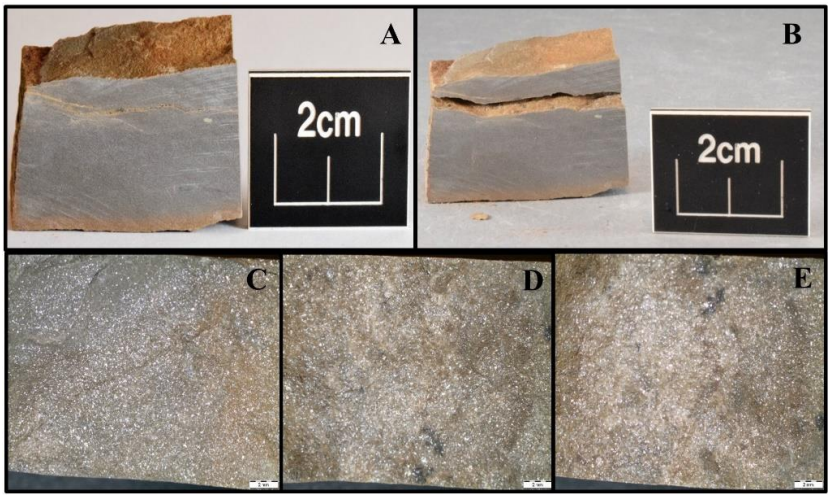

Figure 4.5 - BB1 (1) before (A) and after the experiment (B). Binocular microscope images of the original stone surface (C), the underside of the original surface (D) and the newly exposed stone surface

A pre-existing microcrack can be seen in Figure 4.5 (A) taken before the experiment, running the length of the sample close to the surface. In Figure 4.5 (B), taken after the experiment, the surface above the microcrack has become detached from the stone. Figure 4.5 C, D and E

were taken using a binocular microscope (2mm scale). As evidenced in D and E, the microcrack appears to have failed along a distinct mica abundant joint within the stone.

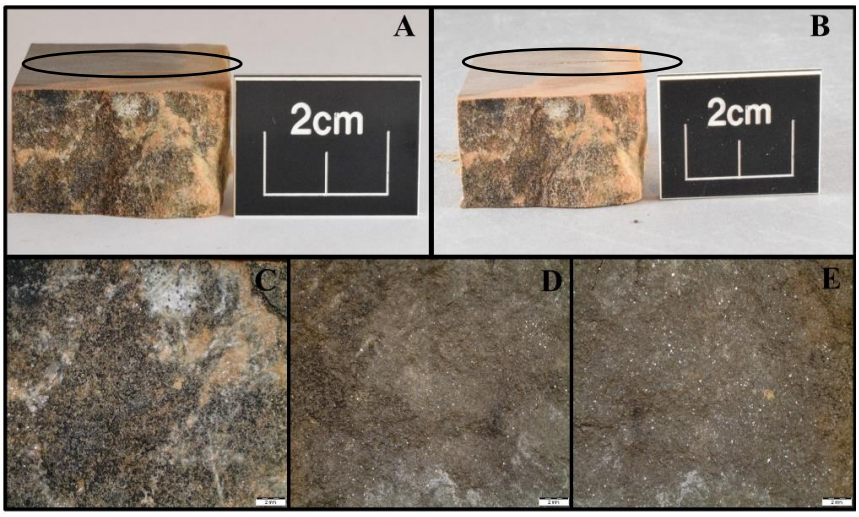

Figure 4.6 - BB3 (8) before the experiment (A), surface loss seen at depth after the experiment (B). Original stone surface (C), the underside of the original surface (D) and newly exposed surface (E)

Similar in character to Figure 4.5, a faint microcrack can be seen (circled) in Figure 4.6 (A) taken before the experiment, running the length of the sample at a depth of approximately 1cm. In Figure 4.6 (B), taken after the experiment, a considerable amount of stone above this pre-identified weakness has become detached. Figure 4.6 C, D and E were taken using a binocular microscope (2mm scale). Figure 4.6 D and E show that a similar failing has occurred in this sample as the sample shown in Figure 4.5, whereby the stone has failed along a distinct mica rich joint, leading to significant stone loss.

Visible changes to the Torridonian Sandstone from Clachtoll are less apparent, as evidenced in Figure 4.7 and Figure 4.8.

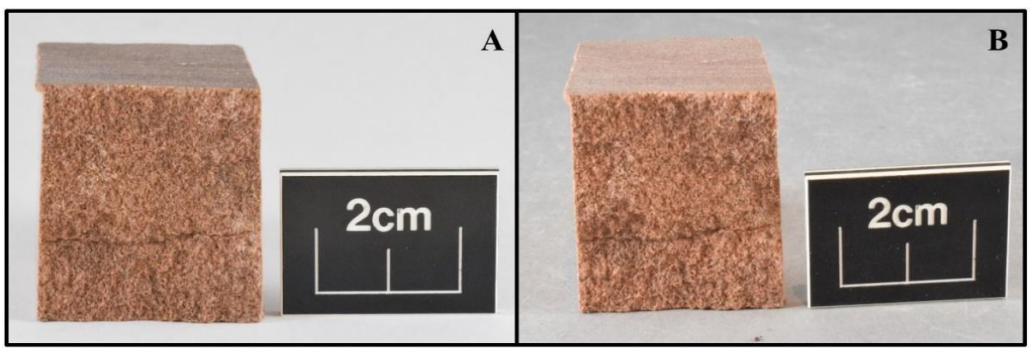

Figure 4.7 - CB2 (5) before (A) and after (B) CEF experiment. Granular loss seen at the bottom edge of the stone surface (B)

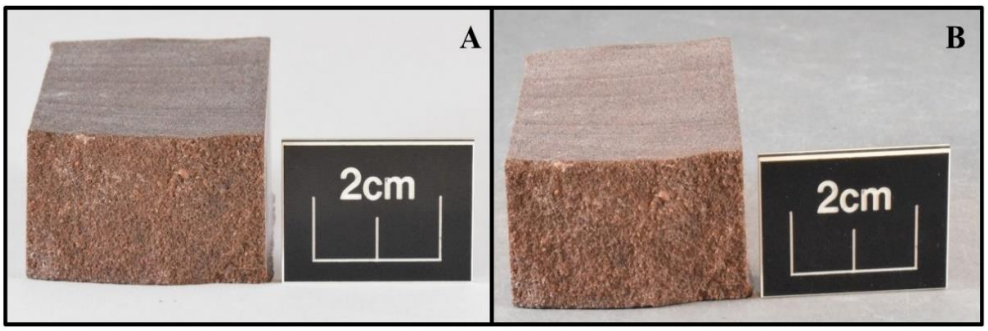

Figure 4.8 - CB3 (9) before (A) and after (B) CEF experiment. Granular loss seen at the bottom edge of the stone surface (B)

No major change is seen in the samples upon completion of the temperature and humidity climate changed year, however, surrounding the exposed surface perimeter there appears to have been a slight loss of stone material, seen most clearly at the bottom edge of the 'after' samples (Figure 4.7 and Figure 4.8).

4.2.2.2 Temperature, Humidity and Precipitation

Borwick samples exposed to temperature, humidity and precipitation show signs of surface salt formation (Figures 4.9 and 4.10).

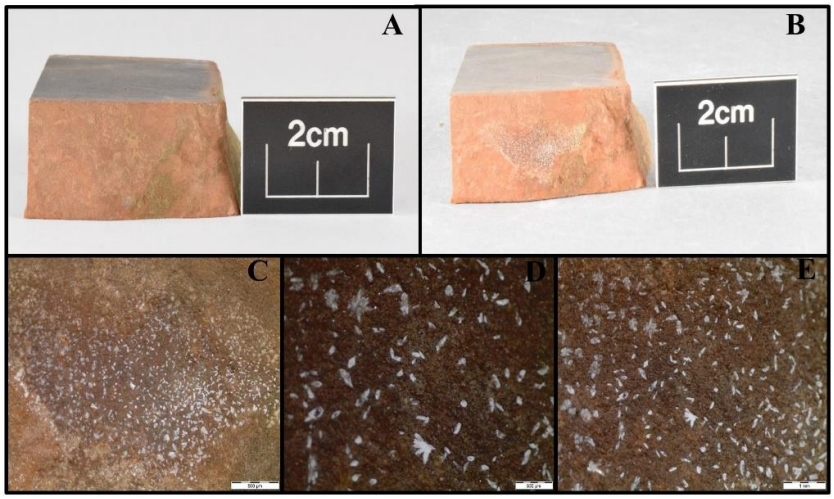

Figure 4.9 - BB2 (6) before (A) and after (B) CEF experiment. Salt formation is seen on the exposed surface of the stone (C, D, E)

Salt formation is particularly prevalent on BB2 (6) shown in Figure 4.9. Before the experiment (Figure 4.9 A), there is no sign of salt on the surface. After completion of the climate change experiment, salt can be seen clearly by the naked eye in Figure 4.9 B as well as under the binocular microscope in Figure 4.9 C, D (500 µm scale) and E (1mm scale).

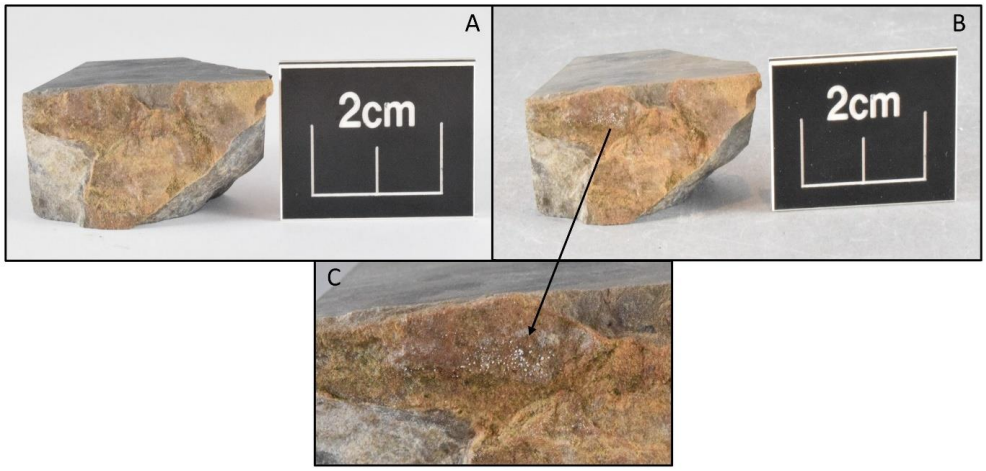

Figure 4.10 - BC3 (9) before (A) and after (B) CEF experiment. Salt formation is seen on the exposed surface of the stone (C)

Salt formation, although less prevalent one BC3 (9) when compared to BB2 (6), is still a clearly identifiable surface change that has occurred through exposure to 2055 climate conditions simulated in the CEF. Conversely, there is very little observable change in the Torridonian Sandstone with the introduction of precipitation to the experiment, aside from potential granular loss at the bottom edge of CB2 (6) (Figure 4.11).

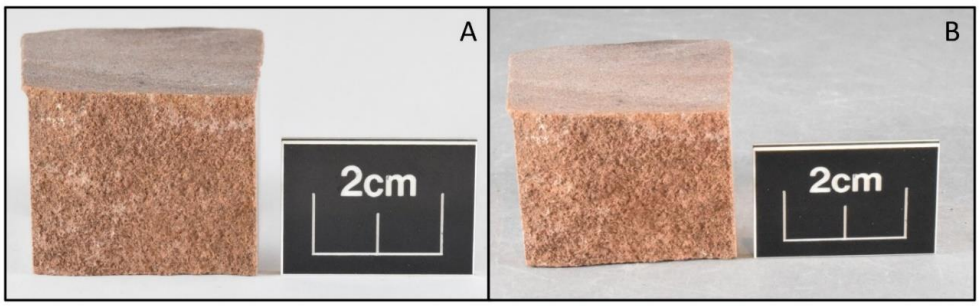

Figure 4.11 - CB2 (6) before (A) and after (B) CEF experiment. Potential granular loss seen at the bottom edge of the sample (B)

4.2.3 Visible Alterations Discussion

The most significant changes reflected in the samples exposed to temperature and humidity fluctuations in the CEF are seen on the surfaces of Borwick Broch stone, which appear considerably more vulnerable to weathering than samples from Clachtoll. Particular areas of weakness appear to be lateral fractures that run parallel with the bedding of the stone, exemplified in Figure 4.5 and Figure 4.6 where two Borwick Broch samples have failed along these weaknesses. Although the microcracks were present before the CEF experiment,

the conditions simulated in the chamber have caused the feature to reach a tipping point and fail, leading to extensive surface loss. Conversely, Borwick control rock shows little to no sign of surface change, indicating that the above surface exposure of stone in Borwick Broch has weathered the material to a sufficiently weak state that the climate change experiment has caused two of the samples to fail. This highlights the importance of the 'memory effect' held within a stone emplaced above the surface compared with rock manifested within geological deposits. The history of stone within a monument is a fundamental aspect of this research, whereby, samples taken from heritage sites are more vulnerable to future weathering due to their weathering history, particularly clearly demonstrated in this experiment with respect to Borwick Broch samples.

The Torridonian Sandstone associated with Clachtoll, by comparison, appears relatively unaffected by the climate change experiment. The only noticeable change upon a comparison of the before and after images is granular loss around the edges of the stone (Figure 4.7 Figure 4.8). This observation is quantified through analysis of mass measurements provided in a subsequent section (Section 4.3 Mass Analysis).

Alterations brought about by the temperature and humidity aspect of the experiment can be characterised as physical changes to the stone such as cracking and granular loss. Conversely, with the addition of precipitation, more of a chemical change occurs, particularly on the surface of the Borwick Broch stone, manifested as salt formation. Despite the abundance of microcracks present in the Stromness Flagstone, none of the samples utilised in the experiment with precipitation failed. All microcracks have an inherent tipping point and it is possible that samples utilised in the temperature and humidity chamber were closer to failure than the samples used in the experiment with added precipitation. Additionally, it cannot be ruled out that sample failure would have occurred regardless of what chamber the failed samples were used in. What is clear, however, is that surface salt formation can be seen exclusively on Borwick samples (Figure 4.9 and Figure 4.10) used in the added precipitation experiment and is seen most clearly on BB2 (6) (Figure 4.9). On both affected samples, the salt has formed in a slight surface depression, once more highlighting the importance of using non-fresh-cut samples in this experiment; surface roughness is a determining factor in the nature and extent of salt formation (Bede, 2000). Weathering as a result of salt crystallisation is controlled primarily by temperature and moisture oscillations. This experiment frequently cycled these parameters, causing salts held within the samples to be mobilised and brought to the surface in solution where drying and subsequent crystallisation could occur, a process

which in turn stimulates granular loss and disaggregation, eventually leading to the occurrence of flaking and even surface loss in extreme cases. As discussed previously in this thesis, in a climate changed future stone may be wetter for longer with increased rainfall and so when drying and subsequent salt crystallisation does occur, it can be more destructive to the stone fabric.

Consistent with findings in the temperature and humidity experiment, the addition of precipitation does not appear to have affected the Clachtoll samples other than potential granular loss.

It is imperative to set findings from the climate change experiment in the context of a control experiment. Similar to outcomes from the experimental chamber, exposure to temperature and humidity in the control chamber elicited physical change on the surface of the Borwick Broch stone (Figure 4.1). Although flaking appears to have occurred, the surface has remained intact, in direct contrast to the same stone type utilised in the climate change experiment which failed (Figure 4.5). This indicates that at present, the Stromness Flagstone is particularly susceptible to weathering while exposed above the surface. However, with exposure to warmer, wetter simulated winter months and warmer, drier simulated summer months associated with climate change in Scotland, the sample exhibits a more destructive response. The Borwick control, Clachtoll Broch and Clachtoll control samples show no change after the control experiment and, most notably in the Clachtoll samples, no granular loss is evidenced around the edges of the samples as was seen in the climate change experiment.

The inclusion of precipitation elicited surface darkening on Borwick and Clachtoll Broch samples, however, no evidence of salt formation is seen on the surface of the Borwick Broch sample, contrasting with the same sample type utilised in the experimental chamber.

4.2.4 Visible Alterations Conclusion

Key changes in the samples can be seen concerning sandstone type, sample location and exposure to differing treatments. In both the experimental chamber and the control chamber, pronounced surface alterations are seen in Borwick Broch samples, indicating that the Stromness Flagstone is more vulnerable to weathering than the Torridonian Sandstone. Furthermore, broch samples have visibly altered more than control samples, indicating that the use of authentic sandstone material from the historic environment is crucial in understanding how sandstone incorporated in historic buildings and monuments will proceed

to weather with exposure to changing temperature, humidity, and precipitation parameters. Had this research solely utilised background geology samples, very little if any alteration would have occurred, as evidenced in the CEF experiments. Additionally, no relatability to pre-weathered culturally significant stone would have been achieved. This finding robustly supports the use of non-fresh-cut sandstone while highlighting that pre-existing weaknesses in the sandstones, brought about by weathering associated with exposure above surface, are particularly susceptible to reaching a tipping point and failing in a climate changed future. As highlighted in the previous section and crucial to this research, stone response in the experimental chamber is more pronounced than in the control chamber, indicating that conditions simulated in the experimental chamber are more detrimental to the sandstone.

Through analysis of the visible changes that have occurred on sandstone utilised in the CEF, it can be concluded that Stromness Flagstone obtained from the built environment is most vulnerable to weathering in a climate changed future when compared with Clachtoll Broch stone and control rock, as well as pristine Stromness Flagstone obtained from the background geology. Furthermore, characteristics such as surface roughness have proved to be a determining factor in the occurrence and extent of surface weathering and salt formation, showcasing the importance of the use of non-fresh-cut samples in this research.

4.3 Mass Analysis

As a basic metric of observing and quantifying change within samples, each one was weighed before and after exposure to weathering simulation treatments. Within the experimental chamber where three samples of each type were exposed to each treatment, mean mass loss and standard deviation across all samples could be calculated (Table 4.1). Mean loss in grams was calculated first, from which a mean percentage loss could be calculated. Within the control experiment, only one sample of each type was exposed to each treatment due to sampling restrictions associated with SMC, limiting the extent of analysis that could occur. Calculated percentage loss was scaled up to a 1kg block and a broch structure (based on Dun Telve Broch which weighs approximately 2000 tons, equivalent to 1814369 kg), the limitation being that these calculations assume percentage loss and sample shape are constant with increasing block size/mass. In reality, however, the diverse shape and characteristics of building stone adds significantly more complexity to any decay model calculation. Table 4.1 is provided below as a simple metric of observing change solely within samples used in the experimental chamber.

Table 4.1 - Indicative mass loss values observed after the climate changed year experiment where three samples of each type were exposed to two different treatments. (T = Temperature, H= Humidity, P = Precipitation). Broch mass = 2,000 Tons (1814369 kg/1814.369 Mg)

Sample	Treatment	Mean Loss (g)	SD (g)	Mean Loss (%)	SD (%)	1kg Block loss (g)	Broch Loss (Mg)
Clachtoll Broch	T & H	0.157	0.178	0.205	0.249	2.05 ± 2.49	3.72 ± 4.51
	T, H & P	0.053	0.025	0.062	0.021	0.62 ± 0.21	1.124 ± 0.38
Clachtoll Control	T & H	0.027	0.006	0.038	0.014	0.38 ± 0.14	0.69 ± 0.25
	T, H & P	0.010	<0.0001	0.016	0.002	0.16 ± 0.02	0.29 ± 0.36
Borwick Broch	T & H	0.057	0.015	0.112	0.029	1.12 ± 0.29	2.03 ± 0.53
	T, H & P	0.083	0.015	0.148	0.030	1.48 ± 0.30	2.69 ± 0.54
Borwick Control	T & H	0.017	0.006	0.041	0.025	0.41 ± 0.25	0.74 ± 0.45
	T, H & P	0.003	0.012	0.007	0.036	0.07 ± 0.36	0.13 ± 0.65

Table 4.1 demonstrates that no obvious trend can be detected in the samples based on their treatment, however, both Clachtoll Broch and Borwick Broch samples appear to lose more mass from the experiment than the control samples. This indicates, as anticipated through physical change analysis, that pre-stressed stone that has been exposed above the surface, is more vulnerable to exacerbated decay compared with rock that has not been removed from the geology and placed in a built structure.

It must be noted that there is a large error associated with the Clachtoll Broch T & H and Borwick Control T, H & P samples. However, in all other samples, the error is relatively constrained. In the experimental chamber (Table 4.1), a small, seemingly negligible loss of material is seen across the samples, likely manifested as a granular loss. Crucially, this has occurred over a single experimental phase designed to mimic one year of real-time exposure. It is important to recognise that seemingly negligible values obtained in this experiment, become significant over the lifetime of a historic building, whereby, through decades of exposure, a sample will reach a tipping point and material loss will be exacerbated. The rate at which any given sample will reach a tipping point could be accelerated through climate change, whereby compounded small-scale change may move an equilibrium over an

accelerated decay threshold. Additionally, when the percentage loss is scaled up to a broch, the numbers become more alarming with up to thousands of kg of stone under threat each year.

This research acknowledges that these are indicative values and the true way in which granular loss impacts an entire structure in a climate changed future cannot be inferred from this analysis alone. However, this data is nevertheless important as the figures obtained are a direct consequence of exposing sandstone to laboratory simulated climate change.

Table 4.2 - Indicative mass loss values observed after the climate changed year control experiment where one sample of each type was exposed to two different treatments. (T = Temperature, H= Humidity, P = Precipitation). Broch mass = 2,000 Tons (1814369 kg/ 1814.369 Mg)

Sample	Treatment	Loss (g)	Loss (%)	1kg block loss (g)	Broch Loss (Mg)
Clachtoll Broch	T & H	0.020	0.030	0.300	5.44
	T, H & P	0.040	0.050	0.500	9.07
Clachtoll Control	T & H	**GAIN**	**GAIN**	**GAIN**	**GAIN**
	T, H & P	**GAIN**	**GAIN**	**GAIN**	**GAIN**
Borwick Broch	T & H	0.930	1.230	12.300	223.17
	T, H & P	**GAIN**	**GAIN**	**GAIN**	**GAIN**
Borwick Control	T & H	**GAIN**	**GAIN**	**GAIN**	**GAIN**
	T, H & P	0.000	0.000	0.000	0.00

The data presented in Table 4.2 is of limited use due to sampling restrictions. In samples that do exhibit a mass loss, they appear to do so more drastically than samples utilised in the experimental chamber, however, with results only obtained from one sample, no robust conclusion can be drawn.

Although limited in its scope, this is an interesting avenue of research. With a greater number of samples used in both chambers, a clear understanding could be gained as to how different sample types suffer from granular loss through exposure to weathering treatments and crucially if the values obtained from climate sensitised samples vary at all from those exposed to current climate conditions.

From results obtained it can be said with confidence that samples have generally lost mass which can be attributed to granular loss and broch samples appear to be more affected than

control samples, however, the significance of this loss in relation to climate change cannot be determined due to a lack of samples in the control experiment to serve as a baseline.

4.4 Salt Analysis

Salt formation occurred predominantly on the surface of sample BB2 (6) (Figure 4.9), as well as to a limited extent on sample BC3 (9) (Figure 4.10). Therefore, XRD and XRF analyses were undertaken on BB2 (6) where most salt was present.

4.4.1 XRD Analysis

A small amount of material was scraped from a surface section of BB2 (6), including as much salt as possible. This was ground with a mortar and pestle, mixed with acetone, and placed on a sample holder for XRD analysis to occur.

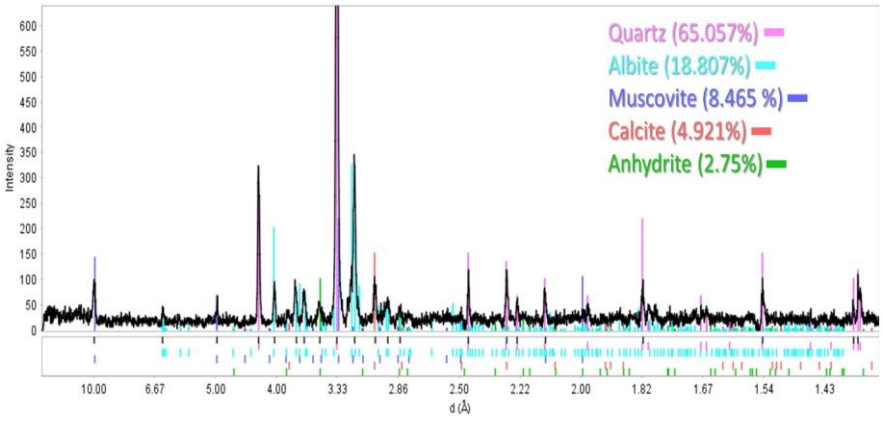

Figure 4.12 - XRD analysis results from salt scraped from the surface of BB2 (6)

Results presented in Figure 4.12 show that a small amount of salt was detected using XRD, namely calcite (4.921%) and anhydrite (2.75%), with the rest of the analysed material being made up of key rock constituents such as quartz, feldspar, and mica.

4.4.2 X-Ray Fluorescence (XRF) Analysis

SEM-EDX analysis was planned on the salt, however, the sample was too large to fit within the sample holder. To avoid cutting the sample which would impede subsequent thin section manufacture, a portable XRF was used. XRF was focused on 3 areas; the side of the sample, the sample surface where no salt is observed and the sample surface where salt is observed. Results of key elements are provided in Table 4.3.

Table 4.3 - BB2 (6) XRF analysis, key element results (%)

Sample	Ca	Ca Error	Mg	Mg Error	S	S Error	Cl	Cl Error	P	P Error
No Salt	0.44	0.066	<LOD	0.854	0.117	0.006	<LOD	0.006	0.197	0.016
No Salt	0.407	0.068	<LOD	0.843	0.133	0.007	<LOD	0.006	0.24	0.017
Side	6.631	0.151	2.084	0.686	0.066	0.006	0.088	0.005	0.125	0.019
Side	6.607	0.146	1.887	0.684	0.078	0.006	0.075	0.005	0.089	0.019
Salt	3.418	0.117	1.506	0.592	0.174	0.012	0.031	0.004	0.316	0.145
Salt	3.89	0.121	1.831	0.62	0.156	0.012	0.039	0.004	0.339	0.144
Salt	3.136	0.117	1.943	0.599	0.194	0.012	0.031	0.004	0.419	0.147

4.4.3 Salt Analysis Discussion

The formation of salt on the surface of samples shown in Figure 4.9 and Figure 4.10 can be attributed to their surface characteristics and incorporation in a CEF experiment, exposing them to climate change conditions. There was no evidence of surface salt before the experiment, however, due to Borwick Broch's coastal location, salt of some kind was likely present within the samples before experimental work. When analysis for trace salts within Borwick Broch samples was conducted in the previous chapter (Figure 3.13), halite and sylvite were the salts discovered. The use of rainwater in the climate change experiment has rehydrated the salt, transporting it in solution to the surface of the stone before evaporation occurred, leaving crystals on distinct areas of the surfaces of BB2 (6) and BC3 (9) (R. C. Murray, 1964; Luo et al., 2019).

As seen in XRD results (Figure 4.12), calcite and anhydrite are the salts identified on sample BB2 (6). The detection of anhydrite, in particular, is unexpected after baseline XRD work, however, its occurrence can be understood as it is an evaporite found commonly in carbonate-rich rocks, including dolomite.

XRF results (Table 4.3) provide greater insight into specific elemental composition within sampled areas and offer a contrast between 3 different sample locations on BB2 (6). As is hypothesised from XRD results, the salt deposit is likely an evaporite. These can be split into three groups: carbonates, sulphates, and chlorites. Of particular relevance to the Stromness Flagstone are carbonates and sulphates due to the high occurrence of these minerals within

the rock type (Bissell, Harold J et al., 2021). Conversely, the chlorite group containing salts such as halite and sylvite can be ruled out; as seen in Table 4.3, chlorine levels are higher on the side of the sample than on the salt itself.

A case can be made for several salts from the carbonate and sulphate groups, including calcite. Although the highest percentage of calcium is seen on the side of the sample, likely influenced by the abundant dolomite cement, it can be seen on comparison of the two surface sites, that calcium is far more abundant in analysed salt sites. Furthermore, calcite is seen in XRD results too (Figure 4.12). Concerning sulphates, it is clear that sulphur percentage is highest on the salt areas of the surface (Table 4.3), meaning it is entirely feasible that salts such as anhydrite and gypsum are present.

A further noteworthy finding is the percentage of phosphorus seen, which is most abundant on the salt surface compared with other sampled sites. Phosphates, however, are most commonly seen in igneous, iron-rich rock types, with several hundred phosphate minerals known to exist, displaying a wide range of characteristics. Of note, phosphorous rich sedimentary rocks do exist in the form of phosphorite, which can be found in sedimentary successions alongside a wide range of minerals, including dolomite (Attfield, 2001; Huminicki and Hawthorne, 2002; Prothero and Schwab, 2004; Porder and Ramachandran, 2013; Valsami-Jones, 2021). As phosphate was not detected in XRD work (Figure 4.12), its presence in XRF results may be due to surface contamination by phosphorous.

Given that the amount of salt that has formed on the surface is extremely low, an exact determination of the salt type cannot be made, however, by process of elimination based on results obtained, it can be seen to be an evaporite from the calcite or sulphite group. It can be hypothesised that the salt present on the surfaces of BB2 (6) and BC3 (9) is a complex mixture of several salts from the aforementioned groups.

4.4.4 Salt Analysis Conclusion

There is no evidence of salt on the surface of any sample before the experiment or on any samples after the control experiment. Its occurrence after the climate change experiment is likely a result of the conditions simulated within the chamber. However, the link between climate change and salt weathering is heavily dependent on rainfall dynamics as well as stone characteristics. This research could not simulate wind-driven rain within the climate chamber which can drive moisture deeper into stone, keeping salt in solution for longer before crystallisation can occur, and exert greater pressure on the surrounding stone constituents.

The salt is pre-existing within the stone before the experiment, it is of interest that conditions simulated in the chamber have caused the observed salt formation, however, its link to climate change is uncertain given the limitations of the chamber.

4.5 Petrographic Thin Section Analysis

Analysis of samples at this stage of the research is focused on weathering indicators and micro-scale features that are likely to have transpired within rock and stone fabrics as a result of their exposure to simulated weathering. Thorough petrographic analysis of each sample type was presented in Chapter 3, including completed petrographic analysis tables, providing extensive detail on sandstone fabric, grain size, grain contacts, cementing, mineralogy, porosity, and percentage composition of rock and stone constituents. These observations are not repeated in this chapter; instead, photomicrograph focused on sample surfaces are presented, showing weathering indicators or lack thereof as compared with baseline analyses undertaken in Chapter 3.

Additionally, through the suite of analytical techniques implemented in Chapter 3, features considered to be potentially vulnerable to weathering and degradation in a climate-changed future were highlighted. Specifically, these include distinct clay layers and microcracks within Clachtoll samples together with dolomite dissolution, volatile sulphide nodules and microcracks present in Borwick samples. Focus is now placed on how these features have reacted to weathering simulations, and if, as hypothesised, they are vulnerable to the climatic change anticipated in Scotland in the coming decades. Furthermore, differences between the weathering of control rock and broch stone are identified together with weathering differences resulting from sample treatment in the CEF (cf. Research Design and Methodology).

The following petrographic thin section analysis is divided into the experimental chamber and control chamber samples with subsections of sample type and treatment exposure, facilitating a discussion and conclusion section.

4.5.1 Experimental Chamber

As presented in Chapter 2, samples utilised in these chambers have been exposed to either temperature and humidity or temperature, humidity and precipitation fluctuations anticipated in Northern Scotland in 2055. Data has been obtained from UKCP18 RCP 8.5 at a high emission scenario at the 50% probability level, in keeping with HES's recent climate change risk assessment (Historic Environment Scotland, 2018b).

4.5.1.1 Clachtoll Temperature and Humidity

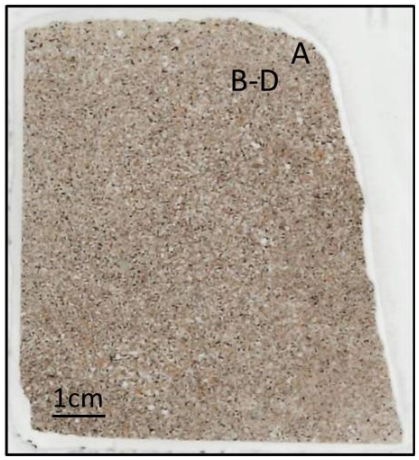

Figure 4.13 - Petrographic thin section scan of CC1 (1), with sites A-D focussing on a microcrack

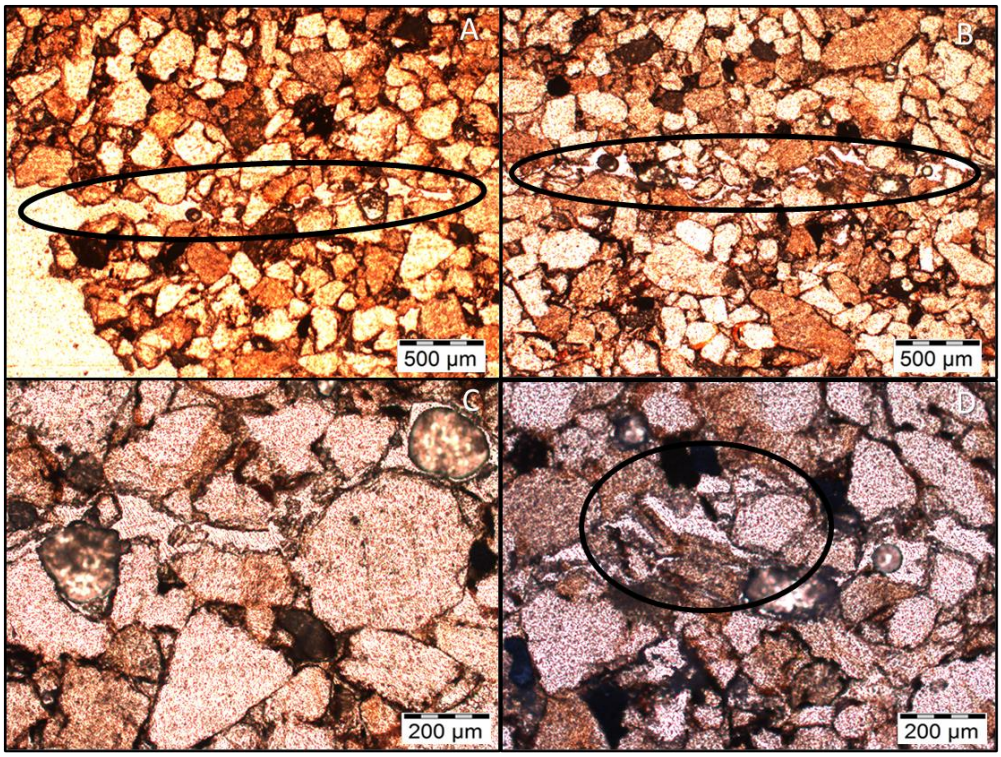

Figure 4.14 - A microcrack is shown at differing magnifications, A and B show that it runs parallel to the sample surface. C and D show that the microcrack has caused quartz grains to fracture (All PPL)

Figure 4.15 - Petrographic thin section scan of CC2 (5), with A and B focussing on two areas of the sample surface

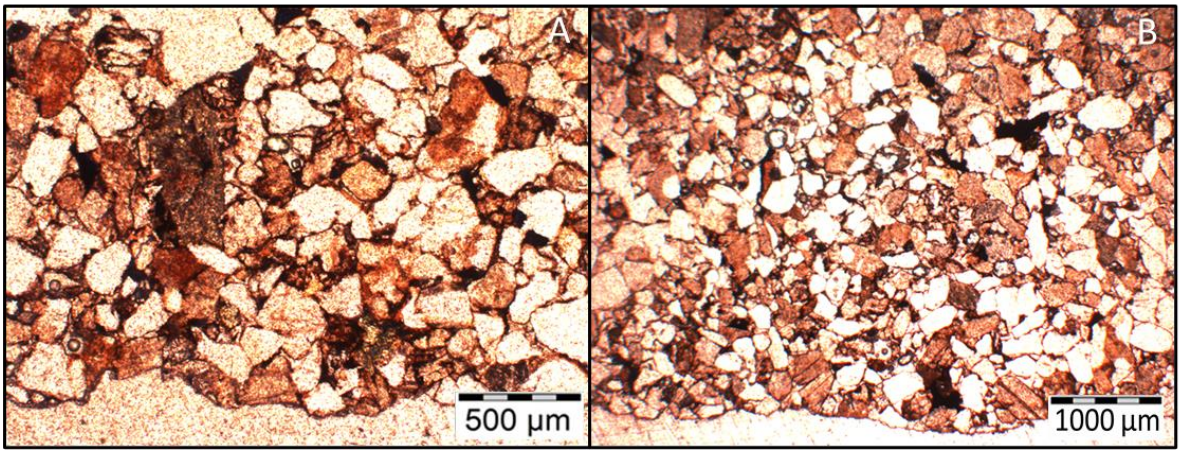

Figure 4.16 - No clear weathering indicators are visible at the surface of CC2 (5) (Both PPL)

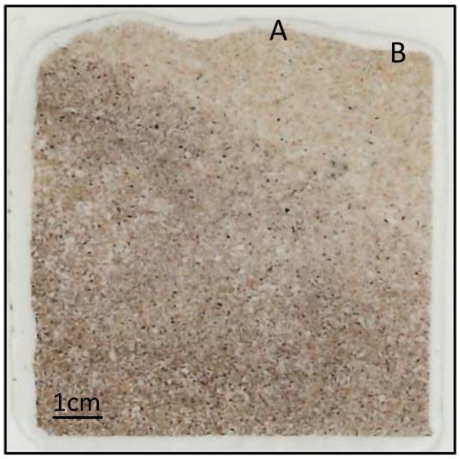

Figure 4.17 - Petrographic thin section scan of CC3 (9), with A and B focussing on two areas of the sample surface

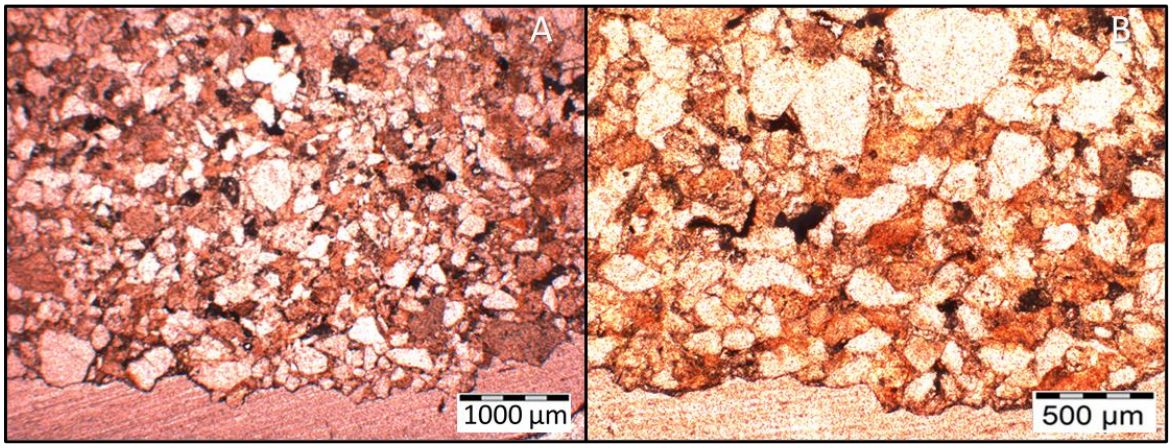

Figure 4.18 - No clear weathering indicators are visible at the surface of CC3 (9) (Both PPL)

Figure 4.19 – Petrographic thin section scan of CB1 (1), with sites A and B focussing on fractured quartz grains while C and D focus on a lateral microcrack

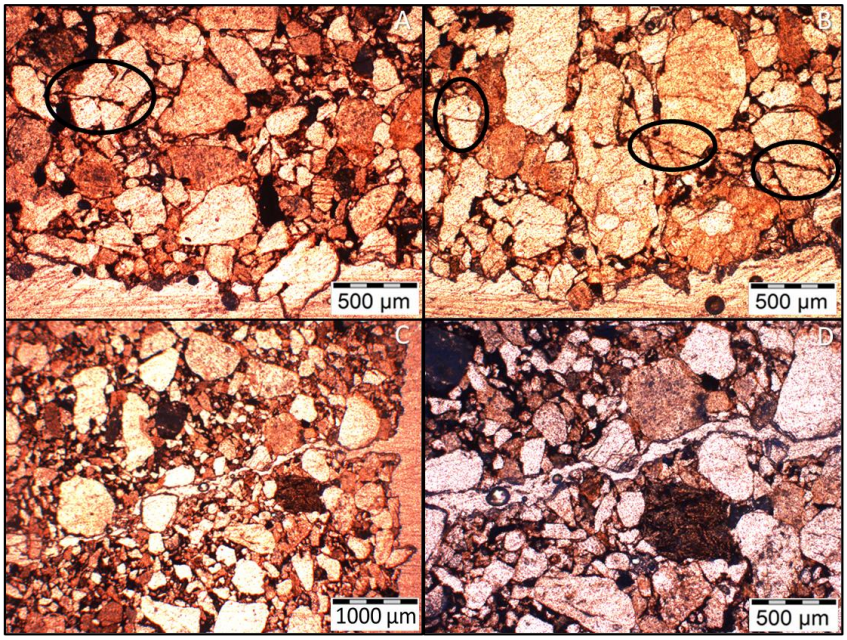

Figure 4.20 - A and B show clear fractures within quartz grains (circled) while C and D highlight a lateral microcrack at depth that meanders around grains (All PPL)

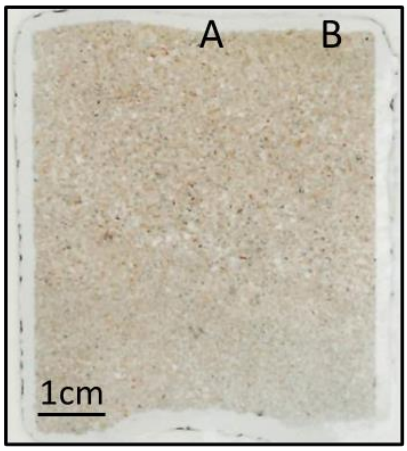

Figure 4.21 - Petrographic thin section scan of CB2 (5), with A and B focussing on two areas of the sample surface

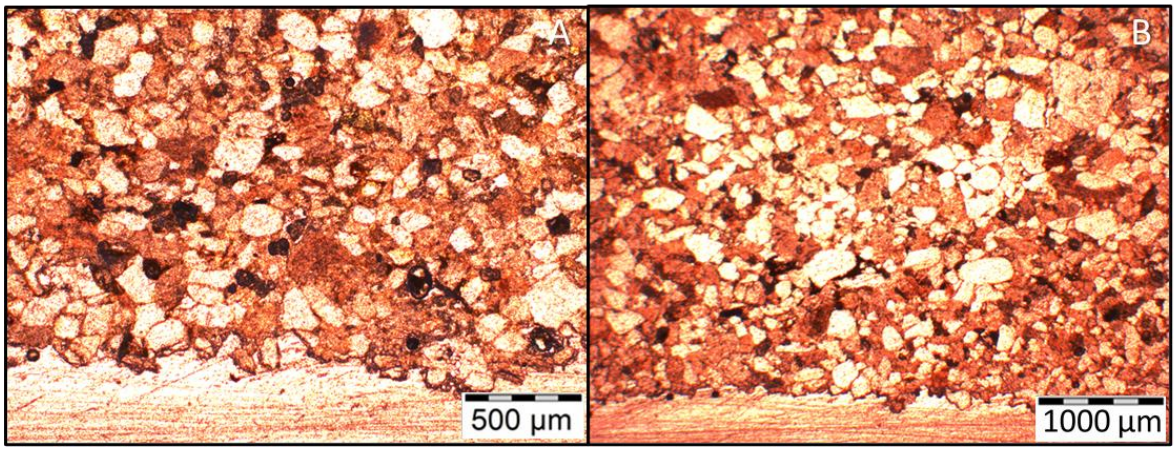

Figure 4.22 - The sample surface of CB2 (5) is robust with no indicators of weathering detected (Both PPL)

Figure 4.23 - Petrographic thin section scan of CB3 (9), with A and B focussing on two areas of the sample surface

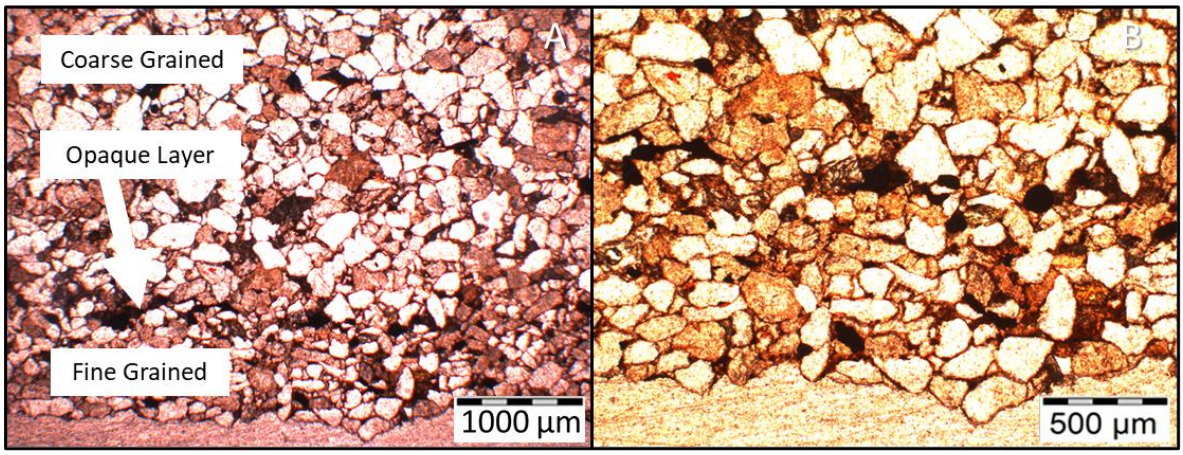

Figure 4.24 - The relatively fine-grained surface of CB3 (9) and its coarse-grained fabric at depth is punctuated by an opaque layer, particularly noticeable in A (labelled) (Both PPL)

Both CC1 (1) (Figure 4.13 Figure 4.14) and CB1 (1) (Figure 4.19 and Figure 4.20) exhibit microcracks, in the former, the microcrack penetrates through quartz grains, while in the latter the feature meanders around grain boundaries, likely following an inherent weakness within the cementing of the stone. This indicates that the microcrack in CC1 (1) has exerted greater force on the rock fabric, generating enough energy to fracture and split quartz grains. It would be unrealistic to assume that these microcracks are a direct consequence of experimental work; similar features were observed in untreated samples in Chapter 3. Regardless of the origin of the microcracks, it is clear that in both instances, the samples remain intact with no sign of surface failure or authigenic clay formation within the microcracks. The Torridonian Sandstone is a robust building stone, nevertheless, microcracks do occur and can be considered areas of weakness, however, experimental work in this instance has not shown these weaknesses to undermine the overall strength of the sandstone after a year of climate change exposure. It stands to reason, nonetheless, that if microcracks are a ubiquitous feature in the sandstone type, as demonstrated, then with accelerating climate change and compounded exposure, they will likely become more prevalent and carry with them a greater chance of triggering partial or complete sample failure.

It is important to make clear that experimental work in this thesis is a snapshot of time within a climate-changed future. A weathering experiment exploring the cumulative effects of decades of exposure would be beneficial in determining whether these microcracks could become significant weak areas that could exacerbate the sandstone's degradation. Future research focused on mimicking prolonged exposure could prove beneficial in efforts to

understand the future degradation of sandstone, however, ensuring realism and relatability of such experiments to real-life weathering conditions is a difficult balance to strike.

A further characteristic of interest is visible in CB3 (9) (Figure 4.23 and Figure 4.24), one of the samples which exhibited granular loss; highlighted and discussed in section 4.2 Visible Alterations. In this instance, however, the occurrence of an opaque layer at the surface of the stone which separates the fine-grained immediate surface of the stone, and the course-grained remainder of the stone can be seen. This feature has, thus far, been observed exclusively in untreated control samples, making CB3 (9) unique. As discussed throughout Chapter 3, these distinct opaque, likely clay-rich bands, are a potential weakness that could lead to a surface loss. As is the case with the aforementioned microcracks in CC1 (1) and CB1 (1), this apparent weakness layer in CB3 (9) has not failed or been altered microscopically as a result of experimental work undertaken. It is important, however, to reaffirm the point that the weathering simulation undertaken is equivalent to a single year of exposure to climate change. It is anticipated that with increased and compounded exposure, these clay layers could indeed be significant weak points and when they reach a tipping point, could prove to exacerbate the degradation of an important building stone in Northern Scotland.

Other samples exposed to the same treatment, namely CC2 (5), CC3 (9) and CB2 (5) display no signs of weathering as a result of experimental work, demonstrating the robustness of the sandstone type. Additionally, these samples do not contain any features within them that can be considered weaknesses. Based on these analyses, it is evident that culturally significant structures built with Torridonian Sandstone can withstand the pressures associated with one simulated year of climate change in Northern Scotland. However, exposure to an experiment that mimics prolonged weathering could have a greater impact on the material and likely more knowledge would be gained into sandstone longevity within a climate changed future.

4.5.1.2 Clachtoll Temperature, Humidity and Precipitation

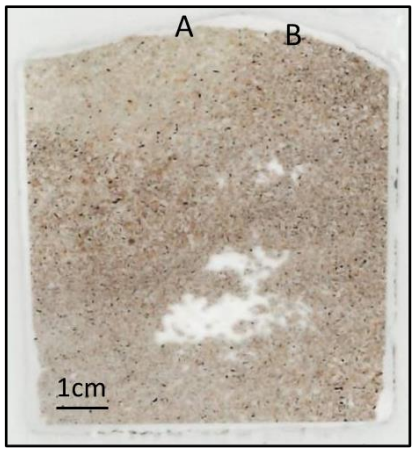

Figure 4.25 - Petrographic thin section scan of CC1 (2), with A and B focussing on two areas of the sample surface

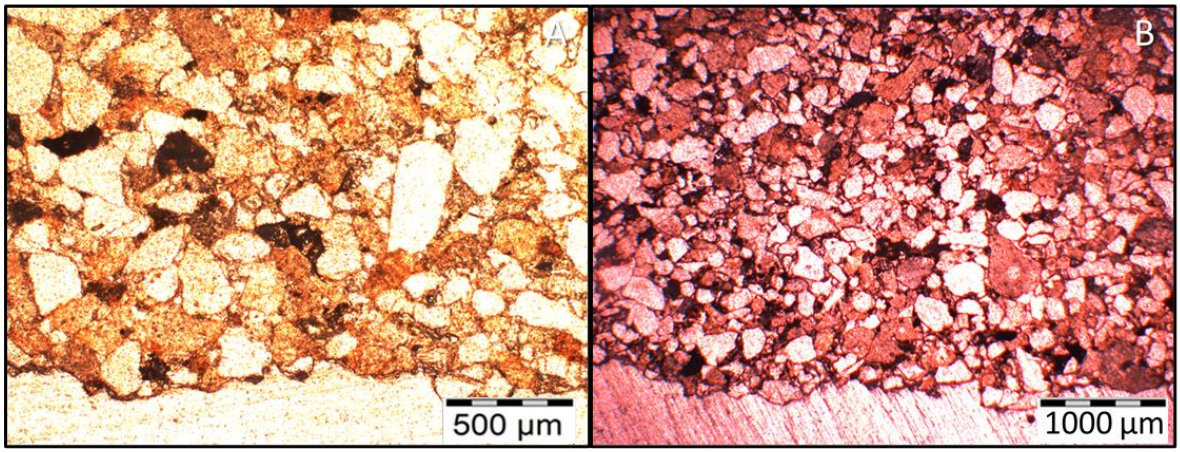

Figure 4.26 - No indicators of weathering are apparent on the surface of CC1 (2) (Both PPL)

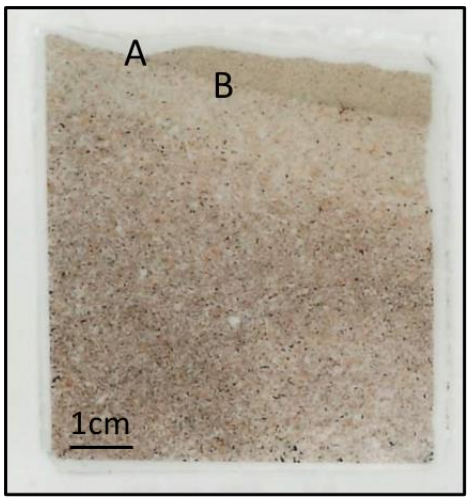

Figure 4.27 - Petrographic thin section scan of CC2 (6), with A and B focussing on grain size fluctuations at the sample's surface

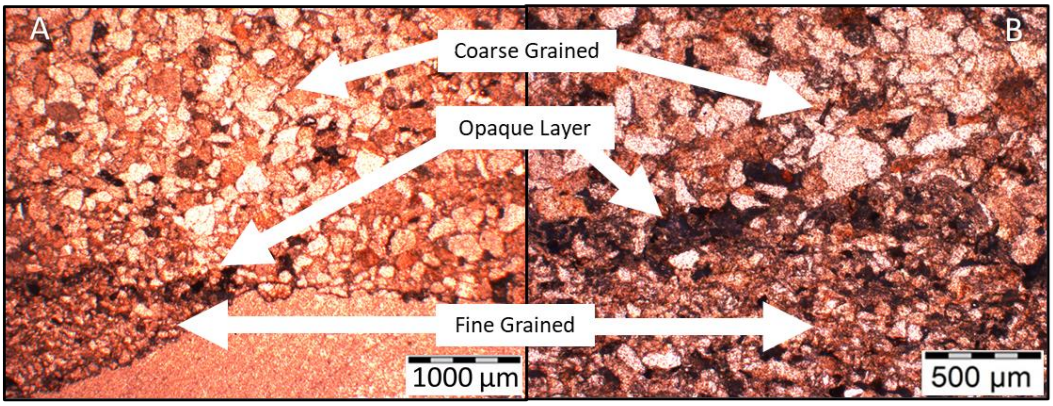

Figure 4.28 - CC2 (6)'s sample surface is characterised by a fine-grained layer, leading to a coarser fabric at depth, punctuated by an opaque clay layer. A shows that the fine-grained layer immediately above the clay material has been lost in one particular area (Both PPL)

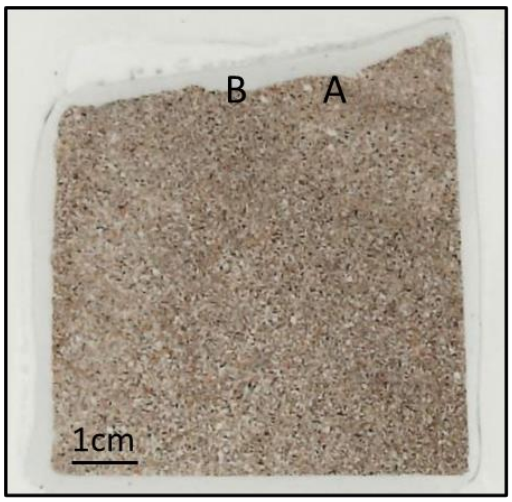

Figure 4.29 - Petrographic thin section scan of CC3 (10), with A and B focussing on two areas of the sample surface

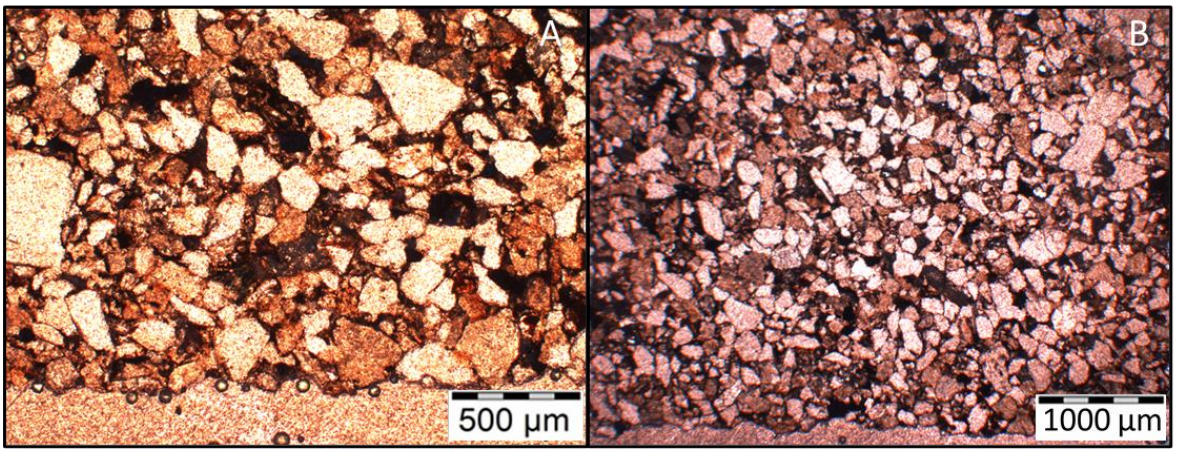

Figure 4.30 - CC3 (10) is rich in an opaque material, however, no weathering indicators can be identified through petrographic thin section analysis (Both PPL)

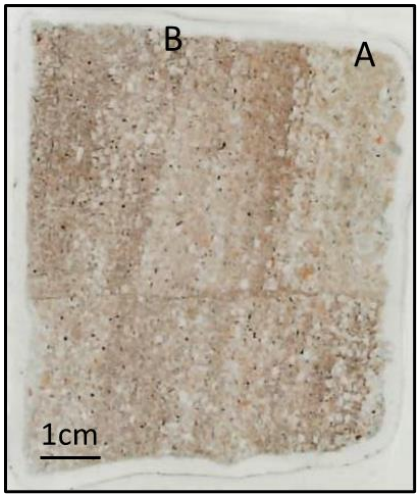

Figure 4.31 - Petrographic thin section scan of CB1 (2), with A and B focussing on two areas of the sample surface

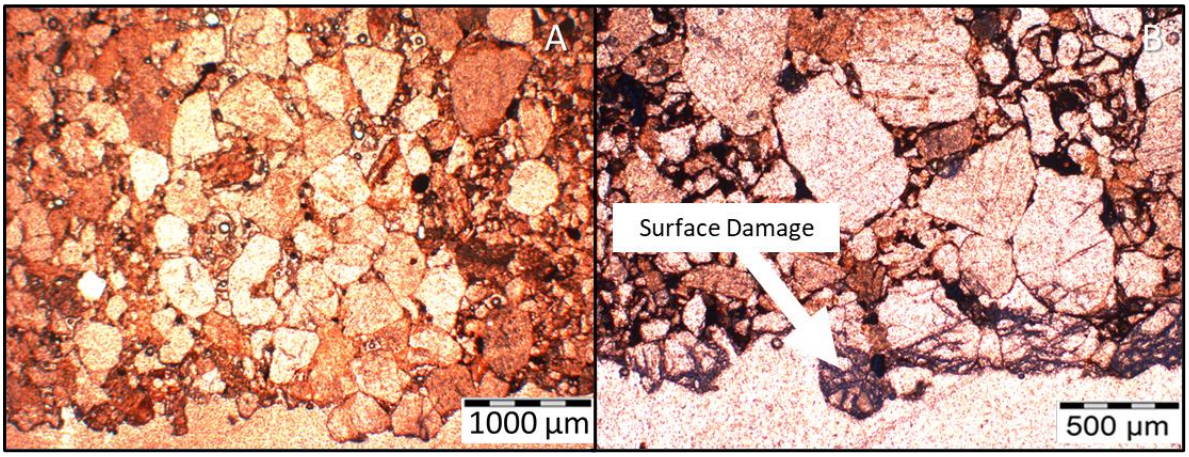

Figure 4.32 - The immediate surface of CB1 (2) appears slightly damaged, this has likely occurred through the thin section manufacturing process (Both PPL)

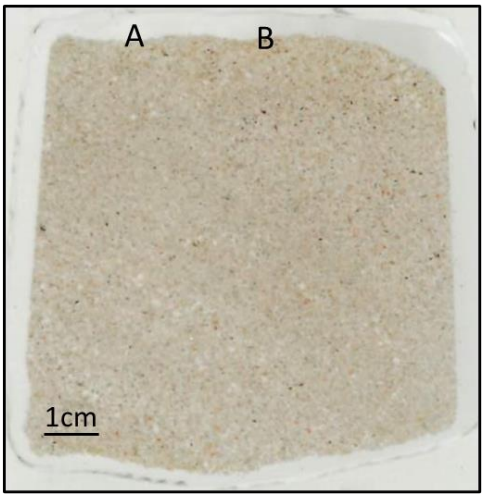

Figure 4.33 - Petrographic thin section scan of CB2 (6), with A and B focussing on two areas of the sample surface

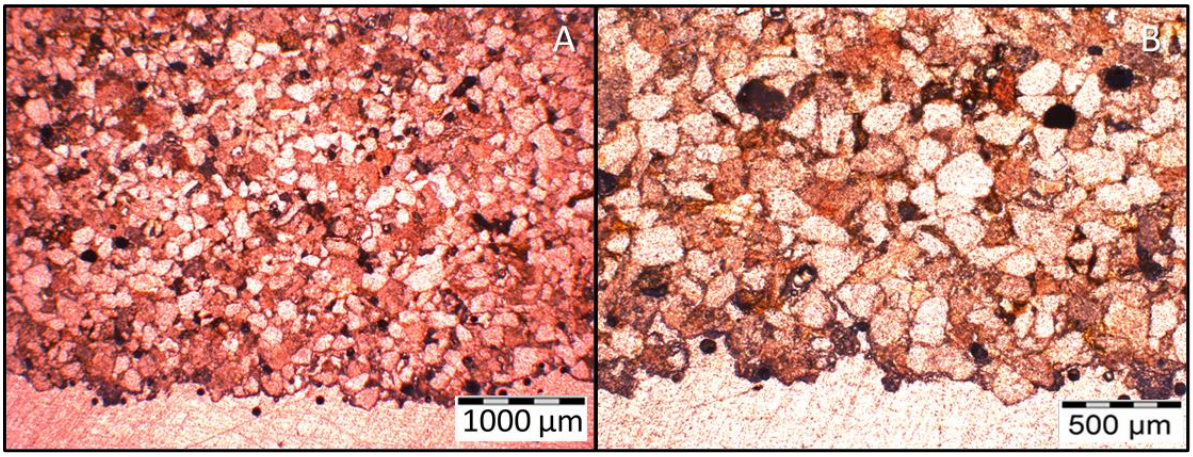

Figure 4.34 - The surface of CB2 (6) appears robust with no indicators of weathering (Both PPL)

Figure 4.35 - Petrographic thin section scan of CB3 (10), with A and B focussing on two areas of the sample surface

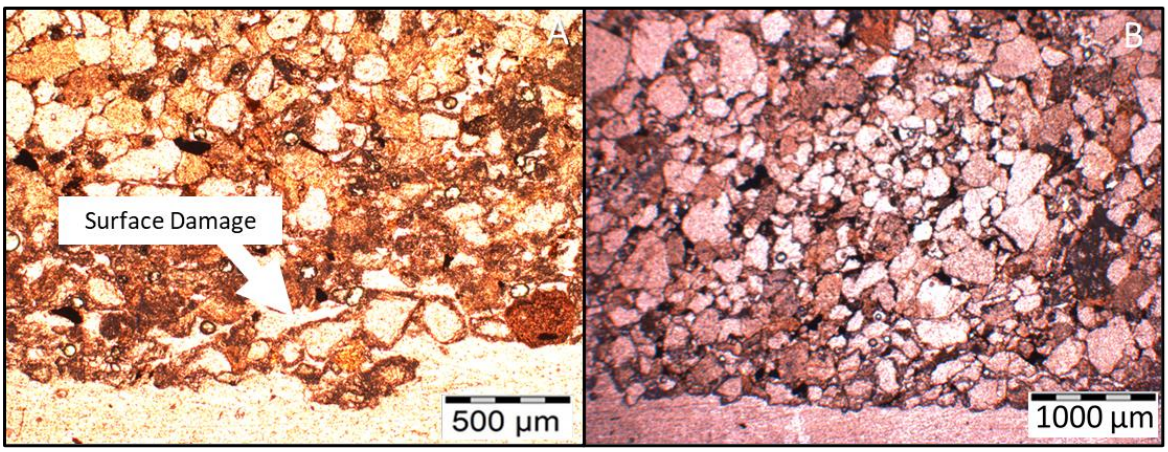

Figure 4.36 - The surface of CB3 (10) appears damaged (A), this has likely occurred during thin section manufacturing. In B, no indicators of weathering are seen (Both PPL)

With the addition of precipitation, there is no evidence that weathering is accelerated to a level beyond the weathering of samples exposed exclusively to temperature and humidity. In CC2 (6) (Figure 4.27 and Figure 4.28), a potential surface loss feature is highlighted.

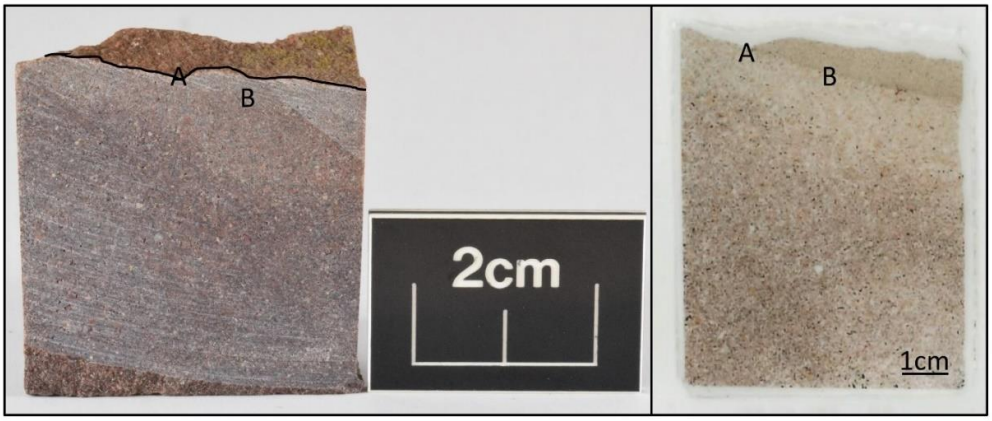

Figure 4.37 - CC2 (6) block before experimental work and petrographic thin section made after experimental work

Figure 4.37 shows the CC2 (6) sample block before experimental work and in a petrographic thin section after experimental work. The same surface loss feature can be seen in the sample block as the thin section by following the superimposed black line on the sample surface and noting the location of photomicrograph (A and B). This feature has not changed markedly as a result of the experiment, affirming the robust nature of the Torridonian Sandstone. Furthermore, aside from CC2 (6), no other samples display any potential new weathering features.

4.5.1.3 Borwick Temperature and Humidity

Figure 4.38 - Petrographic thin section scan of BC1 (1), with A and B focussing on two areas of the sample surface

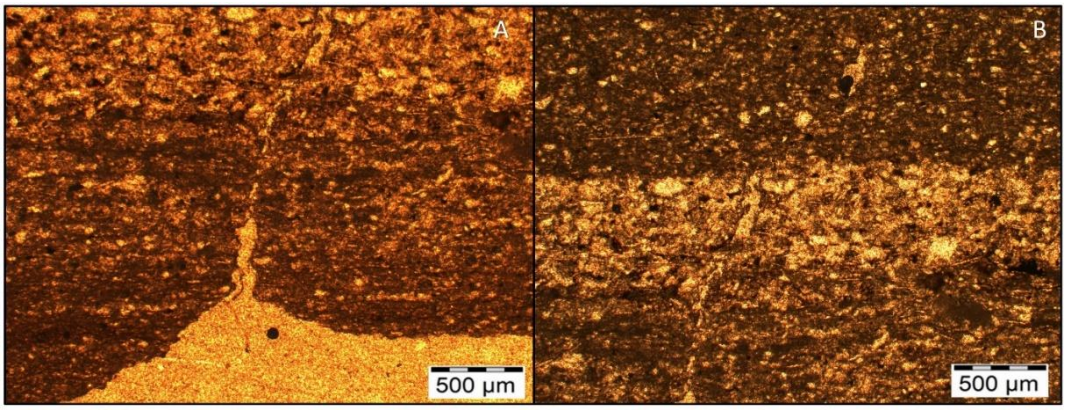

Figure 4.39 - A microcrack is visible extending from the surface of the sample (A) to depth (B), penetrating through different bedding planes within the rock (Both PPL)

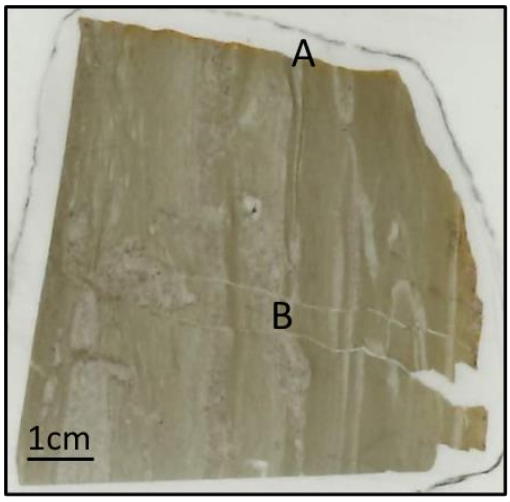

Figure 4.40 - Petrographic thin section scan of BC2 (5) with A focussing on the sample surface and B focused on lateral microcracks at depth

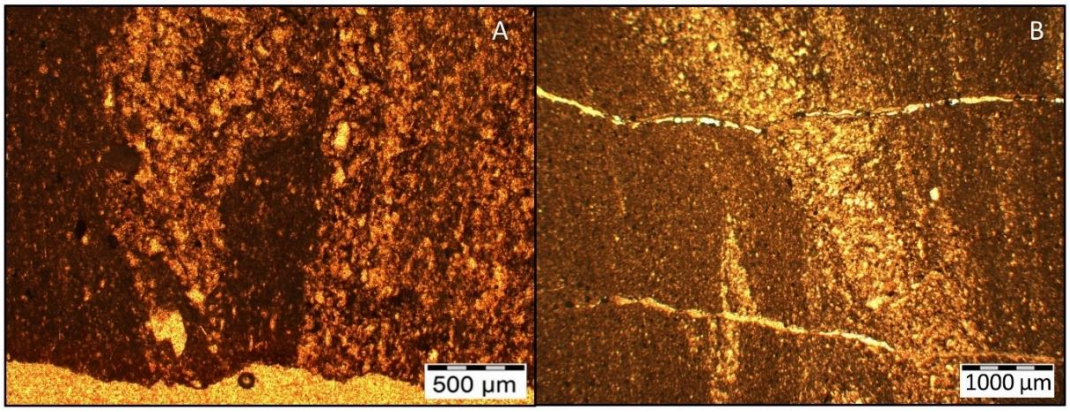

Figure 4.41 - The surface appears intact (A) while lateral microcracks are abundant at depth (Both PPL)

Figure 4.42 - Petrographic thin section scan of BC3 (8), with A and B focussing on two areas of the sample surface where dolomite dissolution appears prevalent

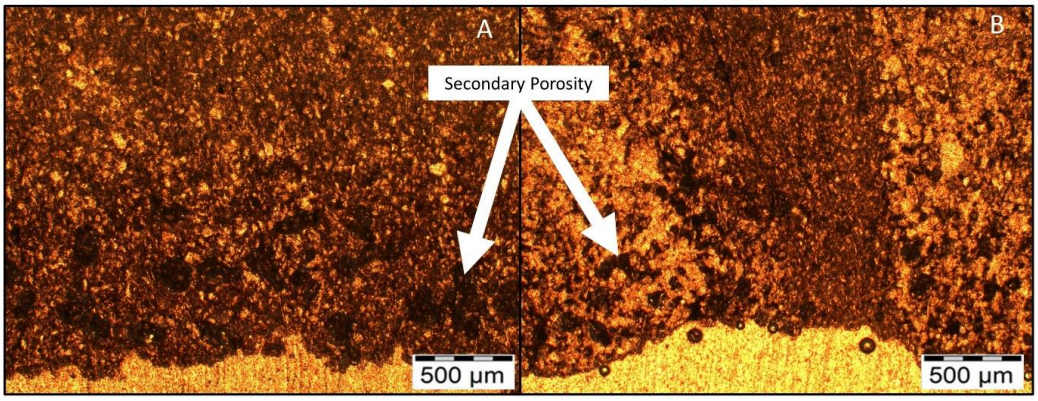

Figure 4.43 - The dark red colour of the material in the thin section photomicrograph makes dolomite dissolution easy to identify. Minor secondary porosity is also visible and labelled (Both PPL)

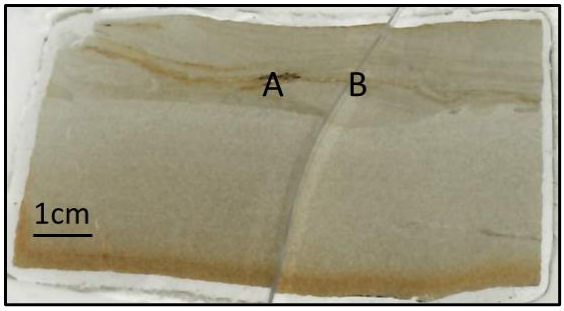

Figure 4.44 - Petrographic thin section scan of BB1 (1) with A and B focussing on two sections of a distinct microcrack that failed during experimental work

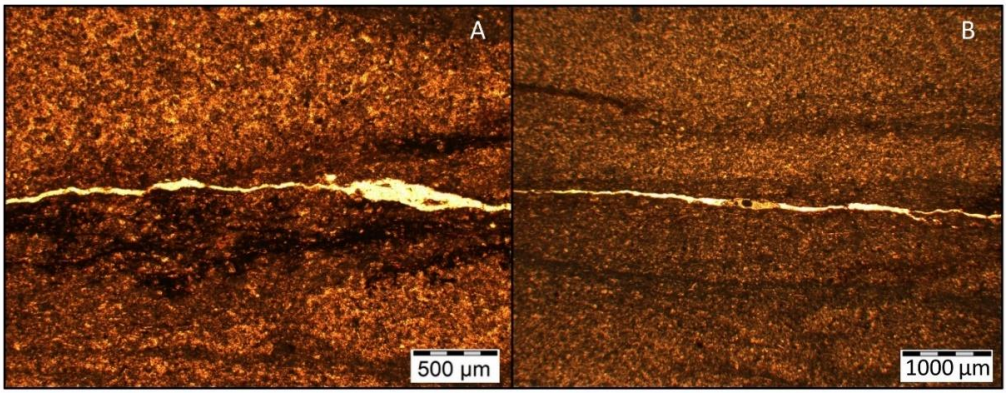

Figure 4.45 - A severe lateral microcrack that failed during experimental work bisects the sample, with dolomite dissolution apparent and surrounding it (Both PPL)

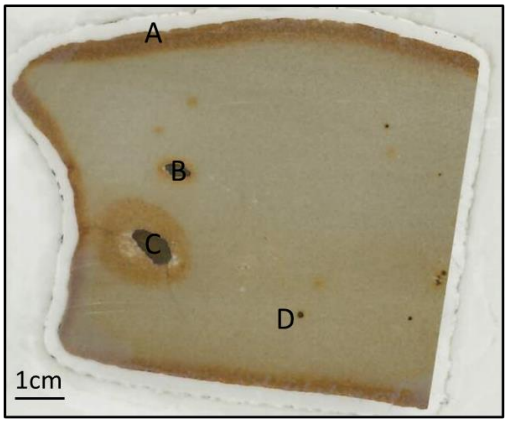

Figure 4.46 - Petrographic thin section scan of BB2 (5). Site A focuses on surface dissolution, while B, C and D focus on distinct sulphide nodules of varying size, scattered throughout the stone fabric

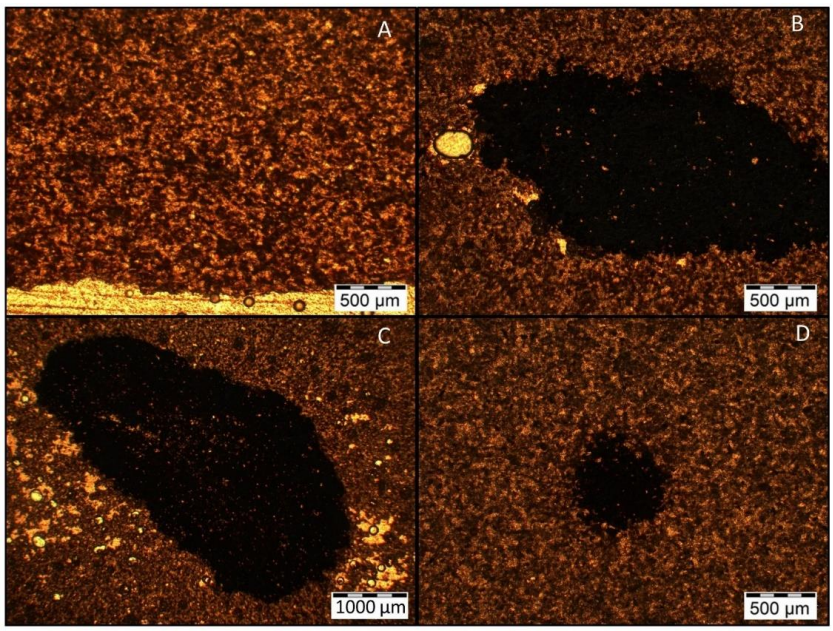

Figure 4.47 - Dissolution is prevalent on the sample's surface (A) and large sulphide nodules are scattered throughout the sample (B, C, D). Considerable dolomite dissolution and secondary porosity are seen surrounding the nodule in C and to a lesser extent in B (All PPL)

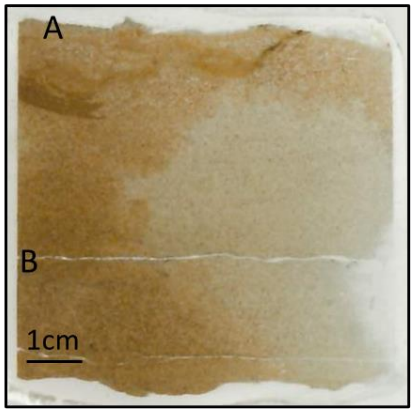

Figure 4.48 - Petrographic thin section scan of BB3 (8) with A focussing on the sample surface and B focussing on a distinct lateral microcrack at depth

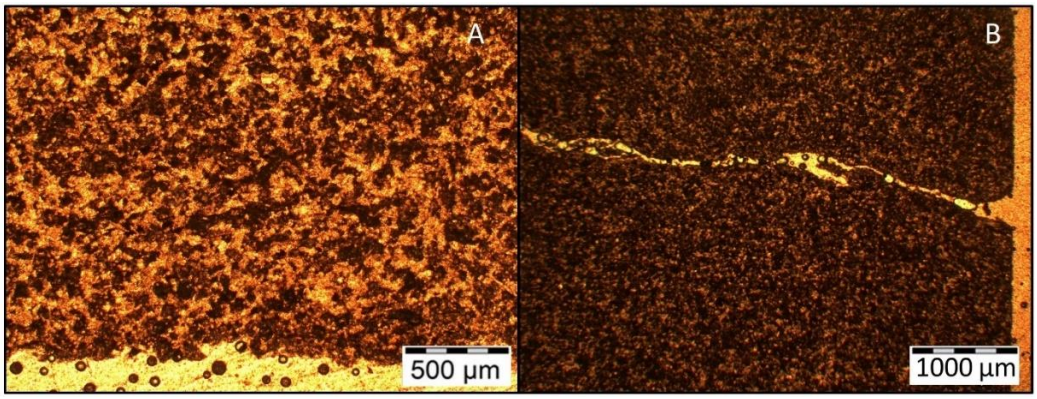

Figure 4.49 - BB3 (8)'s surface appears intact (A); however, the sample is dominated by lateral microcracks, the one photographed in B failed during experimental work (Both PPL)

As highlighted throughout this thesis, Stromness Flagstones are characterised by an abundance of microcracks scattered throughout samples taken. Although obvious weak points within the material, the numerous microcracks within control samples (Figure 4.38 - Figure 4.43), have remained intact throughout experimental work. Interestingly, the same cannot be said for broch samples. As highlighted in section 4.2 Visible Alterations, BB1 (1) (Figure 4.44 and Figure 4.45) and BB3 (8) (Figure 4.48 and Figure 4.49) failed at distinct weak points during the CEF experiment. The thin section photomicrograph (Figure 4.45 and Figure 4.49) clearly show the failing microcracks, which in both instances appear to be surrounded by limited dolomite dissolution, this is seen most clearly in BB1 (1) where it appears that a dark material, likely iron, has precipitated around the microcrack. This contrast between microcracks present in both control and broch samples exposed to the same treatment provides a clear example of the vulnerabilities within pre-weathered samples compared with relatively pristine samples of the same lithology type. This carries important implications for

the longevity of material incorporated within historic monuments; with climate change, the risk of pre-existing weaknesses failing appears greater, demonstrated in this weathering simulation experiment.

BC3 (8) (Figure 4.42 and Figure 4.43) provides the first example in this research of minor secondary porosity formation, triggered by dolomite dissolution. However, secondary porosity is seen most extensively in BB2 (5) (Figure 4.46 and Figure 4.47). Importantly, this has formed around a particularly large sulphide nodule, indicating just how severely the weathering of these features can exacerbate stone material loss through sulphuric acid formation intensifying dolomite dissolution. Interestingly, secondary porosity of this extent has not been observed in untreated samples in Chapter 3, indicating that exposure to climate change conditions has, at least in part, contributed to this phenomenon.

Secondary porosity has been shown in the literature to have a greater volume than primary porosity, having significant negative impacts on a multitude of sandstone properties (Nolansnyder and Parnell, 2019). In specific lithologies, this can be beneficial at depth where large pores can be occupied by liquids such as petroleum (Gluyas, 2004). However, in this field of research, dissolution of the key cementing agent in the stone and subsequent formation of secondary porosity at sample surfaces triggers surface loss and failure of sandstone blocks.

Key findings from this experiment show that broch samples have reacted more severely than control samples to climate change weathering, whereby microcracks have failed and severe secondary porosity has formed as a result of sulphide nodule decay.

4.5.1.4 Borwick Temperature, Humidity and Precipitation

Figure 4.50 - Petrographic thin section scan of BC1 (2) with A focussing on the sample surface and B focussing on a distinct microcrack

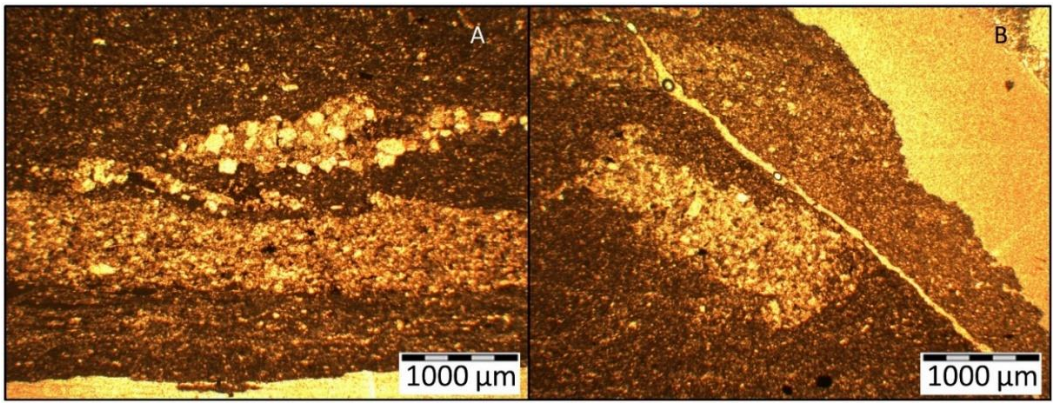

Figure 4.51 - Aside from a surface microcrack in the corner of BC1 (2), weathering indicators such as dissolution are absent (Both PPL)

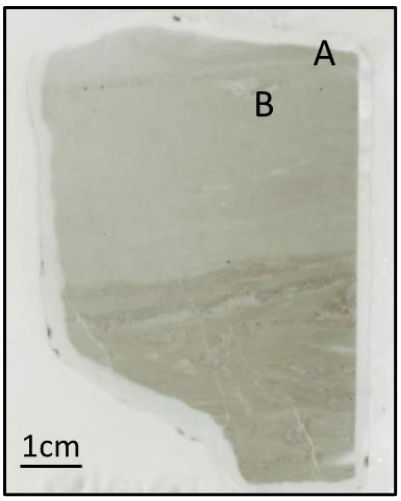

Figure 4.52 - Petrographic thin section scan of BC2 (6), with A focusing on an area of the sample surface and B focussing on vertical microcracks

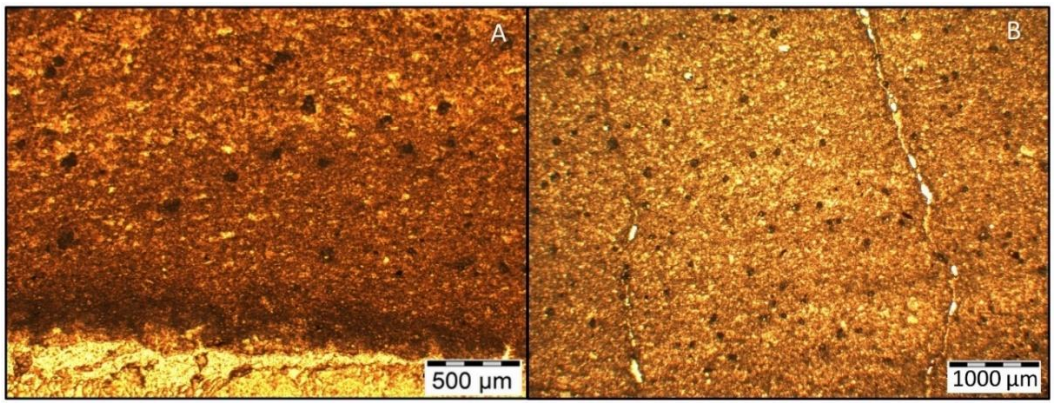

Figure 4.53 - Vertical microcracks are seen at depth within the sample (A), however, the surface does not show any signs of weathering (B) (Both PPL)

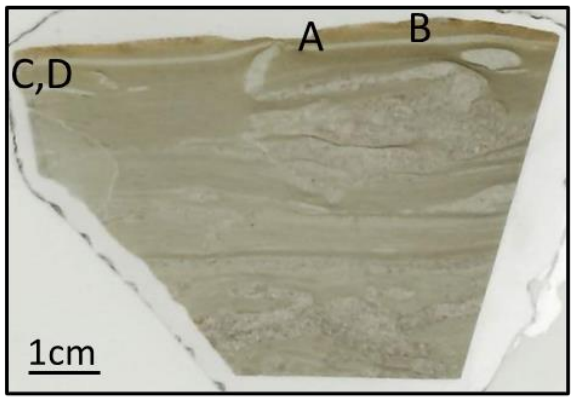

Figure 4.54 - Petrographic thin section scan of BC3 (9), with A and B focussing on two areas of the sample surface while C and D focus on lateral microcracks

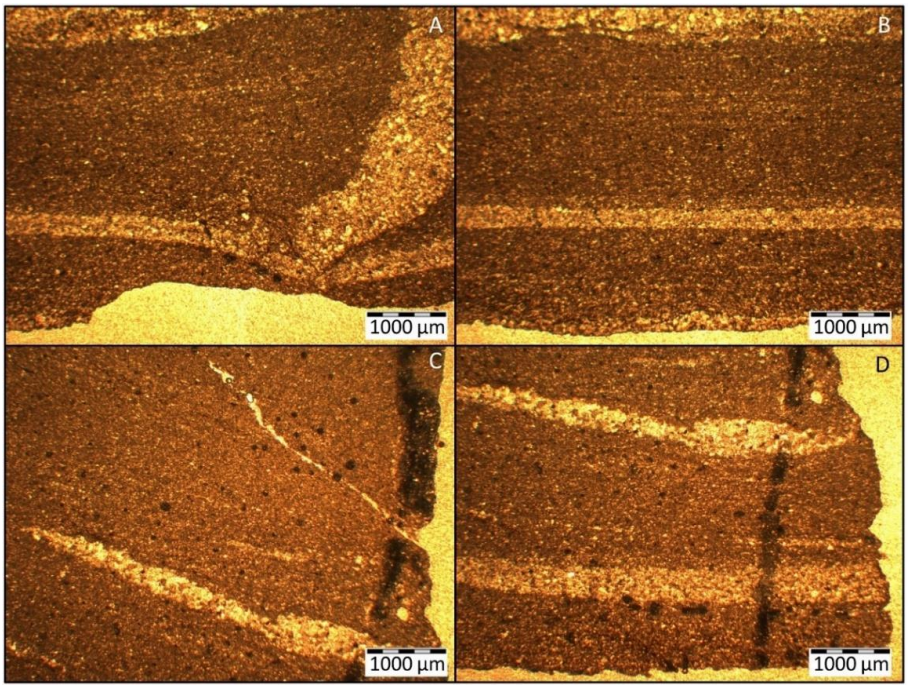

Figure 4.55 - Shown in A, surface loss appears to have occurred in some areas, while other areas remain intact (B). Lateral microcracks and minor evidence of dissolution are seen on the left-hand side of the sample (All PPL)

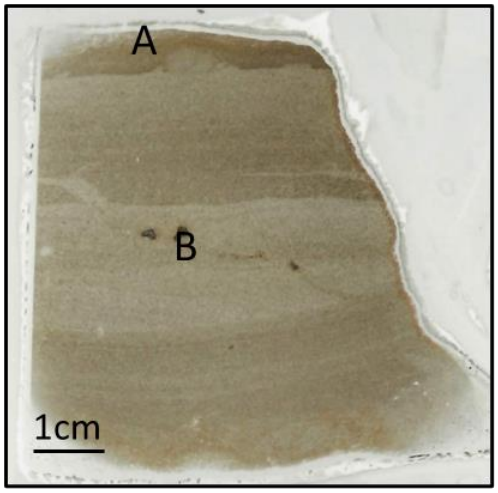

Figure 4.56 - Petrographic thin section scan of BB1 (2), with A focusing on an area of the sample surface and B focussing on a distinct sulphide nodule

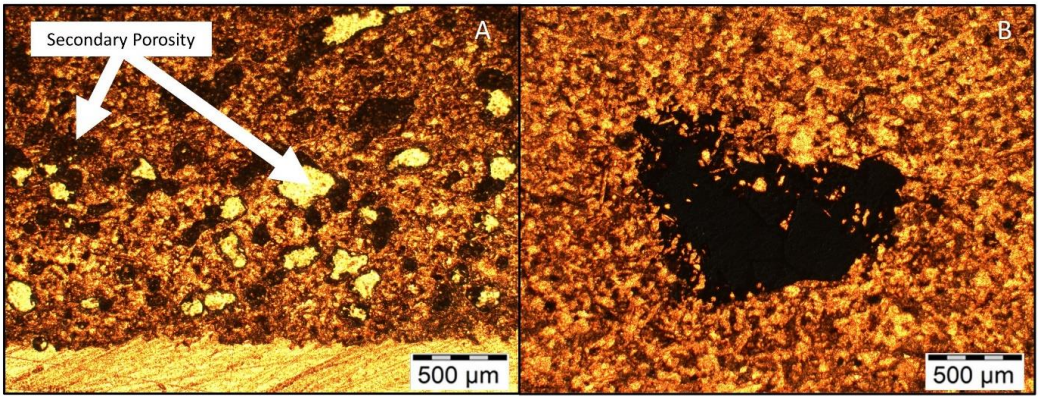

Figure 4.57 - Extensive dissolution and secondary porosity are seen (A), as well as an intact sulphide nodule (B) (Both PPL)

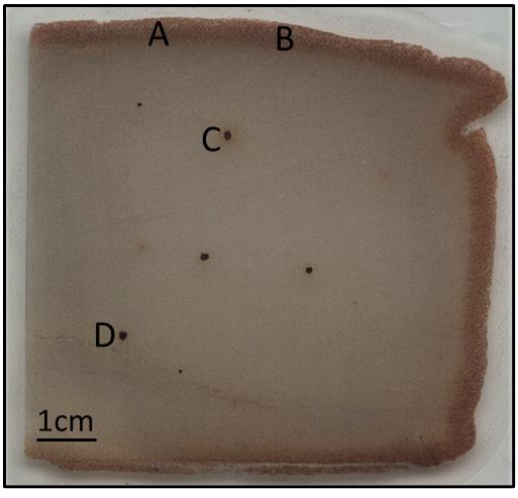

Figure 4.58 - Petrographic thin section scan of BB2 (6), with A and B focussing on two areas of the sample surface while C and D focus on distinct sulphide nodules

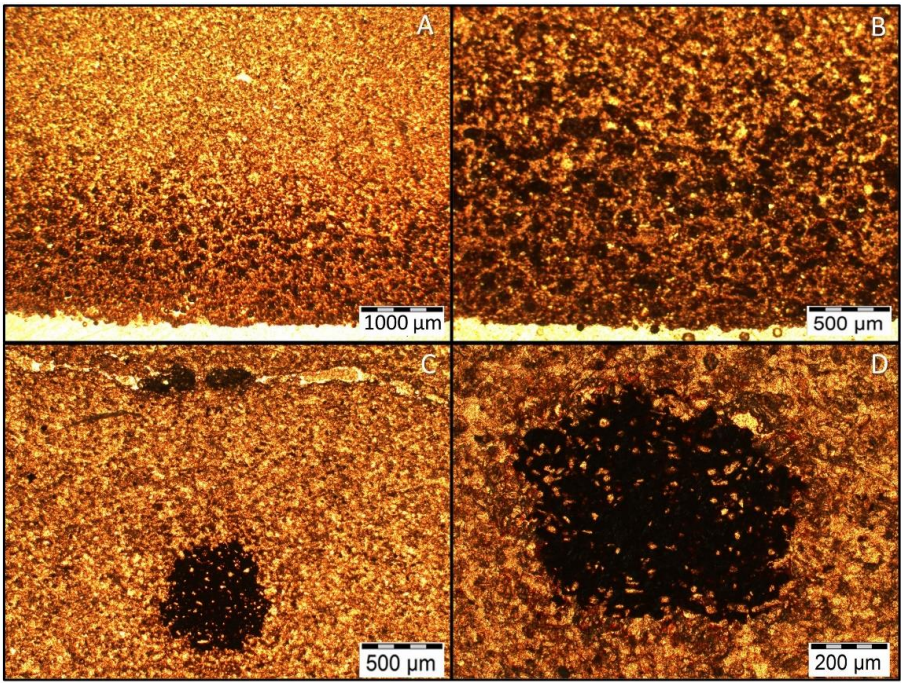

Figure 4.59 - Extensive dissolution and secondary porosity are seen (A and B), as well as intact sulphide nodules (B and D) (All PPL)

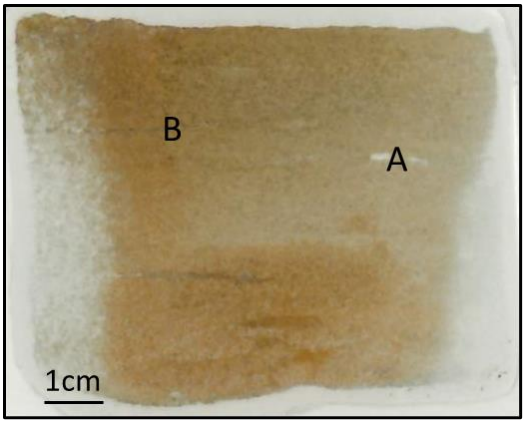

Figure 4.60 - Petrographic thin section scan of BB3 (9), with A and B focussing on two distinct microcracks

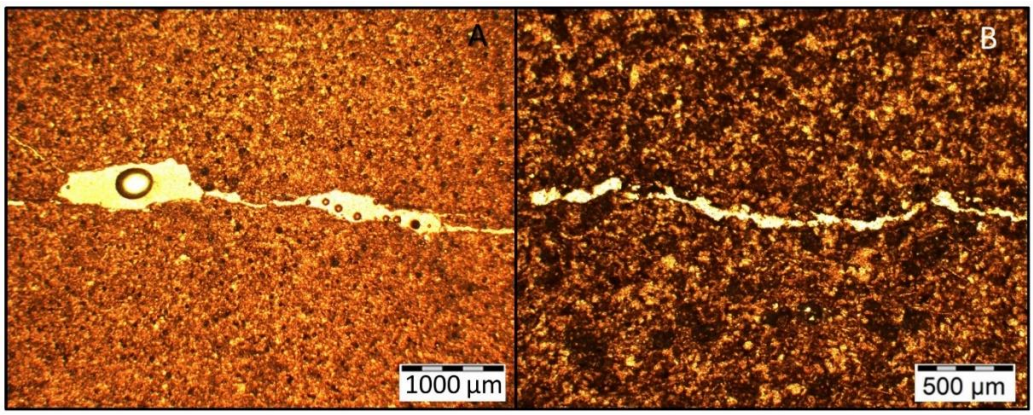

Figure 4.61 - A significant microcrack is shown in A which contains a pore-chamber. The sample is dominated by reddish dissolution features, evidenced in B (Both PPL)

All control samples appear robust after experimental work (Figure 4.50 - Figure 4.55), microcracks in BC1 (2) (Figure 4.50 and Figure 4.51), and BC2 (6) (Figure 4.52 and Figure 4.53) have survived the experiment without any signs of failure. The same can also be said for broch sample BB3 (9) (Figure 4.60 and Figure 4.61), although it appears close to failure, the experiment has not brought the sample to its tipping point, however, given the fragility of the microcrack, it is highly likely that with continued exposure, the sample would have failed.

BB1 (2) (Figure 4.56 and Figure 4.57) exhibits limited dissolution and extensive secondary porosity formation. The latter feature has been identified surrounding sulphide nodules in the other experimental chamber, however, the addition of precipitation in this experiment has potentially exacerbated its formation at the sample surface, whereby precipitation can dislodge and wash stone constituents away in solution. Secondary porosity formation is seen to a less extent in BB2 (6) (Figure 4.58 and Figure 4.59), however, the level of dissolution appears far greater in this sample.

4.5.2 Control Chamber

As presented in Chapter 2, samples utilised in these chambers have been exposed to either temperature and humidity or temperature, humidity and precipitation fluctuations that occurred in Northern Scotland in 2018. Data has been obtained UKCP18 RCP 8.5 at a high emission scenario at the 50% probability level.

4.5.2.1 Clachtoll Temperature and Humidity

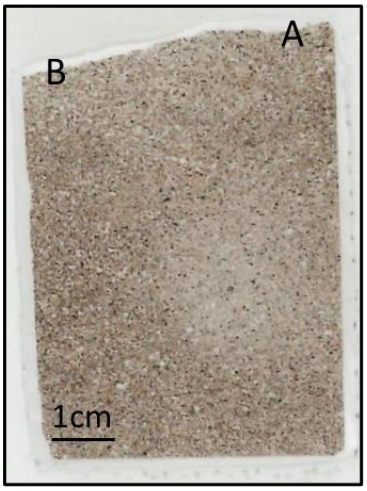

Figure 4.62 - Petrographic thin section scan of CC1 (3)

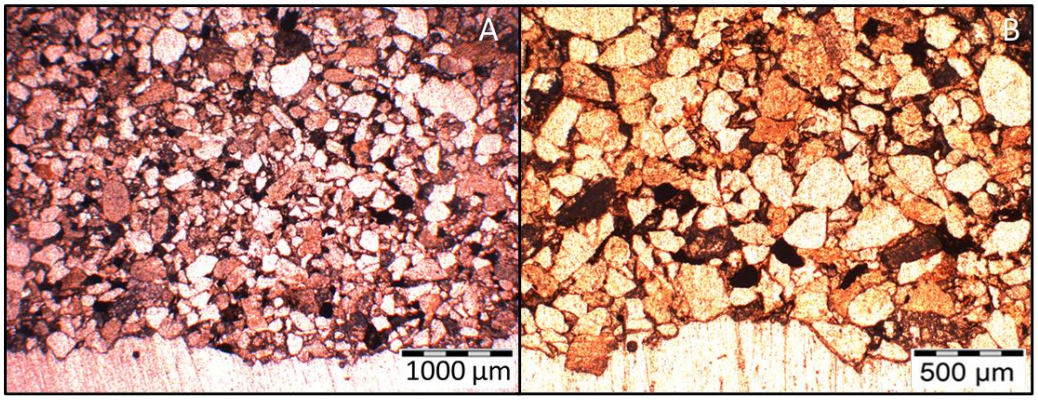

Figure 4.63 - No indicators of weathering are evident in sample CC1 (3), with A and B focussing on two areas of the sample surface (Both PPL)

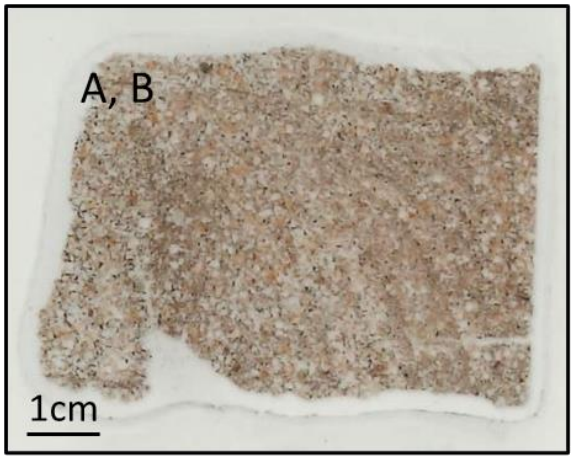

Figure 4.64 - Petrographic thin section scan of CB1 (3), with A and B focussing on a distinct crush zone close to the sample surface

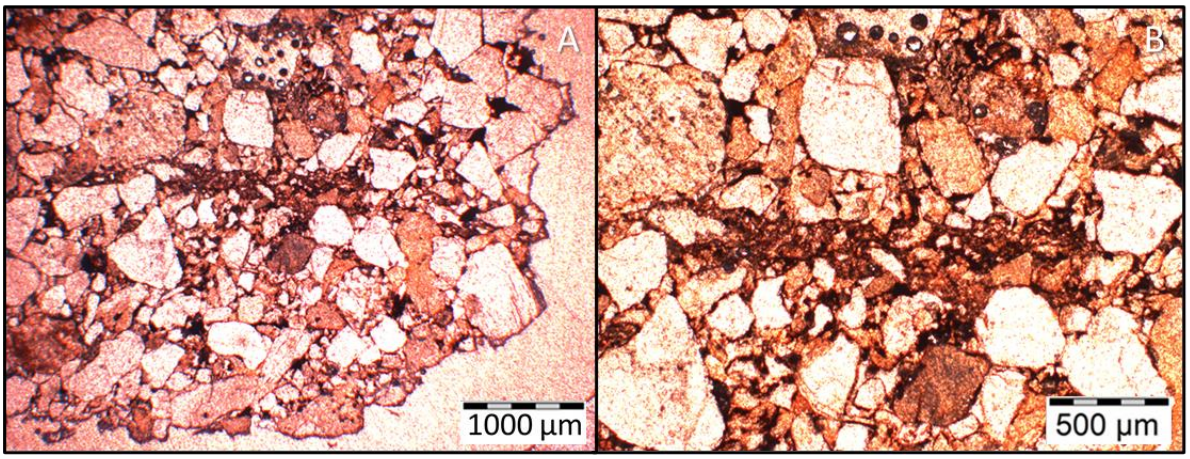

Figure 4.65 - A lateral crush zone is shown in A and B which runs the width of the near-surface. It appears robust with no indicators of weathering or deformation surrounding it (Both PPL)

4.5.2.2 Clachtoll Temperature, Humidity and Precipitation

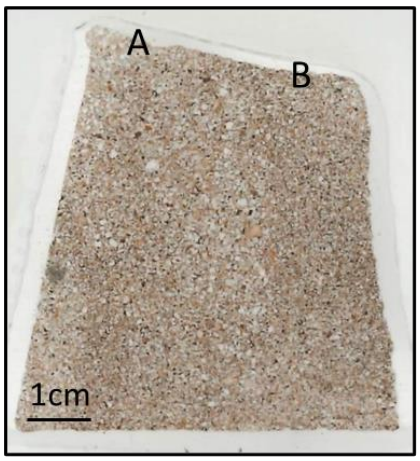

Figure 4.66 - Petrographic thin section scan of CC1 (4), with A and B focussing on two areas of the sample surface

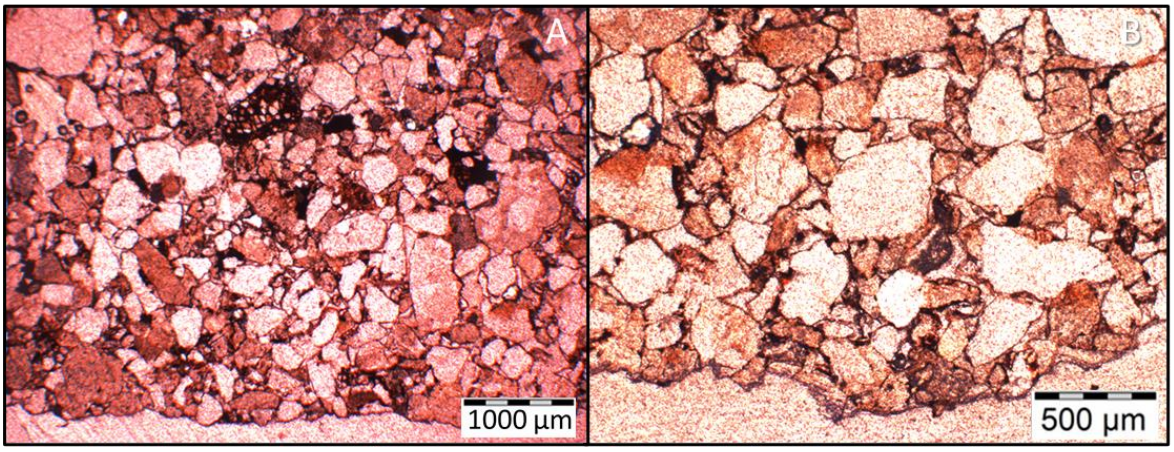

Figure 4.67 - No indicators of weathering are evident in sample CC1 (4) (Both PPL)

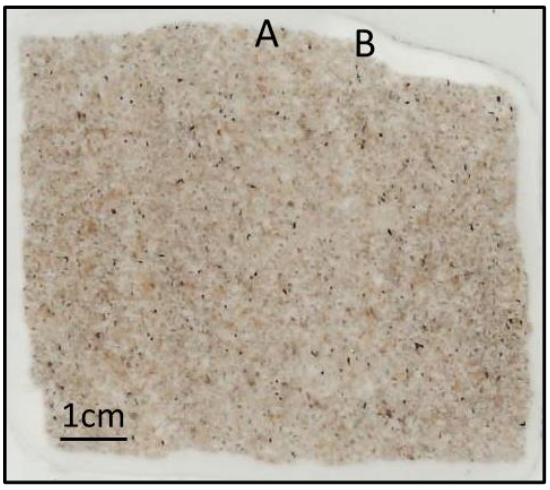

Figure 4.68 - Petrographic thin section scan of CB1 (4), with A and B focussing on two areas of the sample surface

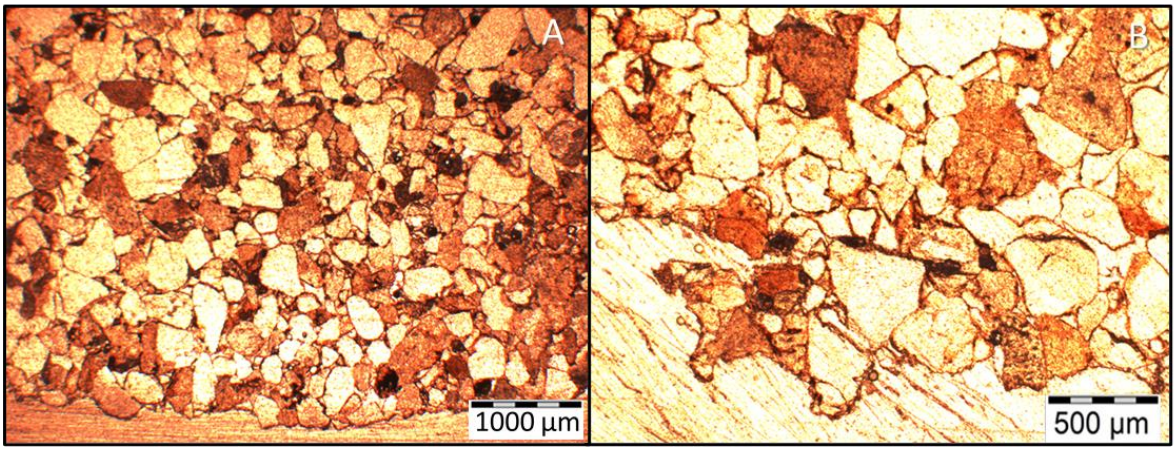

Figure 4.69 - The sample surface has remained intact despite a small microcrack shown in B (Both PPL)

Evidenced through petrographic thin section analysis, all samples utilised in the control experiment for Clachtoll remained intact. Similar to experimental chamber results, there is no apparent microscopic difference between the weathering of samples in the temperature and humidity control chamber and those in the control chamber with added precipitation. Some key features include the crush zone in CB1 (3) (Figure 4.64 and Figure 4.65) which was unaffected by experimental work. There does, however, appear to be a surface microcrack shown in CB1 (4) (Figure 4.69 B), whether this has transpired due to experimental work is uncertain. This research has shown these microcracks to be commonplace in Clachtoll samples. Importantly, the remainder of CB1 (4)'s surface appears intact (Figure 4.69 A).

4.5.2.3 Borwick Temperature and Humidity

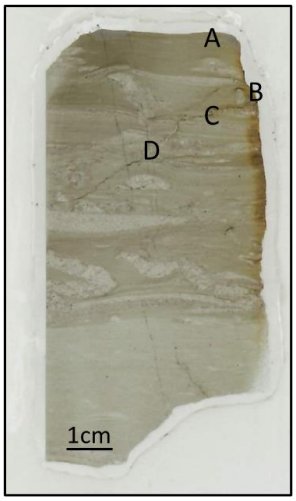

Figure 4.70 - Petrographic thin section scan of BC1 (3). A focuses on the sample surface while B, C and D track distinct microcracks from the right-side edge of the sample (B) through to the centre of the sample (D)

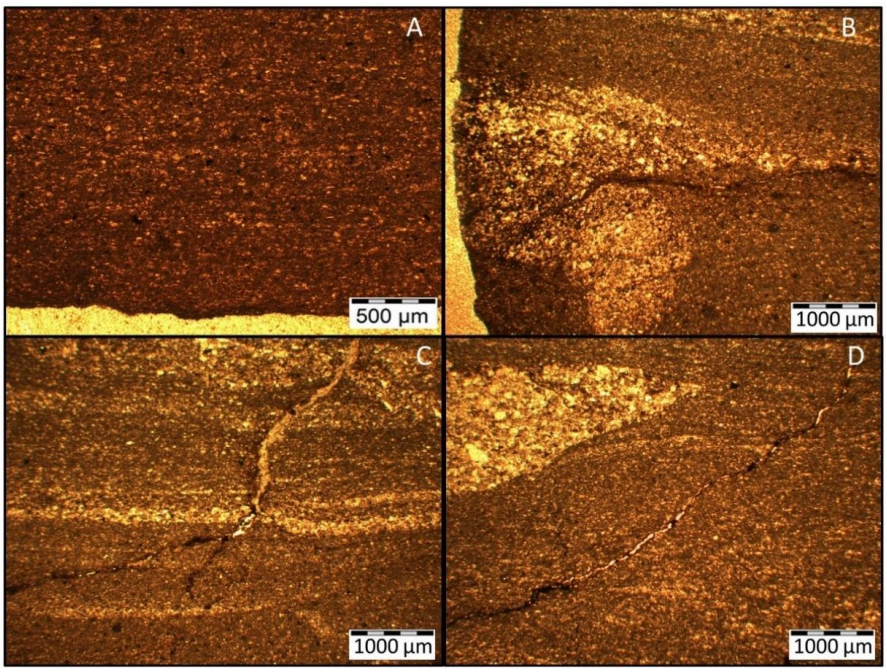

Figure 4.71 - Dolomite dissolution is clear on the right-hand side of the sample (A), the remainder of the rock is abundant in microcracks (B, C, D) (All PPL)

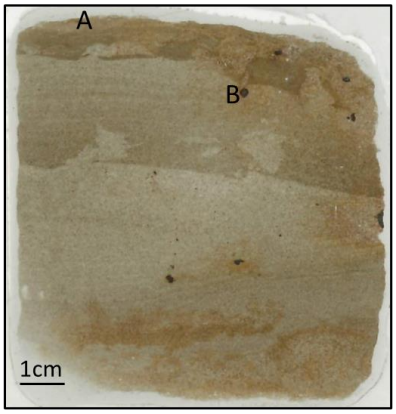

Figure 4.72 - Petrographic thin section scan of BB1 (3), with A focusing on an area of the sample surface and B focussing on a distinct sulphide nodule

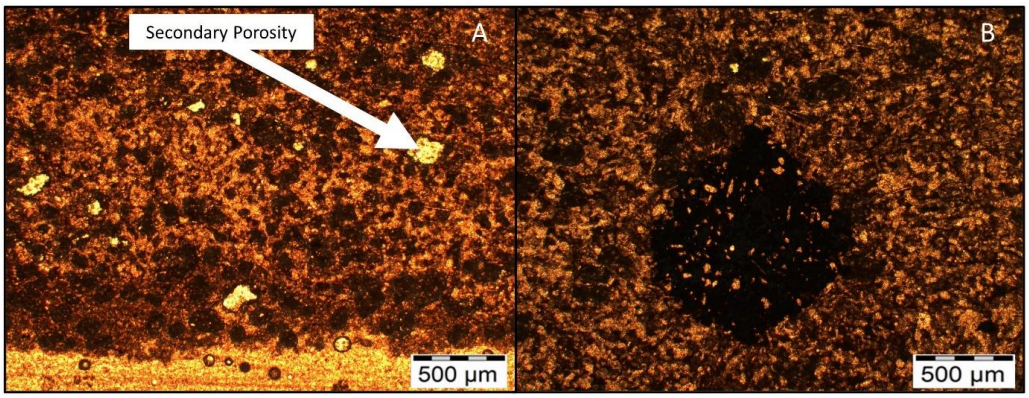

Figure 4.73 - BB1 (3) shows clear signs of surface dissolution (A) characterised by a dark red colour and the presence of secondary porosity. There are multiple sulphide nodules scattered throughout the sample (Both PPL)

4.5.2.4 Borwick Temperature, Humidity and Precipitation

Figure 4.74 - Petrographic thin section scan of BC1 (4), with A and B focussing on two areas of the sample surface

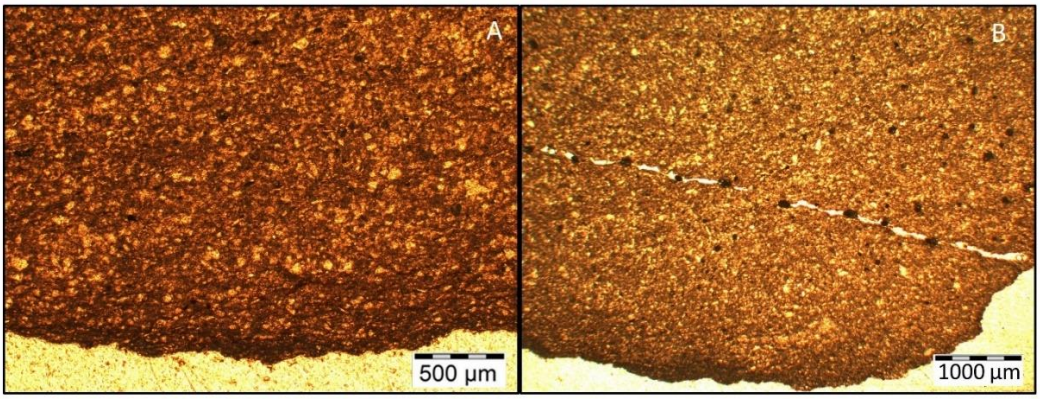

Figure 4.75 - The sample surface appears relatively robust with one minor surface microcrack (Both PPL)

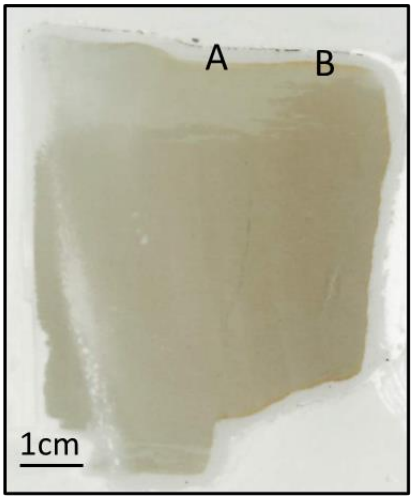

Figure 4.76 - Petrographic thin section scan of BB1 (4), with A and B focussing on two areas of the sample surface

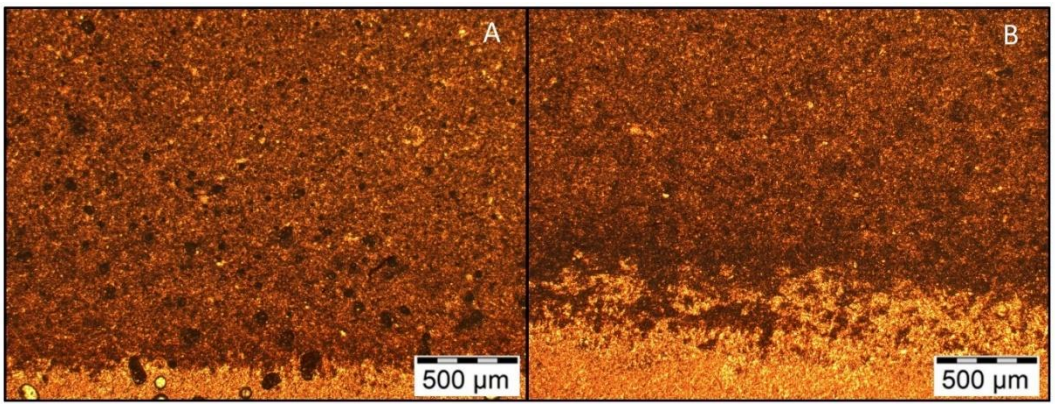

Figure 4.77 - The sample surface is robust with no indicators of weathering (Both PPL)

In both chambers, microscopic evidence of new dolomite dissolution cannot be seen. Furthermore, despite the extensive number of microcracks throughout the samples, they have remained intact. In BB1 (3) (Figure 4.72 and Figure 4.73), used in the temperature and humidity control chamber, secondary porosity is seen to a far lesser extent than in the equivalent sample used in the experimental chamber. Similarly, no secondary porosity is seen surrounding sulphide nodules scattered throughout BB1 (3). Based on these findings, it can be inferred that the exposure of broch samples to climate change conditions, brings about increased weathering in the sample when compared to its use in the control chamber.

4.5.3 Petrographic Thin Section Analysis Conclusion

Findings from petrographic thin section analysis show that in Clachtoll samples, pre-existing weaknesses, namely microcracks and clay layers, have been unaffected by experimental work in both chambers. It has, however, been postulated that with further simulations of weathering exposure these weaknesses could have reached a tipping point. Conversely, in Borwick samples, more indications of weathering are seen, particularly in samples used in the temperature and humidity chamber. Through thin section work, new knowledge has been gained as to why two samples failed, which is explored further through SEM-EDX work in Section 5.6 SEM-EDX Analysis. Furthermore, the volatility of sulphide nodules has been demonstrated in photomicrograph where substantial secondary porosity has formed around the nodule in BB2 (5), a feature not seen in untreated samples. Finally, with added precipitation, surface secondary porosity brought about by dolomite dissolution is seen, indicating that increased rainwater, in turn, increases dissolution rate, prompting the formation of secondary porosity that can lead to surface loss.

In control chambers, Clachtoll samples once again remain intact. More interestingly, the same features that failed or showed signs of weathering in Borwick experimental samples remained intact in control chambers. No microcracks failed, sulphide nodules remained intact and there is considerably less evidence of secondary porosity.

Crucially, it has been demonstrated that broch samples show more signs of weathering than background geology samples and these effects are more pronounced in the experimental chamber. This provides evidence to suggest that in a climate-changed future, culturally significant Scottish sandstone that has been pre-weathered above surface, will be more prone to exacerbated degradation and failure in the future.

It must be noted that detecting truly new weathering features or the degradation of existing ones in climate sensitised samples by analysing petrographic thin sections is complex, not least due to the heterogeneity within, what appear to be, similar sandstone samples. However, due to the formation of a robust baseline for each sample block carried out in Chapter 3, important differences can be detected after experimental work. It would be unreasonable to conclude that all differences noted are entirely a direct consequence of sample exposure to climate change conditions; however, the inferences are clear. If a feature is not seen before, or appears less weathered in untreated samples, but is seen or appears more degraded after experimental work, it is reasonable to conclude that the experiment has at least partially led to this; conclusions made from these analyses are, therefore, robustly supported. Changes in rock and stone samples are subtle over short timescales but are significant when considering compounded exposure within a prolonged climate change future. Through SEM-EDX analysis in the next section, more knowledge is gained into changes within samples noted during petrographic thin section analysis.

4.6 SEM-EDX Analysis

This section follows a similar structure as the SEM-EDX analysis undertaken in Chapter 3 (Section 3.6 SEM-EDX Analysis), whereby a sample scan is presented, showing the location(s) of SEM-EDX mapping. These areas are particular features of interest identified through petrographic thin section analysis. Elemental spectra accompany map data; as discussed in the methods section (Section 2.4.6.3 Scanning Electron Microscope with Emission Dispersive Spectroscopy (SEM-EDX) Analysis), these are sum spectra and, therefore, normalised to 100%, meaning that comparing absolute values across samples incurs error, however, they provide quantification of the percentage compositions of elements

within each analysed area. Interpretation and discussion follow for each sample before an overall conclusion is made on the effects that experimental work has had on focus sandstones, observable through SEM-EDX analysis.

4.6.1 Clachtoll

As highlighted during petrographic thin section work, Clachtoll control and broch samples display very little evidence of weathering associated with their exposure in CEF experiments. Consequently, SEM-EDX work is limited to the following samples that display areas of interest where evidence of weathering is most likely to be discovered:

Experimental Chamber Temperature and Humidity:

CC1 (1), CB3 (9).

Experimental Chamber Temperature, Humidity and Precipitation:

CC2 (6).

Control Chamber Temperature and Humidity:

CB1 (3).

4.6.1.1 Experimental Chamber

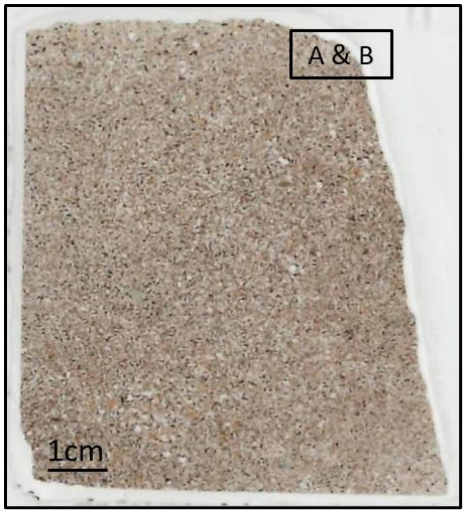

Figure 4.78 - Scan of CC1(1) showing the location of SEM-EDX mapping, focussing on a surface microcrack. Both maps are taken from the same area, map B is at a higher magnification

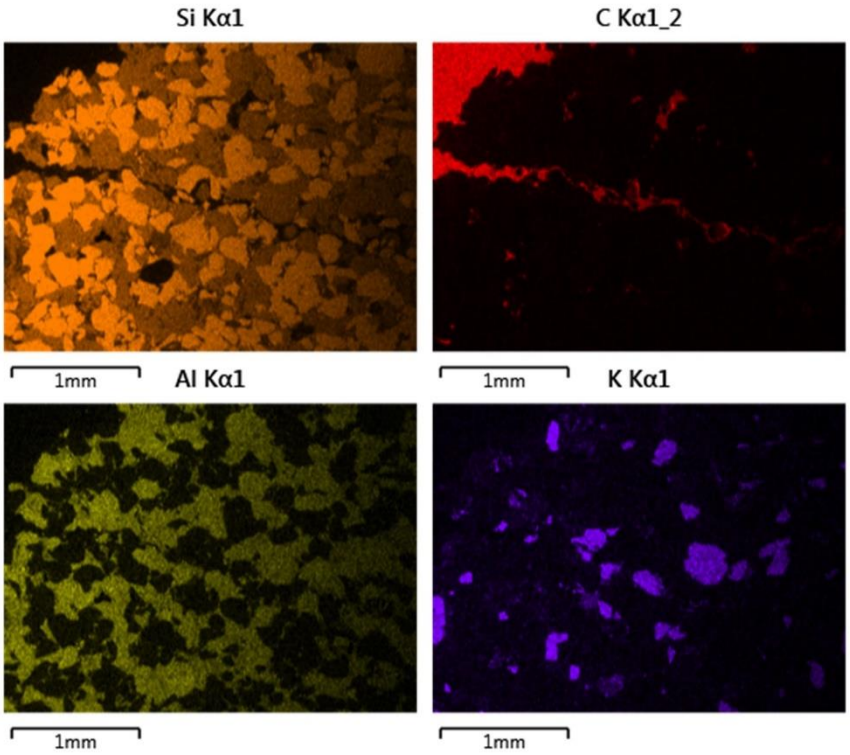

Element	Wt%
O	40.3
C	26.2
Si	24.2
Al	3.3
Na	1.8
Fe	1.5
Mg	0.9
K	0.7
Ca	0.5
Cl	0.3
Ti	0.2

Figure 4.79 - Quartz (Si), C, plagioclase feldspar (Al) and potassium feldspar (K) distribution in the mapped section A of CC1 (1) with normalised elemental proportion (%) of the mapped area

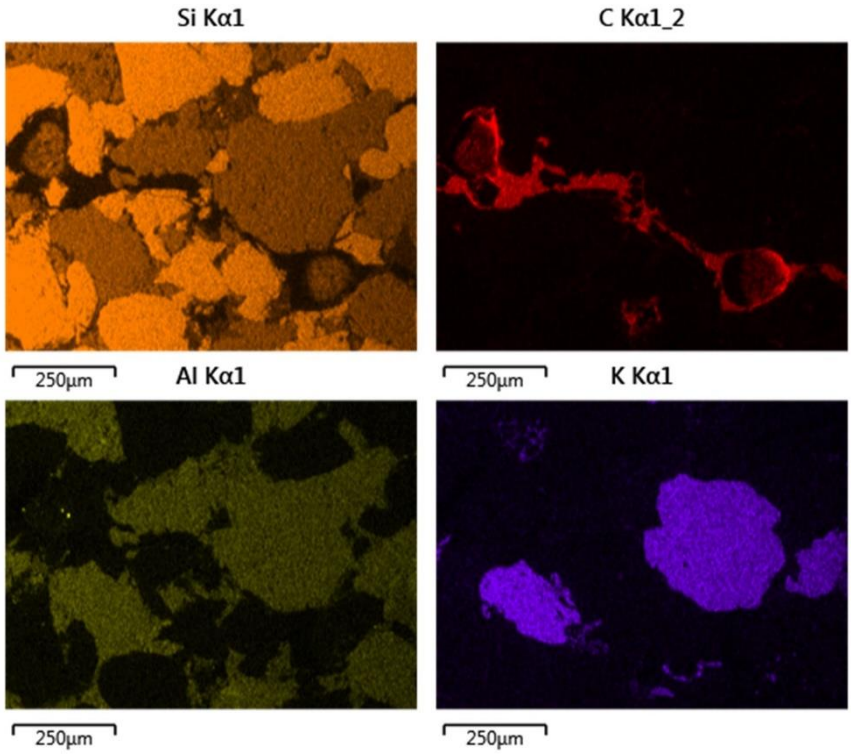

Element	Wt%
O	41
Si	27
C	22.3
Al	3.6
K	1.9
Na	1.5
Fe	1.1
Mg	0.7
Ca	0.4
Cl	0.2
Ti	0.1

Figure 4.80 - Quartz (Si), C, plagioclase feldspar (Al) and potassium feldspar (K) distribution in the mapped section B of CC1 (1) with normalised elemental proportion (%) of the mapped area

SEM-EDX mapping occurred on CC1 (1) to determine whether a microcrack, discovered during thin section analysis, has caused any surface deformation. Figure 4.79 shows the extent of the feature, stretching approximately 3mm into the rock, this is seen most clearly in the carbon map which can be used as a proxy for porosity as it is the signal received from the resin bonding the sample to the glass slide.

What is clear from Figure 4.79, is that the general fabric of quartz and feldspar grains close to the microcrack appear intact. However, on inspection of Figure 4.80 which offers a set of higher magnification maps, localised damage can be seen. The microcrack punctures quartz grains, leaving grain fragments within the newly created pore space. Both feldspar types that are closest to the microcrack exhibit signs of deformation, primarily fracturing. Damage beyond the microcrack location itself cannot be seen, indicating that any deformation caused is extremely limited in scope. Furthermore, from maps and spectra, the microcrack does not appear to have triggered the formation of authigenic clay within the secondary pore space.

It can be said, therefore, that although the microcrack has occurred with considerable force, enough to fracture quartz and feldspar grains, the damage associated with the microcrack is limited. Two reasons can be put forward in explaining this: firstly, it is possible that the microcrack is fresh and has occurred relatively recently, or the rock fabric is extremely robust and the microcrack has not caused significant damage to undermine this. If the feature is fresh, there is potential that it has formed during the experiment, however, as microcracks have been seen in untreated samples, this cannot be confirmed. Of principal importance, exposure to laboratory simulated climate change has not led to any considerable damage to the material arising from the microcrack, whether it transpired during the experiment or not. Given the robustness of the sandstone demonstrated in SEM-EDX maps, it is clear that it would take great force or prolonged exposure to extreme conditions to cause this sample to fail.

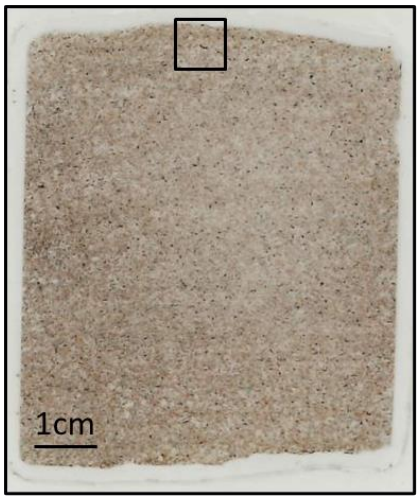

Figure 4.81 - Scan of CB3 (9) showing the location of SEM-EDX mapping, focussing on a potential surface weakness

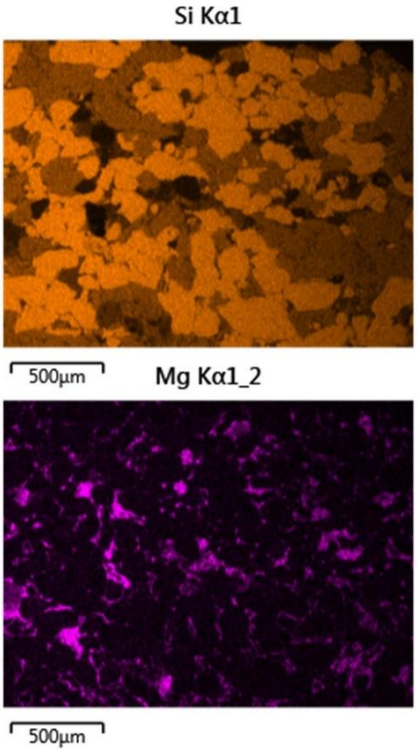

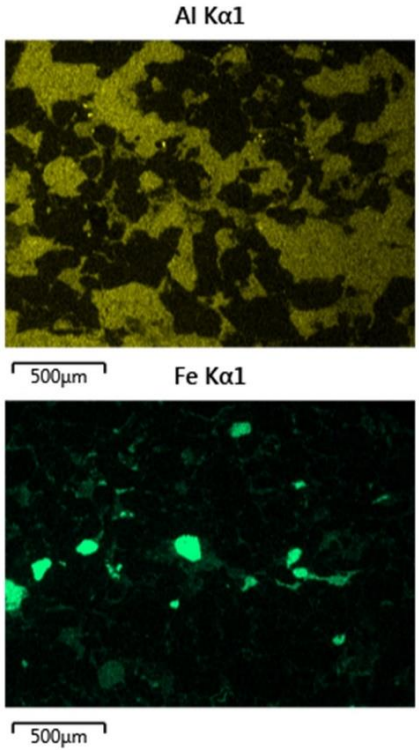

Element	Wt%
O	42.7
Si	29.1
C	17.9
Al	3.5
Fe	2.6
Na	1.8
Mg	0.9
K	0.7
Ca	0.4
Ti	0.2
Cl	0.1

Figure 4.82 - Quartz (Si), plagioclase feldspar (Al), Mg and Fe distribution in the mapped section of CB3 (9) with normalised elemental proportion (%) of the mapped area

The mapping of CB3 (9) focuses on an opaque surface layer observed during thin section work. From Figure 4.82, this can be seen to be composed of iron, with traces of magnesium. Similar features have been mapped and discussed in untreated samples and showcase some of the variability within the Torridonian Sandstone. Although predominantly grain supported, the occurrence of iron oxide cement is seen and adds to the robustness of the sandstone.

However, iron seen in this instance appears to consist of distinct nodules, indicating that they have formed through precipitation in geological deposits, or are derived from underlying Lewisian Gneiss. Crucial to this thesis, however, the iron band does not appear to be an area of weakness that could be exacerbated in a climate changed future.

Figure 4.83 - Scan of CC2 (6) showing the location of SEM-EDX mapping, focussing on an opaque layer that separates fine and coarse-grained material

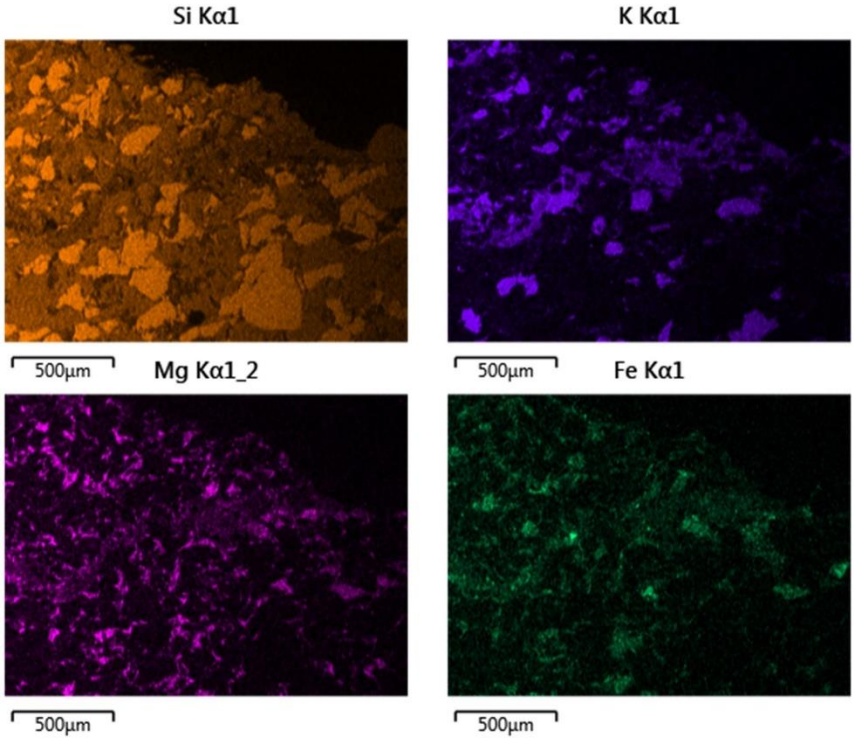

Element	Wt%
O	40.6
C	25.9
Si	21
Al	4.9
Na	2.1
K	1.5
Fe	1.3
Mg	1.2
Ca	0.7
Ti	0.4
Cl	0.3

Figure 4.84 - Quartz (Si), potassium feldspar (K), Mg and Fe distribution in the mapped section of CC2 (6) with normalised elemental proportion (%) of the mapped area

Similar to CB3 (9), the focus of SEM-EDX mapping on CC2 (6) is on an opaque layer, however, in this instance, the opaque layer is a distinct band that separates fine material at the

sample's immediate surface, and coarse material at depth. It contrasts starkly to the iron nodule rich opaque layer seen in CB3 (9), with the map for CC2 (6) (Figure 4.84) showing the fluid-like structure of iron, magnesium, and potassium, whereby they appear to constitute a continuous layer within the sample rather than discrete grains. This feature has been observed and characterised in untreated control samples, from which it was determined that this is likely an illite clay layer.

Clay layers have been pinpointed in Chapter 3 baseline work as a potential weakness area within the Torridonian Sandstone. As discussed during thin section work, the scan in Figure 4.83 shows that at the top left of the slide, an area of the surface has been lost. Although the surface failure did not transpire during the experiment, CC2 (6) demonstrates that this clay banding feature does fail.

Weathering processes that have occurred to date, will continue to occur in the future, however, in the context of a climate changed future, these processes are likely to occur more rapidly. Therefore, with prolonged exposure, it is feasible that surface failure along distinct clay layers could be exacerbated and undermine the robustness of the sandstone type. Additional, laboratory simulated weathering of Torridonian Sandstone focused on longer-term exposure, would be necessary to determine just how destructive climate change could be on the material, particularly sections which contain distinct clay layers.

4.6.1.2 Control Chamber

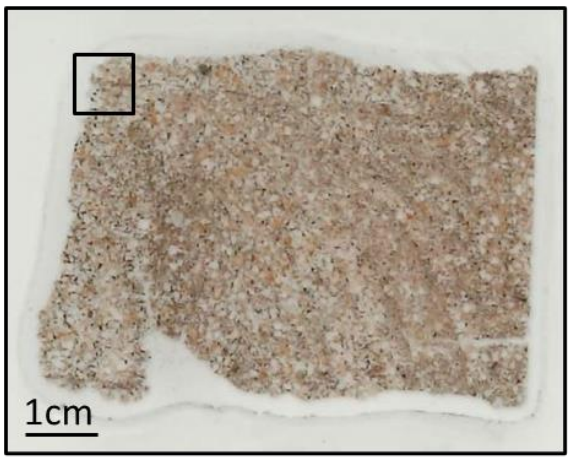

Figure 4.85 - Scan of CB1 (3) showing the location of SEM-EDX mapping, focussing on a horizontal surface crush zone

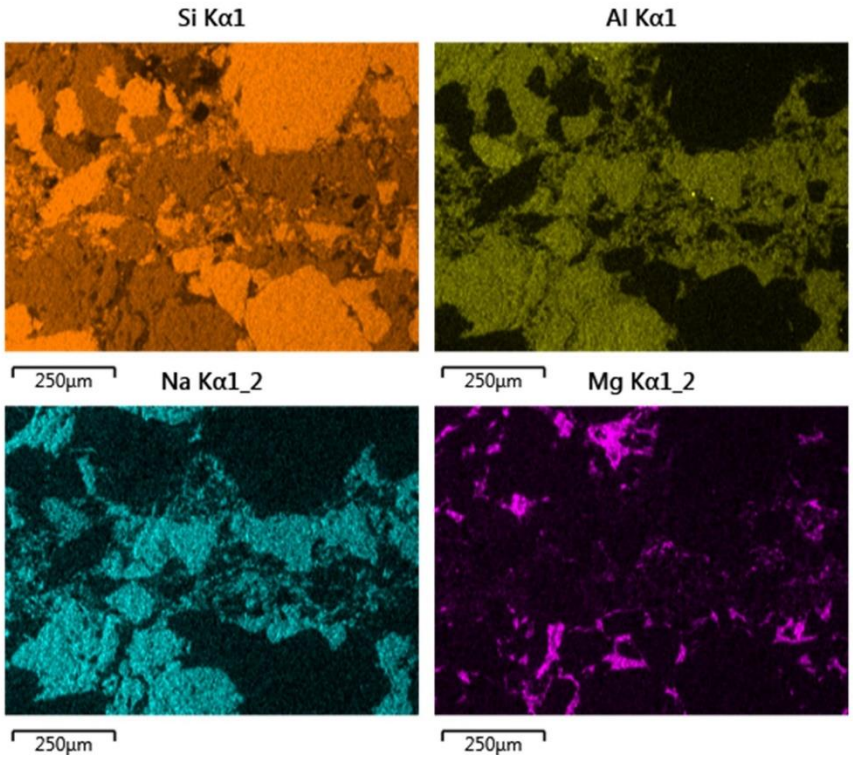

Element	Wt%
O	44.2
Si	30.6
C	14.4
Al	4.7
Na	2.7
Fe	1.6
K	1.1
Ca	0.3
Ti	0.2
Ni	0.1
Mn	0.1

Figure 4.86 - Quartz (Si), plagioclase feldspar (Al), Na and Mg distribution in the mapped section of CB1 (3) with normalised elemental proportion (%) of the mapped area

To understand the structure and chemistry of crush zones which are common in the Torridonian Sandstone, and to determine if any weathering features are associated with them, mapping of a specific section of CB1 (3) occurred. From Figure 4.86, the feature appears to be dominated by crushed quartz. Sodium and potassium can be seen, and their percentages appear high in this area, indicating the presence of albite. Individual grains appear to be held within a fluid structure, perhaps indicating the presence of clay or feldspar dissolution. Crucially, no signs of deformation can be seen around the structure, and they do not appear to be areas of weakness as hypothesised.

4.6.1.3 Clachtoll SEM-EDX Conclusion

Torridonian Sandstone has been negligibly affected at most by exposure to a climate changed year, however, SEM-EDX mapping has been useful in investigating the response of key features to experimental conditions. Mapping was focused on a surface microcrack, opaque layers and a crush zone. Despite a lack of evidence of deformation surrounding the microcrack, there is potential that it occurred as a result of experimental work, regardless, the damage caused is limited in scope and does not appear to undermine the robustness of the material. Two contrasting opaque layers showcase variability within the sandstone, with CB3

(9) containing iron nodules, whereas the iron present in CC2 (6) appears more fluid in structure alongside feldspar components. The latter opaque layer has been characterised as a clay layer, and it has been hypothesised that features such as these could be distinct weakness zones within the sandstone type. Finally, the crush zone seen in CB1 (3) appears completely intact after experimental work.

Knowledge gained into the weathering of Torridonian Sandstone in a climate changed future is limited, due to the extremely robust nature of the material coupled with short-term exposure to simulated weathering. Deeper understandings of the stone fabric have been gained and the only ubiquitous feature within the sandstone that appears to be prone to any kind of degradation is distinct clay layers. The rate at which these features fail remains unknown, and it is suggested that prolonged exposure experiments focused on clay layer failure should be undertaken to understand this more fully. In the scope of this analysis, however, it does not appear that Torridonian Sandstone is under immediate threat from future climate change.

4.6.2 Borwick

Due to the comparatively quicker rate of weathering in Stromness Flagstone when compared with Torridonian Sandstone, more extensive SEM-EDX mapping could occur on particular weathered features of interest, including those that failed as a result of the CEF experiment. SEM-EDX mapping occurred on the following samples, exposed to different treatments within the climate changed year experiment and control:

Experimental Chamber Temperature and Humidity:

BC2 (5), BC3 (8), BB1 (1), BB2 (5), BB3 (8).

Experimental Chamber Temperature, Humidity and Precipitation:

BB1 (2), BB2 (6) BB3 (9).

Control Chamber Temperature and Humidity:

BB1 (3).

4.6.2.1 Experimental Chamber

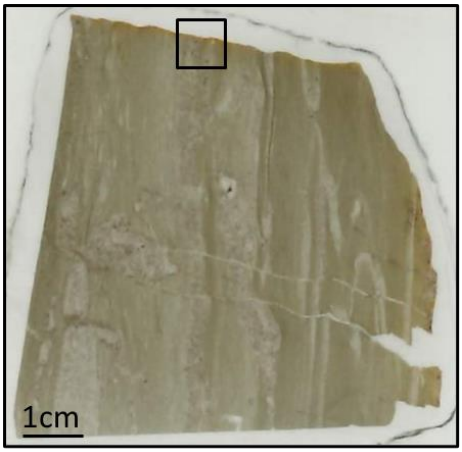

Figure 4.87 - Scan of BC2 (5) showing the location of SEM-EDX mapping, focussing on the surface exposed in the CEF

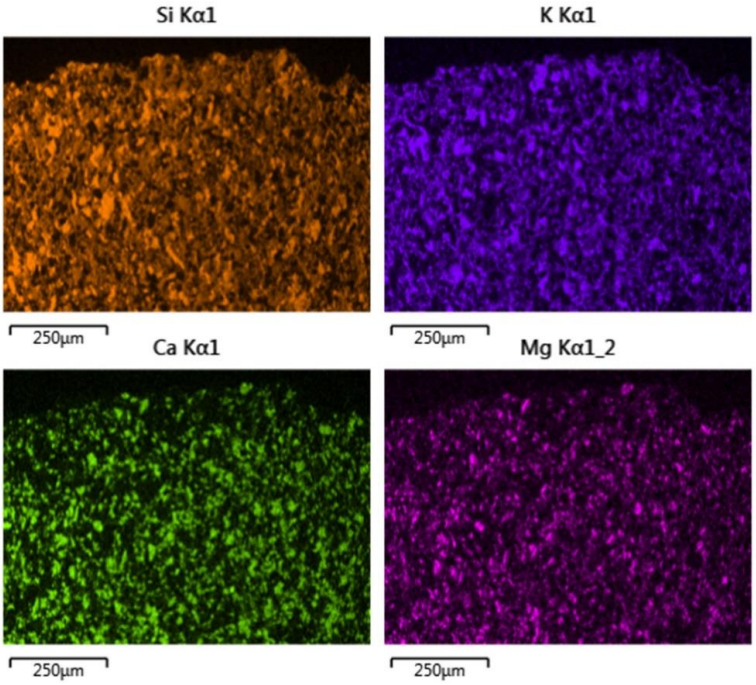

Element	Wt%
O	37.6
C	31.8
Si	14.8
Al	4.1
Ca	4
K	2.9
Fe	2
Mg	1.3
Na	0.7
Cl	0.3
Ti	0.2

Figure 4.88 - Quartz (Si), potassium feldspar (K), Ca and Mg distribution in the mapped section of BC2 (5) with normalised elemental proportion (%) of the mapped area

Figure 4.89 - Scan of BC3 (8) showing the location of SEM-EDX mapping, focussing on the surface exposed in the CEF

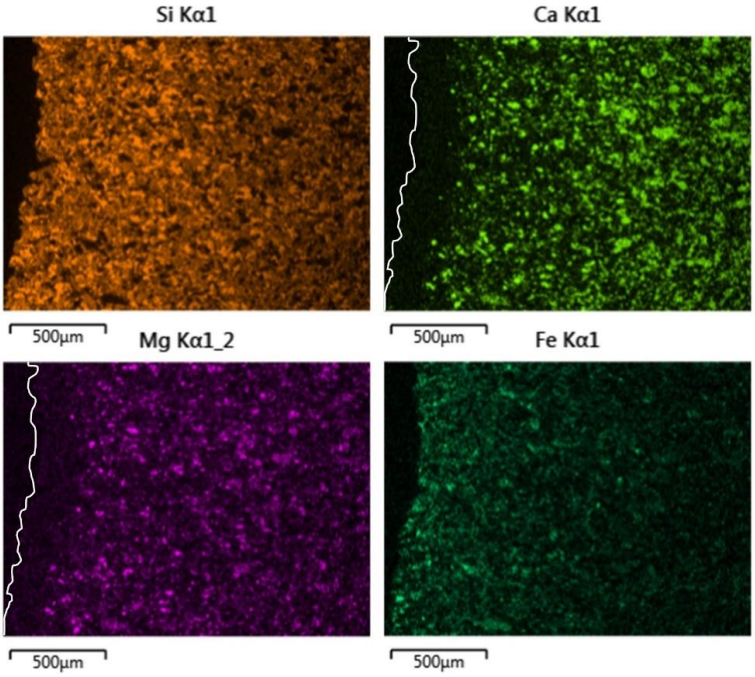

Element	Wt%
O	37.8
C	31.3
Si	15.9
Al	4.1
Ca	3.1
K	2.8
Fe	2.4
Mg	1.1
Na	0.9
Cl	0.3
Ti	0.2

Figure 4.90 - Quartz (Si), Ca, Mg and Fe distribution in the mapped section of BC3 (8) with normalised elemental proportion (%) of the mapped area. Surface line added to Ca and Mg map to highlight dissolution within the upper area of the sample

In spectra provided for BC2 (5) and BC3 (8) (Figure 4.88 and Figure 4.90), calcium, and magnesium account for 4% and 1.3% respectively in the former and 3.1% and 1.1% in the latter, additionally, the abundance of iron is greater in BC3 (8). All of these factors are indicative of greater dolomite dissolution in BC3 (8). However, as noted in Chapter 2 (Section 2.4.6.3 Scanning Electron Microscope with Emission Dispersive Spectroscopy (SEM-EDX) Analysis) and figure captions, spectra percentage has been normalised to 100%, consequently, comparing absolute values is not completely reliable as they are affected by

factors such as sample porosity and the amount of resin (C) detected and can, therefore, only be utilised as a guide. Greater insight into the extent of surface dissolution between samples can be visualised on comparison of the SEM-EDX maps, whereby, dissolution in BC2 (5) can be seen to be considerably more extensive than in BC3 (8). Key dolomite minerals are seen throughout the majority of BC2 (5)'s surface, while they are absent within the surface of BC3 (8). Iron enrichment at the surface of BC3 (8) is visualised in Figure 4.90, giving a reason for the distinct red coloured crust. A narrative can be built around these findings. Likely, the surface of BC2 (5) exposed in the CEF was not outward facing while within the background geology, therefore, its extraction and subsequent exposure in the CEF is the first time this rock face has been subjected to climatic conditions. Conversely, the depth of dissolution in BC3 (8) indicates that the exposed surface in the experiment has been prior exposed while held within the geology. Ideally, control rock surfaces exposed in the CEF will have had no prior exposure, however, given the complexity of sampling and the inherent difficulty of extracting pristine rock from the background geology, this is not always possible. Additionally, before a petrographic thin section has been manufactured, it is difficult to determine which face is truly pristine. In terms of the scope of this research, it can be said with confidence that BC2 (5) is as close to pristine as possible.

The lack of dissolution in BC2 (5) compared to BC3 (8) has been highlighted, however, this research focuses on small scale early indications of a change or acceleration in weathering with exposure to a climate changed future. Although dolomite appears intact at BC2 (5)'s surface, a slight reduction in key mineral intensities in the map data can be observed at the very immediate surface. Findings solely from SEM-EDX mapping indicate that exposure in the CEF has potentially created a very thin dolomite dissolution zone at the immediate surface of BC2 (5), further image analysis work is conducted in a subsequent section (4.6.2.3 ImageJ Analysis) to quantify this finding.

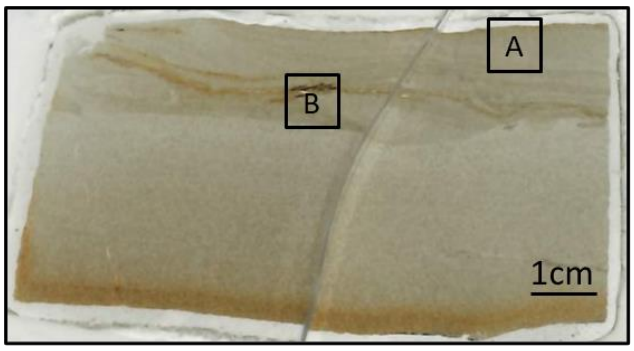

Figure 4.91 - Scan of BB1 (1) showing the location of SEM-EDX mapping, focussing on the surface exposed in the CEF (A) and an area that failed during experimental work (B)

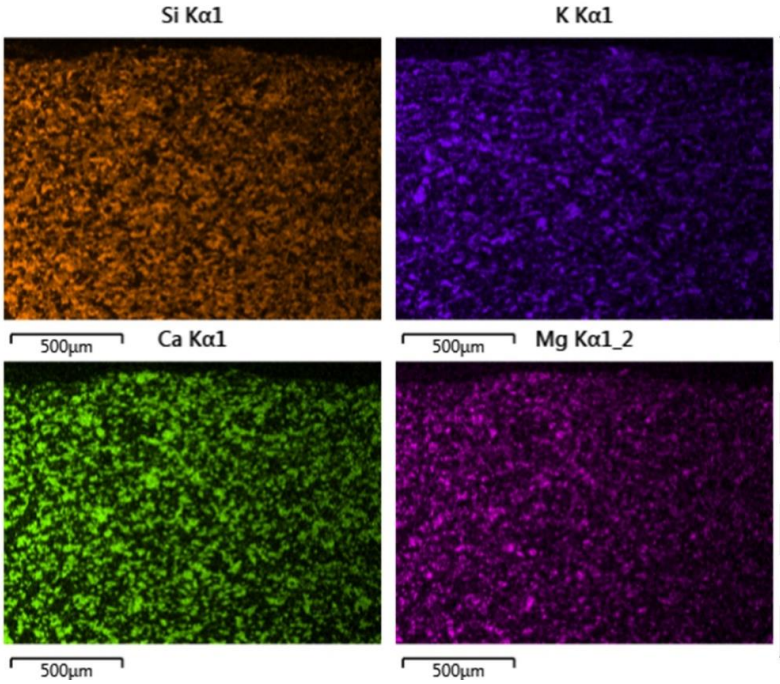

Element	Wt%
C	37.4
O	33.3
Si	13.3
Ca	5.2
Al	3.4
Fe	2.7
K	2.1
Mg	1.3
Na	0.8
Cl	0.3
Ti	0.2

Figure 4.92 - Quartz (Si), Potassium Feldspar (K), Ca and Mg distribution in the mapped section A of BB1 (1) with normalised elemental proportion (%) of the mapped area

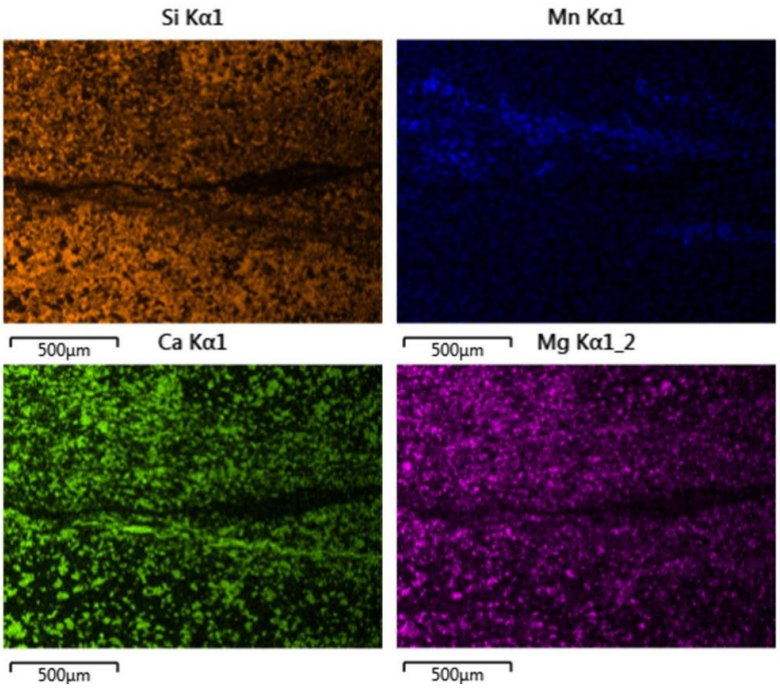

Element	Wt%
O	38.5
C	27.6
Si	15.9
Ca	5.6
Al	4.1
Fe	2.9
K	2.3
Mg	1.4
Na	0.9
Mn	0.3
Ti	0.3

Figure 4.93 - Quartz (Si), Mn, Ca, and Mg distribution in the mapped section B of BB1 (1) with normalised elemental proportion (%) of the mapped area

From the scan of BB1 (1), the sample surface exposed in the CEF displays little sign of weathering when compared to the opposite side, indicating that it has not been outward facing while within Borwick Broch. Calcium and magnesium appear intact at the immediate

surface as seen in Figure 4.92, however, the main feature of interest in this sample is the failure of a pre-existing microcrack, mapped in Figure 4.93. It was hypothesised that this failure had transpired as a result of rainwater penetration into the pore space generated by the microcrack, triggering dolomite dissolution, weakening the stone fabric surrounding the feature, causing it to fail as a result of CEF exposure. However, as seen in the map presented (Figure 4.93), there is no drastic loss of dolomite. It could be argued, therefore, that this appears to be a physical failure, rather than a chemical one. The rock type is abundant in microcracks associated with its deposition and alteration over geological time, based on the calcium and magnesium signal, it appears that the feature has failed without significant dissolution having occurred.

Before arriving solely at this conclusion, the presence of manganese noted in Figure 4.93 must be considered. This is of interest as it is an element not generally seen in sample spectra, with iron being far more common. Manganese is, however, closely related to the dissolution of dolomite in the same way as iron. It is noted in a 2012 report on Liddle's Quarry, an important source of Stromness Flagstone, that manganese had formed on joint surfaces. Rainwater that travels along distinct joints and microcracks comes into contact with dolomite, causing dissolution. When this occurs, iron and, in this case, manganese, is released and redeposited on joint surfaces, causing a distinct red dissolution colour to surround the joint. Therefore, although there does not appear to be a lack of calcium or magnesium surrounding the microcrack, the presence of manganese is evidence that limited dolomite dissolution has occurred and could have contributed to the failure of the microcrack (Gillespie and Tracey, 2012). The failure is, therefore, likely to be a result of the physical failure of a pre-existing weakness, exacerbated by minor dolomite dissolution, evidenced by the presence of manganese.

Crucially, it appears that the conditions simulated within the climate changed CEF chamber, have been sufficient to cause the sample's failure. This result in itself was unexpected as this research is focused on small scale, early indications of change. In this instance, however, a dramatic loss of stone material is seen. It must be noted that the state of the microcrack before experimental work was unknown, aside from the fact that the sample was intact. It was likely close to failure, with one cycle in the CEF chamber enough to cause it to fail. This finding has significant implications for Borwick Broch stone containing similar features, with repeated exposure to climate change conditions, it is feasible that more such features will fail, potentially with increased regularity.

From these findings, the weathering and degradation of Stromness Flagstone can be considered twofold, where distinct surface dissolution weakens the exposed face of the material, while, over time, pre-existing microcracks and bedding planes fail at depth, making the lithology highly prone to both chemical and physical decay.

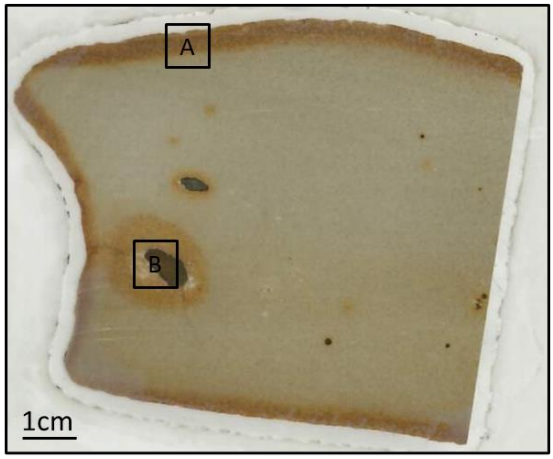

Figure 4.94 - Scan of BB2 (5) showing the location of SEM-EDX mapping, focussing on the surface exposed in the CEF (A) and a sulphide nodule (B)

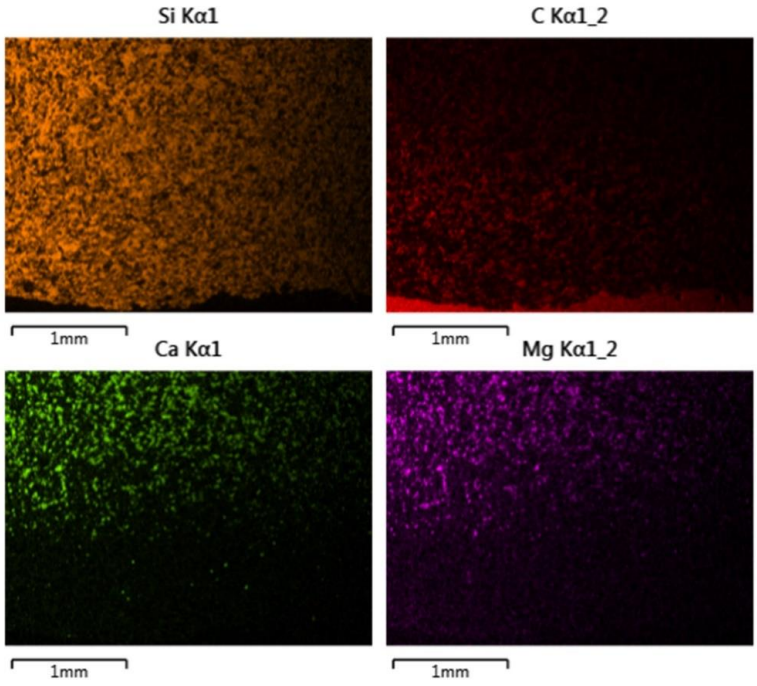

Element	Wt%
O	38
C	31.7
Si	19.3
Al	3.2
Fe	2.4
Ca	1.8
Na	1.3
K	1.1
Mg	0.6
Cl	0.3
Ti	0.2

Figure 4.95 - Quartz (Si), C, Ca, and Mg distribution in the mapped section A of BB2 (5) with normalised elemental proportion (%) of the mapped area

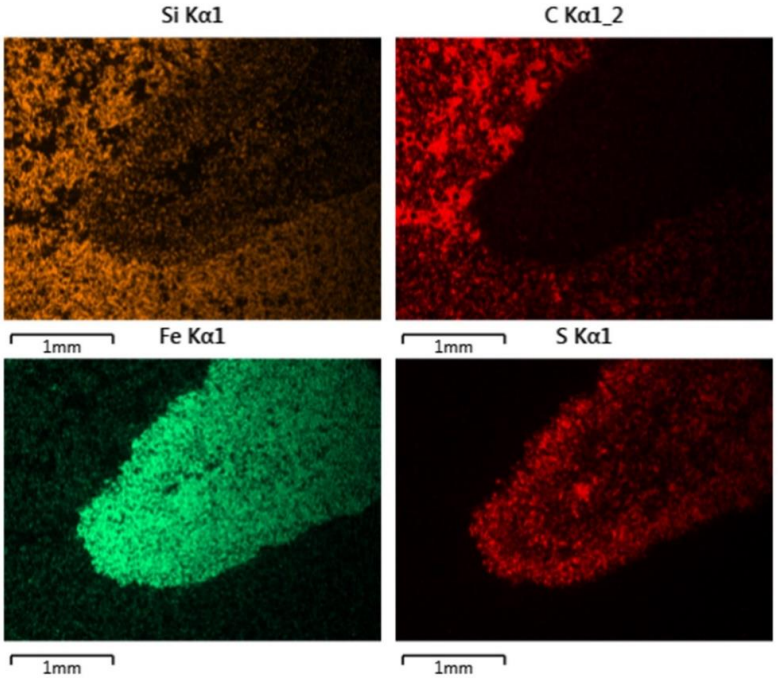

Element	Wt%
C	35.2
O	31.8
Fe	12.3
Si	11.8
S	3.9
Al	2.4
Na	1
K	0.8
Cl	0.4
Ca	0.3
Ti	0.1

Figure 4.96 - Quartz (Si), C, Fe, and S distribution in the mapped section B of BB2 (5) with normalised elemental proportion (%) of the mapped area

There are two key features of interest in BB2 (5): surface dissolution and sulphide nodule weathering. Figure 4.95 showcases the diminished level of calcium and magnesium at the upper surface of the stone, travelling to a considerable depth which is quantified in the ImageJ section (4.6.2.3 ImageJ Analysis). Furthermore, a carbon map is provided in the figure, which is a proxy for secondary porosity, this is also investigated further through image analysis, however, it appears that as calcium and magnesium decrease, carbon increases, showcasing that dolomite dissolution is generating secondary porosity at the surface of the broch stone.

A weathered area surrounding a sulphide nodule is mapped in Figure 4.96, although the iron and sulphur signals suggest that the nodule itself is intact, there is considerable dissolution and secondary porosity formation around the nodule. This indicates that when sulphide nodules weather and generate sulphuric acid which exacerbates dissolution, a small quantity of the acid is sufficient to cause significant damage to the surrounding stone fabric as is seen in this instance. This showcases the volatility of sulphide nodules and just how damaging they are to the stone structure; with little to no evidence of the nodule itself weathering, but significant stone loss evidenced by the prevalence of carbon in the SEM-EDX map.

In baselining work undertaken in Chapter 3 that focused on sulphide nodules, the surrounding stone fabric was intact, however, under exposure to climate change conditions in the CEF, it appears to have triggered enough sulphuric acid formation to cause significant damage to the surrounding stone. It can be said, therefore, that short time exposure to climate change conditions has caused slight weathering of the nodule itself, which, in turn, has caused significant weathering and dissolution of the stone material surrounding the nodule, evidenced by extensive secondary porosity.

This finding adds to the knowledge of how the Stromness Flagstone weathers in a plethora of ways. As discussed in previous samples, surface dissolution and the failure of microcracks at depth are highly detrimental to the material, in addition, it appears that weathering is exacerbated considerably by the presence of sulphide nodules, highlighting just how at risk the stone is from climate change and associated intensification of weathering.

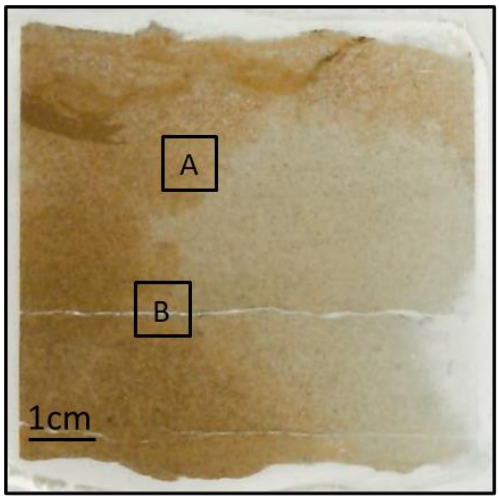

Figure 4.97 - Scan of BB3 (8) showing the location of SEM-EDX mapping, focussing on the stone's general fabric (A) that can be compared with the failed microcrack (B)

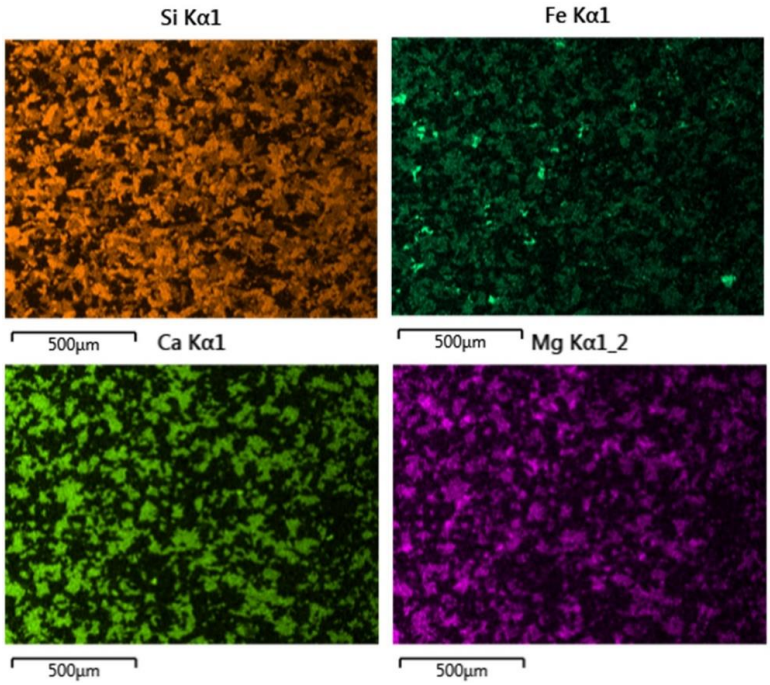

Element	Wt%
O	44.4
Si	21.4
C	13.9
Ca	7.2
Al	3.8
Fe	3.8
Mg	2
K	1.9
Na	1.3
Ti	0.3
Ni	0.1

Figure 4.98 - Quartz (Si), Fe, Ca, and Mg distribution in the mapped section A of BB3 (8) with normalised elemental proportion (%) of the mapped area

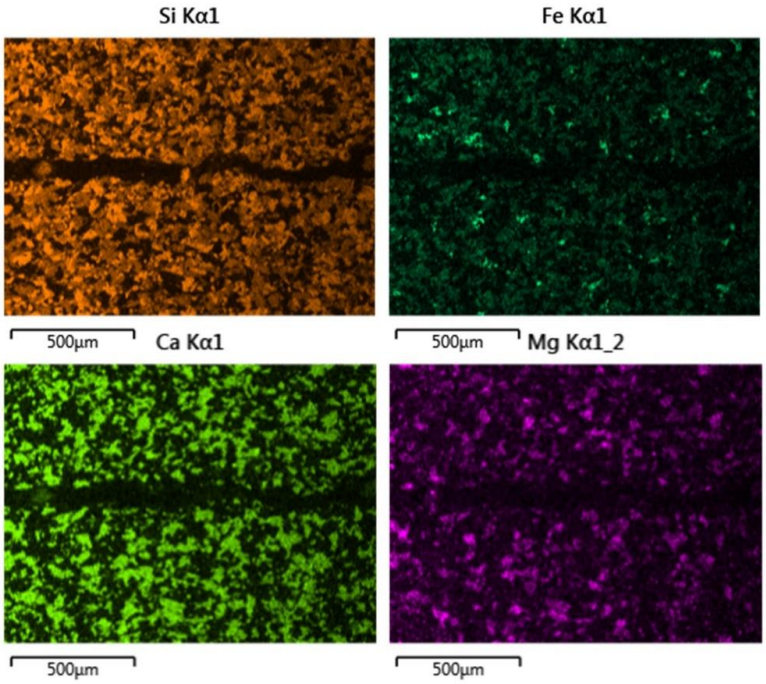

Element	Wt%
O	40.4
C	23.7
Si	17.6
Ca	6.1
Fe	3.8
Al	3.7
K	1.8
Na	1.2
Mg	1.2
Cl	0.2
Ti	0.2

Figure 4.99 - Ca and Mg distribution in the mapped section B of BB3 (8) with normalised elemental proportion (%) of the mapped area

A failure is seen in BB3 (8), similar to that which is seen in BB1 (1). The first set of maps and spectra (Figure 4.98) associated with BB3 (8) is focused on the general fabric of the stone, taken in what appears to be an unweathered area of the material and provides an

important comparison when analysing the map and spectra associated with sample site B (Figure 4.99). The distribution and structure of calcium, magnesium and iron follow the same pattern in both mapped areas. Moving towards the microcrack in Figure 4.99, all elements remain present, there is no sign of dissolution or concentrated iron build up. These findings indicate that there is very little if any chemical alteration leading to the failure of the pre-existing microcrack. Instead, it can be attributed to a physical characteristic within the stone. The Stromness Flagstone is characterised by these weaknesses, of importance in this research, the exposure of BB3 (8) to climate changed conditions has caused sufficient strain on the weakness, enough for it to fail. This has severe implications on the longevity of this stone as part of a culturally significant monument in a climate changed future.

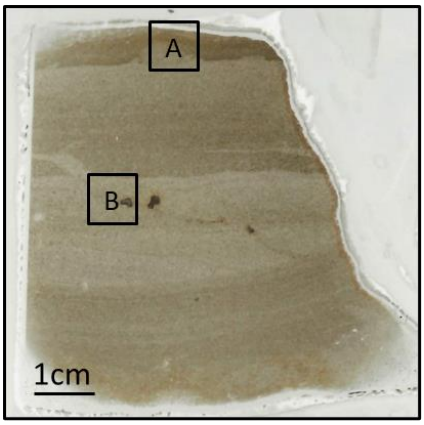

Figure 4.100 - Scan of BB1 (2) showing the location of SEM-EDX mapping, focussing on the surface exposed in the CEF (A) and a sulphide nodule (B)

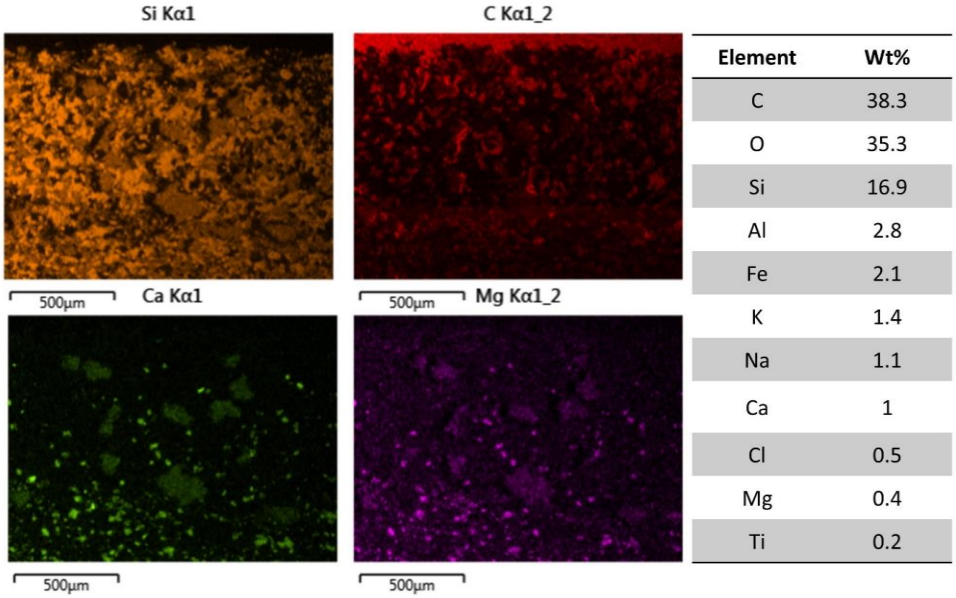

Element	Wt%
C	38.3
O	35.3
Si	16.9
Al	2.8
Fe	2.1
K	1.4
Na	1.1
Ca	1
Cl	0.5
Mg	0.4
Ti	0.2

Figure 4.101 - Quartz (Si), C, Ca, and Mg distribution in the mapped section A of BB1 (2) with normalised elemental proportion (%) of the mapped area

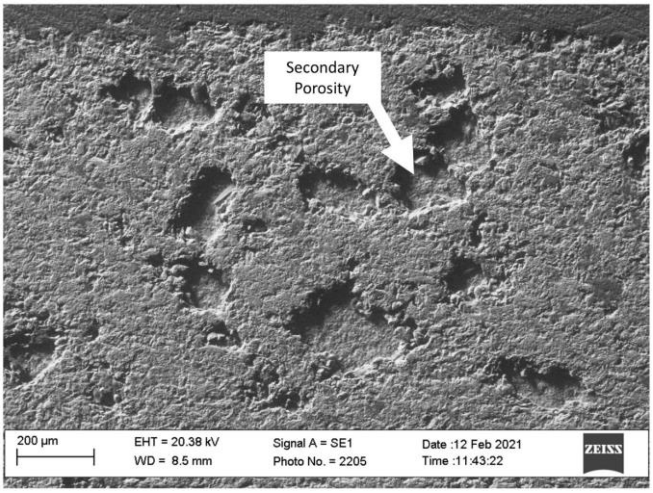

Figure 4.102 – Secondary electron (SE) image of mapped section A of BB1 (2), showing extensive secondary porosity formation

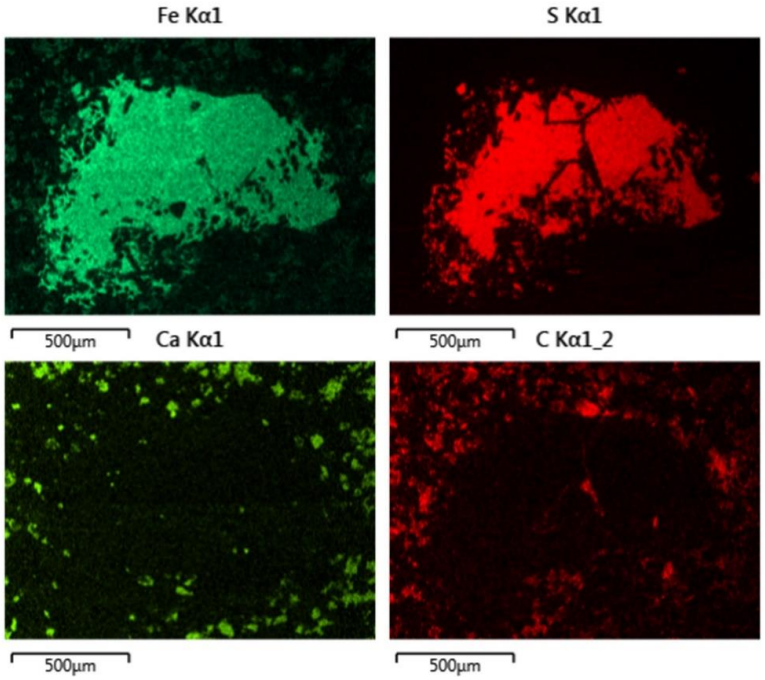

Element	Wt%
O	31.7
C	19.8
Si	16.4
Fe	15.6
S	10.4
Al	2.5
Ca	1.3
K	1.2
Na	1
Cl	0.1

Figure 4.103 - Fe, S, Ca, and C distribution in the mapped section B of BB1 (2) with normalised elemental proportion (%) of the mapped area

The surface map of BB1 (2) is characterised by dolomite dissolution and extensive secondary porosity formation; more prevalent here than in BB2 (5). The secondary porosity appears as a loss of discrete grains, an indication that dissolution is leading to quartz and feldspar granular loss as the cement is no longer present to a sufficient level that can hold the stone fabric together (Figure 4.101 and Figure 4.102). This feature is not seen at the surface of untreated broch samples, meaning that it can be postulated that exposure to climate change conditions has triggered, to a certain extent, increased dolomite dissolution, secondary porosity

formation and granular loss. Potentially giving a reason for the more extensive granular loss is the fact that this sample was utilised within the temperature, humidity, and precipitation chamber. It is feasible that the addition of simulated rainfall allows loose grains to be removed in solution. Further image analysis work in section 4.6.2.3 ImageJ Analysis aids in the quantification of this dissolution surface.

An important feature within this sample is the mapped sulphide nodule (Figure 4.103), unlike the same feature discussed in sample BB2 (5), the nodule in this instance displays more signs of internal fracturing, particularly noticeable in the sulphur signal, with secondary porosity seen within the nodule itself. The effect of this, however, in the dissolution of surrounding dolomite is less prevalent in terms of dolomite dissolution and secondary porosity formation. It can be hypothesised that although in general, all sulphide nodules are labile, some nodules have greater inherent volatility due to factors such as size, structure, and proximity to joints/microcracks from which they can be exposed to rainfall.

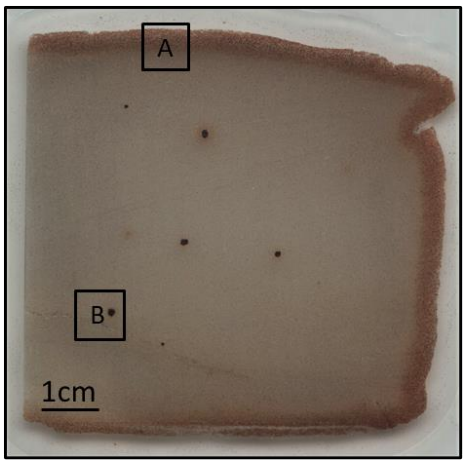

Figure 4.104 - Scan of BB2 (6) showing the location of SEM-EDX mapping, focussing on the surface exposed in the CEF (A) and a nodule and microcrack at depth (B)

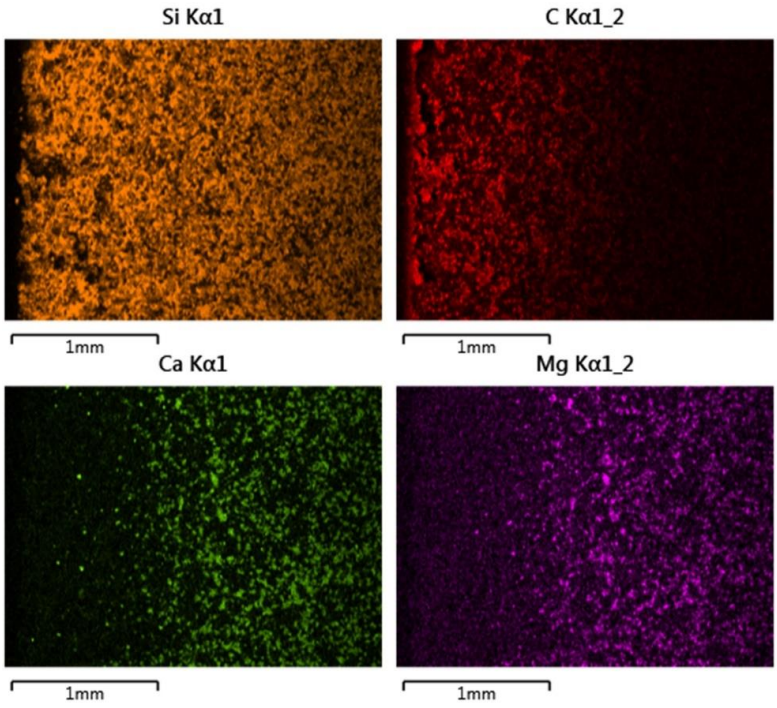

Element	Wt%
O	39.5
C	26
Si	19.9
Al	3.3
Fe	2.9
Ca	2.5
Rb	2.1
Na	1.3
K	1.2
Mg	0.8
Ti	0.2

Figure 4.105 - Quartz (Si), C, Ca, and Mg distribution in the mapped section A of BB2 (6) with normalised elemental proportion (%) of the mapped area

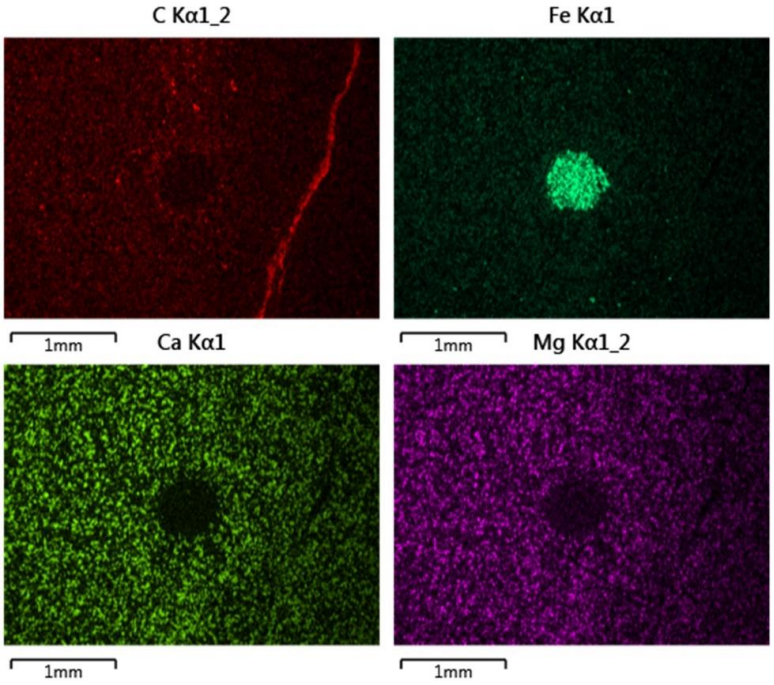

Element	Wt%
O	43.1
Si	22.5
C	17.2
Ca	5
Fe	3.8
Al	3.8
Na	1.6
Mg	1.5
K	1.2
Ti	0.2
Ni	0.1

Figure 4.106 - C, Fe, Ca, and Mg distribution in the mapped section B of BB2 (6) with normalised elemental proportion (%) of the mapped area

The mapping of BB2 (6) showcases the reduction of key dolomite minerals, corresponding with an increase in secondary porosity at the sample surface. The mapped dissolution surface in BB2 (6) (Figure 4.105 and Figure 4.106) is very similar in characteristic to BB2 (5)

utilised in the temperature and humidity chamber. The addition of precipitation does not appear to have affected the depth of the feature; however subsequent image analysis quantifies this more accurately. Interestingly, in BB2 (5), severe weathering of sulphide nodules is noted, conversely, in BB2 (6) (Figure 4.106), the same features appear intact, with minimal secondary porosity formation and no detectable dolomite dissolution surrounding the nodule.

A microcrack can also be observed in BB2 (6) (Figure 4.106), this appears to be a physical joint within the sample, whereby no dolomite dissolution is seen surrounding the feature, evidenced by intact calcium and magnesium signals as well as no observable precipitation of iron surrounding the microcrack.

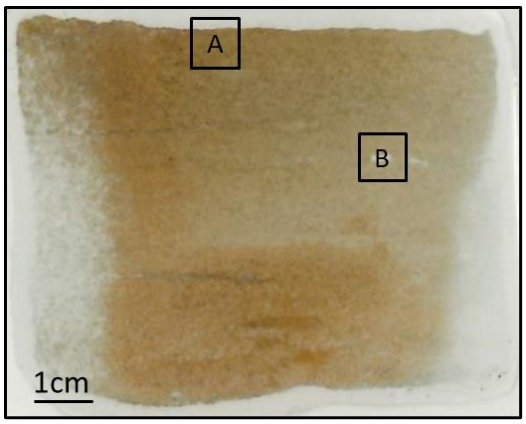

Figure 4.107 - Scan of BB3 (9) showing the location of SEM-EDX mapping, focussing on the surface exposed in the CEF (A) and a microcrack at depth (B)

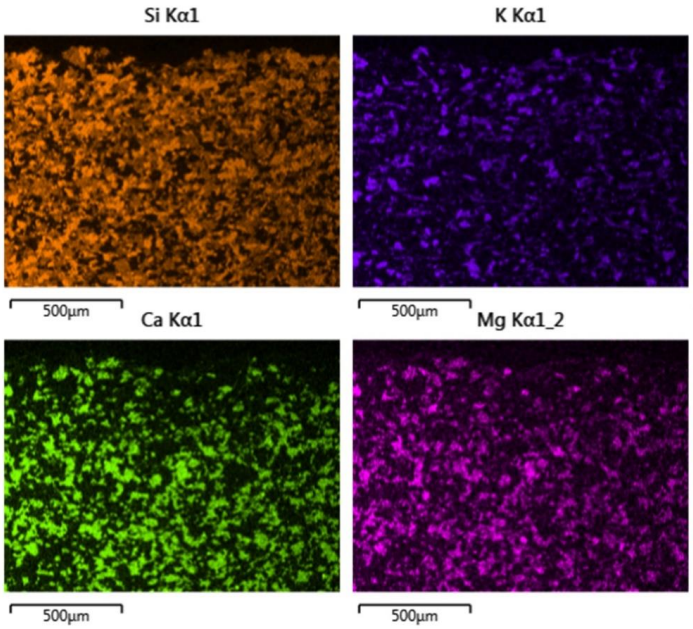

Element	Wt%
O	39.3
C	28.4
Si	16.6
Ca	4.6
Al	3.4
Fe	3.3
K	1.5
Mg	1.3
Na	1.1
Cl	0.3
Ti	0.2

Figure 4.108 - Quartz (Si), potassium feldspar, Ca, and Mg distribution in the mapped section A of BB3 (9) with normalised elemental proportion (%) of the mapped area

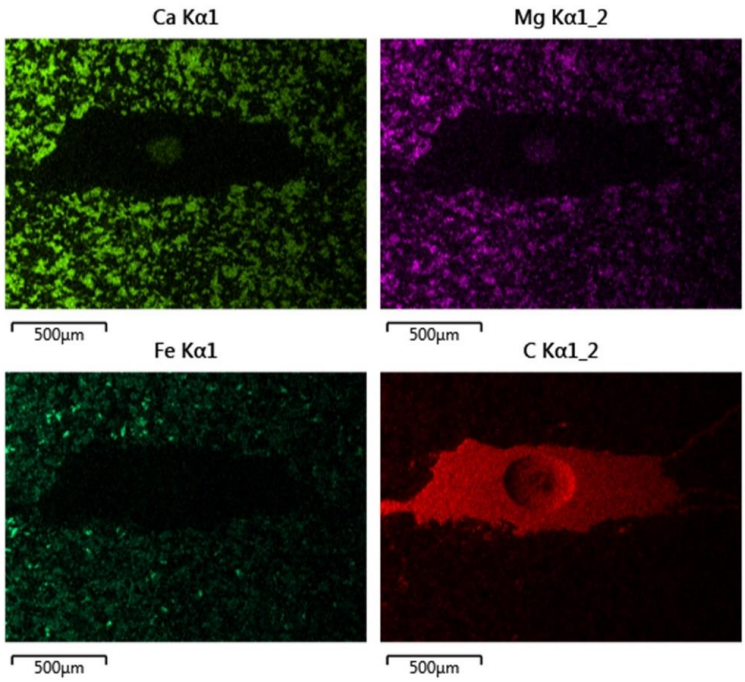

Element	Wt%
O	36.5
C	35.6
Si	13.1
Ca	4.7
Fe	3
Al	2.9
K	1.4
Mg	1.3
Na	0.9
Cl	0.4
Ti	0.2

Figure 4.109 - Ca, Mg, Fe, and C distribution in the mapped section B of BB3 (9) with normalised elemental proportion (%) of the mapped area

BB3 (9) displays two types of common weaknesses within the Stromness Flagstone, namely surface dissolution of dolomite evidenced in Figure 4.108 and microcracks along distinct joints within the stone shown in Figure 4.109. Dissolution seems to be minimal and does not appear close to surface failure. The microcrack varies from similar features seen in other samples, instead of being a continuous microcrack of similar width, there are distinct pore chamber features joined together by a thin microcrack. Unlike BB1 (1) and BB3 (8), BB3 (9) remained intact during experimental work, despite having a significant pre-existing microcrack running the width of the sample. Analysis of Figure 4.109 can aid in understanding this. Contrary to failed samples, there is no evidence of dissolution whatsoever, calcium and magnesium remain completely intact immediately surrounding the microcrack and there is no observable iron abundance. Furthermore, the carbon signal highlights that no secondary porosity has formed surrounding the pore chamber.

Although this microcrack appears to be a distinct weak point, the material surrounding the feature appears intact despite exposure to climate change temperature, humidity, and precipitation conditions. It can be inferred that precipitation has not been significant enough to penetrate through the microcrack and exacerbate its failure. However, sample geometry plays an important role in this, due to the non-fresh cut nature of samples, the shape of the sample can expose or indeed protect specific areas of weakness. Furthermore, as factors such

as wind-driven rain cannot be simulated in the chamber, it is possible that with increased precipitation force from different angles, rainwater could penetrate the weaknesses such as microcracks, triggering dissolution and, eventually, the sample's failure. Additionally, with the increased cycling of climate change conditions in the CEF, it is feasible that the microcrack would have reached its tipping point, similar to BB1 (1) and BB3 (8). As far as the scope of this weathering simulation, the sample has remained intact.

4.6.2.2 Control Chamber

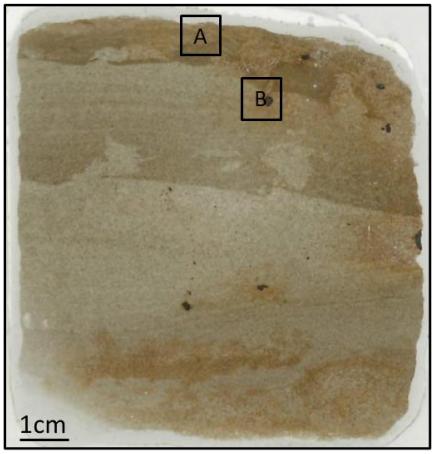

Figure 4.110 - Scan of BB1 (3) showing the location of SEM-EDX mapping, focussing on the surface exposed in the CEF (A) and a sulphide nodule (B)

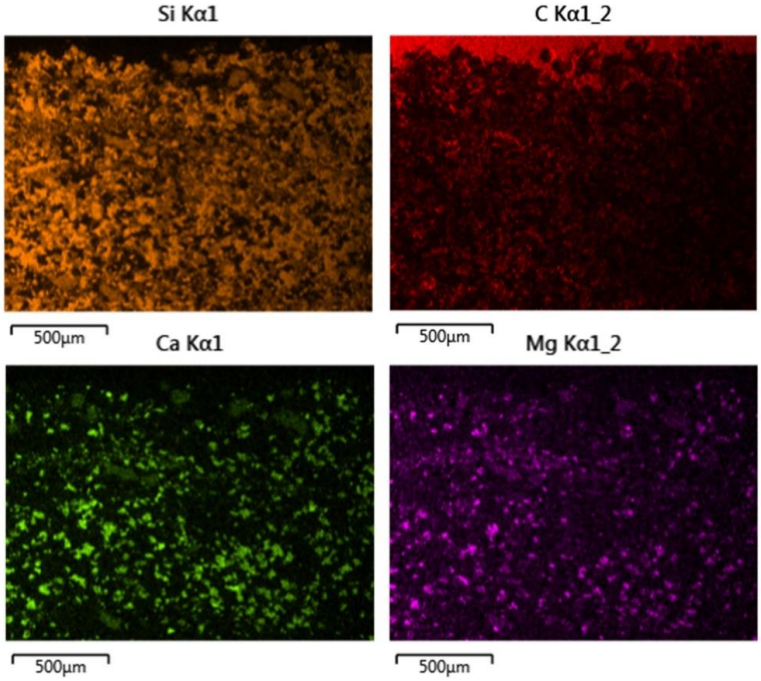

Element	Wt%
C	36.8
O	35.9
Si	15.9
Al	2.9
Fe	2.6
Ca	2.1
K	1.4
Na	0.9
Mg	0.6
Cl	0.4
Ti	0.2

Figure 4.111 - Quartz (Si), C, Ca, and Mg distribution in the mapped section A of BB1 (3) with normalised elemental proportion (%) of the mapped area

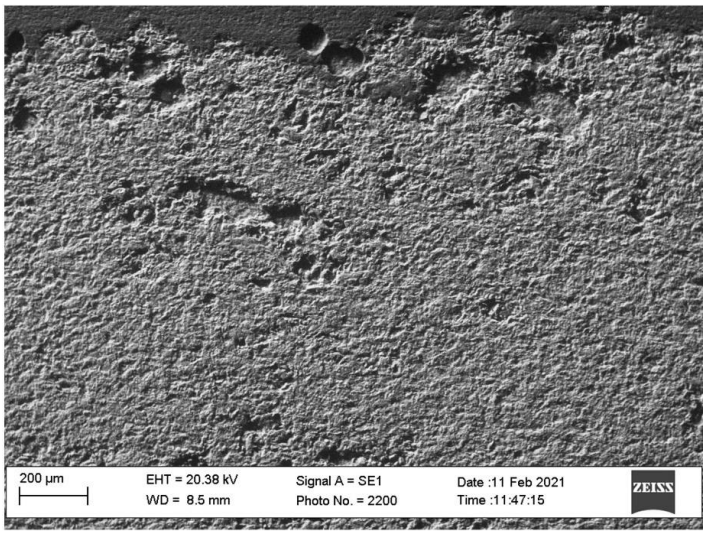

Figure 4.112 – Secondary electron (SE) image of mapped section A of BB1 (3)

Important contrasts can be made between BB1 (3) (Figure 4.110 - Figure 4.112) and BB1 (2) (Figure 4.100 - Figure 4.103) discussed in the previous section. Similar features are seen on both samples, namely surface dolomite dissolution and secondary porosity formation. However, the extent of these features appears reduced in BB1 (3) which was utilised in the control chamber when compared with BB1 (2) which was incorporated within the climate change chamber. From SEM-EDX mapping (Figure 4.111) it can be seen that calcium and magnesium levels are diminished at the immediate surface and grain-like losses can be seen here and in the secondary electron image (Figure 4.112). As highlighted, these features appear less extensive than they do in BB1 (2) utilised in the experimental chamber. This finding has significant implications for the rate of dolomite dissolution in a climate changed future. It can be hypothesised based on findings from this research that with exposure to climate change conditions in Scotland, dolomite dissolution and subsequent secondary porosity formation will be increased compared to how these processes occur at present. This is explored further through image analysis. The mapped section B focuses on a distinct sulphide nodule within proximity of the sample surface (Figure 4.113).

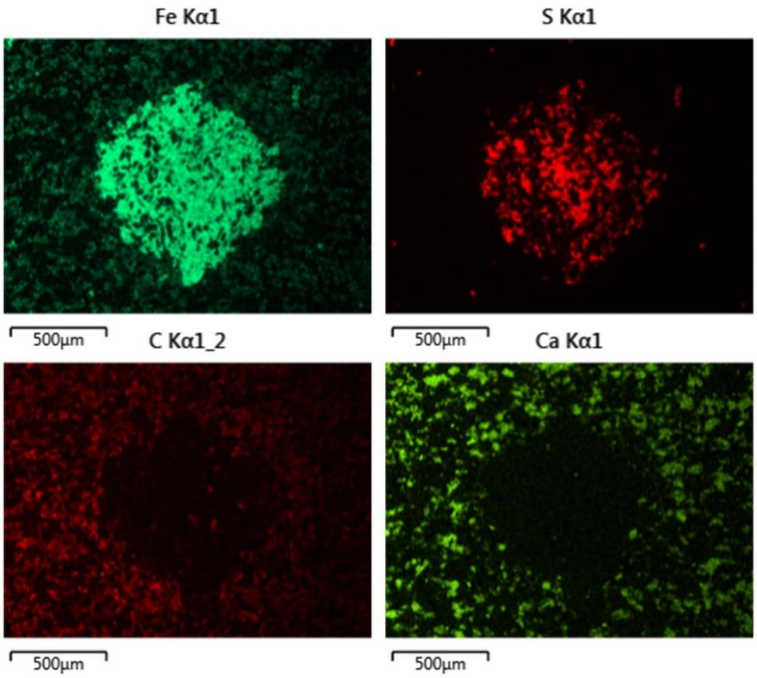

Element	Wt%
O	36.8
C	23.8
Si	17.1
Fe	10.9
Al	2.9
Ca	2.5
S	2.4
K	1.3
Na	1
Mg	0.8
Cl	0.2

Figure 4.113 - Fe, S, C, and Ca distribution in the mapped section B of BB1 (3) with normalised elemental proportion (%) of the mapped area

This nodule appears no different to nodules seen in untreated samples, secondary porosity does surround the feature, however, appears sparser than the secondary porosity that surrounds BB2 (5) which was used in the experimental chamber. This suggests that sulphide nodule exposed to climate change conditions will cause more extensive weathering in surrounding stone fabric than occurs under present climatic conditions.

4.6.2.3 ImageJ Analysis

This section follows the same structure as section 3.6.2.3 Borwick ImageJ Analysis, whereby key elements are transformed using the auto-threshold function in ImageJ to quantify and visualise their distribution and fluctuating abundance within specific sample areas. This process has occurred on a selection of sample surfaces from Borwick that are presented in the previous SEM-EDX analysis section. Particular focus is placed on the depth of dolomite dissolution, iron-enriched surfaces, and secondary porosity. The following samples have been analysed in this way:

Experimental Chamber Temperature and Humidity:

BC2 (5), BC3 (8), BB2 (5).

Experimental Chamber Temperature, Humidity and Precipitation:

BB1 (2), BB2 (6).

Control Chamber Temperature and Humidity:

BB1 (3).

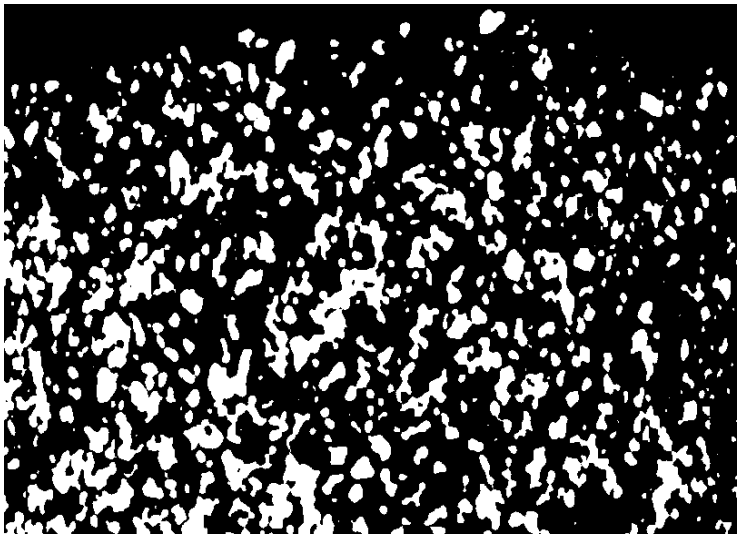

Figure 4.114 - BC2 (5) mapped section auto-threshold image of Mg distribution. The map has been cropped to the immediate surface of the sample

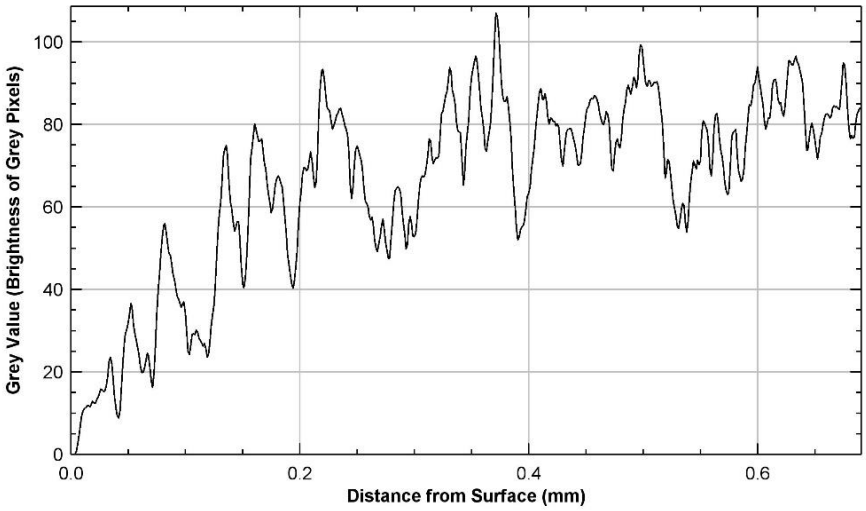

Figure 4.115 - Intensity of grey pixels (Mg) with progression from the sample surface to 0.7mm depth showing diminished Mg at sample surface to a depth of 0.2mm

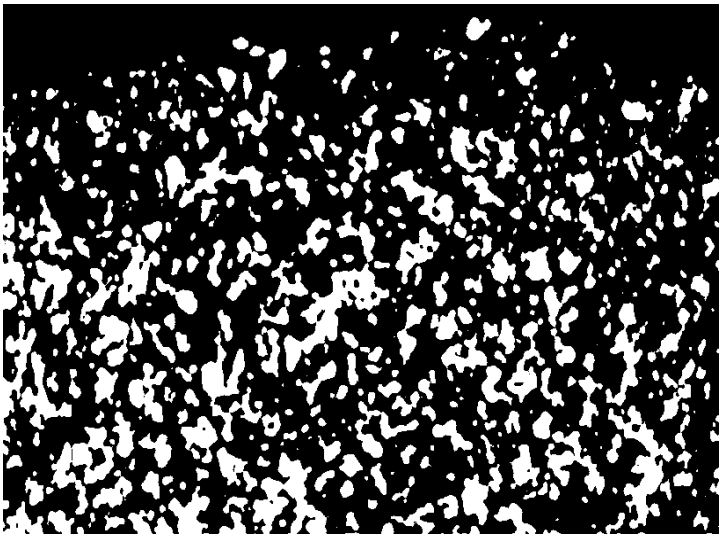

Figure 4.116 - BC2 (5) mapped section auto-threshold image of Ca distribution. The map has been cropped to the immediate surface of the sample

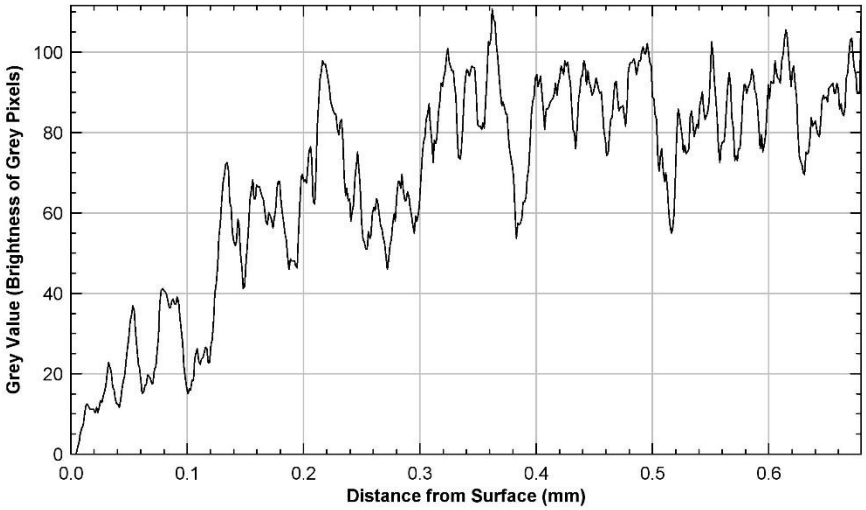

Figure 4.117 - Intensity of grey pixels (Ca) with progression from the sample surface to 0.68mm depth, showing diminished Ca at the sample surface to a depth of 0.2mm

Image analysis on BC2 (5) has been aimed at further quantifying surface dissolution identified during SEM-EDX mapping. Crucially, through ImageJ analysis, distance can be attributed to the depth of dissolution and the abundance of key elements can be plotted. The grey intensity of magnesium (Figure 4.115) and calcium (Figure 4.117) follow an extremely similar pattern. Both elements show a low grey value in the first 0.15mm of the sample before increasing to and maintaining a value above 40, reaching as high as 100 in places. Furthermore, this pattern can be visualised in auto-threshold images for each element (Figure 4.114 and Figure 4.116) whereby magnesium and calcium accumulations are sparse and smaller in size at the surface than they are at depth.

These results indicate that dissolution has occurred at the immediate surface of the rock, although not penetrating to any considerable depth. It cannot be said with complete certainty, but it can be hypothesised with confidence that surface dissolution in this instance is likely attributable to exposure in the experimental chamber and can be considered an important early indication of future weathering in pristine Stromness Flagstone. Had this surface been exposed while in the geology before experimental work, the dissolution surface would have been considerably more extensive, similar to that of BC3 (8) discussed below. However, the dissolution zone is a fraction of a millimetre in depth, indicating that it has occurred through the simulated weathering experiment. The sample is still intact, and its robustness not undermined by the limited extent of dolomite dissolution, however, this provides insight into how fragile the Stromness Flagstone is, one simulation of a climate changed year has been enough to trigger surface dissolution. It is important to build on this finding with the increased cycling of climate change conditions on a larger scale, longer-term CEF experiment.

It can also be seen that calcium and magnesium follow an analogous pattern, therefore, in subsequent samples, data from only one of the elements is provided.

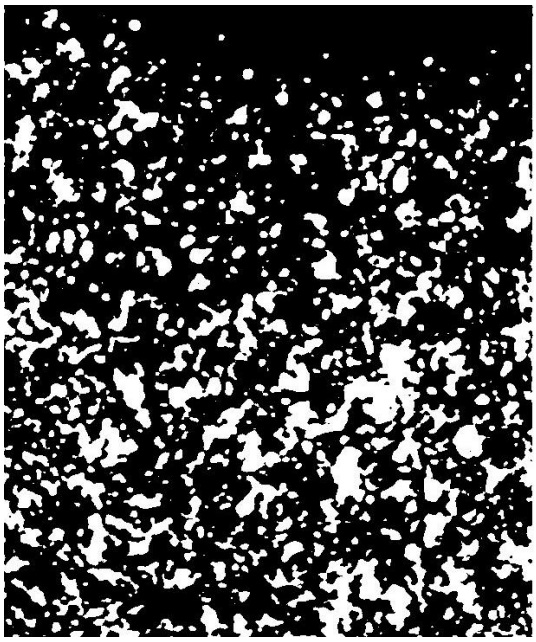

Figure 4.118 - BC3 (8) mapped section auto-threshold image of Ca distribution. The map has been rotated and cropped to the immediate surface of the sample

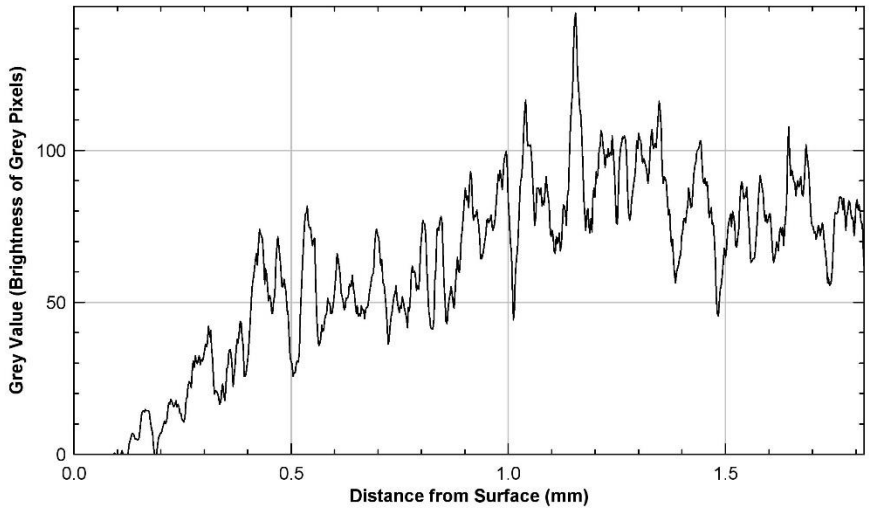

Figure 4.119 - Intensity of grey pixels (Ca) with progression from the sample surface to 1.8mm depth, showing diminished Ca at the sample surface to a depth of 0.5mm

Figure 4.118 and Figure 4.119 for BC2 (3) provide contrast to the figures presented for BC2 (5). In the auto-threshold image, calcium is sparse at the surface and to a considerable depth before it begins to appear with more abundance. The depth is quantified in Figure 4.119, where the calcium grey value increases very gradually and takes around 1mm for it to remain above 50, affirming the hypothesis developed through mapping analysis that this surface has been prior exposed to climatic conditions at the surface of a geological outcrop.

Figure 4.120 - BC3 (8) mapped section auto-threshold image of Fe distribution. The map has been rotated and cropped to the immediate surface of the sample

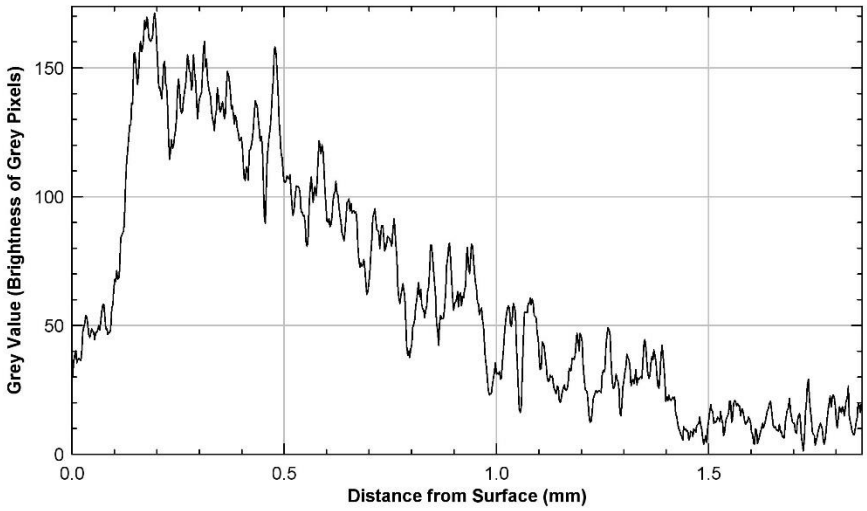

Figure 4.121 - Intensity of grey pixels (Fe) with progression from the sample surface to 1.9mm depth, showing increased Fe abundance to a depth of 1-1.5mm

In the absence of dolomite, iron can be seen within the dissolution zone, providing the dark red/rust colour on the surface of the sample. The grey value (Figure 4.121) peaks at around 170 before slowly reducing to background levels at a depth of around 1.5mm. Untreated control samples do not display the same level of surface dissolution, it is, therefore, difficult to disentangle the effects of the experiment from the effects of prior exposure as part of the background geology. This sample does, however, help to legitimise the results obtained from BC2 (5) that the small level of dissolution seen can be attributable to experimental conditions, as if the sample had been exposed as part of the background geology, the dissolution zone would be expected to be closer to 1mm in depth.

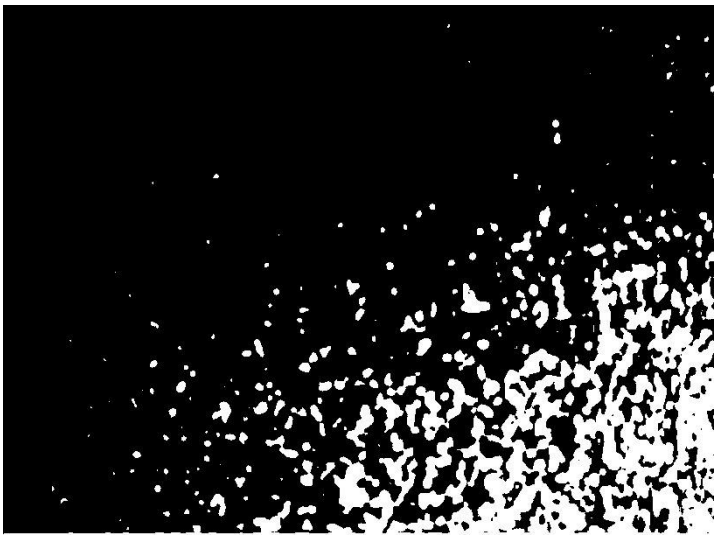

Figure 4.122 - BB2 (5) mapped section (A) auto-threshold image of Mg distribution. The map has been rotated and cropped to the immediate surface of the sample

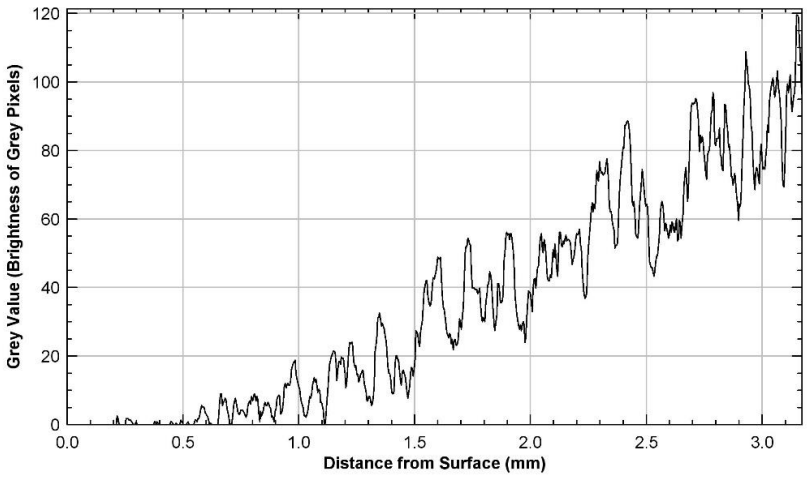

Figure 4.123 - Intensity of grey pixels (Mg) with progression from the sample surface to 3.2mm depth, showing diminished Mg at the sample surface to a depth of 1.5-2mm

Figure 4.124 - BB2 (5) mapped section (A) auto-threshold image of C distribution. The map has been rotated and cropped to the immediate surface of the sample

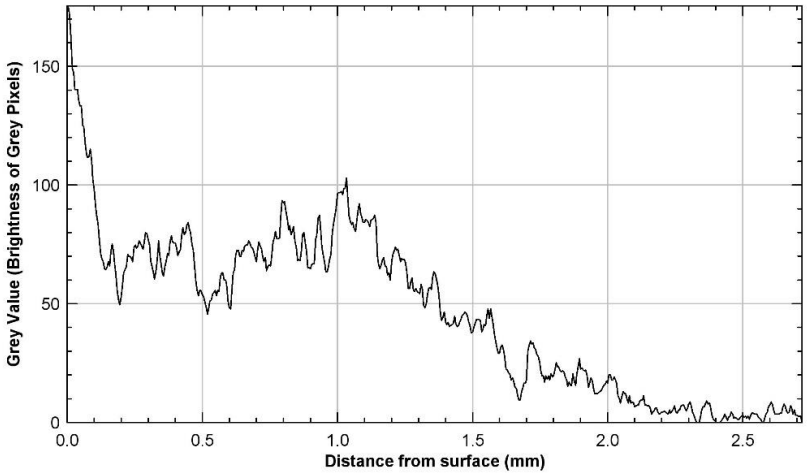

Figure 4.125 - Intensity of grey pixels (C) with progression from the sample surface to 2.7mm depth, showing increased C at the sample surface to a depth of 1-1.5mm

Extensive dolomite dissolution (Figure 4.122 and Figure 4.123) is seen at the surface of BB2 (5) as well as secondary porosity formation (Figure 4.124 and Figure 4.125). It can be seen that in the upper 1.5mm of stone, magnesium has a grey value predominantly below 20, it is not until after this depth that it increases steadily, eventually reaching 120 at 3.2mm depth. The opposite is seen in the carbon signal, it remains above 50 until approximately 1.3-1.5mm depth, before tailing off towards zero at around 2.5mm. The same depth of dolomite dissolution is seen in the untreated BB2 sample; therefore, it cannot be concluded that exposure to climate change conditions simulated within the CEF has caused any detectable deepening or worsening of dolomite dissolution. However, as is seen in the case of BC2 (5), the scale of dissolution attributable to experimental work can be less than 0.1mm, which is difficult to detect on a sample that already displays a dissolution zone of 1.5mm. It could, therefore, be the case that the dissolution zone has increased slightly but cannot be detected through this method of analysis.

The following ImageJ analysis is focused on comparisons between BB1 (2) used in the experimental chamber and BB1 (3) utilised in the control chamber.

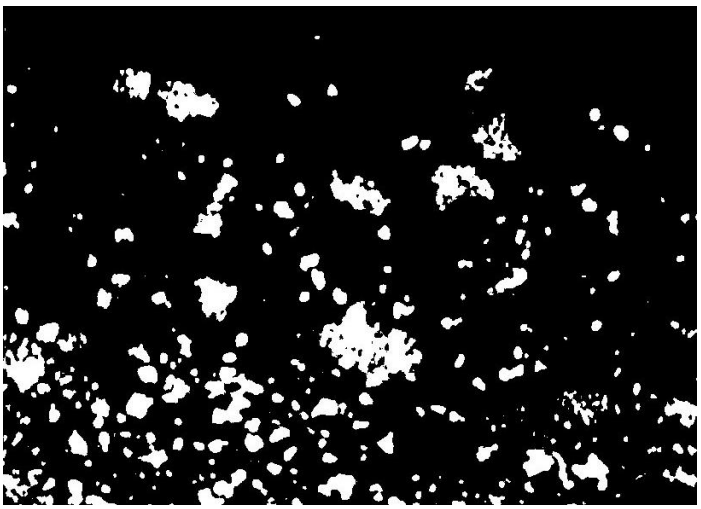

Figure 4.126 - BB1 (2) mapped section (A) auto-threshold image of Ca distribution. The map has been cropped to the immediate surface of the sample

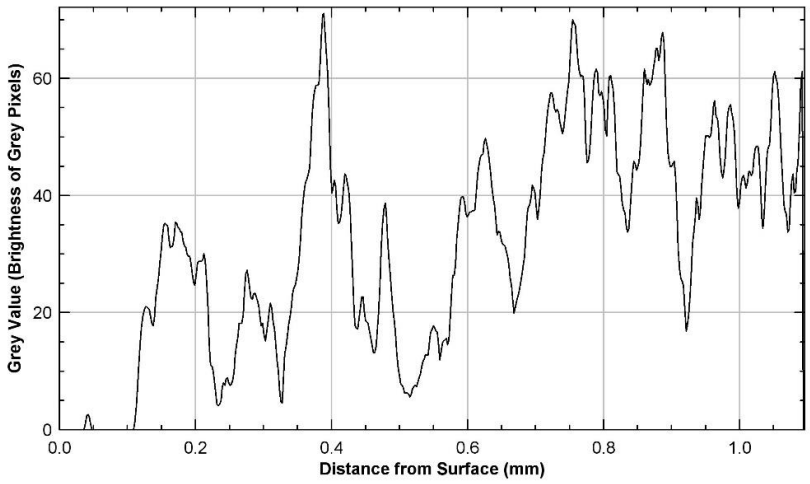

Figure 4.127 - Intensity of grey pixels (Ca) with progression from the sample surface to 1.2mm depth, showing erratic grey value due to granular loss

The calcium grey value peaks and troughs considerably in the mapped section (Figure 4.127), going from close to 0 to between 40 and 60 within 0.2mm. This is in keeping with the granular loss that is seen within the surface of the sample. Relatively large grains are lost, while others remain, resulting in an erratic grey value that fluctuates considerably over short distances. It appears to become steady after around 0.8mm. This trend is similarly seen on observation of magnesium in BB1 (3) presented below (Figure 4.128 and Figure 4.129).

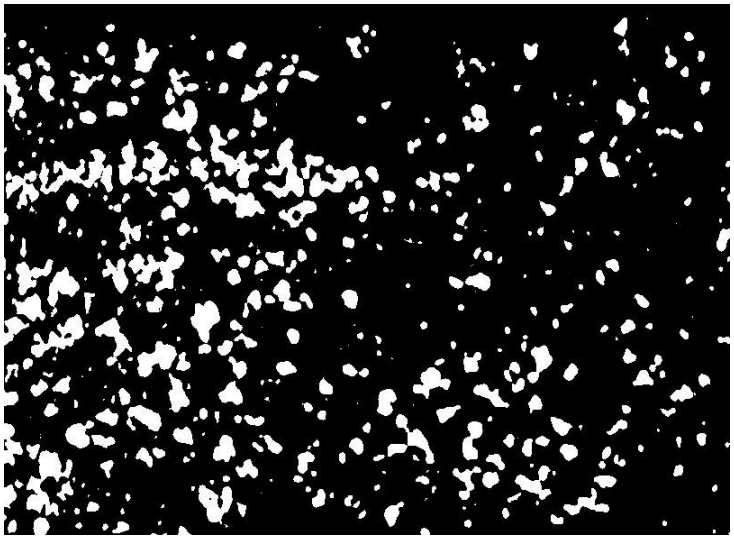

Figure 4.128 - BB1 (3) mapped section (A) auto-threshold image of Mg distribution. The map has been cropped to the immediate surface of the sample

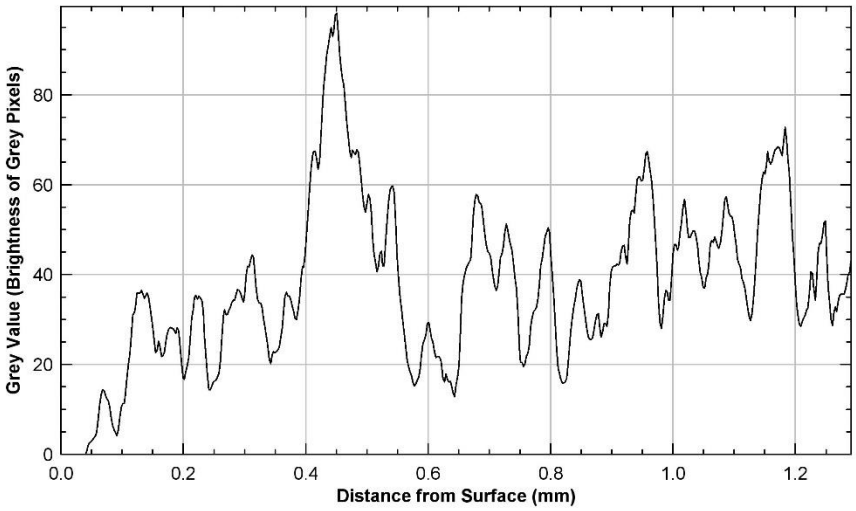

Figure 4.129 - Intensity of grey pixels (Mg) with progression from the sample surface to 1.3mm depth, showing erratic grey value due to granular loss

Although it appeared in the SEM-EDX analysis section, particularly in the secondary electron images presented (Figure 4.102 and Figure 4.112) that BB1 (2) exhibits more significant granular loss than BB1 (3), on observation of the auto-threshold images and grey value graphs presented above (Figure 4.127 - Intensity of grey pixels (Ca) with progression from the sample surface to 1.2mm depth, showing erratic grey value due to granular loss and Figure 4.129), it is difficult to come to the same conclusion. Therefore, instead of presenting individual grey value graphs for these samples, the carbon signal data for each sample has been extracted from ImageJ and plotted together on the same graph. Auto-threshold images and graphed grey value data is presented below (Figure 4.130 and Figure 4.131).

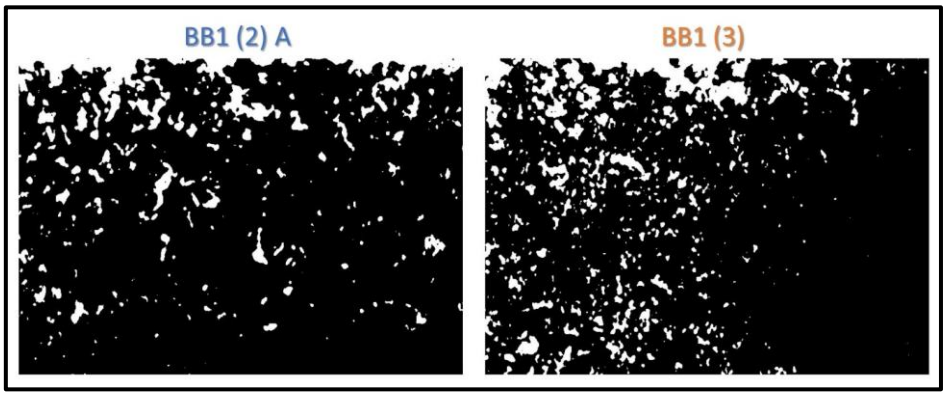

Figure 4.130 - BB1 (2) and BB1 (3) auto-threshold images of C distribution. The maps have been cropped to the immediate surface of the samples

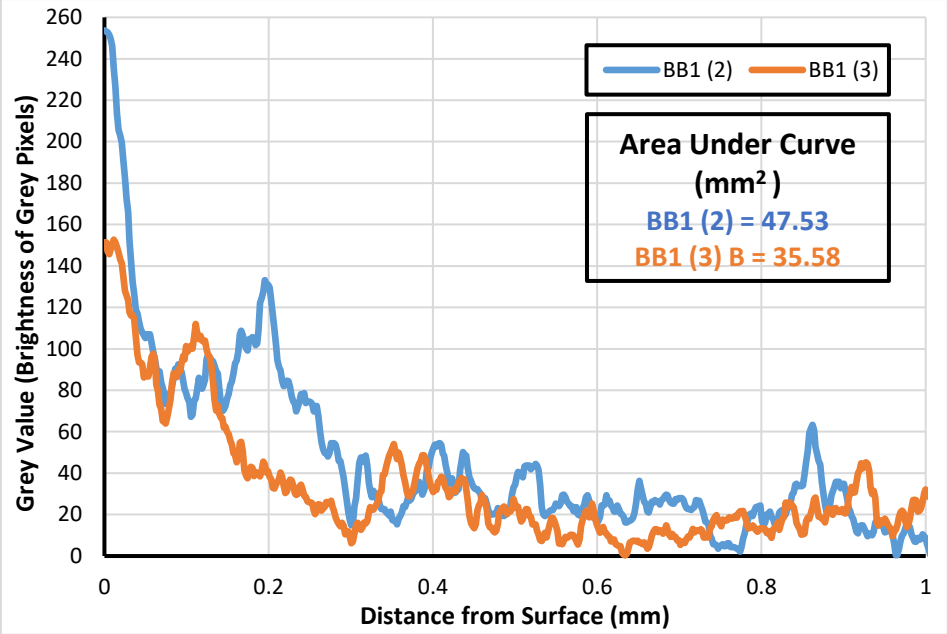

Figure 4.131 - Intensity of grey pixels (C) with progression from BB1 (2) and BB1 (3) sample surfaces to 1mm depth. Area under curve (mm^2) results are also presented.

It can be seen from Figure 4.136 that both samples follow a relatively similar grey value pattern, however, for the majority of the graph, the blue line representing BB1 (2) sits above the orange line representing BB1 (3), indicating that secondary porosity (carbon) levels are higher in BB1 (2) which was utilised in the experimental chamber. Both of these samples have been obtained from the same larger block, it is therefore interesting that secondary porosity is amplified in the sample exposed to climate change conditions. Based on this observation, it can be hypothesised that dissolution and subsequent secondary porosity formation will be exacerbated in a climate changed future when compared to the present. This observation is supported by the area under curve calculations provided within Figure 4.136, demonstrating that the area under BB1 (2)'s curve is the largest, representing a higher grey value across the plotted area when compared with BB1 (3). However, due to the destructive nature of sampling and analysis, it is not possible to say with certainty that the secondary porosity was identical in each sample before exposure to climate change conditions.

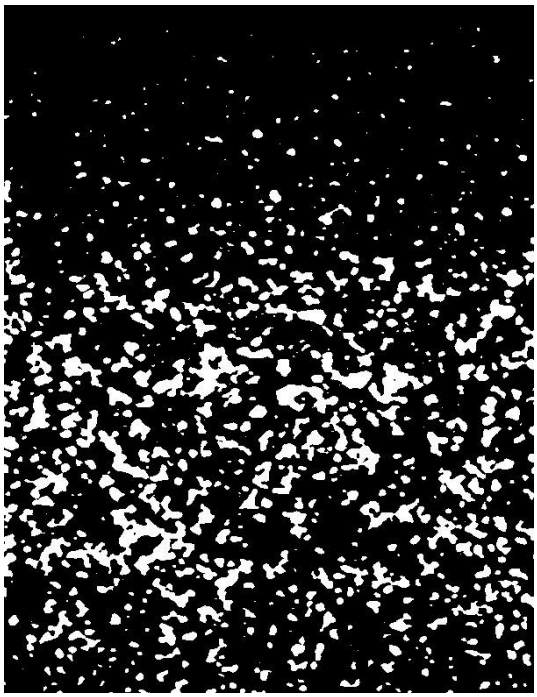

Figure 4.132 - BB2 (6) mapped section auto-threshold image of Mg distribution. The map has been rotated and cropped to the immediate surface of the sample

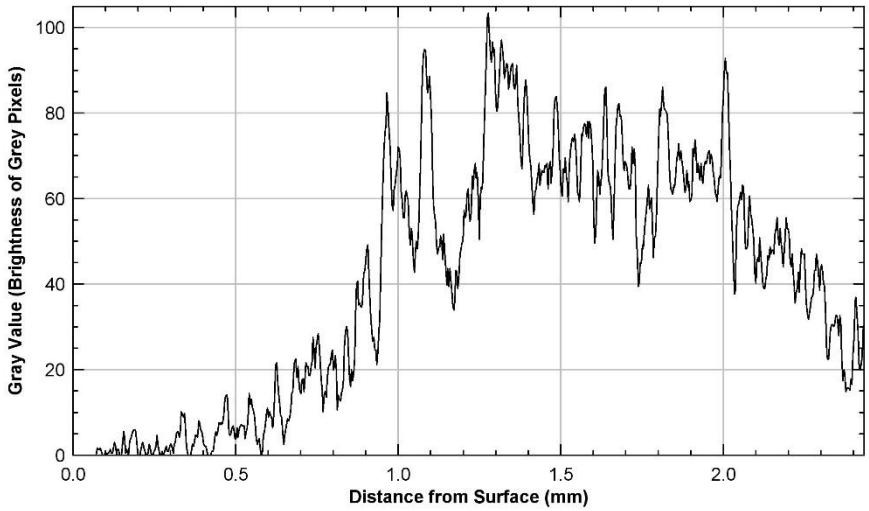

Figure 4.133 - Intensity of grey pixels (Mg) with progression from the sample surface to 2.4mm depth, showing diminished Mg from the sample surface to 1mm depth

It can be seen from Figure 4.132 and Figure 4.133 that magnesium levels are extremely low at the immediate surface of the sample, indicative of dolomite dissolution. At a depth of approximately 1mm the grey value begins to increase rapidly, indicating a more intact dolomite cement.

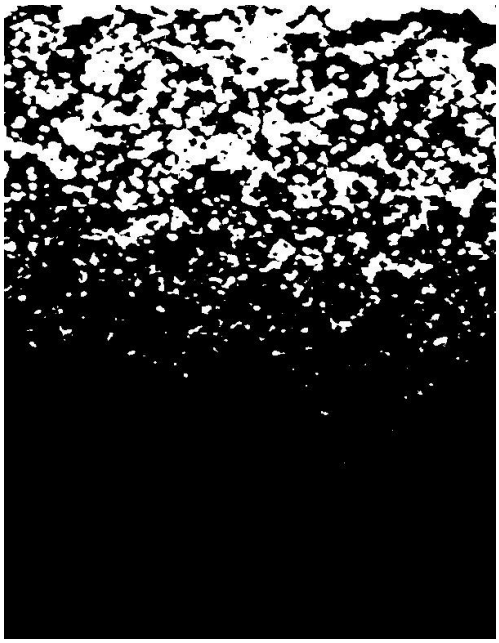

Figure 4.134 - BB2 (6) mapped section auto-threshold image of C distribution. The map has been rotated and cropped to the immediate surface of the sample

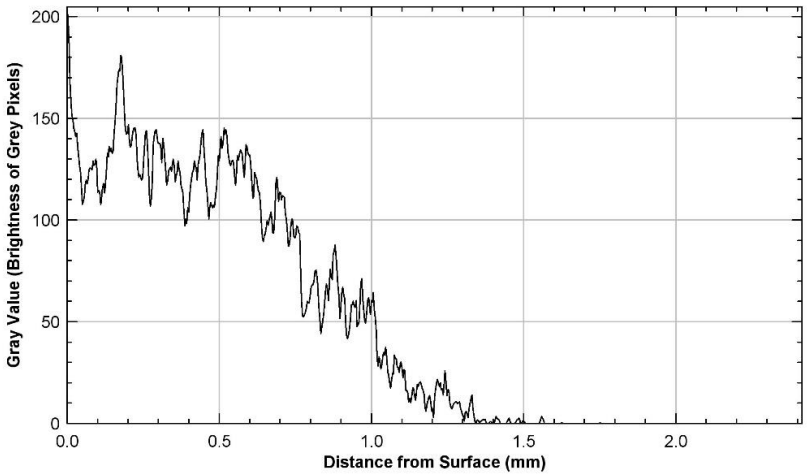

Figure 4.135 - Intensity of grey pixels with progression from the sample surface to 2.4mm depth showing increased C abundance from the sample surface to 1mm depth

The carbon signal indicating secondary porosity is shown in Figure 4.134 and Figure 4.135 contrasts with the magnesium signal presented above. Where magnesium is absent, carbon is abundant. Secondary porosity slowly declines with depth and shows a marked reduction in grey value at 1mm, the depth at which magnesium begins to increase steadily. A dissolution depth of approximately 1mm is commonplace across climate sensitised and untreated Borwick Broch samples, therefore, it cannot be inferred that dissolution depth has increased as a result of simulated climate change.

4.6.2.4 Borwick SEM-EDX Conclusion

Key findings have been discussed from SEM-EDX mapping and ImageJ analysis associated with Borwick samples. A new dissolution zone has been presented in BC2 (5) which appears to have transpired as a result of experimental conditions. The dissolution zone is approximately 0.15mm in size, although extremely small, this is exactly the kind of finding anticipated in the research design, focused on early indications of small-scale weathering. Unfortunately, BC3 (8), although from the background geology, has undergone some degree of dissolution through exposure, this has, however, provided a contrast to BC2 (5) which has aided significantly in the discovery of its dissolution zone.

Microcracks that failed during experimental work in BB1 (1) and BB3 (8) have been characterised. In the former, it appears to be a combined physical and chemical breakdown evidenced by manganese formation whereas, in the latter, evidence suggests the failure is entirely physical. Crucially, it is clear that both samples have failed as a result of their exposure to experimental conditions. Similar features are not identified in the control experiment, indicating that with exposure to future climate change conditions in Scotland, Stromness Flagstone with pre-existing joints/microcracks will be more prone to failure than they are at present.

In BB2 (5) and BB2 (6), it has been difficult to determine whether the dissolution zone has deepened which highlights the issue with inherently destructive sample analysis, the depth of the dissolution zone cannot be known exactly before experimental work, instead, this research is reliant on comparisons made to baseline work. As seen in the case of BC2 (5), new dissolution zones can be extremely small scale and are particularly difficult to identify. However, a key finding in BB2 (5) is the significant weathering of stone fabric surrounding the analysed sulphide nodule. No examples as extreme as this are seen in any untreated or control exposed samples. Exemplifying this, BB2 (6)’s and BB1 (3)’s sulphide nodules appear unaffected by exposure in the control chamber.

BB3 (9) has a distinct microcrack feature characterised by several relatively large pore chambers connected by a microcrack extending the width of the sample. From mapping, there does not appear to be any dissolution immediately surrounding the microcrack chamber, giving a reason why it remained intact despite being exposed to climate change conditions in the CEF.

Finally, comparisons made between BB1 (2) utilised in the experimental chamber and BB1 (3) in the control chamber give evidence to suggest that dissolution and subsequent secondary porosity formation is accelerated in a climate changed future compared to the present day. This indicates that Stromness Flagstone, particularly broch stone, will be more susceptible to surface weathering in the future.

The combined use of SEM-EDX and ImageJ has been particularly powerful in gaining new understandings of Borwick samples. A depth of knowledge has been obtained into the effects of climate change, in all samples analysed, it appears that experimental work has had a greater effect on samples than control exposure, evidenced in the formation of dissolution zones, sample failures, the volatile weathering of sulphide nodules and the formation of secondary porosity.

4.7 Chapter Conclusion

This chapter has focused on robust analyses of samples from Clachtoll and Borwick that have been exposed to a simulation of weathering, with control, informed by UKCP18 data for 2055 in Northern Scotland. A summary of findings is detailed in the tables below for the control chamber (Table 4.4) and experimental chamber (Table 4.5).

Table 4.4 - Summary of findings from 'A Climate Changed Year' control chamber

Control Chamber	Treatment	Visible Alterations	Mass Loss per kg	Thin Section Analysis	SEM-EDX	ImageJ Analysis
Borwick Control	T+H	Surface flaking on BB1 (3)	**GAIN**	No Substantial evidence of new weathering.		
	T+H+P	No change	0.000	Limited surface dissolution and secondary porosity formation in BB1 (3).		
Borwick Broch	T+H	No change	12.300	No Substantial evidence of new weathering.		
	T+H+P	Surface darkening on BB1 (4)	**GAIN**			
Clachtoll Control	T+H	No change	**GAIN**	No substantial evidence of weathering in any Clachtoll samples. Microcracks, crush zones and opaque layers have not observably weathered through control chamber exposure.		
	T+H+P	Surface darkening on CC1 (4)	**GAIN**			
Clachtoll Broch	T+H	No change	0.300			
	T+H+P	No change	0.500			

Table 4.5 - Summary of findings from 'A Climate Changed Year' experimental chamber

Experimental Chamber	Treatment	Visible Alterations	Mass Loss per kg	Thin Section Analysis	SEM - EDX	ImageJ Analysis
Borwick Control	T+H	No change	0.41 ± 0.25	Potential new dissolution in BC2 (5).		
	T+H+P	Surface salt formation on BC3 (9).	0.07 ± 0.36	No Substantial evidence of new weathering.		
Borwick Broch	T+H	Two sample failures – BB1 (1) & BB3 (8).	1.12 ± 0.29	Failure of BB3 (8) appears entirely physical. Extensive sulphide nodule weathering in BB2 (5).		
	T+H+P	Surface salt formation on BB2 (6).	1.48 ± 0.30	Dissolution has influenced the failure of BB1 (1). Extensive surface dissolution and secondary porosity formation in BB1 (2).		
Clachtoll Control	T+H	No change	0.38 ± 0.14	No substantial evidence of weathering. Microcracks, crush zones and opaque layers have not observably weathered through climate change experiment exposure.		
	T+H+P	No change	0.16 ± 0.02			
Clachtoll Broch	T+H	Granular loss.	2.05 ± 2.49			
	T+H+P	Granular loss.	0.62 ± 0.21			

Throughout, results from all analyses indicate clearly that Stromness Flagstone weathers more rapidly and destructively than Torridonian Sandstone in a climate changed future. Moreover, broch samples are seen to weather more readily and destructively than control samples and weathering is accelerated in the experimental chamber when compared to the control chamber.

This is evidenced firstly during the analysis of physical alterations where the most significant changes are seen in Borwick Broch samples, not least through the failure of two samples, while Clachtoll samples remained robust aside from minimal granular loss. These observations are compounded by weight analysis undertaken, although indicative values when scaled, at the experimental level greater weight loss is seen in climate sensitised broch samples.

Salt formation is seen extensively on BB2 (6) and to a very limited level on BC3 (9), both of which were exposed to climate change temperature, humidity, and precipitation conditions.

Conversely, no salt formation was noted on any samples upon the completion of the control experiment.

Petrographic thin section, SEM-EDX and ImageJ analyses showcase the robustness of Torridonian Sandstone and the comparative weakness of Stromness Flagstone. No substantial change is seen in the former, while in the latter, a deeper understanding is gained into sample failure, secondary porosity formation and sulphide nodule weathering. Again, weathering features are amplified in climate sensitised Borwick Broch samples. It is highlighted that Stromness Flagstone, particularly samples originating from Borwick Broch, weather in a multitude of ways including through dolomite dissolution, microcrack failure and the volatile decay of sulphide nodules. These features render the material extremely vulnerable to continued and exacerbated weathering as a result of climate change, having serious implications on the longevity of historic buildings constructed from the material.

As mentioned throughout this chapter, there are several shortcomings associated with CEF experiments, in that, not every real-world process can be mimicked accurately, and exposure time is extremely short, therefore, the scale of any change in rock and stone material is reduced. It can be said, therefore, that any response noted in samples through laboratory simulation of climate change will be amplified in an environmental setting due to factors such as storm events and wind-driven rain. Results from CEF work likely underestimate the true effects of climate change, which raises extreme concern particularly for Stromness Flagstone that has been pre-weathered as part of a culturally significant monument.

5 30-Year Seasonal Climate Change Simulation

5.1 Chapter Introduction

Results and interpretation of the second climate change experiment are presented in this chapter. Samples have been exposed to 30 years (2025-2055) of seasonal climate change fluctuations (experimental chamber) and in a separate chamber, a control experiment has exposed samples to 30 repeated cycles of 2018 seasonal fluctuations (control chamber), allowing comparisons to be made between sample responses related to their different simulated climate exposure. The experimental work in this chapter completes the sample set of 'sensitised' sandstone that will be analysed in this research to determine the impacts of climate change on sandstone heritage in Scotland, with a focus on Torridonian and Devonian building stone.

Based on previous findings relating to the baseline condition of the focus sandstones and inherent strengths and vulnerabilities showcased in Chapters 3 and 4, the analytic focus of this Chapter is to determine the effects that increased climate change exposure has on each sandstone type. This chapter follows a similar structure to Chapter 4, whereby analysis begins at the macro-scale where apparent physical surface changes are presented through a comparison of before and after images, additionally, a new analytical method is utilised in this chapter after an assessment was made of methods used in the previous chapter. It was found that identifying any surface colour changes on samples used in the first CEF experiment was difficult, and a more quantifiable method was required, therefore, a Chroma Meter has been used on samples before and after their incorporation in each chamber to determine any potential colour change that can be undetectable to the naked eye (Section 2.4.5.2.1 Climate Change Experiment 2: Chroma Meter). Mass change data is analysed to determine if any mass loss in the samples has occurred, relatable to their treatment. An evaluation of micro-scale change is undertaken through petrographic thin section analysis and SEM-EDX mapping with subsequent ImageJ analysis. As in the previous chapter and with the added benefit of Chroma Meter, it is anticipated that early indicators of a weathering change as a result of prolonged climate change exposure will be identified in the samples.

5.2 Visible Alterations

To gain an initial understanding of any obvious change that has occurred to the samples, comparisons have been made between before and after images. These images illustrate the clearest physical alterations before micro-scale analyses occurred.

5.2.1 Experimental Chamber (30-Year Seasonal Climate Change)

Physical alterations resulting from exposure in the experimental chamber are provided below. It is clear that weathering features are more pronounced in Borwick samples than in Clachtoll samples.

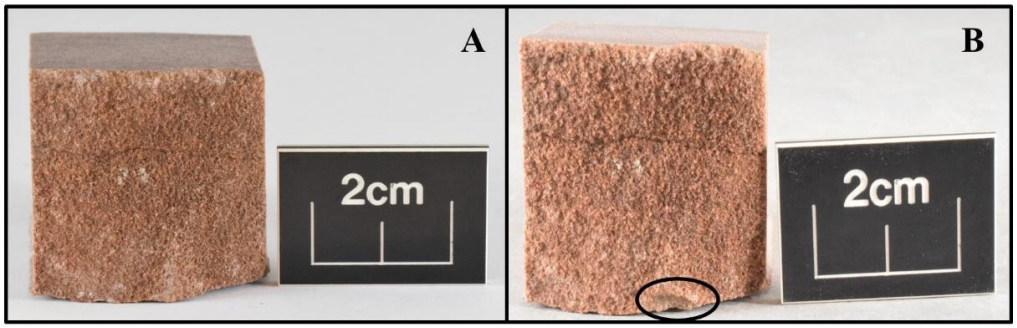

Figure 5.1 - CB2 (7) before (A) and after (B) CEF experiment. Granular loss is circled at the base of the sample (B)

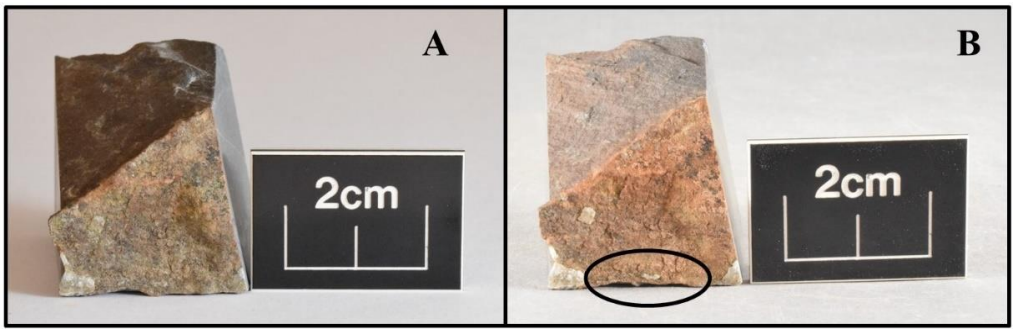

Figure 5.2 - BC2 (7) before (A) and after (B) CEF experiment. Granular loss is circled at the base of the sample (B)

CB2 (7) is the only Clachtoll sample that shows any physical alteration as a result of the climate change experiment, characterised as granular loss on one area of the exposed face (Figure 5.1). A similar feature is circled in BC2 (7) Image B, characterised by granular loss on a single area of the exposed surface (Figure 5.2).

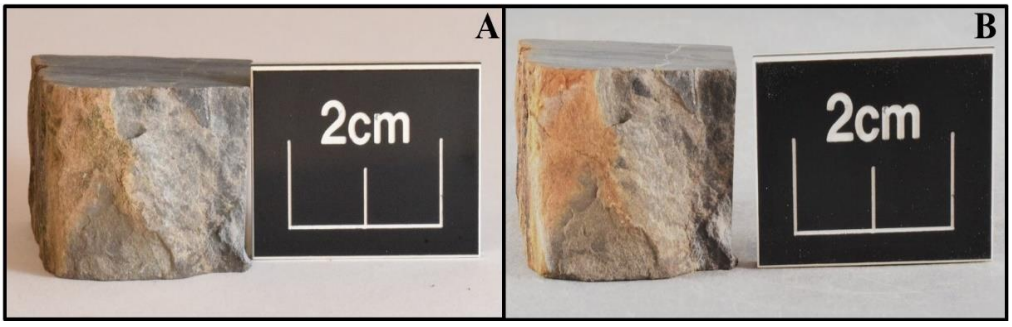

Figure 5.3 - BC3 (10) before (A) and after (B) CEF experiment. Colour change is seen on the left of the sample where it appears to have become lighter (B)

A distinct colour change appears on the surface of BC3 (10), particularly on the left edge of the sample where a distinct white band can be seen running the length of the surface edge (Figure 5.3). This has been quantified through Chroma Meter work presented in Section 5.3 Chroma Meter.

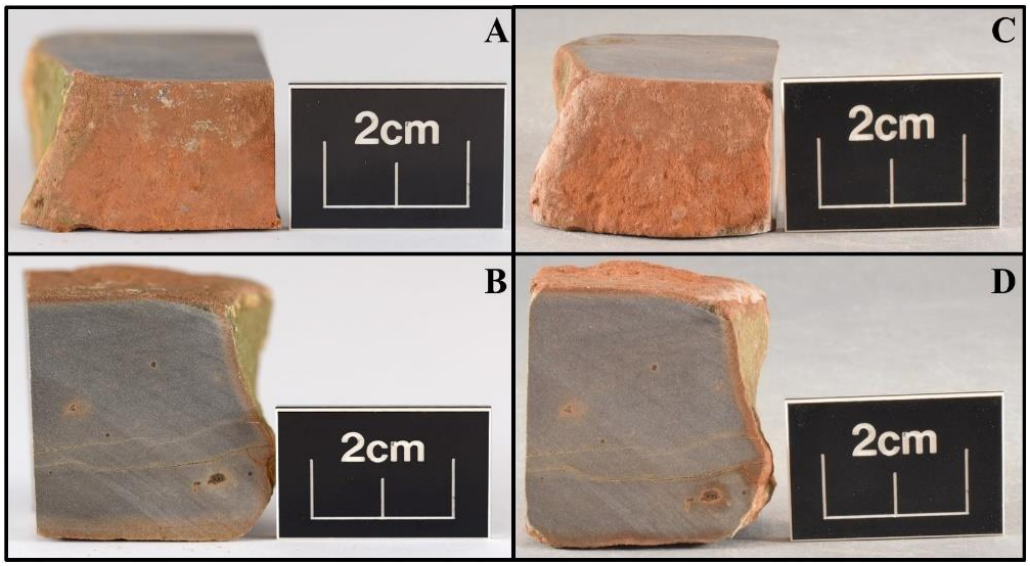

Figure 5.4 - BB2 (7) before (A, B) and after (C, D) CEF experiment. Colour change and surface alteration seen on comparison of (A) and (C). Sulphide nodule weathering seen on comparison of (B) and (D)

Out of the entire sample set, the most significant surface alteration is seen on BB2 (7). After the experiment, the exposed surface has altered markedly through granular loss and colour change. Furthermore, the sulphide nodule on the bottom right of the cross-section face appears to have decayed and there is clear evidence of reddening around the microcrack that extends the width of the sample, indicative of dolomite dissolution (Figure 5.4).

5.2.2 Control Chamber (‘2018’ Experiment)

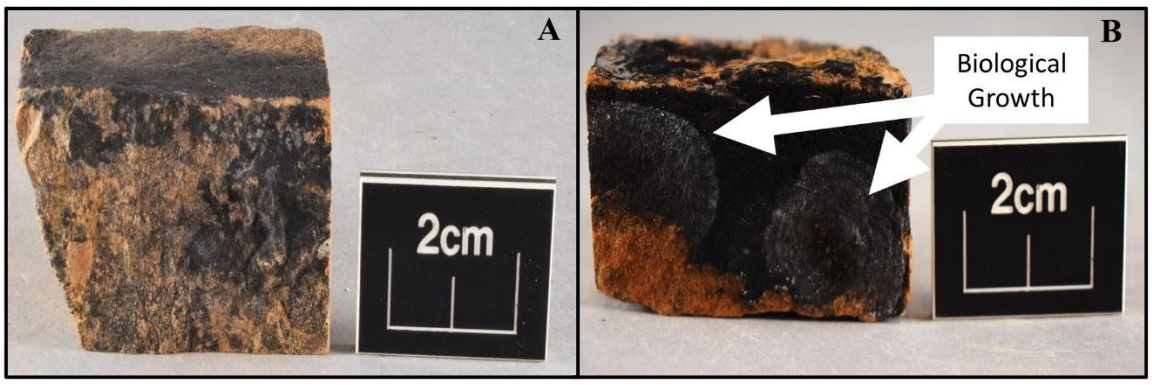

Figure 5.5 - BB3 (11) before (A) and after (B) CEF experiment. Biological growth seen on the non-exposed face (top of A); main face shown in B

Although the exposed surface exhibited no discernible change, one of the non-exposed faces of BB3 (11) shows clear biological growth after the experiment, characterised as two ringed features covering most of the face (Figure 5.5).

5.2.3 Visible Alterations Discussion

Clear alterations are observed on 4 of the 8 samples used in the experimental chamber:

- 0 out of 2 Clachtoll Control Samples
- 1 out of 2 Clachtoll Broch Samples
- 2 out of 2 Borwick Control Samples
- 1 out of 2 Borwick Broch Samples

The only indication of surface change on Torridonian Sandstone is noted on the surface of CB2 (7), where evidence of granular loss is noted. Granular loss has been outlined in baseline work as a potential weakness within the sandstone type, which is showcased in this instance. However, the loss of material at the sample surface is localised and only visible on one of the four Clachtoll samples incorporated within the experiment, reaffirming the strength of the Torridonian Sandstone, even when exposed to rapidly fluctuating climatic conditions. Mass loss analysis will quantify this more fully and micro-scale analyses will allow smaller scale granular loss to be detected that cannot be seen by the naked eye on comparison of before and after images.

As expected, samples of Stromness Flagstone weathered more extensively than Torridonian samples. Granular loss is prevalent, so too are colour changes which will be quantified through chroma meter work. The most distinct changes as a result of experimental exposure are seen on BB2 (7) (Figure 5.4), where a plethora of weathering indicators have been identified, including an increase in surface roughness which can severely exacerbate stone deterioration. Colour changes are visible on specific areas of the stone surface which alter the physical appearance of a building stone and can detract from the aesthetic appeal of a structure. Perhaps most significantly, however, is the apparent decay of a sulphide nodule present within the sample (Figure 5.6). Although this face was not the focus surface in the experiment, the sulphide nodule at the bottom right of the face appears to have weathered substantially and exacerbated dolomite dissolution immediately surrounding the feature.

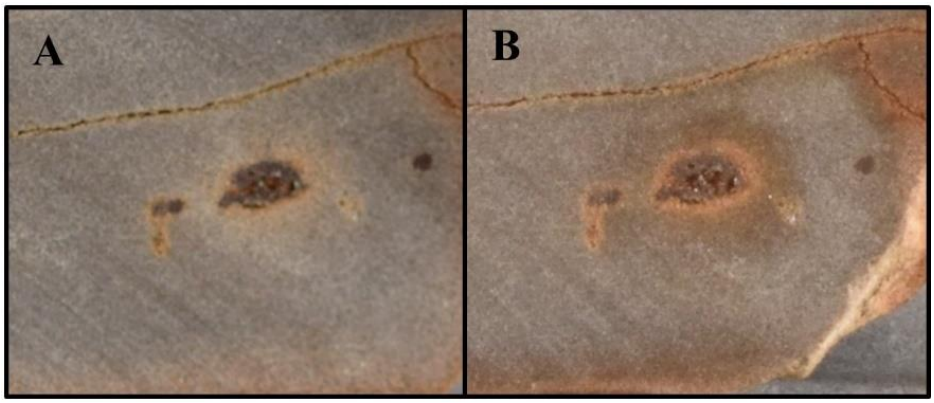

Figure 5.6 - BB2 (7) sulphide nodules before (A) and after the CEF experiment (B), highlighting significant reddening around the feature in B

The area surrounding the nodule and indeed the microcrack running the width of the sample is a clear example of dolomite dissolution. As determined in Chapter 3, dolomite dissolution is a slow process that can be exacerbated by acidic conditions, such conditions can be generated by the weathering of sulphide which produces sulphuric acid. The introduction of precipitation to the experiment has likely caused this reaction to take place.

In the control chamber, the only stone that exhibits any clear alteration is BB3 (11) (Figure 5.5). However, the change is not on the exposed surface, instead, there appear to be two separate but similar biological growths, it remains unknown whether these are algal, bacterial, or fungal, however, they have likely occurred indirectly through the precipitation regime used in the experiment, whereby water has become trapped between the stone itself and the protective film wrapped around it, inadvertently creating ideal conditions for this type of biological growth to form.

5.2.4 Visible Alterations Conclusion

Visible alterations have been shown and discussed above. As anticipated, the Stromness Flagstone utilised in the experiment has weathered at a more pronounced rate than the Torridonian Sandstone. Alterations seen are not as extensive as anticipated based on previous experimental work, highlighting the heterogeneity present within the same sandstone types. All samples remained intact with no significant signs of failure; however, a key aspect of this research is its relatability to above surface weathering processes, where small-scale indications of future weathering are investigated. Instead of subjecting samples to unrealistic conditions to find their breaking point or to, at least, exacerbate weathering, this research

exposes samples to robustly supported climate data to observe more subtle weathering alterations that the historic environment will face, which have been showcased in this section.

5.3 Chroma Meter

5.3.1 Before Experiment

The chroma meter is a useful analytical method in quantifying colour changes that have occurred in the samples as a result of their use in this climate change experiment. Colour change can be subjective and subtle differences can be difficult to quantify with accuracy. To overcome this, the colour of each surface to be exposed in the CEF was determined before the experiment, following the methodology procedure described in Chapter 2. The resulting data obtained were plotted on a colour wheel (Figure 5.7).

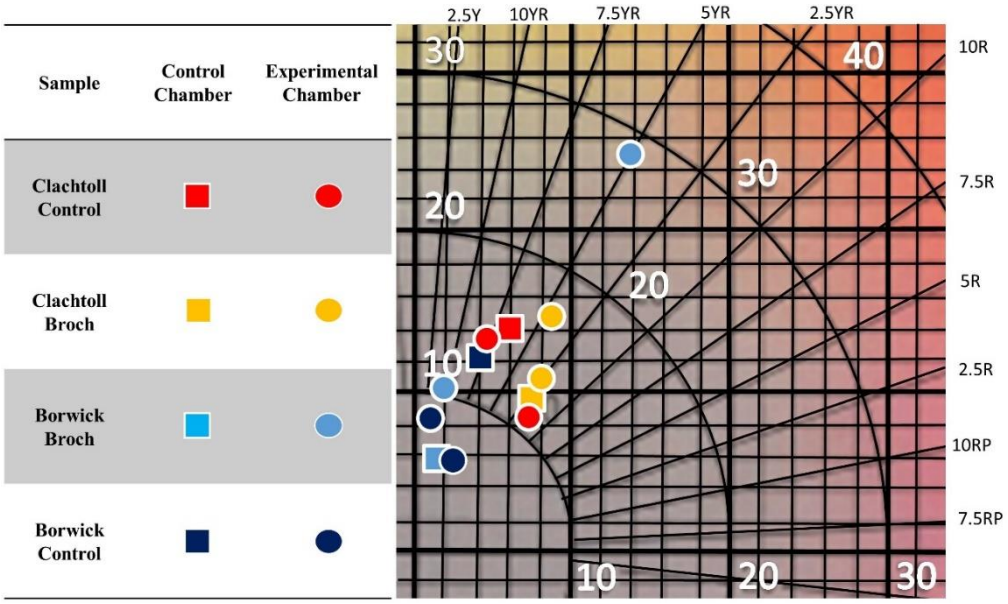

Figure 5.7 - Colour data plotted on a colour wheel for samples before their use in CEF control and experimental chambers

The data presented in Figure 5.7 acts as the baseline for each sample, upon completion of experiments the samples are analysed again, and any changes will be plotted. The legend presented above applies to Figure 5.7, Figure 5.8 and Figure 5.9

5.3.2 Experimental Chamber (30-Year Seasonal Climate Change)

Figures presented in this section (Figure 5.8 and Figure 5.9) show the change in L*, a* and b* values, relative to chroma meter data obtained before the experiment (Figure 5.7).

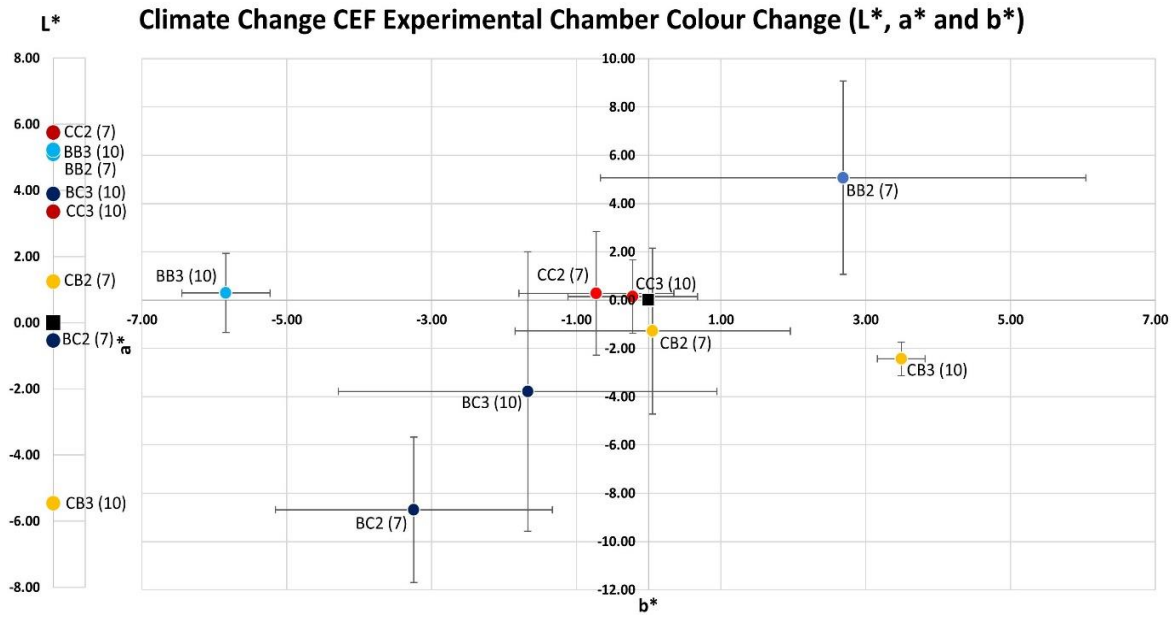

Figure 5.8 - L, a*, and b* change after CEF experiment. Before the experiment baseline for each sample is point 0,0 marked with a black square. The location of each sample on the plot represents their colour change compared to before the experiment*

Both Clachtoll control samples have positive L* values indicating they have become lighter in colour, particularly CC2 (7), however, neither sample exhibit any substantial a* or b* change. Of the Clachtoll broch samples, CB3 (11) displays a distinct negative L* value, indicative of surface darkening taking place. Furthermore, the sample has a positive a* value and slightly negative b* indicating that a reddening and blueing process has occurred. Crucially, the error bars for these colour changes are very small. Conversely, CB2 (7) has become slightly lighter with no robust a* or b* change detected.

BC2 (7) and BC3 (10) show signs of greening and blueing with negative a* and b* values, particularly in the former. BC2 (7) shows very little L* change, while BC3 (10) has become lighter with a positive L* value. Each of the Borwick broch samples shows similar L* changes, becoming lighter in colour. BB3 (10) displays a distinct greening effect characterised by a negative a* value with a small error while BB2 (7) lies in the positive region of the a* and b* graph indicating reddening and yellowing, although it must be noted that there is a large error associated with this observation.

5.3.3 Control Chamber ('2018' Experiment)

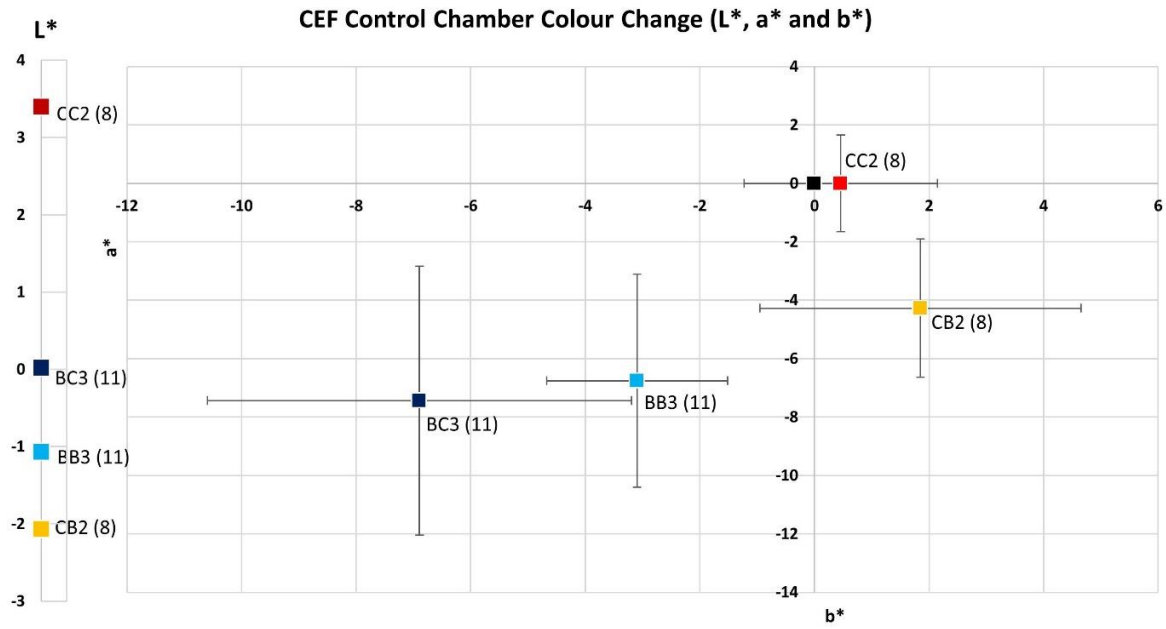

Figure 5.9 - L, a*, and b* change after CEF control experiment. Before the experiment for each sample is point 0,0 marked with a black square on a* and b* figure. The location of each sample on the plot represents their colour change compared to before the experiment*

Like the experimental chamber, the Clachtoll control sample has a positive L* value indicative of becoming lighter in colour, albeit to a lesser extent than the experimental sample, while the a* and b* parameters remain relatively unchanged. CB2 (8) can be seen to have become darker while a reddening and blueing process has occurred, like the CB2 sample used in the experimental chamber.

BC3 (11) shows no L* change, with the a* and b* values following the same greening and blueing process that occurred in the experimental chamber Borwick control samples. BB3 (11) shows significantly less change than the samples in the experimental chamber, with only a slight darkening, greening and blueing taking place with a high error associated with the a* and b* values.

5.3.4 Chroma Meter Discussion

It must be noted that there is an inherent error associated with the application of the chroma meter in this research due to the non-fresh cut nature of the samples. Their surfaces are heterogeneous, displaying a range of colours across them. This is an important feature of the samples as this research is interested in the 'memory effect' held within the broch and background geology sensitised stone and the implication this effect carries for future

weathering. To reduce error, sampling occurred in the same location before and after the experiment, which has been effective for some of the samples.

In this research, some key changes have been identified on samples taken from the background geology and those that have undergone surface alteration through their exposure in a culturally significant monument. A clear trend appears in that although samples in the experimental chamber and control chamber react similarly, the reaction is exacerbated in the experimental chamber. This is seen clearly with the Clachtoll control, Borwick control and broch samples which show higher L* values in the experimental chamber and, additionally, the Clachtoll broch sample darkens less in the control chamber.

The a* and b* values follow a similar change trajectory in both chambers, with slightly more change seen in the experimental chamber. BB3 (10) in the experimental chamber shows the clearest greening with very little associated error, while the control experiment counterpart only shows slight greening. Similarly, CB3 (11), which, like BB3 (10) has a very low error associated with the colour change, has a positive a* value, seen to a reduced extent in the control chamber. No discernible change between chambers occurs in the Clachtoll and Borwick control samples, indicating that broch samples, having been exposed to above surface weathering over ca. 2000 years are more vulnerable to future weathering and associated surface alteration.

5.3.5 Chroma Meter Conclusion

The chroma meter was implemented in this climate change experiment to aid in the quantification of colour change, in favour of determining change through analysis of before and after images as was the case in the first experiment. There is a large error associated with some samples as anticipated due to the heterogeneous nature of the samples utilised. Nevertheless, some of these errors are small and results indicate a distinct colour change, particularly in the case of BB3 (10) and CB3 (11).

Clear trends are observed which have important implications for this research. Although samples in both chambers follow the same general trends, colour change appears to be exacerbated in the experimental chamber indicating that climate change has the potential to increase discolouration of culturally significant stone utilised in the historic environment. Furthermore, broch samples appear to react more substantially than control samples, particularly for the a* and b* parameters, indicating that the ‘memory effect’ held within stone that has a history of exposure above ground, is important in influencing future change

in the stone. These two key findings, when combined, suggest that culturally significant stone that has been exposed above the surface will discolour more significantly in a climate changed future, having potentially negative implications on the aesthetics of historic monuments. Mineral alterations are an integral process that contribute to colour changes in sandstones. Pronounced changes are seen upon exposure to extreme heat such as fire-related events, as demonstrated in the literature where heating leads to increased reddening of sandstone, associated with the presence of iron-bearing minerals (Hager, 2014; Hajpál and Török, 2002; Kompaníková et al., 2014). Despite an extensive web-based search, no research can be found which focuses on colour changes that occur during long-term exposure to climatic conditions, such as while sandstone is incorporated within the built environment. This is, therefore, an important area where more research should be conducted.

5.4 Mass Analysis

The same mass analysis was conducted at the end of this experiment as was conducted for the climate changed year presented in Chapter 4. The data provided below serves as a simple metric to quantify change between samples exposed to experimental and control conditions as well as allowing comparisons to be made between samples originating from the background geologies associated with each site, and the brochs themselves. Due to sampling restrictions, the sample count is lower for this experiment, however, it retains the realism of using culturally significant material. In the experimental chamber (Table 5.1), two samples of each type were exposed to simulated climate change seasonal weathering for the next 30 years (2025-2055), while in the control chamber (Table 5.2), one sample of each type was exposed to repeated 2018 conditions for 30 cycles, simulating 30 years.

Table 5.1 provides mean mass loss in grams from which the mean percentage mass loss was calculated. The calculated loss was then scaled up to represent a 1kg block and a broch structure, with the caveat that % loss is constant with increasing block size and mass.

Table 5.1 - Indicative mass loss values observed after the 30-year seasonal climate change experiment. Broch weight = 2,000 Tons (1814369 kg / 1814.369 Mg)

Sample	Mean Loss (g)	Mean Loss (%)	1kg Block Loss (g)	Broch Loss (Mg)
Clachtoll Broch	0.11	0.13	1.30	2.36
Clachtoll Control	0.07	0.09	0.90	1.63
Borwick Broch	0.92	1.57	15.70	28.49
Borwick Control	0.03	0.06	0.60	1.08

As only one sample of each type was used in the control chamber, Table 5.2 provides both the loss in grams and percentage loss for each sample. This loss was similarly scaled up to a 1kg block and a broch structure.

Table 5.2 - Indicative mass loss values observed after the 30-year seasonal climate change control experiment where one sample of each type was exposed. Broch weight = 2,000 Tons (1814369 kg / 1814.369 Mg)

Sample	Mean Loss (g)	Mean Loss (%)	1kg Block Loss (g)	Broch Loss (Mg)
Clachtoll Broch	0.05	0.06	0.60	1.08
Clachtoll Control	0.05	0.05	0.50	0.91
Borwick Broch	0.03	0.04	0.40	0.73
Borwick Control	0.02	0.03	0.30	0.54

Table 5.1 and Table 5.2 both show that in each treatment and sample type, mass loss has occurred. In each case, the average loss in the experimental chamber is greater than the loss exhibited in the control chamber. Furthermore, results from both experiments show that broch samples exhibit greater mass reduction than control samples.

Results described in this analysis continues to follow the trend highlighted throughout this research; the pre-weathered stone that has been exposed above the surface is prone to decay at a quicker and more destructive rate than samples that have been gathered from the background geology. Additionally, based on these results, both rock and stone samples will be more prone to mass loss in a climate change future than at current climatic conditions.

Although mass loss change is small, continued exposure, particularly to climate change conditions will bring samples towards a tipping point, where sandstone failure could occur more rapidly, having potentially destructive implications on the historic environment.

As these are simply indicative mass losses based on observations from relatively few samples, the only robust conclusion that can be drawn from this analysis is that samples generally appear to lose mass, most likely through granular loss, after exposure to weathering conditions. Other factors that could contribute to mass loss include dissolution, however, due to the duration of exposure, this would be an extremely small-scale loss. Additionally, fluctuations in the quantity of water held within micropores could affect sample mass, however, porosity (%) in each sandstone type is extremely low as demonstrated in Chapter 2, reducing potential water ingress/water holding capacity of the sandstone. Interestingly, it appears that samples exposed to climate change futures experience greater losses than those exposed to current conditions. Continued research in this area, whereby a greater quantity of samples is utilised, could provide more robust results, however, creating such an experiment with culturally significant material is not currently possible due to sampling restrictions associated with the SMC process.

5.5 Petrographic Thin Section Analysis

With a robust understanding of how samples have reacted to experimental work undertaken in Chapter 4, petrographic thin section analysis at this stage is about gaining insight into how existing weathering features and inherent weaknesses may proceed to weather in the long term when exposed to rapid cycling of climatic conditions.

Focus is placed on whether weathering features are more widespread or destructive as a result of increased exposure to simulated weathering. As highlighted throughout this thesis, these features include distinct clay layers and microcracks within Clachtoll samples, as well as dolomite dissolution, volatile sulphide nodules and microcracks present in Borwick samples. In this section, any differences between the weathering of control rock and broch stone are identified, together with weathering differences resulting from sample treatment in the experimental chamber versus the control chamber (cf. Research Design and Methodology).

photomicrograph focused primarily on sample surfaces are presented, showing weathering indicators or lack thereof. From this analysis, specific areas of interest are outlined, where focused SEM-EDX mapping occurred (Section 5.6 SEM-EDX Analysis).

The following petrographic thin section analysis is divided into the experimental chamber and control chamber samples with subsections of sample type, facilitating a discussion and conclusion section.

5.5.1 Experimental Chamber (30-Year Seasonal Climate Change)

5.5.1.1 Clachtoll

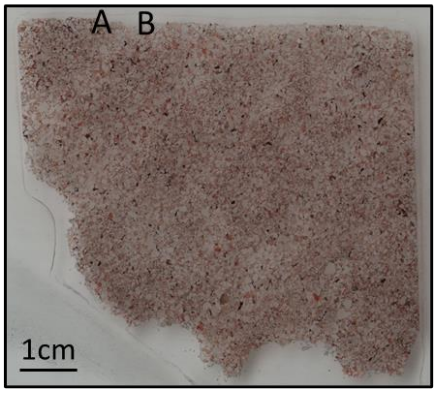

Figure 5.10 - Petrographic thin section scan of CC2 (7), with A and B focussing on a microcrack at the sample surface

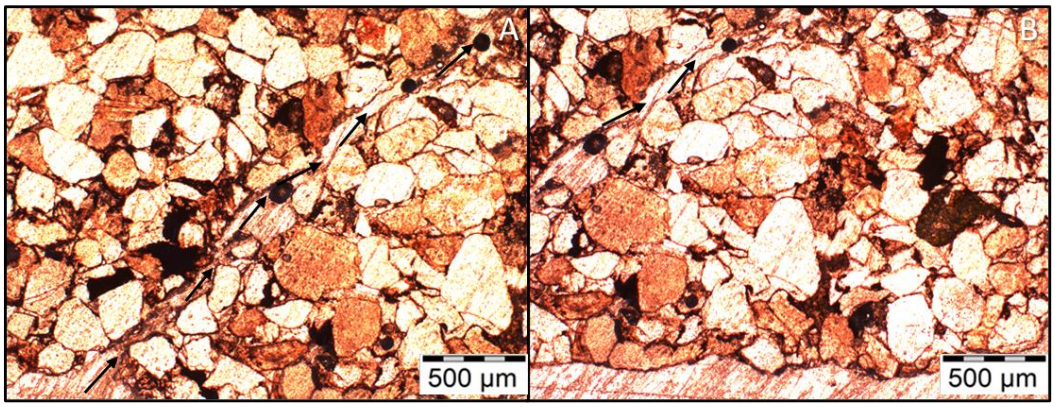

Figure 5.11 - A vertical microcrack is seen in the upper left corner of CC2 (7) (A – marked with arrows), aside from this, the sample surface is intact (B) (Both PPL)

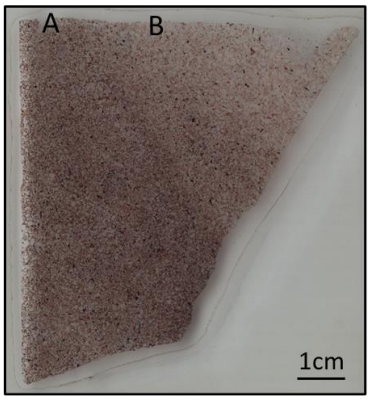

Figure 5.12 - Petrographic thin section scan of CC3 (11) with A and B focussing on two areas of the sample surface

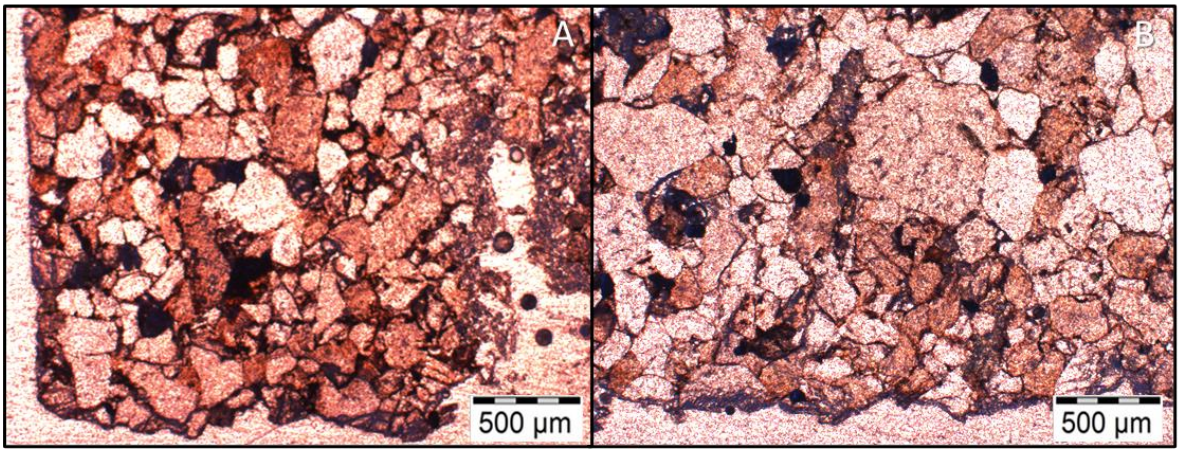

Figure 5.13 - Manufacturing damage seen on CC3 (11)'s surface; in unaffected areas the sample appears intact (left-hand side of A) (Both PPL)

Figure 5.14 - Petrographic thin section scan of CB2 (7), with A and B focussing on two areas of the sample surface

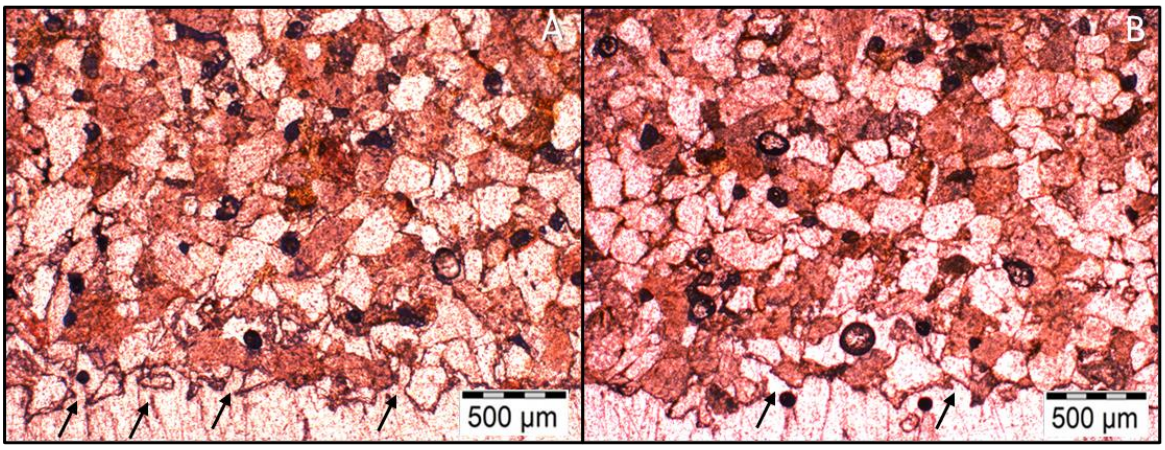

Figure 5.15 - Evidence of granular loss is marked at different locations on the surface of CB2 (7) (Both PPL)

Figure 5.16 - Petrographic thin section scan of CB3 (11), with A and B focussing on two areas of the sample surface

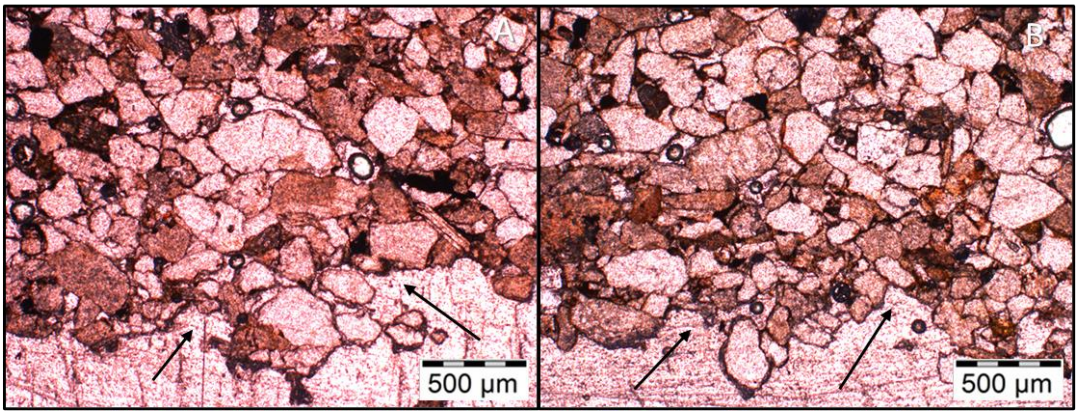

Figure 5.17 - Evidence of granular loss is indicated at the surface of CB3 (11) (Both PPL)

As shown throughout this thesis, both control and broch samples from Clachtoll appear generally unaffected by weathering processes, with little evidence of weathering associated with above surface exposure or simulated climate change. The aim of this experiment with focus on the Torridonian Sandstone has been to expose samples to more prolonged, rapid cycling of climate conditions to determine if this elicits a greater weathering response from the material. Through petrographic thin section analysis of samples from the experimental chamber, potential evidence of increased weathering can be seen.

Very little insight is gained through analysis of CC3 (11) (Figure 5.12 and Figure 5.13) due to manufacturing damage, however, in the undamaged areas of the surface, it appears intact. In CC2 (7) (Figure 5.10 and Figure 5.11), however, the occurrence of a vertical microcrack originating at the sample surface is of particular interest. It has been noted in baseline work that lateral microcracks are relatively common in the Torridonian Sandstone, conversely, vertical microcracks have not been noted in analysed samples until now. Moreover, Clachtoll

samples from the background geology have been seen to be extremely robust, therefore, such a feature, carrying implications for water ingress, freeze-thaw, and granular loss, is unexpected. A key caveat of findings from this research is the lack of knowledge about whether this feature was already present before experimental work. It can be said, however, that given the lack of vertical microcracks seen in any Clachtoll sample leading up to this point, there is potential that exposure to more extreme cycling of climate change has initiated a response within the rock that has at least contributed to the formation, deepening, or widening of this feature. SEM-EDX mapping in section 5.6 SEM-EDX Analysis is utilised to more fully understand the microcrack, however from thin section analysis it appears to be a physical failure within the material, meandering around quartz grains as opposed to puncturing through them, indicating a low level of force has been required to create it.

Both CB2 (7) (Figure 5.14 and Figure 5.15) and CB3 (11) (Figure 5.16 and Figure 5.17) appear to display indications of increased granular loss compared with baseline samples analysed in Chapter 3. Loose grain fragments are noted at the sample surfaces and areas are indicated on relevant figures where sections of the surface have been lost. The occurrence of granular loss has been pinpointed as one of the few weakness within Clachtoll samples, evidenced through comparison images and mass loss analysis. It can be seen clearly in these samples that at the surface, grains have become detached through a weakening of the grain supported fabric of the stone, causing secondary porosity formation and the loss of some small surface sections. This is seen particularly in CB3 (11) which was investigated further through SEM-EDX analysis to determine the depth of granular loss (Section 5.6 SEM-EDX Analysis).

It is difficult to quantify how much degradation in Clachtoll samples is attributable to climate change exposure, however, with comparison to baseline samples and samples utilised in the climate change year experiment in Chapter 4, key differences have been outlined. The occurrence of a vertical microcrack in CC2 (7) is particularly significant as no other Clachtoll samples display this feature. Therefore, it can be inferred that it has at least in part been initiated by climate change exposure. Subsequent analysis of samples utilised in the control chamber for this experiment allows additional comparisons to take place.

5.5.1.2 Borwick

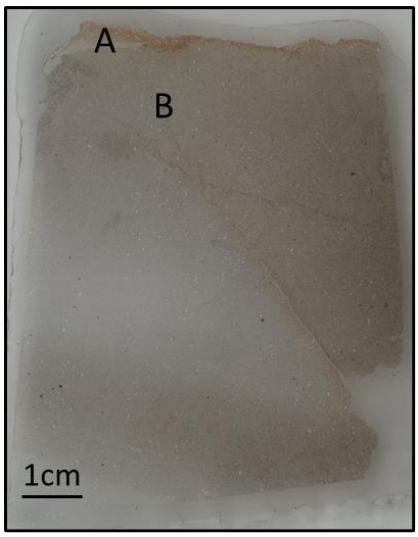

Figure 5.18 - Petrographic thin section scan of BC2 (7), with A and B focussing on distinct microcrack features

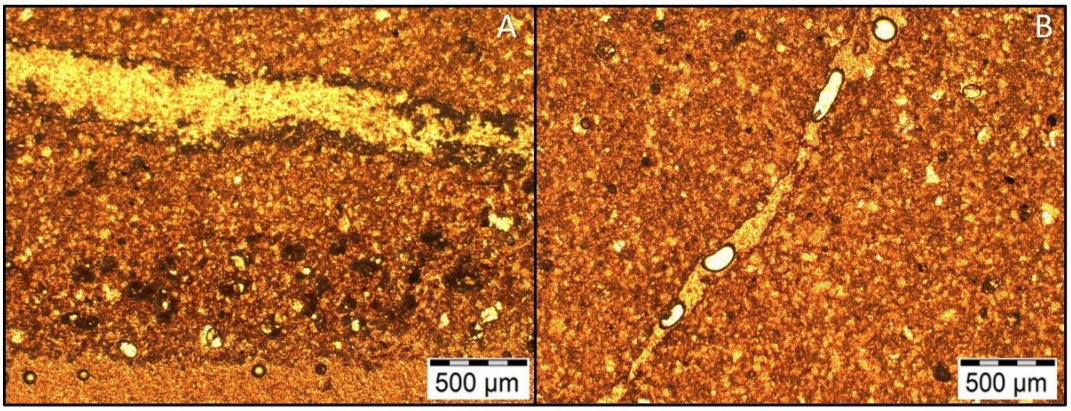

Figure 5.19 - A horizontal surface microcrack (A), as well as a vertical microcrack extending to depth, is seen in BC2 (7) (Both PPL)

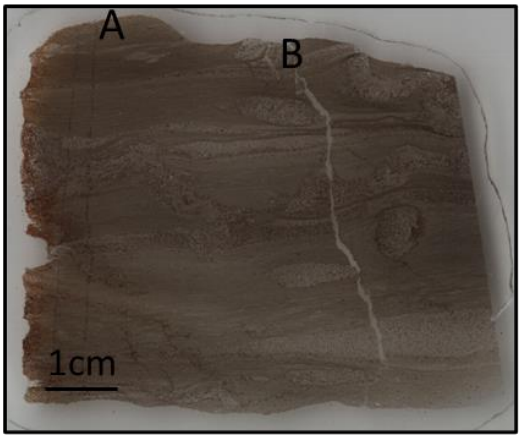

Figure 5.20 - Petrographic thin section scan of BC3 (10), with A and B focussing on two areas of the sample surface

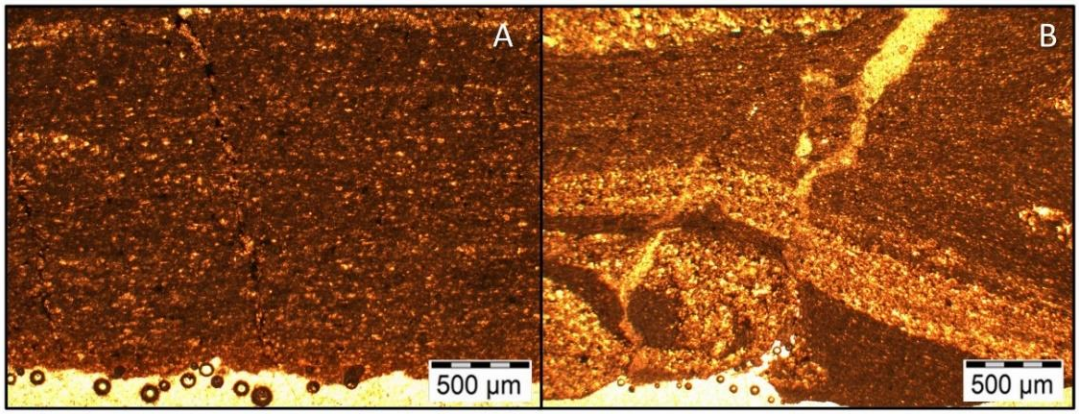

Figure 5.21 - The sample surface of BC3 (10) appears relatively intact (A), aside from a significant vertical microcrack extending deep into the sample (B) (Both PPL)

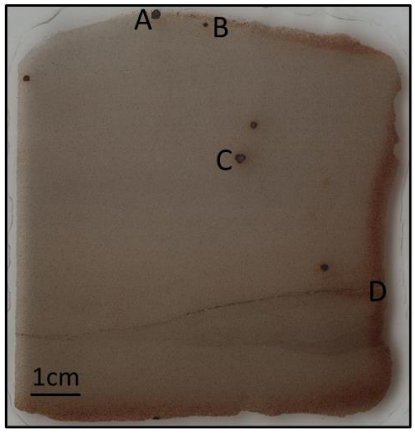

Figure 5.22 - Petrographic thin section scan of BB2 (7), with A and B focussing on two areas of the sample surface, C focussing on a sulphide nodule and D on a microcrack at depth

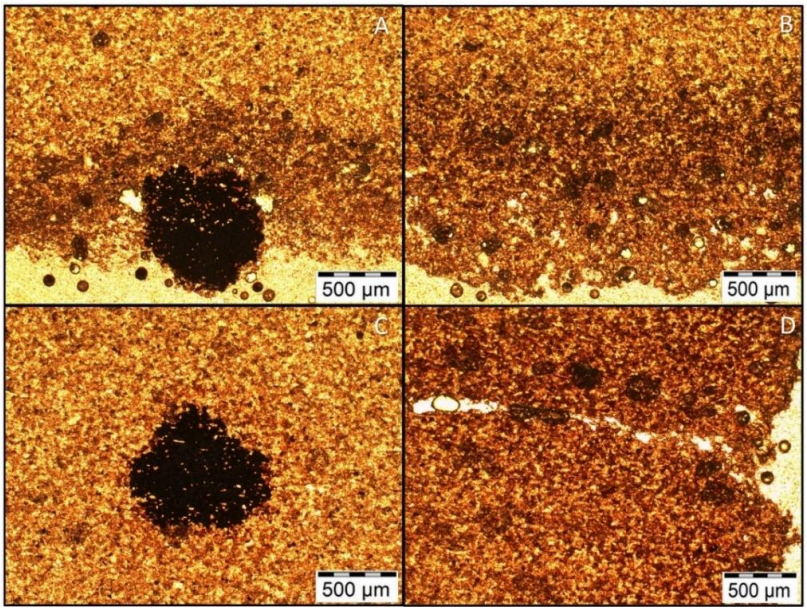

Figure 5.23 - Intact sulphide nodules are seen throughout BB2 (7) (A, C). At the surface, there is evidence of dissolution with secondary porosity (B). A horizontal microcrack at depth can be seen extending the width of the sample (D) (All PPL)

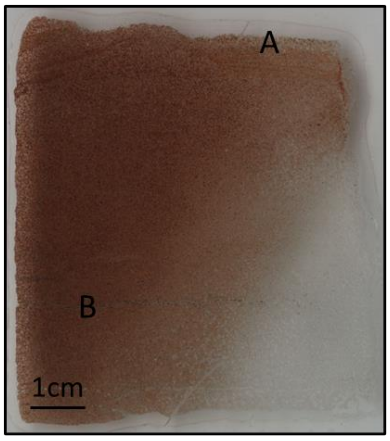

Figure 5.24 - Petrographic thin section scan of BB3 (10) with A focussing on potential secondary porosity at the sample surface and B focussing on an opaque layer at depth

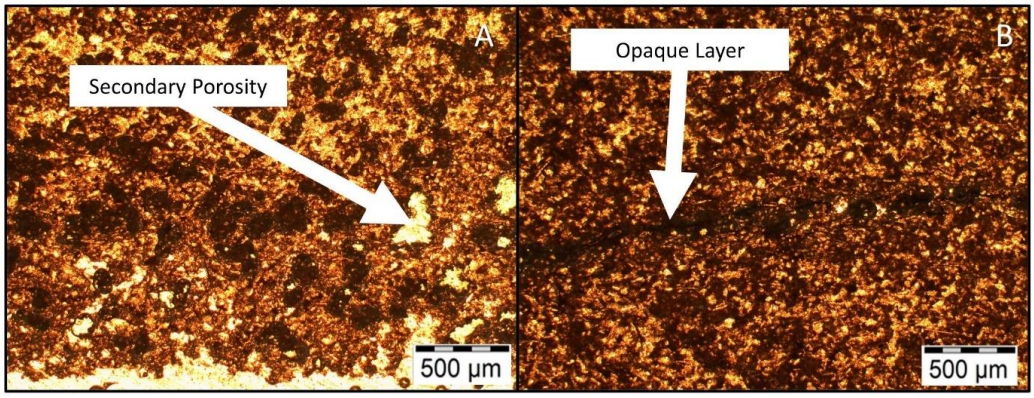

Figure 5.25 - Dissolution and secondary porosity are seen at BB3 (10)'s surface (A). At depth, there is a distinct opaque layer (B) (Both PPL)

Stromness Flagstone samples have been shown to be particularly vulnerable to weathering in a climate changed future. With this knowledge, it was hypothesised that exposure to rapid and prolonged cycling of climate conditions would elicit a destructive response from the material. As seen through petrographic analysis, samples have remained intact despite the occurrence of some significant weathering features.

BC2 (7) (Figure 5.18 and Figure 5.19) displays several notable microcracks. At the surface of the sample (Figure 5.19 A), a severe microcrack is visible which appears extremely close to failure, while in Figure 5.19 B, a vertical microcrack extends the length of the sample. It appears that these features are close to intersecting which could result in complete failure of the sample. A vertical microcrack is also noted in BC3 (10) (Figure 5.21 B), which appears close to penetrating through the entire sample and causing significant material loss. In control samples discussed in Chapter 3 baseline work and Chapter 4 climate sensitised analysis, some evidence of vertical microcracking is noted. However, in the limited samples that do display

this feature, they can be characterised as being extremely fine and limited in length. Conversely, in BC2 (7) and BC3 (10) which have been exposed to prolonged climate change cycling, the microcracks are wider and longer, indicating that conditions simulated in the CEF have potentially had a destructive effect on microcrack characteristics, bringing them closer to failure. In terms of dolomite dissolution, SEM-EDX analysis is undertaken on BC3 (10) in Figure 5.20 A to determine if any new dissolution has occurred, attributable to sample exposure in the CEF (Section 5.6 SEM-EDX Analysis). Conversely, in BC2 (7), the depth of dissolution indicates prior exposure while within the geology, making any inferences of the effect of experimental exposure difficult to determine.

BB2 (7) (Figure 5.22 and Figure 5.23) displays all vulnerabilities associated with Stromness Flagstone Broch stone, namely the presence of sulphide nodules, surface dissolution, and a lateral microcrack. However, all of these features appear intact despite exposure in the CEF experimental chamber. From Figure 5.23 A and C, sulphide nodules show little sign of weathering, which is particularly unexpected in the former due to its location at the surface of the stone, in direct contact with precipitation.

In the thin section scan of BB2 (7), reddening can be seen surrounding the nodule at C, however, this is not reflected in thin section images. SEM-EDX mapping is used on this feature to determine if any early indications of weathering are present. A potential reason for the lack of weathering seen in thin section work is that nodules, although numerous, are small in size and potentially less volatile as a result. In terms of surface dissolution, there is no evidence to suggest it has deepened as a result of experimental work. The stability of the microcrack at depth is appraised through SEM-EDX mapping.

It is important at this point to reference Figure 5.4 and Figure 5.6 provided earlier in this chapter, where clear weathering is seen surrounding a nodule located beneath the microcrack marked at D in Figure 5.23. This nodule is not seen in thin section analysis, indicating that during manufacturing the sample face containing the weathered nodule has been lost, giving a reason for the relatively unaffected state of BB2 (7) as a result of experimental work. This highlights the importance of a multifaceted methodological approach; whereby multiple techniques are combined to minimise data loss and maximise understandings gained into sample weathering.

Dissolution depth appears significant at the surface of BB3 (10) (Figure 5.24 and Figure 5.25), this is quantified through SEM-EDX mapping and subsequent image analysis.

Similarly, SEM-EDX analysis is required to understand the composition of fine opaque infill areas seen throughout the sample, an example of which is shown in Figure 5.25 B. Petrographic thin section analysis has been useful in the identification of these features; however, SEM-EDX mapping is crucial in understanding and quantifying them more fully.

5.5.2 Control Chamber ('2018' Experiment)

5.5.2.1 Clachtoll

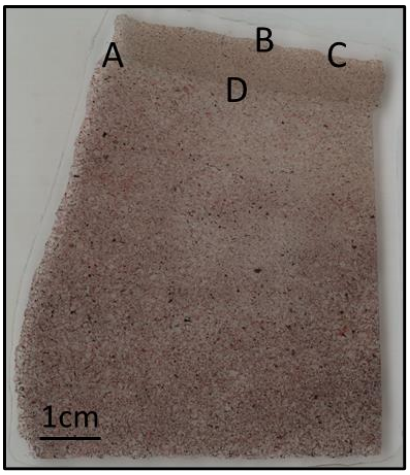

Figure 5.26 - Petrographic thin section scan of CC2 (8), with A and D focussing on a grain size transition punctuated by a clay layer, B and C focus on two areas of the sample surface

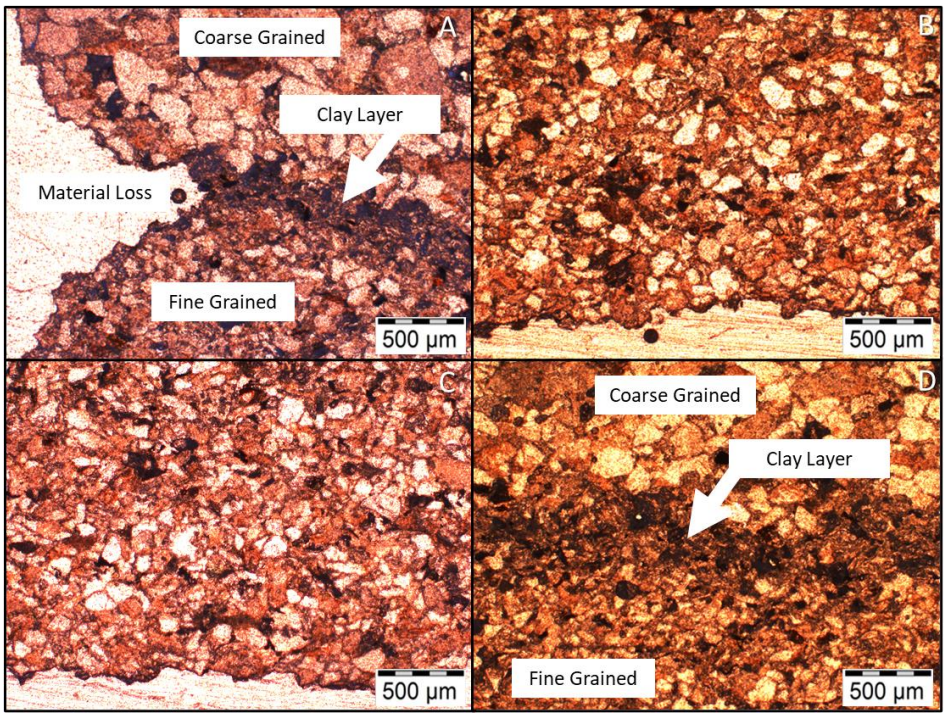

Figure 5.27 - Evidence of material loss is seen at the edge of CC2 (8) (A), while the upper surface appears intact (B, C). There is a distinct surface clay, separating fine material at the immediate surface and more coarse material at depth (D) (All PPL)

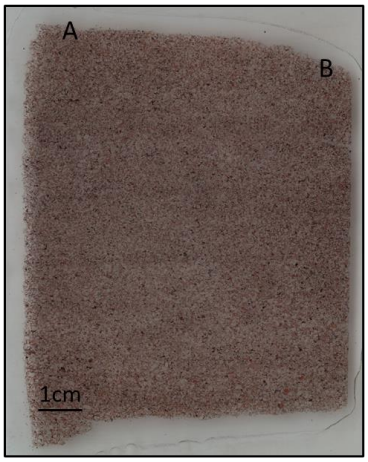

Figure 5.28 - Petrographic thin section scan of CB2 (8), with A and B focussing on two areas of the sample surface

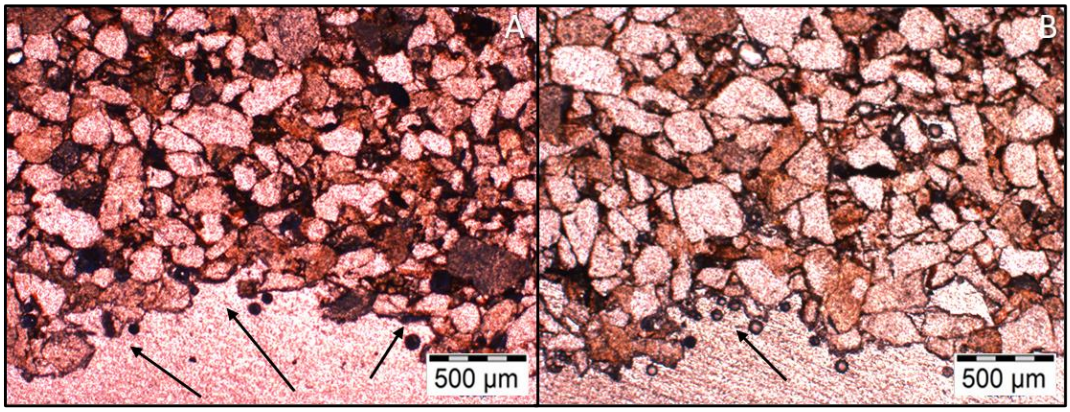

Figure 5.29 - Evidence of granular loss is indicated at the surface of CB2 (8) (Both PPL)

CC2 (8) (Figure 5.26 and Figure 5.27) contains a common feature within Clachtoll control samples; a surface transition from fine-grained to coarse-grained material, punctuated by a distinct clay band. From Figure 5.27 A, it appears that material loss has occurred at the edge of the sample within the clay band area, while the fine and coarse material sit proud of the clay layer, indicating that it weathers more readily when exposed. In baseline work and Chapter 4 experimental work, this same feature remains intact. In this instance, although no failure has occurred, loss of material can be observed, and it can be hypothesised that increased cycling of current climatic conditions has elicited this response within the material. This indicates that clay layers, although generally robust, do have a greater susceptibility to granular loss than the general fabric of the sandstone. Additionally, if this material loss is occurring in simulated 2018 conditions, it stands to reason that with climate change, the occurrence of this loss will only increase and intensify.

CB2 (8) (Figure 5.28 and Figure 5.29) displays evidence of surface granular loss, similar to that seen in the experimental chamber. Through visual analysis, no determination can be made as to what samples display more extensive granular loss, therefore, this is investigated further through comparative SEM-EDX analysis with associated ImageJ analysis.

5.5.2.2 Borwick

Figure 5.30 - Petrographic thin section scan of BC3 (11), with A focussing on the sample surface and B focussing on a vertical microcrack at depth

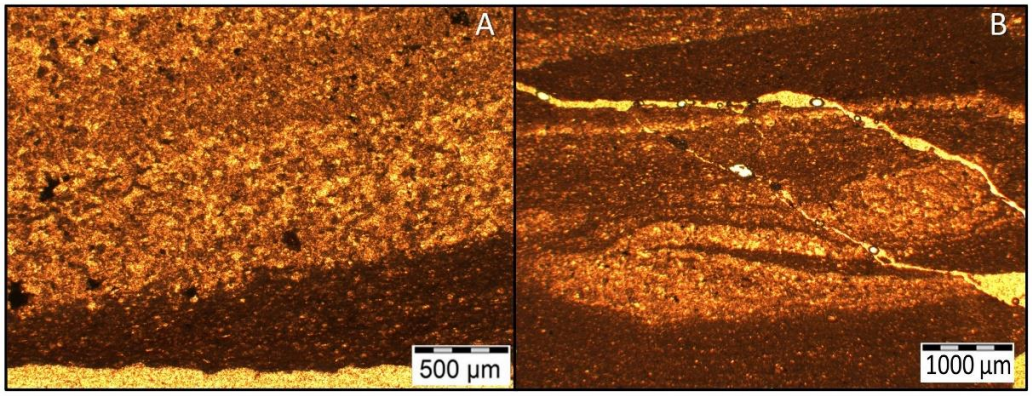

Figure 5.31 - The sample surface of BC3 (11) appears intact (A), while there are distinct horizontal microcracks at a depth of approximately 2cm (B) (Both PPL)

Figure 5.32 - Petrographic thin section scan of BB3 (11), with A and B focussing on two areas of the sample surface

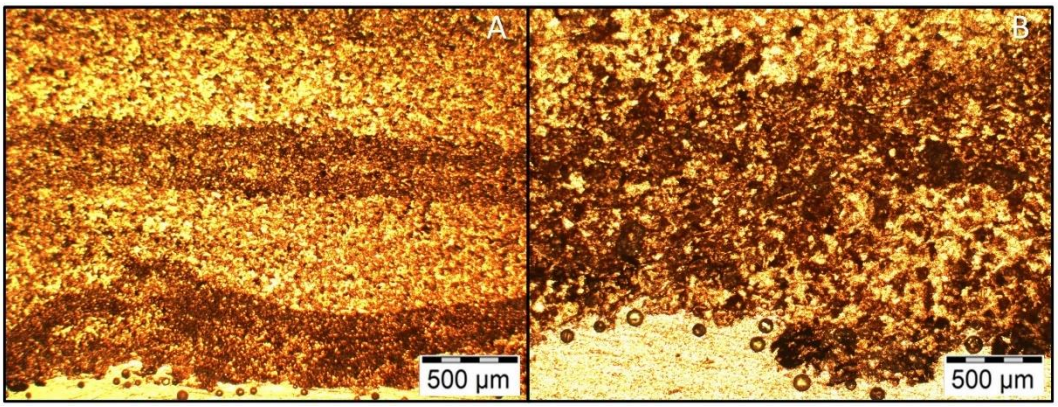

Figure 5.33 - Evidence of dissolution is seen across the surface of BB3 (11), evidenced by a distinct reddish colour seen in both photomicrograph; particularly prevalent at site B (Both PPL)

Comparisons can be made between climate sensitised samples and those exposed to repeated cycling of 2018 conditions. In BC3 (11) (Figure 5.30 and Figure 5.31), no surface dissolution is evident, however, it will take focused SEM-EDX analysis to quantify this at the micro-scale. Microcracks present within the sample (Figure 5.31 B) run parallel to bedding and are characteristic of Borwick control microcracks seen throughout analysis undertaken in this research. They contrast starkly to microcrack features highlighted in climate sensitised control samples, which are wider and run perpendicular to sample bedding.

The surface of BB3 (11) (Figure 5.32 and Figure 5.33) appears intact although dissolution characterised by a light reddish colour is seen across the entire sample surface, however, no secondary porosity is evident in photomicrograph. Furthermore, when instances of extreme dissolution and secondary porosity formation in Borwick Broch stone have been presented previously in this thesis, a dark red colour change is noticeable, in BB3 (11), however, it appears distinctly lighter, indicating that although dissolution has taken place, it has not reached a level that is detrimental to the integrity of the stone. Both of these observations are investigated and quantified through SEM-EDX work.

5.5.3 Petrographic Thin Section Analysis Conclusion

Contrary to anticipated findings, it appears from thin section analysis that control samples from both sites display the greatest evidence of degradation as a consequence of experimental conditions. At Clachtoll, a vertical microcrack is seen in CC2 (7), a feature not previously identified in any Clachtoll baseline or climate sensitised samples. Similarly, in both Borwick control samples, extensive microcracks are visible, including a vertical microcrack in BC3

(10) which is more severe than the typical microcracks associated with the Stromness Flagstone. Moreover, these features noted in the experimental chamber are not reflected in samples utilised in the control chamber. Instead, no microcracking is evident in Clachtoll control rock and only minimal horizontal microcracks are noted in Borwick control samples. What is interesting from the control chamber is the weathering of a distinct clay layer in CC2 (8), indicating that with prolonged exposure, even to current climatic conditions, the clay material is lost at a quicker rate than the surrounding stone fabric. This suggests that in a climate change future, this will continue, perhaps at an exacerbated rate, reaffirming the hypothesis that clay layers are distinct weaknesses within the Torridonian Sandstone and can lead to surface failure.

Concerning broch stone, Clachtoll samples appear to have suffered from surface granular loss in both chambers, SEM-EDX mapping is necessary to quantify the depth of this loss for any conclusion to be made surrounding which chamber has elicited a greater weathering effect from the stone. Unexpectedly, Borwick Broch samples, despite containing several weaknesses, appear to have been negligibly impacted by experimental work. Subsequent analysis is focused on potential sulphide nodule weathering and the chemistry of opaque material. However, as far as petrographic thin section analysis work goes, no clear indication of new weathering can be identified, reflected too in the control chamber broch sample.

In summary, it appears that although all samples remained intact, increased cycling of climate change conditions has primarily initiated a response in control samples. Degradation within the Torridonian control samples is identified for the first time in this thesis, indicating that although the material remains intact when subject to short term exposure, in the long term, features like vertical microcracks and more extensive granular loss could become prevalent. In the case of Borwick, the control samples appear very close to failure, primarily through vertical and horizontal microcracks. Counterintuitively, broch samples appear relatively unaffected. Focus now is on SEM-EDX mapping and subsequent image analysis, from which deeper understandings are gained into highlighted weathering features.

5.6 SEM-EDX Analysis

5.6.1 Clachtoll

5.6.1.1 Experimental Chamber (30-Year Seasonal Climate Change)

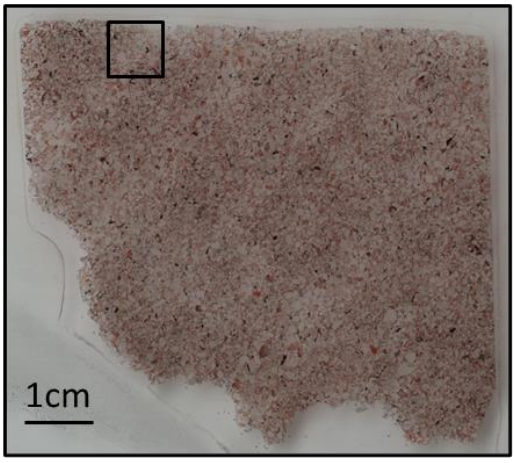

Figure 5.34 - Scan of CC2 (7) showing the location of SEM-EDX mapping, focussing on a surface vertical microcrack

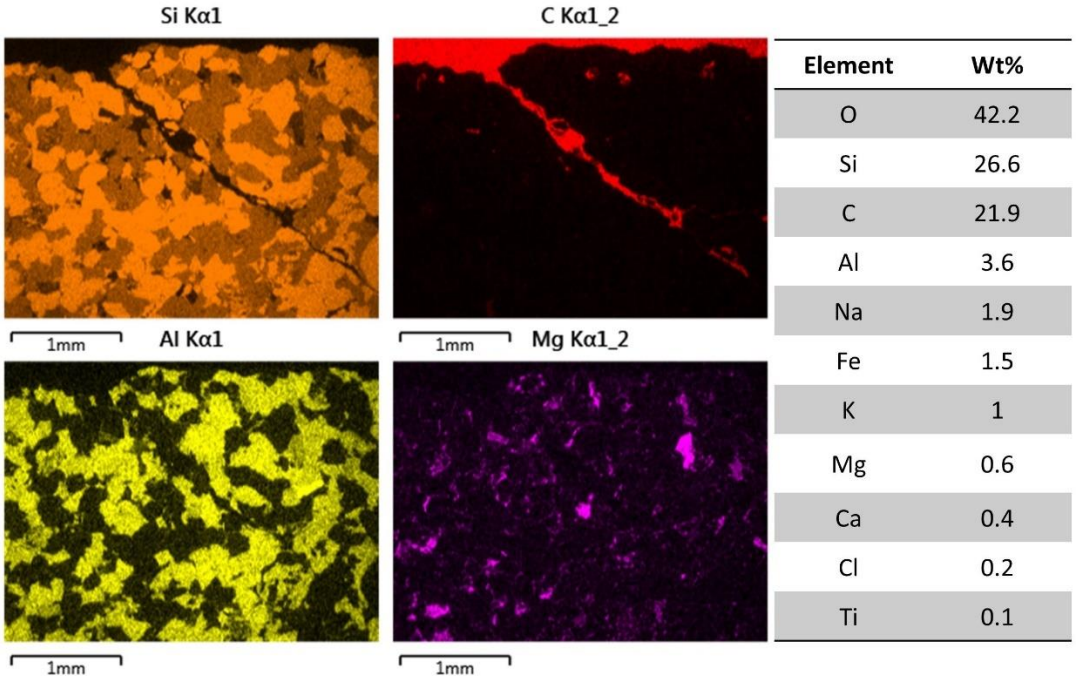

Element	Wt%
O	42.2
Si	26.6
C	21.9
Al	3.6
Na	1.9
Fe	1.5
K	1
Mg	0.6
Ca	0.4
Cl	0.2
Ti	0.1

Figure 5.35 - Quartz (Si), C, plagioclase feldspar (Al) and Mg distribution in the mapped section of CC2 (7) with normalised elemental proportion (%) of the mapped area

CC2 (7) (Figure 5.34) displays a clear ~3mm long vertical microcrack, identified during petrographic thin section analysis. Through SEM-EDX work, however, the chemical structure of the rock material either side of the microcrack is visualised and can be

understood more clearly. Contrary to observations made during thin section analysis, it appears as though the process of cracking has exerted considerable force on the stone fabric, evidenced by fractured quartz and feldspar grains; sections of which now occupy areas of the porosity generated by the microcrack (Figure 5.35). The impact of this feature is limited in scope, whereby the key sandstone mineral components appear intact immediately surrounding the microcrack. Furthermore, as established during baseline work, magnesium-rich compounds work as a minor cementing component within the sandstone and the Mg signal appears completely intact surrounding the microcrack, indicating structural strength remains present within the majority of the sample. However, the microcrack itself can be considered a weak point, stretching approximately 3mm into the rock, leaving it exposed to rainwater ingress, allowing subsequent wetting and drying cycles and freeze-thaw action to occur, which could be severely detrimental to the material in the long term.

As there is no evidence of vertical microcracking in samples analysed before CC2 (7), it can be postulated that there has been an existing weakness within the rock fabric which has been exacerbated by simulated climate change conditions. In previous experimental work that exposed samples to one year of weathering, the Torridonian Sandstone remained intact, although potential weaknesses were highlighted. It appears, however, that increased experimental exposure has elicited a greater weathering effect in the material, evidenced by this vertical microcrack. It can be concluded, based on findings from this experiment and relating specifically to CC2 (7), that although the sandstone is extremely stable and weaknesses within the rock fabric do not fail readily, decades of compounded exposure could cause significant weaknesses to form, such as the one evidenced in CC2 (7). These features, as highlighted, could cause the structural integrity and longevity of Torridonian Sandstone to reach a tipping point. The effects of climate change will likely quicken the rate at which these features form and exacerbate sandstone failure.

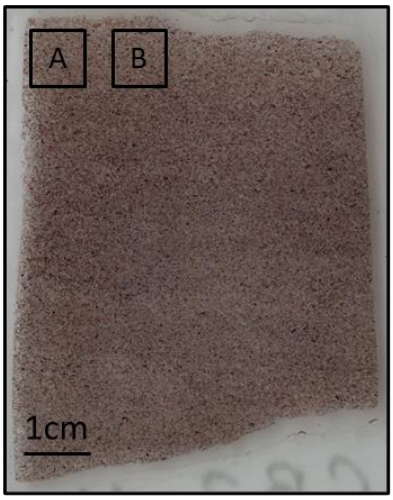

Figure 5.36 - Scan of CB3 (11) showing the locations of SEM-EDX mapping, focussing on surface granular loss

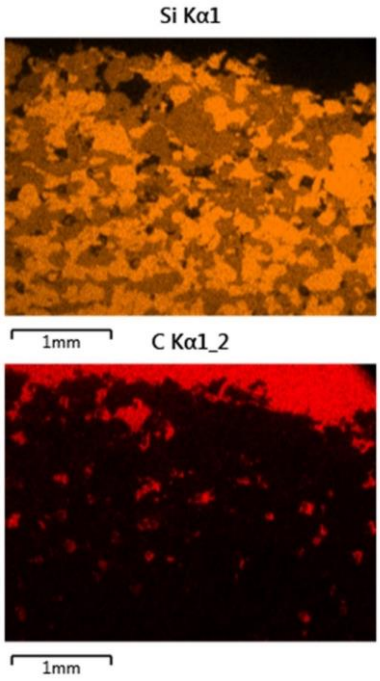

Element	Wt%
O	40.4
C	30.3
Si	21.8
Al	3.1
Na	1.7
Fe	0.9
K	0.8
Mg	0.5
Ca	0.3
Ca	0.3
Ti	0.1

Figure 5.37 - Quartz (Si) and C distribution in the mapped section A of CB3 (11) with normalised elemental proportion (%) of the mapped area

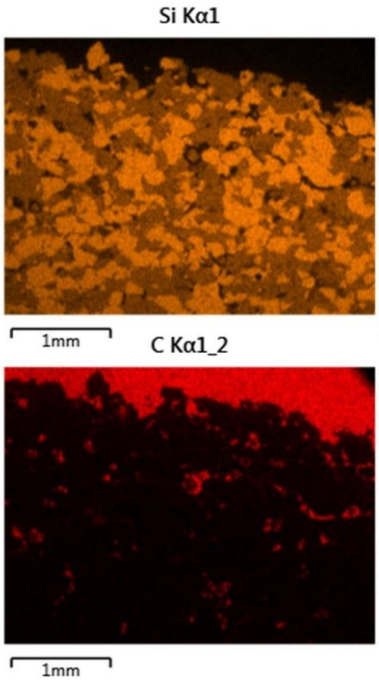

Element	Wt%
O	40.2
C	31.2
Si	20.9
Al	3.1
Na	1.7
Fe	1
K	0.7
Mg	0.5
Cl	0.3
Ca	0.2
Ti	0.1

Figure 5.38 - Quartz (Si) and C distribution in the mapped section B of CB3 (11) with normalised elemental proportion (%) of the mapped area

Two sections of CB3 (11)'s surface were mapped (Figure 5.37 and Figure 5.38). Granular loss can be visualised through the fragmented appearance of quartz and the occurrence of resin (carbon) where quartz is absent. This feature is quantified through ImageJ analysis to understand the depth and distribution of granular loss (5.6.1.3 Clachtoll ImageJ Analysis). Furthermore, to understand whether exposure to climate change conditions triggers increased granular loss, comparisons are made between CB3 (11) and CB2 (8) utilised in the control chamber (5.6.1.2 Control Chamber ('2018' Experiment)).

5.6.1.2 Control Chamber (‘2018’ Experiment)

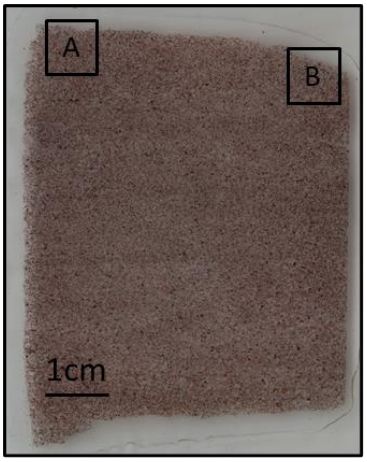

Figure 5.39 - Scan of CB2 (8) showing the locations of SEM-EDX mapping, focussing on surface granular loss

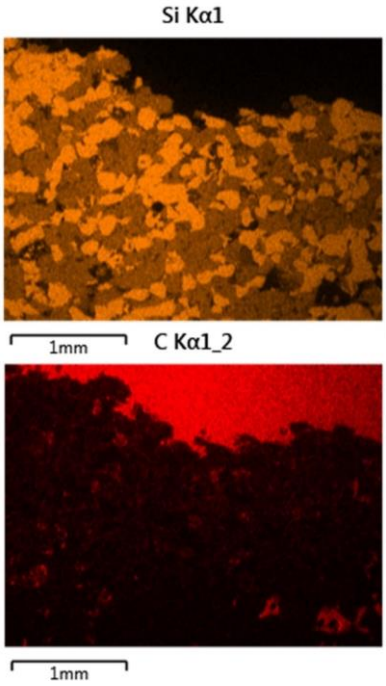

Element	Wt%
C	36.9
O	36.5
Si	18.7
Al	2.9
Na	1.4
Fe	1.2
K	0.8
Mg	0.6
Cl	0.4
Ca	0.3
Ti	0.1

Figure 5.40 - Quartz (Si) and C distribution in the mapped section A of CB2 (8) with normalised elemental proportion (%) of the mapped area

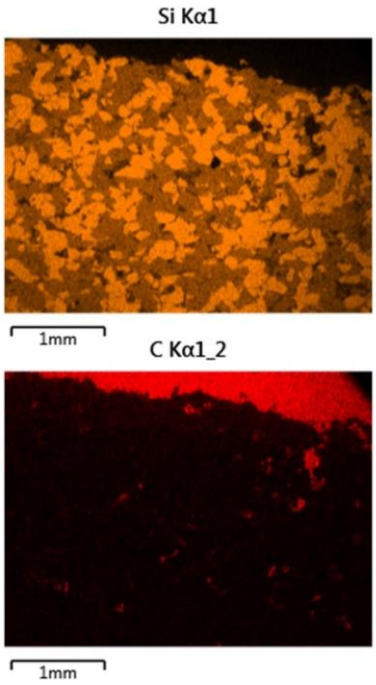

Element	Wt%
O	40.2
C	31.2
Si	20.9
Al	3.1
Na	1.7
Fe	1
K	0.7
Mg	0.5
Cl	0.3
Ca	0.2
Ti	0.1

Figure 5.41 - Quartz (Si) and C distribution in the mapped section B of CB2 (8) with normalised elemental proportion (%) of the mapped area

Similar to CB3 (11) used in the experimental chamber, two areas of CB2 (8)'s surface were mapped and are presented above (Figure 5.40 and Figure 5.41). The granular loss appears less prevalent in this sample than in CB3 (11), however, as discussed in the previous section, ImageJ analysis quantifies this in the following section.

5.6.1.3 Clachtoll ImageJ Analysis

A key finding from the petrographic thin section and SEM-EDX analysis on Clachtoll samples exposed in the CEF chamber is the extent of granular loss that has occurred. ImageJ analysis has been conducted on the surface of two samples, namely CB3 (11) and CB2 (8), that have been utilised in the experimental and control chambers, respectively. The focus element in determining the presence of surface loss and secondary porosity is carbon, which is the signal received from the resin on the slide that the sample is mounted to. For each location of surface mapping on CB3 (11) and CB2 (8), the carbon map has been cropped to the sample's immediate surface before auto-thresholding occurred in ImageJ. In thin section and SEM-EDX work, it appeared that granular loss is more extensive in the experimental sample, reflected too in the auto-threshold images presented below (Figure 5.42).

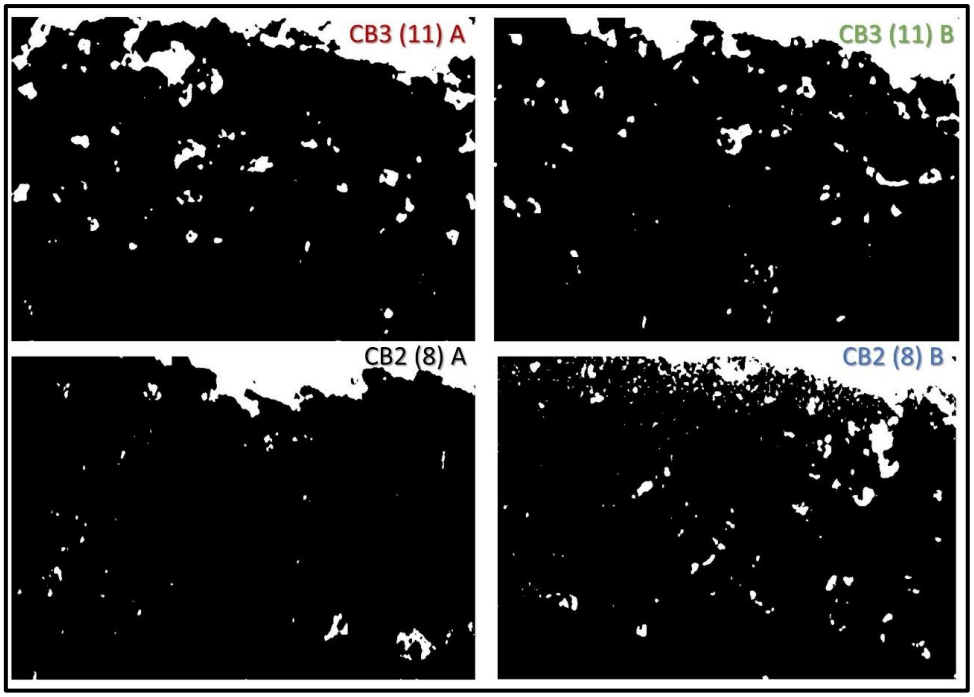

Figure 5.42 - Carbon auto-threshold images of CB3 (11) and CB2 (8) mapped surfaces. The maps have been cropped to the immediate surface of the samples

On observation of the auto-threshold images, it appears that the focus element of carbon that is expressed in white appears more widespread and persistent at depth in both CB3 (11)'s sample sites. Conversely, and particularly in CB2 (8) A, carbon appears to diminish rapidly below the immediate surface. Analysis of these images is subjective, therefore, to quantify the level of carbon, the grey value representing the brightness of white pixels representing carbon has been plotted (Figure 5.43).

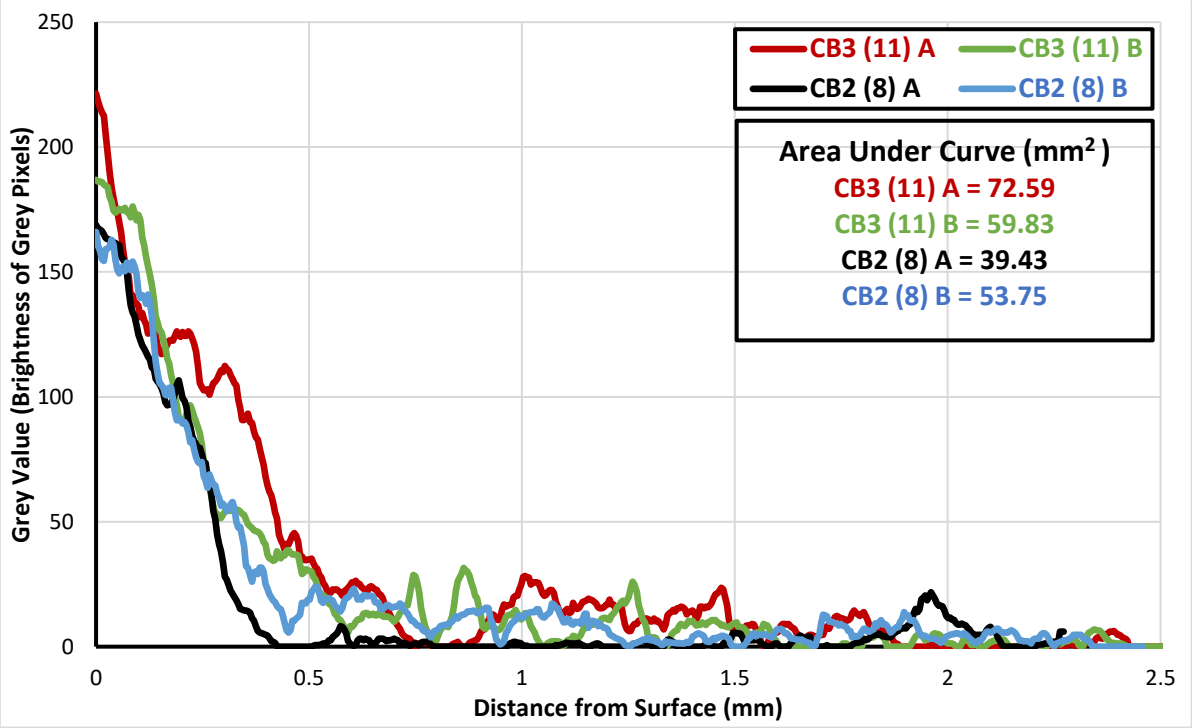

Figure 5.43 - Intensity of grey pixels (C) with progression from sample surfaces to 2.5mm depth. Area under curve (mm^2) results are also presented

The grey value for each sample site has been plotted on the same graph to allow comparisons to be made. It must be noted that the grey value presented at 0mm will be slightly inflated due to a small area of the glass slide above the sample map being unavoidably included, however, the general pattern of carbon in the upper 2.5mm of each sample at two separate locations can be visualised and quantified.

Each sample follows a similar pattern; however, key differences can be identified. The red and green lines representing CB3 (11) A and B respectively remain at a higher grey value for longer at the immediate surface of the stone, while the black and blue lines representing CB2 (8) A and B respectively descend toward zero at a more rapid rate; CB2 (8) A reaches a grey value of 0 at approximately 0.4mm depth while CB2 (8) B remains negligibly above zero at the same depth. This indicates that granular loss at the immediate surface of the stone is more extensive in CB3 (11), utilised in the experimental chamber.

The grey values associated with CB2 (8) remain close to zero for the remainder of the measured area, aside from several minor increases in CB2 (8) B and one pronounced increase at approximately 1.9mm depth in CB2 (8) A. Although close to zero, CB3 (11) A and B lines

can be seen to sit above the CB2 (8) lines, with three pronounced spikes in CB3 (11) A at approximately 0.75mm, 0.85mm and 1.25mm depth.

Findings from ImageJ analysis support initial non-quantified observations that granular loss depicted by carbon distribution is seen more extensively in the climate sensitised experimental sample when compared with the control exposed sample. This is further supported by the area under curve calculations presented within Figure 5.43 where it can be seen that the area is higher beneath the focus areas of CB3 (11). Although the differences appear minor, this research is concerned with small scale differences and observed changes between climate sensitised and control samples, which, in this instance showcase potentially increased granular loss in a climate changed future.

5.6.1.4 Clachtoll SEM-EDX Conclusion

SEM-EDX mapping with associated ImageJ analysis has deepened insight into the effects of simulated climate change on Torridonian Sandstone from the background geology and Clachtoll Broch. It has been postulated that the occurrence of a vertical microcrack in CC2 (7), a feature not seen in any other Clachtoll samples has in part transpired through simulated climate change exposure. Although the surrounding fabric remained unaffected, evidenced by the presence of intact mineral grains and magnesium cement, the feature could be significantly detrimental to the longevity of the sandstone in a climate changed future. Additionally, a robust comparison of granular loss severity has been made between CB3 (11) and CB2 (8), with the former being exposed in the experimental chamber and the latter in the control chamber. Evidence gathered through auto-threshold images, grey values and area under the curve calculations suggests that granular loss is increased upon exposure to a climate changed future.

5.6.2 Borwick

5.6.2.1 Experimental Chamber (30-Year Seasonal Climate Change)

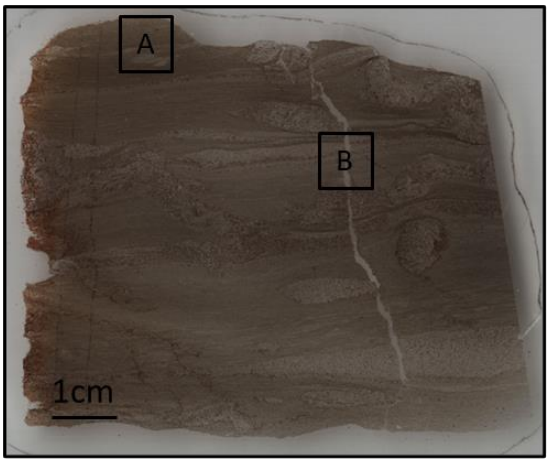

Figure 5.44 - Scan of BC3 (10) showing the locations of SEM-EDX mapping, focussing on surface dissolution (A) and a vertical microcrack (B)

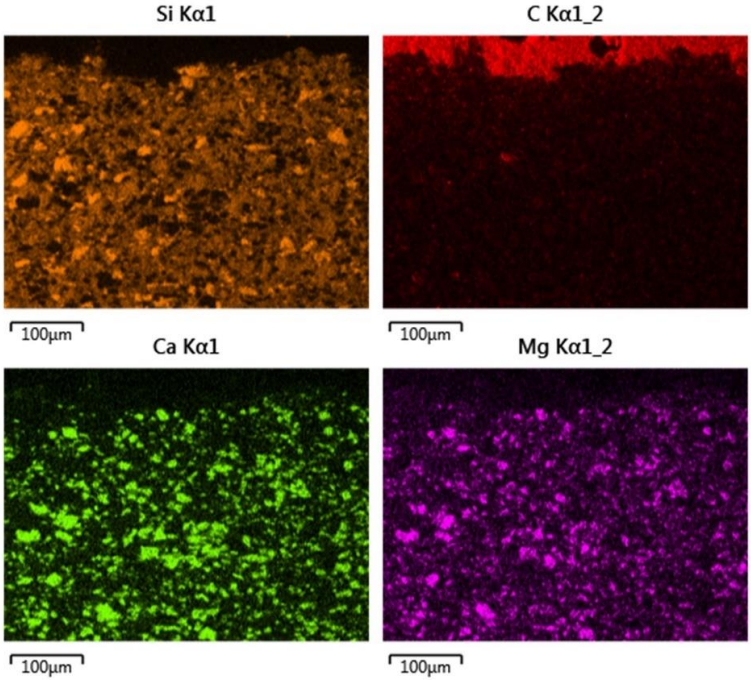

Element	Wt%
O	37.9
C	30.6
Si	14.1
Al	5.5
K	3.8
Ca	3.5
Fe	1.8
Mg	1.4
Na	0.7
Cl	0.3
Ti	0.3

Figure 5.45 - Quartz (Si), plagioclase feldspar (Al), Ca and Mg distribution in the mapped section A of BC3 (10) with normalised elemental proportion (%) of the mapped area

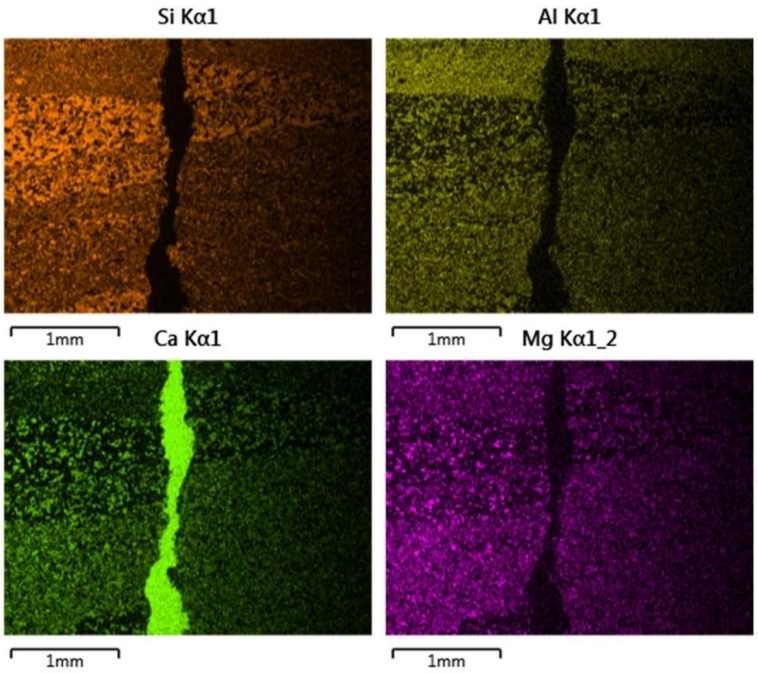

Element	Wt%
O	44.4
Si	19.3
C	13.6
Ca	8.7
Al	4.8
K	3.1
Fe	2.5
Mg	2
Na	1
Yb	0.3
Ti	0.2

Figure 5.46 - Quartz (Si), plagioclase feldspar (Al), Ca and Mg distribution in the mapped section B of BC3 (10) with normalised elemental proportion (%) of the mapped area

Upon inspection of BC3 (10) (Figure 5.44), it is clear that the face on the left-hand side has been prior exposed when part of the background geology, and the upper face, has likely not. Therefore, mapping was undertaken to determine whether any potentially new dissolution has occurred on the pristine side of the sample through CEF exposure (Figure 5.45). It can be seen that the immediate surface of BC3 (10) shows signs of diminished calcium and magnesium, indicative of dolomite dissolution. However, from the carbon map, no secondary porosity appears to have formed, indicating that the surface is in the very early stages of dissolution. This potential finding is quantified through ImageJ analysis (5.6.2.3 Borwick ImageJ Analysis).

The dominant microcrack feature within the sample is mapped in Figure 5.46. In each of the four elemental maps, clear displacement of bedding planes can be seen, however, no dissolution is apparent, indicating that this is a physical weakness within the rock sample. Of significance, this appears to be a severe weakness within the sample that is not characteristic of microcracks observed in baseline Stromness Flagstone samples, indicating that its depth and width has at least in part been influenced by simulated climate change conditions.

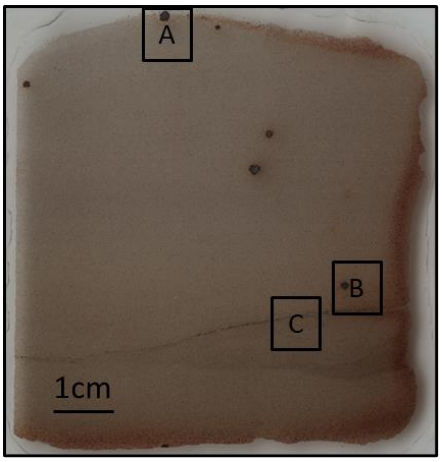

Figure 5.47 - Scan of BB2 (7) showing the locations of SEM-EDX mapping, focussing on two sulphide nodules (A and B) as well as a microcrack (C)

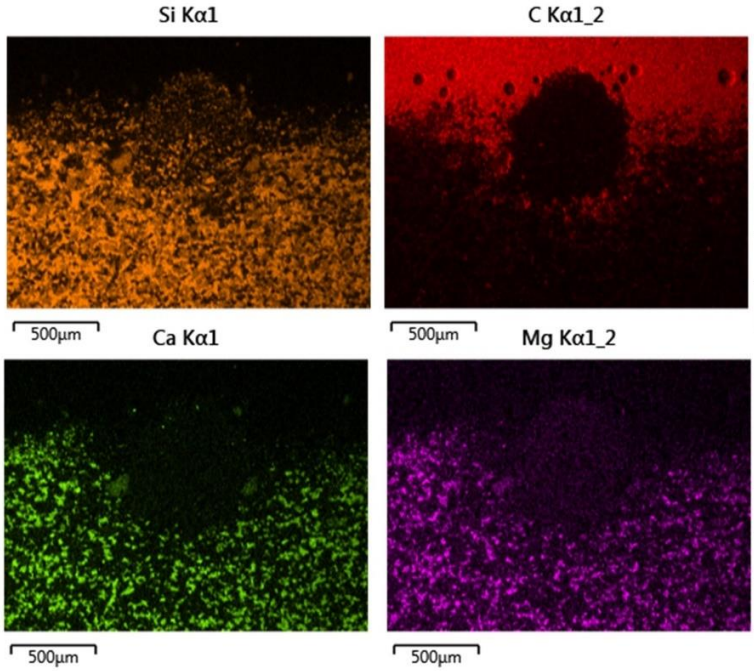

Element	Wt%
C	43.1
O	32.4
Si	11.2
Fe	4.5
Al	2.1
Ca	1.9
S	1.9
Na	0.8
K	0.7
Mg	0.6
Cl	0.6

Figure 5.48 - Quartz (Si), C, Ca, and Mg distribution in the mapped section A of BB2 (7) with normalised elemental proportion (%) of the mapped area

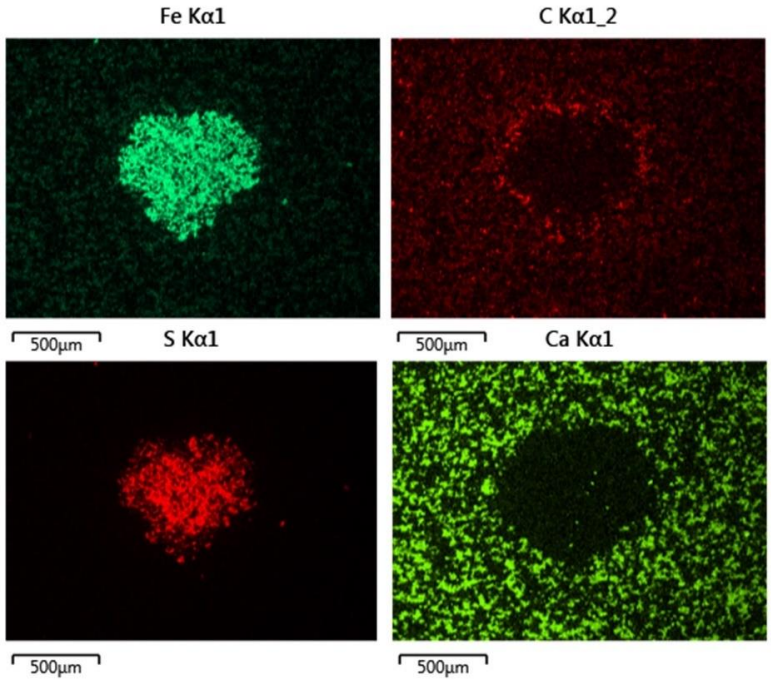

Element	Wt%
O	42.1
Si	22.2
C	15.2
Fe	5.6
Ca	4.5
Al	3.6
S	2.4
Na	1.6
Mg	1.4
K	1.1
Ti	0.2

Figure 5.49 - Iron (Fe), C, S, and Ca distribution in the mapped section B of BB2 (7) with normalised elemental proportion (%) of the mapped area

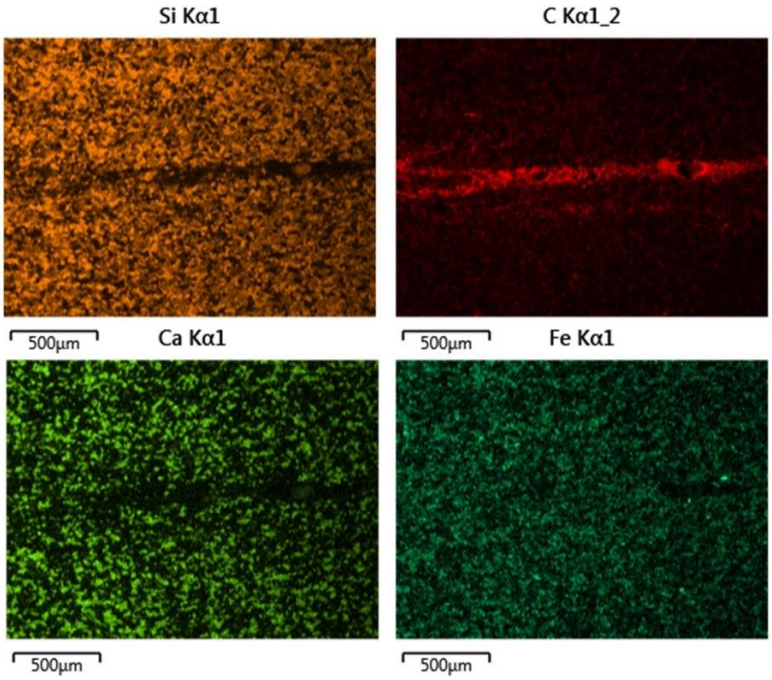

Element	Wt%
O	45.4
C	23.9
Si	20.6
Ca	5.1
Fe	2.9
K	1.7
Ti	0.2
Cl	0.2
Mn	0.1

Figure 5.50 - Quartz (Si), C, Ca, and Iron (Fe) distribution in the mapped section C of BB2 (7) with normalised elemental proportion (%) of the mapped area

As mentioned during petrographic thin section analysis, BB2 (7), despite containing multiple weaknesses associated with Borwick Broch stone, appeared relatively unaffected by experimental work. However, based on SEM-EDX mapping, some weathering effects can be

seen. The surface nodule mapped in Figure 5.48 appeared unweathered in thin section observations. Showcasing the importance of multiple analysis methods, however, a distinctly dolomite depleted, carbon-rich ring can be seen surrounding the surface nodule. Although the nodule has not weathered as extensively as anticipated, this finding indicates that it has weathered surrounding stone fabric to a limited extent. A similar feature is mapped in Figure 5.49 where carbon, indicative of secondary porosity, can be seen surrounding a sulphide nodule, although no significant dissolution of dolomite (calcium) can be seen. Finally, the microcrack at depth is mapped in Figure 5.50, although dolomite appears intact, a concentration of iron can be seen around the microcrack indicating some dissolution has occurred, however, this has not been extensive enough to cause the feature to fail. ImageJ analysis has, therefore, been undertaken to quantify the iron signal around the microcrack.

As noted in thin section work, BB2 (7) appears heavily weathered on the comparison of before and after images presented at the beginning of this chapter (Figure 5.6). Unfortunately, it appears this surface has been lost and the face exposed in the CEF chamber has been lost. Nevertheless, sulphide nodule weathering that had gone undetected in thin section work has been noted and microcrack dissolution has been highlighted.

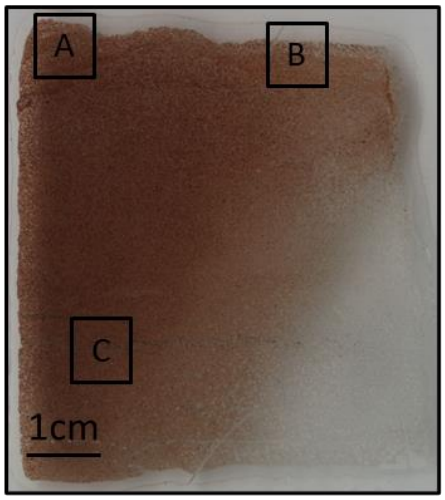

Figure 5.51 - Scan of BB3 (10) showing the locations of SEM-EDX mapping, focussing on two areas of the sample surface (A and B) as well as an opaque layer at depth (C)

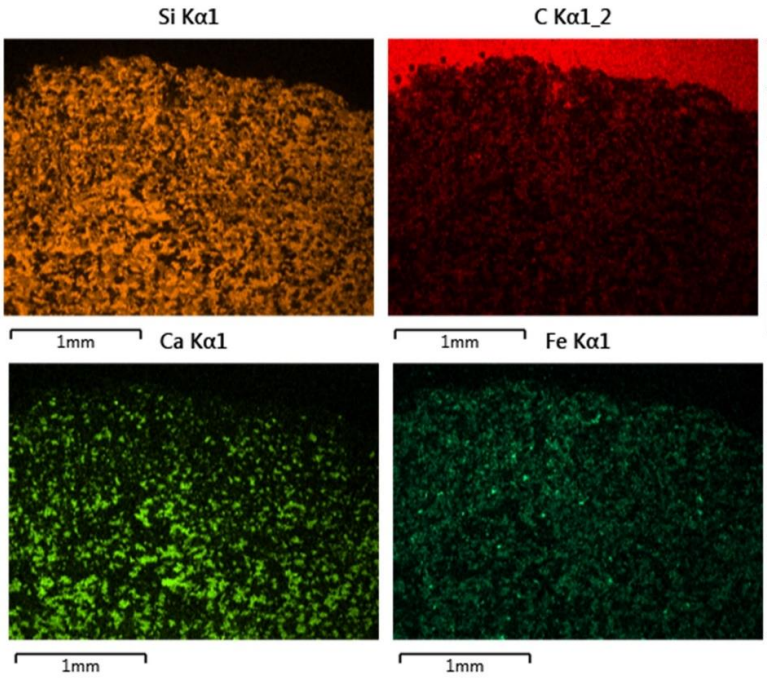

Element	Wt%
O	36.8
C	35.5
Si	15.6
Fe	3
Al	2.7
Ca	2.7
K	1.2
Na	1
Mg	0.7
Cl	0.4
Ti	0.2

Figure 5.52 - Quartz (Si), C, Ca, and Iron (Fe) distribution in the mapped section A of BB3 (10) with normalised elemental proportion (%) of the mapped area

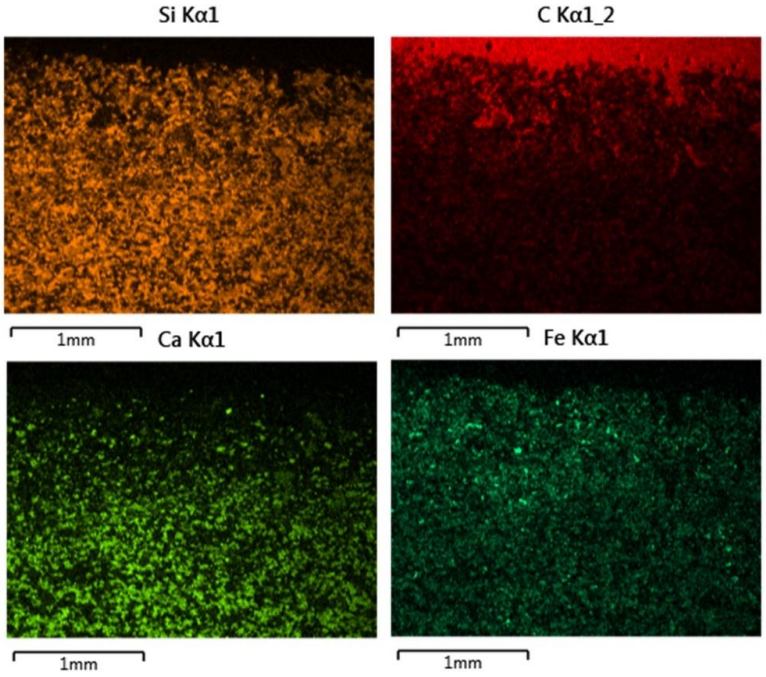

Element	Wt%
C	36.9
O	36.3
Si	13.7
Ca	3.3
Fe	3.2
Al	2.8
K	1.3
Na	1
Mg	0.7
Cl	0.5
Ti	0.3

Figure 5.53 - Quartz (Si), C, Ca, and Iron (Fe) distribution in the mapped section B of BB3 (10) with normalised elemental proportion (%) of the mapped area

Two areas of BB3 (10)'s surface have been mapped (Figure 5.52 and Figure 5.53), focussing on surface dissolution and secondary porosity formation, which appears most extensive in Figure 5.53, where diminished calcium and increased amounts of carbon and iron are seen.

ImageJ analysis has been implemented to quantify this feature and comparisons are made between this sample and BB3 (11) presented in the following section which was exposed in the control chamber associated with this experiment.

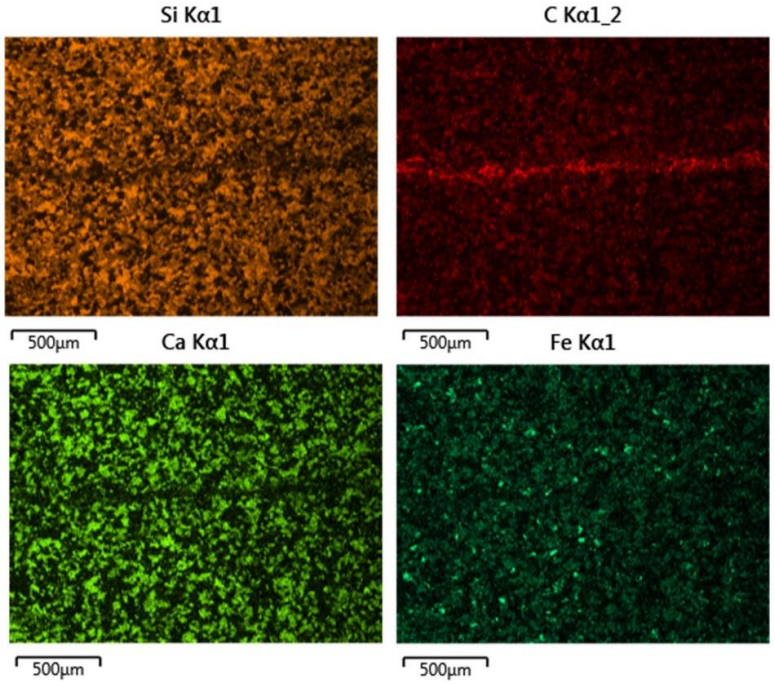

Element	Wt%
O	41
C	22.7
Si	18.4
Ca	5.5
Fe	4
Al	3.8
K	1.8
Na	1.3
Mg	1.1
Ti	0.2
Cl	0.1

Figure 5.54 - Quartz (Si), C, Ca, and Iron (Fe) distribution in the mapped section C of BB3 (10) with normalised elemental proportion (%) of the mapped area

Dark material at depth is mapped in Figure 5.54, this does not appear to be a microcrack despite the carbon signal suggesting that to be the case, instead, it appears to be a product of the manufacturing process that has adhered to the thin section, therefore, no further analysis took place on this feature.

5.6.2.2 Control Chamber (‘2018 Experiment’)

Figure 5.55 - Scan of BC3 (11) showing the locations of SEM-EDX mapping, focussing a potential dissolution area at the surface

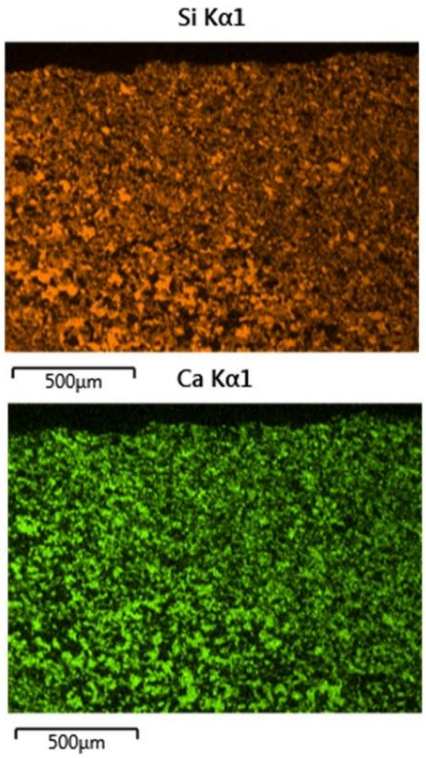

Element	Wt%
O	40.7
C	25.2
Si	15.3
Ca	6.1
Al	4.2
K	2.7
Fe	2.4
Mg	2
Na	0.8
Ti	0.2
Cl	0.2

Figure 5.56 - Quartz (Si), Iron (Fe) Ca, and Mg distribution in the mapped section of BC3 (11) with normalised elemental proportion (%) of the mapped area

One area of BC3 (11)'s surface has been mapped to determine whether any new dissolution has occurred as a result of CEF exposure in the control chamber. From SEM-EDX mapping alone (Figure 5.56), this does not appear to be the case, nonetheless, ImageJ analysis is undertaken in section 5.6.2.3 Borwick ImageJ Analysis to quantify this fully.

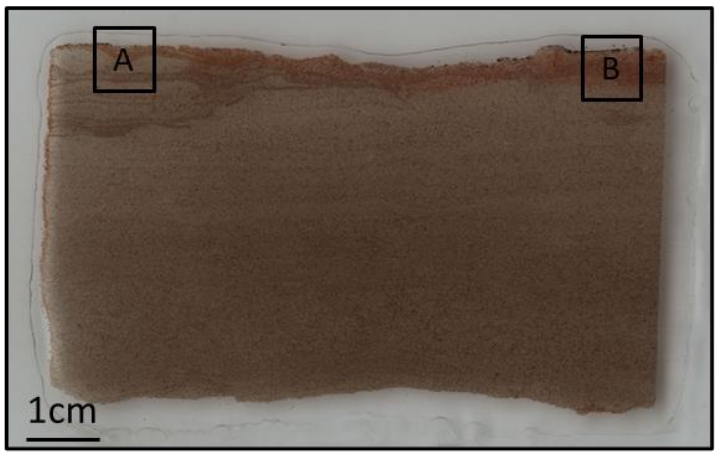

Figure 5.57 - Scan of BB3 (11) showing the locations of SEM-EDX mapping, focussing on two areas of the sample surface (A and B)

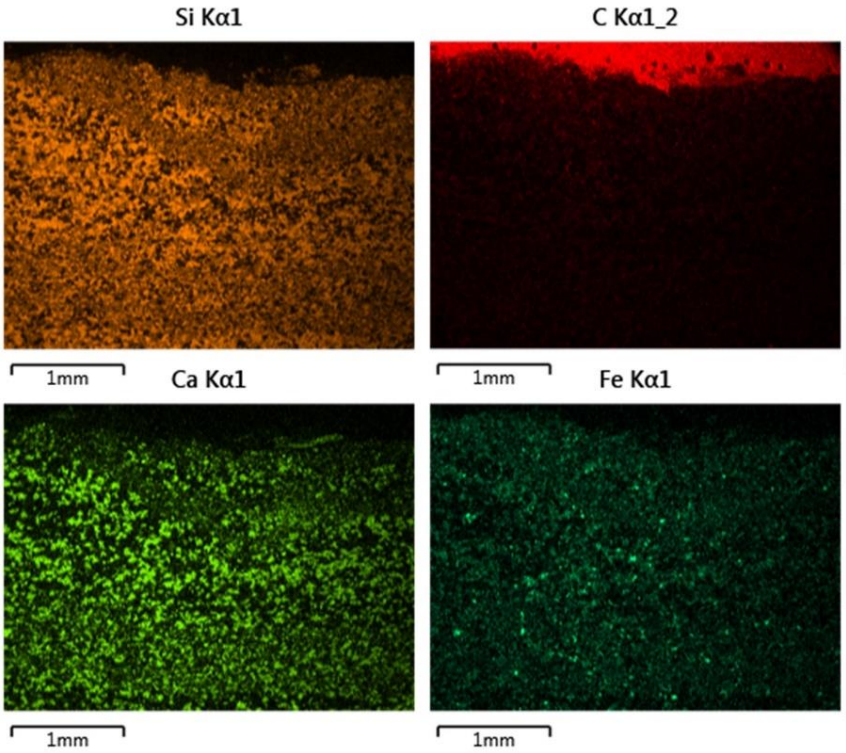

Element	Wt%
O	39.6
C	27.5
Si	17.8
Ca	3.6
Fe	3.5
Al	3.5
K	1.6
Na	1.2
Mg	1.1
Ti	0.2
Cl	0.2

Figure 5.58 - Quartz (Si), Iron (Fe), Ca, and Mg distribution in the mapped section A of BB3 (11) with normalised elemental proportion (%) of the mapped area

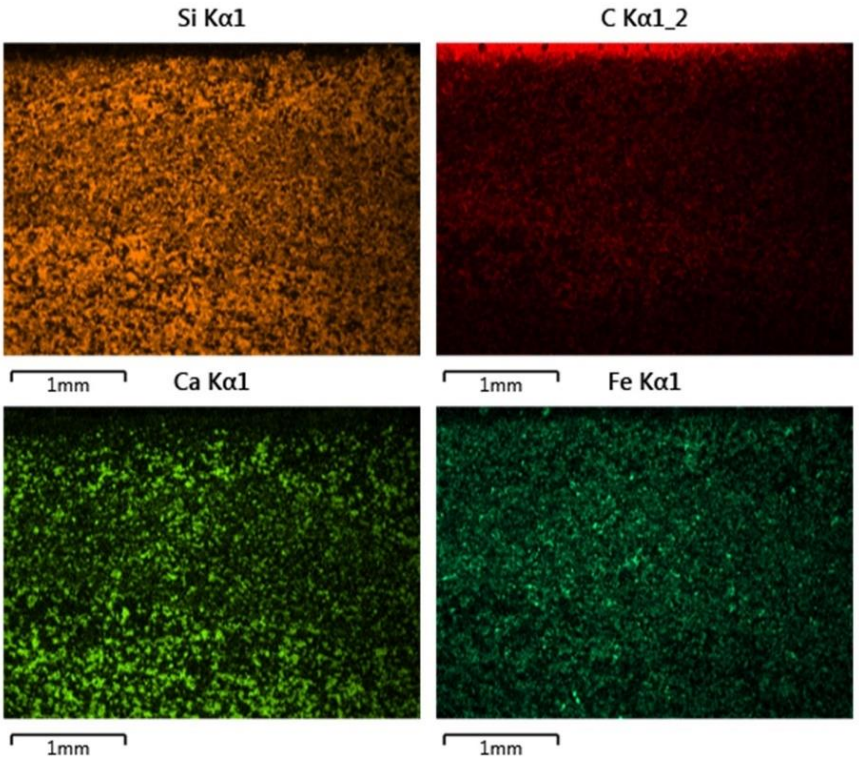

Element	Wt%
O	37.9
C	30.6
Si	14.1
Al	5.5
K	3.8
Ca	3.5
Fe	1.8
Mg	1.4
Na	0.7
Cl	0.3
Ti	0.3

Figure 5.59 - Quartz (Si), C, Ca, and Fe distribution in the mapped section B of BB3 (11) with normalised elemental proportion (%) of the mapped area

Two areas of BB3 (11)'s surface have been mapped (Figure 5.58 and Figure 5.59), and focus is placed on dolomite dissolution. As mentioned in the discussion section associated with BB3 (10), comparisons are made between these two samples to determine whether greater surface dissolution has occurred in BB3 (10) due to its exposure in the experimental chamber. On observation of SEM-EDX mapping alone, this appears to be the case; ImageJ analysis will allow this to be assessed more robustly.

5.6.2.3 Borwick ImageJ Analysis

Key findings based on petrographic thin section and SEM-EDX analysis on Borwick samples exposed to simulated weathering are quantified using ImageJ analysis. Focus is placed on potential new dissolution zones observed on the surfaces of BC3 (10) (experimental chamber) and BC3 (11) (control chamber), the chemistry of a microcrack at depth in BB2 (7) and a comparison of surface granular loss on BB3 (10) and BB3 (11) utilised in the experimental and control chambers, respectively. Findings from this analysis aid in the quantification of new weathering features while allowing comparisons to be made between the effects on samples exposed in the experimental chamber versus those exposed in the control chamber.

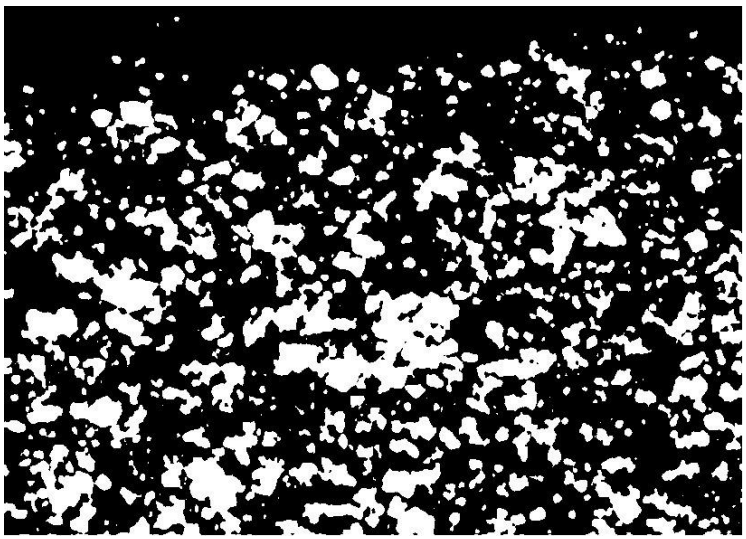

Figure 5.60 - BC3 (10) mapped section (A) auto-threshold image of Ca distribution. The map has been cropped to the immediate surface of the sample

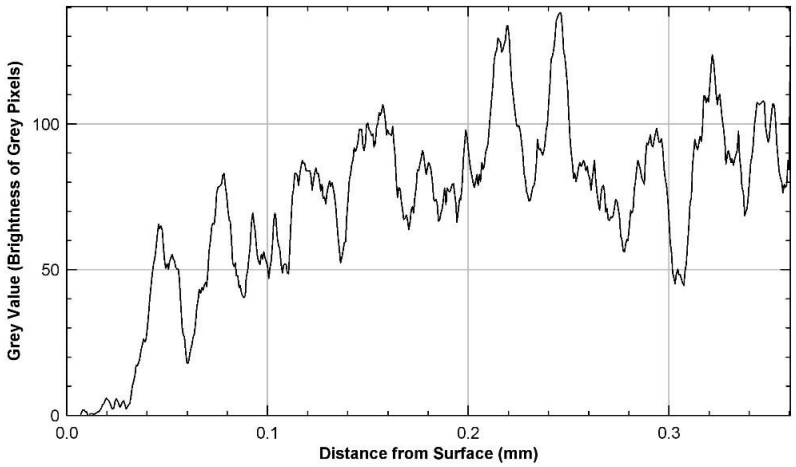

Figure 5.61 - Intensity of grey pixels (Ca) with progression from the sample surface to 0.36mm depth showing diminished Ca to a depth of 0.04mm

Figure 5.62 - BC3 (10) mapped section (A) auto-threshold image of C distribution. The map has been cropped to the immediate surface of the sample

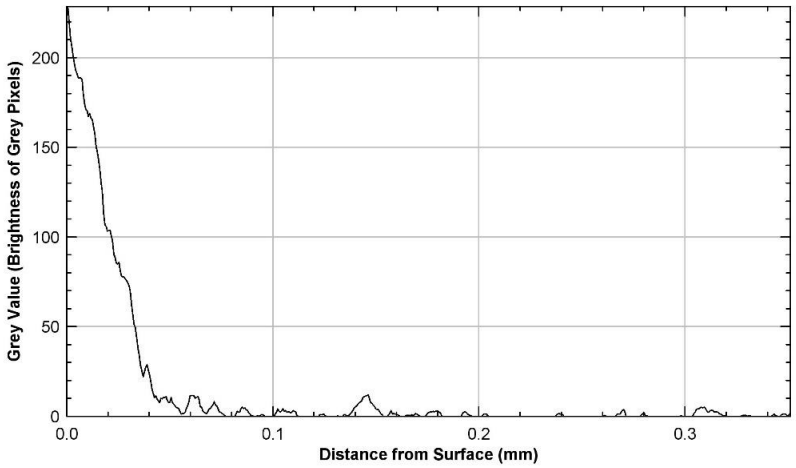

Figure 5.63 - Intensity of grey pixels (C) with progression from the sample surface to 0.36mm depth showing increased C abundance to a depth of 0.04mm

Determining a new dissolution zone attributable to laboratory simulated climate change exposure is difficult since it cannot be said with certainty that the observed dissolution was not present before experimental work. However, on the thin section scan of BC3 (10) (Figure 5.20), it is clear that the surface on the left-hand side of the sample has been the exposed side, while the surface exposed in the CEF appears unexposed and pristine. It can be said with confidence, therefore, that dissolution, if detected in the climate sensitised surface, can be attributed to laboratory treatment. In auto-threshold images, Figure 5.60 and Figure 5.62, a slight reduction in calcium can be seen at the surface of the sample, while a slight increase in carbon can also be seen. Quantified in the grey value maps provided in Figure 5.61 and Figure 5.63, it appears that diminished calcium and enhanced carbon is seen in the upper 0.04mm of the mapped area. This represents an extremely small dissolution zone, enhancing the likelihood that it has occurred in the CEF; if the surface had been subject to continued exposure in the environment, the dissolution depth would be considerably deeper. In terms of this experiment, the sample has been exposed to 30 years of condensed seasonal climate fluctuations which have left a seemingly negligible mark on the exposed surface of the rock. As has been highlighted throughout this thesis, effects seen on samples exposed to laboratory simulated climate change will be more pronounced in the environment, however, it is clear that based on 0.04mm of dissolution over 30 years, it would take centuries for any considerable dissolution zone to develop that could cause significant surface loss and trigger the failure of a culturally significant sandstone block incorporated within a monument or building. As an additional method of quantification and comparison, BC3 (11) is analysed for the same surface feature further on in this section to see if the same effect occurred on a sample exposed in the control chamber.

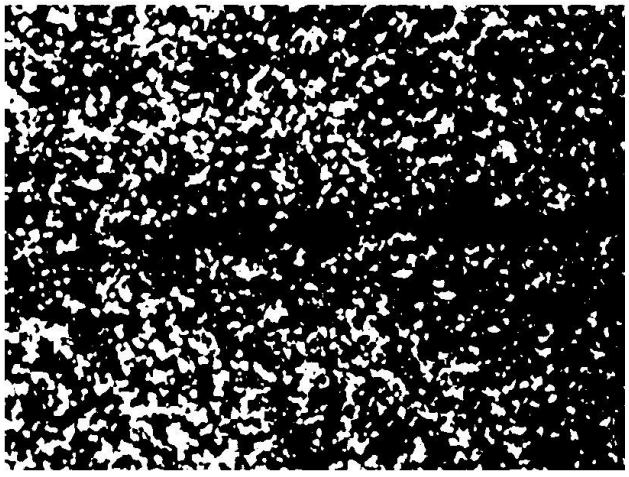

Figure 5.64 - BB2 (7) mapped section (C) auto-threshold image of Ca distribution. The map has been cropped to the immediate surface of the sample

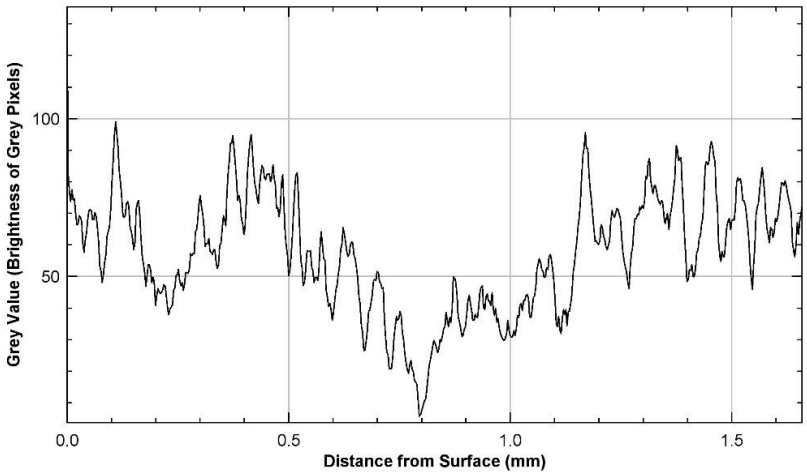

Figure 5.65 - Intensity of grey pixels (Ca) with progression from the sample surface to 1.7mm depth, showing sustained diminished Ca at a depth of 0.5-1.2mm

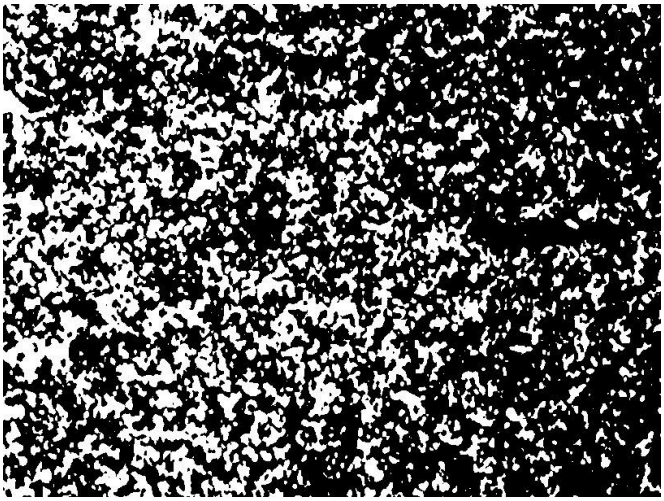

Figure 5.66 - BB2 (7) mapped section (C) auto-threshold image of Fe distribution. The map has been cropped to the immediate surface of the sample

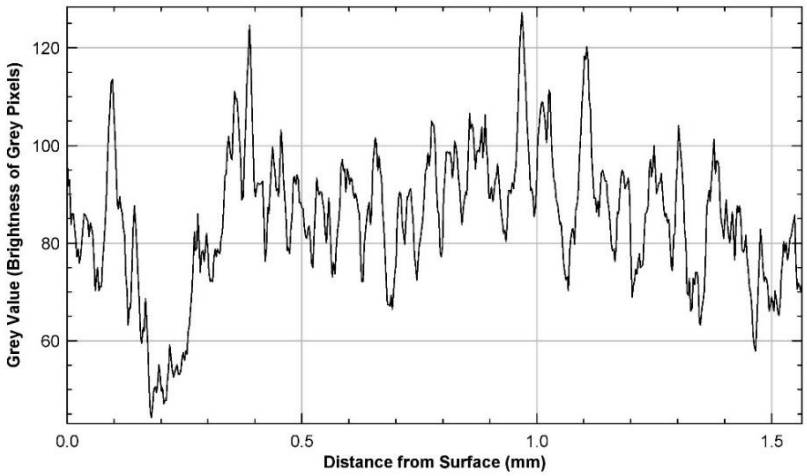

Figure 5.67 - Intensity of grey pixels (Fe) with progression from the sample surface to 1.7mm depth, showing enhanced Fe abundance at either side of the microcrack (0.4mm and 1-1.2mm)

The microcrack feature can be most clearly seen in the calcium auto-threshold image presented in Figure 5.64, while in the iron auto-threshold image (Figure 5.66), the feature is difficult to pinpoint. Grey value graphs provided for calcium and iron in Figure 5.65 and Figure 5.67 respectively, prove useful in determining the physical and chemical characteristics of the area surrounding the microcrack. The feature itself can be seen to begin at a depth of 0.5mm within the mapped area and end at approximately 1.2mm, with the start point characterised by a pronounced reduction in calcium and simultaneous increase in iron, with the opposite being true for the endpoint. Over the approximate 0.7mm representing the microcrack itself, iron remains present while the grey value for calcium steadily reduces to zero at 0.8mm. The fact that iron is highest at either side of the microcrack indicates that dissolution is occurring, and iron is being precipitated in localities immediately surrounding the microcrack, while dolomite is undergoing dissolution. This indicates that although the microcrack is a physical failure, dissolution is occurring which could exacerbate decay around an already weak area within the stone's fabric. Concerning climate change, an increase in precipitation could increase dissolution, making the Stromness Flagstone, which is abundant in these features, more prone to weathering and subsequent failure.

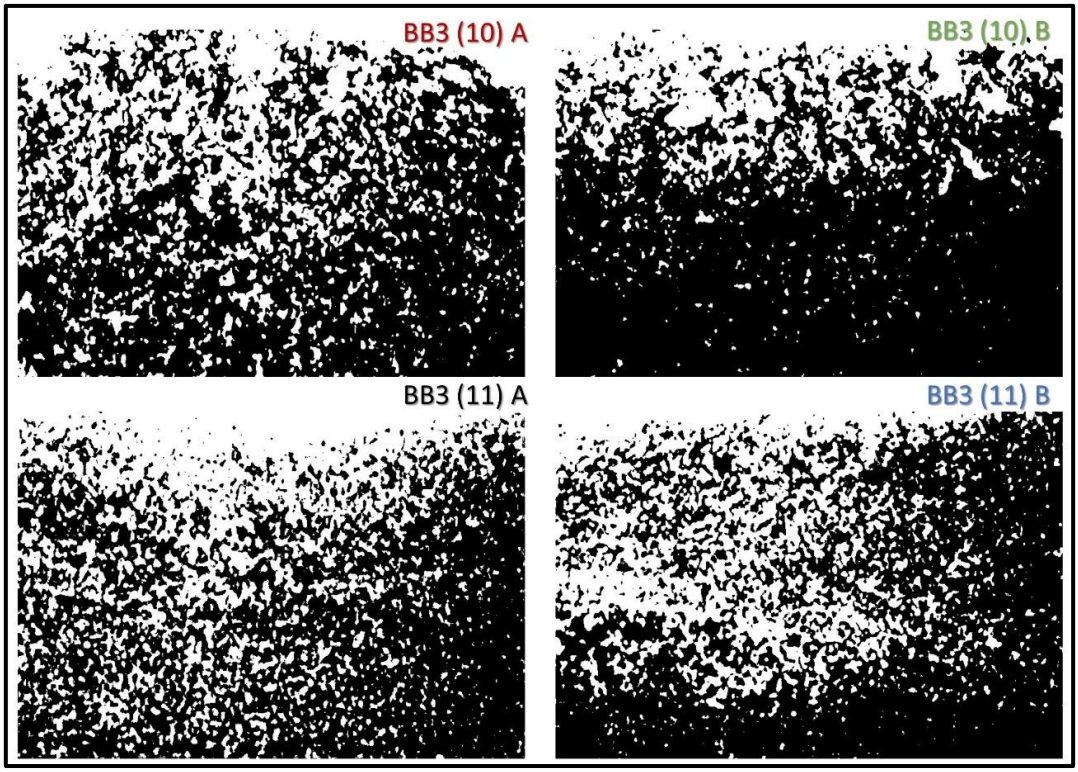

Figure 5.68 - Carbon auto-threshold images of BB3 (10) and BB3 (11) mapped surfaces. The maps have been cropped to the immediate surface of the samples

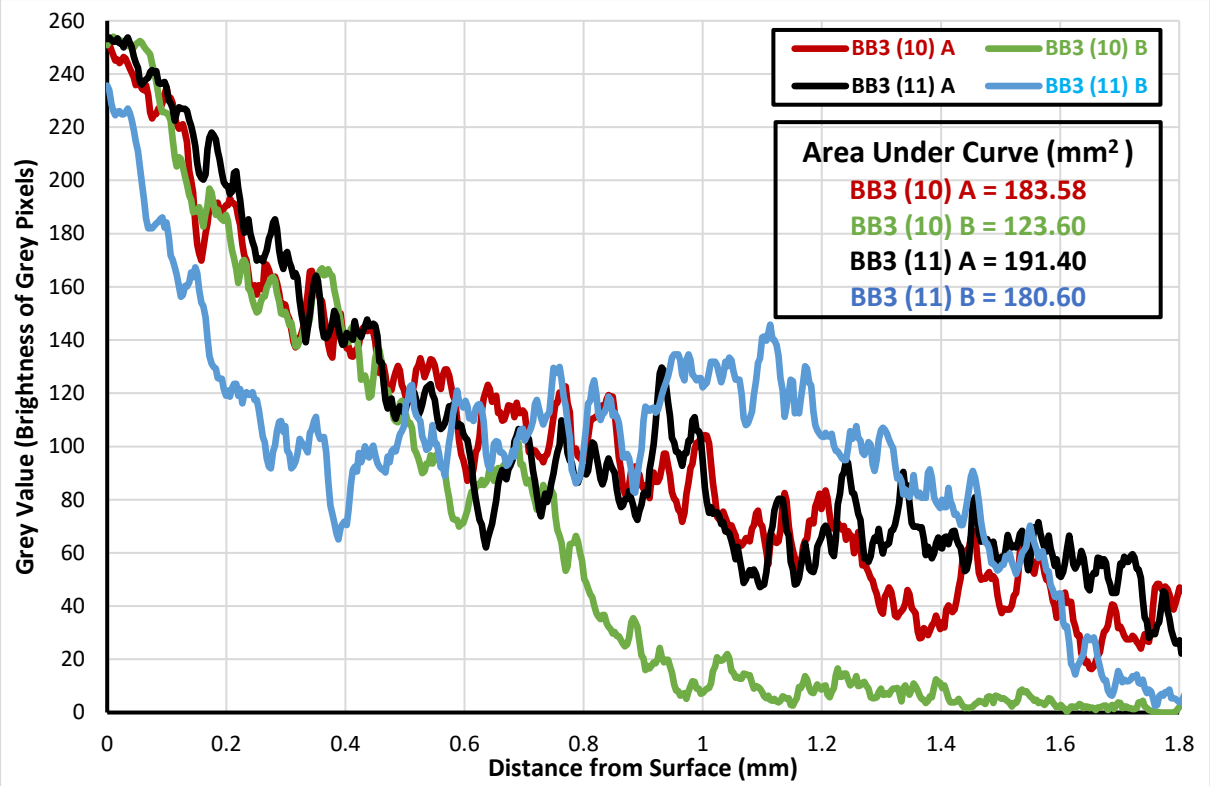

Figure 5.69 - Intensity of grey pixels (C) with progression from sample surfaces to 1.8mm depth. Area under curve (mm^2) results are also presented

From auto-threshold images provided in Figure 5.68, it can be seen that dissolution and subsequent secondary porosity formation is abundant in all mapped areas. In the experimental sample, BB3 (10), dissolution is particularly prevalent at the immediate surface of the stone, however, this diminishes with depth, particularly in BB3 (10) B. Conversely, both BB3 (11) sample sites show a more sustained presence of carbon with distance from the immediate surface. This observation is supported and quantified by grey value data presented in Figure 5.69. The red and black lines representing BB3 (10) and (11) A respectively follow an extremely similar pattern. The importance of the area under the curve calculation becomes clear at this point, quantifying a slight difference between the two sample areas, with BB3 (11) A having a slightly greater area under the curve value, indicative of increased secondary porosity across the sampled area.

The main difference, however, can be observed in BB3 (10) and (11) B plots, whereby the former tracks considerably higher than the latter until around 0.6mm, at which point the lines cross over as BB3 (10) B descends towards zero and BB3 (11) plateaus at a grey value between 80 and 140 until approximately 1.4mm depth before decreasing steadily to zero.

It can be concluded, therefore, that both samples display extensive secondary porosity. In the experimental sample, this feature is more pronounced at the immediate surface of the stone, while in the control sample, although secondary porosity is less prevalent at the sample surface, it is sustained to a greater depth.

Any determination as to whether experimental work has influenced dissolution depth and secondary porosity would be difficult to put forward with any great confidence given the exposure history of the samples. It can be seen that both samples have remained intact as a result of experimental work, highlighting that despite a dissolution depth of between 1 and 1.5mm across mapped areas, this has not been substantial enough for any sample failure to occur through experimental or control exposure.

Figure 5.70 - BC3 (11) mapped section auto-threshold image of Ca distribution. The map has been cropped to the immediate surface of the sample

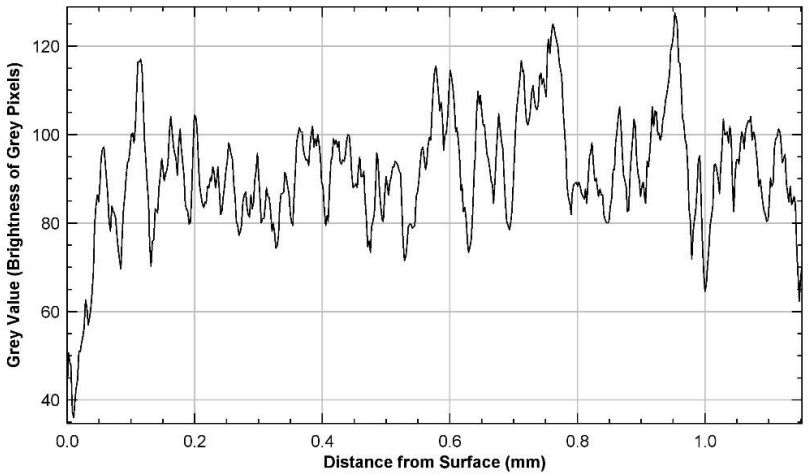

Figure 5.71 - Intensity of grey pixels (Ca) with progression from the sample surface to 1.15mm depth showing diminished Ca at sample surface to a depth of 0.1mm

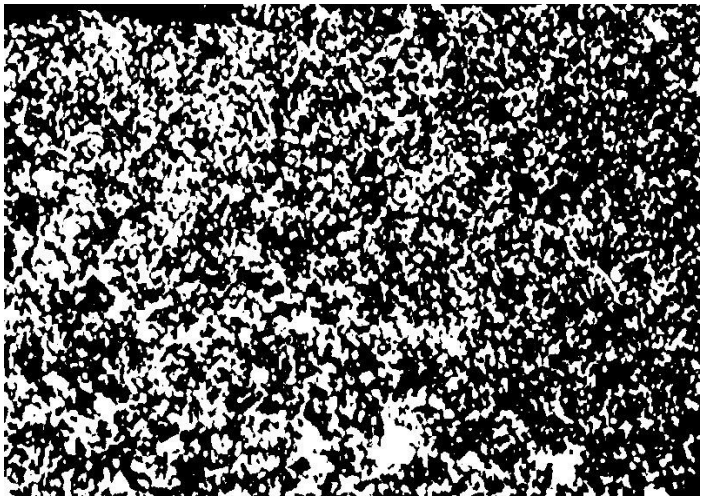

Figure 5.72 - BC3 (11) mapped section auto-threshold image of Fe distribution. The map has been cropped to the immediate surface of the sample

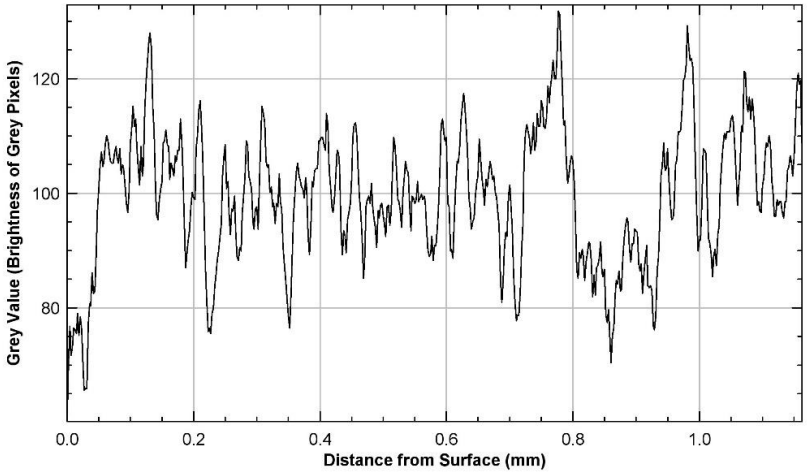

Figure 5.73 - Intensity of grey pixels (Fe) with progression from the sample surface to 1.15mm depth showing slightly increased Fe abundance at 0.15mm

In BC3 (11), no carbon was detected during SEM-EDX mapping of the surface of the sample, therefore, iron, which precipitates as a result of dissolution, has been analysed instead. From auto-threshold images of calcium and iron (Figure 5.70 and Figure 5.72), no apparent evidence of surface dissolution can be seen. Grey values for each element have been mapped (Figure 5.71 and Figure 5.73) and slight evidence of diminishing calcium and increasing iron that is characteristic of dolomite dissolution can be observed. However, this can be attributed to a section in the upper left corner of the auto-threshold images which represents the glass slide being unavoidably included in the grey value analysis. It can be seen that the grey value for iron remains predominantly between 80 and 120 for the entire depth of the mapped area which could perhaps indicate dolomite dissolution, however, as calcium levels do not

diminish at the immediate surface, it can be concluded that no dolomite dissolution has occurred. This is an important finding which provides an interesting comparison with BC3 (10) discussed prior, which showed evidence of minor surface dissolution after exposure in the experimental chamber. However, in BC3 (11) exposed in the control chamber, a similar feature cannot be seen. This indicates that exposure in the experimental chamber elicits a slightly more destructive response than exposure in the control experiment.

5.6.2.4 Borwick SEM-EDX Conclusion

Analysis undertaken in this section has allowed robust comparison between climate sensitised samples and those that were utilised within a control experiment. In BC3 (10) incorporated in the experimental chamber, an extremely small scale, but potentially new dissolution zone has been detailed, found at the immediate surface of the sample going to a depth of 0.04mm. The size of this feature indicates that dissolution can be an extremely slow process, particularly in samples obtained from the background geology, however, this research focuses on small scale indications of weathering, therefore, a finding as minor as this one is anticipated. Moreover, in comparison with BC3 (11) exposed in the control chamber, no evidence of any new small-scale surface dissolution is evident. Based on these findings it appears that dissolution, although a slow onset process, could be exacerbated by climate change conditions. Additionally, what appears to be a negligible dissolution zone, could greatly influence the longevity of the stone with increased exposure in the real environment. As detailed previously in this thesis, any weathering change resulting from a CEF experiment can be considered the absolute minimum weathering change that would occur in the natural environment, given the parameters such as wind-driven rain or a storm event that cannot be replicated in a laboratory within the scope of this research.

Insight into BB2 (7) was limited to the chemistry of the microcrack located at depth within the sample, SEM-EDX mapping and ImageJ analysis has showcased that dolomite dissolution and precipitation of iron has occurred surrounding the microcrack, weakening it. Although simulated climate change has not caused the sample to fail, it can be said that it has accelerated dolomite dissolution.

Finally, a comparison was made between the depth of dissolution in BB3 (10) and BB3 (11) utilised in the experimental and control experiment, respectively. It was determined that although both samples show extensive dissolution, they can be characterised differently. In BB3 (10) dissolution is more severe at the immediate surface but reduces significantly

beyond that. Conversely, in BB3 (11), dissolution is less severe at the surface but is sustained to a greater depth within the sample.

5.7 Chapter Conclusion

Knowledge of the strengths and weaknesses associated with each sandstone type has been gained through baseline work undertaken in Chapter 3 and short-term climate change exposure conducted in Chapter 4. Based on this, it was hypothesised that with increased climate change exposure simulated in this chapter, greater understandings would be gained into how specific weaknesses within each sandstone type would react to the long-term effects of simulated climate change.

Throughout this thesis, the strength of Torridonian Sandstone has been showcased, while the comparative weakness of Stromness Flagstone has similarly been presented. Concerning the former, this chapter has aimed to determine whether, although the material does not weather readily, longer-term exposure would elicit a response from identified weaknesses, including microcracks and distinct clay layers. While in the latter, it has been a case of determining how weak the material is when exposed to long term climate change conditions, given its destructive response to shorter-term exposure in Chapter 4.

A summary of key findings from each chamber is presented in Table 5.3 and Table 5.4, with relevant summary text provided below.

Table 5.3 - Summary of key findings from control chamber ('2018' experiment)

Control Chamber	Visible Alterations	Chroma Meter	Mass Loss per kg (g)	Thin Section Analysis	SEM-EDX	ImageJ Analysis
Borwick Control	No Change	Potential a* and b* decrease in BC3 (11)	0.60	No substantial evidence of weathering		
Borwick Broch	Biological growth on BB3 (11)	Potential a* and b* decrease in BB3 (11)	0.50	Dissolution and secondary porosity in BB3 (11) seen to a greater extent than experimental chamber sample		
Clachtoll Control	No Change	L* increase	0.40	No substantial evidence of weathering		
Clachtoll Broch	No Change	L* decrease. Potential a* increase, b* decrease	0.30	Granular loss identified in CB2 (8) to a lesser extent than experimental chamber sample		

Table 5.4 - Summary of key findings from experimental chamber (30-year seasonal climate change)

Experimental Chamber	Visible Alterations	Chroma Meter	Mass Loss per kg (g)	Thin Section Analysis	SEM-EDX	ImageJ Analysis
Borwick Control	Granular loss on BC2 (7)	Minor change with large error in BC2 (7) & BC3 (10)	1.30	Potential minor new dissolution zone identified in BC3 (10)		
Borwick Broch	Surface flaking and sulphide nodule weathering on BB2 (7)	Significant change in BB3 (10) L*, a* and b* values	0.90	Dissolution and secondary porosity in BB3 (10) to a lesser extent than control chamber sample		
Clachtoll Control	No Change	Negligible a* and b* change, L* increase	15.70	Vertical microcracking identified in CC2 (7)		
Clachtoll Broch	Granular loss on CB2 (7)	Clear b* increase in CB3 (11)	0.60	Evidence of increased granular loss in CB3 (11) compared with a control experiment sample		

Analyses in this chapter began at the macro-scale with observations made through comparisons of before and after images, it was shown that physical change was limited to minor granular loss in Clachtoll samples, while in Borwick samples, granular loss, colour changes and increased dissolution was highlighted. Chroma Meter and mass loss analyses helped to quantify observations made in the physical change section, showcasing that colour change and mass loss is most prevalent in climate sensitised broch samples, particularly those originating from Borwick Broch.

Turning to the micro-scale, greater insight into sample strength as a result of experimental treatment was gained through petrographic thin section analysis, SEM-EDX mapping and ImageJ analysis. Thin section work allowed microfeatures to be picked out, namely vertical microcracking in a Clachtoll control sample as well generally increased granular loss in the Torridonian Sandstone. In Borwick samples, wide vertical microcracking, surface dissolution and sulphide nodule stability were highlighted. These features were mapped on the SEM-EDX and quantified using ImageJ; insight emerged to suggest that the vertical microcrack in CC2 (7) had occurred with significant force, enough to fracture sandstone mineral components, however, the damage is limited to the immediate microcrack site. Additionally,

quantification of granular loss determined that it has occurred to a greater depth in the climate sensitised CB3 (11), compared with CB2 (8) utilised in the control chamber. In Borwick samples, a minor new potential dissolution zone of 0.04mm was identified in climate sensitised BC3 (10) while in BC3 (11), no similar feature was identified after exposure in the control experiment, inferring that dissolution rate may increase marginally in a climate changed future, compared to present. Additionally, dolomite dissolution was identified and quantified surrounding a microcrack in BB2 (7). Dissolution depth and secondary porosity formation were compared between BB3 (10) and BB3 (11), showing that this feature was sustained to a greater depth in the latter, which was exposed in the control chamber.

Increased cycling of seasonal climate change exposure has had a lesser effect on samples than anticipated, showcased through the overall stability of samples utilised in experimental work. However, focussing on the small-scale change, macro-scale observations indicate that degradation as a result of climate change exposure is more pronounced than change that has occurred in the control chamber, especially relating to samples originating from Borwick broch. However, through micro-scale analyses, notable changes are highlighted from samples used in both the experimental and the control chambers.

Undoubtedly, this chapter would have benefitted from an increased number of samples, however, this was not possible due to SMC restrictions and a trade-off emerged between sample quantity and relatability to the historic environment. Despite this, a methodological approach has been tested and insight gained into the effects that climate change may have on each building stone type. Chapter 6 will follow on from these analyses and begin appraising the longevity of Torridonian and Devonian building stone based on findings from Chapters 3-5.

6 Synthesis Chapter

6.1 Chapter Introduction

The principal aim of this thesis has been to understand the future effects of climate change on two important Scottish sandstone types; Torridonian Sandstone and Stromness Flagstone, utilised in the construction of Clachtoll and Borwick Brochs respectively, and with wider representation in nearby built structures.

To achieve this, their baseline characteristics were extensively appraised, as presented in Chapter 3, alongside their inherent strengths and potential weaknesses. Samples of each sandstone type were then exposed to climate changed futures in two innovative weathering simulations presented in Chapters 4 and 5. Each sample went through extensive and multifaceted macro/micro-scale analyses to build up a clear understanding of how these sandstones may proceed to weather in a climate changed future in Scotland.

This final chapter presents the key findings from research undertaken, relevant to sandstone type and sample treatment. Based on these findings, decay models are presented for each sandstone over the next century, which helps to inform potential conservation strategies. Leading on from this, an evaluation of methods utilised in this study is provided, alongside limitations encountered. Finally, recommendations for future research to build on this thesis and continue to develop understandings of the threats of climate change on sandstone heritage sites in Scotland are suggested.

6.2 Key Findings

Table 6.1 brings together the most significant findings from Chapters 4 and 5 and allows comparisons to be made between experiments. In both control chambers, sample response was extremely limited, particularly in the climate changed year experiment, with surface flaking in a Borwick Control sample the only apparent alteration. In the 30-year change control chamber, sample response is slightly amplified through a potential increase in dissolution evidenced in a Borwick Broch sample, together with clear surface colour changes in Clachtoll samples.

Table 6.1 - Summary table of key findings from each CEF experiment

	CONTROL CHAMBER		EXPERIMENTAL CHAMBER	
	Climate Changed Year	**30-Year Change**	**Climate Changed Year**	**30-Year Change**
Borwick Control	Surface flaking, slight surface dissolution.	No substantial evidence of new weathering.	Trace surface salt formation. Potential new surface dissolution.	Granular loss and potential new surface dissolution.
Borwick Broch	No Substantial evidence of new weathering.	Increased dissolution and secondary porosity formation.	Failure of two samples along distinct microcracks. Surface salt formation.	Surface flaking, sulphide weathering, significant colour changes.
Clachtoll Control	No substantial evidence of new weathering.	L* increase.	No substantial evidence of new weathering.	Vertical microcracking.
Clachtoll Broch	No substantial evidence of new weathering.	L* decrease. Less granular loss than experimental chamber samples.	Minimal surface granular loss.	B* yellowing and more extensive surface granular loss.

Crucially, the most significant responses, are seen in samples exposed to climate change futures. In the climate changed year experimental chamber, two Borwick Broch samples failed. Moreover, surface salt formation occurred exclusively on samples used in this chamber and most extensively on a Borwick Broch sample. These findings indicate that pre-weathered material in historic monuments is most susceptible to weathering associated with future climate change.

The response from Clachtoll samples is far less severe, it is only in the 30-year change experimental chamber that the most prominent signs of increased weathering are seen, whereby vertical microcracks were noted for the first time in control samples and more extensive granular loss was seen in broch samples.

Given the dramatic impacts that one year of climate change exposure had on Borwick Broch samples, it was anticipated that a simulation of 30-years of seasonal climate change would elicit even more pronounced changes in the material. However, this did not transpire as demonstrated by the relative lack of Borwick weathering features noted in Table 6.1. Of significance to this research, however, effects appear marginally more pronounced with exposure to simulated climate change conditions than repeated 2018 conditions in the control

chamber. This is evidenced by increased weathering in Borwick Control samples and a multitude of different weathering features noted in Borwick Broch samples, including flaking of surface material, sulphide nodule weathering and colour changes. However, new surface dissolution has potentially occurred to a more pronounced level in the control chamber.

Potentially giving a reason for the fact that 30-years of simulated climate change exposure did not elicit the weathering response hypothesised in Borwick samples, is sample randomness. It is feasible that the samples utilised in the first climate change experiment had more inherent weaknesses within them and these weaknesses were closer to reaching a decay tipping point. As demonstrated throughout this thesis, intra-block heterogeneity is unavoidable given the complex and manifold way that sandstone weathers, however, to mitigate this, samples used in each experiment originate from the same source and from the same larger sample blocks where possible. Although counter-intuitive, it is also possible that based on findings observed from the climate changed year experiment, exposure to gradual but concentrated climate change elicits a greater weathering response in Borwick samples. The opposite can be said for Clachtoll samples, whereby one year of exposure had negligible weathering effects, however, with increased cycling of climatic conditions, some prior pinpointed weaknesses such as granular loss began to occur at a more pronounced rate. The two sandstone types are distinctly different as demonstrated in Chapters 2 and 3 of this thesis, therefore, the fact they have responded differently to each treatment is expected and adds to the complexity of safeguarding different heritage sites from future climate change.

The most clear and significant finding from this research, as demonstrated throughout analyses undertaken, is that generally, weathering is more pronounced in experimental chambers where samples are exposed to climate change temperature, humidity and in some cases precipitation conditions. Moreover, these weathering effects are amplified in samples that originate from broch structures, highlighting clearly that the past exposure history of a culturally significant building stone greatly influences its longevity within a climate changed future. This is particularly clear in Borwick Broch Stromness Flagstone where significant changes such as sample failure have occurred. Although the contrast is less stark, Clachtoll Broch samples do appear to weather at an increased rate than control samples in a climate changed future.

From key findings, it is apparent that Torridonian building stone will have greater longevity than Stromness Flagstone in the cultural environment. However, as demonstrated in decay

models provided in the following section, each sandstone type is vulnerable to accelerated weathering in a climate changed future.

6.3 Decay Models

Informed by how broch stone from each site has weathered through CEF experiments undertaken in this research, indicative decay models have been produced. The models focus on expected stone decay phenomena at 10, 30 and 50-100 year intervals from present, specific to each sandstone type (Figure 6.1).

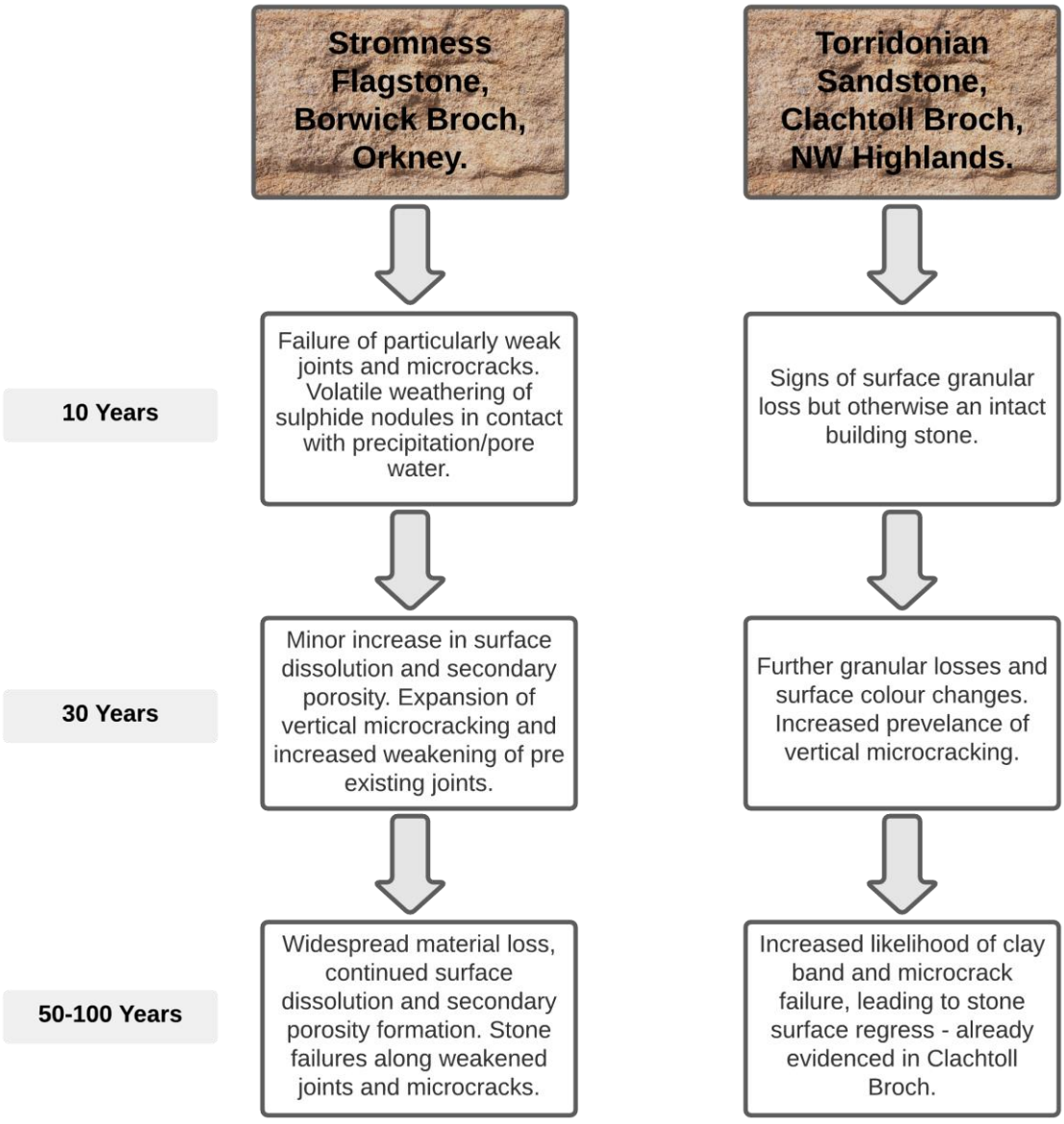

Figure 6.1 - Indicative decay models for Borwick and Clachtoll Broch stone in a climate changed future without conservation measures in place, based on findings from experimental work undertaken

Decay models for sandstone are seen in the literature, however, by nature, are extremely complex and are influenced by a multitude of factors. Different sandstone types will decay differently, efforts have been made, such as by Smith et al., 2011 to produce a decay model for sandstone in general, however, the heterogeneity of the material, even within the same sandstone type, makes this a difficult task. Exemplified throughout this thesis; Stromness Flagstone and Torridonian Sandstone decay differently, they have distinctive weaknesses and decay patterns that occur at varying rates. Therefore, rather than producing a decay model for sandstone in general, Figure 6.1 provides a more specific decay pathway for two contrasting sandstone types, considering their strengths and weaknesses that have been identified throughout this research project.

After 10 years of climate change exposure, failure of particularly weak microcracks and joints is highly probable in Borwick Broch stone, evidenced through the failure of two samples in the first CEF experiment. Additionally, particularly volatile sulphide nodules, primarily those located close to microcracks within the stone that precipitation can penetrate, will begin to weather. The resulting sulphuric acid will exacerbate dolomite dissolution and secondary porosity formation surrounding such features, which will begin to undermine the structural integrity of the stone. This process will not be linear, over time the most vulnerable sulphide nodules will oxidise and a new equilibrium will be achieved within the stone. However, as demonstrated in experimental work, Stromness Flagstone is prone to surface failure and when this occurs, a fresh surface is exposed. This will uncover previously protected nodules and they will be subjected to precipitation, causing them to weather.

Conversely, Torridonian Sandstone will remain intact with little observable change after 10 years of exposure, other than minor granular loss that does not negatively impact the structural integrity of the stone.

It appears through experimental work that a slight weathering hiatus occurs in Borwick Broch samples after 30 years of exposure, whereby the susceptible microcracks and joints have already failed, and the more intact microcracks can withstand a few decades of exposure. During this time, dissolution will continue at a relatively slow rate at stone surfaces and surrounding microcracks. Additionally, there is potential that vertical microcracks will widen and deepen within the stone, increasing failure susceptibility. In the environment, however, this apparent reduction in dramatic weathering effects may not occur to the same extent as seen in the 30-year change experiment. It could be the case that factors associated with being

part of a structure could exacerbate or even protect against decay, depending on factors such as type and abundance of biological cover and the location of a building stone within the structure. Moreover, particularly aggressive storm events could intensify weathering and bring samples closer to failure. In Clachtoll Broch samples, subtle colour changes may occur, and an increased rate of granular loss is probable, evidenced through the 30-year change experiment results. Additionally, the occurrence of vertical microcracking is seen exclusively in samples sensitised to 30-years of climate change, potentially weakening the stone's structure. However, it can be said with confidence that the building stone will remain intact after 30 years of climate change exposure.

With progression towards 50-100 years of climate change exposure, the decay pathway of each stone type becomes more speculative as this forecasts beyond the scope of the experimental design. Therefore, assumptions have been made based on the strengths and weaknesses exhibited in each stone type and how they have reacted in both climate change experiments. The likelihood of identified weaknesses failing has been appraised, from which informed postulations have been made with the caveat that the decay model can be updated, assuming the condition of the two building stone types is monitored in the coming decades. In Borwick samples, more widespread stone losses will likely occur as previously intact joints and microcracks begin to suffer from increased dissolution and water ingress, potentially exposing previously unweathered sulphide nodules which will rapidly weather, causing extensive secondary porosity formation and, eventually, the loss of stone material through surface flaking and microcrack failure. In Clachtoll samples, vertical microcracks and distinct clay bands have been identified, although these remained intact after experimental work, it was demonstrated that these features are distinct weaknesses that could reach a tipping point in a climate changed future. The failure of these would lead to stone surface regress, a feature already evidenced in Torridonian Sandstone structures, including Clachtoll Broch (Figure 6.2 and Figure 6.3) and Tanera Mòr Herring Station (Figure 6.4).

Figure 6.2 - Clachtoll Broch wall face, packing stone sits proud of larger face bedded blocks, some examples of which are highlighted. The block shown in Figure 6.3 is circled

Figure 6.3 - Face bedded block within Clachtoll Broch, showing signs of extensive surface cracking and flaking

Surface regress is apparent in Clachtoll Broch, where face bedded building stones are held in place by surrounding packing stones that are oriented along their bedding plane. Examples of face bedded stone regress are highlighted in Figure 6.2. While within a culturally significant monument for millennia (Clachtoll Broch), considerable surface loss is seen. A close up of a face bedded building stone in Clachtoll Broch is provided in Figure 6.3. Surface cracking is seen extensively across the face of the stone and areas where stone material has been lost as a result of surface failures are visible. Clachtoll Broch has stood since the Iron Age, meaning these blocks have been in situ for approximately 2000 years, suggesting that stone decay of this kind is a very slow process. However, an example is provided below of a similar face bedded Torridonian Sandstone structure on Tanera Mòr, an island located in Loch Broom in the Inner Hebrides. The building in question is a ruined 18th Century Herring Station that was

abandoned in the mid-20th Century. Although a far more contemporary structure when compared with Clachtoll Broch, the same face bedded stone regress is seen (Figure 6.4).

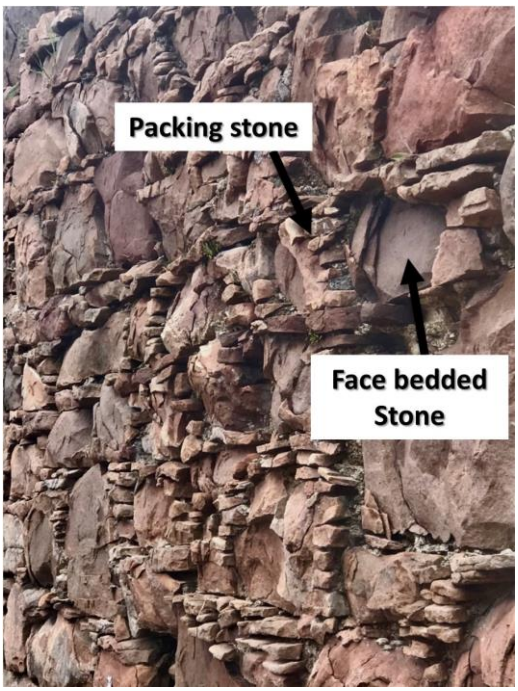

Figure 6.4 - Face bedded Torridonian Sandstone at Tanera Mòr Herring Station. Packing stones sit proud of the larger face bedded block. Image courtesy of Timothy Meek

This example from Tanera Mòr highlights once more that face bedded Torridonian Sandstone manifested within a built structure suffers from surface losses, causing the packing stones to sit proud of the larger face bedded blocks. It must be noted, therefore, that although Torridonian Sandstone from Clachtoll Broch remained intact and appeared robust during CEF experiments, when exposed in the real environment, decay may occur at an accelerated rate, especially in a climate changed future.

What is clear throughout this study and incorporated within the decay models presented (Figure 6.1), is that these two types of sandstone weather in different ways at different rates. A decay model simply applied to sandstone, in general, is not specific enough for building conservation. Consequently, constructing more focused sandstone decay models, specific to sandstone type and weathering history is crucial. In turn, more nuanced decay models allow for more site-specific conservation strategies to be produced.

6.3.1 Conservation Strategies

The manifold way that sandstones weather has been made clear throughout this thesis and accelerated decay of pre-weathered building stone is predicted in a climate changed future.

Therefore, conservation strategies must be highly specific and take into consideration; sandstone type, structure type, location, and weathering history, all of which are essential factors that influence future decay. Given the cultural significance of stone-built heritage in Scotland, conservation strategies must be minimally invasive while ensuring site authenticity and longevity are not compromised, which can be a difficult balance to strike.

Brochs are especially difficult to protect given their age, structure, and level of decay to date, however, the following section provides site-specific suggestions for Borwick and Clachtoll Brochs as well as wider suggestions for structures composed of the same stone types.

6.3.1.1 Stromness Flagstone, Borwick Broch

The coastal location of Borwick Broch on top of a rocky promontory as well as its ruinous state makes it especially difficult to conserve, both at a structural level and building stone level. Given the vulnerability of Stromness Flagstone to accelerated weathering in a climate changed future, compounded by increased coastal erosion and rising sea level predicted in the coming decades (Harkin *et al.*, 2020), Borwick Broch is at severe risk of being lost entirely, with various decay mechanisms at play. Relating to the future of Borwick Broch, the vulnerability of coastal sites to erosion in a climate changed future has become a key area of investigation for HES, who have constructed an adaptive intervention hierarchy, delineating the options available to them for the conservation of vulnerable coastal sites in their care (Figure 6.5: Harkin et al., 2020).

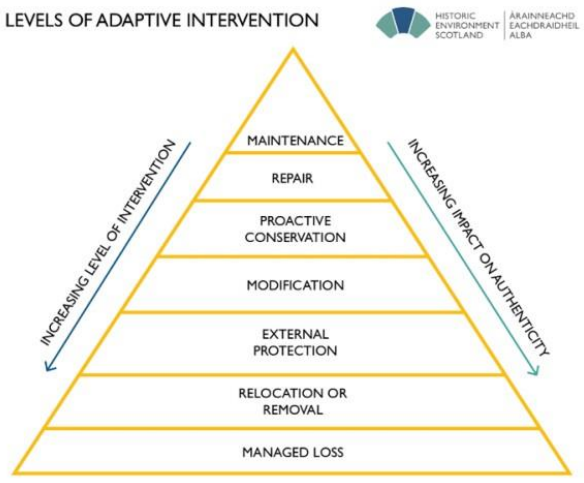

Figure 6.5 - The different levels of adaptive intervention used in the management of coastal heritage assets, and the level of intervention and associated impact on authenticity they have. (Copyright Historic Environment Scotland)

As detailed in Chapter 2 (2.3.2 Borwick Broch, Orkney), Borwick has been the subject of extensive periodic archaeological investigation, providing some degree of preservation by record. Recently, a 3D model has been produced of the site and is available to view online at Sketchfab. Based on this and informed by Figure 6.5 taken from Harkin *et al.*, 2020, managed loss and preservation by record is likely to be the best way forward to ensure that despite the likelihood of material loss, knowledge of the site is retained. Other options include the relocation of the structure further inland, however, this could undermine the authenticity of the site.

At the building stone level and specifically relating to this thesis, the inherent vulnerability of the broch stone to decay is clear, moreover, in a climate changed future, findings from this research showcase that the material will weather at an exacerbated rate through a plethora of identified weaknesses such as dolomite dissolution, failure of microcracks/joints and the weathering of sulphide nodules. To prevent further stone degradation, a hard engineered solution such as the construction of a protective structure around the broch would be necessary to protect the stone from weathering accelerants such as precipitation, however, this would be difficult to legitimise given the ruinous state of the broch and would detract from the authenticity of the site.

Protecting the stone itself from degradation is therefore difficult, however, suggestions to increase the longevity of the site can be put forward. Partial collapse of the seaward facing broch wall has occurred, given the plethora of archaeological spoil surrounding the site, this material could feasibly be incorporated in a rebuilding effort, bringing the collapsed wall back to the same height as the surrounding broch walls. Alternatively, fresh flagstone could be utilised in a partial rebuild, but this too could detract from the authenticity of the site given the contrast between pristine flagstone and material which has suffered from decay since the Iron Age. Additionally, a replacement for particularly badly weathered stone within the structure could be sought from archaeological spoil.

Findings from this research can be applied beyond the scope of Borwick Broch and aid in the conservation of more contemporary structures that are composed of the same building material. Stromness Flagstone from Liddle's Quarry has been used in the construction of buildings and structures around Orkney's mainland (Gillespie and Tracey, 2012). At present, the material is vulnerable to weathering and in a climate change future, this will only intensify. Therefore, key indicators of decay must be monitored on Stromness Flagstone

structures, such as surface reddening indicative of dolomite dissolution, flaking caused by microcrack/joint failures and the weathering of distinct sulphide nodules. These phenomena can be seen as indications that the sandstone is deteriorating, and potential stone replacement or stone covering should be considered.

6.3.1.2 Torridonian Sandstone, Clachtoll Broch

Contrasting with Borwick Broch, Clachtoll Broch lends itself well to preservation. It has been extensively excavated by AOC Archaeology, who have uncovered increased knowledge of the past use of the building, adding greatly to the cultural significance and importance of the site, highlighting it as one of the most significant broch structures in Scotland. Rubble has been removed from the interior of the broch and visitors can easily walk around the site and admire its high degree of preservation. Although coastally located and therefore vulnerable to coastal erosion, exemplified by the partial collapse of its seaward facing wall, it is protected to an extent by underlying geology that slopes away from the site towards the sea. Given the likelihood of the loss of coastal broch sites such as Borwick, Clachtoll could be utilised as an exemplar coastal broch due to its comparatively high degree of preservation. Clachtoll Broch could feasibly become a visitor attraction similar to more well-known sites such as the Broch of Gurness on Orkney, but with increased accessibility given its location close to the North Coast 500. In terms of conservation practices to further enhance the site, a great deal of archaeological spoil is located close to the site and, like Borwick, a partial rebuild of the collapsed seaward facing wall would enhance the site. The broch itself is not protected in any way from human activity. This could incur increased damages and loss of material, therefore, measures to protect the site from such activity should be considered, such as the installation of a perimeter wall/fence. Provided earlier in this chapter, Figure 6.2 and Figure 6.3 showcase surface regress and surface cracking of the Torridonian building stone, although this does not appear to undermine the overall structural robustness of the broch, should further surface losses occur, potential removal of particularly badly damaged stone should be considered. Again, like Borwick, suitable material within archaeological spoil would be an adequate source of stone replacement.

Relating to other Torridonian Sandstone structures, conservation suggestions can be put forward. As highlighted earlier in section 6.3 Decay Models, Torridonian Sandstone may weather to an increased rate in the environment. Using Tanera Mòr as an example again, the benefit of surface finish in protecting the sandstone is clear to see.

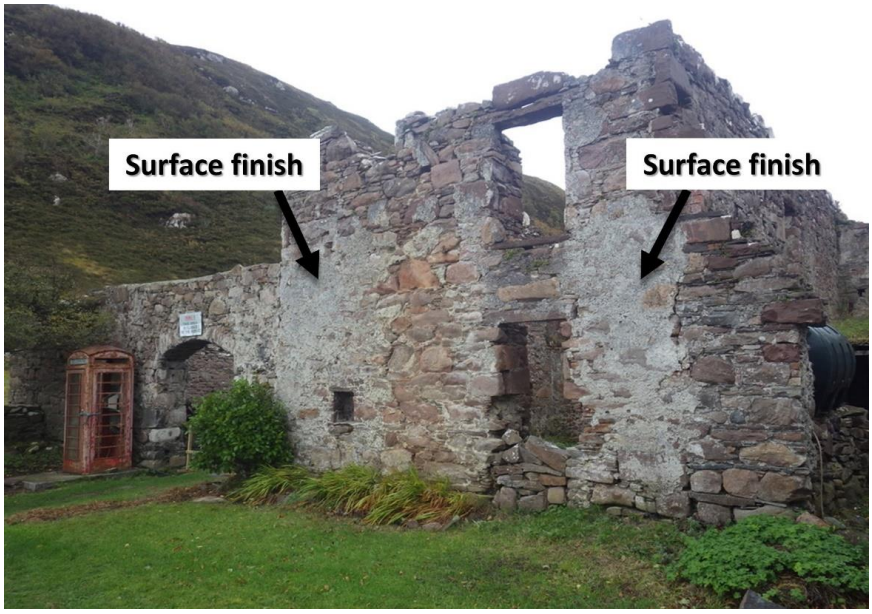

Figure 6.6 - Tanera Mòr Herring Station building, comparative lack of Torridonian Sandstone weathering seen on areas of the building that have a surface finish. Image courtesy of Timothy Meek

Comparisons made between Figure 6.6 and Figure 6.4 showcase the protective qualities of surface finish. In Figure 6.4, as highlighted, face bedded stone has suffered from surface loss leading to stone regress. Conversely, as demonstrated in Figure 6.6, areas of stone protected by surface finish remain intact and do not suffer from surface regress. Applying a surface finish could be an important factor in ensuring the longevity of structures composed of Torridonian Sandstone. However, in the case of Clachtoll Broch, a historically bare stone building, applying surface finish would lack authenticity. In the wider environment, buildings such as the Herring Station at Tanera Mòr which can be seen to have been covered by a surface finish in the past, a feasible conservation strategy would be to reapply such a finish and protect the face bedded stone from further regress and decay.

6.4 Evaluation of Research

This section brings together the completed aims and objectives that were set out in Chapter 1 through a robust analysis of the literature and associated gaps present. As is the case in any study, it is important also to reflect on limitations encountered, which contribute to future research recommendations.

6.4.1 Completed Aims and Objectives

As established in Chapter 1, knowledge on rock and stone decay has steadily increased in recent decades, however, key gaps in the literature were established as follows:

- Analysis tends to focus on fresh-cut stone, sacrificing relatability to the built environment.
- Stone is exposed to temperature extremes to elicit a weathering response within samples, sacrificing relatability to real climatic conditions.
- When undertaken, weathering simulations are rarely informed by climate data.
- Temperate climates are underrepresented, despite containing a plethora of culturally significant stone-built sites.

As a result, the following aims and objectives were put in place for this research, to address relevant literature gaps and enhance this important study area. Text beneath each set of aims and objectives ties in key findings from this research project:

- Generate a new and innovative research design that retains relatability to the built environment and climate projection data
    - Obtain SMC to access culturally significant sandstone samples from Clachtoll and Borwick Brochs. As a baseline, associated geology samples will also be collected.
    - Incorporate relevant climate projection data from UKCP18 in the creation of controlled environment facility experiments.

Scheduled monument consent was successfully obtained, allowing removal of material from archaeological spoil associated with each site, giving this research undeniable relatability to the built environment, which is severely lacking in the literature. Additionally, climate data was obtained from the UKCP18 database, ensuring this research had relatability with real climate data. RCP 8.5 was used for each CEF experiment, which is the most extreme climate projection scenario and most relatable to future climate change in Scotland.

- Understand the effects of climate change on the weathering of sandstone heritage sites in Scotland
    - Conduct in depth petrographic analyses on Torridonian Sandstone and Stromness Flagstone to determine their key characteristics, degree of weathering to date and specific strengths/weaknesses
    - Undertake two innovative climate change experiments, exposing samples to simulated weathering conditions anticipated between 2025 and 2055

    - Analyse sample response using a suite of analytical techniques to create sandstone specific decay models for the next century and provide information on potential conservation strategies

All sandstone samples were robustly characterised and analysed using a plethora of techniques. Clear weaknesses were identified upon comparison of geology rock and broch stone, specific to each sandstone type. These included microcracks, sulphide nodules and dolomite dissolution in Stromness Flagstone, as well as microcracks and distinct clay layers in Torridonian Sandstone.

Two CEF experiments were undertaken, the non-fresh-cut surface of each sandstone sample played a significant role in their weathering while incorporated in CEF experiments. This was clearly demonstrated by weathering features such as surface flaking, surface failure and salt formation in Borwick samples as well as granular loss in Clachtoll samples, which would have been extremely unlikely occurrences had fresh-cut samples been used. The pre-weathered surface of a historic building stone has been a vital feature in experimental work, without it, any conclusions drawn from this research and applied to the broch structures would lack robust backing.

Sample response was analysed using many differing techniques to build up an evidence-based decay model, specific to each sandstone type. It became clear that, despite being exposed to the exact same parameters, sample response was far more pronounced in Stromness Flagstone, when compared with Torridonian Sandstone. This highlights the importance of a more nuanced approach to understand stone material response in a climate changed future and site-specific conservation plans.

- Evaluate the effectiveness of this research design and make suggestions for the future that can enhance this study area
    - Evaluate the effectiveness of the CEF in exposing samples to climate change conditions
    - Evaluate the SMC process and the limitations it has on stone weathering research

The CEF has been highlighted as a useful technique for exposing samples to climate change conditions, as demonstrated throughout this study. A substantial number of stone weathering simulation experiments in the literature were conducted in extreme conditions. In some instances, this was achieved through laboratory simulated exposure to extreme conditions,

and in others through the study of rock and stone material in extreme environments such as deserts. As highlighted in Chapter 1, these studies are important in gaining an overall understanding of how different rock types and building stones weather, however, of importance to this research, they offer very little relatability to the cultural environment. Building stones largely do not experience the sorts of temperature extremes that are simulated in the literature and a study focussing on realistic, data-driven climate exposure has been missing. What is clear from this research, is that exposure to more realistic conditions, such as those obtained through RCP8.5 from UKCP18, does elicit a response in samples used. Although less extreme, the responses are more realistic to how building stone will weather in a climate changed future. These responses have been described as early warning indicators of future weathering and are incorporated within specific decay models (Figure 6.1).

Sample number has been the greatest limiting factor in this research and is discussed at length in the following section. Due to restrictions placed by the SMC process, access to culturally significant stone material is difficult, even for legitimate scientific research. As the overarching influence of climate change becomes clear, access to pre-weathered stone is vital as scientific efforts intensify to understand building material response in a climate changed future.

6.4.2 Limitations

An acknowledgement of limitations is required to robustly assess the methodological approach utilised. In doing so, this helps to pave the way for future research while raising questions and considerations which control to an extent the advancement of important research in this field, such as the obtainment of culturally significant material for legitimate scientific investigation.

6.4.2.1 Scheduled Monument Consent (SMC)

To ensure the relatability of this research project to the built environment, SMC was sought to obtain culturally significant material from broch sites across Scotland (detailed in Section 2.4.1 Scheduled Monument Consent: Obtaining Culturally Significant Sandstone). Although sandstone type at Borwick and Clachtoll Brochs was known, within each sandstone type there is an inherent range of compositionally differing material, relating to mineralogy, petrography and degree of weathering to date, leading to intra-site heterogeneity (Mottershead *et al.*, 2003). Illustrating this, the coastal location of each study site and the typical broch structure (Figure 6.7), specific areas within each of the Iron Age towers will

have been exposed to different weathering rates and environmental phenomena, leading to compositional differences evidenced throughout each broch. Such areas were determined to include the inner and outer broch walls, the land-facing, and sea-facing walls, as well as differences that can be attributed to the height of building stones within the structure, ranging from the base to the top of each broch wall. As highlighted in Chapter 1, differences in building stone weathering condition and quality are highly influenced by microclimates and biological cover that can be markedly different within a single structure; these impacts similarly affect intra-site sandstone composition. To account for this, SMC was sought to obtain samples directly from the broch structures, in order for the exact location and exposure history of each sample within each broch to be known.

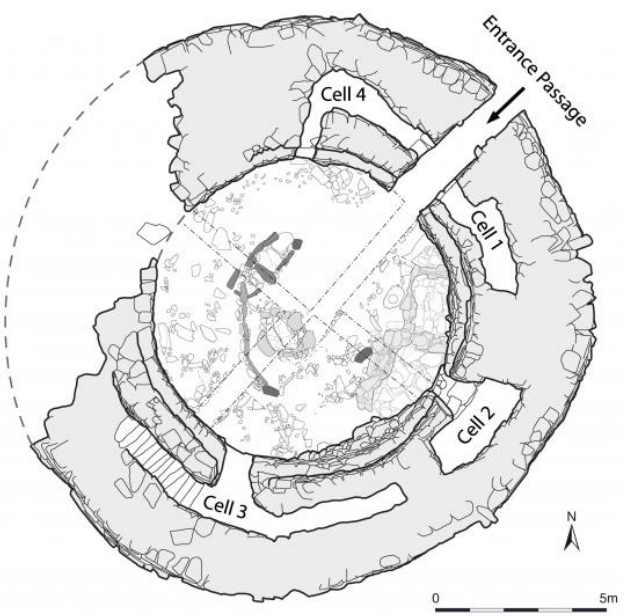

Figure 6.7 - Clachtoll Broch plan, with an outer wall (16.1m) and inner wall (8m) diameter, added (AOC Archaeology)

Ultimately, the SMC process prohibited any sample collection from the broch structures themselves. Instead, permission was granted for archaeological spoil material associated with each site to be taken, therefore, samples could not be attributed to a specific area within the broch, but only the broch in general. SMC became one of the most limiting factors influencing this thesis as a trade-off emerged between obtaining culturally significant material to incorporate in climate change experiments and the number of samples that could be taken from broch sites. Therefore, sample number was sacrificed for experimental work to be intrinsically linked to the built environment. Although a reduction in sample number had

implications on the robustness of results, this was seen as the only way to predict climate change impacts on culturally significant sandstone, while testing innovative laboratory-based climate change simulations. As established, if fresh-cut stone were used then the memory-effect held within culturally significant stone would have been lost, which has proved to be a determining factor in building stone weathering.

SMC is undoubtedly an important process that helps to safeguard Scotland's many scheduled monuments while ensuring that any work conducted does not sacrifice the authenticity of a site or cause unnecessary degradation to a site. It has, however, been detrimental to this research and greatly limited sample number incorporated within experimental work.

There is no doubt that this research would have been enhanced by increased sample number and knowledge of where samples were located within the broch. Therefore, it could be argued that for legitimate scientific research such as this, more stone material should be sacrificed with the overall objective of prolonging and protecting the site from future climate change.

Study sites utilised in this research are ruins and have suffered from extensive degradation for approximately 2000 years, with many of the building stones now located outside of the broch as archaeological spoil or reused within surrounding modern structures and drystone walls. Moreover, no relatability to the built environment is achieved from fresh-cut samples obtained from quarries and only limited relatability to building stone history is achieved by sampling from archaeological spoil. To know how heritage sites will respond to climate change, access is needed to pre-weathered sandstone. Of course, this does not mean overexploitation of building stone and removal of large volumes of culturally significant material from a structure. However, it could be argued that ruined sites such as some brochs could be utilised as a source of weathered stone for legitimate scientific investigation. To retain authenticity, samples of sandstone taken from the broch structure could be replaced by spoil heap material to ensure no additional site degradation occurs.

6.4.2.2 Climate Chambers

CEF chambers were utilised to expose samples to a systematic simulation of climate change conditions predicted for Scotland in the coming decades. In doing so, this tested an innovative methodology, aimed at understanding material decay in a climate changed future, while there is still time to generate conservation plans to protect sites from any potential acceleration of weathering detected during the experiments. It was acknowledged that effects

seen in sandstones as a result of these experiments would likely be the minimum anticipated response, compared with real climatic conditions experienced in the built environment.

The CEF allowed temperature, humidity and precipitation exposure in a climate changed future to be mimicked, however, there are several shortcomings with the chambers. Firstly, there was an inability to recreate wind-driven rain and storm events which have the potential to increase sample weathering (Briggen *et al*., 2009) and exacerbate the failure of identified sample weaknesses. Without the wind-driven rain aspect, in particular, the effect of precipitation on samples was likely limited as it lacked the suitable force to penetrate microcracks or exacerbate granular loss. Additionally, although sample exposure was supported by UKCP18 data, this made for a very constrained experiment in that temperature was confined between the predicted daily minimum and maximum values. However, in reality, climatic conditions are more variable and factors such as frost, overnight freezing and anomalous days of increased/reduced temperature do occur. Efforts could be made to mimic such events; however, this brings about a degree of subjectivity to the experiment and strays from climate data. Therefore, ensuring relatability to the real environment while sticking to predicted climate data in such experiments is a difficult balance to strike. With increased sample number, more experiments could have been run to account for this and expose samples to different climate scenarios, providing more robust results.

A further important note is that samples utilised, while in the built environment are exposed to a plethora of factors that can exacerbate decay and cannot be mimicked within a CEF experiment. These factors include but are not limited to increased biological colonisation, chemical weathering while exposed to atmospheric conditions such as air pollution caused by anthropogenic activity, increased freeze-thaw and salt weathering cycles, changes in air pressure, human interference, structure microclimates and vertical cracking brought about by load pressure within a building (Schaffer, 2016; Siegesmund *et al*, 2002; Warke et al., 2006). As it is not possible to recreate such conditions within a CEF, an acknowledgement must be made that any effect of climate change simulation witnessed in the experiments, would be amplified in the built environment. Small scale changes outlined in this research that are seen to be driven by climate change, therefore, have the potential to elicit a more dramatic weathering response in the built environment where the stone is exposed to a multitude of other pressures. As showcased, a building stone is under considerable pressures while in a structure, therefore, the added implications of climate change could trigger accelerated decay by exacerbating weathering processes that occur in the built environment.

Despite highlighted limitations surrounding the obtainment of culturally significant material and the confines of using a CEF to simulate climate change, the innovative methodological design used in this thesis undoubtedly paves the way for future climate simulation-based research projects. Relevant recommendations for subsequent research are provided in the next section.

6.5 Recommendations for Future Research

Although the primary aim of this research has been to understand the future effects of climate change on sandstone heritage in Scotland, alongside this, it has tested an innovative methodological approach designed to expose building stone to simulated weathering conditions. In doing so, clear evidence has been presented to showcase that broch stone exposed to climate changed futures elicits increased weathering, when compared to control samples and control experiment responses, indicating that the application of CEF chambers has been successful in this research. However, several limitations have been identified in the previous section and these help to pave the way for vital future research to occur.

One of the key requirements of any subsequent research in this field will be to ensure maximum relatability to the built environment, achieved to an extent in this study through the use of broch stone from archaeological spoil. However, further research that utilises material from a known location within a structure would be highly beneficial, as the past weathering of the stone would be more clearly understood before any experimental work. The SMC process would hinder such sampling, reaffirming the need to consider whether, for legitimate scientific research aimed at safeguarding Scotland's built sandstone heritage, increased access to building stone is required. It has been suggested in this chapter that access to ruinous sites such as certain brochs, would provide a source of culturally significant sandstone, with ample archaeological spoil available to replace any stone taken from the structure itself. Failing that, archaeological spoil material, as demonstrated in this research, can be considered a useful source of culturally significant stone for scientific research, and should be favoured over fresh-cut stone.

One of the most limiting factors in this research is the small sample set used, which is difficult to overcome due to SMC restrictions. Future research should strive to utilise an increased number of samples in any climate change simulation work; however, this is not always possible, especially when sandstone is sourced from culturally significant sites. It may be the case, therefore, that future research will have to make do with a small sample set,

which could be a significant limiting factor in the advancement of this research field. Alternative stone sources should be explored before using fresh-cut stone. As mentioned, these include archaeological spoil or stone found outside of a scheduled monument boundary that has been removed from the immediate monument site through human activity. If no suitable alternative can be found, fresh-cut stone could be pre-weathered through an initial CEF experiment, designed to bring the block to a suitably weathered state that would be comparable to exposure in a historic structure. A thorough analysis of the focus structure would be required to retain as much relatability to the structure as possible and ensure a realistic research design and methodology.

Turning to the CEF chambers, they are highly programmable and can be tailored to very specific and complex weathering simulations, however, are limited to temperature and humidity parameters, with a precipitation component included by opening the chamber and spraying samples with rainwater. For a more robust experimental design, customising a CEF chamber with a water inflow that can be sprayed onto samples inside the chamber at varying pressures and angles would be particularly beneficial, although would likely incur significant cost. This would, however, prevent the need to open the chamber at any point during experimental work, furthermore, simulated rainfall would be more comparable to the environment that a historic monument is located in. Additionally, varying the force of rainwater being sprayed on samples could be used to mimic storm events, which are predicted to occur with increased frequency in a climate changed future. Another approach that could be considered is the construction of small drystone walls within climate chambers. These test structures would increase relatability to the built environment by incorporating structural stressors that blocks are exposed to in historic monuments. The impact of conservation techniques could similarly be tested, such as the performance of external wall finishes in mitigating weathering effects in sandstone, brought about by climate change. An experiment exposing bare stone and lime wash coated stone to climate change conditions and comparing sample responses would be beneficial in achieving this (Meek and Addyman, 2019).

This research has shown that CEF chambers can be well suited in research that mimics complex climate change conditions in a laboratory-controlled fashion. Future research can utilise the methodological design of this thesis as a guide while considering the limitations and recommendations that have been put forward in this chapter. An ideal subsequent research project should include more samples that contain an inherent relatability to the built

environment, ideally taken from a ruinous structure or archaeological spoil in keeping with SMC restrictions. With an increased sample number, more experiments with more replicates could be conducted, exposing a wide range of building stone to multiple climate change scenarios informed by UKCP18 data. Additionally, with necessary engineering knowledge and funding, a CEF chamber could be suitably altered to include an automatic rainfall regime that can mimic storm events and wind-driven rain to enhance the experiment's relatability to the outdoor environment. Furthermore, small scale test structures could be used within chambers for added realism. Finally, CEF chambers are versatile enough to be applied to any stone decay simulation, including experiments designed to inform conservation practices for specific stone types, including assessments of protective stone coverings.

6.6 Chapter Conclusion

This research project has addressed significant literature gaps concerning stone weathering and has exposed culturally significant sandstone and associated control material to predicted climate change conditions in innovative CEF experiments, robustly informed by climate change data. Comparisons made between climate sensitised, 2018 sensitised and baseline material have demonstrated that pre-weathered stone is most susceptible to exacerbated weathering in a climate changed future. This is particularly evident in Stromness Flagstone samples taken from Borwick Broch, while Torridonian Sandstone samples from Clachtoll Broch show comparatively fewer signs of future weathering.

It has been made clear that the focus sandstones in this research weather differently, each with their own weaknesses which reach failure tipping points at varying rates. Therefore, producing a general sandstone decay model would have been inherently flawed, instead, indicative decay models have been generated that are specific to each sandstone type and based on findings from CEF experiments. These models have given insight into how focus sandstones will likely proceed to weather in a climate changed future, allowing informed conservation strategies to be postulated.

Both sites are at risk of being lost through increased coastal erosion, evidenced by seaward facing wall failures. As mentioned throughout this chapter, archaeological spoil associated with each site could be incorporated in a partial rebuild of collapsed walls, however, any hard engineered mitigation attempt would be extremely costly and difficult to implement, especially at Borwick Broch which stands on top of a promontory. Therefore, preservation by record has been highlighted as a vital practice to ensure that in the event of partial or

complete site loss, as much knowledge as possible is obtained from the site. It has also been suggested that Clachtoll Broch, given its coastal location and cultural significance evidenced by AOC archaeology work, could be a significant visitor attraction, serving as a well-preserved example of a coastal broch, should sites like Borwick become lost, too severely damaged, or too dangerous to access.

In addition to broch conservation, findings from this research can aid in the preservation of other structures composed of the same sandstone material. This can be achieved through the identification of key weathering indicators in Stromness Flagstone such as surface reddening and flaking, while in Torridonian Sandstone, extensive surface cracking can be seen as an indicator of potential surface regress. Stone replacement is suggested for particularly badly weathered building stone, while the clear benefit of applied surface finish in preventing stone regress in face bedded Torridonian Sandstone has been shown.

An evaluation of research undertaken has demonstrated that this project has addressed multiple literature gaps while implementing and assessing an innovative methodological approach that can enhance understandings of stone decay in a climate changed future. The most limiting factor has undoubtedly been the low sample number, which is a trade-off taken to ensure the cultural significance of material utilised. It is suggested that access to increased quantities of culturally significant material, particularly from ruined structures, could significantly advance this research field. The climate chambers performed well in this research and provided a platform to expose samples to predicted climate changed futures with associated control. Methods of enhancing future CEF experiments have been highlighted, including the engineering of chambers to include automatic rainfall systems, providing the ability to assess sample response to simulated storm events in a laboratory setting. It is suggested that future research should focus on the analysis of culturally significant material in favour of fresh-cut stone. Should access to cultural material be blocked through SMC, archaeological spoil can be used as a proxy, ensuring subsequent studies retain relevance to the built, historic environment. Additionally, there is very much a need to expose samples to realistic climate parameters, informed by robust climate data, and move away from exposing samples to climatic extremes that are not experienced in the built environment. This gives more focussed, site-specific insight into how culturally significant sandstone is likely to weather in a climate changed future.

In summary, this research project has demonstrated, through the application of innovative CEF experiments, that exacerbated weathering of Scotland's sandstone heritage is likely to occur in a climate changed future, whereby specific sandstone weaknesses will reach decay tipping points at a quicker rate than they have in the past. Crucially, different sandstone types will continue to weather at different rates, meaning a general sandstone decay pathway approach is not specific enough to safeguard Scotland's diverse sandstone heritage. Instead, highly specific decay models related to precise strengths, weaknesses, and exposure histories of building stone are crucial. From these considerations, relevant management plans can be considered which seek to limit stone decay in a way that does not detract from site authenticity. Finally, for this important study field to advance and prove useful in the preservation of historic monuments, future studies must incorporate pre-weathered culturally significant material and consider the overarching influence that climate change will have on exacerbating weathering of historic building stone. This research argues that any conservation plans that fail to incorporate these vital factors, will become increasingly obsolete in a climate changed future. Therefore, specific to Scotland, findings from this research indicate that there must be a shift in SMC procedures to allow for legitimate scientific research of culturally significant stone. Moreover, heritage science research and conservation strategies must ensure maximum relatability to the built environment and the climate that one of Scotland's most important assets will be exposed to in decades to come.

7 References

Abd Mutalib, M. *et al.* (2017) 'Scanning Electron Microscopy (SEM) and Energy-Dispersive X-Ray (EDX) Spectroscopy', in *Membrane Characterization*. Elsevier Inc., pp. 161–179. doi: 10.1016/B978-0-444-63776-5.00009-7.

Abollino, O. *et al.* (2008) 'Interaction of metal ions with montmorillonite and vermiculite', *Applied Clay Science*, 38(3–4), pp. 227–236. doi: 10.1016/j.clay.2007.04.002.

Adger, W. N. *et al.* (2012) 'Cultural dimensions of climate change impacts and adaptation', *Nature Climate Change*. Nature Publishing Group, 3(2), pp. 112–117. doi: 10.1038/nclimate1666.

Al-Saad, Z. and Abdel-Halim, M. A. H. (2001) 'Laboratory evaluation of various types of mortars for the conservation of Qasr al-Bint monument, Petra-Jordan', *Engineering Structures*. Elsevier, 23(8), pp. 926–933. doi: 10.1016/S0141-0296(00)00115-2.

Allen, J. R. L. (1982) 'Soft-sediment deformation structures', *Developments in Sedimentology*, 30, pp. 343–393. doi: 10.1016/S0070-4571(08)71019-7.

Arrhenius, S. (1896) *On the Influence of Carbonic Acid in the Air upon the Temperature of the Ground, Philosophical Magazine and Journal of Science Series*. Available at: http://www.globalwarmingart.com/ (Accessed: 9 June 2020).

Attfield, J. P. (2001) 'Phosphates', in *Encyclopedia of Materials: Science and Technology*. Elsevier, pp. 6896–6901. doi: 10.1016/B0-08-043152-6/01222-5.

Barrett, J. C. (1981) 'Aspects of the Iron Age in Atlantic Scotland. A case study in the problems of archaeological interpretation', *Proceedings of the Society of Antiquaries of Scotland*, 111(Hodson 1980), pp. 205–219. Available at: https://s3.amazonaws.com/academia.edu.documents/35758693/Barrett_1981_-_Aspects_of_the_Iron_Age_in_Atlantic_Scotland.pdf?AWSAccessKeyId=AKIAIWOWYYGZ2Y53UL3A&Expires=1517491054&Signature=rvH6wkDiSRF0AoaJBzNgWTE4NWc%3D&response-content-disposition=inline%3B (Accessed: 1 February 2018).

Barthelmy, D. (2012) *Mineralogy Database, Choice Reviews Online*. doi: 10.5860/choice.45-0296.

Bede, E. A. (2000) '2Characterization of surface morphology of carbonate stone and its effect on surface uptake of SO', in *Proceedings of the 9th International Congress on Deterioration and Conservation of Stone*. Elsevier, pp. 303–311. doi: 10.1016/b978-044450517-0/50112-4.

Bendle, J. M., Palmer, A. P. and Carr, S. J. (2015) 'A comparison of micro-CT and thin section analysis of Lateglacial glaciolacustrine varves from Glen Roy, Scotland', *Quaternary Science Reviews*. Pergamon, 114, pp. 61–77. doi: 10.1016/J.QUASCIREV.2015.02.008.

Berchin, I. I. *et al.* (2017) 'Climate change and forced migrations: An effort towards recognizing climate refugees', *Geoforum*. Pergamon, 84, pp. 147–150. doi: 10.1016/J.GEOFORUM.2017.06.022.

Bissell, Harold J. , Crook, Keith A.W. , Beck, Kevin Charles , Haaf, Ernst ten , Folk, Robert Louis and Schwab, F. L. (2021) 'Sedimentary rock', *Britannica*. Available at: https://www.britannica.com/science/sedimentary-rock/Evaporites (Accessed: 9 February 2021).

Bjørlykke, K. (1998) 'Clay Mineral Diagenesis in Sedimentary Basins — A Key to the Prediction of Rock Properties. Examples from the North Sea Basin', *Clay Minerals*, 33(1), pp. 15–34. doi: 10.1180/claymin.1998.033.1.03.

Bonazza, A. *et al.* (2009) ‘Mapping the impact of climate change on surface recession of carbonate buildings in Europe’, *Science of The Total Environment*. Elsevier, 407(6), pp. 2039–2050. doi: 10.1016/J.SCITOTENV.2008.10.067.

Boone, M. A. *et al.* (2014) ‘3D mapping of water in oolithic limestone at atmospheric and vacuum saturation using X-ray micro-CT differential imaging’, *Materials Characterization*. Elsevier Inc., 97, pp. 150–160. doi: 10.1016/j.matchar.2014.09.010.

BRE (2020) *British Stone testing and assessment - Stone list*. Available at: https://projects.bre.co.uk/ConDiv/stonelist/stonelist.html (Accessed: 30 April 2020).

Briggen, P. M., Blocken, B. and Schellen, H. L. (2009) ‘Wind-driven rain on the facade of a monumental tower: Numerical simulation, full-scale validation and sensitivity analysis’, *Building and Environment*. Pergamon, 44(8), pp. 1675–1690. doi: 10.1016/j.buildenv.2008.11.003.

Brimblecombe, P., Grossi, C. M. and Harris, I. (2011) ‘Climate Change Critical to Cultural Heritage’, in *Survival and Sustainability, Environmental Earth Sciences*, pp. 91–101. doi: 10.1007/978-3-540-95991-5.

British Geological Survey (2005) *Building with Scottish stone*.

British Standard Institution (2006) ‘BS EN 1936:2006 Natural stone test methods - Determination of real density and apparent density, and of total and open porosity’.

British Standard Institution (2008) *BS EN 13755:2008 Natural stone test methods - Determination of water absorption at atmospheric pressure*. doi: 10.1017/CBO9781107415324.004.

Budel, B. *et al.* (2004) ‘Reshaping of sandstone surfaces by cryptoendolithic cyanobacteria: bioalkalization causes chemical weathering in arid landscapes’, *Geobiology*. Blackwell Science Ltd, 2(4), pp. 261–268. doi: 10.1111/j.1472-4677.2004.00040.x.

Bull, P. A. and Morgan, R. M. (2013) ‘The Scanning Electron Microscope in Geomorphology’, in *Treatise on Geomorphology*. Academic Press, pp. 257–261. doi: 10.1016/B978-0-12-374739-6.00387-0.

Bullock, P. *et al.* (1985) *Handbook for soil thin section description, International Society of Soil Science*. Waine Research Publications. Available at: https://books.google.com/books/about/Handbook_for_Soil_Thin_Section_Descripti.html?id=ONdOAQAAIAAJ (Accessed: 23 October 2021).

Bunaciu, A. A., Udriştioiu, E. gabriela and Aboul-Enein, H. Y. (2015) ‘X-Ray Diffraction: Instrumentation and Applications’, *Critical Reviews in Analytical Chemistry*. Taylor and Francis Ltd., pp. 289–299. doi: 10.1080/10408347.2014.949616.

Cameron, S. *et al.* (1997) *Biological Growths on Sandstone Buildings*. Available at: file:///C:/Users/dcm5/Downloads/TAN 10 - Biologcal Growths on Sandstone Buildings - Control .pdf.

Cavers, G., Barber, J. and Heald, A. (2015) *Clachtoll Broch Conservation Strategy and Research Design*. Available at: http://portal.historicenvironment.scot/document/600000975 (Accessed: 5 February 2018).

Cavers, G., Heald, A. and Barber, J. (2011) ‘Excavation and Consolidation of Clachtoll Broch’, pp. 1–30. Available at: http://ldap.aocarchaeology.com/PDF/Clachtoll.pdf (Accessed: 2 February 2018).

Coleman, N. T., LeRoux, F. H. and Cady, J. G. (1963) ‘Biotite - Hydrobiotite - Vermiculite in soils’, *Nature*, 198(4878), pp. 409–410. doi: 10.1038/198409c0.

Colman, S. M. (1981) ‘Rock-weathering rates as functions of time’, *Quaternary Research*. No longer published by Elsevier, 15(3), pp. 250–264. doi: 10.1016/0033-5894(81)90029-6.

Craig, G. Y. (Gordon Y. and Geological Society of London. (1991) *Geology of Scotland*. Geological Society.

Dayal, A. M. and Varma, A. K. (2017) ‘Exploration Technique’, in *Shale Gas: Exploration and Environmental and Economic Impacts*. Elsevier Inc., pp. 65–93. doi: 10.1016/B978-0-12-809573-7.00005-6.

DEFRA (2021) *UKEAP: Precip-Net- Defra, UK*. Department for Environment, Food and Rural Affairs (Defra), Nobel House, 17 Smith Square, London SW1P 3JR helpline@defra.gsi.gov.uk. Available at: https://uk-air.defra.gov.uk/networks/network-info?view=precipnet (Accessed: 23 October 2021).

Dewanckele, J. *et al.* (2012) ‘4D imaging and quantification of pore structure modifications inside natural building stones by means of high resolution X-ray CT’, *Science of the Total Environment*, 416, pp. 436–448. doi: 10.1016/j.scitotenv.2011.11.018.

Dixon, J. L., Heimsath, A. M. and Amundson, R. (2009) ‘The critical role of climate and saprolite weathering in landscape evolution’, *Earth Surface Processes and Landforms*. John Wiley & Sons, Ltd., 34(11), pp. 1507–1521. doi: 10.1002/esp.1836.

Doehne, E. (2002) ‘Salt weathering: A selective review’, *Geological Society Special Publication*, 205, pp. 51–64. doi: 10.1144/GSL.SP.2002.205.01.05.

Dupont, L. and Van Eetvelde, V. (2013) ‘Assessing the potential impacts of climate change on traditional landscapes and their heritage values on the local level: Case studies in the Dender basin in Flanders, Belgium’, *Land Use Policy*. Pergamon, 35, pp. 179–191. doi: 10.1016/j.landusepol.2013.05.010.

El-Gohary, M. A. (2017) ‘Environmental impacts: Weathering factors, mechanism and forms affected the stone decaying in Petra’, *Journal of African Earth Sciences*. Pergamon, 135, pp. 204–212. doi: 10.1016/j.jafrearsci.2017.08.020.

Fatorić, S. and Seekamp, E. (2017) ‘Are cultural heritage and resources threatened by climate change? A systematic literature review’, *Climatic Change*. Springer Netherlands, 142(1–2), pp. 227–254. doi: 10.1007/s10584-017-1929-9.

Fettes, D. J. and Mendum, J. R. (1987) ‘The evolution of the Lewisian complex in the Outer Hebrides’, *Geological Society Special Publications*. Geological Society of London, 27(1), pp. 27–44. doi: 10.1144/GSL.SP.1987.027.01.04.

Fitzner, B., Heinrichs, K. and La Bouchardiere, D. (2003a) ‘Weathering damage on Pharaonic sandstone monuments in Luxor-Egypt’, *Building and Environment*. Pergamon, 38(9–10), pp. 1089–1103. doi: 10.1016/S0360-1323(03)00086-6.

Fitzner, B., Heinrichs, K. and La Bouchardiere, D. (2003b) ‘Weathering damage on Pharaonic sandstone monuments in Luxor-Egypt’, *Building and Environment*. Elsevier BV, 38(9–10), pp. 1089–1103. doi: 10.1016/S0360-1323(03)00086-6.

Folk, R. L. (1980) ‘Petrology of Sedimentary Rocks’, *Image (Rochester, N.Y.)*. Hemphill Publishing Company, (1974), pp. 3–4. Available at: https://repositories.lib.utexas.edu/handle/2152/22930 (Accessed: 20 October 2021).

Forino, G., MacKee, J. and von Meding, J. (2016) ‘A proposed assessment index for climate change-related risk for cultural heritage protection in Newcastle (Australia)’, *International Journal of Disaster Risk Reduction*. Elsevier, 19, pp. 235–248. doi: 10.1016/j.ijdrr.2016.09.003.

Francioni, F. and Lenzerini, F. (2008) *The 1972 World Heritage Convention : a commentary*. Oxford University Press. Available at: http://cadmus.eui.eu/handle/1814/8508 (Accessed: 8 December 2017).

Galán, E. and Ferrell, R. E. (2013) 'Genesis of Clay Minerals', in *Developments in Clay Science*. Elsevier B.V., pp. 83–126. doi: 10.1016/B978-0-08-098258-8.00003-1.

Gariano, S. L. and Guzzetti, F. (2016) 'Landslides in a changing climate', *Earth-Science Reviews*. Elsevier, pp. 227–252. doi: 10.1016/j.earscirev.2016.08.011.

Geng, J. *et al.* (2018) 'Temperature dependence of the thermal diffusivity of sandstone', *Journal of Petroleum Science and Engineering*. Elsevier, 164, pp. 110–116. doi: 10.1016/J.PETROL.2018.01.047.

George E. Williams (1966) 'Planar Cross-Stratification Formed by the Lateral Migration of Shallow Streams', *SEPM Journal of Sedimentary Research*. Society for Sedimentary Geology, Vol. 36(3), pp. 742–746. doi: 10.1306/74d7155a-2b21-11d7-8648000102c1865d.

Georgescu, M. S. *et al.* (2017) 'Heritage and Climate Changes in Romania: The St. Nicholas Church of Densus, from Degradation to Restoration', in *Energy Procedia*. Elsevier, pp. 76–85. doi: 10.1016/j.egypro.2017.09.374.

Ghilardi, M. and Boraik, M. (2011) 'Reconstructing the holocene depositional environments in the western part of Ancient Karnak temples complex (Egypt): A geoarchaeological approach', *Journal of Archaeological Science*. Academic Press, 38(12), pp. 3204–3216. doi: 10.1016/j.jas.2011.06.007.

Gillespie, M. R. and Tracey, E. A. (2012) *Liddle's Quarry, Orkney: a resource evaluation and assessment of past and possible future uses of extracted stone*. Available at: http://nora.nerc.ac.uk/id/eprint/501037/1/OR12070.pdf (Accessed: 25 January 2018).

Gillespie, M. R. and Tracey, E. A. (2016) *Scotland's building stone industry: a review*. Available at: www.bgs.ac.uk/gsni/ (Accessed: 23 April 2020).

Global Monitoring Laboratory (2020) *Global Monitoring Laboratory - Carbon Cycle Greenhouse Gases*. Available at: https://www.esrl.noaa.gov/gmd/ccgg/trends/ (Accessed: 9 June 2020).

Gluyas, J. (2004) 'Sedimentary Rocks: Sandstones, diagenesis and porosity evolution', in *Encyclopedia of Geology*. Elsevier Inc., pp. 141–151. doi: 10.1016/B0-12-369396-9/00309-9.

Gomez-Heras, M. and McCabe, S. (2015) 'Weathering of stone-built heritage: A lens through which to read the Anthropocene', *Anthropocene*. Elsevier, pp. 1–13. doi: 10.1016/j.ancene.2015.12.003.

Goudie, A. and Viles, H. A. (1997) *Salt weathering hazard*. Wiley.

Grossi, C. M., Brimblecombe, P. and Harris, I. (2007) 'Predicting long term freeze-thaw risks on Europe built heritage and archaeological sites in a changing climate'. doi: 10.1016/j.scitotenv.2007.02.014.

Hager, I. (2014) 'Sandstone colour change due to the high temperature exposure', in *Advanced Materials Research*. Trans Tech Publications, pp. 411–415. doi: 10.4028/www.scientific.net/AMR.875-877.411.

Hajpál, M. (2002) *Changes in Sandstones of Historical Monuments Exposed to Fire or High Temperature, Fire Technology*.

Hajpál, M. and Török, Á. (2004) 'Mineralogical and colour changes of quartz sandstones by heat', in *Environmental Geology*. Springer, pp. 311–322. doi: 10.1007/s00254-004-1034-z.

Hall, K. (1986) ‘Rock moisture content in the field and the laboratory and its relationship to mechanical weathering studies’, *Earth Surface Processes and Landforms*. John Wiley & Sons, Ltd, 11(2), pp. 131–142. doi: 10.1002/esp.3290110204.

Hall, K. and André, M.-F. (2003) ‘Rock thermal data at the grain scale: applicability to granular disintegration in cold environments’, *Earth Surface Processes and Landforms*. John Wiley & Sons, Ltd., 28(8), pp. 823–836. doi: 10.1002/esp.494.

Hall, K., Guglielmin, M. and Strini, A. (2008) ‘Weathering of granite in Antarctica: II. Thermal stress at the grain scale’, *Earth Surface Processes and Landforms*. John Wiley & Sons, Ltd., 33(3), pp. 475–493. doi: 10.1002/esp.1617.

Hall, K. and Hall, A. (1996) ‘Weathering By Wetting and Drying: Some Experimental Results’, *Earth Surface Processes and Landforms*. John Wiley & Sons, Ltd, 21(4), pp. 365–376. doi: 10.1002/(SICI)1096-9837(199604)21:4<365::AID-ESP571>3.0.CO;2-L.

Hall, K., Lindgren, B. S. and Jackson, P. (2005) ‘Rock albedo and monitoring of thermal conditions in respect of weathering: some expected and some unexpected results’, *Earth Surface Processes and Landforms*. John Wiley & Sons, Ltd., 30(7), pp. 801–811. doi: 10.1002/esp.1189.

Hall, K., Thorn, C. and Sumner, P. (2012) ‘On the persistence of “weathering”’, *Geomorphology*. Elsevier, pp. 1–10. doi: 10.1016/j.geomorph.2011.12.024.

Harkin, D. *et al.* (2020) ‘Impacts of climate change on cultural heritage’, *MCCIP Science Review*, pp. 616–641. doi: 10.14465/2020.arc26.che.

Haugen, A. and Mattsson, J. (2011) ‘International Journal of Climate Change Strategies and Management Preparations for climate change’s influences on cultural heritage Preparations for climate change’s influences on cultural heritage’, *International Journal of Climate Change Strategies and Management International Journal of Climate Change Strategies and Management Iss International Journal of Climate Change Strategies and Management*, 3(1), pp. 386–401. Available at: https://doi.org/10.1108/17568691111175678 (Accessed: 20 November 2017).

Hedges, J. W. and Bell, B. (1980) ‘That tower of Scottish prehistory-the broch’, *Antiquity*. Cambridge University Press, 54(211), pp. 87–94. doi: 10.1017/S0003598X00043064.

Heinrichs, K. (2008) ‘Diagnosis of weathering damage on rock-cut monuments in Petra, Jordan’. doi: 10.1007/s00254-008-1358-1.

Historic Environment Scotland (2011) *Traditional Building Skills - A Strategy for Sustaining and Developing Traditional Building Skills in Scotland*. Available at: www.historic-scotland.gov.uk (Accessed: 23 April 2020).

Historic Environment Scotland (2012) ‘A Climate Change Action Plan for Historic Scotland’, pp. 1–13. Available at: https://www.historicenvironment.scot/media/2611/climate-change-plan-2012.pdf (Accessed: 18 December 2017).

Historic Environment Scotland (2016) *Short Guide: Climate Change Adaptation for Traditional Buildings*. Available at: https://www.historicenvironment.scot/archives-and-research/publications/publication/?publicationId=a0138f5b-c173-4e09-818f-a7ac00ad04fb (Accessed: 21 April 2020).

Historic Environment Scotland (2017a) *A Climate Change Risk Assesment Of The Properties In Care Of Historic Purpose And Scope*.

Historic Environment Scotland (2017b) *Annual Operating Plan 2017-18*. Available at: https://www.historicenvironment.scot/media/4030/annual-operating-plan-2017-18.pdf

(Accessed: 18 December 2017).

Historic Environment Scotland (2018a) *Annual Operating Plan 2018-19*. Available at: https://www.historicenvironment.scot/archives-and-research/publications/publication/?publicationId=aabb21ef-36b0-4746-9712-a8c700d4290a.

Historic Environment Scotland (2018b) *Climate Change Risk Assessment*. Edinburgh. Available at: https://www.historicenvironment.scot/archives-and-research/publications/publication/?publicationId=55d8dde6-3b68-444e-b6f2-a866011d129a (Accessed: 16 January 2018).

Historic Environment Scotland (2018c) *Yesnaby, Broch Of Borwick | Canmore, CANMORE*. Available at: https://canmore.org.uk/site/1660/yesnaby-broch-of-borwick (Accessed: 5 February 2018).

Historic Environment Scotland (2019a) *A Guide To Climate Change Impacts | Historic Environment Scotland*. Available at: https://www.historicenvironment.scot/archives-and-research/publications/publication/?publicationId=843d0c97-d3f4-4510-acd3-aadf0118bf82 (Accessed: 21 April 2020).

Historic Environment Scotland (2019b) *Annual Operating Plan 2019-20*. Available at: https://www.historicenvironment.scot/archives-and-research/publications/publication/?publicationId=33fc749a-60c8-4402-bcfb-aa2400d24241.

Historic Environment Scotland (2019c) *Climate Risk Assessment for the Heart of Neolithic Orkney World Heritage Site*. Available at: https://www.historicenvironment.scot/archives-and-research/publications/publication/?publicationId=c6f3e971-bd95-457c-a91d-aa77009aec69 (Accessed: 21 April 2020).

Hosono, T. *et al.* (2006) 'Salt weathering of sandstone at the Angkor monuments, Cambodia: identification of the origins of salts using sulfur and strontium isotopes', *Journal of Archaeological Science*. Academic Press, 33(11), pp. 1541–1551. doi: 10.1016/j.jas.2006.01.018.

Hulme, M. *et al.* (1999) 'Relative impacts of human-induced climate change and natural climate variability', *Nature*. Nature Publishing Group, 397(February), pp. 688–691. doi: 10.1038/17789.

Huminicki, D. M. C. and Hawthorne, F. C. (2002) 'The Crystal Chemistry of the Phosphate Minerals', *Reviews in Mineralogy and Geochemistry*. GeoScienceWorld, 48(1), pp. 123–253. doi: 10.2138/rmg.2002.48.5.

ICOMOS (1964) *The Venice Charter 1964, IInd International Congress of Architects and Technicians of Historic Monuments*. Available at: https://www.icomos.org/charters/venice_e.pdf (Accessed: 8 December 2017).

Ielpi, A. and Ghinassi, M. (2015) 'Planview style and palaeodrainage of Torridonian channel belts: Applecross Formation, Stoer Peninsula, Scotland', *Sedimentary Geology*. Elsevier, 325, pp. 1–16. doi: 10.1016/j.sedgeo.2015.05.002.

IPCC (2018) *Global warming of 1.5°C*. Available at: https://www.ipcc.ch/site/assets/uploads/sites/2/2019/06/SR15_Full_Report_High_Res.pdf (Accessed: 20 September 2019).

Irving, E. and Runcorn, S. K. (1957) 'Analysis of the Palaeomagnetism of the Torridonian Sandstone Series of North-West Scotland. I', *Philosophical Transactions of the Royal Society A: Mathematical, Physical and Engineering Sciences*. The Royal Society, 250(974), pp. 83–99. doi: 10.1098/rsta.1957.0013.

Jamison, C. *et al.* (2010) *Mapping the spatial distribution of precipitation, biological soiling, and decay on monuments in Northern Ireland: towards understanding long-term stone response to moisture, Proceedings XIX Congress of the Carpathian-Balkan Geological Association*.

Johnston, B., McKinley, J. and Warke, P. (2019) 'Comparative investigation of the spatial distribution of past weathering impacts on sandstone masonry', *Geomorphology*. Elsevier, 324, pp. 25–35. doi: 10.1016/J.GEOMORPH.2018.09.022.

Johnstone, G. S. and Mykura, W. (1989) *British Regional Geology: The Northern Highlands of Scotland*. Fourth Edi. Edinburgh: Crown.

Kanamaru, T. *et al.* (2018) 'The weathering of granitic rocks in a hyper-arid and hypothermal environment: A case study from the Sør-Rondane Mountains, East Antarctica', *Geomorphology*. Elsevier, 317, pp. 62–74. doi: 10.1016/J.GEOMORPH.2018.05.015.

Keeling, C. D. *et al.* (1976) 'Atmospheric carbon-dioxide variations at Mauna-Loa Observatory, Hawaii', *Tellus*, 28(6), pp. 538–551. doi: 10.1111/j.2153-3490.1976.tb00701.x.

De Kock, T. *et al.* (2015) 'A pore-scale study of fracture dynamics in rock using X-ray micro-CT under ambient freeze-thaw cycling', *Environmental Science and Technology*. American Chemical Society, 49(5), pp. 2867–2874. doi: 10.1021/es505738d.

Kompaníková, Z. *et al.* (2014) 'Sandstone alterations triggered by fire-related temperatures', *Environmental Earth Sciences*. Springer Verlag, 72(7), pp. 2569–2581. doi: 10.1007/s12665-014-3164-2.

de la Torre, M. A. *et al.* (1991) 'Fungi in weathered sandstone from Salamanca cathedral, Spain', *Science of the Total Environment, The*. Elsevier, 107(C), pp. 159–168. doi: 10.1016/0048-9697(91)90257-F.

Lai, J. *et al.* (2018) 'A review on pore structure characterization in tight sandstones', *Earth-Science Reviews*. Elsevier, 177, pp. 436–457. doi: 10.1016/J.EARSCIREV.2017.12.003.

Lenzerini, F. (2011) 'Intangible Cultural Heritage: The Living Culture of Peoples', *European Journal of International Law*. Oxford University Press, 22(1), pp. 101–120. doi: 10.1093/ejil/chr006.

Liu, X. *et al.* (2017) 'Pore-scale characterization of tight sandstone in Yanchang Formation Ordos Basin China using micro-CT and SEM imaging from nm- to cm-scale', *Fuel*. Elsevier, 209, pp. 254–264. doi: 10.1016/J.FUEL.2017.07.068.

Manabe, S. *et al.* (1967) 'Thermal Equilibrium of the Atmosphere with a Given Distribution of Relative Humidity', *http://dx.doi.org/10.1175/1520-0469(1967)024<0241:TEOTAW>2.0.CO;2*. doi: 10.1175/1520-0469(1967)024<0241:TEOTAW>2.0.CO;2.

Marey Mahmoud, H. H. *et al.* (2011) 'Characterization of plasters from ptolemaic baths: New excavations near the Karnak Temple Complex, Upper Egypt', *Archaeometry*. Blackwell Publishing Ltd, 53(4), pp. 693–706. doi: 10.1111/j.1475-4754.2010.00572.x.

Martínez-Martínez, J. *et al.* (2013) 'Non-linear decay of building stones during freeze-thaw weathering processes', *Construction and Building Materials*. Elsevier, 38, pp. 443–454. doi: 10.1016/j.conbuildmat.2012.07.059.

Martínez-Martínez, J. *et al.* (2017) 'Stone weathering under Mediterranean semiarid climate in the fortress of Nueva Tabarca island (Spain)', *Building and Environment*. Pergamon, 121, pp. 262–276. doi: 10.1016/J.BUILDENV.2017.05.034.

McCabe, S. *et al.* (2011) 'The "Greening" of Natural Stone Buildings:Quartz Sandstone

Performance as a Secondary Indicator of Climate Change in the British Isles?', *Atmospheric and Climate Sciences*. Scientific Research Publishing, Inc, 01(04), pp. 165–171. doi: 10.4236/acs.2011.14018.

McCabe, S. *et al.* (2013) 'Changing climate, changing process: Implications for salt transportation and weathering within building sandstones in the UK', *Environmental Earth Sciences*. Springer-Verlag, 69(4), pp. 1225–1235. doi: 10.1007/s12665-013-2278-2.

McCabe, S. *et al.* (2015) 'Building sandstone surface modification by biofilm and iron precipitation: emerging block-scale heterogeneity and system response', *Earth Surface Processes and Landforms*, 40(1), pp. 112–122. doi: 10.1002/esp.3665.

McCabe, S., Smith, B. J. and Warke, P. A. (2007) 'Preliminary observations on the impact of complex stress histories on sandstone response to salt weathering: Laboratory simulations of process combinations', *Environmental Geology*. Springer-Verlag, 52(2), pp. 269–276. doi: 10.1007/s00254-006-0476-x.

McCaughie, D. *et al.* (2020) 'Baselining Sandstone Heritage for Conservation in a Climate Change(d) Future', in *Seigesmund, S. & Middendorf, B. (EDS.): Monument Future: Decay and Conservation of Stone. Proceedings of the 14th International Congress on the Deterioration and Conservation of Stone. Volume I and II. Mitteldeutscher Verlag 2020.*, pp. 717–722.

McGreevy, J. P. (1985) 'A preliminary scanning electron microscope study of honeycomb weathering of sandstone in a coastal environment', *Earth Surface Processes and Landforms*. John Wiley & Sons, Ltd, 10(5), pp. 509–518. doi: 10.1002/esp.3290100509.

McKay, C. P., Molaro, J. L. and Marinova, M. M. (2009) 'High-frequency rock temperature data from hyper-arid desert environments in the Atacama and the Antarctic Dry Valleys and implications for rock weathering', *Geomorphology*. Elsevier, 110(3–4), pp. 182–187. doi: 10.1016/j.geomorph.2009.04.005.

McKerrow, W. S., Mac Niocaill, C. and Dewey, J. F. (2000) 'The Caledonian Orogeny redefined', *Journal of the Geological Society*. Geological Society of London, 157(6), pp. 1149–1154. doi: 10.1144/jgs.157.6.1149.

Mckirdy, A. (2010) 'Orkney and Shetland A Landscape Fashioned by Geology'. Available at: www.snh.gov.uk (Accessed: 25 January 2018).

Mckirdy, A. and Crofts, R. (2010) *Scotland: The Creation of its Natural Landscape*. Scottish National Heritage. Available at: http://www.snh.org.uk/pdfs/publications/geology/scotland.pdf (Accessed: 23 January 2018).

Mcmillan, A. and Hyslop, E. (2008) *The City of Edinburgh - Landscape in Stone*.

Meek, T. and Addyman, T. (2019) *Technical Paper 10 | Historic Environment Scotland | History*. Available at: https://www.historicenvironment.scot/archives-and-research/publications/publication/?publicationid=9fc7b2b3-e3a1-4b4c-8b5b-aa8b00908af2 (Accessed: 11 May 2021).

van der Meer, J. J. M. and Menzies, J. (2011) 'The micromorphology of unconsolidated sediments', *Sedimentary Geology*. Elsevier, 238(3–4), pp. 213–232. doi: 10.1016/J.SEDGEO.2011.04.013.

Menzies, J. *et al.* (2010) 'Micromorphology: as a tool in the detection, analyses and interpretation of (glacial) sediments and man-made materials', *Proceedings of the Geologists' Association*. Elsevier, pp. 281–292. doi: 10.1016/j.pgeola.2010.07.005.

Met Office (2018) *UKCP18 Guidance: How to use the UKCP18 land projections, Met*

Office. Available at: www.metoffice.gov.uk (Accessed: 27 April 2021).

Met Office (2019) *UK Climate Projections: Headline Findings*. Available at: www.metoffice.gov.uk (Accessed: 27 April 2021).

Mirza, M. M. Q. (2003) 'Climate change and extreme weather events: Can developing countries adapt?', *Climate Policy*, 3(3), pp. 233–248. doi: 10.3763/cpol.2003.0330.

Mol, L. and Viles, H. A. (2010) 'Geoelectric investigations into sandstone moisture regimes: Implications for rock weathering and the deterioration of San Rock Art in the Golden Gate Reserve, South Africa', *Geomorphology*. Elsevier, 118(3–4), pp. 280–287. doi: 10.1016/j.geomorph.2010.01.008.

Mol, L. and Viles, H. A. (2012) 'The role of rock surface hardness and internal moisture in tafoni development in sandstone', *Earth Surface Processes and Landforms*. John Wiley & Sons, Ltd, 37(3), pp. 301–314. doi: 10.1002/esp.2252.

Moses, C., Robinson, D. and Barlow, J. (2014) 'Methods for measuring rock surface weathering and erosion: A critical review', *Earth-Science Reviews*. Elsevier, pp. 141–161. doi: 10.1016/j.earscirev.2014.04.006.

Mosoarca, M. *et al.* (2017) 'Failure analysis of historical buildings due to climate change', *Engineering Failure Analysis*. Pergamon, 82, pp. 666–680. doi: 10.1016/j.engfailanal.2017.06.013.

Mottershead, D. *et al.* (2003) 'The influence of marine salts, aspect and microbes in the weathering of sandstone in two historic structures', *Building and Environment*. Pergamon, 38(9–10), pp. 1193–1204. doi: 10.1016/S0360-1323(03)00071-4.

Mustoe, G. E. (1983) 'Cavernous weathering in the Capitol Reef Desert, Utah', *Earth Surface Processes and Landforms*. John Wiley & Sons, Ltd, 8(6), pp. 517–526. doi: 10.1002/esp.3290080603.

Mykura, W. (1976) *British Regional Geology: Orkney and Shetland*. First Edi. Edinburgh: Crown.

Nicholson, D. T. and Nicholson, F. H. (2000) 'Physical deterioration of sedimentary rocks subjected to experimental freeze–thaw weathering', *Earth Surface Processes and Landforms*. John Wiley & Sons, Ltd, 25(12), pp. 1295–1307. doi: 10.1002/1096-9837(200011)25:12<1295::AID-ESP138>3.0.CO;2-E.

Nolansnyder, D. R. and Parnell, J. (2019) 'Comparative pore surface area in primary and secondary porosity in sandstones', *Journal of Petroleum Science and Engineering*. Elsevier, 172, pp. 489–492. doi: 10.1016/j.petrol.2018.09.095.

Nong, X. and Towhata, I. (2017) 'Investigation of mechanical properties of soft rock due to laboratory reproduction of physical weathering process', *Soils and Foundations*. Elsevier, 57(2), pp. 267–276. doi: 10.1016/J.SANDF.2016.12.004.

Oguchi, C. T. (2013) 'Weathering Rinds: Formation Processes and Weathering Rates', in *Treatise on Geomorphology*. Elsevier, pp. 98–110. doi: 10.1016/B978-0-12-374739-6.00067-1.

Oliver, G. J. H., Wilde, S. A. and Wan, Y. (2008) 'Geochronology and geodynamics of Scottish granitoids from the late neoproterozoic break-up of Rodinia to Palaeozoic collision', *Journal of the Geological Society*, 165(3), pp. 661–674. doi: 10.1144/0016-76492007-105.

Owen, G. (1995) 'Soft-sediment deformation in Upper Proterozoic Torridonian Sandstones (Applecross Formation) at Torridon, northwest Scotland', *Journal of Sedimentary Research A: Sedimentary Petrology & Processes*. GeoScienceWorld, 65(A65(3)), pp. 495–504. doi:

10.1306/d4268108-2b26-11d7-8648000102c1865d.

Owen, G. and Moretti, M. (2011) 'Identifying triggers for liquefaction-induced soft-sediment deformation in sands', *Sedimentary Geology*, 235(3–4), pp. 141–147. doi: 10.1016/j.sedgeo.2010.10.003.

Owen, G. and Santos, M. G. M. (2014) 'Soft-sediment deformation in a pre-vegetation river system: the Neoproterozoic Torridonian of NW Scotland', *Proceedings of the Geologists' Association*. Elsevier, 125(5–6), pp. 511–523. doi: 10.1016/J.PGEOLA.2014.08.005.

Ozguven, A. and Ozcelik, Y. (2013) 'Investigation of some property changes of natural building stones exposed to fire and high heat', *Construction and Building Materials*, 38, pp. 813–821. doi: 10.1016/j.conbuildmat.2012.09.072.

Papida, S., Murphy, W. and May, E. (2000) 'Enhancement of physical weathering of building stones by microbial populations', *International Biodeterioration and Biodegradation*. Elsevier, 46(4), pp. 305–317. doi: 10.1016/S0964-8305(00)00102-5.

Paradise, T. R. (2002) 'Sandstone weathering and aspect in Petra, Jordan', *Zeitschrift für Geomorphologie*, 46(1), p. 1017. Available at: https://www.researchgate.net/profile/Thomas_Paradise/publication/286021419_Sandstone_weathering_and_aspect_in_Petra_Jordan/links/5672d8b608ae04d9b099af00/Sandstone-weathering-and-aspect-in-Petra-Jordan.pdf (Accessed: 27 November 2017).

Paradise, T. R. T. R. (2005) 'Petra revisited: An examination of sandstone weathering research in Petra, Jordan', *SPECIAL PAPERS-GEOLOGICAL SOCIETY OF America*. Geological Society of America, 390, pp. 39–49. doi: 10.1130/0-8137-2390-6.39.

Park, R. G. (2005) 'The Lewisian terrane model: a review', *Scottish Journal of Geology*. Geological Society of London, 41(2), pp. 105–118. doi: 10.1144/sjg41020105.

Parmesan, C. and Yohe, G. (2003) 'A globally coherent fingerprint of climate change impacts across natural systems', *Nature*. Nature Publishing Group, 421(6918), pp. 37–42. doi: 10.1038/nature01286.

Pope, G. A., Dorn, R. I. and Dixon, J. C. (1995) 'A New Conceptual Model for Understanding Geographical Variations in Weathering', *Annals of the Association of American Geographers*. Blackwell Publishing Ltd, 85(1), pp. 38–64. doi: 10.1111/j.1467-8306.1995.tb01794.x.

Pope, G. A. and Rubenstein, R. (1999) 'Anthroweathering: Theoretical Framework and Case Study for Human-Impacted Weathering', *Geoarchaeology - An International Journal*. John Wiley & Sons, Ltd, 14(3), pp. 247–264. doi: 10.1002/(SICI)1520-6548(199903)14:3<247::AID-GEA2>3.0.CO;2-6.

Porder, S. and Ramachandran, S. (2013) 'The phosphorus concentration of common rocks-a potential driver of ecosystem P status', *Plant and Soil*, 367(1–2), pp. 41–55. doi: 10.1007/s11104-012-1490-2.

Přikryl, R. *et al.* (2003) 'Experimental weathering of marlstone from Přední Kopanina (Czech Republic)—historical building stone of Prague', *Building and Environment*. Pergamon, 38(9–10), pp. 1163–1171. doi: 10.1016/S0360-1323(03)00073-8.

Prothero, D. R. and Schwab, F. (2004) *Sedimentary Geology*. 3rd edn. W.H. Freeman & Company. Available at: https://books.google.co.uk/books/about/Sedimentary_Geology.html?id=vlG-BGZhZrAC&redir_esc=y (Accessed: 9 February 2021).

R. C. Selley (1965) 'Diagnostic Characters of Fluviatile Sediments of the Torridonian

Formation (Precambrian) of Northwest Scotland', *SEPM Journal of Sedimentary Research*. Society for Sedimentary Geology, Vol. 35(2), pp. 366–380. doi: 10.1306/74d7127b-2b21-11d7-8648000102c1865d.

Rainbird, R. H. (2001) 'Detrital zircon geochronology and provenance of the Torridonian, NW Scotland', *Journal of the Geological Society*. Geological Society of London, 158(1), pp. 15–27. doi: 10.1144/jgs.158.1.15.

Reedy, C. L. (1994) 'Thin-section Petrography in Studies of Cultural Materials', *Journal of the American Institute for Conservation*. Routledge, 33(2), pp. 115–129. doi: 10.1179/019713694806124793.

Reidsma, P. *et al.* (2010) 'Adaptation to climate change and climate variability in European agriculture: The importance of farm level responses', *European Journal of Agronomy*. Elsevier, 32(1), pp. 91–102. doi: 10.1016/j.eja.2009.06.003.

Rimstidt, D. D. and Vaughan, D. J. (2003) 'Pyrite oxidation: A state-of-the-art assessment of the reaction mechanism', *Geochimica et Cosmochimica Acta*, 67(5), pp. 873–880. doi: 10.1016/S0016-7037(02)01165-1.

Ritchie, A. and Royal Commission on the Ancient and Historical Monuments of Scotland. (1996) *Orkney (Exploring Scotland's Heritage)*. Stationery Office.

Romankiewicz, T. (2016) 'Land, Stone, Trees, Identity, Ambition: the Building Blocks of Brochs', *Archaeological Journal*, 173(1), pp. 1–29. doi: 10.1080/00665983.2016.1110771.

Rössler, M. (2006) 'World Heritage cultural landscapes: A UNESCO flagship programme 1992 – 2006', *Landscape Research*. Routledge , 31(4), pp. 333–353. doi: 10.1080/01426390601004210.

Røyne, A. *et al.* (2008) 'Controls on rock weathering rates by reaction-induced hierarchical fracturing', *Earth and Planetary Science Letters*. Elsevier, 275(3–4), pp. 364–369. doi: 10.1016/j.epsl.2008.08.035.

Ruedrich, J. *et al.* (2011) 'Moisture expansion as a deterioration factor for sandstone used in buildings', *Environmental Earth Sciences*. Springer-Verlag, 63(7–8), pp. 1545–1564. doi: 10.1007/s12665-010-0767-0.

Saleh, S. A. *et al.* (2006) 'Study and Consolidation of Sandstone: Temple of Karnak, Luxor, Egypt', *Studies in Conservation*. Taylor & Francis, Ltd.International Institute for Conservation of Historic and Artistic Works, 37(2), p. 93. doi: 10.2307/1506401.

Schaffer, R. J. (2016) *The Weathering of Natural Building Stones*, *The Weathering of Natural Building Stones*. doi: 10.4324/9781315793771.

Selley, R. C. (1966) 'Petrography of the Torridonian Rocks of Raasay and Scalpay, Inverness-shire', *Proceedings of the Geologists' Association*, 77(3), pp. 293–313. doi: 10.1016/S0016-7878(66)80036-6.

Siedel, H. *et al.* (2010) 'Sandstone weathering in tropical climate: Results of low-destructive investigations at the temple of Angkor Wat, Cambodia', *Engineering Geology*. Elsevier, 115(3–4), pp. 182–192. doi: 10.1016/j.enggeo.2009.07.003.

Siegesmund, S., Weiss, T. and Vollbrecht, A. (2002) 'Natural stone, weathering phenomena, conservation strategies and case studies: Introduction', *Geological Society Special Publication*, 205, pp. 1–7. doi: 10.1144/GSL.SP.2002.205.01.01.

Singurindy, O. and Berkowitz, B. (2003) 'Flow, dissolution, and precipitation in dolomite', *Water Resources Research*. American Geophysical Union, 39(6). doi: 10.1029/2002WR001624.

Smith, B. J., McCabe, S., *et al.* (2011) ‘A commentary on climate change, stone decay dynamics and the “greening” of natural stone buildings: New perspectives on “deep wetting”’, *Environmental Earth Sciences*. Springer-Verlag, 63(7), pp. 1691–1700. doi: 10.1007/s12665-010-0766-1.

Smith, B. J., Srinivasan, S., *et al.* (2011) ‘Near-surface temperature cycling of stone and its implications for scales of surface deterioration’, *Geomorphology*. Elsevier, 130(1–2), pp. 76–82. doi: 10.1016/j.geomorph.2010.10.005.

Smith, B. J., Gomez-Heras, M. and McCabe, S. (2008) ‘Understanding the decay of stone-built cultural heritage’, *Progress in Physical Geography*, pp. 439–461. doi: 10.1177/0309133308098119.

Steffen, W., Crutzen, P. J. and McNeill, J. R. (2007) ‘The anthropocene: Are humans now overwhelming the great forces of nature?’, *Ambio*, pp. 614–621. doi: 10.1579/0044-7447(2007)36[614:TAAHNO]2.0.CO;2.

Stewart, A. D. (1982) ‘Late Proterozoic rifting in NW Scotland: the genesis of the “Torridonian”.’, *Journal of the Geological Society*. Geological Society of London, 139(4), pp. 413–420. doi: 10.1144/gsjgs.139.4.0413.

Stewart, A. D. and Donnellan, N. C. B. (1992) ‘Geochemistry and provenance of red sandstones in the Upper Proterozoic Torridon Group in Scotland’, *Scottish Journal of Geology*. Geological Society of London, 28(2), pp. 143–153. doi: 10.1144/sjg28020143.

Stoessell, R. K. and Pittman, E. D. (1990) ‘Secondary porosity revisited: the chemistry of feldspar dissolution by carboxylic acids and anions’, *American Association of Petroleum Geologists Bulletin*. American Association of Petroleum Geologists, 74(12), pp. 1795–1805. doi: 10.1306/0C9B25D3-1710-11D7-8645000102C1865D.

Sumaila, U. R. *et al.* (2011) ‘Climate change impacts on the biophysics and economics of world fisheries’, *Nature Climate Change*. Nature Publishing Group, pp. 449–456. doi: 10.1038/nclimate1301.

Sutton, J. and Watson, J. (1950) ‘The pre-Torridonian metamorphic history of the Loch Torridon and Scourie areas in the north west Highlands, and its bearing on the chronological classification of the Lewisian.’, *Quarterly Journal of the Geological Society*. Geological Society of London, 106(1–4), pp. 241–307. doi: 10.1144.

Theodossopoulos, D. *et al.* (2012) ‘The Achievement of Structural Stability in the Drystone Iron- Age Broch Towers in North Scotland’, *Nuts and bolts of construction history*, 3(Aoc 2011), pp. 1–10. Available at: https://www.researchgate.net/profile/Dimitris_Theodossopoulos/publication/267381667_The_Achievement_of_Structural_Stability_in_the_Drystone_Iron-Age_Broch_Towers_in_North_Scotland/links/54ebc0e90cf2ff89649e56ea/The-Achievement-of-Structural-Stability-in-t (Accessed: 2 February 2018).

Titchen, S. M. (1996) ‘On the construction of “outstanding universal value”: Some comments on the implementation of the 1972 UNESCO World Heritage Convention’, *Conservation and Management of Archaeological Sites*. Routledge, 1(4), pp. 235–242. doi: 10.1179/135050396793138971.

Topal, S. and Özkul, M. (2014) ‘Soft-sediment deformation structures interpreted as seismites in the kolankaya formation, denizli basin (SW Turkey)’, *Scientific World Journal*. Hindawi Publishing Corporation. doi: 10.1155/2014/352654.

Trewin, N. H. (2002) *The Geology of Scotland, The Geology of Scotland*. The Geological Society of London. doi: 10.1144/gos4p.

Tucker, H. and Carnegie, E. (2014) ‘World heritage and the contradictions of “universal value”’, *Annals of Tourism Research*. Pergamon, 47, pp. 63–76. doi: 10.1016/J.ANNALS.2014.04.003.

Turkington, A. V. (1998) ‘Cavernous weathering in sandstone: lessons to be learned from natural exposure’, *Quarterly Journal of Engineering Geology and Hydrogeology*. Geological Society of London, 31(4), pp. 375–383. doi: 10.1144/GSL.QJEG.1998.031.P4.11.

Turkington, A. V. and Paradise, T. R. (2005) ‘Sandstone weathering: A century of research and innovation’, *Geomorphology*, pp. 229–253. doi: 10.1016/j.geomorph.2004.09.028.

Turnbull, M. J. M., Whitehouse, M. J. and Moorbath, S. (1996) ‘New isotopic age determinations for the Torridonian, NW Scotland’, *Journal of the Geological Society*. Geological Society of London, 153(6), pp. 955–964. doi: 10.1144/gsjgs.153.6.0955.

UKCP (2019) *UK Climate Projections: Headline Findings*.

UNESCO (1972) ‘Convention Concerning the Protection of the World Cultural and Natural Heritage’, *General conference seventeenth session*, 1(November), pp. 135–145. doi: 10.1111/j.1468-0033.1973.tb02056.x.

UNESCO (2007a) ‘Case studies on climate change and World Heritage’. Paris, p. 82. Available at: http://whc.unesco.org/en/activities/473/ (Accessed: 18 December 2017).

UNESCO (2007b) *UNESCO World Heritage Centre - Series*. Paris. Available at: http://whc.unesco.org/en/series/22/ (Accessed: 18 December 2017).

UNESCO (2007c) *World Heritage Centre - Development of Policy Document on Impacts of Climate Change and World Heritage*. Paris. Available at: http://whc.unesco.org/en/CC-policy-document/ (Accessed: 18 December 2017).

Vallega, A. (2003) ‘The coastal cultural heritage facing coastal management’, *Journal of Cultural Heritage*. Elsevier Masson, 4(1), pp. 5–24. doi: 10.1016/S1296-2074(03)00004-9.

Valsami-Jones, E. (2021) ‘Phosphates’, in *Encyclopedia of Geology*. Elsevier, pp. 422–427. doi: 10.1016/B978-0-08-102908-4.00032-1.

Vecco, M. (2010) ‘A definition of cultural heritage: From the tangible to the intangible’, *Journal of Cultural Heritage*. Elsevier Masson, 11(3), pp. 321–324. doi: 10.1016/j.culher.2010.01.006.

Veerle, C. *et al.* (2009) ‘Multi-disciplinary characterisation of a sandstone surface crust’, *Science of the Total Environment*, 407(20), pp. 5417–5427. doi: 10.1016/j.scitotenv.2009.06.040.

Viles, H. A. (2005) ‘Microclimate and weathering in the central Namib Desert, Namibia’, *Geomorphology*, 67(1-2 SPEC. ISS.), pp. 189–209. doi: 10.1016/j.geomorph.2004.04.006.

Viles, H. A. (2013) ‘4.2 Synergistic Weathering Processes’, in *Treatise on Geomorphology*. Elsevier, pp. 12–26. doi: 10.1016/B978-0-12-374739-6.00057-9.

Viles, H. A. and Cutler, N. A. (2012) ‘Global environmental change and the biology of heritage structures’, *Global Change Biology*, 18(8), pp. 2406–2418. doi: 10.1111/j.1365-2486.2012.02713.x.

Vincent, B. *et al.* (2018) ‘Diagenesis of Rotliegend sandstone reservoirs (offshore Netherlands): The origin and impact of dolomite cements’, *Sedimentary Geology*. Elsevier B.V., 373, pp. 272–291. doi: 10.1016/j.sedgeo.2018.06.012.

Warke, P. A., McKinley, J. and Smith, B. J. (2006) ‘Variable weathering response in sandstone: Factors controlling decay sequences’, *Earth Surface Processes and Landforms*.

John Wiley & Sons, Ltd., 31(6), pp. 715–735. doi: 10.1002/esp.1284.

Warke, P.A., McKinley, J. and Smith, B. J. (2006) 'Weathering', in *Fracture and Failure of Natural Building Stones*. Dordrecht: Springer Netherlands, pp. 313–327. doi: 10.1007/978-1-4020-5077-0_20.

Warke, P. A. and Smith, B. J. (1998) 'Effects of direct and indirect heating on the validity of rock weathering simulation studies and durability tests', *Geomorphology*, 22(3–4), pp. 347–357. doi: 10.1016/S0169-555X(97)00078-0.

Warren, J. (2000) 'Dolomite: Occurence, evolution and economically important associations', *Earth Science Reviews*, 52(1–3), pp. 1–81. doi: 10.1016/S0012-8252(00)00022-2.

Waters, C. N. *et al.* (2016) 'The Anthropocene is functionally and stratigraphically distinct from the Holocene', *Science*. American Association for the Advancement of Science. doi: 10.1126/science.aad2622.

Watt, G. R. and Thrane, K. (2001) 'Early Neoproterozoic events in East Greenland', *Precambrian Research*. Elsevier, 110(1–4), pp. 165–184. doi: 10.1016/S0301-9268(01)00186-3.

Watt, W. G. T. (1882) 'Notice of the Broch Known As Burwick or Borwick, in the Township of Yescanabee and Parish of Sandwick, Orkney', *'Proceedings of the Society' (of Antiquaries of Scotland)*, 16, pp. 442–450. Available at: http://archaeologydataservice.ac.uk/archiveDS/archiveDownload?t=arch-352-1/dissemination/pdf/vol_016/16_442_450.pdf (Accessed: 5 February 2018).

Wedekind, W. and Ruedrich, J. (2006) 'Salt-weathering, conservation techniques and strategies to protect the rock cut facades in Petra/Jordan', in *Heritage, Weathering and Conservation: Proceedings of the International Conference*, pp. 261–268. Available at: http://www.academia.edu/3883158/Salt-weathering_conservation_techniques_and_strategies_to_protect_the_rock_cut_façades_in_Petra_Jordan (Accessed: 27 November 2017).

Weibel, R. and Friis, H. (2004) 'Opaque minerals as keys for distinguishing oxidising and reducing diagenetic conditions in the Lower Triassic Bunter Sandstone, North German Basin', *Sedimentary Geology*, 169(3–4), pp. 129–149. doi: 10.1016/j.sedgeo.2004.05.004.

Williams, G. E. and Schmidt, P. W. (1997) 'Palaeomagnetic dating of sub-Torridon Group weathering profiles, NW Scotland: Verification of Neoproterozoic palaeosols', *Journal of the Geological Society*. Geological Society of London, 154(6), pp. 987–997. doi: 10.1144/gsjgs.154.6.0987.

Williams, R. B. G. and Robinson, D. A. (1981) 'Weathering of sandstone by the combined action of frost and salt', *Earth Surface Processes and Landforms*. John Wiley & Sons, Ltd, 6(1), pp. 1–9. doi: 10.1002/esp.3290060102.

Wilson, M. D. and Pittman, E. D. (1977) 'Authigenic Clays in Sandstones: Recognition and Influence on Reservoir Properties and Paleoenvironmental Analysis', *SEPM Journal of Sedimentary Research*. Society for Sedimentary Geology, Vol. 47. doi: 10.1306/212f70e5-2b24-11d7-8648000102c1865d.

Xiao, M. *et al.* (2018) 'Feldspar Dissolution and Its Influence on Reservoirs: A Case Study of the Lower Triassic Baikouquan Formation in the Northwest Margin of the Junggar Basin, China', *Geofluids*. Hindawi Limited, 2018, pp. 1–19. doi: 10.1155/2018/6536419.

Yatsu, E. (1988) *Nature of Weathering, The; An Introduction*. Sozosha. Available at:

https://books.google.co.uk/books?id=-BsLAQAAIAAJ (Accessed: 20 November 2017).

Young, A. R. M. (1987) ‘Salt as an agent in the development of cavernous weathering’, *Geology*. GeoScienceWorld, 15(10), p. 962. doi: 10.1130/0091-7613(1987)15<962:SAAAIT>2.0.CO;2.

Young, R. and Young, A. (1992) ‘Introduction’, in *Sandstone Landforms*. 1st edn. Springer-Verlag Berlin Heidelberg, pp. 1–12. doi: 10.1007/978-3-642-76588-9_1.

Yuan, G. *et al.* (2015) ‘Feldspar dissolution, authigenic clays, and quartz cements in open and closed sandstone geochemical systems during diagenesis: Typical examples from two sags in Bohai Bay Basin, East China’, *AAPG Bulletin*. American Association of Petroleum Geologists, 99(11), pp. 2121–2154. doi: 10.1306/07101514004.

Yuan, G. *et al.* (2017) ‘Reactive transport modeling of coupled feldspar dissolution and secondary mineral precipitation and its implication for diagenetic interaction in sandstones’, *Geochimica et Cosmochimica Acta*. Pergamon, 207, pp. 232–255. doi: 10.1016/J.GCA.2017.03.022.

Zalasiewicz, J. *et al.* (2008) ‘Are we now living in the Anthropocene’, *GSA Today*. Geological Society of America, 18(2), p. 4. doi: 10.1130/gsat01802a.1.

Zhu, C. (2005) ‘In situ feldspar dissolution rates in an aquifer’, *Geochimica et Cosmochimica Acta*. Elsevier Ltd, 69(6), pp. 1435–1453. doi: 10.1016/j.gca.2004.09.005.

8 Appendices

Appendix A: Sandstone Physical Characteristics (Chapter 3)

8.1 Raw Data

Below are the data obtained from sandstone physical characteristic measurements, used to calculate apparent density, open porosity, and water absorption of each sandstone type. The methodological procedure is outlined in section 2.4.3 Determining the Physical Characteristics and results are presented in section 3.2 Sandstone Physical Characteristics.

Table 8.1 - Clachtoll samples physical characteristics raw data 1

Clachtoll Sample	Dry Specimen (g) (Md)	Saturated Specimen (g) (Ms)	Weight of Specimen Under Water (g) (Mh)	Vacuum Saturated Specimen (g)
C1	89.32	89.96	55.44	79.09
C2	38.50	38.87	23.92	54.18
C3	68.64	69.25	42.82	66.60
C4	79.89	80.70	49.31	66.81
C5	70.46	71.09	43.81	68.66
C6	91.20	92.05	56.28	59.80
Mean	**73.00**	**73.65**	**45.26**	**65.86**

Table 8.2 - Clachtoll samples physical characteristics raw data 2

Clachtoll Sample	Water Absorption at Atmospheric Pressure (%) (Ab)	Open Porosity (%) (Po)	Apparent Density (Kg/m^3) (Pb)
C1	1.5	4.03	2652.76
C2	1.2	3.15	2673.98
C3	1.3	3.42	2643.94
C4	1.1	2.93	2687.11
C5	1.3	3.57	2738.52
C6	1.6	4.2	2648.62
Mean	**1.3**	**3.55**	**2674.15**
SD	**0.2**	**0.5**	**35.6**

Table 8.3 - Borwick samples physical characteristics raw data 1

Borwick Sample	Dry Specimen (g) (Md)	Saturated Specimen (g) (Ms)	Weight of Specimen Under Water (g) (Mh)	Vacuum Saturated Specimen (g)
B1	77.88	79.06	49.79	89.96
B2	53.56	54.19	34.22	38.86
B3	65.82	66.67	41.85	69.26
B4	66.14	66.86	42.32	80.71
B5	67.79	68.67	43.99	71.10
B6	58.87	59.80	37.64	92.02
Mean	**65.0**	**65.9**	**41.6**	**73.65**

Table 8.4 - Borwick samples physical characteristics raw data 2

Borwick Sample	Water Absorption at Atmospheric Pressure (%) (Ab)	Open Porosity (%) (Po)	Apparent Density (Kg/m3) (Pb)
B1	0.7	1.85	2579.72
B2	1	2.47	2567.53
B3	0.9	2.31	2589.26
B4	1	2.58	2537.44
B5	0.9	2.31	2575.1
B6	0.9	2.38	2541.97
Mean	**0.9**	**2.32**	**2565.17**
SD	**0.1**	**0.25**	**20.99**

Appendix B: CEF Data

8.2 Climate Changed Year Data (Chapter 4)

Data provided below are the temperature and humidity fluctuations that occurred in the CEF experiment for a ‘Climate Changed Year’ and associated control (Table 8.5 and

Table 8.6).

Table 8.5 - CEF experimental data for 'Climate Changed Year' experiment

Week	Humidity (%)	00:00 - 01:00	01:00 - 02:00	02:00 - 03:00	03:00 - 04:00	04:00- 05:00	05:00- 06:00
1	86	3°C	3°C	3°C	4°C	4°C	4°C
2	85	2°C	2°C	2°C	2°C	3°C	3°C
3	84	3°C	3°C	3°C	3°C	4°C	4°C
4	83	3°C	3°C	4°C	4°C	4°C	5°C
5	83	6°C	6°C	7°C	7°C	8°C	8°C
6	85	11°C	11°C	12°C	12°C	13°C	13°C
7	88	12°C	12°C	13°C	13°C	14°C	14°C
8	87	14°C	14°C	14°C	14°C	15°C	15°C
9	87	11°C	11°C	12°C	12°C	13°C	13°C
10	87	10°C	10°C	10°C	11°C	11°C	12°C
11	86	7°C	7°C	7°C	8°C	8°C	8°C
12	86	2°C	2°C	2°C	2°C	3°C	3°C

06:00- 07:00	07:00- 08:00	08:00- 09:00	09:00- 10:00	10:00- 11:00	11:00- 12:00	12:00- 13:00	13:00- 14:00
4°C	4°C	5°C	5°C	5°C	6°C	6°C	6°C
3°C	4°C	4°C	4°C	4°C	5°C	5°C	5°C
4°C	5°C	5°C	5°C	6°C	6°C	7°C	7°C
5°C	5°C	6°C	6°C	7°C	7°C	8°C	8°C
9°C	9°C	10°C	10°C	11°C	12°C	13°C	13°C
14°C	14°C	15°C	16°C	17°C	18°C	18°C	18°C
15°C	15°C	16°C	16°C	16°C	17°C	17°C	17°C
16°C	16°C	17°C	17°C	18°C	18°C	19°C	20°C
14°C	14°C	15°C	15°C	15°C	16°C	16°C	16°C
12°C	13°C	13°C	13°C	13°C	14°C	14°C	14°C
8°C	9°C	9°C	9°C	9°C	10°C	10°C	10°C
3°C	3°C	4°C	4°C	4°C	5°C	5°C	5°C

14:00-15:00	15:00-16:00	16:00-17:00	17:00-18:00	18:00-19:00	19:00-20:00	20:00-21:00	21:00-22:00	22:00-23:00	23:00-00:00
6°C	6°C	6°C	5°C	5°C	5°C	4°C	4°C	3°C	3°C
5°C	5°C	5°C	4°C	4°C	4°C	3°C	3°C	3°C	2°C
6°C	6°C	6°C	5°C	5°C	5°C	5°C	4°C	4°C	3°C
8°C	7°C	7°C	6°C	6°C	5°C	5°C	5°C	4°C	4°C
13°C	12°C	12°C	11°C	10°C	9°C	9°C	8°C	8°C	7°C
17°C	17°C	17°C	16°C	16°C	15°C	14°C	14°C	13°C	12°C
16°C	16°C	16°C	15°C	15°C	14°C	14°C	13°C	13°C	13°C
20°C	19°C	18°C	18°C	17°C	17°C	16°C	15°C	15°C	14°C
16°C	15°C	15°C	15°C	14°C	14°C	13°C	12°C	12°C	12°C
14°C	14°C	13°C	13°C	12°C	12°C	11°C	11°C	10°C	10°C
10°C	10°C	9°C	9°C	8°C	8°C	7°C	7°C	7°C	7°C
5°C	5°C	4°C	4°C	3°C	3°C	2°C	2°C	2°C	2°C

Table 8.6 - CEF control data for 'Climate Changed Year' experiment

Week	Humidity (%)	00:00 - 01:00	01:00 - 02:00	02:00 - 03:00	03:00 - 04:00	04:00-05:00	05:00-06:00
1	84	1°C	1°C	1°C	2°C	2°C	3°C
2	84	1°C	1°C	1°C	2°C	2°C	3°C
3	81	4°C	4°C	4°C	4°C	5°C	5°C
4	81	4°C	4°C	4°C	5°C	5°C	5°C
5	79	5°C	5°C	6°C	6°C	7°C	7°C
6	82	9°C	9°C	10°C	10°C	11°C	11°C
7	85	12°C	12°C	12°C	12°C	13°C	13°C
8	86	11°C	11°C	11°C	12°C	12°C	13°C
9	88	9°C	9°C	9°C	10°C	10°C	11°C
10	88	8°C	8°C	8°C	9°C	9°C	9°C
11	90	3°C	3°C	3°C	3°C	4°C	4°C
12	88	2°C	2°C	2°C	3°C	3°C	4°C

06:00-07:00	07:00-08:00	08:00-09:00	09:00-10:00	10:00-11:00	11:00-12:00	12:00-13:00	13:00-14:00
3°C	3°C	4°C	4°C	4°C	5°C	5°C	5°C
3°C	3°C	4°C	4°C	4°C	5°C	5°C	5°C
5°C	6°C	6°C	7°C	7°C	8°C	8°C	8°C
6°C	6°C	7°C	7°C	8°C	8°C	9°C	9°C
7°C	8°C	8°C	9°C	9°C	10°C	11°C	11°C
12°C	12°C	12°C	13°C	13°C	14°C	14°C	15°C
14°C	14°C	15°C	15°C	16°C	16°C	17°C	17°C
13°C	14°C	14°C	15°C	15°C	16°C	16°C	16°C
11°C	12°C	12°C	13°C	13°C	14°C	14°C	14°C
9°C	9°C	10°C	10°C	10°C	11°C	11°C	11°C
4°C	4°C	5°C	5°C	5°C	6°C	6°C	6°C
4°C	4°C	4°C	5°C	5°C	5°C	5°C	5°C

14:00-15:00	15:00-16:00	16:00-17:00	17:00-18:00	18:00-19:00	19:00-20:00	20:00-21:00	21:00-22:00	22:00-23:00	23:00-00:00
5°C	5°C	5°C	4°C	4°C	3°C	3°C	2°C	2°C	2°C
5°C	5°C	5°C	4°C	4°C	3°C	3°C	2°C	2°C	2°C
7°C	7°C	7°C	6°C	6°C	5°C	5°C	4°C	4°C	4°C
9°C	8°C	8°C	7°C	7°C	6°C	6°C	5°C	5°C	5°C
11°C	10°C	10°C	9°C	9°C	8°C	8°C	7°C	7°C	6°C
15°C	15°C	14°C	14°C	12°C	12°C	11°C	11°C	10°C	10°C
17°C	16°C	16°C	16°C	15°C	14°C	14°C	13°C	13°C	12°C
16°C	16°C	15°C	15°C	14°C	13°C	13°C	12°C	12°C	11°C
14°C	14°C	13°C	13°C	12°C	12°C	11°C	11°C	10°C	9°C
11°C	11°C	10°C	10°C	10°C	9°C	9°C	8°C	8°C	8°C
6°C	6°C	5°C	5°C	5°C	4°C	4°C	3°C	3°C	3°C
5°C	5°C	5°C	4°C	4°C	4°C	3°C	3°C	2°C	2°C

8.3 30-Year Seasonal Climate Change Experiment Data (Chapter 5)

Data provided below are the exact temperature and humidity fluctuations that occurred in the CEF experiment for the 30-year seasonal climate change experiment (Table 8.7) and the associated control chamber (Table 8.8).

Table 8.7 - CEF data for '30-Year Seasonal Climate Change' experiment

Season Year/Time	00:00-06:00	06:00-11:00	11:00-16:00	16:00-21:00	21:00-00:00	Humidity (%)
Winter 2025	2°C	4°C	6°C	5°C	3°C	87.8
Spring 2025	3°C	6°C	8°C	7°C	5°C	80.9
Summer 2025	11°C	14°C	17°C	15°C	12°C	82.8
Autumn 2025	8°C	10°C	12°C	10°C	9°C	87.7
Winter 2026	1°C	2°C	5°C	3°C	2°C	88.3
Spring 2026	4°C	7°C	9°C	6°C	4°C	79.3
Summer 2026	9°C	12°C	15°C	13°C	11°C	83.2
Autumn 2026	8°C	9°C	12°C	11°C	9°C	86.7
Winter 2027	1°C	3°C	4°C	3°C	2°C	91.4
Spring 2027	3°C	6°C	8°C	7°C	5°C	82.3
Summer 2027	11°C	14°C	17°C	15°C	13°C	82.0
Autumn 2027	6°C	8°C	10°C	9°C	8°C	86.2
Winter 2028	2°C	3°C	5°C	4°C	3°C	87.5
Spring 2028	3°C	5°C	8°C	6°C	4°C	79.6
Summer 2028	10°C	12°C	15°C	13°C	11°C	84.4
Autumn 2028	8°C	10°C	12°C	10°C	9°C	88.3
Winter 2029	2°C	4°C	6°C	5°C	3°C	85.6
Spring 2029	4°C	6°C	9°C	7°C	5°C	79.6
Summer 2029	11°C	14°C	17°C	16°C	13°C	82.2
Autumn 2029	7°C	9°C	11°C	9°C	8°C	86.8
Winter 2030	1°C	3°C	5°C	4°C	3°C	86.8
Spring 2030	4°C	6°C	9°C	8°C	5°C	82.3
Summer 2030	12°C	15°C	18°C	15°C	13°C	83.6
Autumn 2030	8°C	10°C	12°C	10°C	9°C	87.0
Winter 2031	4°C	5°C	7°C	6°C	5°C	84.9

Spring 2031	4°C	7°C	10°C	8°C	5°C	79.6
Summer 2031	11°C	15°C	17°C	15°C	14°C	83.1
Autumn 2031	7°C	9°C	11°C	10°C	8°C	88.5
Winter 2032	2°C	3°C	5°C	4°C	2°C	87.8
Spring 2032	3°C	5°C	8°C	6°C	4°C	82.6
Summer 2032	10°C	13°C	16°C	14°C	13°C	82.9
Autumn 2032	7°C	9°C	12°C	10°C	9°C	87.5
Winter 2033	2°C	4°C	6°C	5°C	3°C	86.2
Spring 2033	4°C	7°C	9°C	8°C	6°C	82.3
Summer 2033	12°C	15°C	19°C	17°C	14°C	80.4
Autumn 2033	8°C	10°C	12°C	11°C	10°C	88.5
Winter 2034	2°C	4°C	6°C	5°C	4°C	87.7
Spring 2034	4°C	7°C	9°C	8°C	5°C	79.7
Summer 2034	10°C	13°C	15°C	14°C	11°C	83.7
Autumn 2034	9°C	10°C	12°C	10°C	9°C	88.9
Winter 2035	2°C	4°C	6°C	5°C	4°C	86.2
Spring 2035	4°C	7°C	10°C	8°C	5°C	80.3
Summer 2035	11°C	14°C	17°C	15°C	12°C	80.9
Autumn 2035	8°C	10°C	12°C	11°C	8°C	85.9
Winter 2036	3°C	5°C	7°C	5°C	3°C	84.2
Spring 2036	4°C	6°C	9°C	8°C	5°C	82.7
Summer 2036	10°C	13°C	15°C	14°C	11°C	84.0
Autumn 2036	8°C	10°C	12°C	10°C	9°C	87.1
Winter 2037	0°C	2°C	3°C	2°C	1°C	86.9
Spring 2037	4°C	6°C	8°C	7°C	6°C	82.9
Summer 2037	10°C	13°C	16°C	15°C	12°C	84.5
Autumn 2037	8°C	10°C	12°C	11°C	9°C	88.9
Winter 2038	1°C	3°C	5°C	3°C	2°C	88.6
Spring 2038	3°C	5°C	8°C	7°C	4°C	82.1
Summer 2038	12°C	15°C	18°C	16°C	13°C	84.0
Autumn 2038	9°C	11°C	13°C	12°C	10°C	89.0
Winter 2039	1°C	3°C	5°C	4°C	2°C	89.2

Spring 2039	4°C	7°C	9°C	8°C	6°C	81.3
Summer 2039	11°C	14°C	17°C	15°C	13°C	83.0
Autumn 2039	8°C	10°C	12°C	11°C	9°C	87.7
Winter 2040	2°C	4°C	6°C	4°C	3°C	84.9
Spring 2040	4°C	8°C	11°C	9°C	6°C	77.4
Summer 2040	12°C	15°C	18°C	16°C	13°C	81.9
Autumn 2040	9°C	11°C	14°C	13°C	10°C	87.6
Winter 2041	2°C	4°C	6°C	5°C	3°C	87.9
Spring 2041	4°C	7°C	10°C	9°C	5°C	82.7
Summer 2041	11°C	14°C	17°C	15°C	13°C	82.7
Autumn 2041	7°C	9°C	11°C	10°C	8°C	88.2
Winter 2042	3°C	4°C	6°C	5°C	4°C	84.3
Spring 2042	4°C	6°C	9°C	7°C	5°C	83.0
Summer 2042	11°C	15°C	18°C	16°C	13°C	81.1
Autumn 2042	7°C	10°C	12°C	11°C	8°C	86.3
Winter 2043	2°C	4°C	6°C	5°C	3°C	84.6
Spring 2043	4°C	6°C	8°C	6°C	5°C	83.2
Summer 2043	10°C	14°C	17°C	15°C	12°C	81.9
Autumn 2043	9°C	11°C	13°C	11°C	10°C	90.2
Winter 2044	3°C	4°C	5°C	4°C	3°C	87.0
Spring 2044	5°C	8°C	10°C	9°C	6°C	79.4
Summer 2044	11°C	14°C	17°C	15°C	12°C	83.7
Autumn 2044	8°C	9°C	11°C	10°C	9°C	87.9
Winter 2045	1°C	3°C	5°C	4°C	2°C	87.5
Spring 2045	4°C	6°C	9°C	7°C	5°C	83.9
Summer 2045	11°C	14°C	17°C	16°C	13°C	83.3
Autumn 2045	8°C	10°C	12°C	11°C	9°C	86.4
Winter 2046	1°C	3°C	4°C	3°C	2°C	87.5
Spring 2046	3°C	5°C	8°C	6°C	4°C	82.8
Summer 2046	11°C	14°C	16°C	15°C	12°C	84.8
Autumn 2046	8°C	10°C	12°C	11°C	9°C	87.6
Winter 2047	2°C	4°C	6°C	4°C	3°C	83.7

Spring 2047	5°C	7°C	10°C	8°C	6°C	80.5
Summer 2047	10°C	14°C	17°C	15°C	13°C	81.6
Autumn 2047	9°C	11°C	13°C	12°C	10°C	88.1
Winter 2048	1°C	3°C	4°C	3°C	°2°C	90.6
Spring 2048	4°C	6°C	9°C	7°C	5°C	81.6
Summer 2048	11°C	14°C	17°C	15°C	12°C	83.6
Autumn 2048	7°C	10°C	12°C	11°C	8°C	88.6
Winter 2049	3°C	5°C	7°C	5°C	3°C	84.6
Spring 2049	4°C	7°C	9°C	8°C	5°C	81.9
Summer 2049	12°C	15°C	19°C	16°C	15°C	82.3
Autumn 2049	9°C	11°C	13°C	11°C	9°C	87.9
Winter 2050	2°C	4°C	5°C	4°C	3°C	88.8
Spring 2050	4°C	7°C	9°C	8°C	5°C	81.3
Summer 2050	12°C	14°C	17°C	15°C	14°C	83.8
Autumn 2050	9°C	11°C	13°C	11°C	10°C	88.7
Winter 2051	2°C	4°C	6°C	4°C	3°C	85.1
Spring 2051	4°C	7°C	10°C	9°C	6°C	80.2
Summer 2051	12°C	16°C	19°C	18°C	14°C	80.6
Autumn 2051	8°C	10°C	12°C	11°C	9°C	87.0
Winter 2052	2°C	4°C	5°C	4°C	3°C	87.1
Spring 2052	3°C	5°C	8°C	6°C	4°C	83.4
Summer 2052	11°C	14°C	17°C	16°C	12°C	85.3
Autumn 2052	10°C	12°C	14°C	13°C	12°C	87.2
Winter 2053	2°C	4°C	5°C	4°C	3°C	86.4
Spring 2053	3°C	6°C	8°C	7°C	5°C	80.9
Summer 2053	11°C	14°C	17°C	16°C	13°C	83.0
Autumn 2053	8°C	10°C	12°C	10°C	9°C	88.0
Winter 2054	2°C	3°C	5°C	4°C	3°C	88.0
Spring 2054	5°C	7°C	10°C	7°C	6°C	81.5
Summer 2054	11°C	14°C	17°C	15°C	12°C	82.8
Autumn 2054	8°C	10°C	12°C	11°C	8°C	87.5

Table 8.8 - CEF data for '30-Year Seasonal Climate Change' experiment

Season Year/Time	00:00-06:00	06:00-11:00	11:00-16:00	16:00-21:00	21:00-00:00	Humidity (%)
Winter 2018	2°C	4°C	6°C	5°C	4°C	85.8
Spring 2018	4°C	7°C	9°C	8°C	5°C	80.5
Summer 2018	11°C	13°C	16°C	14°C	12°C	84.2
Autumn 2018	7°C	8°C	11°C	9°C	7°C	88.8

Appendix C: Sample Mass Data

8.4 Climate Changed Year (Chapter 4)

Presented below are raw sample mass measurements taken before and after the 'Climate Changed Year' experiment, outlined in section 2.4.5.1 Climate Change Experiment 1: 'Climate Changed Year', with results presented and discussed in section 4.3 Mass Analysis.

Table 8.9 - Sample mass before and after 'Climate Changed Year' experiment, exposed to 2055 N. Scotland temperature and humidity parameters

Sample	Mass Before(g)	Mass After (g)
CB1 (1)	73.44	73.08
CB2 (5)	84.42	84.34
CB3 (9)	96.14	96.11
CC1 (1)	71.80	71.77
CC2 (5)	59.49	59.46
CC3 (9)	87.94	87.92
BB1 (1)	37.25	37.21
BB2 (5)	82.04	81.97
BB3 (8)	42.09	42.03
BC1 (1)	46.12	46.11
BC2 (5)	61.62	61.60
BC3 (8)	28.81	28.79

Table 8.10 - Sample mass before and after 'Climate Changed Year' control, exposed to 2018 N. Scotland temperature and humidity parameters

Sample	Mass Before(g)	Mass After (g)
CB1 (3)	71.6	71.58
CC1 (3)	56.51	56.54
BB1 (3)	75.85	74.92
BC1 (3)	38.71	38.75

Table 8.11 - Sample mass before and after 'Climate Changed Year' experiment, exposed to 2055 N. Scotland temperature humidity and precipitation parameters

Sample	Mass Before(g)	Mass After (g)
CB1 (2)	66.46	66.43
CB2 (6)	92.78	92.70
CB3 (10)	91.18	91.13
CC1 (2)	72.17	72.16
CC2 (6)	65.05	65.04
CC3 (10)	56.81	56.80
BB1 (2)	65.76	65.66
BB2 (6)	68.77	68.69
BB3 (9)	39.95	39.88
BC1 (2)	29.64	29.65
BC2 (6)	49.29	49.28
BC3 (9)	29.36	29.35

Table 8.12 - Sample mass before and after 'Climate Changed Year' control, exposed to 2018 N. Scotland temperature, humidity, and precipitation parameters

Sample	Mass Before(g)	Mass After (g)
CB1(4)	73.47	73.43
CC1(4)	139.36	139.43
BB1(4)	97.79	97.91
BC1(4)	72.51	72.51

8.5 '30-Year Seasonal Climate Change' (Chapter 5)

Presented below are raw sample mass measurements taken before and after the '30-Year Seasonal Climate Change' experiment, outlined in section 2.4.5.2 Climate Change Experiment 2: '30-Year Seasonal Climate Change, with results presented and discussed in section 5.4 Mass Analysis.

Table 8.13 - Sample mass before and after 30-year seasonal climate change experiment, exposed to 2025-2055 N. Scotland seasonal fluctuations of temperature and humidity with wetting

Sample	Mass Before(g)	Mass After (g)
CB2 (7)	101.09	100.93
CB3 (11)	62.71	62.65
CC2 (7)	50.01	50
CC3 (11)	70.89	70.77
BB2 (7)	59.35	57.57
BB3 (10)	35.45	36.4
BC2 (7)	56.05	56.03
BC3 (10)	32.24	32.21

Table 8.14 - Sample mass before and after 30-year seasonal climate change control experiment, exposed to repeated 2018 N. Scotland seasonal fluctuations of temperature and humidity with wetting

Sample	Mass Before(g)	Mass After (g)
CB2 (8)	90.87	90.82
CC2 (8)	92.29	92.24
BB3 (11)	85.7	85.67
BC3 (11)	64.95	64.93

Appendix D: Chroma Meter

8.6 Chroma Meter Data (Chapter 5)

Presented below are raw colour measurements of L*, a*,b* and c* taken before and after the '30-Year Seasonal Climate Change' experiment, with associated colour change. The methodological procedure for this analysis is outlined in section 2.4.5.2.1 Climate Change Experiment 2: Chroma Meter and results are presented in section 5.3 Chroma Meter.

Table 8.15 - Chroma Meter experimental chamber samples before and after 30-year seasonal climate change experiment in Chapter 5, with associated L*, a* and b* change

	Before Experiment				After Experiment				Change		
Sample	**L***	**a***	**b***	**c***	**L***	**a***	**b***	**c***	**L* change**	**a* change**	**b* change**
CC2 (7)	44.75	5.13	13.55	14.49	35.17	6.67	15.84	17.19	9.58	-1.54	-2.29
	41.83	4.40	13.14	13.86	36.16	4.78	8.83	10.04	5.67	-0.38	4.31
	41.46	5.24	14.34	15.27	38.46	5.04	14.39	15.25	3.00	0.20	-0.05
	42.20	4.41	13.76	14.45	38.54	4.16	15.17	15.73	3.66	0.25	-1.41
	42.11	4.46	13.83	14.53	35.30	6.60	12.98	14.56	6.81	-2.14	0.85
Mean	**42.47**	**4.73**	**13.72**	**14.52**	**36.73**	**5.45**	**13.44**	**14.55**	**5.74**	**-0.72**	**0.28**
Standard Deviation	**1.31**	**0.42**	**0.44**	**0.50**	**1.66**	**1.13**	**2.79**	**2.70**	**2.63**	**1.07**	**2.56**

CC3 (10)	40.35	9.07	11.64	14.76	36.98	7.90	9.24	12.16	3.37	1.17	2.40
	37.44	6.49	7.85	10.19	33.95	6.80	7.89	10.42	3.49	-0.31	-0.04
	39.24	7.41	8.64	11.38	36.20	8.00	9.53	12.44	3.04	-0.59	-0.89
	40.19	7.28	8.96	11.54	35.87	7.37	8.21	11.03	4.32	-0.09	0.75
	35.80	6.66	7.44	9.99	33.27	7.94	8.92	11.94	2.53	-1.28	-1.48
Mean	**38.60**	**7.38**	**8.91**	**11.57**	**35.25**	**7.60**	**8.76**	**11.60**	**3.35**	**-0.22**	**0.15**
Standard Deviation	**1.95**	**1.02**	**1.64**	**1.91**	**1.57**	**0.51**	**0.69**	**0.85**	**0.66**	**0.90**	**1.52**
CB2 (7)	39.17	8.98	14.72	17.24	40.18	8.71	16.41	18.58	-1.01	0.27	-1.69
	40.43	9.15	15.57	18.06	30.29	5.88	10.92	12.40	10.14	3.27	4.65
	39.89	8.69	14.60	16.99	42.09	10.10	18.35	20.95	-2.20	-1.41	-3.75
	46.00	8.66	16.21	18.38	43.46	9.58	18.31	20.66	2.54	-0.92	-2.10
	38.20	8.78	14.39	16.86	41.47	9.72	17.91	20.38	-3.27	-0.94	-3.52
Mean	**40.74**	**8.85**	**15.10**	**17.51**	**39.50**	**8.80**	**16.38**	**18.59**	**1.24**	**0.05**	**-1.28**
Standard Deviation	**3.06**	**0.21**	**0.77**	**0.68**	**5.28**	**1.71**	**3.15**	**3.58**	**5.43**	**1.90**	**3.43**
CB3 (10)	37.47	8.40	11.69	14.40	44.75	5.13	13.55	14.49	-7.28	3.27	-1.86
	36.43	7.94	10.89	13.48	41.83	4.40	13.14	13.86	-5.40	3.54	-2.25
	36.56	8.62	11.72	14.55	41.46	5.24	14.34	15.27	-4.90	3.38	-2.62
	35.76	7.63	10.22	12.75	42.20	4.41	13.76	14.45	-6.44	3.22	-3.54
	38.84	8.50	11.95	14.66	42.11	4.46	13.83	14.53	-3.27	4.04	-1.88

Mean	**37.01**	**8.22**	**11.29**	**13.97**	**42.47**	**4.73**	**13.72**	**14.52**	**-5.46**	**3.49**	**-2.43**
Standard Deviation	**1.19**	**0.42**	**0.72**	**0.82**	**1.31**	**0.42**	**0.44**	**0.50**	**1.53**	**0.33**	**0.69**
BC2 (7)	37.62	1.74	6.59	6.82	38.60	4.32	14.18	14.82	-0.98	-2.58	-7.59
	36.08	1.43	6.20	6.36	36.90	6.51	17.25	18.44	-0.82	-5.08	-11.05
	38.88	2.05	6.80	7.10	41.07	2.92	11.91	12.26	-2.19	-0.87	-5.11
	37.71	0.93	5.20	5.28	37.50	6.27	17.69	18.77	0.21	-5.34	-12.49
	38.44	1.56	6.46	6.65	37.39	3.91	13.64	14.19	1.05	-2.35	-7.18
Mean	**37.75**	**1.54**	**6.25**	**6.44**	**38.29**	**4.79**	**14.93**	**15.70**	**-0.55**	**-3.24**	**-8.68**
Standard Deviation	**1.07**	**0.41**	**0.63**	**0.70**	**1.67**	**1.55**	**2.47**	**2.82**	**1.23**	**1.91**	**3.01**
BC3 (10)	53.82	0.52	7.35	7.37	50.35	5.99	19.38	20.28	3.47	-5.47	-12.03
	51.85	2.59	13.17	13.42	47.48	2.11	11.51	11.70	4.37	0.48	1.66
	50.44	0.75	7.69	7.73	46.03	0.47	7.24	7.26	4.41	0.28	0.45
	50.74	0.68	7.39	7.42	46.11	1.01	8.96	9.02	4.63	-0.33	-1.57
	50.43	1.07	8.57	8.64	47.85	4.38	16.00	16.59	2.58	-3.31	-7.43
Mean	**51.46**	**1.12**	**8.83**	**8.91**	**47.56**	**2.79**	**12.62**	**12.97**	**3.89**	**-1.67**	**-3.78**
Standard Deviation	**1.44**	**0.84**	**2.47**	**2.57**	**1.75**	**2.33**	**5.02**	**5.40**	**0.86**	**2.61**	**5.78**
BB2 (7)	49.68	13.48	24.41	27.88	47.19	9.39	17.95	20.26	2.49	4.09	6.46
	50.86	13.95	25.28	28.87	45.39	14.62	24.32	28.38	5.47	-0.67	0.96
	50.78	13.95	25.35	28.93	42.79	7.75	15.71	17.52	7.99	6.20	9.64

	50.58	14.02	25.57	29.16	45.26	15.12	24.81	29.05	5.32	-1.10	0.76
	49.83	13.99	24.77	28.45	45.60	9.07	17.27	19.51	4.23	4.92	7.50
Mean	**50.35**	**13.88**	**25.08**	**28.66**	**45.25**	**11.19**	**20.01**	**22.94**	**5.10**	**2.69**	**5.06**
Standard Deviation	**0.55**	**0.22**	**0.47**	**0.50**	**1.58**	**3.42**	**4.24**	**5.37**	**2.01**	**3.35**	**4.01**
BB3 (10)	38.83	1.91	11.83	11.98	30.02	7.39	9.74	12.23	8.81	-5.48	2.09
	40.76	2.23	13.06	13.25	34.57	8.75	12.09	14.92	6.19	-6.52	0.97
	38.74	2.13	10.38	10.60	33.00	7.29	9.29	11.81	5.74	-5.16	1.09
	34.40	1.79	9.28	9.45	34.27	8.24	11.36	14.03	0.13	-6.45	-2.08
	35.18	1.86	8.84	9.03	29.93	7.45	9.44	12.03	5.25	-5.59	-0.60
Mean	**37.58**	**1.98**	**10.68**	**10.86**	**32.36**	**7.82**	**10.38**	**13.00**	**5.22**	**-5.84**	**0.29**
Standard Deviation	**2.69**	**0.19**	**1.76**	**1.76**	**2.25**	**0.64**	**1.26**	**1.39**	**3.16**	**0.61**	**1.64**

Table 8.16 - Chroma Meter control chamber samples before and after experiment with associated L*, a* and b* change

	Before Control Experiment				**After Control Experiment**				**Change**		
Sample	**L***	**a***	**b***	**c***	**L***	**a***	**b***	**c***	**l* change**	**a* change**	**b* change**
CC2 (8)	41.25	6.02	15.32	16.46	43.93	6.76	14.76	16.23	-2.68	-0.74	0.56
	45.44	6.90	15.84	17.28	34.99	4.40	13.40	14.10	10.45	2.50	2.44
	43.67	6.34	11.86	13.45	34.99	4.40	13.40	14.10	8.68	1.94	-1.54
	41.19	4.98	12.85	13.78	42.06	6.37	14.38	15.73	-0.87	-1.39	-1.53
	44.94	6.73	15.78	17.16	43.55	6.74	15.72	17.10	1.39	-0.01	0.06
Mean	**43.30**	**6.19**	**14.33**	**15.62**	**39.90**	**5.73**	**14.33**	**15.45**	**3.39**	**0.46**	**0.00**
Standard Deviation	**2.00**	**0.76**	**1.85**	**1.86**	**4.54**	**1.23**	**0.98**	**1.33**	**5.85**	**1.69**	**1.66**
CB2 (8)	38.81	5.72	8.23	10.02	43.93	6.76	14.76	16.23	-5.12	-1.04	-6.53
	41.50	9.10	11.71	14.83	34.99	4.40	13.40	14.10	6.51	4.70	-1.69

	40.86	8.83	11.26	14.31	34.99	4.40	13.40	14.10	5.87	4.43	-2.14
	28.93	5.36	7.64	9.33	42.06	6.37	14.38	15.73	-13.13	-1.01	-6.74
	39.06	8.91	11.46	14.52	43.55	6.74	15.72	17.10	-4.49	2.17	-4.26
Mean	**37.83**	**7.58**	**10.06**	**12.60**	**39.90**	**5.73**	**14.33**	**15.45**	**-2.07**	**1.85**	**-4.27**
Standard Deviation	**5.11**	**1.87**	**1.96**	**2.69**	**4.54**	**1.23**	**0.98**	**1.33**	**8.28**	**2.80**	**2.37**
BC3 (11)	44.88	4.27	13.06	13.74	43.19	9.39	17.95	20.26	1.69	-5.12	-4.89
	43.72	4.66	12.64	13.47	45.39	14.62	24.32	28.38	-1.67	-9.96	-11.68
	46.94	4.52	12.86	13.63	42.79	7.75	15.71	17.52	4.15	-3.23	-2.85
	41.94	3.43	11.74	12.23	45.26	15.12	24.81	29.05	-3.32	-11.69	-13.07
	44.83	4.60	12.56	13.38	45.60	9.07	17.27	19.51	-0.77	-4.47	-4.71
Mean	**44.46**	**4.30**	**12.57**	**13.29**	**44.45**	**11.19**	**20.01**	**22.94**	**0.02**	**-6.89**	**-7.44**
Standard Deviation	**1.83**	**0.51**	**0.50**	**0.61**	**1.34**	**3.42**	**4.24**	**5.37**	**2.94**	**3.70**	**4.60**
BB3 (11)	26.96	0.97	4.51	4.61	20.84	1.63	5.48	5.72	6.12	-0.66	-0.97
	33.93	1.82	7.44	7.66	35.89	5.47	15.65	16.58	-1.96	-3.65	-8.21
	28.55	1.22	5.55	5.68	34.52	6.11	16.48	17.58	-5.97	-4.89	-10.93
	27.58	1.00	4.67	4.78	30.34	3.62	11.28	11.85	-2.76	-2.62	-6.61
	36.80	2.54	9.60	9.93	37.58	6.20	16.68	17.80	-0.78	-3.66	-7.08
Mean	**30.76**	**1.51**	**6.35**	**6.53**	**31.83**	**4.61**	**13.11**	**13.90**	**-1.07**	**-3.10**	**-6.76**
Standard Deviation	**4.36**	**0.67**	**2.16**	**2.25**	**6.70**	**1.96**	**4.80**	**5.17**	**4.46**	**1.58**	**3.64**